J. M. CARPENTER
Intense Pulsed Neutron Source
MAY
Action
File DESK

PROCEEDINGS OF THE 4TH MEETING OF INTERNATIONAL COLLABORATION ON ADVANCED NEUTRON SOURCES (ICANS-IV)

KEK, TSUKUBA, OCTOBER 20-24

KENS REPORT II

March 1981

Edited by

Yoshikazu ISHIKAWA
Noboru WATANABE
Yasuo ENDOH
Nobuo NIIMURA
John M. NEWSAM

NATIONAL LABORATORY FOR

J. M. CARPENTER
Intense Pulsed Neutron Source

APR 14 1981

Action_____
File_____

Proceedings
of the 4th Meeting of International Collaboration
on
Advanced Neutron Source

Oct 20-24, 1980

National Laboratory for High Energy Physics

Oho-Machi, Tsukuba-gun, Ibaraki-ken, 305 Japan

Sponsored by

National Laboratory for High Energy Physics

and the

Japan Society of Promotion of Science

Property of Jack M. Carpenter
Please return to IPNS Library
Building 360 - Room E101

PREFACE

The fourth meeting of the laboratories involved in the International Collaboration on Advanced Neutron Sources (ICANS-IV) was held at the National Laboratory for High Energy Physics (KEK) from 20 to 24 October 1980. The meeting was organized under the auspices of both KEK and Japan Society for Promotion of Science. This was the first formal ICANS meeting to be held since the ICANS membership was enlarged, and it was attended by ninety people from seven countries. The program was broadly divided into the two topics of Target Station and Instruments which were discussed in parallel sessions. It is noteworthy that three new projects of continuous or quasi-continuous spallation neutron sources were presented at the meeting and that experimental results already obtained at the spallation neutron sources were reported for the first time by three laboratories. This indicates that our collaboration program has progressed to the second stage.

The Organizing Committee for the meeting consisted of T. Kamei (KEK), K. Kikuchi (KEK), N. Watanabe (KEK), A. Masaike (KEK), M. Kimura, S. Hoshino (ISSP), K. Suzuki (Tohoku Univ.), K. Tsukada (Nihon Univ.), Y. Mori (KEK), H. Sasaki, (KEK, Chairman) and Y. Ishikawa (Tohoku Univ. ICANS Contact). A Steering Committee for the meeting was also organized consinsting of J. Carpenter (Argonne), G. J. Russell (Los Alamos), A. Carne (Rutherford), C. G. Windsor (Harwell), G. S. Bauer (Julich), J. M. Newsam (Tohoku), Y. Nakahara (JAERI), Y. Endoh (Tohoku), N. Niimura (Tohoku), N. Watanabe and ourselves. The members of this committee helped us to make a workshop-style meeting possible in our country by giving appropriate advice on the final program, promoting the meeting discussions and, finally, by writing summary reports of each session. All of their efforts are gratefully acknowledged. The format of this

report was determined in a special meeting attended by the members of the Steering Committee, which was held at Sendai on 27, October.

The authors of many of the papers from Japan owe a particular debt to J. M. Newsam who has personally devoted a lot of time to reading our manuscripts and providing many helpful suggestions and advice. We would also like to thank many of the staff in both the Research and Administration Departments at KEK for their continuous assistance in managing the meeting which was in fact the first international conference to be held at KEK. Finally we express our sincere gratitude to T. Nishikawa, the Director General of KEK, for his support and encouragement which made it possible for the ICANS-IV meeting to be realized at KEK.

H. SASAKI

Y. ISHIKAWA

CONTENTS

Welcome Address T. Nishikawa

I REVIEWS OF PROJECTS

Present Status and Future Development of WNR 1
G. A. Keyworth

The IPNS Program at Argonne National Laboratory. 16
D. L. Price, N. J. Swanson, J. M. Carpenter and C. W. Potts

Progress Report on the Construction of the Spallation Neutron Source at the Rutherford and Appleton Laboratories 28
G. Manning

The Status of the German Spallation Source Project 42
W. Klose and H. Stillor

Spallation Neutron Source at SIN 56
C. Tschalär

The Booster Synchrotron Utilization Facility at KEK. 77
H. Sasaki

Present Status of the KENS Facility. 89
Y. Ishikawa

Summary

Report of Status of Spallation Neutron Source Projects 102
J. M. Carpenter and Y. Ishikawa

II TARGET STATIONS

General

Summary of Results from the ZING-P' Pulsed Neutron Source. 105
J. M. Carpenter and IPNS Program Staff

Status of IPNS Construction 131
N. J. Swanson

Review of SNS Target Station 136
A. Carne

Layout of the Target Station for the German High Power Spallation Neutron Source Project 154
G. S. Bauer

KENS Target Station 181
N. Watanabe, S. Ikeda and Y. Ishikawa

KENS Cold Neutron Source
S. Ikeda, Y. Ishikawa and K. Inoue 200

Physics

Measurements of Spallation Target-Moderator-Reflector Neutronics at the Weapons Neutron Research Facility 210
G. J. Russel, M. M. Meier, J. S. Gilmore, R. E. Prael, H. Robinson and A. D. Taylor

Some General Results from a Calculation of a TRAM Assembly . . . 242
F. Atchison

Theoretical Studies Related to Spallation Target Physics 249
D. Filges, T. Armstrong, P. Cloth, R. D. Neef, M. Kloda, and G. Sterzenbach

Some Remarks on the Neutronics of Spallation Targets 259
W. E. Fischer and B. Sigg

High Energy Neutrons from 500 MeV Protons on Lead 277
I. M. Thorson and L. Moritz

Studies on High Energy Spallation and Fission Reactions 286
Y. Nakahara

Studies of Cold Neutron Sources for Spallation Targets 302
W. Reichardt

Engineering

Engineering, Activity Handling and Emergency Considerations for a Rotating High Power Target 313
H. Stechemesser and G. S. Bauer

Materials Problems in Beam Windows and Structural Components of the SNQ-Target 323
W. Lohmann

Liquid Metal Target Development for the German Neutron Source (SNQ) 333
H. J. Hoffmann, P. E. Huber and M. Pieshe

Free Convection Liquid Metal Target 343
C. Tschalär

Molten-Salt Target and Blanket Concept 349
K. Furukawa, K. Tsukada and Y. Nakahara

Shield and Radioactivity

KENS Radiation Shield 355
S. Ban and H. Hirayama

Beam Hole Design 359
W. S. Howells

Some Comments on Beam-tube Shielding 360
C. G. Windsor

Cost of Radiation Shielding 366
M. M. Barbier

KENS Radiation Activity: Structural Materials 376
H. Hirayama and S. Ban

Radioactivity and Radiolysis of the Solid Methane Used as a Cold Neutron Moderator in the KENS Target Assembly 381
K. Kondo and K. Hozumi

Experimental Studies of the Induced Radioactivities in a Uranium Target 392
K. Katoh, S. Ban, H. Hirayama, S. Ikeda, K. Irie, K. Kondo, M. Miyajima, S. Satoh, N. Watanabe and S. Yamaguchi

BSF Beam Control System 406
Y. Irie

Summaries

Summary of Target Physics Discussions 413
G. J. Russel

Summary on Target Engineering 415
G. S. Bauer

Summary on Discussion on Moderators with Grooved Surface 423
G. S. Bauer

Summary of Meetings on Energy Deposition in Moderators, Shielding, Activation and Safety 426
A. Carne

A Comment on Energy Deposition in the KENS Cold Moderator 433
N. Watanabe

III INSTRUMENTATION

General Papers

Instrument Development for Materials Science Research at WNR . . . 434
J. Eckert, R. N. Silver, A. Soper, P. J. Vergamini, J. Goldstone, A. Larson, P. A. Seeger and J. Yarnell

IPNS Neutron Scattering Instrument Development 460
C. S. Borso, R. Brenner, T. O. Brun, J. M. Carpenter, R. K. Crawford, J. E. Epperson, G. P. Felcher, D. G. Hinks, G. Holmblad, J. D. Jorgensen, R. Kleb, G. A. Lander, M. H. Mueller, G. E. Ostrowski, C. A. Pelizzari, F. J. Rotella, A. J. Schultz, M. G. Strauss, R. G. Teller F. Williamson and T. G. Worlton

Neutron Scattering Facilities at the Tohoku University Electron LINAC 485
K. Suzuki, N. Niimura, T. Kajitani, K. Kai, Y. Endoh, S. Tomiyoshi, K. Yamada and S. Yamaguchi

Instrument Development at the Harwell Linac 494
C. Windsor

Choppers and Guides

The Phasing of Fast Mechanical Neutron Beam Choppers to the SNS . . 499
T. J. L. Jones and J. H. parker

Neutron Guides 507
W. G. Williams and J. Penfold

Characteristics of KENS Cold Neutron Guide Tube 521
J. Mizuki, Y. Endoh, Y. Ishikawa and S. Ikeda

Total Scattering Instruments

Liquid Diffraction 531
W. S. Howells

The High Intensity Total Scattering Spectrometer (HIT) 539
N. Watanabe, T. Fukunaga, T. Shinohe, K. Yamada and T. Mizoguchi

The Powder Diffractometers 549
M. W. Johnson

The Low Q Spectrometer for the Rutherford Laboratory Spallation Neutron Source 556
R. J. Stewart

Small Angle Scattering Spectrometer (KENS-SAN) 563
Y. Ishikawa, M. Furusaka, M. Arai, N. Niimura, S. Ikeda and K. Hasegawa

Inelastic Scattering Spectrometers

A Medium Energy Inelastic Spectrometer for SNS 576
A. D. Taylor

High Energy Inelastic Spectrometer 580
B. C. Boland

High Throughput Inelastic Spectrometer 584
R. M. Richardson

High Resolution Inelastic Spectrometer 588
C. J. Carlile

Large Analyser Minor Low Energy Spectrometers, LAM(KEK) and LANDAM(HU), and Electron Linac Cold Source 592
K. Inoue, Y. Kiyanagi, M. Kohgi, Y. Ishikawa, N. Watanabe, H. Iwasa, Y. Sakamoto and K. Jinguji

Multi-Analyser Crystals Spectrometer at KENS 600
K. Tajima, K. Kanai, Y. Ishikawa, S. Tomiyoshi and C. G. Windsor

Some Background Measurements on the MAX Spectometer at KENS 607
C. G. Windsor

Polarized Neutrons

Time of Flight Spectrometer with Optical Polariser 609
Y. Endoh, J. Mizuki, Y. Sasaki and H. Ono

Polarized Neutrons 618
W. G. Williams

Neutron Polarization by Polarized Proton Filter 630
S. Ishimoto

Detectors and Data Acquisition Systems

Development of ^{6}Li Glass Scintillator in Japan 635
N. Niimura, A. Matsumoto, M. Kariya and S. Hoshino

Position Sensitive Slow Neutron Detectors Using Fibre Optic Encoding 642
P. L. Davidson and H. Wroe

Data Acquisition and Analysis Systems on SNS 655
M. W. Johnson

KENS Data Acquisition System 663
N. Niimura, M. Kohgi, M. Arai, S. Tomiyoshi, K. Tajima, M. Isobe, M. Furusaka and Y. Fujino

New Instruments

Advantage of Neutron Sources with Time Structure for Special Neutron Spectrometers 671
N. Nücker and W. Schmatz

Some New Instruments Designed to Use the Time Structure of a Quasi Continuous Spallation Neutron Source 678
B. Alefeld

Summaries

Instrumentation 690
C. G. Windsor and Y. Endoh

Data Acquisition and Detectors 704
J. M. Newsam and N. Niimura

Guides, Choppers and Polarised Beams 708
J. M. Newsam and W. G. Williams

Ultra Cold Neutrons

The Ultra Cold Neutron Production at KENS 715
H. Yoshiki

A Neutron Spectrometer for use in the Long Wavelength Limit 723
T. Dombeck

The Operation of an Ultra-Cold Neutron Source at the Argonne ZING-P' Pulsed Neutron Facility 732
T. Dombeck

Construction of KUR Ultra Cold Neutron Source with a Supermirror Neutron Turbine 743
M. Utsuro, S. Shirahama, K. Okumura, Y. Ishikawa and T. Ebisawa

A Comment on the Ultra Cold Neutron Session 758
H. Yoshiki

IV APPENDICES

ICANS-IV Program 760

Common Abbreviations 772

ICANS-IV Participants 774

WELCOME ADDRESS

T. Nishikawa

Director General --- KEK

It is my great pleasure to welcome you all to KEK, the National Laboratory for High Energy Physics in Japan. KEK is an abbreviation of the Japanese name of the Laboratory "Ko-Enerugi Butsurigaku Kenkyusho" or "Ko-E-Ken". I think it is convenient to you to remember the name Ko-E-Ken, if you want to take a taxi or a bus from your hotel to our place. Since 1970, the Japanese Government has constructed a new academic town, Tsukuba, dedicated to scientific research and education. When we came here early 1971 as one of the pioneers of this town, we saw few buildings, shops, school and hospital around this site. Only a country house of an insolvent golf-club provided us the tentative office and the accomodation for our accelerator project. We reached here from the nearest railroad station, Tsuchiura, by driving a car along a narrow curved country road; we called it as the Whisky road.

As the growth of the new town, KEK has increased its activities not only in the field of high energy physics but also in a wide application of the accelerator science. I understand that you have a tour to our facilities scheduled for this afternoon. I hope all of you will actually see our laboratories where we do the work. In particular, you will be interested in the spallation neutron source with the 500 MeV booster beam of the 12 GeV proton synchrotron, i.e. the first principal instrument of our laboratory. The neutron source just completed last June and we call it "KENS". The Booster Synchrotron Utilization Facility also contains the pulsed muon source with a superconducting muon channel and will include the medical science center for cancer therapy and diagnostics.

We are also constructing a synchrotron radiation facility, the "Photon Factory" for applications to various scientific fields. I believe, this facility will provide close and complemental research programs to the pulsed neutron project when it is completed in early 1982. Being encouraged by initial success of the laboratory project, we will proceed with our future plan, TRISTAN, i.e. a large storage ring complex.

Now, this Meeting has been organized by Professor Hiroshi Sasaki, Head of the Booster Synchrotron Utilization Facility, in cooperation with Professors Yoshikazu Ishikawa, Noboru Watanabe and other members of the Organizing Committee. I see that this is number IV in the series of meeting started in 1977 at Argonne National Laboratory where the preliminary plan was discussed between Dr. L.C.W. Hobbis, Dr. R.G. Fluharty, Dr. J.M. Carpenter and Professor M. Kimura. Professor Kimura is also a member of the present Organizing Committee.

In the letter dated on June 16, 1977, Dr. Hobbis addressed to the leading scientists who concern this subject, "I am writing as agreed during the discussion held at ANL---in which we reviewed the areas of common interest in the development of our respective

pulsed neutron source projects. It will clearly be advantageous if we can develop an effective interaction along the lines summarised in the note attached."

It was just the time we were about to start the construction of the beam line from our booster to the proposed pulsed neutron source. When I heard the story from Professor Ishikawa just after he received the letter, I certainly agreed the principle of the proposed plan, however, I was not sure that our project on the spallation neutron source could be well-financed. I am very happy after the successful meetings at Argonne, Rutherford and Los Alamos, now we can host the forth meeting at KEK.

It goes without saying that as the next generation neutron source, the spallation sources undertaken at several active laboratories in the world will provide large interesting areas on the material studies including their dynamical behaviors taking advantage of the narrow time-structures. As an outsider to the field of neutron spectroscopy, I'm not sure how you can maneuver the measurements with such a narrow intense pulsed beam, however I can suggest you that the advanced pulse techniques developed in the field of high energy physics will be also useful for you.

On the other hand, for instance, the ultra-cold neutron source you will develop should be very valuable to measure the neutron dipole moment with an extreme high precision or to investigate the neutron oscillations that are questions of great importance in the present elementary particle physics. Therefore, I am confident that the "International Collaboration on Advanced Neutron Sources" is also the "Interdiscipline Collaboration on Advanced Notable Science".

On behalf of the host institute, I do hope that throughout the meeting you will have a good time and enjoy your stay in this country including the visit to traditional Japanese places. We will do our best to help you for this purpose, and again will say welcome all of you for a wonderful meeting.

Thank you.

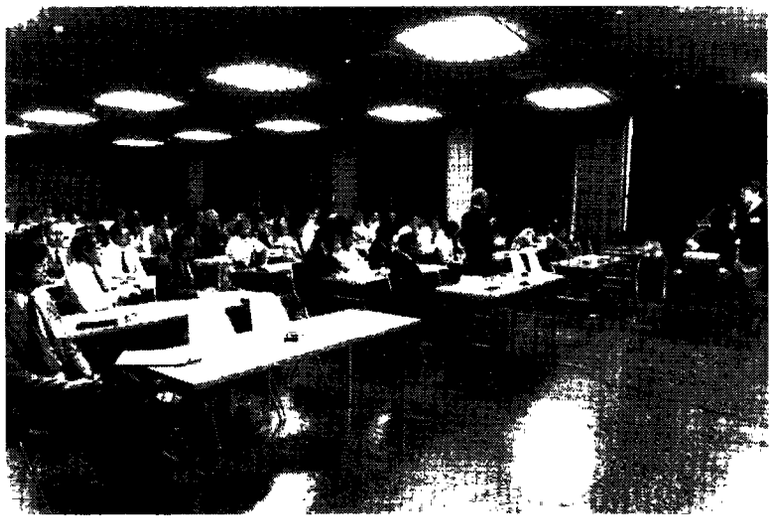

The Plenary Session

The Director-General of KEK

T. Nishikawa

The Presentation of

G.A. Keyworth at the Plenary

Session

I REVIEWS OF PROJECTS

Plenary Session

The papers included in this section were presented at the Plenary session on October 20 as reviews of the neutron source projects at each laboratory. The first three papers summarise the present status of construction of three different pulsed spallation neutron sources, while the next two papers by Prof. W. Klose and Dr. C. Tschalär outline respectively new quasi-continuous and continuous spallation neutron source projects. The last two papers' of this section describe the KEK-Booster Synchrotron Utilization Facility including both the Pulsed Neutron Source Facility (KENS) and the Meson Physics Research Facility (BOOM). Tours of these facilities were organized for the conference participants after the Plenary session. The states of the projects at all of the ICANS laboratories are summarized in the Table of the Summary report which is appended at the end of this section.

PRESENT STATUS AND FUTURE DEVELOPMENT OF WNR

G. A. Keyworth
Los Alamos Scientific Laboratory
Los Alamos, New Mexico 87545 U.S.A.

I. INTRODUCTION

The Los Alamos Weapons Neutron Research/Proton Storage Ring complex (WNR/PSR) will be a major United States facility for the study of condensed matter science, fundamental interaction physics, and nuclear physics. It will serve as a major adjunct to the Los Alamos Meson Physics Facility (LAMPF) and will contribute to its role as a thriving research center.

Our objective in developing the WNR/PSR is to provide a facility and to support the development of research programs of the highest possible quality in several areas of fundamental science of particular current interest. We believe strongly that the existence of a multi-disciplinary scientific program at the WNR/PSR will produce many synergistic interactions between the contributing disciplines that will make the facility exciting and productive.

Current interest in substantiating our theoretical understanding of the nature and role of the weak interaction provokes intense interest in the use of thermal and ultra-cold neutrons both for studying the intrinsic properties of the neutron itself, such as the electric dipole moment, and in the role of the weak interaction in neutron-induced nuclear reactions. The unique properties, including the non-critical nature, of pulsed spallation sources are particularly well suited to the production of intense beams of slow neutrons with minimum background for these studies.

Pulsed spallation sources have another application of intense current interest that is often not fully recognized. During the early stages of development of the WNR research program, it became evident that the future Proton Storage Ring would have a major impact on our ability to do neutrino physics at LAMPF. In experiments where the signal-to-noise ratio is primarily determined by the cosmic ray background, pulse compression has an obvious and direct advantage. Although the neutrino energy spectrum available with LAMPF protons is low compared to other major neutrino producing facilities, the neutrino intensity is

[illegible]ralleled. In addition, current interest in studying the intrinsic [illegible]erties of the neutrino, such as the existence of neutrino "oscillations", l[illegible] a renewed interest to relatively low-energy neutrino sources. This c[illegible]ility of the WNR/PSR will represent a major element of our multi-di[illegible]plinary scientific program.

[illegible]here has been no major new pulsed neutron source constructed in the U[illegible]tates in more than 12 years. A great variety of nuclear physics and [illegible]ar structure questions have arisen that cannot be addressed by existing sources, such as the Oak Ridge Electron Linear Accelerator. The WNR/PSR will provide a source of neutrons from thermal energies to several hundred MeV with an intensity mor than an order of magnitude greater than is currently available with existing sources. Thus, the WNR/PSR represents a major element in the future of our Laboratory's traditional emphasis upon nuclear physics.

In the last 20 years, neutron scattering has amply proven itself as a uniquely powerful tool for studying many of the properties of condensed matter. Although the United States continues to maintain a prominent position in neutron scattering research, superior facilities and support in Europe and elsewhere are rapidly eroding this position. We believe that through the development of the WNR/PSR facility and its attendant research programs the United States will continue to maintain a position at the forefront of neutron scattering research. The WNR/PSR will permit both assessment of the opportunities offered by pulsed spallation sources for neutron scattering as well as achievement of the major requirements specified for the next generation of advanced neutron sources.

A neutron scattering program was initiated at the WNR facility in 1978. The major direction of our program to date has been to explore the performance characteristics of a pulsed spallation source, to develop instruments, and to perform those significant experiments possible with a relatively low ($< 10^{14}$ n/cm^2-s) intensities. The PSR will be completed by 1985 and will increase the peak thermal flux available at the WNR by

two orders of magnitude. At that stage, the United States will possess a pulsed neutron facility with a peak thermal flux significantly greater than the steady-state flux from any research reactor in the world, as well as a completely new regime of epithermal neutron intensity.

The WNR/PSR will be open to both the United States and international scientific communities. LASL has a long history of university contacts and is operated by the University of California under a government contract. The international users program at the present LAMPF facility comprises more than 1000 members.

II. FACILITIES

The LAMPF 800-MeV linac is the world's highest intensity (1 mA) proton accelerator. The already operational WNR facility can only accept less than 1% (< 10 μA) of the LAMPF beam without having undesirably long pulse lengths for time-of-flight techniques. The PSR will compress the LAMPF pulse as well as provide variability in repetition rate, thus enhancing the overall power and versatility of the WNR by 2-3 orders of magnitude for condensed matter research and even more for some other applications such as nuclear and neutrino physics. With relatively minor upgrading of the present WNR target, the WNR/PSR will by 1986 be able to accommodate an average proton current of 100 μA and thus achieve a peak thermal neutron flux of 1.2×10^{16} n/cm^2-s with pulse characteristics optimally matched to experimental time-of-flight requirements for neutrons ranging over ten decades (0.01 eV - 100 MeV) of energy.

A. The Los Alamos Meson Physics Facility

LAMPF consists of a three-stage, high-intensity linear accelerator designed to provide a beam of protons at variable energies up to 800 MeV with an average current of 1 mA. The facility is also designed to permit simultaneous acceleration of beams of H^- ions, that will be required for input to the PSR. The LAMPF pulse profile is characterized by a macro-structure of 120 pulses per second, each approximately 750-μs long for the presently utilized 9% duty factor. Each macropulse in turn has microstructure consisting of a 50-100-ps burst every 5 ns.

The present LAMPF proton current of approximately 600 μA is constrained by target and experimental area considerations, rather than by accelerator capacity. Tests at higher currents have already indicated that the LAMPF accelerator can readily produce more than 1 mA. As with most other major research accelerators in the United States today, budget restrictions limit LAMPF to approximately six months of production per year.

A number of modifications to the LAMPF accelerator are however necessary to permit injection of 100 μA of H^- ions into the PSR. Studies by LAMPF personnel indicate that the necessary modifications can be designed and executed with only minor impact on the present operating features and production schedules. The incremental operating costs for LAMPF to supply 100 μA of H^- to the PSR are estimated to be about 3.5% of the annual LAMPF operating budget.

B. Proton Storage Ring

The function of the PSR is to accumulate relatively long proton pulses from LAMPF and to restructure them into sequences of narrow, intense pulses optimized for the time-of-flight techniques utilized at the WNR. For many nuclear physics applications, pulse widths of approximately 1 ns and high repetition rates are needed for optimum energy resolution and count rates. However, for applications where thermal and epithermal neutrons are required, pulse widths can be several hundred ns but the repetition rate must be low (10-50 Hz) to avoid frame overlap. The PSR is designed to operate in two different modes that separately optimize pulse performance for the high- and low-energy applications. In the high-energy mode, the PSR will accumulate protons in six equally spaced 1-ns long bunches to deliver protons to the target at a 720-Hz repetition rate with an average current of 10 μA. In the low-energy mode, the PSR accumulates protons in a single 270-ns pulse, and ejection is at 12 Hz. Although the presently designed average current level is 100 μA, raising the repetition rate permits a proportional increase in the average current, ultimately permitting delivery of currents significantly greater than 100 μA to an appropriate target facility.

C. Weapons Neutron Research Facility

The WNR facility was designed and built to accept up to 2% (20 μA) of the LAMPF beam. The protons impinge upon a high-Z target producing, through spallation reactions, a polychromatic spectrum of neutrons extending from 800 MeV down to approximately 100 keV. Hydrogeneous moderators adjacent to the target effectively reduce this neutron energy spectrum for low-energy applications. In addition, there is a second, low-current target room which can accommodate proton beams up to 0.1 μA.

The proton beam enters into a service cell in the high-current target where it impinges upon a high-Z target. The service cell permits access to the target in the crypt below. The crypt holds two target assemblies, and four large moderator assemblies which are mounted on remotely controlled mechanisms allowing a variety of target-moderator configurations tailored to the needs of various experimental programs. A 3.8-m-thick target shield surrounds the crypt and limits dose rates to less than 1 mrem/h at its outer surface with 10 μA of 800-MeV protons on target. This shield is penetrated by 12 neutron flight paths. Each penetration consists of a graduated opening that can be filled with collimators and beam shutters as required. Some of these flight paths can be extended outside the experimental room (beyond 15 m) with flight path 1 presently developed to 200 m. The WNR was designed to permit personnel access to the main experimental floor at all times. In order to operate the WNR at the 100-μA level some modest upgrading of the target cell and shield is required.

The long-pulse, low-repetition-rate mode of operation of the PSR can simultaneously accommodate all projected applications except those nuclear physics measurements requiring high-energy neutrons and high resolution. Present and projected scientific emphases indicate that such fundamental interaction measurements as the electric dipole moment of the neutron and determination of the parity-violating component in the n-p system as well as neutrino physics will receive major interest. If an additional, high-current target area is built, then the enormous

potential for neutrino physics achieved by the compression of the LAMPF pulse by > 10^4 can be realized in simultaneous and noninterfering operation with the condensed matter science program. With these considerations, we project that the operating mode will be optimum for the needs of the condensed matter science community at least 80% of the production time. Mechanisms are currently being studied to further increase this fraction through multiplexing techniques. Of course, this projected fraction may be modified by outstanding requirements of particular experiments as evaluated by members of the user community and LASL staff. Such questions surpass disciplinary boundaries in import.

III. RESEARCH

The particular attraction of the WNR/PSR rests in those performance characteristics which open up completely new areas of science. In the following we shall briefly describe the present status of our research efforts and indicate some future directions that appear to be particularly exciting.

A. Weak Interactions

A number of fundamental tests of the role of the weak interaction in nuclear reactions and in nuclear decays remain essential to establishing the validity of current weak-interaction theories. The extremely high peak intensities of neutrons and neutrinos available at the WNR/PSR facility will provide a unique opportunity to explore this fundamental area of research.

It is already possible to conduct some measurements with neutrinos at LAMPF. The PSR, however, will enhance the peak intensity available by nearly a factor of 10^5. There already exists intense interests in the nuclear and particle physics communities to use the PSR for these measurements.

Neutrons themselves also represent a powerful tool by which to measure the weak-interaction component in strong interactions. However, this weak-interaction component is generally a miniscule fraction of the total interaction. Thus, intense beams of very low-energy neutrons are

required to provide adequate statistics and high cross sections. We are currently exploring the feasibility, with encouraging results, of using the WNR beam to explore the parity-violating, weak-interaction component in the fundamental interaction between neutrons and protons by measuring the circular polarization of the gamma-rays resulting from n-p capture.

Another fundamental measurement is the magnitude of the electric dipole moment of the neutron as a measurement of the weak interaction component in this fundamental decay. We are currently collaborating with university researchers to develop techniques to exploit the WNR facility as a source of ultracold neutrons to support this and other measurements.

B. Nuclear Physics

Because of the difficulty in producing and detecting neutrons, the study of nuclear structure using neutrons as a probe is a difficult art. With the advent of the PSR at the WNR facility, sufficient intensity will become available to substantially reduce this inherent difficulty and will permit unprecedentedly high energy resolution.

One of the major experimental tools currently under development at LASL involves using beams of polarized neutrons and polarized targets to explore the role of spin in nuclear reactions through the study of nuclear resonances. We expect this technique to reveal new vistas in our understanding of nuclear structure, as preliminary experiments using polarized neutrons on polarized fissionable nuclei have already revealed.

The PSR will permit us to produce high intensity pulses of high energy neutrons of 1-ns duration to allow measurements with very high energy resolution. For example, as theoretical understanding of quark-gluon models of fundamental nuclear structure evolves, evidence of this radically new picture of nuclear matter may conceivably display itself in aspects of nuclear structure. The unique capability for high-resolution experiments with neutrons at the WNR/PSR will offer a high-precision tool for exploring such microscopic phenomena in nuclear reactions.

C. Condensed Matter Science

1. Motivation

The development of the WNR/PSR pulsed neutron source at Los Alamos and the new synchrotron light sources provide the next generation of

facilities required for the United States to remain at the forefront of condensed matter science in the next decade. The WNR/PSR is the only next generation United States thermal neutron source under construction capable of providing an order of magnitude improvement in peak flux over the highly successful, but aging, research reactors at BNL and ORNL. It will permit us to remain competitive in the 1980's with new pulsed neutron sources at various stages of development throughout the world.

The WNR/PSR will provide access to new areas of scientific research. For example, neutron scattering at epithermal energies ($E > 0.1$ eV) will be practical for the first time because of the several orders of magnitude increase in epithermal flux compared to research reactors ($\phi \sim 1/E$ for WNR/PSR whereas $\phi \sim e^{-E/kT}$ for reactors). The potential applications for using the large energy and momentum transfer possible with epithermal neutrons are vast, ranging from chemical spectroscopy to crystal field levels of magnetic rare-earth atoms.

It should be noted that the WNR/PSR can provide information complementary to that provided by investigations at synchrotron light sources. It will be possible to probe electronic transitions in the characteristic eV range of magnetic materials by coupling to the neutron magnetic moment while synchrotron light permits measurements of electronic band structures in the same range through photoelectron spectroscopy. In general, the new synchrotron light sources and the WNR/PSR will extend the complementary aspects of neutron and x-ray sources into new energy and intensity ranges.

The WNR/PSR will also be complementary to research reactors. For example, hydrogen potentials in metal hydrides as determined through inelastic epithermal neutron scattering are important to understanding hydrogen diffusion as inferred through measurement of quasielastic scattering at reactors.

The pulsed nature of the WNR/PSR source and time-of-flight instrumentation will also offer substantial advantages for many measurements. Examples are powder, amorphous, and liquids diffraction where there is an increase of two orders of magnitude in the number of useful resolution elements over that possible with steady-state experiments.

2. Development of the Neutron Scattering Program

Because of the obvious scientific potential of the WNR source, LASL initiated a new neutron scattering research group in 1978. The present mission and expected development of this group is coupled to the planned improvements in neutron source performance and to a growing role in serving a national user community.

With the neutron source characteristics expected between 1980 and 1985, 11 μA of 800-MeV protons in 8-μs pulses at frequencies up to 120 Hz, the WNR will be a factor of 50-100 more intense than the old Harwell linac upon which is based much of the confidence in the scientific future of pulsed neutron sources. An initial objective during this period will be to develop and test new instrument concepts required for optimal utilization of both the WNR and the much more intense WNR/PSR. This development is required due to limited experience with time-of-flight instrumentation at existing reactors and electron linacs, the unprecedented source characteristics such as the fast neutron background, and advances in technology in areas such as data acquisition and position sensitive detectors that make practical envisioning experiments with millions of resolution elements. As successful instruments are built they will be used to explore those scientific questions to which they are suited.

The changes in neutron source characteristics after PSR operation commences in 1985 will make the WNR a much more versatile and powerful tool for condensed matter research. As discussed above, the WNR/PSR will provide 100 μA of 800-MeV protons to a target in 0.27-μs pulses resulting in a 1.2×10^{16} n/cm^2-s peak thermal flux at a repetition rate of 12 Hz. This capability will also permit an order of magnitude improvement in time-of-flight resolution and in flux for experiments with epithermal neutrons. For example, liquids diffraction studies without the uncertainties of Placzek corrections should be possible. With a peak thermal flux of 10^{16} n/cm^2-s the source will also be competitive with research reactors for most applications in the thermal neutron range. For example, the high intensities will make possible

studies of small volumes of difficult to obtain samples or of difficult to observe phenomena. The low repetition rate and easy implementation of cold moderators will be especially advantageous for experiments with long-wavelength neutrons. Thus, the WNR/PSR will be competitive for polymer studies by small Q scattering, diffusion studies in solids by quasielastic scattering, and surface studies by ultracold neutrons.

At this point, it is easy to continue to speculate on the specific areas of science upon which the WNR/PSR will have the most dramatic impact. However, the history of such predictions shows that much of the best science that will ultimately develop at the WNR/PSR will elude our best prediction. The important considerations are that neutrons are a proven powerful probe of condensed matter, and that the WNR/PSR will provide neutrons at new intensities, energies, and with a time structure that will permit development of new experimental techniques.

Experience with the WNR/PSR will make possible an assessment of the value of yet another regime of neutron intensity potentially available with spallation sources. The WNR/PSR itself will still have considerable capacity for further flux increases because of the 1 mA and greater intrinsic capability of LAMPF.

3. Present Activities in Neutron Scattering

The immediate activities of the neutron scattering program at LASL include a number of experiments that benefit from the unique characteristics of the WNR, support the development of a set of prototype time-of-flight instruments, or support the development of the WNR as a facility. The WNR is now close to being in a production mode for condensed matter research.

The initial inelastic neutron scattering research program has emphasized the study of local phonon modes in solids, and chemical spectroscopy. The most productive research area has been the measurement of the high-energy vibrational spectra of metal hydrides. This information is used to determine hydrogen potentials, hydrogen sites, anharmonicity,

and the effects of phase transitions. These potentials are of particular importance in understanding the probable quantum mechanical origin of fast hydrogen diffusion in these materials.

Preliminary measurements have also been conducted of the spectra of hydrocarbons absorbed on surfaces. These observations should make it possible to monitor the evolution of chemical reactions and to determine bonding sites at surfaces. These results will complement measurements at lower energy transfer performed at reactors. The particular approach we have pursued is to use large surface area materials such as grafoil and dispersed-metal catalysts. Also, we have examined the vibrational spectra of metallic hexamines where severe distortions of NH_3 groups have been indicated. Such measurements are carried out using a crystal analyzer spectrometer which is particularly suited to measurements at large energy ($\Delta E > 0.1$ eV) and large momentum transfers ($\Delta Q > 2\ A^{-1}$).

For future development, we are evaluating concepts such as constant Q and high symmetry spectrometers. These instruments would permit studies of elementary excitations in single crystals. A possible application would be the study of very high stiffness spin wave spectra.

The most versatile instrument for inelastic scattering measurements at pulsed sources will probably be a neutron chopper. We have been experimenting with a 240-Hz chopper with Cd slits acquired from the now defunct MTR reactor. We have accomplished phasing the chopper to the neutron pulses by controlling both the chopper frequency and phase by active damping, and by controlling the firing of LAMPF proton pulses. The chopper has been used to confirm observations made with the crystal analyzer of a 15-MeV splitting of the hydrogen fundamental in TiH_2. The next step is to develop a chopper suitable for high energy transfers ($\Delta E > 0.2$ eV), to construct proper shielding and collimation, and to build a detector bank suited to both large Q scattering, such as required for measurement of the Bose condensate fraction in He II, and very low Q scattering, such as required to minimize recoil broadening in molecular and solid state spectroscopy.

Time-of-flight methods have particular advantages in structural studies of materials in extreme environments. The detector bank can subtend a small solid angle with a restricted view of the sample, and still satisfy the Bragg condition by varying the wavelength. Such a special environment diffractometer is in routine use for the study of the equation of state of Pu at pressures up to 5 kbar and temperatures up to 350° C. We have measured variation of the lattice constant with pressure within the δ phase and have observed large hysteresis effects. The detector bank is "geometrically time focused" so that neutrons of a given energy arrive at all detectors at the same time. The resolution achieved is $\Delta d/d \sim 0.7\%$. With improvements to the instrument currently being implemented, only one hour of beam time will be required to obtain a good pattern.

Another versatile instrument is a general purpose diffractometer which is under development for structural studies of powder, liquid, and amorphous materials. Using detectors at angles between 10° and 150° it is possible to cover the small-Q range important for minimizing Placzek corrections in liquids diffraction as well as the large-Q range important to high resolution powder diffraction and molecular liquids diffraction. This instrument will be electronically time focused. Counts will be recorded for individual detectors and differences in flight times will be compensated for by computer. The electronic time focusing makes it possible to use large solid angles with greatly increased count rates compared to those achievable with a geometrically focused instrument. Another concept that will be tested is "geometric resolution focusing". This technique decreases the solid angle slightly, but allows all detectors within a bank to have the same resolution so that their outputs may be simply combined. For high resolution powder studies, the instrument should attain $\Delta d/d \sim 0.5\%$ and be capable of measuring smaller d-spacings than comparable reactor instruments. This measurement is useful, for example, in determination of parameters of several coexisting phases in a sample where the Bragg peaks are close together. The count rate is expected to be better than the best powder instrument at the ILL and the resolution will be comparable.

The initial experiments in molecular liquids diffraction will explore determination of the hydrogen-hydrogen correlation function in water. This will employ an isotope substitution method to remove first-order Placzek corrections without requiring introduction of models of the inelastic spectra. When combined with the WNR capability to determine the scattering function at very large Q, the experiments will provide a model-free test of theories of water structure.

A single crystal diffractometer based on the Laue time-of-flight method is being developed. This instrument uses a position-sensitive area detector to simultaneously measure many Bragg peaks, as well as to determine the incoherent and diffuse background. The single crystal diffractometer is an example of an instrument made possible by advances in data acquisition. It uses a high speed megaword memory being developed by LASL in collaboration with ORNL. Our initial experiments will involve the determination of hydrogen positions in organometallic catalysts. Another obvious application is to the study of order-disorder transitions in solids. Because of the capability to measure high-index reflections using the high epithermal flux, one can also determine the thermal parameters and lattice anharmonicity in the A-15 superconductors.

The source characteristics of the present WNR are adequate for many moderate resolution experiments. None of the existing instruments suffer significant loss in time-of-flight resolution at 8-μs pulse widths and they do not require long-wavelength neutrons which would produce frame overlap. Further experiments, extending into the epithermal range, may require a lengthening of the flight path or a reduction of the pulse width to achieve adequate resolution, at some sacrifice in intensity. Experiments at longer wavelengths may require either pulse choppers or velocity selectors to avoid frame overlap.

The advent of the PSR will provide pulse widths and repetition rates where time-of-flight resolution is limited only by the moderators and where frame overlap is negligible. It will also make chopper phasing easy by allowing WNR choppers to time the extraction of beam from the PSR.

Future activities in the neutron scattering program will aim toward building special capabilities for exploiting the unique characteristics of the WNR pulsed neutron source. This may include developing neutron polarizers, resonance detectors, and pulsed sample environments. Polarized neutrons have applications in the study of magnetic materials, in the isolation of hydrogen behavior in catalytic systems by scattering resulting in spin flip transition, and the inelastic spectroscopy by the spin-echo method. Resonance detectors may be essential to spectroscopy at several eV energy. Pulsed sample environments will permit kinetic studies such as glass crystallization.

Polarized neutrons and resonance detectors are examples of areas where the multi-disciplinary program pursued at the WNR will contribute directly to the development of a condensed matter research effort. Polarized proton targets are routinely used at LAMPF and the WNR to determine spins of nuclear resonances as well as to explore the nucleon-nucleon system at intermediate energies.

IV. POSSIBLE ADVANCED SPALLATION FACILITY

The uniquely high proton current intensity of at least 1 mA produced by LAMPF provides the basis for an even more advanced and intense spallation neutron source.

If the scientific opportunities appear sufficiently promising, LASL will propose to build a new target area to utilize the full potential of the LAMPF accelerator to achieve yet another major increase in neutron source intensity. Such a facility might use 1000 μA of protons from LAMPF delivered to a new target and would produce a peak thermal flux of between 10^{16} and 10^{17} n/cm^2-s depending upon repetition rate.

An advanced pulsed spallation facility of this type would be considered for development after 1990. It is compatible with current plans under study to develop a post-accelerator to LAMPF for kaon and anti-proton physics. Such an accelerator, perhaps a synchrotron of $\geqslant$ 15-GeV energy, would utilize only 100-μA of the LAMPF current, while dominating the nuclear and particle physics program at LAMPF. Utilizing then the remaining high-current capability intrinsic to LAMPF for a high-current ($\sim$ 1 mA) spallation source would be feasible.

The following would be required to develop this source:

A. LAMPF

LAMPF will have sufficient capacity to provide at least 1 mA of proton current. No additional construction or modification beyond that already implemented or planned for 100-μA PSR operation is expected to be required. The entire scientific opportunities at LAMPF will need to be examined in order to determine the amount of current to be devoted to a spallation neutron source.

B. PSR

The PSR is conservatively designed to accommodate 100-μA average current at 12 Hz. If beam loss is sufficiently low, 400-μA operation could be achieved immediately by operating at 48 Hz. The ultimate capacity of the PSR and the exact nature of any required modifications will only become clear when actual operating experience becomes available. However, we do believe that up to 1-mA operation may be possible with modest modifications.

C. Target Area

The present WNR target area cannot be upgraded in a reasonable manner to accommodate proton currents beyond 100 μA. Thus an entirely new target area would be required for 500-1000-μA operation. It is clear that such a target area would represent the major cost for this spallation source and preliminary studies indicate $40-50 M might be required. These studies also indicate that this target area could accommodate simultaneous use for condensed matter science and neutrino physics, although the need for two shared, high-current targets is not excluded.

The IPNS Program at Argonne National Laboratory

D. L. Price, N. J. Swanson, J. M. Carpenter and C. W. Potts

Argonne National Laboratory
9700 South Cass Avenue
Argonne, Illinois 60439

Introduction

The eighteen-month period since ICANS-III has been a most exciting time for the IPNS Program. It has seen (a) the progress of IPNS-I construction from an empty building to the final stage of a major experimental facility, (b) the completion of the ZING-P' prototype operation with successful resolution of the key technical questions in the design of the IPNS-I facilities and instrumentation, and (c) the upgrade of the accelerator current to a level commensurate with the performance required for IPNS-I start-up. The simultaneous realization of these three goals in a situation of limited resources has called for dedication, ingenuity and excellent teamwork on the part of the people involved.

In the following sections of this paper, we shall briefly summarize the progress achieved in these three areas. Technical accomplishments in the areas of targetry and neutron scattering instrumentation will be covered in separate papers.

The principal components of the IPNS-I facilities are shown in Figs. 1 and 2. Fig. 1 gives a plan view of the accelerator systems and the 500 MeV beam transport line. The 500 MeV transport line and the relocation of the Rapid Cycling Synchrotron extraction into this line are part of the IPNS-I construction project; the other accelerator components were transferred from the DOE High Energy Physics Program. Fig. 2 gives a plan view of the neutron generation systems and research instrumentation, all of which are being built under the construction project, apart from the principal buildings housing these facilities which existed previously.

A. IPNS-I Construction

Progress in all areas of the design and construction indicates high confidence that the IPNS-I facilities will become operational in April 1981. With the shutdown of the ZING-P' program in August 1980 additional resources have been released to work on the transition from the prototype facility to IPNS-I where prototype operations did not allow construction work previously. Details of the progress for the three principal tasks of the IPNS-I projects are given below.

1. Proton Transport System (PTS)

The PTS tunnel was completed within the experiment hall (Building 375) and expanded to the limit of its support pad outside and north of the hall. Included has been the completion of the proton beam dump which will serve as a Faraday cup to accept the full output of the accelerator for operational optimization purposes.

The PTS magnets obtained from ZGS have been refurbished and mounted on newly-procurred precision positioning platforms which will also serve as mobile transport dolleys for installation or removal from the PTS tunnel. Several magnets have been positioned in the completed tunnel and the alignment and vacuum system testing has been started.

With the completion of ZING-P' prototype operations, preparations for joining the PTS tunnel to the synchrotron cavity were begun. This work included removal of accelerator shielding blocks of the south side, excavation of the floor and earth at the cavity-tunnel junction area, placement of the extension of the high-load concrete support pad for the PTS shielding, and the relocation of accelerator power supplies and miscellaneous equipment previously

located at the junction zone. Joining of the PTS tunnel to the accelerator cavity is planned for completion before the inclement winter weather arrives.

Progress is quite satisfactory for the ancillary systems to support the PTS. This work includes the subsystems for beam diagnostics, vacuum, beam control and safety shutdown. Accelerator modifications have been started to modify and relocate the extraction system. These activities are scheduled to be completed at the time when the PTS construction will be finished in February 1981.

2. Neutron Generation System (NGS)

The slow, tedious task of cutting and fitting of the shielding steel around the vessels and neutron beam tubes within the atmospheric control barrier has been completed. Design of the removable shielding to be used within the vessels and neutron beam tubes is complete and procurements have begun.

Fabrication of the components for the first target is progressing on schedule. Assembly of some of these components to form the first target will be performed in October with preoperational testing begun in November. Delivery of the target cooling systems is expected in early October with installation performed shortly thereafter. Mating of these systems to target assemblies is expected in November.

The beryllium reflector assembly and its contained moderator cans for the Neutron Scattering Facility is being fabricated. Delivery of this long lead item is not expected until late January and this work continues to comprise the critical path for the overall construction. The reflector assemblies for the Radiation Effects Facility are being fabricated with delivery expected in October.

Design of all electrical and mechanical facility systems for support of the NGS has been completed. All procurements are underway and installations were begun in September.

All designs for the NGS monitoring and control systems have been completed. All procurements have been placed and most have been received. Installation in the control room, now under construction, is expected to begin in late October.

3. Instruments and Data Acquisition System (DAS)

It is planned that seven neutron scattering instruments will be operational during 1981. Designs were completed for the flight paths of the Special Environment Powder Diffractometer and General Purpose Powder Diffractometer. Bid solicitation for these components was completed and a fabricator selected. Work continues on developing layouts for the High Resolution Medium Energy Chopper Spectrometer scattered flight path housing. This assembly will be obtained by a design and build contract.

Conceptual designs for the Crystal Analyzer Spectrometer and Small Angle Diffractometer are continuing. Detail design work for the Low-Resolution Medium-Energy Spectrometer and Single Crystal Diffractometer will begin shortly.

Progress has been realized in the development for single-ended, linear position-sensitive detectors needed for the two powder diffractometers. Suitable detector systems are expected at the time when the housings are ready to accept them.

Work has begun on the rebuilding and refurbishment of vacuum systems required for the scattering instruments. Most of the vacuum equipment will derive from existing components obtained from completed HEP programs.

Designs for the five required choppers have been completed. A fabricator has begun the machining of the beryllium parts and ordering of other chopper components has been started.

For the DAS activities work continues on the detail design for detector electronics, computer software and computer hardware. A fifth front end computer has been delivered. One computer is being used for program development and detector electronics checkout.

The progress on developing encoding circuits for single-ended linear position-sensitive detectors has been excellent. Close coordination with the detector supplier continues in an effort to optimize the special detector needs for IPNS-I instruments.

4. General Items

At the beginning of August the contractor who began the IPNS-I construction work was dismissed and replaced by a new, inexperienced contractor. Since this action occurred with very short notice, all active subcontracts became invalid and required formalization with the new contractor. This caused some delays while new subcontracts were established. Also, some inefficiencies were encountered due to the changing of supervision. At present most problems have been remedied and harmonious and efficient construction activities appear to have been restored. High rainfall in August and early September caused some delays. However, exceptionally good weather in October has permitted acceleration of the construction activities.

The operations staff for IPNS-I, headed by Bruce Brown, has coordinated the development of the Safety Analysis Report (SAR). This report has been reviewed by committees with information participation by design personnel. The

reviews have resulted in some design improvements. The SAR has been approved by the Laboratory committees and submitted to the Department of Energy (DOE) for approval. With the DOE approval of the SAR on schedule, startup of the facility in April 1981 can be expected.

B. Research and Development

On August 4, we ended operation of ZING-P' to begin final preparation for IPNS-I. ZING-P' was the second prototype pulsed spallation neutron source operated at ANL, following the first experiments (anywhere, as we understand) in 1974 and 1975 on the ZGS Intense Neutron Generator Prototype, ZING-P. Foreseeing completion of the 500 MeV, 30 Hz Rapid Cycling Synchrotron, we conceived (with Motoharu Kimura, our visiting consultant from the Laboratory of Nuclear Science, Tohoku University, Japan) and decided to build this second prototype which was completed in time for startup with the new accelerator in December 1977.

The data acquisition system used for most of the scattering instruments was an ND6600 computer-based multichannel analyzer system with time-of-flight ADC's. George Ostrowski maintained the ND6600 and detectors for this system, and they fulfilled our needs well.

Our goals were to test further the applications of pulsed spallation neutron sources in scattering studies and to develop information needed for design of IPNS. We think we've been very successful in reaching these goals. Starting with low intensity operation with 0.5×10^{12} proton/pulse at 1 Hz, while sharing the injector linac with ZGS, we reached in the end 1.8×10^{12} proton/pulse at 30 Hz in a dedicated mode with reliability of about 90%.

Initially a target of tungsten was used with three Be-reflected room-temperature polyethylene moderators. Later we installed and operated a Zr-clad depleted uranium target and a natural-circulation liquid hydrogen moderator and also made a number of changes in moderator poisoning and decoupling. These developments not only provided a more effective neutron source, but enabled essential measurements relating to IPNS-I design.

Scientists of the Argonne scientific divisions developed and operated five scattering instruments and one general physics experiment. Several fast neutron radiation effects tests were done. An extensive series of measurements of target, moderator, reflector and cooling system tests were carried out, and the source was used as a test-bed for neutron detector tests by Argonne and Rutherford Lab groups.

The table summarizes scattering instrument developments, source measurements, and tests of applications of pulsed spallation neutron sources that we have carried out.

1. Scattering Instrument Development

   Crystal analyzer spectrometer

   Single crystal diffractometer (Time-of-Flight Laue Camera)

   Small angle diffractometer

   High resolution powder diffractometer

2. Fundamental Physics Experiment

   Ultracold neutron generator (for neutron bottle and neutron EDM measurements)

3. Fast Neutron Irradiation

   S_iO_2, carbon

4. Radiation Effects Facility Mock-Up Measurements

   Pb reflector, Ta and U targets

5. Resonance Neutron Radiography

6. Source Measurements

   Total power in W and U targets

   Local power density in U target

   γ + n dose rates in neutron beams

   Total nuclear heating in liquid hydrogen moderator

   Nuclear heating power densities in polyethylene, Be and Pb

   Nuclear heating in boron and Cd-shielded boron decoupler materials

   Absolute neutron beam intensities for W and U targets

   Delayed-neutron fraction

   Neutron spectra for liquid hydrogen and polyethylene moderators

   Neutron pulse widths vs wavelength for liquid hydrogen and polyethylene moderators

   Radioactivity in H_2O cooling system

   H_2 production in cooling system

   Corrosion products in cooling system.

C. Accelerator Operation

The Rapid Cycling Synchrotron (RCS) and 50 MeV Linear Accelerator (linac) really came of age as a 30 Hz pulsed neutron source during the four-month run starting April 1. While all the system components had limited testing at 30 Hz prior to this run, it was very satisfying to see them perform reliably at this frequency over an extended period. The linac, run at 0.3 Hz for many years as

part of the Zero Gradient Synchrotron (ZGS), had less than five hours of breakdown in 2500 hours of scheduled 30 Hz running. The rf, sextupole and extraction improvements installed during the previous shutdown all performed well. The new pulsed transformer septum magnet (the old septum magnet was the Achilles heel of the RCS) logged over 200 million pulses without a problem.

The summary at the end of this article details the RCS performance, but a few highlights should be noted. These include: at 15 Hz -- short-term average of 2.0×10^{12} protons per pulse and eight hour average of 1.9×10^{12} protons per pulse; at 30 Hz -- short-term average of 1.83×10^{12} protons per pulse (8.8 μA) and twenty-four hour average of 1.58×10^{12} protons per pulse (7.6 μA). All the good numbers in the summary were achieved under clean operating conditions such that beam losses during this run were on the average no greater than previous runs at 15 Hz. Some 280 hours of operating time were used in studies to improve the performance of the synchrotron system. A number of reliability problems were also sorted out and appropriate changes made during the machine study periods.

Average target current showed a steady improvement over this run. The temptation to get high beams regardless of beam loss was avoided. Problems of clean beam handling and radiation induced outgassing were faced and conquered gradually as the beam intensity increased. The machine physicists were as eager to see a "clean" operation as were the operators and repair personnel. In the long run, this is the only way a high-flux machine such as the RCS can function.

The upgrade activities (both long-term and short-term) progressed at a reasonable rate considering the attention required by operation and preparation for an assortment of review committees. Improvements planned during the next

six months are: tune control -- a programmable octupole magnet system; rf -- new cavity bias power amplifiers; kicker magnet system -- a new magnet and power supply capable of 50% more kick; and installation of the Penning ion source.

A major activity of the group during the six-month shutdown will be the rearrangement of synchrotron components and shielding to deliver beams to the new IPNS-I target. This major activity along with several thousand man-hours of routine maintenance will make a busy time indeed for the RCS and linac groups.

The IPNS accelerator system operating summary for the period Arpil 1, 1980, through August 4, 1980, is as follows:

ZING-P' scheduled operating time	2465.0 hours
ZING-P' time available	2092.4 hours
Operating efficiency	84.9%
Total protons on target, pulses $>10^{11}$ protons	2.19×10^{20}
Total extracted pulses $>10^{11}$ protons per pulse	1.93×10^{8}
Average protons per pulse on target	1.13×10^{12}
Average current	4.81 μA
Average repetition rate	26.48 Hz
User requested downtime	68.1 hours
User requested operation <30 Hz	46.4 hours

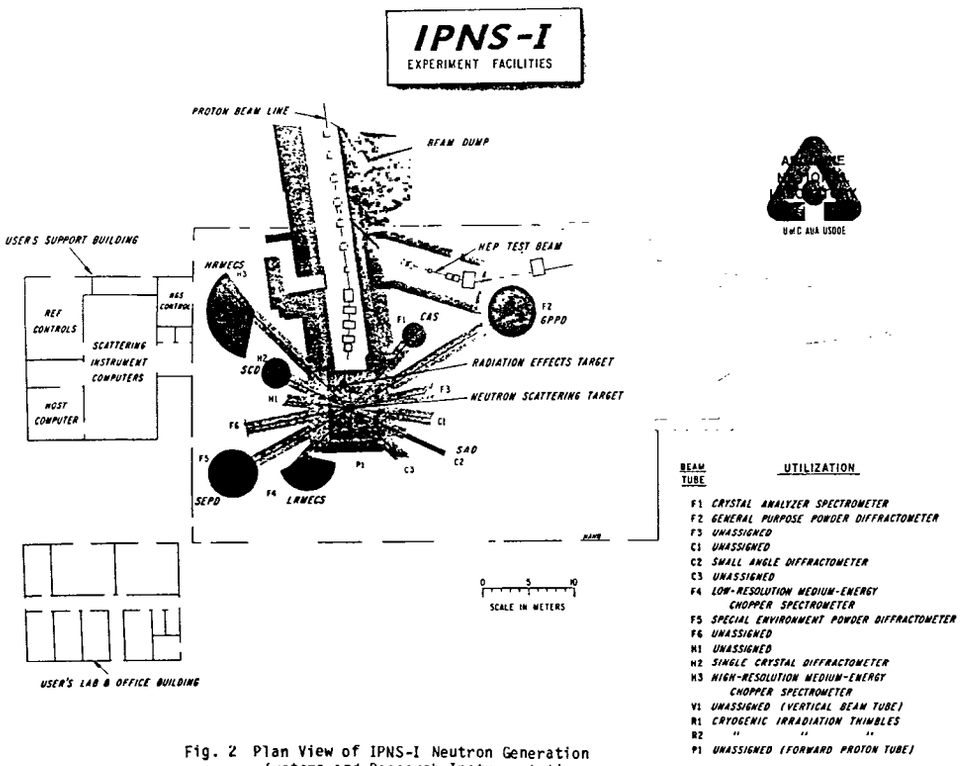

Fig. 2 Plan View of IPNS-I Neutron Generation Systems and Research Instrumentation

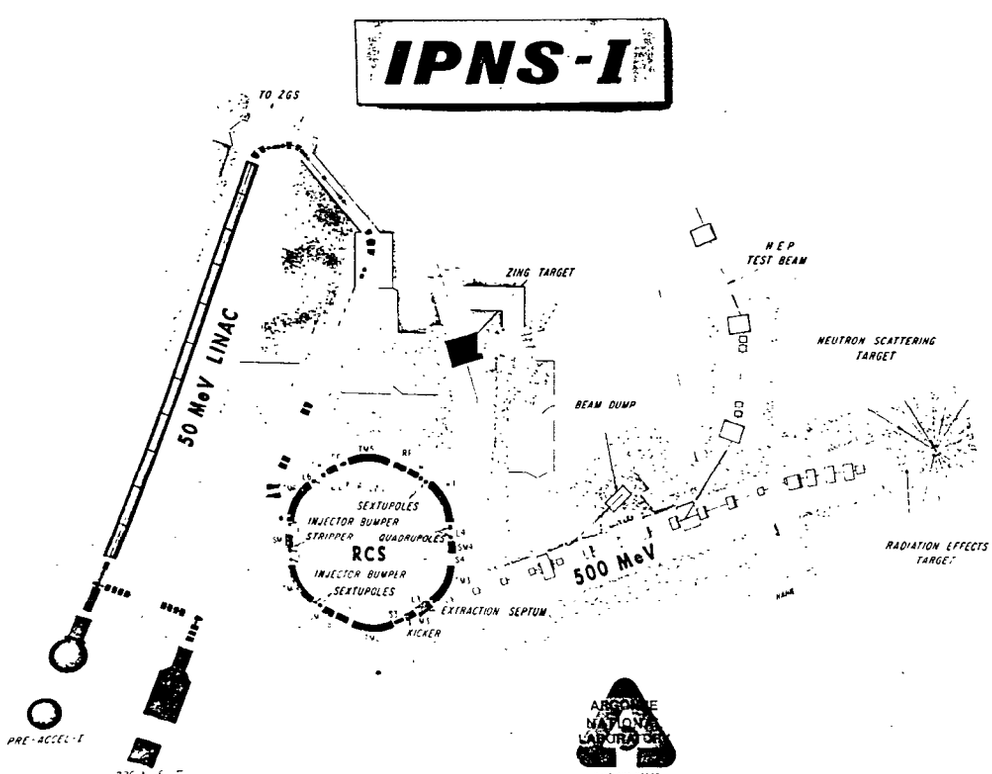

Fig. 1 Plan View of IPNS-I Accelerator Systems and Transport Line to Neutron Generation Systems

PROGRESS REPORT ON THE CONSTRUCTION OF THE SPALLATION NEUTRON SOURCE AT THE RUTHERFORD AND APPLETON LABORATORIES

G MANNING

Rutherford and Appleton Laboratories

1. Introduction.

The delivered version of this talk will report progress largely by showing slides of work completed or work in progress. The written version cannot be the same. It will serve no useful purpose if it provides a logical progression through each item of the machine stating our precise position on the first of October 1980. The procedure I have followed below is to give a general introduction to remind the reader of the specification and main parameters of the machine and to state our current financial approval. I then cover our planned timescale and our philosophy for priorities in that time scale. The remaining sections of the paper provide a statement of what we have achieved, where we are making good progress and perhaps more importantly where we expect problems. No attempt has been made to be complete - items that involve a lot of work are often omitted because their careful coverage will be of no help to others and they would have only lengthened the report.

2. Specification of the SNS.

Table 1 gives the specification of the SNS and some of its basic parameters. The machine will be an 800 MeV, 50Hz proton synchrotron delivering 2.5×10^{13} protons per pulse - an average current of 200 μA. Extraction will be single turn by kicking the beam out in the vertical direction. Each cycle of the machine will provide two pulses of protons of base width 100ns separated by 220 ns - an effective pulse width for neutron experiments of 0.4 μs. The beam will be transported onto a depleted uranium target of 9 cm diameter and 25 cm long and each proton will produce about 25 neutrons - this will provide $\simeq 6 \times 10^{14}$ neutrons per pulse at 50 Hz repetition rate or $\simeq 3\ 10^{16}$ neutrons per second. The neutrons are produced at energies ~ 1 MeV and will be slowed to "thermal" energies in moderators placed immediately above and below the target. 18 beam ports will be provided through the biological shield. The facility can support about 25 neutron beam instruments but financial provision has been made for only about 15.

Figures 1 shows an artist's impression of the facility.

3. Finance and Manpower.

The Laboratory received approval for the construction of the SNS in June 1977. The authorised capital cost for the machine and target station is £11.374M at 1 April 79 prices - this does not include staff costs or the research and development but it does include first line spares. Table 2 gives information on the breakdown.

We have authorisation for £1.804M at 1 April 79 prices to build the first seven of the neutron instruments. The financial plans include a total of £5.7M for the construction of 15 instruments, for computing requirements, sample environments etc. Further authorisation will be sought when detailed designs are ready.

The total financial provision for the SNS provides about £7.2M (at today's prices) per year over the next five years. It is this provision rather than technical matters that determine the construction timescale.

Although the SNS was approved in June 1977 appreciable manpower did not become available until June 1978 with the closure of the 7 GeV proton accelerator (NIMROD) used for High Energy Physics. The current manpower used on the SNS is about 200 and this will decrease over the next few years as construction is completed - the operation crew for the machine and target station will be 105.

Much of the equipment from NIMROD is used for the SNS and a rough estimate of the current value of that equipment is £24M allowing for amortization. Its replacement cost in current prices would be about £43M.

4. Timescale.

A series of milestones has been set for the construction and commissioning of the SNS. These milestones and the dates planned for their achievement are listed below:

1. Early 1982 - Injector complete. 70 MeV H^- beam.
2. Early 1983 - Magnet ring and vacuum complete. Injection line and injection system complete. Some machine diagnostics installed. Injection tests.
3. Mid 1983 - 2 RF stations installed (out of 6). Main magnet power supply working. Acceleration studies at low intensity.
4. Late 1983 - 4 RF stations. Extracted system installed. Extraction studies at low intensity.
5. Early 1984 - With 4 RF stations. Extracted proton beam installed Target Station installed. 600 MeV protons (low intensity) producing neutrons in the target.
6. Late 1984 - 6 RF stations installed. 800 MeV protons (low intensity).
7. ∿ 1986 - Full intensity operation with 800 MeV protons

The philosophy adopted is to give the greatest priority to the early completion of the machine to a stage to study injection, acceleration and extraction at very low intensity (milestones 1 - 3). Second priority is given to providing protons onto a target and provision of some neutrons. Milestone 4 provides 600 MeV protons (determined by the fact that only 4 RF cavities are ready) at an intensity that will be no more than 10% of full design.

Full energy will be reached by late 1984 but full intensity is expected to take some time to achieve because the procedure will be to limit the beam injected so that beam losses are low enough to allow hands-on maintenance. Beam intensity will only be raised as we learn to control beam loss and we estimate that full intensity may not be reached until 1986.

The provision of instruments will have to have the lowest priority and with the present financial plans they are expected to come into operation as indicated below.

	1984	1985	1986	1987
Number installed in that year	4*	4	5	2
Total number installed	4*	8	13	15

* 2 of these will be used on the Harwell Linac from 1981-1984.

If more funds become available the provision will be advanced. It is possible that international collaboration on the SNS could provide a means for improving the instrument provision.

5. Progress Made.

I list below brief notes on progress made in major areas of the project - no attempt is made to be complete nor does the number of words reflect in any way the effort taken.

5.1 Civil Engineering

The Nimrod magnet and experimental halls have been cleared of Nimrod equipment and the necessary modification are well under way. All work should be complete by about April 1981.

5.2 Injector and Injection

Injection is to be made using H^- ions at 70 MeV. 20 mA of H^- will be injected for 470 μs (315 turns). Conversion of the 70 MeV linac from 1 Hz to 50 Hz and from H^+ to H^- is well in hand and we expect to achieve full specification by early 1982. Most of the work to be done is "conventional engineering" and is not breaking new ground. The new areas are the ion source and the stripping foil.

We have constructed a prototype Phillips ion gauge (PIG) ion source of the Russian/Los Alamos/Argonne type, modified to provide water cooling to allow a higher duty cycle. We require 20-40 mA for 500 μs at 50 Hz We have run the source at full duty cycle with 50A arc current for considerable periods and have extracted 40 mA for limited periods but we have not yet analysed the output beam. We have yet to establish running conditions, measure lifetime, caesium consumption, gas consumption etc.

Our requirement for stripping the H^- is for a foil of 50 $\mu g/cm^2$ (about ¼ micron) of 10 cm x 5 cm with one 10 cm edge unsupported. We have placed a development contract with the Fulmer Research Institute and so far they have made an aluminium oxide foil of quarter size and correct thickness and a boron nitrode foil of full size and 4 μ thickness. They are also trying carbon foils. The work will continue.

5.3 Magnets for Synchrotron Ring

Each superperiod of the main ring requires a bending magnet which also focusses horizontally, a singlet quadrupole which focusses vertically, a pair of doublet quadrupoles and a pair of trim quadrupoles. There are 10 superperiods. All of the elements are on order and the present position with each is:

bending magnets (GEC/UK) - prototype due at end of this year,
singlet quadrupole (TESLA/UK) - prototype due early next year,
doublet quadrupoles (LINTOTT/UK) - all the 20 required plus 2 spares are delivered.
trim quadrupoles (DANFYSIK/Denmark) - all the 20 required are delivered. 2 spares plus 2 more to be used as skew quadrupoles are due very soon.

Designs are ready for octupoles ($\lesssim$ 12 required) and for correction dipoles (12 required) but orders have not yet been placed. Space has been reserved in the lattice for sextupoles but we do not expect to need them.

5.4 Magnet Power Supplies

The main ring components (other than trim and correction magnets) are powered in series at 50 Hz from a choke and resonating capacitor system that is already available. Make-up for losses will be from a 1 MVA alternator that we are about to purchase. This will initially be run at mains frequency but can be changed to fixed frequency if necessary at a later stage.

The trim quadrupole power supplies are on order from DANFYSIK, Denmark and the prototype is due soon.

5.5 Main Ring Vacuum

The vacuum vessels in the magnets are to be made from ceramic. Sections of ceramic of the relevant cross section are provided (WADES/UK) with the ends glazed with glass and with dowels to locate adjacent sections. The sections are stacked vertically in a furnace to make a complete chamber and the temperature is raised to 1100°C to form a glass joint between the sections. This work is done in the Laboratory. Three prototype chambers have been made: 60cm chamber for the singlet quadrupole, 3 m chamber for a pair of doublet quadrupoles plus a pair of trim quadrupoles, and a 5 m chamber with a 36° bend for the bending magnet. All are successful and have been pumped to below 10^{-8} Torr (a pressure of 5×10^{-7} Torr is required). Production has now started.

5.6 RF Shields for Main Ring

All of the ceramic vacuum chambers will require RF shields to isolate the beam from the high RF impedance of the laminated magnets. A system has been designed that uses 2 mm diameter stainless steel wires supported by ceramic spacers. The stainless wires follow the envelope of the beam to minimise the RF impedance. These wires are shorted directly to each other at one end and are connected to the next screen via small 0.1μF capacitors at the other end. There will be about 4000 capacitors in the SNS vacuum system. Their radiation resistance is being tested at SIN. A prototype RF shield has been constructed for the bending magnet and is mechanically acceptable but its RF impedance has yet to be measured.

5.7 Main Ring RF

The SNS will have six RF cavities which will be placed in straight sections 2,3,4,7,8,9. A frequency swing from 1.3 - 3.1 MHz is required and this will be achieved by a single turn bias current to 2800A through the ferrite rings of the RF cavities. Power levels of $\simeq$1MW are required and all the cavities have to be accurately controlled in frequency, voltage and phase. Beam compensation will also be needed at full intensity.

A prototype cavity, drive system and bias system is being assembled in the Laboratory and should be ready for test early next year. Reasonable progress has been made on the design and prototype work for the low power RF system that will have to provide the phase and voltage controls.

5.8 Diagnostics

The SNS main ring is to have diagnostics equipment to determine the beam position to an accuracy of a fraction of a millimetre, beam intensity to an accuracy of one thousandth of full intensity and to determine the beam profile. Prototypes have been built and successfully tested for the first two of these and development work is in hand for the profile monitor.

5.9 Extraction

Extraction from the SNS will be achieved by bumping the beam vertically upwards in straight section No 1 and then by using 3 ferrite kicker magnets kicking the beam vertically into a DC septum magnet. The field in these magnets must reach full value in 220 ns and stay flat to 1% for 500 ns.

A prototype kicker magnet and drive system using thyratons is being developed and tested. At the moment the rise time is about 300 ns and further development is proceeding. The system has been tested for 4 x 10^7 pulses and testing is continuing.

5.10 Beam Loss Protection

We believe that the factor that will determine the operational intensity of the SNS will be the control of the beam loss. We intend to limit the beam that is injected so that we can use hands on maintenance for the accelerator. This will mean that the intensity of the SNS will only be raised as we learn to control the beam loss and as we successfully develop beam loss catchers.

We anticipate that at full intensity we will trap about 50% of the injected beam and that the rest will be lost from 70-100 MeV. This leaves 17 kW of beam power to be dumped somewhere. We have studied ways of collecting this lost beam and intend to use thin foils to scatter protons in the wings of the beam followed by beam catchers placed downstream. Both the scattering foils and the beam catchers will be installed on remotely controlled drive systems that can be accurately moved towards the beam. Prototype beam catchers have been made using carbon blocks that are brazed to water cooled copper plates. These catchers are designed to be removed and inserted by remote handling equipment. Space has been reserved to place four such systems in the accelerator for vertical and horizontal losses. A computer simulation of the complete system indicates that about 90% of the injection losses should be collected in this way. We hope to develop the system so that at least 95% can be collected in preferred places and we believe that this will be acceptable. At the start up of the accelerator we will install only the horizontal low energy catchers.

There will also be unavoidable beam loss at extraction. It is impossible to calculate this as it depends upon the detailed shape of the beam way out in the wings. We have based our plans on the assumption that the loss will be 1%. We have studied a scattering foil and collector system for this and intend in the first instance to install a system in the vertical plane in the long straight following the kicker magnets. We have also reserved space for a horizontal system. We have based our radiation calculations on the assumption that we will collect 90% of these extraction losses. We hope to keep losses during acceleration to considerably less than 1%.

We have reserved space in the synchrotron hall so that we can install a shield tunnel around the main ring. This will reduce the irradiation of the synchrotron hall so that the induced activity is at an acceptable level and will shield personnel from radiation from activity induced in the accelerator. We do not intend to install this shield wall in the first instance.

We intend to keep the floor inside the synchrotron ring smooth and clear of obstructions so that we can use remote handling equipment if necessary at a later stage. We will provide no such equipment in the first instance. Magnets,vacuum equipment etc have been designed to make remote handling possible.

5.11 Extracted Proton Beam Line

A design has been made for the beam transport system from the extraction DC septum magnet to the target station. It will use 60 magnets and all but one of these are already available. The shielding for the beam line will use existing steel and concrete and is already being installed.

5.12 Target Station

The target station is designed to provide 18 beam tubes each of which will have an independently operated beam shutter of 2 metres length. Each beam can be equipped with a collimator to look at any one of the four moderators - two above and two below the target. Present thoughts are for one 20K , one 77K and two room temperature moderators. The reflector will be of beryllium and heavy water.

The target will consist of U^{238}plates clad in Zircaloy-2 and cooled by heavy water. The U^{238} plates will vary from 6.5 mm thick to 12.5 mm thick. The cooling gaps will be 1.75 mm wide.

The downstream section of the biological shield can be moved backwards to carry the target, relector and moderators into a remote handling cell. A full scale mock-up of this cell has been assembled and will be used to test and verify all target equipment prior to installation.

The civil engineering of the target station has already started and 2½ metres of steel has been placed beneath ground level to stop ground shine and to ensure that water in the water table is not made radioactive. A neutrino cave 5 x 5 x 3 m^3 has been constructed beneath and to one side of the target at a distance of 7m from the target. The target base plate is to be installed in the next few months.

Full details of the target staion design will be given in later sessions.

5.13 Computer Control

The SNS control system will use four GEC 4070 computers, one as a central computer that will be connected to the control console, the other three will be satellites for the injector/injection, for the main ring and for the EPB/target station. All four computers have been delivered and considerable progress has been made on software and hardware for interfacing and connecting to the SNS equipment. Considerable use will be made of microcomputers for control of specific items of equipment and for data logging, but these will all be interfaced to the 4070 systems.

5.14 Experimental Instruments

Financial approval has been given for the seven instruments listed below:

		authorisation in £K (1/4/79 prices
Low Q spectrometer (small angle scattering)	(LOWQ)	330
High energy transfer spectrometer	(HET)	291
High resolution quasi elastic spectrometer	(IRIS)	354
High resolution powder diffractometer	(HRPD)	284
High intensity powder diffractometer	(HIPD)	164
Liquids and amorphous diffractometer	(LAD)	105
High throughput inelastic spectrometer	(HTIS)	112
		1640
contingency		164
		1804

Two of these (LAD) and (HTIS) will be constructed early in 1981 and will be initially installed on the Harwell electron Linac.

Full details of these seven instruments and of others planned will be given in later sessions.

6. Non Neutron Beam Uses

The extracted proton beam for the SNS has been designed so that an intermediate focus can be formed 20 - 30m upstream of the main uranium target. A thin target can be placed at this intermediate focus and can be used as a source of pions and muons. A design has been made for a pion beam, taken vertically above the target, that could be suitable for bio-medical work. A 5cmthick carbon target will give a beam of about 4×10^8 π^- per second delivered to the final focus. This will produce about 10 rads/min over an irradiation volume of about 500cc.

A second possible beam from the intermediate target is a low momentum muon beam ($\sim$26 MeV/c)for SR work. A conceptual design has been made that could provide at least 10^4 μ^+ per pulse in a 5 nsec time slot.

Other possible non-neutron beam uses of the SNS that are being considered are isotope production, neutrino physics, rare muon decays, radiation damage studies, and neutron radiography. None of these is approved but options have been kept open and possibilities are being studied.

7. Conclusion

The SNS project is now well launched and visible progress is being made in most areas. We expect to start operation in 1984 but do not expect to reach full intensity until 1986. Our progress towards full intensity we believe will be determined by how quickly we can learn to control beam losses.

TABLE 1 MAIN PARAMETERS OF THE SNS

Proton design energy		800 MeV
Proton design intensity		2.5 10^{13} ppp
Nominal repetition frequency		50 Hz
Injection scheme		H^- charge exchange
Injection interval		476 μs
Injection energy		70.4 MeV
Injection intensity		20 mA
Injected beam emittance (area ÷ π)		20 μrad m
Mean radius of synchrotron		26.0 m
Number of superperiods		10
Length of superperiod		16.336 m
Dipole field at 70.4 MeV		0.1764T
Dipole field at 800 MeV		0.697T
Betatron tune (Q_h,Q_v)		4.31, 3.83
Beam emmittance at 70.4 MeV (area ÷ π)	Horizontal	600 μrad m
	Vertical	460 μrad m
Number of RF cavities		6
Magnet currents (DC, AC)		661.5 A, ± 395A
Target material		depleted Uranium
Nominal fast neutron production rate		3 10^{16} neutrons/sec
Nominal neutron current from surface of moderator		10^{13} neutrons eV^{-1} ster s^{-1}

TABLE 2 BREAKDOWN OF THE CAPITAL COST OF THE SNS (1 APRIL 1979 PRICES)

	£K
Injector and injection	900
Synchrotron magnets	1748
Synchrotron power supplies	684
Vacuum system	897
RF and diagnostics	1976
Extraction and extracted proton beam line	771
Controls	435
Services	679
Target, moderators and reflectors	627
Target station shielding	1244
Remote handling for target assembly	238
Machine and target station spares	750
Reserve	425
	11374

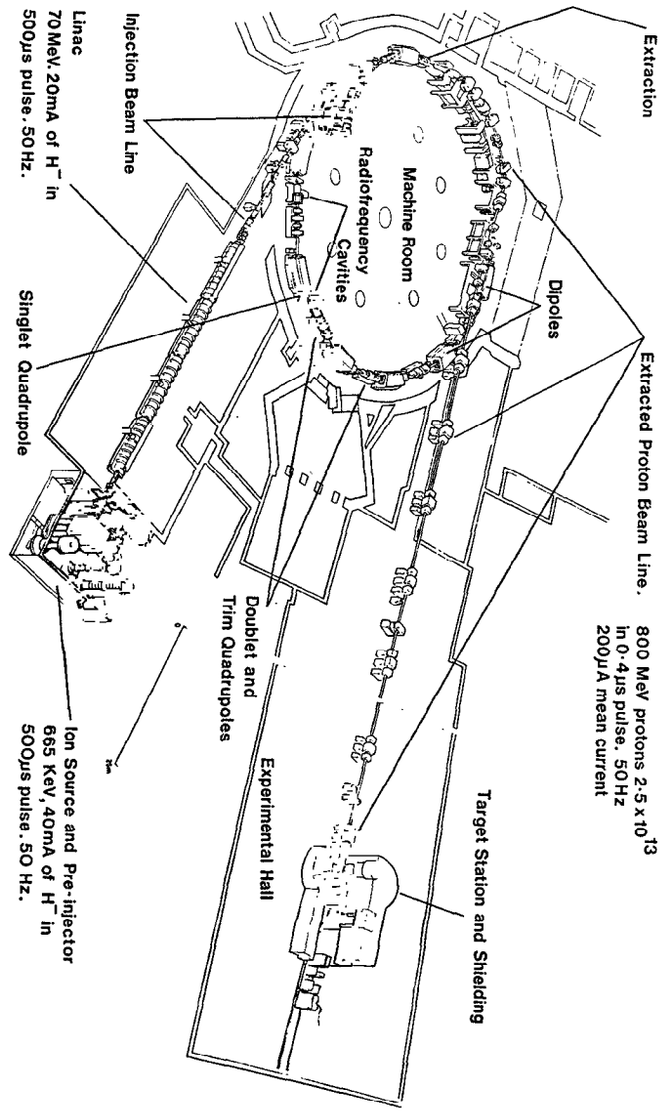

SPALLATION NEUTRON SOURCE

FIGURE 1

The status of the German spallation source project (SNQ).

W. Klose, H. Stiller

KERNFORSCHUNGSZENTRUM KARLSRUHE, GERMANY

KERNFORSCHUNGSANLAGE JÜLICH, GERMANY

1. Progress since ICANS-III

In 1977, the German minister for research and technology (BMFT) appointed a panel of scientists to study future developments for research with neutrons. In 1979, the panel recommended a detailed investigation on the feasibility of a spallation neutron source. This recommendation was based on the fact, that one of the research reactors presently in operation in Germany, the FR-2 in Karlsruhe, is planned to be shut-down in 1981, and that with one exception also all other research reactors in Germany are more than 20 years old. Germany is a partner with the tri-national high flux reactor in Grenoble, France, but the average admission rate for experiments with this neutron source is below 50% already now. There are more than 30 very active research groups in Germany using neutron beams. Thus we need a sufficient potential for neutron research with national installations.

The recommendation of the scientific panel was also based on the belief that, if feasible, a spallation neutron source would have a number of interesting advantages in comparison to a fission source, in particular the flexibility in time structure of the neutron flux. Hence the study was leveled for a spallation source which would yield a time-averaged thermal neutron flux comparable to the one of a high flux reactor, and for a time structure optimized to the needs of the scientific experiments.

Following the recommendation, the BMFT asked the two big German National Nuclear Research Laboratories to organize the project study (fig.1).

A reference-concept was fixed in March 1980 and the different tasks are considered by Karlsruhe and Jülich in collaboration with European research laboratories and industry.

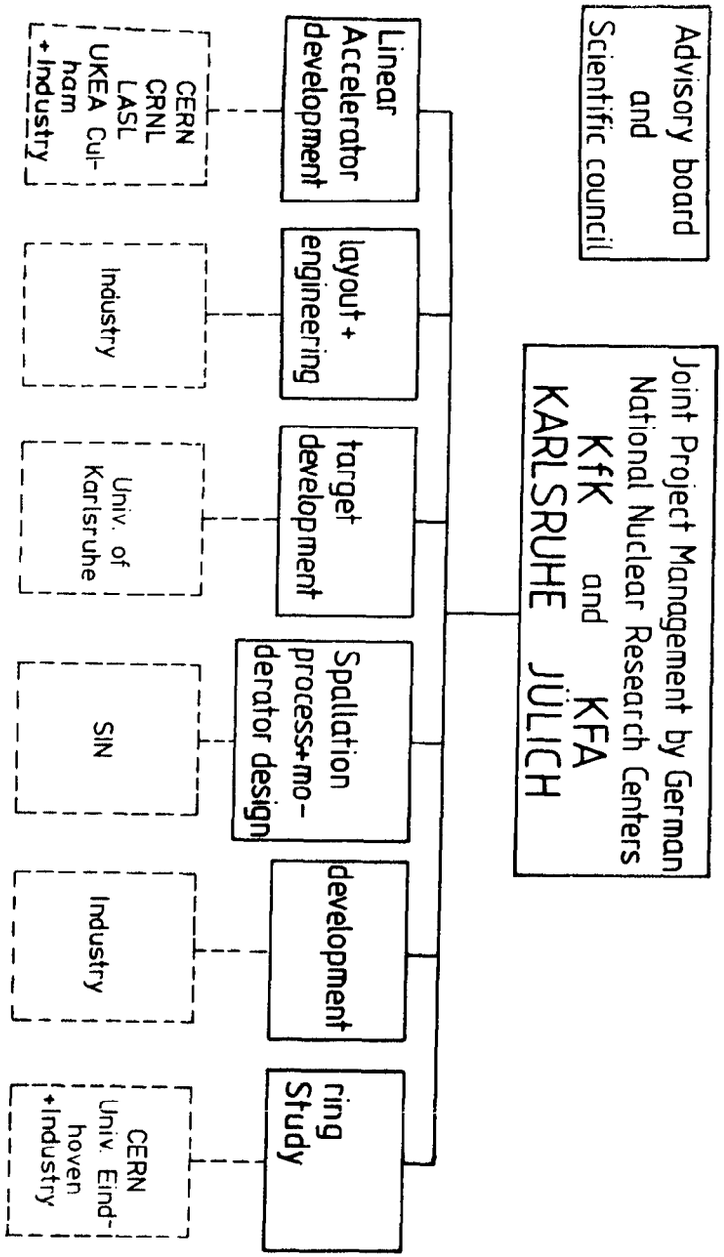

Organigram of the snq project study

Computations as well as measurements which will be described in other papers at this conference have shown that with protons as primary particles and lead as target material a time-averaged thermal neutron flux of 7×10^{14} cm^{-2} sec^{-1} requires a beam power of 5.5 MW in the target. As to the time structure a pulse repetition rate of 100 sec^{-1} appears optimal for time of flight experiments. In view of these two numbers a linear accelerator had to be choosen for the primary particles. Thus the reference concept is based on a linac for protons (fig. 2), a lead target, and two moderators, a fast small volume (H_2O) and a large volume (D_2O) one. The primary pulse width was chosen as small as technically feasible: 0.5 msec. In order to render possible an injection of the beam into a compressor-ring the proton energy was chosen to be 1.1 GeV. Hence a mean current of 5 mA is required, with a peak current of 100 mA (the limit of what seems achievable with present technology).

Future options for the machine include a compressor ring for protons (fig. 3) to compress the pulses from the linac by a factor of 650, gaining a neutron peak flux for the higher thermal and epithermal energy ranges, and - using the protons directly - attracting other research fields.

2. Major goals of the SNQ study.

In fig. 4 you find a birds-eye-view on the presently considered main R&D goals. Detailed information will be provided in several contributions to ICANS-IV by Drs.

G.S. BAUER on the target station
J.E. VETTER on the linear accelerator and liquid metal target development
N. NUECKER on cold neutron sources
B. ALEFELD and N. NUECKER on instrument design to utilize the time structure of the flux.
H. STECHEMESSER, D. FILGES and W. LOHMANN on technical aspects and theoretical considerations.

All authors are affiliated with one of the two national laboratories in Karlsruhe or Jülich.
I should only introduce into the different fields very briefly.

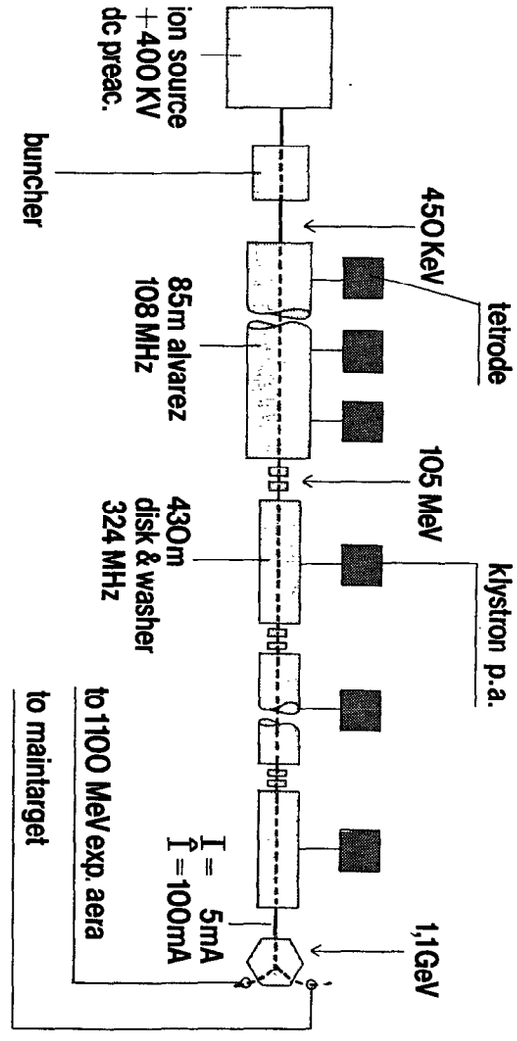

snq-linear accelerator, reference concept

- better knowledge of the spallation process - optimization of target-moderator arrangements - minimization of background radiation	- experiments at SIN and CEN - Saclay (SATURNE) - theoretical and experimental studies
- function test of rotating target (bearings+cooling) - development of liquid-metal target	- prototype to be built - modeling experiments underway
- injection into linear accelerator - beam loss - rf-generation	- analysis, experiments and prototype development in collaboration with CERN, LASL and Valvo
(option 3) compressor ring layout	-design and layout in co-operation with SIN, CERN, Scanditronix

snq

major r+d goals snq - study

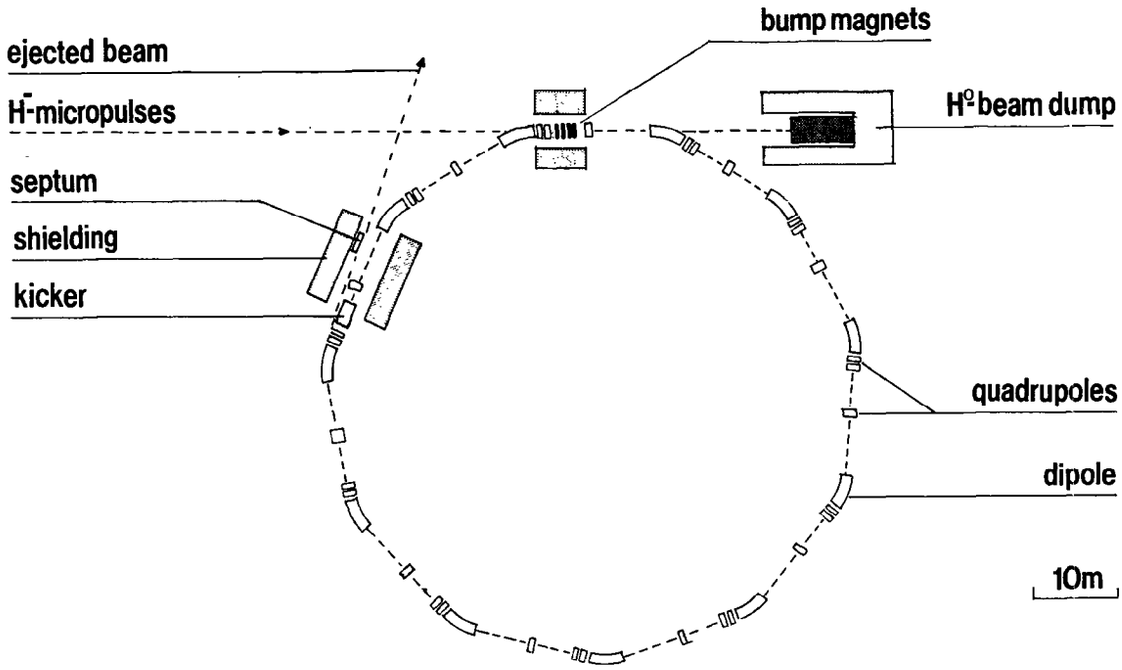

snq

schematic layout of compressor ring

2.1 General

In addition to the flexible time structure of the neutron production, the spallation process offers some further advantages compared to fission-production of neutrons:

- not a critical assembly;
- smaller γ-background;
- more neutrons per event and thus less heat produced per neutron.

For protons as primary particles one has for $0.5 \leq E_p \leq 2.0$ GeV and mass-numbers A (target) > 10 a neutron yield

$$y = a\,(A+b) \cdot (E_p - E_s)$$

a,b depend on geometry and the kind of the target nuclei. A cylindrical target of 10 cm diameter and 60 cm length gives $a=0.1\ (\mathrm{GeV})^{-1}$ and b=20 for lead. So one has y = 20 (for uranium this amounts to 35) for a 1 GeV proton. The heat per neutron produced by a 1 GeV proton in lead is some 20 MeV.

Special drawbacks compared to a reactor are felt with the necessity to put continuously energy into the machine, and with the appearance of very high energy neutrons. About 5% of the neutrons generated are expected with energies above 100 MeV. They have to be filtered out by the time structure and, of course, by sufficient shielding.

2.2 Linear Accelerator

100 mA of peak beam current during macropulses of 500 µs duration have to be accelerated to an energy of 1100 MeV.

The main extrapolation from state of the art is the beam power of 5.5 MW. Beam loss and its consequences have been of primary concern for the linac design. As an example, the operation frequencies of the rf accelerator were chosen lower than usual, leaving large apertures for the beam, provisions for installation of remote handling is provided all along the accelerator, beam diagnostics will be installed at various locations and emittance control will be done at any suitable place along the accelerator.

These precautions aim at keeping the machine accessible for hands-on-maintenance after shut down. This imposes very stringent conditions on the long term beam spill which should not exceed a few watts/m length at highest energies (some 10^{-7} of total beam intensity per m!).
Besides beam loss, considerations of economy and reliability influenced the design parameters.

The reference accelerator consists of:

- Injection, i.e.: ion source, preacceleration, low energy beam transport and beam pulse forming devices
- Alvarez accelerator
- Disk and washer accelerator and high energy beam transport

A magnetic multipole ion source provides 250 mA of total beam current during the beam pulse of about 1 ms duration. After separation of the protons from molecular ions at 50 keV energy level, the beam is transversally shaped and preaccelerated to an energy of 450 keV. Formation of the macro-pulse and matching to the transverse and longitudinal acceptances of the following rf accelerator is done in the low energy beam transport. About 80% of the dc beam can be trapped into the acceleration process.

The Alvarez linac consists of 7 tanks, 12 m long each, fed by 1.7 MW tetrode power amplifiers operating at a frequency of 108 MHz. Most of the technology could be adopted from the GSI heavy ion accelerator (same duty cycle and frequency), and from the CERN new linac (comparable space charge problems).

At 100 MeV transition to the disk and washer accelerator is made, because the drop of acceleration efficiency calls for another type of accelerating structure and a higher frequency.

57tanks, operating at 324 MHz, accelerate the beam with an energy gradient of 3 MeV/m, within Kilpatrick's limit of peak field strenghts. The overall length of the accelerator from injection to the high energy exit thus amounts to about 600 m. The accelerator structure is intersected by quadrupole focusing elements. Rf power is generated in 89 klystron amplifiers designed for 3.7 MW of saturated peak power, each. Development of a suitable klystron and fast control systems is underway in collaboration with industry.

Magnetic field strengths in all optical elements and vacuum conditions were chosen in view of an H^- beam, replacing the protons, when the compressor ring shall be added to the accelerator.

Variable fractions of the beam pulses can be extracted into the 400 MeV and 1100 MeV areas for nuclear physics experiments, whereas most of the pulse will be transmitted to the neutron target.

2.4 Target

The target is designed as a rotating wheel of 2.5 m outer diameter (fig. 5). All target material is mounted on the circumference, the proton beam coming in at right angle to the axis of rotation. The target consists of 9000 individually Al-canned Pb-pins, cooled by water which enters and leaves through the shaft.

The speed of rotation is 0.5 rps. The temperature inside the target pin will stay below 120°C, the life-time is estimated to be more than 20 000 hours of operation at full power.

There are of course considerations to use as target material uranium instead of lead. The rotating wheel concept would permit a large variety of target materials. But there are some serious problems connected with such a choice, which might finally outweigh the advantage of the larger neutron production rate in uranium:

- more power at the target to be cooled off, or use of a smaller beam-current,
- pass a tighter legal approval scheme.

If materials other than lead were ruled out a different target concept also could be considered. Additional development work is done in parallel for a target of liquid Bi-Pb.+)

2.5 Moderators and reflectors

Since the SNQ-project aims to serve a broad range of different users (including irradiation with thermal or fast neutrons), the locations above and below the target-wheel may be used for 2 different moderators: a fast H_2O moderator (with a Pb (or Be)-reflector) below the target for good pulse structure, and a D_2O tank (for a large volume of high flux) above the target wheel. A cold source (probably D_2) will be inserted into the D_2O tank, with neutron guides into a separate hall.

+) H.S.Hoffmann, P.E.Huber, M. Piesche, Liquid Metal Target Development for the German Neutron Source (SNQ), these proceedings

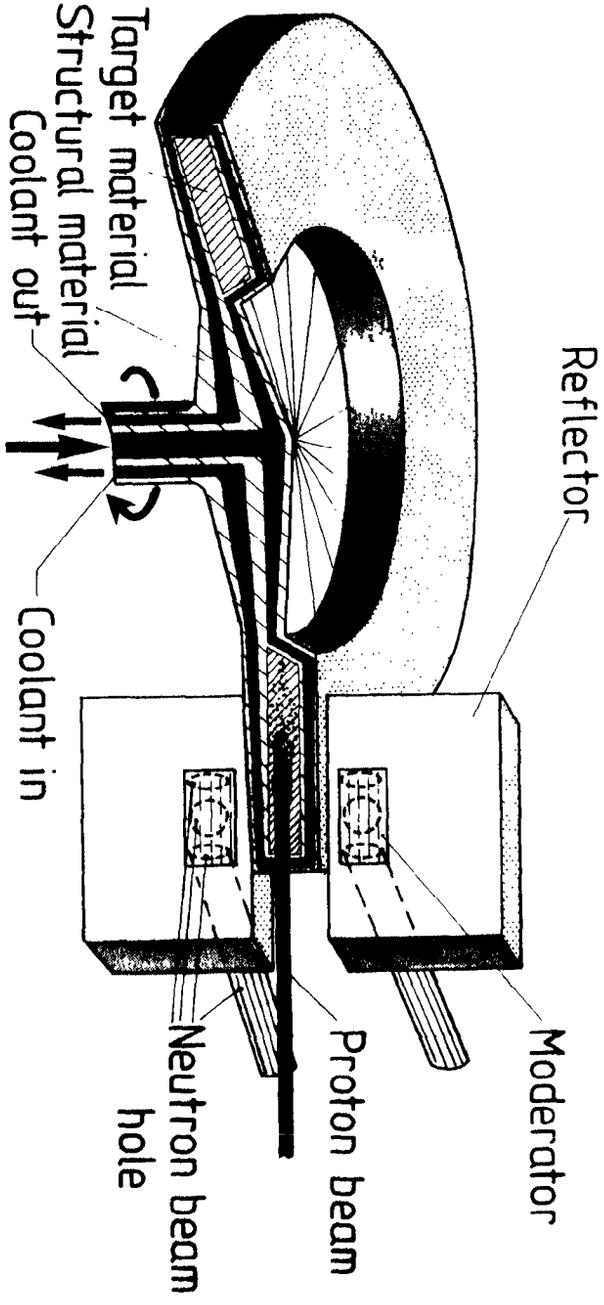

Rotating high power spallation target

2.6 Compressor Ring

If the proton pulses coming at 100 Hz in 0.5 ms bunches from the LINAC were stored in a circular orbit, one could empty this orbit, once completely filled by an accelator macropulse, at one stroke.

For ϕ = 65m one could fill eventually 80% of the orbits length with protons (about $2.7 \cdot 10^{14}$ protons). These protons then could be periodically extracted to give an intensity gain-factor of $\sim$ 650 by keeping just the same average current.

With such a device, neutron pulses with epithermal energies ($\lesssim$ eV-range) and a width of 10 µsec could be obtained, thus opening this energy range for experiments. (TOF: E=1 eV; $\Delta E/E = 10^{-2}$; Δt = 10µsec; flight-length $= \Delta t \cdot (E/\Delta E)\,(8E/m)^{1/2}$ = 30m).

The conceptual design work for this device is done in collaboration with experts from Eindhoven, SIN, CERN, Scanditronix, the responsability given to H. WILLAX, from SIN. Several problems are to be solved:

- Injection (phase space problems)
- Space charge instabilities ($\sim v^{-2} \left(\frac{mo}{m}\right)^3$).

3. Experiments under way in the course of a project verification.

As shown in Fig. 7 some crucial questions are tackled experimentally in collaboration with different laboratories:

Accelerator: CERN, LASL, VALVO
Target: Flux distribution in moderators (SIN)
Flux distribution for fast neutrons (SATURNE)
Spallation process: SIN, SATURNE.

4. Science connected with the use of SNQ.

Neutron experiments (physics, chemistry, biology) are the spear-head of the justification for such an expensive installation. Most types of experiments will be better off compared to the ILL-HFR. One could group the neutron scattering experiments into four classes:

(1) Experiments only using the mean flux (irradiation): gain factor 1

(2) Experiments using the mean flux, making profit from gating synchronously with the pulse to reduce background noise and higher order contamination (e.g. from a monochromator) estimated gain factor 2

(3) Thermal time-of-flight experiments, making full use of the peak flux gain factor 18 (without the compressor-ring)

(4) New types of experiments.

With the compressor-ring, another factor between 2 and 3 could be gained for time of flight measurements with thermal neutrons. The gain will be enormous for neutrons with energies above 0.1 meV. This gain, together with the fact that the pulse structure of the beam itself is appropriate for time of flight measurements with neutrons of such energies, renders the electron volt region accessible to neutron spectroscopy.

I will here not go into the details of solid state physics in this spectral range (electronic band structures via $\chi(Q,\omega)$, high excitation of local moments, high $\hbar\omega$, molecular excitations in solids or fluids, structural analysis of fluids and amorphous solids with high Q), but instead mention some physics based on μ^+-particles, neutrinos, and direct use of the primary protons. μ^+ as well as ν are produced by primary protons:

$$p + A \rightarrow \pi^{\pm} + \ldots$$

$$\pi^{\pm} \rightarrow \mu^{\pm} + \nu_\mu\,(\bar{\nu}_\mu) \qquad \tau_\pi = 2.6 \cdot 10^{-8}\ \text{sec}$$

$$\mu^{\pm} \rightarrow e^{\pm} + \nu_e + \bar{\nu}_\mu\,(\bar{\nu}_e + \nu_\mu) \qquad \tau_\mu = 2.2 \cdot 10^{-6}\ \text{sec}$$

A suitable target may produce 99% of the neutrinos from stopped pions. The different life-times τ_π and τ_μ are to be used in connection with the pulse-structure of the beam to separate pion or muon-decay events.

4.1 Solid state physics by muons.

Fundamentally, one can use the charge or the magnetic moment of the muons for probing solid state behavior.
The Larmor frequency for muon-spin rotation (μSR) is : $\omega_L/H = 2\mu_\mu/\hbar$ = 85.5 KHz/Gauss. Since muons are emitted polarized parallel (or anti-parallel) to the pion-momentum, one can measure the change in spin-direction by non-symmetric distribution of positrons after the muon decay.

4.1.1 To probe internal magnetic fields (ferromagnetics, paramagnetic metals (Knight-shift), one could

either directly follow the e^+-intensity oscillations in a fixed detector after μSR. A spallation source with a "compressed" (accumulated) beam of small pulse width (e.g. 10^{-7}sec) could lead to the detection of small ω_L ie. small H not accessible with only the muon-lifetime 2.2 μsec.

or choose an external field, so that ω_L equals the pulse-repetition frequency (100 Hz). Thus all muons would oscillate in phase, if not internal fields would cause deviations.
The precision of the measurements is directly proportional to the beam intensity (1o-1oo ppm Knight shift obtainable).

If the muons would show a fast diffusion in a random magnetic lattice, on the average there would be no effect on the muon spin. Traps for muons would then lead to a visible effect.
Again, short pulses from the accumulator would allow the detection of very small effects (e.g. relaxation rates during depolarization in a longitudinal external field).

4.1.2 Channeling of π^+ or μ^+.

There is a pronounced correlation between the decay-spectrum and the crystal axes. Perfect crystals show maximum intensity for thermalized μ^+ or π^+ on interstitials along the "channels" in the lattice. Defects, especially holes trap the muons and reduce the intensity along close packed chains. High intensity is necessary. There is practically no noise for that measurements.

4.2 Neutrino-physics.

Pion-decay neutrinos come with 30 MeV, those from muon-decay with less than 53 MeV.
A neutrino flux of $\phi_\nu \sim 2.5 \cdot 10^9$ cm^{-2} scc^{-1} in 5m distance from the target could be expected for an accumulated SNQ-p-beam. That would allow to reduce the lower limit for measurements of mass-differences between neutrinos $\Delta^2 := m_2^2 - m_1^2$, to ≥ 0.03 $(eV)^2$ [instead of $\Delta^2 > 1$ $(eV)^2$ available now.]
Inelastic scattering of neutrinos at nuclei

$$\nu_\mu + (A,Z)\ [T,I] \rightarrow \nu_\mu + (A,Z)^+\ [T',I']$$

(T: isospin, I:spin)

e.g. $^7Li\ (\nu,\nu')^7\ Li^*$ or ^6Li, ^{12}C, ^{19}F could be detected by the γ-particles emitted from A^+. Thus, nuclear physics with <u>neutral-neutrino-currents</u> could be performed, unique in the sense that neutrinos cannot change the nucleon-configuration in the target by either strong or electromagnetic interaction (as all other probes would do). Here you see the importance of the separation of neutrinos from pion and muon decays.
Using clean muon-neutrinos after pion-decay allows the determination of model free matrix-elements. (cf. T.W. Donnelly, R.D. Peccei, Neutral Current Effects in Nuclei, Physics Reports <u>50</u>, 1, (1979)).

4.3 Nuclear physics with protons.

- (p,2p)-, (p,pn)-reaction for $300 \leq E_p \leq 500$ MeV (internal structure of the nucleus)
- few nucleon reactions for better understanding of internal dynamics of few-nucleon-systems
- (p,pα)-reactions for cluster-structure at the surface of nuclei.

We feel, that the goals in n-scattering physics as well as in nuclear and solid state physics as mentioned provide an interesting challenge to all of us to put this new type of instrument into being with all efforts possible, as soon as possible.

SPALLATION NEUTRON SOURCE AT SIN

C. Tschalär

Schweizerisches Institut Für Nuklear-forschung

1. Accelerator

The meson factory SIN (Schweizerisches Institut für Nuklear-forschung) started operation in February 1974. It was built as a research facility mainly for nuclear and particle physics using high flux beams of pi-mesons and muons as probes. These particles are produced by a primary proton beam which is accelerated first by a sector focussing injector cyclotron to 72 MeV and then by a separated magnet isochronous ring cyclotron to a fixed energy of 595 MeV (Fig. 1). At present, beam currents of 0.1 to 0.15 mA are used routinely and 0.2 mA peak has been achieved in short-time trials. The beam has a macro-duty cycle of 100 %. The micropulses are about 0.5 ns long and are separated by 20 ns.

Since the available current from the present injector is limited to a few tenths of milliamperes, it was decided to build a new injector (II) which is now under construction. It is a ring cyclotron similar to the main accelerator but with four sector magnets instead of eight. It is in turn fed by a Cockroft-Walton injector of 0.8 MeV. The current capacity of injector II is expected to be beyond 2 mA.

The main cyclotron (ring) should be able to accelerate about

0.5 mA using existing hardware. The limitation is beam loading of the four RF acceleration cavities. A boost of the RF power from the present 0.6 MW to about 2 MW is planned, which would allow beam currents of 1 to 2 mA. Beam losses in the accelerator are not expected to be a serious limitation since extraction efficiencies of 99.98 % are routine today.

In order to be able to handle proton beams of more than about 0.2 mA, the external proton beam channel and the two meson production targets have to be upgraded. The second target station (thick target E) and the beam dump will be rebuilt entirely such that the waste beam after target E can be either deflected into the dump or extracted through the dump shielding and injected into a neutron source placed in a new East Hall adjacent to the main experimental hall. Depending on the thickness of target E (5 to 10 cm of graphite), 50 % to 75 % of the primary proton beam will reach the neutron source.

2. Choice of neutron source

In principle the quasi continuous beam from the SIN cyclotrons could be pulsed (kHz or slower) by either a fast chopper, a buncher at the injector or a compressor (storage ring) in the extracted beam. The fast chopper would reduce the average current to incompetitive levels and the acceleration of bunched pulses is difficult and limited to peak currents well below 10 mA. Both these modes would further handicap meson experiments severely. A compressor ring for the waste beam is

extremely difficult to conceive because of the large phase space of the beam and a compressor for a partial beam split off from the main beam would again suffer from low average beam. Furthermore, the cost of a compressor ring would be comparable to the cost for the entire neutron source.

For these reasons it was decided to build a continuous spallation source at SIN for a proton current of 1 to 2 mA using a first generation target made from non-fissionable material. Calculations and measurements have shown that thermal neutron fluxes comparable to medium flux reactors can be expected. Since spallation sources release much less power per neutron produced, a cold neutron source (liquid D_2 moderator) can be placed closer to the region of maximum neutron flux than in a reactor. Estimates suggest that this feature together with modern cold source design and optimized coupling to neutron guides would yield cold neutron fluxes comparable with those of existing high flux reactors. A cold source of about 30 l of liquid D_2 is therefore included in the concept of the SIN neutron source.

3. Source concept

3.1 Lay-out

The proposed layout of the SIN neutron source is shown in Fig. 2. The proton beam enters the target at an incline of about 5 % to the horizontal. Beside areas for about 6 thermal neutron ports, a large area is provided for experiments with

cold neutrons.

3.2 Target concepts

3.2.1 Target material

A first generation target is to be made of a liquid lead-bismuth eutectic (LBE). The well known advantages of LBE are a high spallation neutron yield as well as a low thermal neutron absorption cross section which allows relatively large targets and beam diameters and thus lower power densities. Low melting point (123° C), large liquid phase temperatur range (∿ 1'400° C), zero volume change on freezing and a well known corrosion behaviour make LBE ideal for use as a circulating target which eliminates heat transfer and radiation damage problems in the target proper.

3.2.2 Beam window

An unavoideable requirement for a liquid target is a beam entrance window. Even in the case of a proton beam plunging vertically onto a "free" surface of an LBE target, a thin window is generally needed to hold back vapors and gases from the hot target. Feasability of a beam window depends primarily on the question of radiation damage to the window material. Since graphite (either pyrolytic graphite or normal graphite coated by pyrolytic graphite) is an ideal material for windows from the termo-mechanical and neutron physics point of view, samples have been irradiated with the SIN proton beam. As a first test, a 3 mm thick disk of normal graphite was irradiated by a 100 µA-beam of about 0.2 cm^2 cross section at about 1'200° C

for 200 hours yielding an irradiation density of 100 mAh/cm^2. The sample showed no visible damage or distortion. Detailed structure studies are in progress. A sample of pyrolytic graphite of 6 mm thickness was irradiated in the same beam at 1'500 - 2'000° C for 800 hours and a sample of high grade pyrographite is currently included in the A5-target at LAMPF (0.4 mA of protons at 800 MeV). Results of both tests are expected by the end of the year. Based on the irradiation density of the first sample, a minimal life time of about 2'000 mAh can be assumed for a graphite window in a typical proton beam of 5 cm diameter. For a conical graphite window of a thickness of 5 mm which is cooled on one surface, calculations yield thermal strains below 10 % of the breaking strain. If the same window is cooled by radiation only, the strain is even less and the maximal temperature about 2'000° C which is acceptable for graphite.

Thus a graphite entrance window to a liquid target, even under pressures of a few bar, seems eminently feasible. Since it provides great freedom of choice of target and source geometries and allows to design compact targets with accordingly modest requirements on handling and service facilities, it was adopted in all concepts of the SIN neutron source.

3.3.3 Forced convection target

In the present concept for the LBE target, the LBE is pumped through the target by a mechanical pump and cooled by an external heat exchanger. The target, shown in Fig. 3, is a

cylindrical vessel centered on the proton beam. The LBE enters concentrically around a conical entrance window, cooled by the LBE, and returns again concentrically along the wall of the vessel. The target vessel is placed inside a cylindrical helium container which acts as a confinement. The unit is attached to a cylindrical shielding block about the beam vacuum chamber. Together they constitute the target plug which can be uncoupled from the beam vacuum and the LBE circuit and extracted from the source by a remotely controlled shielding cask. The loaded cask is lifted out of the proton channel by crane and then transported to a hot cell for service or repair on the target. A similar arrangement is used at present for servicing the meson production targets at SIN.

The LBE circuit is shown schematically in Fig. 4. The target is at the highest point of the circuit in order to minimize the pressure on the target window. The circuit, including the sloping target section, is layed out in such a way that the entire LBE content drains into a shielded reservoir as soon as the pump is turned off. The vertical section of the circuit has the effect, among other things, that in case of a leak through the window, the pump runs dry after about 20 % of the LBE content of the circuit are lost and prevents the rest from being pumped out through the leak, even if the pump is not stopped.

The entire LBE circuit is encased in a containment filled with helium gas. The gas is also used to preheat the circuit at startup.

The LBE system is therefore inhearently safe: Even if all detection devices and active control measures fail, the target vessel is drained automatically of its LBE content in case of leaks, pump failures or stoppages, thus preventing an explosion due to oberheating by the beam. Even a simultaneous failure of both LBE and helium windows would at worst result in part of the LBE content to flow down the beam pipe and be caught in a shielded dump. Emergency cooling of the activated LBE is not necessary as the total power emitted by the reaction products is estimated to be less than about 1 % of the beam power.

Preliminary data for the LBE system are shown in table 1.

Table 1:

Flow data for a forced convection LBE target

LBE circuit		Entrance window	
beam power	1 MW	heat density	500 W/cm^3
r.m.s. beam diameter	5 cm	surface heat flux density	250 W/cm^2
LBE flow rate	4 l/s	heat transfer number	1.2 W/cm^2 K
LBE temperature range		max. window temperature	500° C
170° C - 340° C		LBE pressure at window	1 bar
LBE pump pressure	3.5 bar		

3.3 Source structure

The structure of the proposed neutron source is shown in Fig. 5 - 7. The target is embedded in a cylindrical heavy water moderator tank with a vertical axis, a diameter of

2.5 m and a volume of about 12m^3. Horizontal beam tubes for thermal neutrons originating above and below the target tube extend out radially within an angular region of about 45°-135° on both sides of the proton beam. A cold source in the shape of a cryogenic container filled with about 30 l of liquid deuterium is placed directly on top of the target. The expected power of about 1 kW deposited in the cold source per mA of proton beam is removed by a vertical D_2-heat pipe system with a condensor on top of the shielding.

The source is shielded by a cylindrical stack of cast iron of about 6 m outer radius. It contains the neutron beam tubes and beam shutters. It is surrounded by a layer of additional shielding made essentially of iron and concrete of 1-2 m thickness which can be individually adjusted and designed to suit the experiments. The cylindrical part of the shielding is extended in the direction downstream from the target to shield against the intence flux of forwardly produced high energy neutrons.

4. Alternative source concepts

4.1 Free convection target

In order to simplify the proposed LBE system, we studied the possibility of a sealed target vessel extending at an incline through the inner layer of the shielding. At the bottom end of the cylindrical vessel the proton beam enters through a conical graphite window as in the case of the forced convection target.

The top half is cooled by an array of cooling pipes thus setting up a convection current in the LBE. A schematic drawing of a vertical target version is shown in Fig. 8. The target vessel should be long enough (~4m) such that the residual activation at the top end is low enough to permit manual decoupling of the vaccum connection, the cooling pipes and monitoring devices. The entire target vessel is then handled and serviced like the target plug of the forced convection system.

First calculations show that, once a stationary convection current is reached, flow rates and temperatures similar to the forced convection case can be achieved. Estimated for the start up phase of the convection current indicate that initial temperatures close to the evaporation point would be reached if the full power of the beam would be switched on at once. However, the rather large latent heat of evaporation of LBE would prevent evaporation even in this extreme case. Thus a free convection target, especially a vertical one, seems to be possible for SIN beams. It would considerably reduced the complexity and cost of a spallation target system and will therefore be investigated in more detail.

4.2 Vertical beam lay-out

In alternative source lay-out has been studied at SIN featuring an entirely cylindrical source geometry centered on a vertical proton beam entering from the bottom (see Fig. 9 and 10). In

contrast to the "free target surface" concept with a vertical beam entering from the top as was proposed elsewhere, the SIN version allows genuine 360°-access to the neutron source analogons to a reactor without the exceedingly expensive bridge structure required to support a shielded proton channel over the experimental area. Instead only a slit trench in the floor of the neutron source hall is required into which the proton beam descends beneath to source and is then bent upwards by a large bending magnet. The slit trench is covered by a modest amount of heavy shielding to protect the experimental area above it. From the technical point of view the vertical beam concept would allow an optimal geometry for a free convection target. Furthermore, in case of a window failure the LBE would be collected in the slit trench thus reducing the danger of wide-spread contamination.

Although the vertical beam concept is somewhat more expensive, it offers a significiant increase in available thermal beam ports. It is therefore studied further as an alternative to the horizontal beam version.

5. Performance

In the past year extensive measurement of neutron spectra and fluxes from a mock-up spallation source were carried out on the 1nA proton beam at SIN. Targets of Lead-Bismuth and of U^{238} in various shapes were studied without moderator and with light

and heavy water moderators and simulated neutron beam pipes in various geometries. Preliminary results for the LBE target surrounded by a beryllium multiplier and placed in a D_2O moderator of about 1 m radius indicate that a realistic flux of about 10^{14} n/cm^2 mAs can be expected for 600 MeV protons.

6. Timetable

The present long range planning for the development of SIN facilities calls for completion of injector II by early 1983, upgrading of the proton beam to 2mA capacity by late 1984, installation of the RF power booster of the ring cyclotron by late 1985 and completion of the neutron source by 1986. Proton currents of 1mA or larger are also expected by 1986.

Scientific opinion on the proposed neutron source and response from potential users has been almost unanimously positive. In view of this and the relatively modest cost, the odds are very much in favour of the project. A decision is scheduled for January 1981.

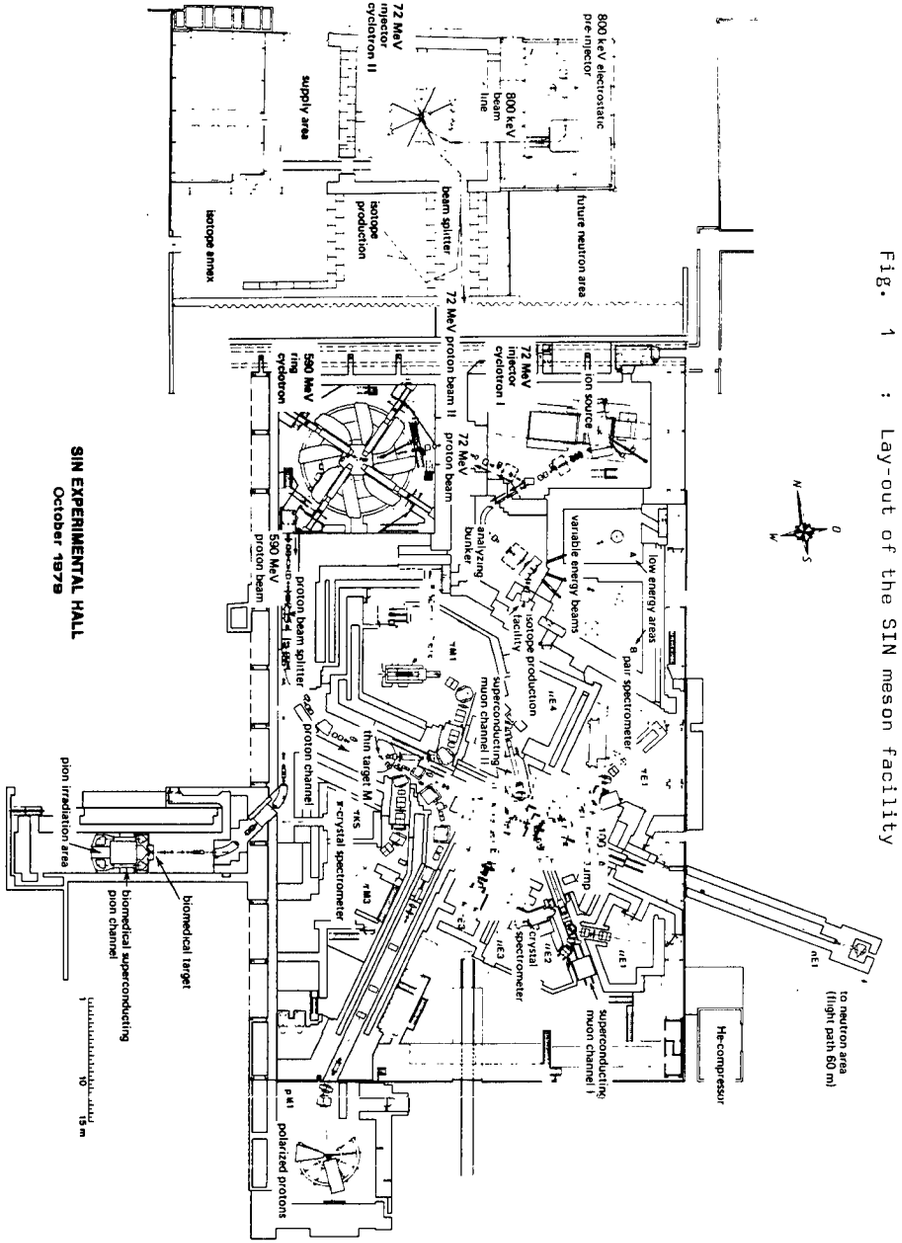

Fig. 1 : Lay-out of the SIN meson facility

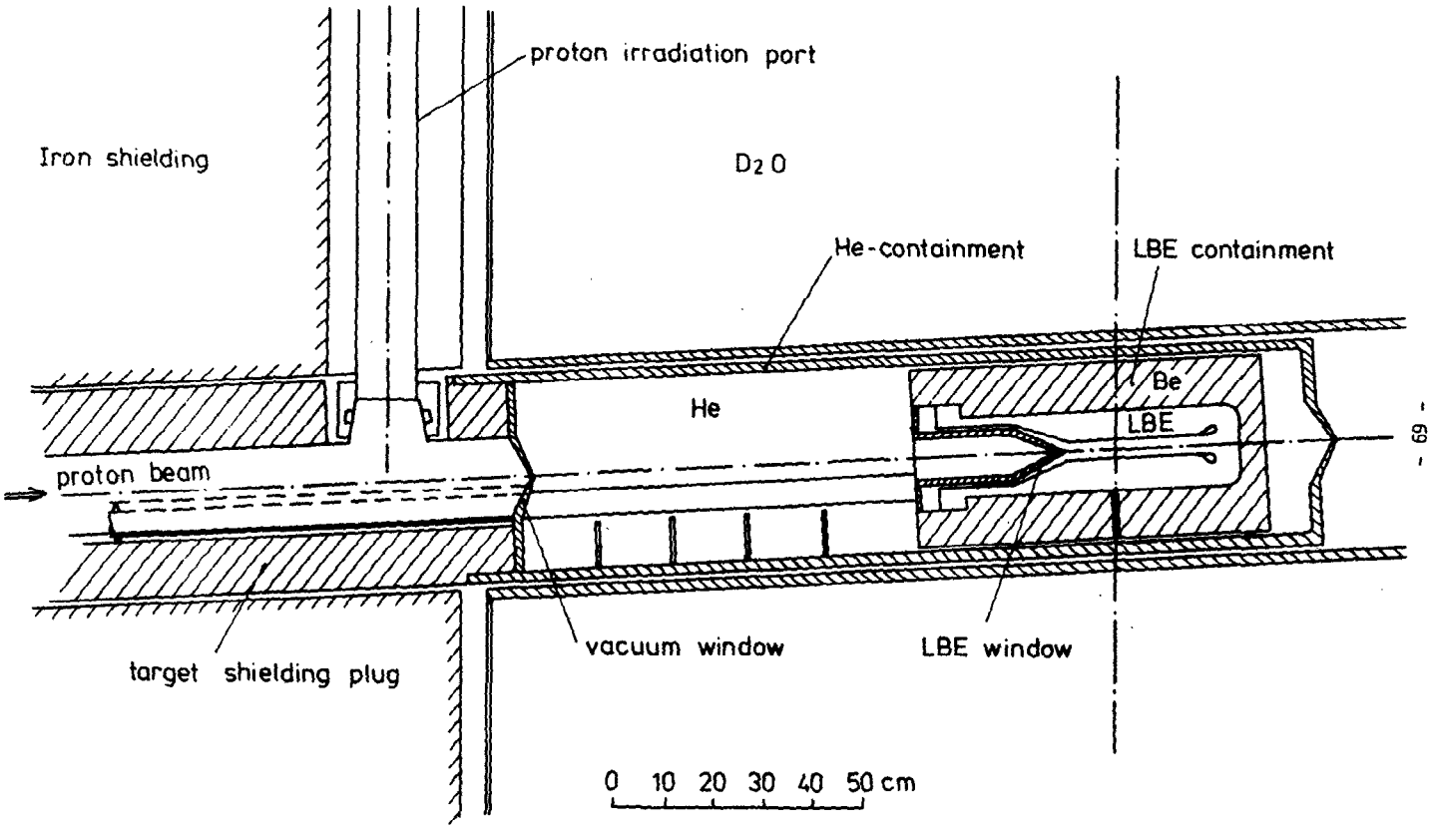

Fig. 3 : Cross section through a forced convection LBE target

Fig. 2 : Lay-out of the SIN spallation neutron source

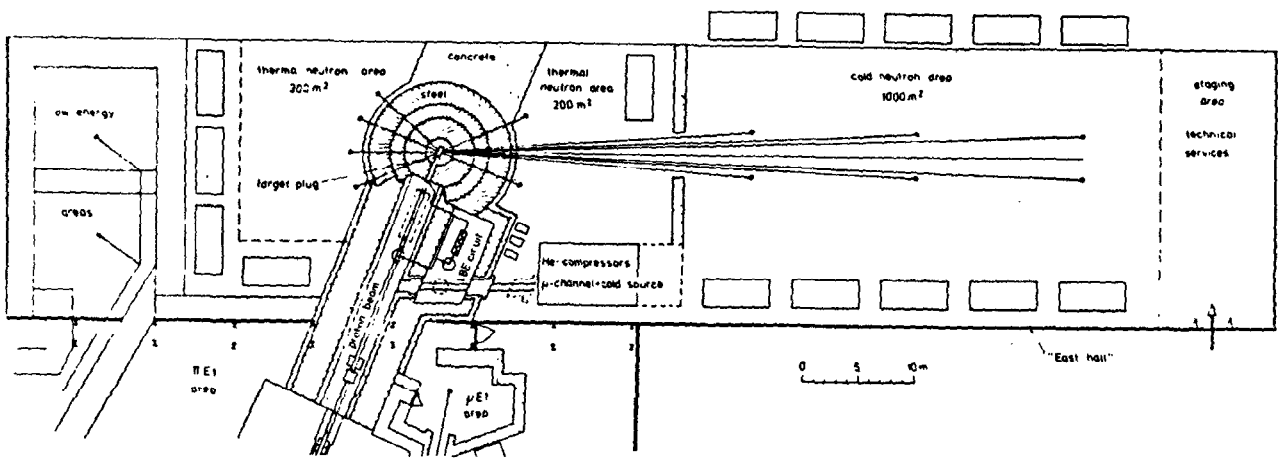

Fig. 5 : Vertical cross section through the source (proton beam plane)

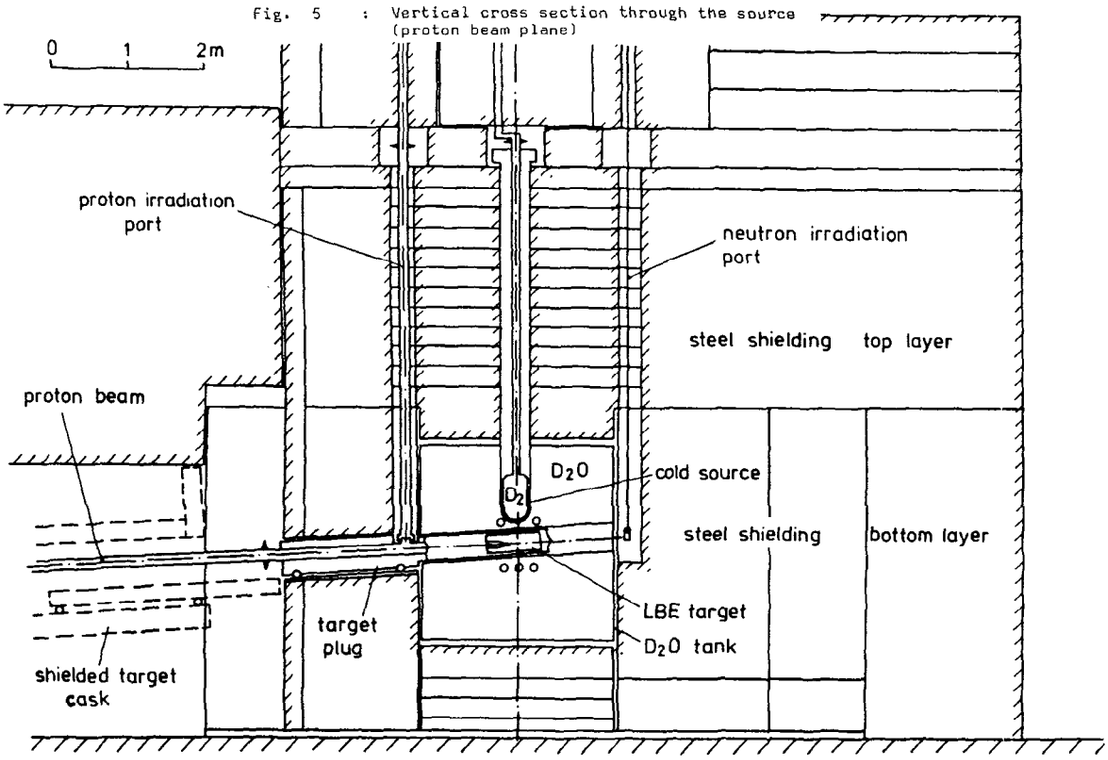

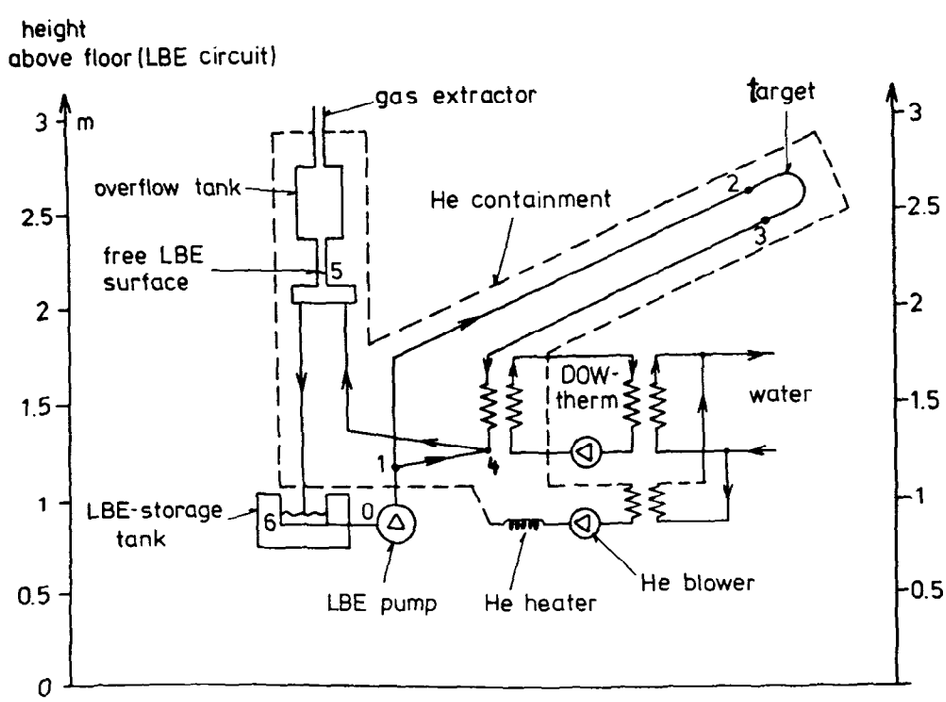

Fig. 4 : Schematic LBE circuit

Fig. 6 : Vertical cross section through the source (perpendicular to proton beam)

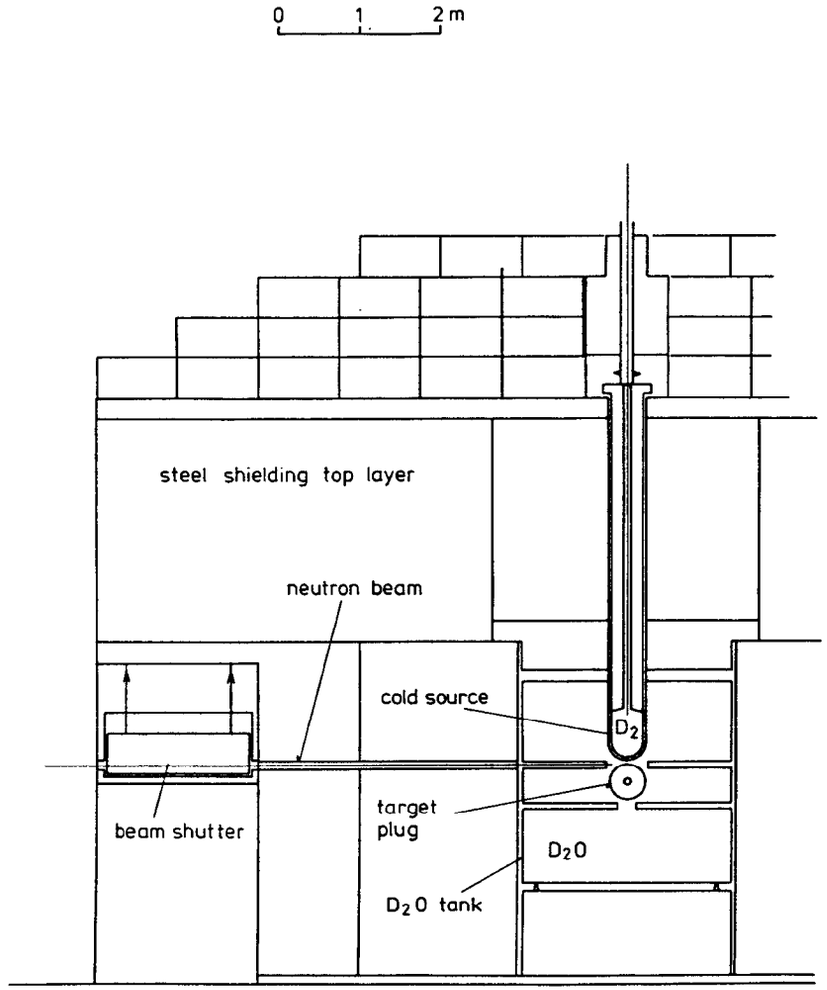

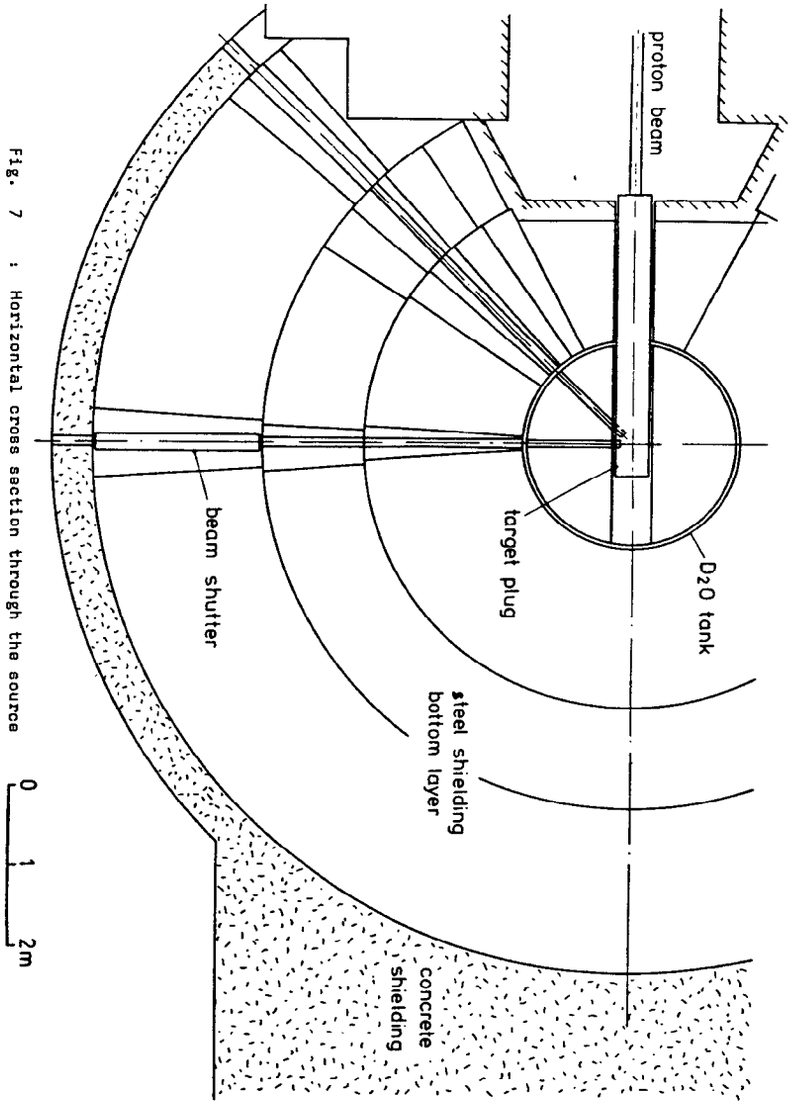

Fig. 7 : Horizontal cross section through the source

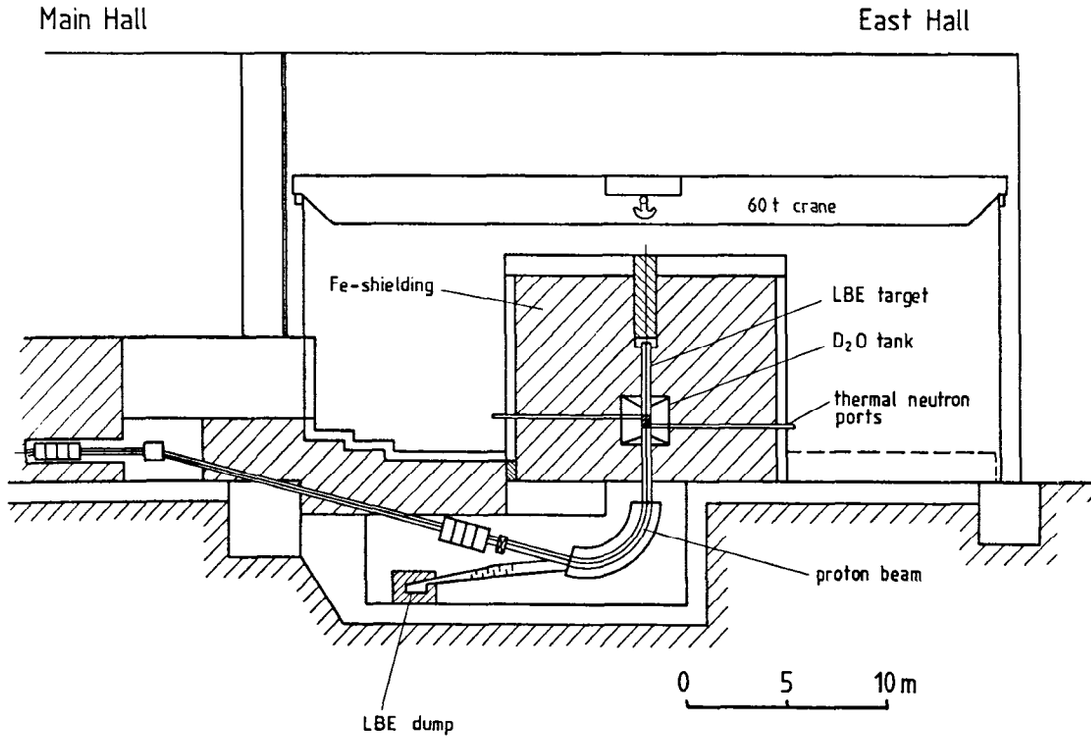

Fig. 9 : Vertical beam concept of a neutron source; vertical cross section

Fig. 8

Free Convection LBE Target

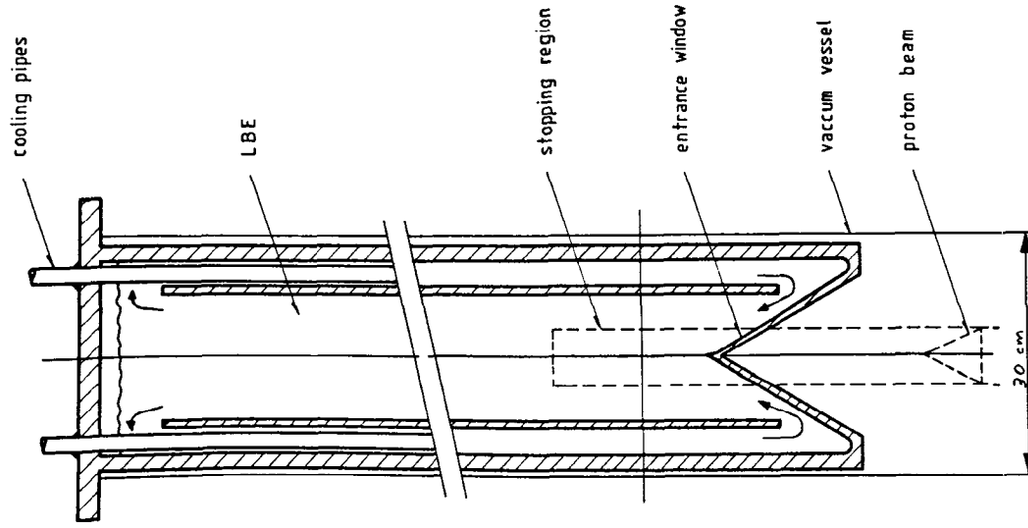

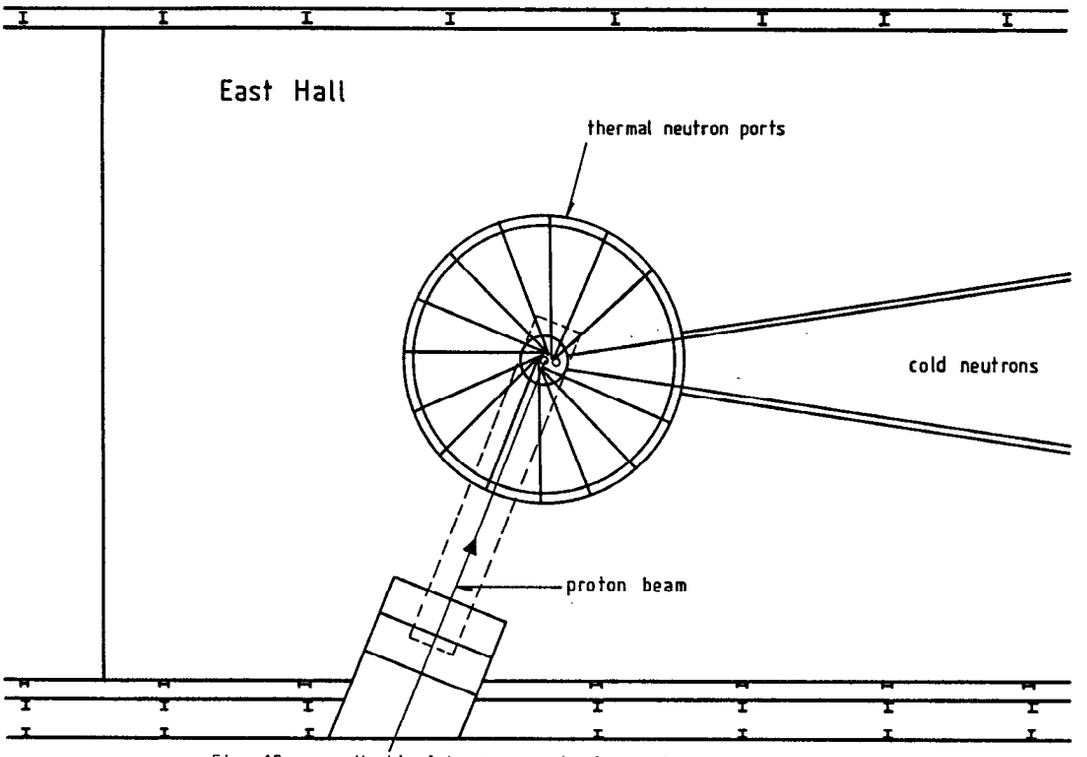

Fig. 10 : Vertical beam concept of a neutron source; horizontal cross section

THE BOOSTER SYNCHROTRON UTILIZATION FACILITY AT KEK

H. Sasaki

National Laboratory for High Energy Physics

1. Overall Summary

The Booster Synchrotron Utilization Facility (BSF) was established to provide a pulsed neutron source facility (KENS), a meson physics research facility (BOOM) and high-energy proton and neutron beams for medical and biological purposes (PARMS). According to schedule, on June 18, 1980, the BSF which had been under construction since 1978, came into operation. Preliminary surveys indicated that the production of thermal, epithermal and cold neutrons from the tungsten target for the neutron scattering experiments was satisfactory. On July 16, one month after delivery of the first beam, protons from the booster synchrotron were switched to the meson experimental area and the emergence of pulsed meson and muon beams from a 6 m long 5 Tesla superconducting solenoid was confirmed. Initial operation of the new Booster facility during the one and half months up to the end of July was devoted to confirmation and adjustment of various design parameters. Adjustment and improvement of the apparatus will be continued during the second half of this year and the new facility will be regularly open to users from the beginning of the next fiscal year. The proposal for medical use of the booster beam, which was submitted to the government through the University of Tsukuba, was approved last

April and construction of the facility will start shortly.

2. Booster Synchrotron and its Injector System

Operation of a 20 Hz rapid-cycling 500 MeV Booster Synchrotron as an injector for the 12 GeV proton synchrotron commenced in December 1974. Design parameters of the synchrotron are listed in Table 1. The design goal of a beam intensity of 6×10^{11} protons per pulse was achieved in June 1977. During the summer of 1979 the vacuum chamber of the main synchrotron was replaced and the maximum beam intensity in the main ring exceeded 4×10^{12} protons per pulse the last May. A consequence of the increased acceptance of the main ring is that the booster synchrotron operates with above the initial design intensity. During the initial shared operation of the booster with the main ring synchrotron 47 pulses every 2.4 seconds were delivered to BSF as shown in Fig. 1. The effective rate for BSF was thus about 16 Hz.

Conversion of the injection scheme in the booster synchrotron from the present multi-turn injection to charge exchange injection with a H^- ion beam is under consideration. By this new scheme, not only will the ordinary proton beam intensity be increased, but the acceleration of polarized proton beams will also become possible. The development of a H^- ion source and design of such an injection system for the booster synchrotron are now in progress. Measurements of the proton beam life time in the multi-traverse through a 120 $\mu g/cm^2$ carbon foil stripper set in the booster ring indicate that it will be possible to inject a H^- ion beam of 150 turns into the booster. This would give rise to an estimated circulating beam current of about 1.5 A in the booster just after the injection process

for a 15 mA H^- injected ion beam. The circulating current is only about 0.4 A with the present multi-turn injection scheme. A trial H^- ion source on a test stand is now delivering a 15 mA H^- ion beam for a duration of 150 μsec.

3. Proton-Beam Line

Fig. 2 shows the layout of Booster Synchrotron Utilization Facility including the booster synchrotron and the beam line to the facility. The length of the beam line from the booster to the neutron production target is about 150 m. The beam line consists of two parts; the beam-dump line and a new line extending from the beam dump to BSF. A pulsed bending magnet on the injection course to the main ring separates the proton-beam pulses of 50 nsec from the main ring injection beam and directs them towards the beam dump located outside the accelerator enclosure. The beam-dump line makes a vertical detour around a cable pit containing feeder lines for the main ring magnets and it is designed to fulfill achromatic conditions in the vertical plane at the exit from the vertical bending magnet located just before the beam dump. The proton beam may be switched in one of three directions by another pulsed switching magnet situated about 40 m downstream from the beam dump. If the magnet is switched off the beam hits directly the spallation neutron target. By supplying power to the magnet the beam may be switched either to the meson experimental area or to the secondary proton beam line for medical purposes. The beam line contains several π-sections in addition to the achromatic and matching sections. At the exit from the matching section, which is located downstream from the beam-dump line, the beam is focussed into an appropriate size for the

respective production target to which it is transfered through π-sections.

All the evacuated beam pipes including the bellows and gaskets in the BSF beam line are manufactured from aluminium alloy with the exception of the ceramic chamber and stainless steel squared bellows of the pulsed switching magnet. The residual radioactivity in aluminium induced on exposure of the 500 MeV proton beam is much lower than that in stainless steel.

The monitor system for the beam line consists of fifteen beam-profile monitors and ten intensity monitors inclusive of those on the beam-dump line. It is possible to measure the beam emittance and twiss parameters without disturbing the beam transportation.

During normal operation of the accelerator, 38 proton-beam pulses within each main ring repetition period of 2.4 sec are available for BSF, each 50 nsec beam pulse containing about 6×10^{11} protons. These pulses are distributed to the pulsed neutron source facility, the meson physics research facility and medical use in accordance with the prescribed program.

4. Pulsed Neutron Source Project

Construction of the pulsed neutron source (KENS), which utilizes the pulsed proton beam from the KEK 500 MeV booster synchrotron, started in 1977. Neutron beams ranging in energy from eV to meV are provided by spallation in a tungsten target and using moderators of polyethylene at room temperature and solid methane at 20 K, and a Be reflector about 200 kg in weight. The target assembly is placed at the centre of a large biological shield consisting of a heavy-concrete fixed shield and a movable section

composed of iron and concrete blocks. Thirteen neutron beam holes are installed in the biological shield. Each of these, except for three supplying cold neutrons to the guide tubes, is equipped with a 0.9 m long iron shutter. The three neutron guide tubes which transport cold neutrons to the cold neutron experimental area have a 9 m long curved section with a cross section of 20 x 50 mm^2 and a radius of curvature of 820 m. Ni float glass is used for the neutron reflector in the guide tube, which transmits the neutrons with wave lengths more than 4 Å. A tail cutter is also installed at the exit of the cold neutron beam hole to admit only those neutrons with wave lengths less than 12 Å. Five spectrometers for thermal, epithermal and cold neutron scattering experiments and a data acquisition system have already been designed and constructed. The installed spectrometers are as follows: Small Angle Neutron scattering instrument (SAN), TOF spectrometer with Optical Polarizer (TOP), Low energy Large Analyzer Mirror spectrometer (LAM), Multi Analyzer Crystal neutron spectrometer (MAX) and High Intensity Total scattering spectrometer (HIT). The emphasis of the research conducted at the pulsed neutron source will be on condensed matter in non-equilibrium states, transient phenomena and the structures of liquid and amorphous materials under normal and extreme conditions such as high pressure or low temperature.

5. Meson Physics Research Facility (BOOM)

In 1978, the Meson Science Laboratory was established in the Faculty of Science, Univ. of Tokyo. Representing a branch of that laboratory, the facility called BOOM (Booster Meson facility) has been established as one of the three major projects of BSF (Meson,

Neutron and Medical). The final goal of the BOOM project is to create a meson experimental facility and research program based on the maximum use of the unique pulsed time structure provided by BSF. μSR studies using pulsed muons are the central area of study. Fig. 3 shows the layout of the meson experimental area.

The main apparatus in BOOM is a pulsed muon channel, which is characterized by a superconducting solenoid representing the $\pi\mu$ decay section. The pion injector consists of a quadrupole triplet and a single bending magnet placed at a zero degree take-off angle with 75 mstr acceptance. A Be target 3 cm in diameter and 12 cm long is normally used for pion production. The superconducting solenoid, which is 6 m long, 12 cm internal diameter and with a central field of 5 T, is indirectly cooled by supercritical He. In the extraction channel of the muon beam, a QQ-B-Q-B-QQ type achromatic scheme is applied. This provides good beam focussing properties. The number of μ^+ produced in the preliminary experiment was estimated to be 2.5 x 10^4/pulse or 5 x 10^5/sec. For the μ^- intensity, this number should be divided by a factor of 3. The comparison between the negative muon intensities at the muon channels of the major meson factories as shown in Fig. 4. The average intensity of our channel is relatively low but still competitive. However, the instantaneous intensity is really huge, easily 3 orders of magnitude larger than that of the LAMPF stopped muon channel.

The newly completed pulsed μSR facility is therefore quite satisfactory in both intensity and quality. There are several types of μSR experiments which can be studied effectively only by this facility and, in addition to μSR measurements, there are also other

experimental projects to which our pulsed muon beam may be effectively applied.

Table 1 Design Parameters of KEK Booster

Structure	
Type of Focusing	Combined-Function
Focusing Order	FDFO
Energy and Magnetic Field	
Max. Kinetic Energy	500 MeV
Max. Field at Equilibrium Orbit	11.018 kG
Injection Kinetic Energy	20 MeV
Injection Field at Equilibrium Orbit	1.969 kG
Repetition Rate	20 Hz
Physical Dimensions	
Average Radius	6 m
Circumference	37.70 m
Bending Radius	3.3 m
Number of Magnets	8
Orbit Parameters	
Profile Parameter	3.664 m^{-1}
Number of Betatron Oscillation per Revolution	
Horizontal	2.2
Vertical	2.3
Average Momentum Compaction Factor	0.1877
Total Transition Energy over Rest Energy	2.308
Transition kinetic Energy	1.23 GeV
Maximum and Minimum β	
$\beta_{H.max}$	3.40 m
$\beta_{V.max}$	8.25 m
$\beta_{H.min}$	1.48 m
$\beta_{V.min}$	1.55 m
Maximum Dispersion Function	1.40 m

Apertures of Magnets and Acceptance	
Useful Semi-Aperture of Magnets	
Horizontal	50 mm
(Good Field Region	63 mm)
Vertical	30 mm
Height of Magnet Gap at Equilibrium Orbit	76 mm
Acceptance at 20 MeV	
Horizontal	56 mm.mrad
Vertical	10 mm.mrad
Emittance at 500 MeV	
Horizontal	112 mm.mrad
Vertical	15 mm.mrad
RF Acceleration	
Revolution Frequency	
at Injection	1.617 MHz
at Final Energy	6.031 MHz
Intensity Estimation	
Incoherent Space Charge Limit	2.6×10^{12} ppp*
Coherent Space Charge Limit	4.3×10^{12} ppp
Design Intensity	6×10^{11} ppp
(Final Goal	1.1×10^{12} ppp)

*ppp : protons/pulse

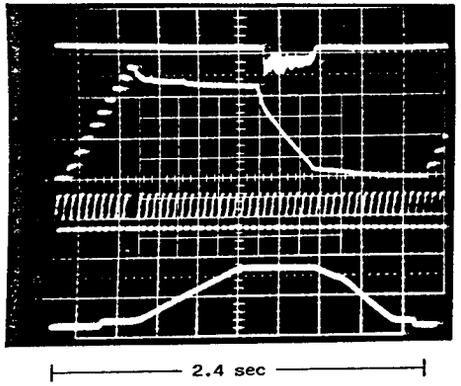

Fig. 1 Proton beam currents
in MR synchrotron and booster synchrotron

1st trace: Extracted proton beam from MR
2nd trace: Circulating proton beam in MR
3rd trace: Circulating proton beam current in the booster
4th trace: Magnetic field of MR

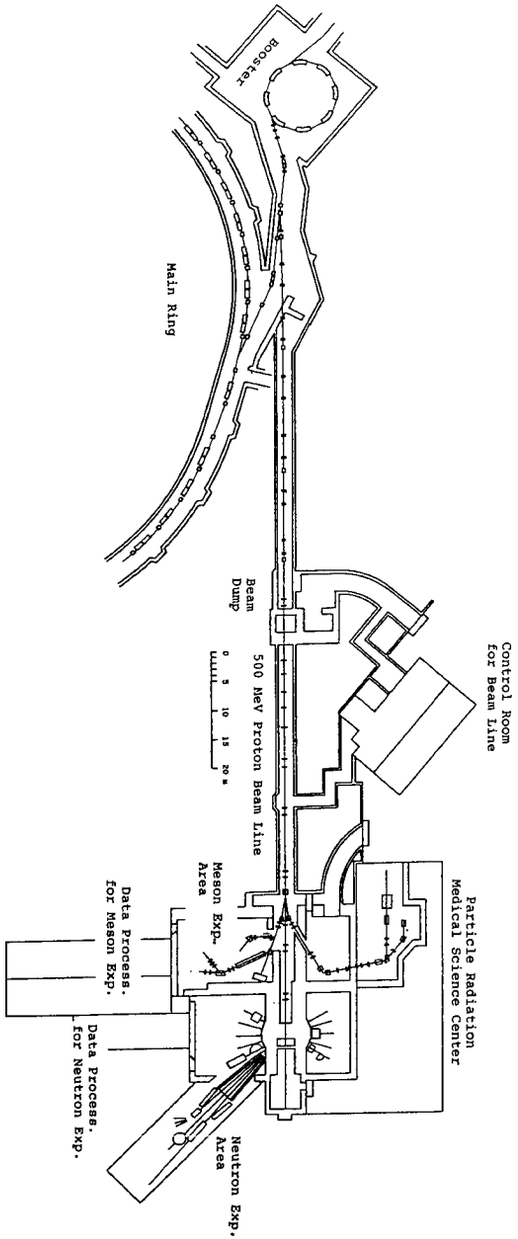

Fig. 2 Layout of Booster Synchrotron Utilization Facility and booster synchrotron

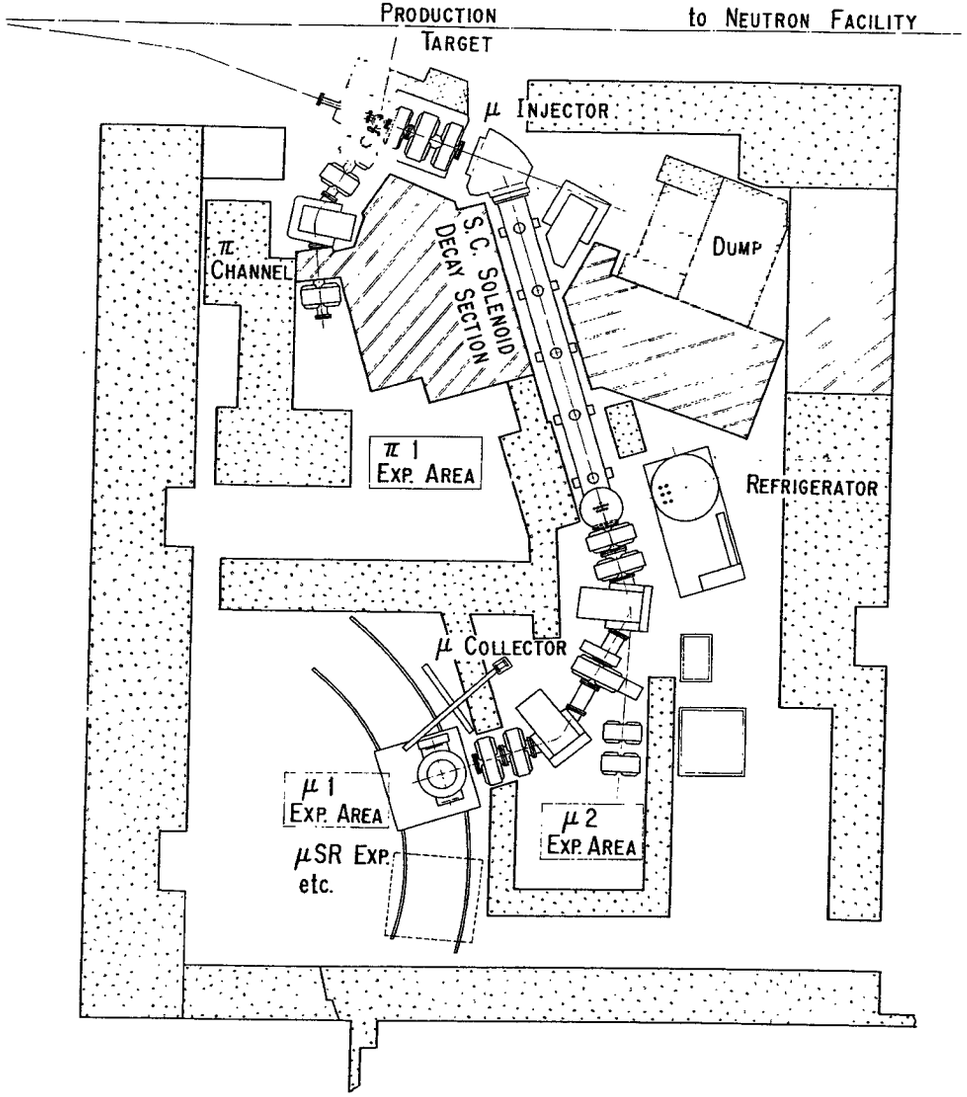

Fig. 3 Layout of the meson experimental area

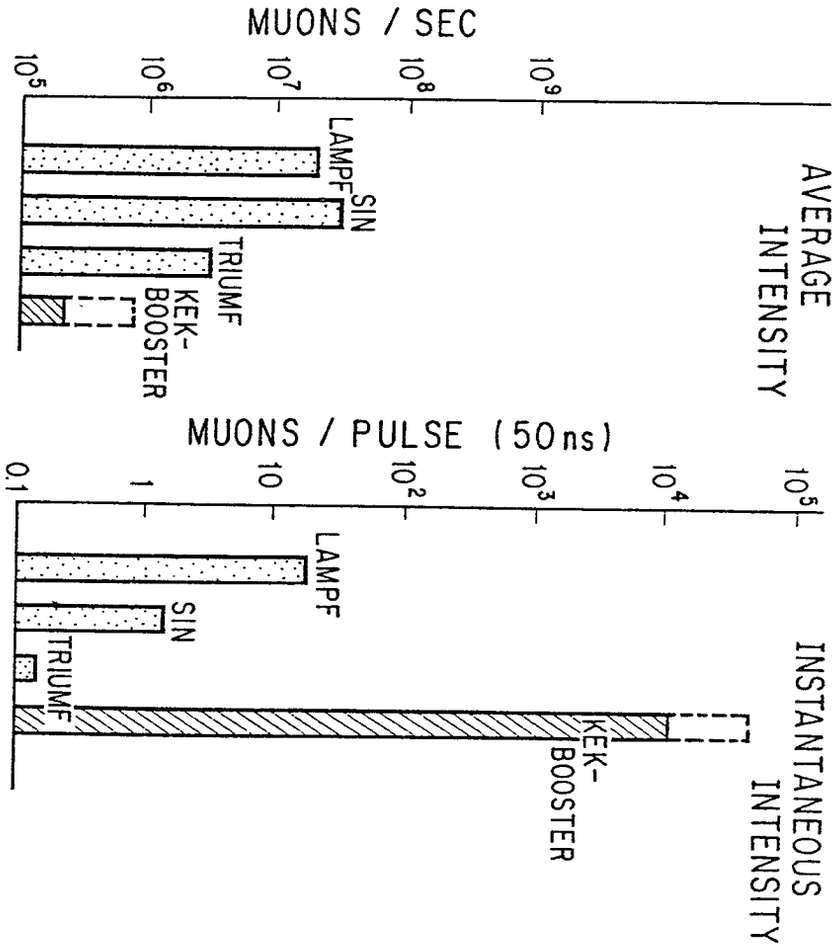

Fig. 4 Negative muon intensity at the major meson factories. Design value is shown by broken line.

PRESENT STATUS OF THE KENS FACILITY

Y. Ishikawa

Physics Department, Tohoku University, Sendai

§1. Facility

Construction of the neutron scattering research facility-(KENS) was completed at the end of March, 1980, as a part of the KEK-Booster Synchrotron Utilization Facility. The layout of the constructed facility, as shown in Fig. 1, is close the that envisaged in the original proposal.[1,2] It consists of three rooms - the main experimental area, the cold neutron experimental area and the data acquisition room. The neutron source is located near to the center of the main experimental area and the biological shield which surrounds the source effectively devides this hall into two areas, A and B. Nine beam tubes, H_1 to H_9 which glance at the normal moderator deliver thermal and epithermal neutrons to these two areas. Four further beam tubes, which view the cold moderator transfer cold neutrons either directly to area B (C_4) or to the cold neutron experimental area via three neutron guide tubes, (C_1, C_2, C_3). Five spectrometers HIT, MAX, LAM-40, SAN and TOP are already installed around the neutron source as displayed in Fig. 1. The present appearance of the facility is indicated in the photographs (Figs. 2-5) of these experimental areas and the data acquisition room which were taken recently. Approval for operation of the facility was obtained

at the end of May and the first proton beams arrived at the neutron target on June 18. We still remember vividly the impressive experience we had on that day. Early in the morning, we were informed that the beam line magnets would be switched on at about 10:00 a.m. Anticipating that initially a small fraction of the full proton beam would arrive at the target, we had decided to place a He^3 counter at the exit of a beam tube in order to detect the small neutron flux produced by the first proton beam and we watched the data diplay panel in vain for about an hour. At 11:00 we were surprised to receive a telephone call from the operation center asking "Are you aware that the full proton beams are already reaching on your target?" Nearly the full proton beam had arrived at our target at the moment of switching on the magnets and our He^3 counter had therefore been saturated from the outset.

The proton beam size at the target was found to be 52 x 45 mm^2 (defined as within positions of 1/50 intensity) as displayed in Fig. 6. This is acceptably small compared with the target size $78^H \times 57^V$ mm^2. Figure 7 is the first neutron diffraction pattern obtained from an iron block and the spectrum of incoherent elastic scattering from a polyethylene plate measured on that day by using a single He^3 counter. These results convinced us that neutron beams were really being emitted from our new spallation source.

The following day the cold neutron moderator was cooled to 17K during operation of the source and the first cold neutron beams were detected at the exits of the neutron guides on June 20. Since then the KENS neutron source has been operating routinely without problems until the time of the present report. In the intervening period, many data on the neutron source have been accumulated,

together with experimental data from the operating spectrometers. This paper briefly summarises these results. More detailed discussions can be found in the other papers comprising this KENS report.

§2. Target Assembly

The KENS neutron source employs a tungsten target cooled by pure water.[1] The neutron flux emitted from the ambient and cold moderators was measured by means of activation of Au foils. By normalizing the fluxes with respect to the number of fast neutrons emitted from the source, the conversion ratios of the fast to epithermal and cold neutrons for our moderator-reflector system were determined to be 5.26×10^{-3} (n/str.eV.p) for 1 eV neutrons and 3.12×10^{-2} (n/str.p) respectively. These values are somewhat smaller than our original estimate of the intensity of the KENS neutron source, but they are still reasonable compaired with the expected value at other spallation neutron sources. The 47 equivalent peak flux intensities of the cold (3 meV), thermal (81 meV) and epithermal (1 eV) neutrons on the moderator surface were estimated to be 1.6×10^{15}, 5.7×10^{14} and 2.6×10^{14} (n/cm^2-sec-eV) respectively at full power operation (6×10^{11} PPP x 38 P/2.5 sec). The neutron energy spectra from moderators were also determined by measuring the incoherent scattering from V metal.

§3. Biological Shield

The radiation levels on the surface of the biological shield

and at the beam stopper were measured to be 0.6 mR/hr and 0.8 mR/hr respectively, in accordance with the design value of less than 1 mR/hr. Radiation levels in the experimental areas A and B were found to be below 2 mR/hr even when the shutters of the three beam tubes H_3, H_5, C_4 were completely open. Access to the spectrometers is, therefore, allowed even during operation time as we had originally expected.

§4. Cold Neutron Source[3]

The cold neutron source has been operating successfully throughout the whole available machine time. Using a small cryogenerator (PGH 105) of 40 W and a 7 m long He gas transfer tube the cold moderator can be cooled to 16.8K. The temperature of the moderator increases only by one degree during full power operation of the neutron source. The heat deposited by radiation inside the moderator was calculated to be 1W for a proton beam intensity of 7.3×10^{12} proton sec^{-1} which is in good agreement with our earlier estimate. The extend of decomposition of the methane in the moderator by radiation was found to be rather small. The methane gas returned to the reservoir tank from the moderator contained only 0.14% hydrogen after one weeks' operation. The total number of spallation neutrons entering the moderator during this time was about 1.4×10^{18} ns. The extent of this decomposition is only 1/50 of that found after a similar effective operation of the Hokkaido cold neutron source which is installed at an electron LINAC. This suggests that the decomposition in the latter case is mainly due to γ ray radiation. The above results are quite encouraging and they allow us the

possibility to increase the intensity of spallation neutrons without changing the present cooling system. The time and energy spectra of the cold neutrons emitted from the cold neutron source were also measured.

§5. Cold Neutron Guide Tubes

Three bent guide tubes of the cross section 20 x 50 mm^2 transport neutrons to the cold neutron experimental area. At the entry of three guides there are three tail cutters which admit only neutrons within the wave range 4-12 Å or 3-11 Å. The intensity of cold neutrons at the exit of the guides was estimated by activation of a Au foil to be about 1×10^5 n cm^{-2} sec^{-1}, which is in approximate agreement with that calculated from at the moderator and the guide geometry the flux. More accurate measurements of the absolute value of the intensity of cold neutron flux are in progress to find out the real transmission factor of our guide tubes. The energy spectrum and spatial distribution of the cold neutron beams at the exits of the guides have also been measured.

§6. Spectrometers and Data Acquisition System

Five spectrometers, HIT, MAX, LAM-40, SAN and TOP have already been installed at the facility as shown in Fig. 1. The TOF data recorded by these spectrometers is accumulated in a computer OKITAC-50/60 (575 KB-IC) via a separate time analyzer for each spectrometer.

HIT is the high intensity total scattering spectrometer which

was designed so as to optimise the speed of the measurement.[4] Fifty 1/2" diameter He^3 counters and a special electronic device for the amplifiers have unable the counting rate to be increased up to 5 nts/μsec. The scattering from a standard amorphous sample (5 gr) can then be measured up to 50 $Å^{-1}$ with good statistics in a few minutes.

MAX is the multi-analyzer crystal spectrometer with inverted geometry which is equipped with fifteen separate analyzer crystals.[5] If appropriate values for the scattering and analyzer angles are selected, the spectrometer can be used to perform energy scans along any desired direction in the reciprocal space. The constant Q mode of operation is, therefore, possible and complete magnon or phonon dispersion relations in a Brillouin zone can be probed at one time. The phonon scattering from an iron single crystal was measured with good S/N ratio in 48 hrs.

LAM-40 is the large analyzer mirror spectrometer equipped with four large PG analyzer mirrors.[6] The spectrometer is suitable for measuring the quasi-elastic scattering from hydrogen containing materials at a medium resolution (60 μeV-200 μeV). A beautiful quasi-elastic scattering profile of these materials can be obtained in one hour.

SAN, the small angle scattering spectrometer, is installed at the exit of guide tube C_1. Equipped with a two dimensional PSD which may be moved inside a vacuum chamber and with fifteen He^3 counters set at six different fixed positions, the spectrometer can measure simultaneously the scattering in a wide range of momentum transfer from 3×10^{-3} to 4 $Å^{-1}$. By virtue of the pulsed of the incident beam the separation or measurement of inelastic scattering

will be possible without significant modification. The small angle scattering from a sample as an Al-10%Zn alloy may be measured with a good S/N ratio in the space of a few minutes.

TOP is the TOF cold polarized neutron spectrometer installed also at the exit of a guide tube C_1. The incident pulsed white beam of neutrons polarized by means of total reflection from a Soller slit package composed of thin films of an Fe-Co alloy on a polymer support. The polarization direction is reversed by a Drapkin type spin flipper and a flipping ratio of 11 has been achieved as monitored by the 111 Bragg reflection from a Cu Heusler alloy. The spectrometer is currently being used to study the interface magnetism in the bilayer crystals of FePd or FeZr.

Two further spectrometers called FOX and PEN are at a late stage of design and will be installed in early 1981. The former is a conventional four cycle single crystal diffractometer, while the latter is a polarized epithermal neutron spectrometer in which polarization is achieved by transmission of the neutron beam through a dynamically polarized proton filter.

§7. System for Operation and Research

The KENS facility is unique in that it was constructed without there being permanent staffs for the project in KEK. Even now the number of permanent staff is limited to be three so that the neutron source, cold neutron source and the five spectrometers must be maintained by the KENS research group which consists mainly of outside people. Seven spectrometer groups have been organized corresponding to the seven existing spectrometers and those belonging

to each group have an obligation both to maintain and improve their spectrometer as well as acting as a 'local contact' when persons outside the group wish to use the machine. Because of this arrangement about 70% of the total machine time is allocated to the spectrometer group. Further subdivision of the machine time within the group is made by group leader, which makes research scheduling somewhat flexible. In each year all proposals including those from each spectrometer group are presented to KEK before the end of February. These proposals were examined by the Neutron Scattering Committee composed of eight specialists from different fields and following their decision final approval may be given by Advisory Council for Scientific Policy and Management via Committee for the Utilization of BSF.

References

1) Y. Ishikawa and N. Watanabe, KEK Report 78-19 (1978)
2) H. Sasaki, N. Watanabe and Y. Ishikawa, KENS Report I (1980) 1
3) Y. Ishikawa and S. Ikeda, KENS Report I (1980) 19
4) N. Watanabe, K. Yamada, M. Misawa and T. Mizoguchi, KENS Report I (1980) 73
5) K. Tajima, Y. Ishikawa and S. Tomiyoshi, ibid. 86
6) K. Inoue, Y. Kiyanagi, M. Kohgi and Y. Ishikawa, ibid. 127
7) Y. Ishikawa, S. Ikeda, M. Furusaka and N. Niimura, ibid. 101
8) Y. Endoh and Y. Ishikawa, ibid. 149

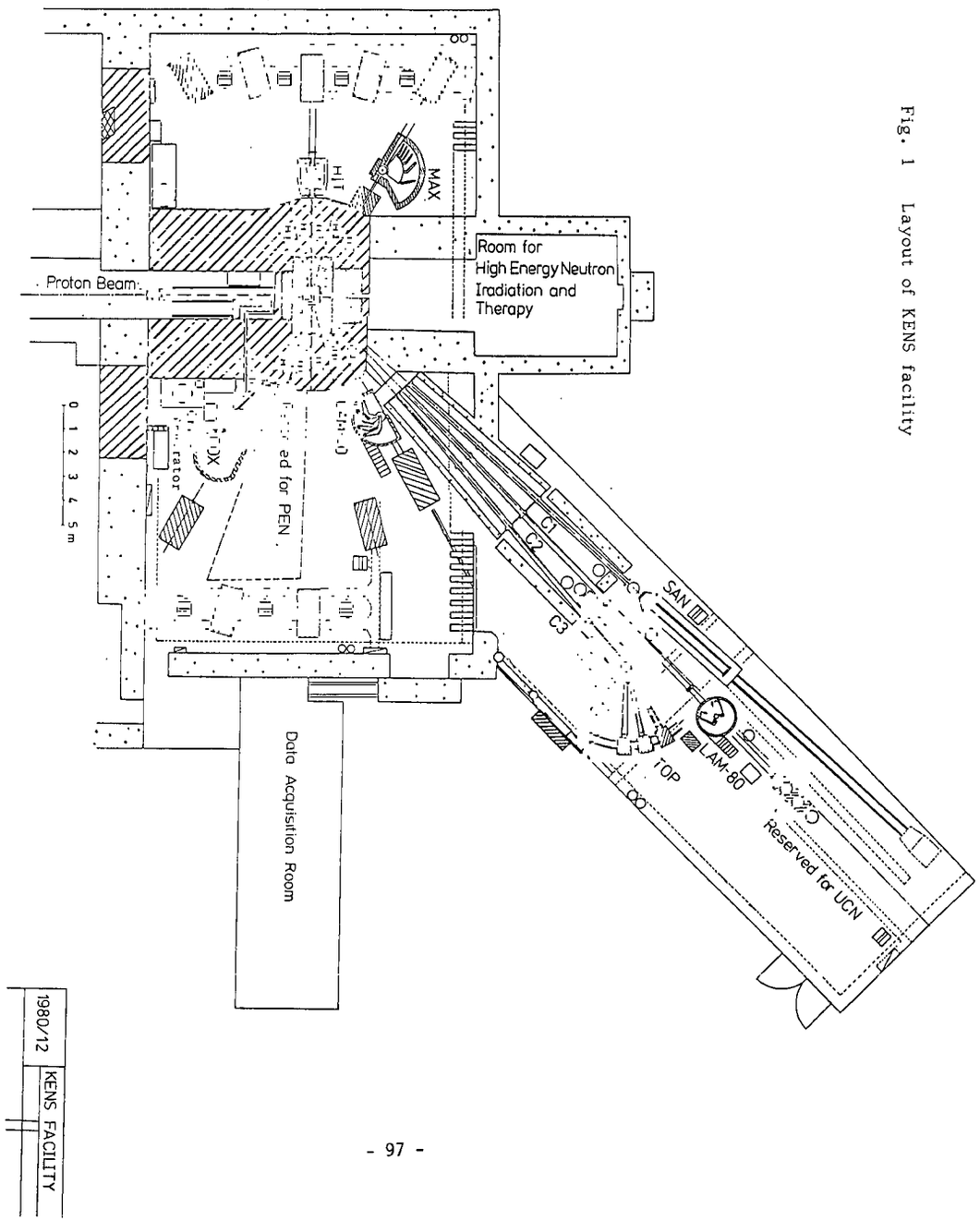

Fig. 1 Layout of KENS facility

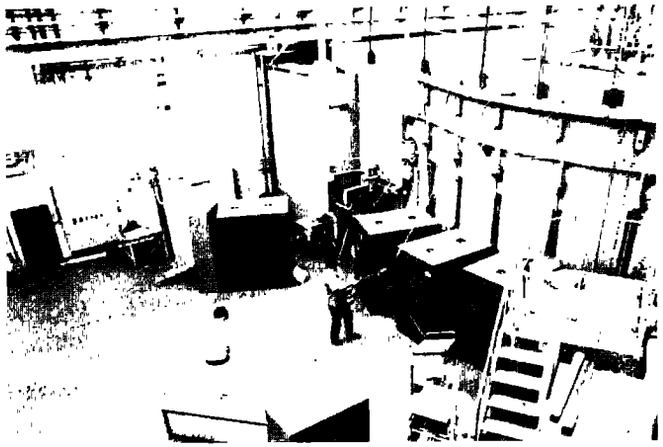

Fig. 2 Photograph of main experimental area A with LAM on the right hand side

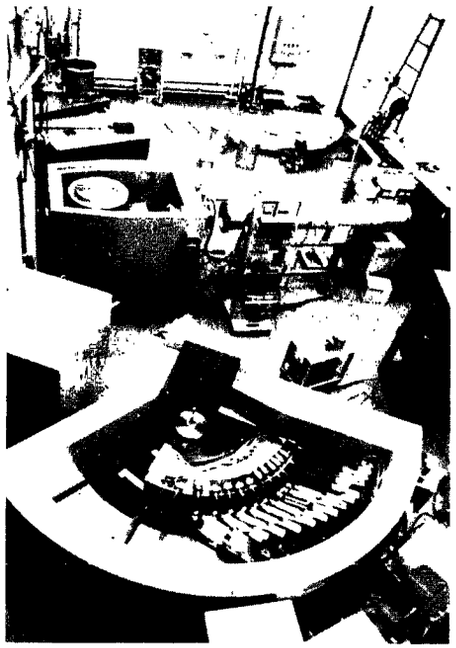

Fig. 3 Photograph of main experimental area B with HIT and MAX (below)

Fig. 4 Photograph of cold neutron experimental area with SAN (left) and TOP (right)

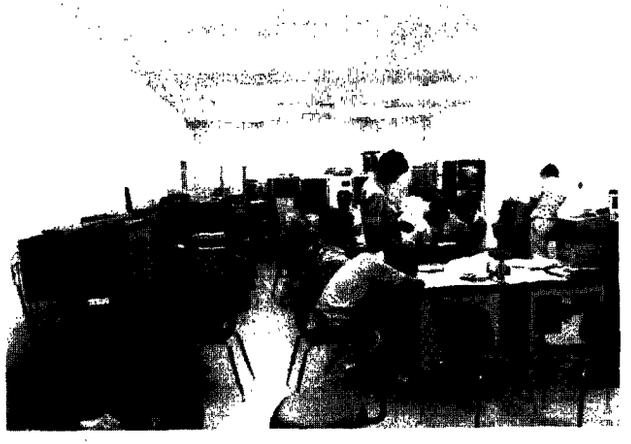

Fig. 5 Photograph of data acquisition room

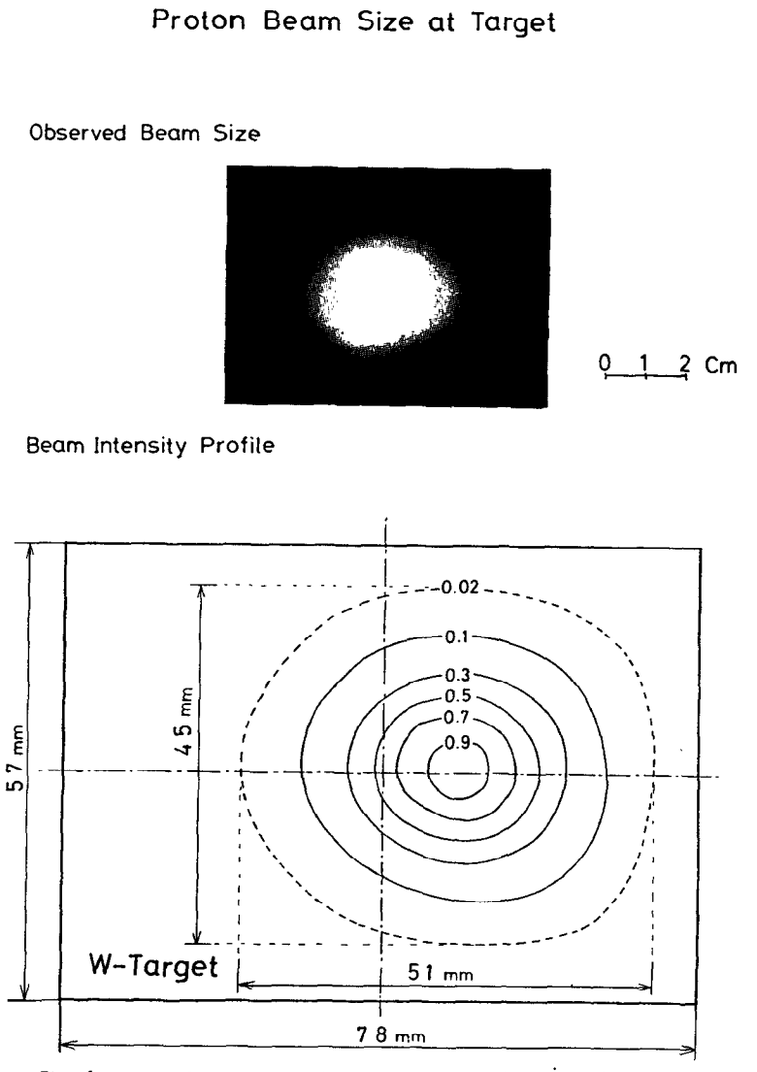

Fig. 6 Proton beam size on the neutron target (above) and beam intensity profile (below)

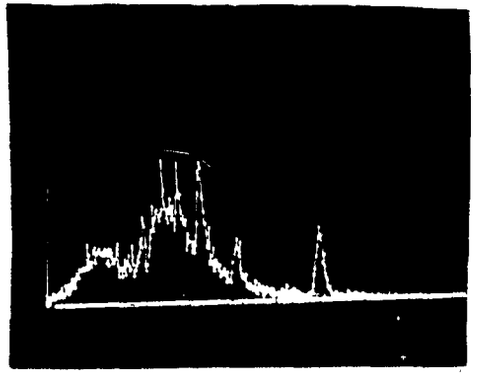

(a)

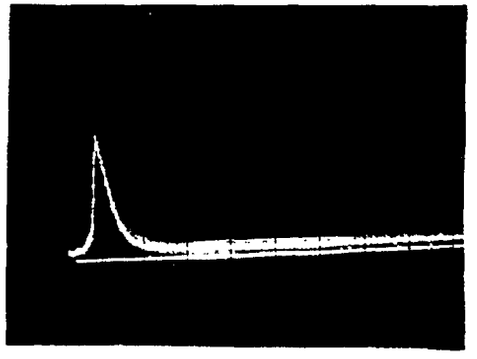

(b)

Fig. 7 First neutron scattering data from the KENS facility measured on June 18, 1980

(a) iron block (b) polyethylene plate

Summary of the Plenary Session

Reports of Status of Spallation

Neutron Source Projects

J. M. Carpenter and Y. Ishikawa

This session showed the growing world-wide interest in steady, quasi-steady and pulsed spallation neutron sources. The six projects on which we heard status reports ranged from those which are in the process of conceptual design, to those which have been completed, with one, the ZING-P' prototype, already shut down after accomplishing its purpose. The table lists the projects, the characteristics of the sources, and their status. The TRIUMF project is included in the table for completeness, although no report was given in this session, since there have been no recent new developments since the ICANS-III meeting. The detailed reports from each laboratory should be consulted for further information.

Spallation Neutron Source Projects

Laboratories	Source	Location	Characteristics	Status
KEK	KENS	Tsukuba, Japan	500 MeV protons Synchrotron (shared) 2μA, pulsed 20 Hz, τ_s=0.1μs W target CH_2 and Solid CH_4 moderators.	Completed June 1980
LASL	WNR	Los Alamos, USA	800 MeV protons Linac (shared) 6μA, pulsed 120 Hz, τ_s=8.μs W, Ta targets.	Completed '77
	WNR/PSR		800 MeV (H^- injection) LINAC-storage ring (shared) 100μA pulsed 12 Hz, τ_s=.27μs	Full instensity 1986
ANL	ZING-P'	Chicago, USA	300 & 500 MeV protons (H^- injection) Synchrotron 8μA, pulsed 30 Hz, τ_s=0.1μs U Target	Startup 1977, closed 1980
	IPNS-I		500 MeV protons (H^- inject.) Synchrotron 22μA, pulsed 45 Hz, τ_s=0.1μs, U Target, Liq. H_2 and CH_4 moderators.	Startup 1981 Full current ~1983
	IPNS-II		800 MeV protons (H^- inject.) Synchrotron 500μA, τ_s=0.2μs 60 Hz, pulsed	Decision deferred
Rutherford - Appleton Lab	SNS	Chilton, UK	800 MeV protons (H^- inject.) Synchrotron 200μA, pulsed 50 Hz τ_s=.27μs U Target	Low current 1983 Full intensity 1986
KFA	SNQ	To be determined	1.1 GeV protons Linac 5mA, quasi-steady 100 Hz, τ_s=500μs Lead or Liq. Pb-Bi target Options: add H^- compressor ring	Design study to be completed early 1981 project completion ~1991
SIN	TNS	Villigen, Switzerland	600 MeV protons Cyclotron 1-3 mA, steady Liq. Pb-Bi target	Full Current 1986
TRIUMF	TNF	Vancouver, Canada	600 MeV protons Cyclotron 140μA, steady Liq. Lead target D_2O & H_2O moderators. Option: quadruple current.	Completed 1976

Most of the reported design and construction activity seems at this stage to be devoted to the sources themselves rather than instruments. This probably reflects the facts that the sources require the longer time to design and construct and that commitments on instruments can be held for later to make possible the needed evaluation of new concepts and development of new components in instrumentation. Nevertheless, instruments appear to come on line with the completion of the sources. Some exciting instrumentation developments are appearing to exploit the characteristics of the new sources. Instruments on the operating sources are already providing new scientific results.

Each project addresses a different mix of applications, according to the capabilities and needs of the community served. While the primary applications discussed in this meeting were neutron scattering (and in the case of IPNS, fast neutron radiation damage) research, other applications of these installations were also discussed. A partial list includes medium energy (meson) physics, muon spin resonance, pion therapy, neutrino physics isotope production and nuclear physics. Most of these applications are mutually exclusive, thus require time sharing of the primary accelerator beam.

In earlier meetings, we were in many cases grouping for factors of two in evaluating source parameters, and quite ignorant of some important questions. Now we are asking for accuracy at the level of, say, 20%, and have identified and quantitatively answered many more important questions than before. At the same time, we have begun to get gratifying scientific results from some of the new instruments and are becoming able to assess more convincingly the scientific productivity of spallation neutron sources.

This steady progress is the coming to fruition of the new generation of advanced neutron sources.

T. Nishikawa and W. Close

Informal Discussions

H. Sasaki, R. Jameson and S. Fukumoto

Coffee Break

G. Russell, Y. Ishikawa, A. Carne

T. Broome and T. Nishikawa

Coffee Break

N. Swanson, T. Armstrong, N. Watanabe

K. Katoh, M. Furusaka

II TARGET STATIONS

The target sessions were mainly devoted to presentations and discussions on Target-Moderator-Reflector assemblies. The detailed design of such assemblies at each laboratory as well as the results of their operation at the completed neutron sources were presented on the morning of Tuesday, October 21st. The afternoon of that day was devoted to discussions on the neutronics of the assembly. The problem of radio activation were discussed mainly on the morning of Thursday, October 23rd. The meeting program is given in Appendix I. The course and outcome of the sessions are summarized by three reporters. Their summaries appear at the end of this section.

Energy deposition in cold moderators was one of the intensively discussed topics following the presentation of early results obtained from the KENS cold moderator which had suggested an energy deposition ten times greater than previous estimates. This problem was, however, settled by a subsequent measurement at KENS which yielded a value for the energy deposition similar to that found by other groups as described in the comment of Watanabe. Grooved moderators were proved to be another interesting topic for discussion as is clear from the summary report of Bauer.

Two important contribution on accelerator development which do not appear below were presented on Wednesday, October 22nd. They are "Review of Accelerator Development at LASL Relevant to Intense Neutron Source" by R.A. Jameson (LASL) and " A Linear Accelerator for the German Spallation Neutron Source (SNQ)" by J.E. Vetter (KFK, Karlsruhe). Unfortunately, because of a severe limitation on space, those two papers could not be included in these proceedings and those who are interested in these papers are therefore requested to contact the authors directly.

Summary of Results from the ZING-P' Pulsed Neutron Source

J.M. Carpenter and IPNS Program Staff *

Argonne National Laboratory

9700 South Cass Avenue

Argonne, Illinois 60439

* The number of people who have made important contribution to this work is so large that it is impractical to include a complete list of authors' names.

Summary of Results from the ZING-P' Pulsed Neutron Source

J.M.Carpenter and IPNS Program Staff

Our goals in operating ZING-P' were to test further the applications of pulsed spallation neutron sources in scattering studies and to develop information needed for design of IPNS. Starting with low intensity operation, with 0.5×10^{12} proton/pulse at 1 Hz, while sharing the injector linac with ZGS, we reached in the end 1.8×10^{12} proton/pulse at 30 Hz in a dedicated mode with reliability of about 90%. (See above summary of ZING-P' Operation.)

Scientists of the Argonne scientific divisions developed and operated five scattering instruments and one general physics experiment. An extensive series of measurements of target, moderator, reflector and cooling system performance were carried out, and the source was used as a test-bed for neutron detector tests by Argonne and Rutherford Lab groups.

The table summarizes source measurements and tests of applications of pulsed spallation neutron sources that we have carried out.

Source Measurements

- Total power in W and U targets
- Local power density in U target
- γ + n dose rates in neutron beams
- Total nuclear heating in liquid hydrogen moderator
- Nuclear heating power densities in polyethylene, Be and Pb
- Nuclear heating in boron and Cd-shielded boron decoupler materials
- Absolute neutron beam intensities for W and U targets
- Delayed-neutron fraction
- Neutron spectra for liquid hydrogen and polyethylene moderators

Neutron pulse widths vs wavelength for liquid hydrogen and polyethylene moderators

In the following we give some of the results of these measurements.

Uranium Target

The Uranium target is shown below. The material was depleted Uranium (0.2% ^{235}U), with Zerconium cladding applied in a Hot Isostatic Pressure (diffusion) bonding process. Four stainless steel-clad, MgO-insulated Cu-constantan thermocouples were let into ELOXed holes in the Uranium.

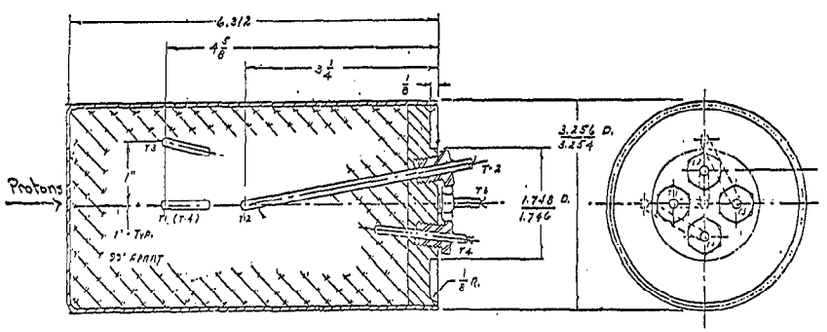

The ZING-P' Uranium Target

(Dimensions in inches)

The target and moderator arrangement of ZING-P' are shown in the figure below:

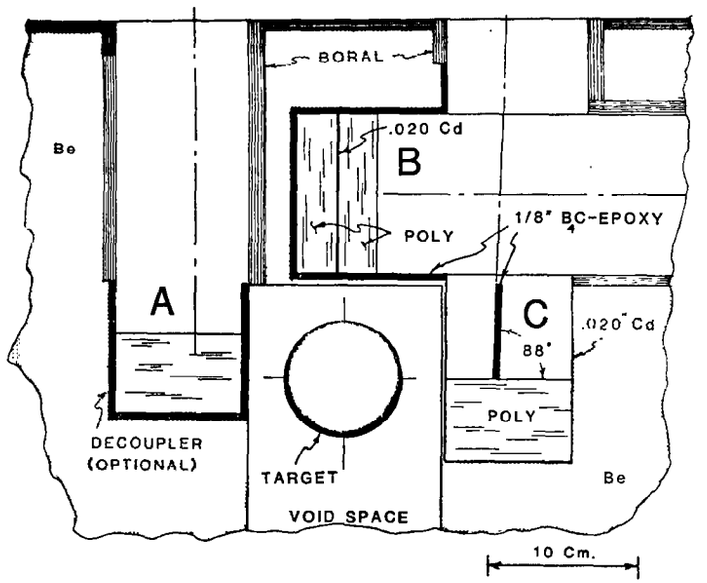

The ZING-P' target-moderator configuration.

The data acquisition system was a Nuclear Data ND6600 computer-based multichannel analyzer system, using eight time of flight ADC's providing 4K channels for each of 4 inputs. Input/output devices were a magnetic tape, paper tape, line printer and a removable disk, and one CRT terminal. Signals were transmitted using optically-decoupled cables to minimize noise pickup.

ZING-P' Operating Record

From the time of turnon, ZING-P' and the RCS were continuously improved. Starting in December 1977, delivering about .5 x 10^{12} protons per pulse at 1 Hz (.08 μA) to a W target, we reached week-long averages of 1.5 x 10^{12} protons per pulse, at 30 Hz (7.2 μA) on a U target. On a 24 hour basis we reached 7.6 μA, and for a few minutes, a current of 9.6 μA at 30 Hz (nearly 2 x 10^{12} protons/pulse). The U target increased the neutron beam intensities by about x2 over the intensities for the W target. During the first part of the history, the machine delivered 500 MeV protons. In the later part, we lowered the energy to 300 MeV to minimize the effects of lossy extraction while the intensity reached its highest levels. Extraction system improvements will enable 500 MeV operation at the higher intensities when IPNS-I is turned on.

The following figures summarize the recent operating history.

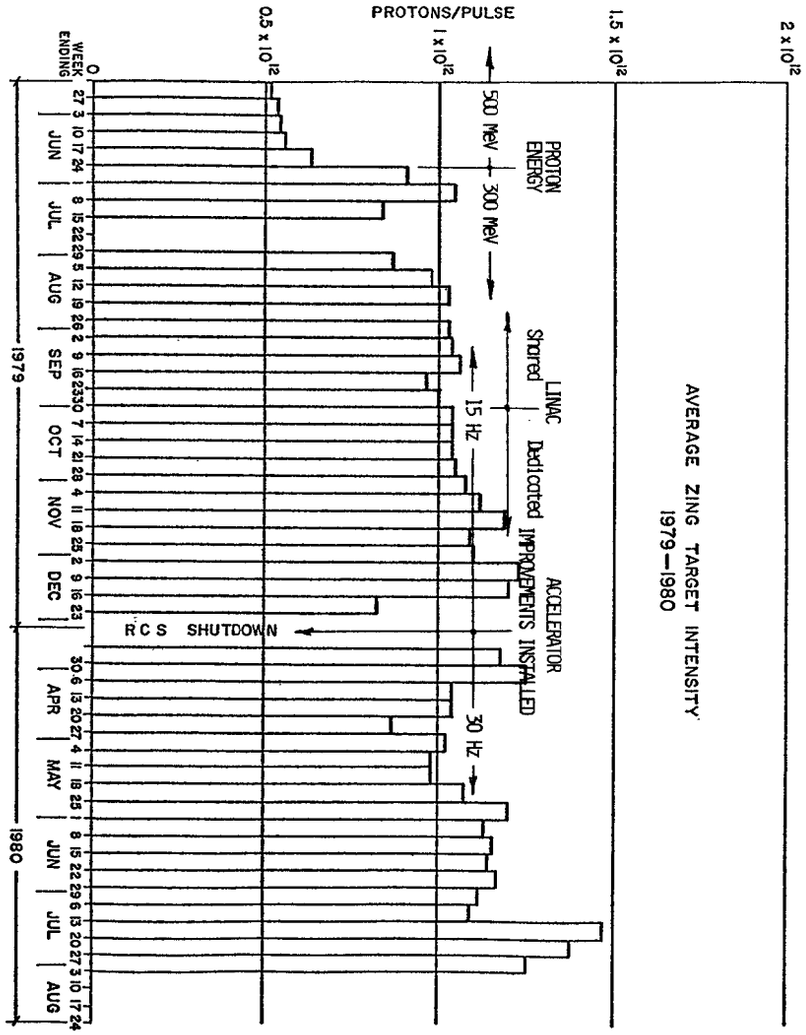

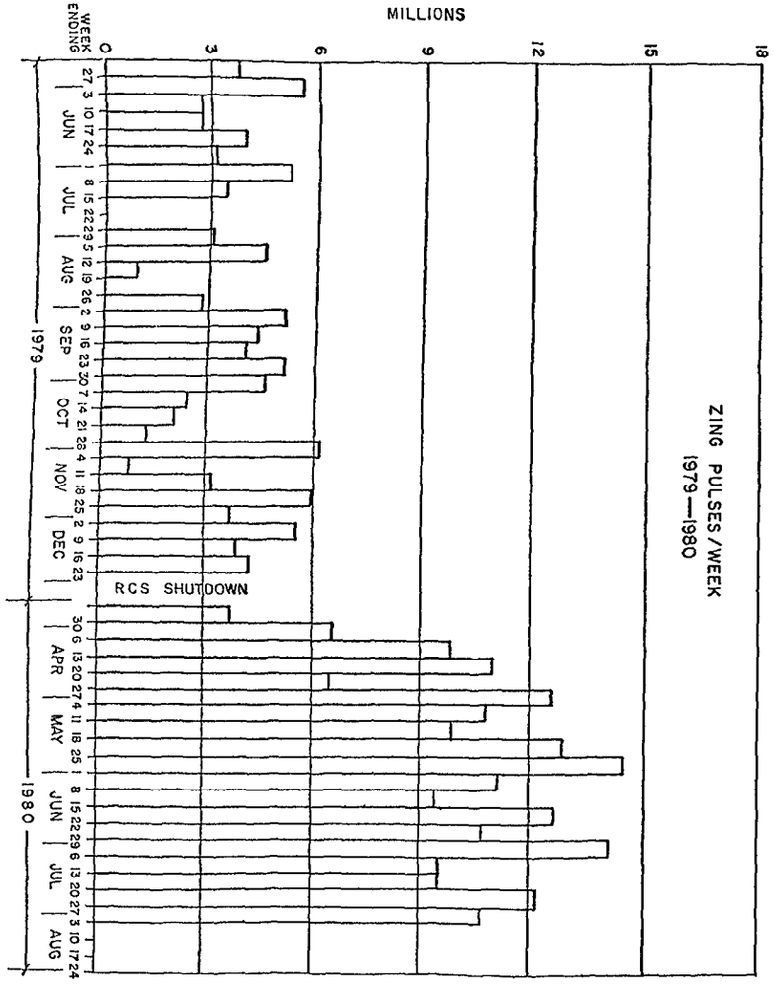

Liquid Hydrogen Moderator

Cold neutrons for the first stage of an ultracold neutron experiment were produced by a liquid hydrogen moderator installed in place of the original polyethylene moderator for beam V-2 at ZING-P'. The liquid hydrogen moderator and the refrigeration system shown schematically in the figure operated essentially trouble free since its installation.

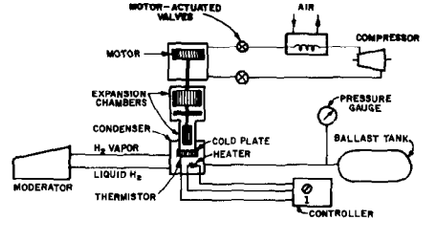

The ZING-P' Liquid Hydrogen Moderator System

The moderator, which had a volume of 368 cm^3 was connected through recirculating tubes to the condenser. Liquid H_2 flows to the condenser under natural circulation. Hydrogen was condensed by a cold plate chilled by cold helium provided by a Displex refrigerators were operated in parallel (only one is shown in Fig.2). The refrigerators operated steadily at constant power.

The moderator was connected through an open gas line to a 0.29 m^3 ballast tank. Temperature was controlled by a controller which sensed the temperature of a thermistor in the condenser. The H_2 system was charged when the system was warm to a pressure of 37 psia. This ensured that when the moderator was cold,

it was filled with liquid when the controlled temperature was the same as the temperature of liquid hydrogen at a pressure of 16 psia. This small overpressure relative to atmosphere was maintained to prevent inward leakage of condensable gases (air).

The moderator was of somewhat irregular shape to fit the geometric constraints of the ZING-P'reflector, shield and beam pipes. The 3° slope of the top plate provided that vapor bubbles flow readily to the vapor oulet. The insulating vacuum space contained several layers of aluminized glass-fiber paper as radiation shielding. The moderator container was supported by ceramic standoffs from the vacuum enclosure.

Radiation Effects Facility Mockup

The proton beam from RCS was directed through the normal target position of ZING-P' (the ZING-P' target was removed) to a shielded location downstream, for test of a mockup of the fast neutron Radiation Effects Facility.

Neutron spectra, fluxes and flux gradients were measured in a mock-up at ZING-P' using 478 MeV protons bombarding solid targets of tantalum and depleted uranium. The targets were surrounded by a thick lead neutron reflector. Neutron spectra were determined from multifoil activation by spectrum unfolding using the STAYSL computer code. The materials and geometry of the mock-up were selected so that neutron production and transport could be easily calculated theoretically by the HETC and VIM computer codes.

A simplified chematic of the target system and dosimetry positions is shown in the Figure. The targets were watercooled solid cylinders of Ta or Zircaloy clad ^{238}U. Each target was irradiated separately while centrally located in a Pb cask, which provided 25 cm of neutron reflector. The integrated proton beam

current and profile was measured by activation of Al foils at the entrance to the Pb cask. The neutron spectra for each target was determined by 28 neutron reactions. The neutron spectrum from the ^{238}U target is shown in the Figure. The neutron flux distributions were measured along and perpendicular to the targets by 11 neutron reactions.

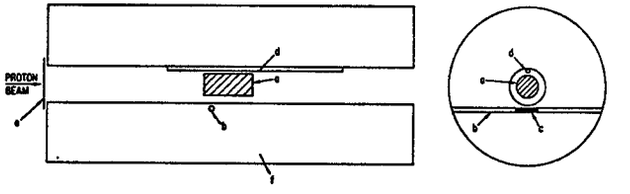

Schematic of the radiation effects target-reflector mock-up: a Ta or ^{238}U target, b. perpendicular neutron dosimetry position, c. primary neutron dosimetry position, d. parallel neutron dosimetry position, e. Al foil for p^+ dosimetry, f. Pb reflector.

The exact geometric and material arrangement of each target system was modeled for computer calculation of the neutron spectra, fluxes and flux gradients. The measured proton beam profile was used as input to each calculation. The figure compares the measured and calculated neutron spectra for the ^{238}U target system. The calculations are in good agreement with the experimental results. In the mock-up configuration, the ^{238}U target produces 50% more neutrons that the Ta target. The neutron spectrum is affected by the reflector material. The (n,xn) reactions in the Pb reflector also increase the neutron flux.

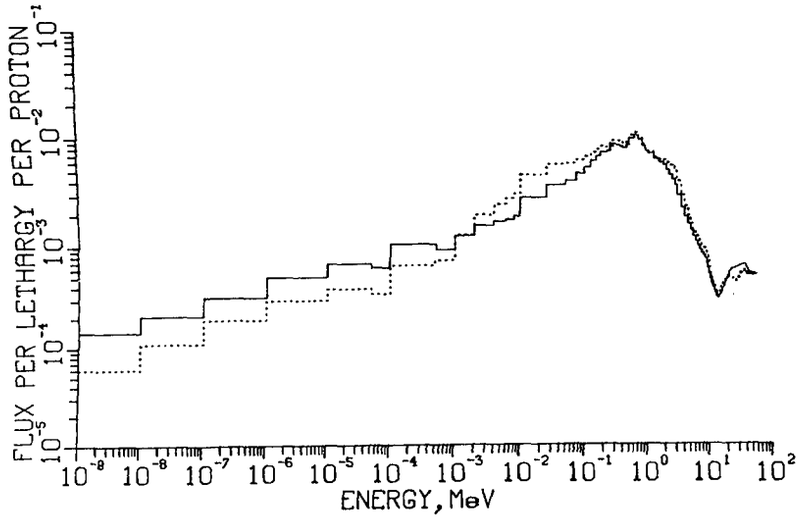

Spallation neutron spectra for the ^{238}U target. The solid line is calculated and the dotted line is experimental.

Source Measurements

Total Power Measurements in W and U Targets

The total power deposited in these targets was measured using the arrangement described in the diagram. The energy deposited is the net of energy carried in by protons, energy released by nuclear reactions, the separation energy of particles produced, and the kinetic energy of escaping particles. Proton beam intensities were monitored by the $^{27}Al(p,x)^{22}Na$ reaction.

ARRANGEMENTS FOR MEASURING TOTAL POWER IN ZING-P' TARGETS

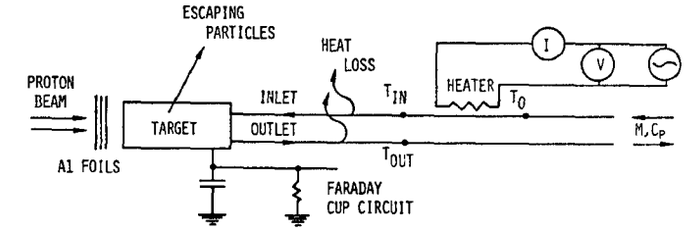

The results are tabulated below.

Total Power in Zing-P' Targets

Target (Proton Energy)	Total Power/Beam Power
U (300 MeV)	1.5
U (500 MeV)	1.5
W (500 MeV)	.94

The results are about 30% higher than were predicted by our HETC and VIM codes.

Local Power Density in the U Target

Four thermocouples were embedded in the ZING-P' U target. The power density at each thermocouple location was determined from obervations of the rate of temperature change when the proton beam was instantaneously turned off after steady operation. Then, the power density at point $\underline{r}$ is, quite rigorously

$$p(\underline{r}) = -\rho C \left(\left.\frac{dT(\underline{r})}{dt}\right|_{t=o^+} - \left.\frac{dT(\underline{r})}{dt}\right|_{t=o^-} \right)$$

The lag in response of the thermocouples (about 2 seconds) produces the major uncertainty in our results, since this makes it difficult to determine the initial rate of temperature change. We have made "best-fit" corrections to the data, to account for this effect. The proton beam profile was determined from a Teflon-foil autoradiograph. The results are summarized below, and compared with predictions of HETC and VIM codes.

Measured Power Densities

Thermocouple	Position (r,z),cm	Power Density w/cm^{3}μA	Thermocouple Lag time, sec
TC1	0.0, 4.1	3.75-6.46	1.75-2.85
TC2	0.0, 7.6	.049-.074	1.8-2.5
TC3	2.5, 4.1	.79-1.33	2.5-4.0
TC4	2.5, 4.1	1.00-1.17	.95-1.1

These results are subject to random error due to the thermocouple lag correction procedure, which gives rise to the large range of results. The results are still tentative as we continue our efforts to refine them.

Computed Power Densities, w/cm^{3}μA

FWHM of Proton Beam	TC1	TC2	TC3 & 4
1.95	7.5 ± .2	.17 ± .02	.41 ± .02
2.25	6.4 ± .2	.17 ± .02	.60 ± .02
2.30	5.7 ± .2	.16 ± .02	.63 ± .02

The measurements are uncertain ± 20% since they are based on Faraday-cup measurement of the proton intensity. The calculations contain about ± 10% error from HETC. These errors both appear in the results as scale factors. The HETC-VIM results have not been connected here to give the observed total power -- this factor is 1.30, to give the observed ratio actual power/beam power = 1.5.

Gamma Ray and Neutron Dose Rates in the Neutron Beams

The total dose rate due to gamma rays and neutrons from the U target was determined using thermoluminescent detectors, in beam H-2 of ZING-P', 18 meters from the source viewing the entire moderator. We found the following results:

Proton Energy	Dose Rate mrad/hr-μA	Dose Rate x (Distance)^2 rad-m^2/hr-μA
300 MeV	62.	20.
500 MeV	230.	74.5

The proton beam intensity was determined using the target Faraday cup circuit, thus the results are uncertain by ± 20%.

Total Nuclear Heating in the Liquid Hydrogen Moderator

Energy deposited by neutrons, gamma rays and other particles produces heat which must be removed from moderators. We have measured the heat deposited in the 368 cm^3 liquid hydrogen moderator by using it as a gas thermometer to observe the rate of pressure increase when the refrigerator is turned off. The proton beam intensity was monitored using the target Faraday cup circuit, therefore results are uncertain by ± 20%. The target was Uranium and the proton energy 300 MeV. The result is

$$P = 100 \text{ mW}/\mu\text{A} \quad .$$

No decoupling material surrounded the moderator, and a 5 cm thick Be reflector-filter topped the moderator.

Nuclear Heating of Moderator and Reflector Materials

Neutron and gamma ray induced heating have been measured in a position 11.5 cm from the Uranium target as shown below. The proton energy was 300 MeV.

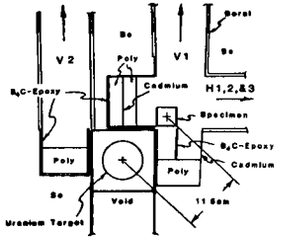

The ZING-P' target-moderator configuration for moderator-reflector measurements. The distance from target center-line to the center of the specimen used for heating measurements was 11.5 cm, as roughtly depicted above.

A thermocouple was used to determine the rate of temperature rise in a well-insulated specimen, and the power density inferred from the relation

$$p = \rho C\left(\frac{dT}{dt}\bigg|_{t=o^+} - \frac{dT}{dt}\bigg|_{t=o^-}\right)$$

which applies after startup of the proton beam at time o.

The results are summarized below and are in reasonable agreement with first-principles estimates

Material	Power Density
CH_2	1.2 $mW/cm^3 \mu A$
Be	.3 $mW/cm^3 \mu A$
Pb	1.7 $mW/cm^3 \mu A$

The proton beam was monitored by the installed target Faraday cup circuit, and the results are therefore subject to about ±20% error. The power densities are expected to scale according to the neutron production rate in the target.

Decoupler Heating

Decoupler materials (Cd, Boron, etc.) needed to prevent long-lived thermal neutrons in the reflector from broadening the pulses from the moderator, are heated by neutron capture processes. This heating is difficult to estimate analytically, yet may require provision for cooling. We have measured the power deposited in decouplers of Boron-fiber-aluminum composite materials at ZING-P', in a position adjacent to the fact of the polyethylene horizontal beam moderator. The proton energy was 300 MeV, and the target was U. An insulated specimen of the composite material with area density $.68 \times 10^{21}$ B^{10}/cm^2 backed with 5 cm Be (to simulate reflector material) was instrumented with a thermocouple and the rate of temperature change upon change of proton beam power was determined. The results give area power densities:

composite only: .74 $mw/cm^2 \mu a$ (±10%)

with .5mm Cd shielding: .32 $mw/cm^2 \mu a$ (±10%)

The heat capacity per unit area for the boron composite was assumed to be .0355 $cal/°C\text{-}cm^2$. The horizontal beam moderator was 5 x 10 x 10 cm^3 slab of polyethylene, poisoned by .5mm Cd 2.5 cm below the surface.

The result is in reasonable agreement with first-principle estimates.

Absolute Neutron Beam Currents

Epithermal neutron beam currents were measured using Au foil resonance activation, with the ZING-P' Uranium target and for 315 and 489 MeV protons. The proton beam intensity was monitored using the $^{27}Al(n,x)$ ^{22}Na reaction. The results are tabulated below, with the results of HETC-VIM calculations. We computed for two cases, assuming theoretical Be density for the reflector, and assuming 75% density (closer to the truth, since the stacking of the Be blocks in the reflector left considerable voids.

Beam Currents Measured by Gold Foil Activation at ZING-P'

(Units of n/ster-μA-s)

Ep = 489 MeV

Moderator	Experimental	Calculated (100% Be)	Calculated (75% Be)
A: liq. H_2 (no filter)	3.02×10^{10}	3.78×10^{10}(3.18)	3.00×10^{10}(2.52)*±.65
		α = .043	α = .068
B: Polyethylene		1.94×10^{10}	2.01×10^{10} ± .7
		α = .048	α = .052
C: Polyethylene	2.38×10^{10}	2.89×10^{10}(2.43)*	2.61×10^{10}(2.20)*±.65

Ep = 315 MeV

Moderator	Experimental	Calculated
A: liq. H2 (no filter)	1.17×10^{10}	$1.39 \times 10^{10} \pm .04 (1.18)$*
B: Polyethylene	0.88×10^{10}	$0.68 \times 10^{10} \pm .02$
C. Polyethylene	1.00×10^{10}	$1.12 \times 10^{10} \pm 0.4 (0.93)$*

*Corrected for area viewed by the beam tube, as though intensity were uniformly distributed across the moderator surface.

The results of experiment and calculation correlate quite well, the calculations with 100% and 75% Be densities seem to bracket the measurements.

Measurements of The Delayed-Neutron Fraction in The Uranium Target

When fissionable material (^{238}U, ^{232}Th, etc.) is used as target in a pulsed spallation neutron source, delayed neutrons are produced from certain "precursor" fission fragments which decay by neutron emission following one or more steps of beta decay. Energetic photons emitted from beta-decaying products of fission and spallation processes can also induce delayed neutrons through (γ, n) reactions in materials such as ^{9}Be and ^{2}D which may be close to the primary source. The delay half-lives range from fractions of a second to 1 min for precursor fission fragments, and from a few seconds up to several days, with 98% less than 1 min for fission product gamma rays interacting with ^{9}Be. When the interpulse time is short by comparison with these delay times, delayed neutrons constitute a nearly steady source (unless there exist yet-undiscovered, shorter-lived precursors) of neutrons between source pulses.

We made two measurements, in beam V-2 of ZING-P', with the U target in place. For the "SIGNAL" run, the detector was open to the beam from the moderator, and surrounded by B_4C and ^{10}B shielding. For the "BACKGROUND" run, the detector was

surrounded by the same shielding, but closed to the beam by 10 cm of ^{10}B shielding. A 1-mm-thick Corning 7740 boron glass filter plate (6.4×10^{20} B/cm^2) was placed in the beam to diminish the counting rate due to long-wavelength neutrons from the prompt pulse, which would obscure the delayed neutrons at long times. The detector was a low-efficiency BF_3 beam monitor detector. The moderator was a 10 x 10 x 5-cm^3 slab of polyethylene at 300 K decoupled by 4×10^{21} ^{10}B/cm^2. The assembly was surrounded by beryllium reflector material. The proton energy was 301. MeV.

The figure shows the net counting rate as a function of time. The delayed neutron fraction β is taken as the ratio of the number of counts in the "prompt" peak (which reflects the wavelength distribution of neutrons) and the total number of counts in the constant part of the distribution. The result is

$$\beta = .0053$$

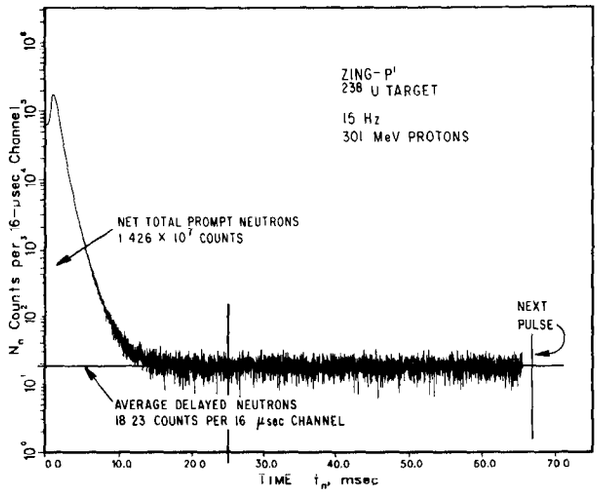

This fraction is not expected to be a strong function of proton energy. At this level, delayed-neutron background will not be a problem in most slow neutron experiments using neutron beams derived from a ^{238}U target.

Studies of a Grooved Moderator

A grooved moderator was placed in Beam V-1 (Moderator C) of ZING-P'. The moderator was of polyethylene, ρ = .915 gm/cm^3, overall 10 x 10 x 5 cm, with 1-cm wide x 2-cm deep grooves placed 1 cm apart on the viewed surface. The moderator was reflected by Be, decoupled by .020" Cd, and was unpoisoned. We measured the intensity vs. wavelength, normalized against that in an unaffected beam from moderator B in beam H-1. We also measured the time structure of the pulses using a time-focussed crystal spectrometer with a Germanium (220) crystal (d = 2.0003 A) and Bragg angle of 168.9°. Comparisons of normalized spectra and pulse width were made between the grooved moderator and the previously-installed, flat, 10 x 10 x 5 cm unpoisoned CH_2 moderator (its condition is described elsewhere in this summary). The moderators were not cooled, and the temperature of the moderators was not measured, but near ambient (300.C).

The figures below compare the time distributions measured for the grooved moderator and the flat moderator at λ = 1.991 A.

We find that the pulse from the grooved moderator starts at the same time as that from the flat moderator, but rises more slowly, and for λ = 4.02 A, peaks at a time roughly equal to the flight time across the groove depth. The exponential decay time (1/e) of the longest-lived mode is 50.8 μs for the flat moderator and 41.7 μs for the grooved moderator (average for three wavelengths). The grooved moderator pulse decays more rapidly, but rises more slowly, thus is broader, but more symmetric than the flat moderator pulse. The figure shows the pulse FWHM vs E for the two moderators.

Comparisons of the spectra indicate that the grooved moderator produces higher beam currents. The table below indicates ratios of spectral intensities for various energy ranges; adjustment has been made for detector efficiency.

Comparison of Intensities for Grooved and Flat Moderators

	Intensity (grooved/flat)
I_{Th}	1.10
$EI(E)_{1ev}$	1.24
I_{Total} (E<1.ev)	1.13

The moderating ratios were

$$I_{Th}/EI(E)_{1ev} = \begin{cases} 4.46 \text{ (Grooved)} \\ 4.75 \text{ (Flat)} \end{cases}$$

The spectral temperatures were also determined:

$$E_T = \begin{cases} 33.4 \text{ meV (388 K) (Grooved)} \\ 36.9 \text{ meV (428 K) (Flat)} \end{cases}$$

GROOVED MODERATOR RAW PULSE WIDTH DATA

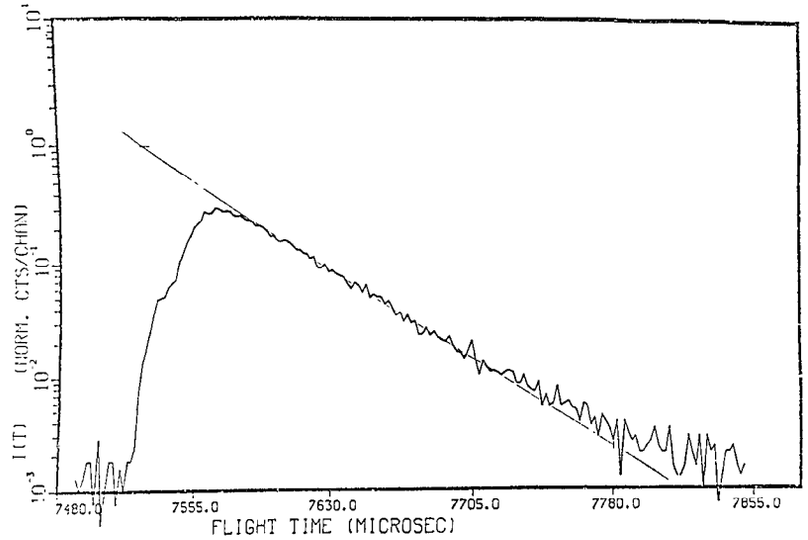

FLAT MODERATOR RAW PULSE WIDTH DATA

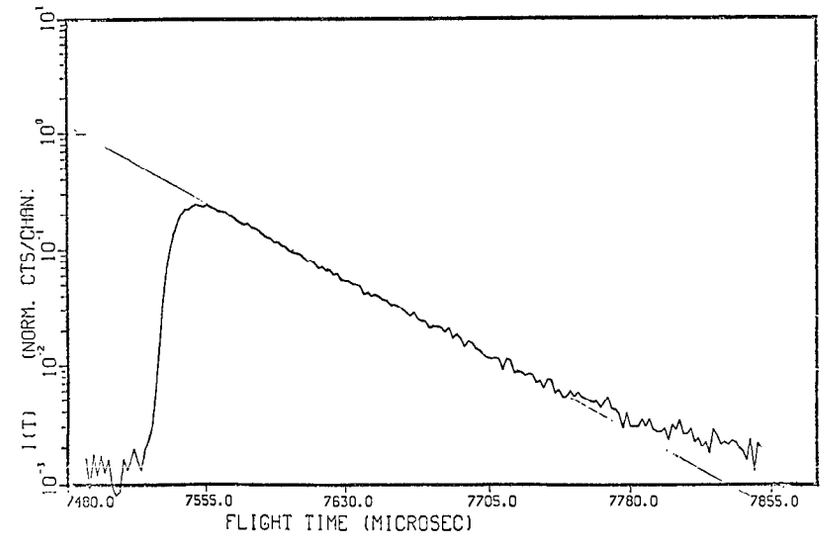

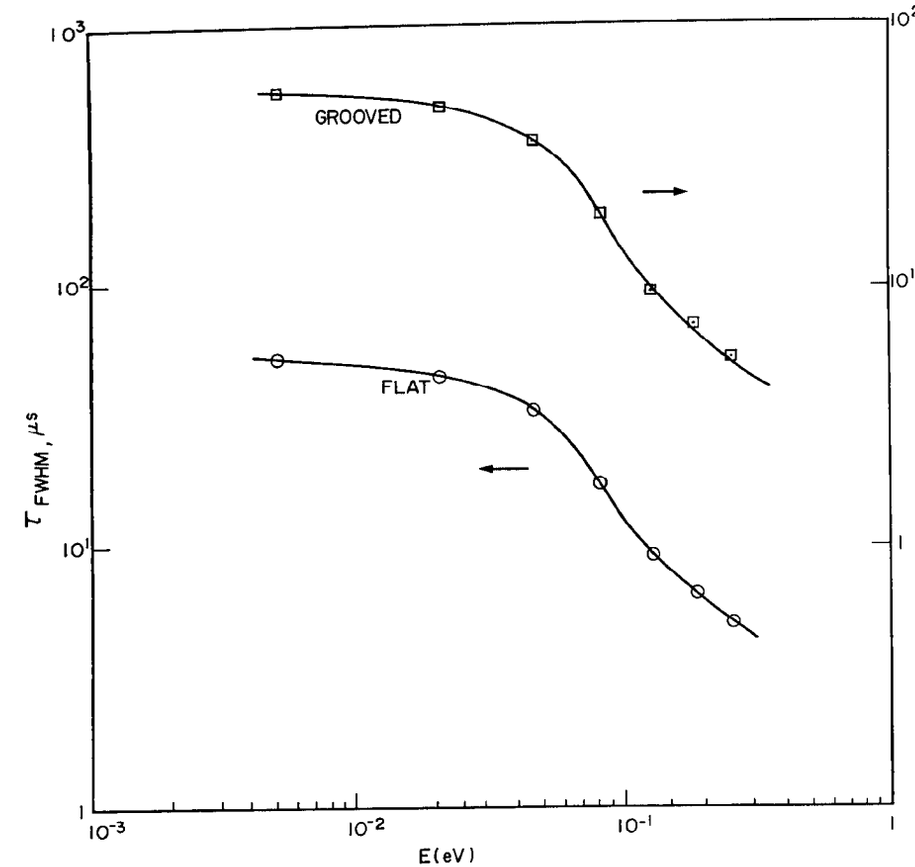

Summary

We found that the grooved moderator produces higher neutron beam currents, a broader, more-symmetric pulse, and lower spectral temperature than the flat moderator. This indicates useful possibilities for improving moderator performance, but also shows the need for further experimental and theoretical study.

Examination of an Irradiated Polyethylene Moderator

The CH_2 moderator of Beam V-1 of ZING-P' (Moderator C of the diagram) has been removed and examined. The moderator had been in place from the start of ZING-P' until 10 June 1980, and endured a fluence of about 1.5×10^{18} n/cm^2, most of it since March 1980, during irradiation of the U target with 300 MeV protons, and was surrounded by Be and decoupled by Cd. The moderator was not cooled, and we do not know the temperatures reached.

Physical Appearance

The moderator was completely balck in appearance. An oily substance had collected on the surface, which crystallized after about 1 month. A crack had appeared on one edge.

Density

The density of the original material was .915 gm/cm^3. After irradiation, the density was .97 gm/cm^3.

Radioactivity

A sample of the polyethylene material was subjected to γ-ray spectral analysis, about 2 months after removal from ZING-P'. Radionuclide concentrations were found to be

^{7}Be: 4.1 μCi/gm CH_2

^{65}Zn: 2.8 nCi/gm CH_2

The Zinc presumably was an activated impurity. The ^{7}Be was presumably created by fast neutron (and perhaps proton) spallation of Carbon. It must be concluded that Tritium at a level of around .2 μCi/gm CH_2 is also present, (although it would not have been observed in the γ spectrum) since it would be created by mechanisms similar to those producing ^{7}Be.

Carbon-Hydrogen Analysis

Six samples of irradiated material were examined. The average H/C ratio was found to be 1.784 H/C. H and C constituted an average 97.3 w% of the total mass. The remainder is presumably Oxygen, which was not determined in our tests. The unirradiated material had an H/C ratio of 2.08 H/C. (Errors are approximately .5%.) The oily material had an H/C ratio of 1.54 H/C, while H and C constituted 46% of the mass, but it was not chemically identified.

The proton densities computed for the unirradiated and irradiated materials are thus

$$n_H = \begin{cases} .0736 \text{ protons/cm}^3 \text{ (irradiated)} \\ .0814 \text{ protons/cm}^3 \text{ (unirradiated)} \end{cases}$$

These results indicate that room-temperature, organic moderators sustain substantial damage in spallation neutron sources. However, their performance, up to the level of damage we observed, did not significantly deteriorate.

IPNS-I

Status of IPNS Construction

N.J. Swanson, Argonne National Laboratory

Progress in all areas of the design and construction indicates high confidence that the IPNS-I facilities will become operational in April 1981. With the shutdown of ZING-P' program in August 1980 additional resources have been released to work on the transition from the prototype facility to the where prototype operations did not allow construction work previously. Details of the progress for the three principal tasks of the IPNS-I projects are given below.

Proton Transport System (PTS)

The PTS tunnel was completed within the experiment hall (Building 375) and expanded to the limit of its support pad outside and north of the hall. Included has been the completion of the proton beam dump which will serve as a Faraday Cup to accept the full output of the accelerator for operational optimization purposes.

The PTS magnets obtained from ZGS have been refurbished and mounted on newly-procurred precision positioning platforms which will also serve as mobile transport dolleys for installation or removal from the PTS tunnel. Several magnets have been positioned in the completed tunnel and the alignment and vacuum system testing has been started.

With the completion of ZING-P' prototype operations preparations for joining of the PTS tunnel to the synchrotron cavity were begun. This work included removal of accelerator shielding blocks of the south side, excavation of the floor and earth at the cavity-tunnel junction area, placement of the extension of the high-load concrete support pad for the PTS shielding, and the relocation of accelerator power supplies and miscellaneous equipment

previously located at the junction zone. Joining of the PTS tunnel to the accelerator cavity is planned for completion before the inclement winter weather arrives.

Progress is quite satisfactory for the ancillary systems to support the PTS. This work includes the subsystems for beam diagnostics, vacuum, beam control and safety shutdown. Accelerator modifications have been started to modify and relocate the extraction system. These activities are scheduled to be completed at the time when the PTS construction will be finished in February 1981.

Neutron Generation System (NGS)

The slow, tedious task of cutting and fitting of the shielding steel around the vessels and neutron beam tubes within the atmospheric control barrier has been completed. Design of the removable shielding to be used within the vessels and neutron beam tubes is complete and procurements have begun.

Fabrication of the components for the first target is progressing on schedule. Assembly of some of these components to form the first target will be performed in October with preoperational testing begun in November. Delivery of the target cooling systems is expected in early October with installation performed shortly thereafter. Mating of these systems to target assemblies is expected in November.

The beryllium reflector assembly and its contained moderator cans for the Neutron Scattering Facility is being fabricated. Delivery of this long lead item is not expected until late January and this work continues to comprise the critical path for the overall construction. The reflector assemblies for the Radiation Effects Facility are being fabricated with delivery expected in October.

Design of all electrical and mechanical facility systems for support of the NGS has been completed. All procurements are underway and installations were begun in September.

All designs for the NGS monitoring and control systems have been completed. All procurements have been placed and most have been received. Installation in the control room, now under construction, is expected to begin in late October.

Instruments and Data Acquisition System (DAS)

It is planned that seven neutron scattering instruments will be operational during 1981. Designs were completed for the flight paths of the Special Environment Powder Diffractometer and General Purpose Powder Diffractometer. Bid solicitation for these components was completed and a fabricator selected. Work continues on developing layouts for the High Resolution Medium Energy Chopper Spectrometer scattered flight path housing. This assembly will be obtained by a design and build contract.

Conceptual designs for the Crystal Analyzer Spectrometer and Small Angle Diffractometer are continuing. Detail design work for the Low-Resolution Medium-Energy Spectrometer and Single Crystal Diffractometer will begin shortly.

Progress has been realized in the development for single-ended, linear position-sensitive detectors needed for the two powder diffractometers. Suitable detector systems are expected at the time when the housings are ready to accept them.

Work has begun on the rebuilding and refurbishment of vacuum systems required for the scattering instruments. Most of the vacuum equipment will derive from existing components obtained from completed HEP programs.

Designs for the five required choppers has been completed. A fabricator has begun the machining of the beryllium parts and ordering of other chopper components has been started.

For the DAS activities work continues on the detail design for detector electronics, computer software and computer hardware. A fifth front end computer has been delivered. One computer is being used for program development and detector electronics checkout.

The progress on developing encoding circuits for single-ended linear position-sensitive detectors has been excellent. Close coordination with the detector supplier continues in an effort to optimize the special detector needs for IPNS-I instruments.

General Items

At the beginning of August the contractor who began the IPNS-I construction work was dismissed and replaced by a new, inexperienced contractor. Since this action occurred with very short notice, all active subcontracts became invalid and required formalization with the new contractor. This caused some delays while new subcontracts were established. Also, some inefficiencies were encountered due to the changing of supervision. At present most problems had been remedied and harmonious and efficient construction activities appear to have been restored. High rainfall in August and early September caused some delays. However, exceptionally good weather in October has permitted acceleration of the construction activities.

The operation staff for IPNS-I hase coordinated the development of the Safety Analysis Report (SAR). This report has been reviewed by committees with information participation by design personnel. The reviews have resulted

in some design improvements. The SAR has been approved by the Laboratory committees and will now be submitted to the Department of Energy (DOE) for approval. With the DOE approval of the SAR on schedule, startup of the facility in April 1981 can be expected.

Review of SNS Target Station

A Carne
Rutherford and Appleton Laboratories, Chilton, Nr Didcot, Oxon, UK

1. Introduction

Aspects of the SNS Target Station have been described in the reports of the previous ICANS meetings; particularly of the ICANS III meeting at LASL, USA, in March 1979(1), also of an informal meeting on Targets for Spallation Sources held at Jülich, West Germany, June 1979(2). It is the purpose of this review to report progress and modifications over the last 12-18 months.

Figure 1 shows the SNS Target Station and its relation to the rest of the SNS facility. The Target Station consists broadly of four parts: Target, Target Assembly, Bulk Shield and Shutter System, and Remote Handling Facility. These will be described in the following sections.

2. Target

2.1 Target Physics

The target will consist of a number of parallel plates of uranium clad in Zircaloy-2 and cooled by D_2O, the whole being contained in an Inconel pressure vessel. Plate thickness of the uranium varies according to the energy deposition and is limited by metallurgical requirements; plate diameter has been determined to be 90 mm to maximise the epithermal neutron current from the moderator, as can be seen in Figure 2. Detailed computational studies have been made of the target and target assembly and some of the results are contained in Table 1. For the expected 200 μA, 800 MeV proton beam incident on the target the total thermal load is 230 kW; 209 kW is due to the uranium itself, of which fission contributes about 110 kW. There are 24.7 sub-15 MeV neutrons escaping from the effective surface of the cylinder containing the plates. The growth and decay of target activity are shown in Figures 3 and 4. Some 1200 nuclides contribute to the total of 0.86 MCi (corresponding decay heating 8.7 kW) after 6 months' continuous

irradiation. Activity due to the Zircaloy-2 cladding is 9.5kCi. After storage to allow a one year cooling period, the total activity and decay power in the target are 3.2 kCi and 14W respectively; in particular the α-activity is 54 Ci. Short-lived nuclides in the coolant will give a saturation activity of 6.3 Ci/l and will result in a total of 500 Ci in the "external" cooling circuits. Some short-lived neutron emitters will be present. Long-lived nuclides are ^3H (0.06 Ci/l after 2 years' irradiation), from oxygen spallation, and ^7Be (0.1 Ci/l); contributions from ^{14}C and ^{10}Be being negligible.

2.2 Target Engineering

The development of bonding between the uranium and the Zircaloy-2 cladding has concentrated on two techniques readily available in the UK. The first technique, liquid phase bonding, has the attraction of obviating the β-quench. Tests were done using tin and lead sputter coatings on the uranium and Zircaloy-2, and metallic interlayers. No successful bonds were obtained. The second technique, hot diffusion bonding, relies on direct pressure, 7 N/mm^2 at 800°C for 1 hour, on the pure materials. Three target plates were produced with satisfactory bonds, which failed during subsequent processing (β-quenching, forming) due to differential contraction. Though the second method has possible solutions, a new program of work is being initiated using the most economic and promising process, hot isostatic pressure bonding.

The cooling mechanism for the target is nucleate boiling. Figure 5 shows the flow/pressure drop characteristics for cooling gaps ranging from the initial 1.75 mm to 1.0 mm. The coolant operational parameters will be velocity 5.5 m/sec, pressure 2.75 bars, T_{sat} 131°C and T_{bulk} 38°C. Figure 6 shows a plan of the actual target, including data on plates and cooling. The maximum power density in the uranium is 0.77kW/cm^3 with a corresponding centre line temperature of 348°C. The chosen maximum allowable temperature of 400°C gives a safety margin of 30% on power or 15% on beam width. The peak heat transfer rate required is 250 W/cm^2; for the given coolant parameters this is 1/3 of the experimentally measured burn-out. It can be seen from Figure 6 that there will be 3 inlet and 3 outlet channels and that the plate cooling channels are in groups of three. This method reduces the total quantity of coolant required (537 litres including the external cooling system), yet allows adequate monitoring of the cooling

parameters. Individual gap closures of 0.25 mm can be detected by the pressure and flow monitors. Flow diagrams of the overall cooling system have been completed.

3. Target Assembly

The Target Assembly contains 4 moderators: 2 above the target and 2 below, in wing geometry. Each moderator is surrounded on all but its exit faces by decoupler and the whole array is contained within a beryllium and heavy water reflector. Neutron beam ports through the reflector are also lined with decoupler. The disposition of the moderators is shown in the isometric view of the target assembly, Figure 7, and a total of 18 neutron beams can be served by these moderators. The dimensions, material, and temperature of each moderator have been chosen to match the requirements of the instruments. The actual moderators and their characteristics are shown in Table 2. The coupling factors quoted are for the so-called "reference design" dimensions of all the moderators of 100 x 100 x 50 mm^3. Moderators built to the maximum dimensions indicated will allow increases in flux by factors of approximately 1.4 Type A, 1.2 Type B, 1.3 Type C and 1.3 Type D respectively. The flux calculations have assumed a decoupler energy of about 36 eV for the A, B, D moderators. The final optimisation of dimensions and decoupler energies has still to be done, and Figure 8 indicates some of the scope. For the high resolution, Type B, moderator material and temperature are also very important. This moderator ideally extends the slowing down region to the longest possible wavelength, has low frequency modes and large hydrogen density. Recent studies have concluded that metal hydrides (eg TiH_2) are not suitable. The favoured material at the present is cooled and poisoned methane. For the Type C moderator with the longest possible wavelengths (4Å-10Å range) a para-hydrogen moderator at 20K will be used, with a cadmium decoupler of about ½ eV decoupling energy. The relaxation of decoupler strength and dimensions has allowed a doubling of moderator flux compared to the reference design.

Table 2 also indicates the expected total thermal loads in the moderators due to all effects. The values for the Type B (methane, 20 or 77K) and Type C (p-H_2, 20K) represent formidable technical, safety and cost problems.

The "reference" decoupling energy of 36 eV corresponds to a ^{10}B density of 0.01 atoms/$Å^3$ and is obtained by a 10 mm thick layer of natural B_4C powder of density 1.1 g/cm^3. The total power deposited in the decoupler is about 9 kW, with a peak power density of 4W/cm^3. This is due mainly to the $^{10}B\ (n,\alpha)^7\ Li$ reaction; this also liberates 13 litres of He per year. Total activity due to short lived products in the decoupler is 530 Ci.

The reflector is constructed to give 80% by volume beryllium, the rest being filled with D_2O to act as both reflector and coolant. The overall dimensions, 680 x 500 x 790 mm^3, have been chosen to allow at least 250 mm of effective reflector material around each moderator. Total power deposited in the reflector is 7.2 kW, 60% of this being due to high energy particles from the target. Tritium production in the D_2O in the reflector will result in an activity of 0.3 Ci/l after 2 years' operation.

Detailed flow measurements on the ambient water moderator have been made to ensure the temperature stability of ± 0.3% can be obtained. Proper location of the inlet and outlet pipes has ensured that there are no unswept regions. Measurements have shown that at the operating pressure of 1.68 bars the neutron exit face of the moderator, 3 mm thick aluminium, will deflect about 0.18 mm, which is acceptable. No detailed work has been done on the cryogenic moderators.

Layout design of the whole assembly has been done. Design of the reflector is almost complete and it will be built in 5 basic layers using 27 mm diameter rods. The beryllium has been obtained, but machining is not due to be done till 1982.

4. Bulk Shield and Shutter System

The target station bulk shield can be seen in Figure 9 and consists of 4 parts: 1) target void, 2) shutter vessel, 3) outer shield, and 4) plinth. Items 2 and 3 constitute the bulk biological shield whose function is to reduce the radiation level at the outer surface to less than 0.1 mrem/hr. Through the shield are 18 neutron beam lines, each of which can be closed by an independently operated shutter.

4.1 Target Void

The target void vessel is cylindrical, 1.6 m radius by 3.8 m high, and provides a contained helium atmosphere around the target. The helium will flow in a closed cooling circuit at about 0.4 m^3/sec to remove the 5kW of heat deposited in the vessel walls. For containment the helium will be at reduced pressure (- 5.5 mbar). Modern codes of practice require the vessel, including its windows, to be a vacuum vessel so it will have walls of mild steel clad on the inside face with stainless steel, overall thickness about 12 mm. The windows will be mounted in frames which can be oriented to view an upper or lower moderator and will be maintained by remote handling techniques from the inside. Each window will, in practice, be a double window of thickness 2 x 0.5 mm aluminium, of cross-section 190 x 190 mm^2, to allow complete viewing of a moderator by an inclined neutron beam line of 10 cm aperture.

The target void vessel floor is of stainless steel of conical shape, connected at its centre with a double walled stainless steel drain-pipe leading to external emergency dump tanks. The radiation levels at the middle of the empty target void vessel due to induced activity in the walls will rise to about 130 rem/hr.

4.2 Shutter Vessel

On either side of the target void vessel is a shutter vessel, each containing 9 shutters on nominal 13° centres. The shutters, when closed, reduce the radiation level in the beam at 10 m to 2.5 mrem/hr and so allow access when the proton beam is on. The shutters are made of iron and concrete and have dimensions 4.5 m x 2 m x 0.28 m, weighing about 22 tonnes each. Because of crane limitations in the experimental hall each shutter is in 3 sections, the centre one of which has a 200 x 200 m^2 hole in which the beam collimator is mounted, with its own helium or vacuum, atmosphere. A 250 mm vertical movement of the shutters is provided by mechanical jacks. Vertical Location is expected to be better than 1 mm and stability $\sim$ 0.2 mm. Between the shutters is wedge shaped steel shielding, with removable iron and concrete shielding above.

The shutter vessels themselves have only the inner face of steel (the target void vessel), the other faces being concrete. Energy deposition

is about 6.5 kW in each vessel and this will be removed by flowing air, rather than by closed circuit helium proposed earlier. These last features lead to a considerable simplification and saving in cost, but also bring problems of their own. Vertical stability of the shutters is now twice the previously reported value of 0.1 mm but is still acceptable. Cooling by air, at a rate of 5 volume changes per minute, results in a specific activity of 83 μCi/l. Present plans are to feed this air along the extracted beam line enclosure, to be diluted with the air in the magnet hall prior to venting.

4.3 Outer Shield

The outer shield extends from the shutter vessel to a radius of 5.9 m. This gives a total shield thickness of 4.4 m of iron and concrete. On the outer surface of the shield the radiation level will be less than 0.1 mrem/hr, except in those sections containing the neutron beams when the radiation levels may reach 6 mrem/hr and will be increased further close to the neutron beam lines. In these regions the shielding will be supplemented by loose blocks. The outer 0.25 m of the bulk shield will be concrete loaded with 1% boron.

As reported previously, a feature of the outer shields is the use of inserts to allow local reconfiguration of the beam lines. These shielding inserts are ready to go out for manufacture.

4.4 Plinth

The plinth forms the foundation for the target station and the remote handling cell. Overall dimensions are 17 m x 12 m x 3 m. On either side are caverns, one of which will contain the emergency dump tanks for the target void vessel. The plinth consists of a reinforced concrete tank 0.75 m thick (containing a water seal), filled with iron and concrete. The iron used was mainly magnet sectors of the former NIMROD accelerator, 3 layers deep. A rigid pillar is incorporated into the plinth to form the basic datum from which the target station and experimental area survey grid are set out. Figure 10 shows the plinth and the embedded magnet sectors can be clearly seen. The next stage in this construction is to add a reinforced concrete raft on which will lie the machined base plates for the shutter system.

5. Remote Handling Facility

Immediately downstream of the bulk shield is the remote handling cell. The target assembly is mounted on a cantilever frame from a movable iron and concrete shielding door about 5.5 m thick. Beyond the shielding door are trolleys carrying the pipework and services. When it is necessary to remove the target assembly the whole system of door and trolleys rolls back on rails until the target assembly is located in the remote handling cell. Work on the components of the target assembly is done using conventional master-slave-manipulators; viewed directly through zinc bromide windows with exit faces 550 x 550 mm^2 and supplemented by TV cameras.

The major source of activity in the remote handling cell will be the target itself. Assuming it takes 1 hour to withdraw the target, the dose rate at 1 m is then about 10^6 mrem/hr. The walls of the remote handling cell will be 1.6 m of ordinary concrete. The zinc bromide windows will also be 1.6 m thick. The dose rate will be less than 1 mrem/hr at the outside face of the windows allowing prolonged use of the manipulators. Irradiated targets will be stored in a tank within the remote handling cell for periods up to about 12 months. As many as 3 targets can be stored at any one time. A target will be removed for disposal via a well into an existing service tunnel under the experimental hall. Ventilation for these systems is being designed in accordance with the United Kingdom codes of practice.

The base of the remote handling cell and the disposal well have been built as part of the construction of the target station foundation. A full scale mock remote handling cell has been recently completed to study in detail the problems of handling the components of the target assembly. As a design philosophy all components intended for the target assembly will be proven in this mock-up cell. Prototypes, including a target and its coupling flanges, for testing in this cell are now being assembled.

6. Timescale

The rate of design and construction of the target station (indeed the whole of the SNS) are determined by program manpower and financial profiles. Within the overall project are 6 "milestones" the last two of

which are of special importance to the target station: early 1984, 600 MeV protons at low intensity to provide the first neutrons; late 1984, 800 MeV protons at low intensity. Full intensity operation with 800 MeV protons is expected by about 1986. We look forward to these dates with no little eagerness!

7. Acknowledgements

This review summarises the work of members of the SNS Target Station Group, particularly Francis Atchison, Tim Broome, Dave Clarke, John Hogston, Mike Holding, Bernard Poulten, Ken Roberts, and Ron Wimblett; also Andrew Taylor of Neutron Division. It is a pleasure to record their continued efforts and enthusiasm.

8. REFERENCES

1. ICANS III, LASL, USA, March 1979. Papers by A D Taylor, R W Wimblett and A Carne.

2. Meeting on "Targets for Neutron Beam Spallation Sources" Jülich, West Germany, June 1979. Papers by F Atchison, T A Broome, A D Taylor and A Carne.

TABLE 1

Input Beam Protons, 800 MeV, 2.5×10^{13} ppp, 50 Hz, I mean = 200 μA
Beam diameter 70 mm, $I = I_o(1-(r/r_o)^2)$

1. TARGET

a. Power:

Prompt in Uranium	200 kW
Nuclide decay	8.7
Zircaloy-2 cladding	6.4
Coolant	5.2
Inconel Vessel	7.0
Total (rounded)	230 kW

b. Activity:

Irradiation		Post Irradiation			
t_i	Total(MCi)	t_c	P(kW)	α-act^y(kCi)	Total(MCi)
1 day	0.65	1 min	4	1	0.65
1 month	0.82	1 hour	1.4	0.6	0.4
6 months	0.86	1 day	0.5	0.47	0.2
		1 month	0.2	0.22	0.03
		1 year	0.014	0.54	0.003

c. Coolant Activity:

Short lived products in external circuit	500Ci
tritium	35Ci (2 years)
^{7}Be	60Ci

2	REFLECTOR	Power	7.2 kW
3.	MODERATORS	Power total	1 kW
4.	DECOUPLERS	Power total	8.9 kW

5. ESCAPE PARTICLES

Low Energy Neutrons (< 15 MeV)	1.3×10^{16}/sec	1.4 kW
High Energy Neutrons (15-800MeV)	1.0×10^{15}/sec	14 kW
Protons	2.8×10^{13}/sec	0.6 kW
Mesons	2.5×10^{12}/sec	0.018 kW
Total energy carried away		16 kW

TABLE 2

Moderators

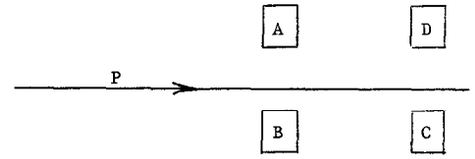

A	B	C	D
H_2O 300K	CH_4 ? 20 - 77K	p-H_2 20K	H_2O ? 300K
High intensity at at expense of resolution	High resolution slowing down spectrum	Long wavelength 4-10A	(as required)
w 12	11.5	11	11
h 12	11.5	12	12
d 6	5	8	6
Est total power 368 W	283	240	250
design for 440 W	380	330	290
Decoupler B_4C(∿1eV)	B_4C (1eV)	Cd(∿½eV)	B_4C(∿1eV)
Coupling factor $\times 10^{-4}$ n/eV/sr/100cm^2/n_f			
2.2	1.8	2.0	1.3
Neutrons per SNS pulse at 1eV/sr/100cm^2			
1.4×10^{11}	1.1×10^{11}	1.3×10^{11}	0.8×10^{11}

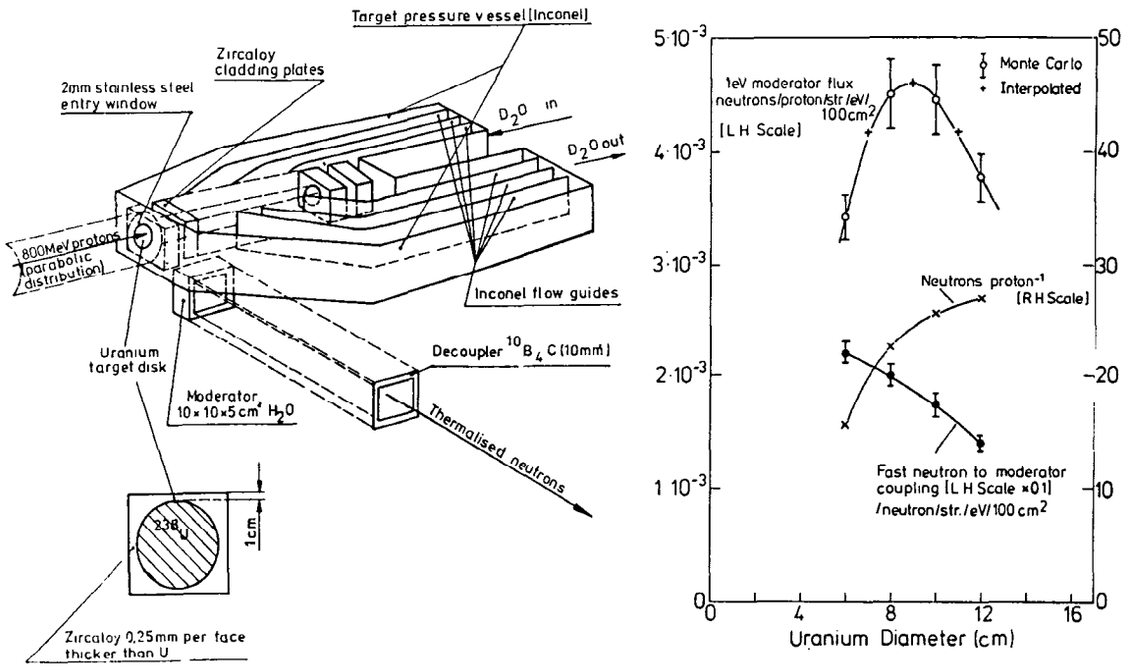

Fig. 2. OPTIMISATION OF TRANSVERSE DIMENSIONS OF SNS TARGET.

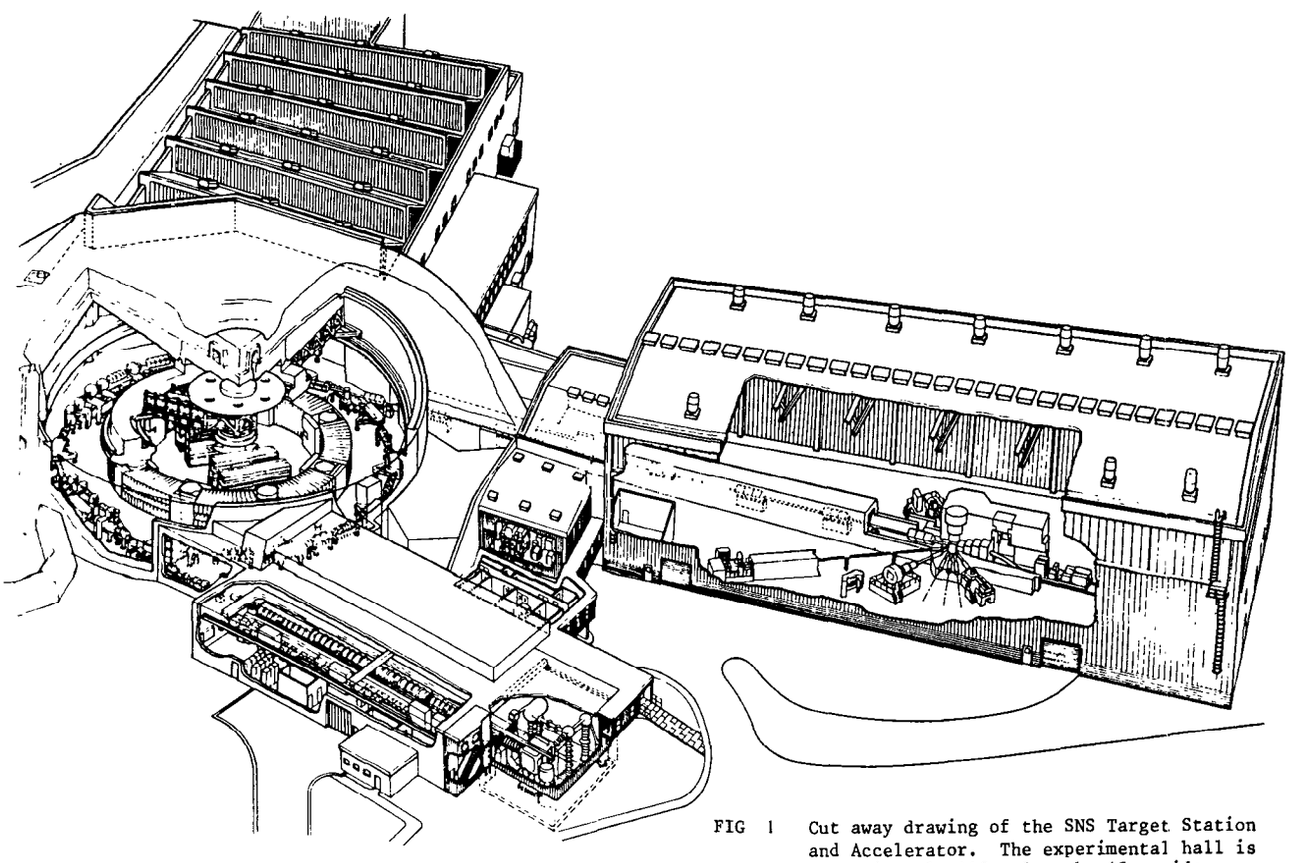

FIG 1 Cut away drawing of the SNS Target Station and Accelerator. The experimental hall is approximately 110 m long by 45 m wide

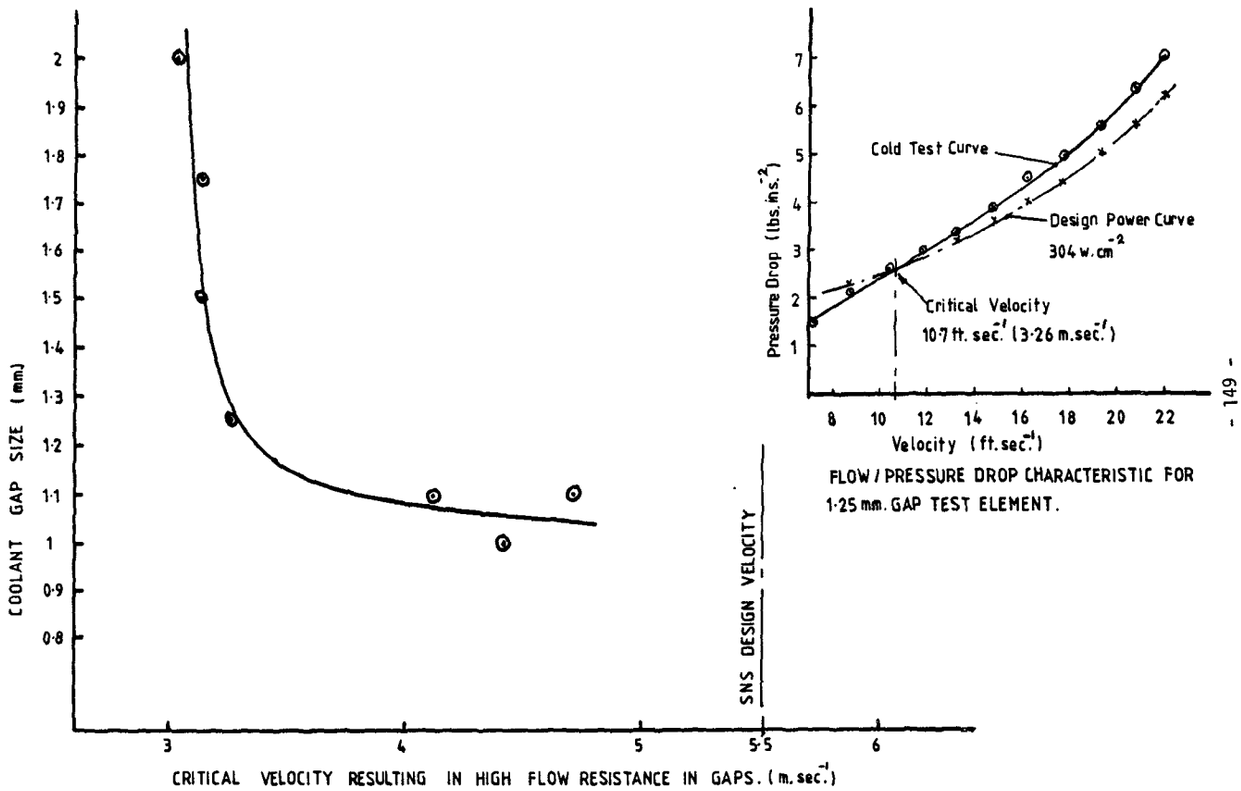

Fig.5. FLOW CHARACTERISTICS AND CRITICAL VELOCITY OF SNS TARGET COOLING CHANNEL.

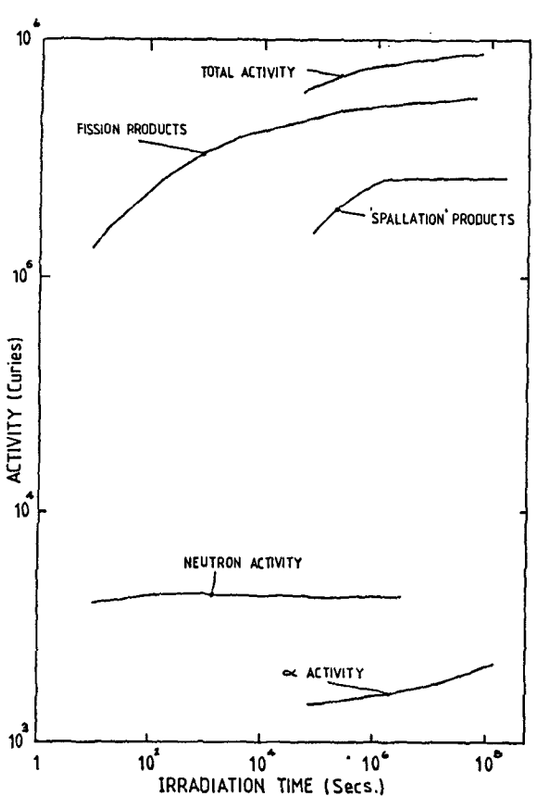

Fig.3. GROWTH OF ACTIVITY IN SNS TARGET.

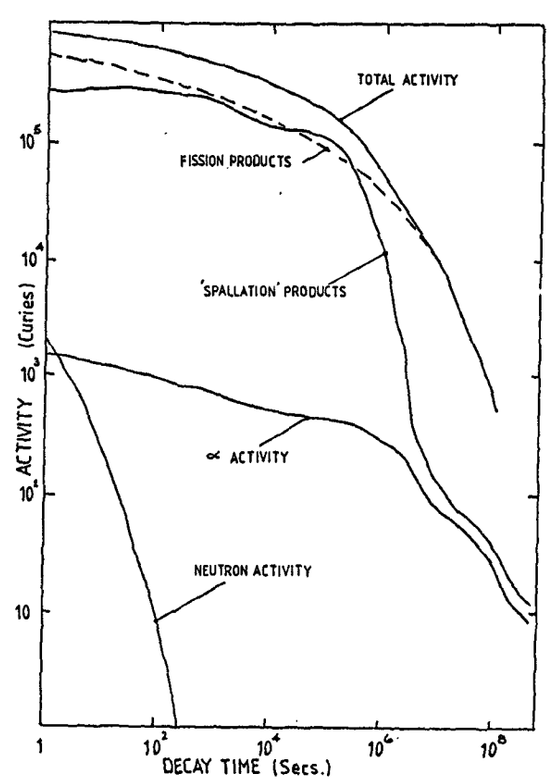

Fig. 4. DECAY OF ACTIVITY IN SNS TARGET.

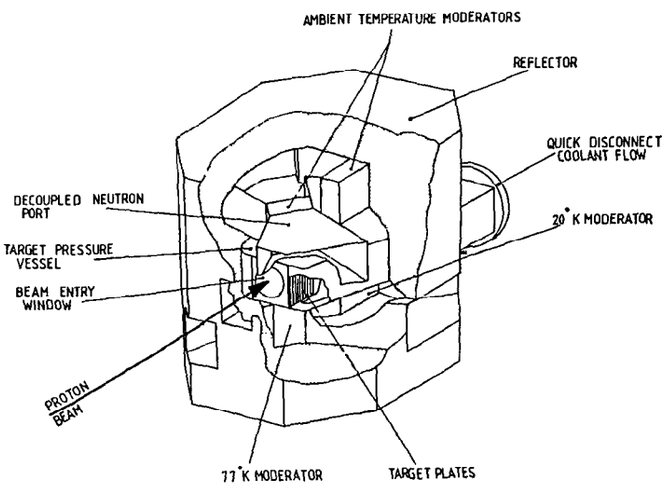

FIG. 7 PROPOSED TARGET ASSEMBLY WITH FOUR WING MODERATORS

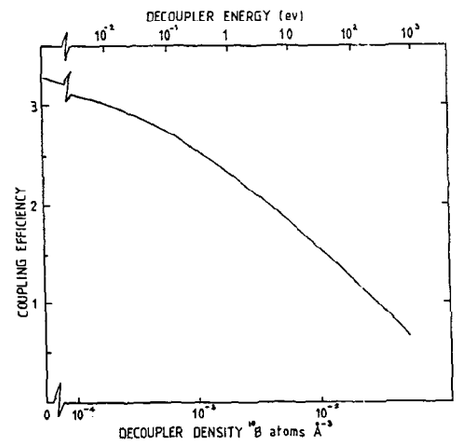

Fig. 8 MODERATOR COUPLING EFFICIENCY AND DECOUPLER DENSITY.

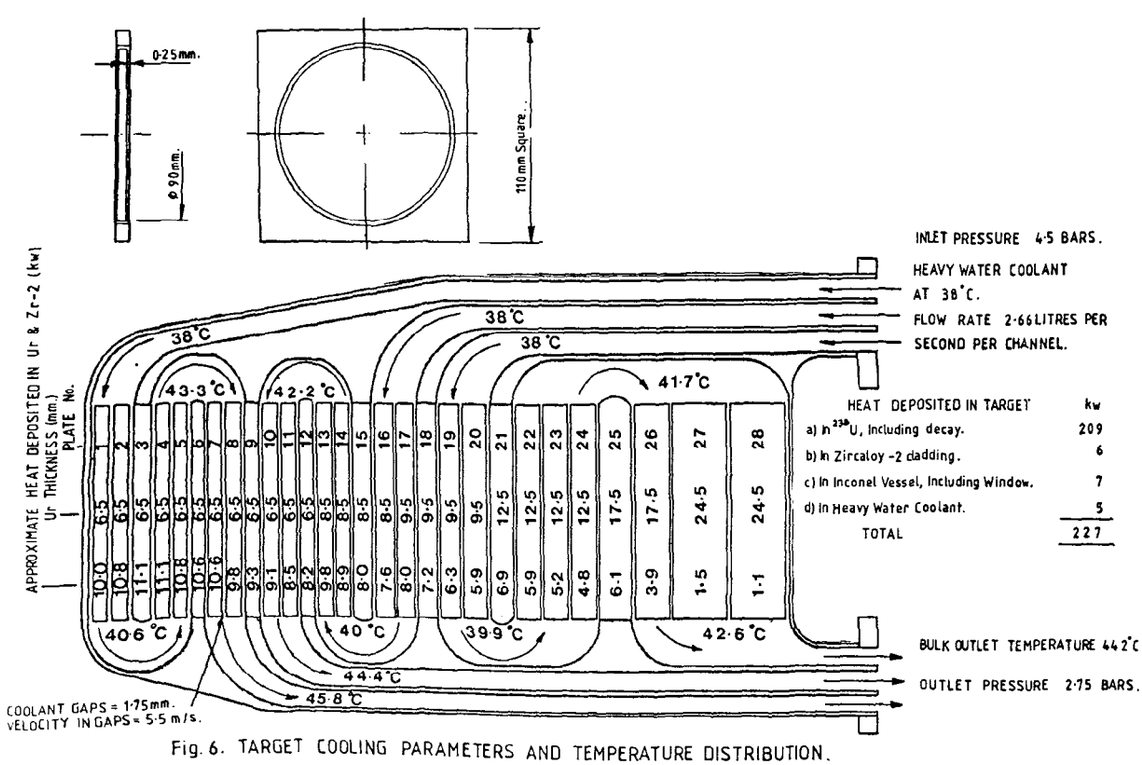

Fig. 6. TARGET COOLING PARAMETERS AND TEMPERATURE DISTRIBUTION.

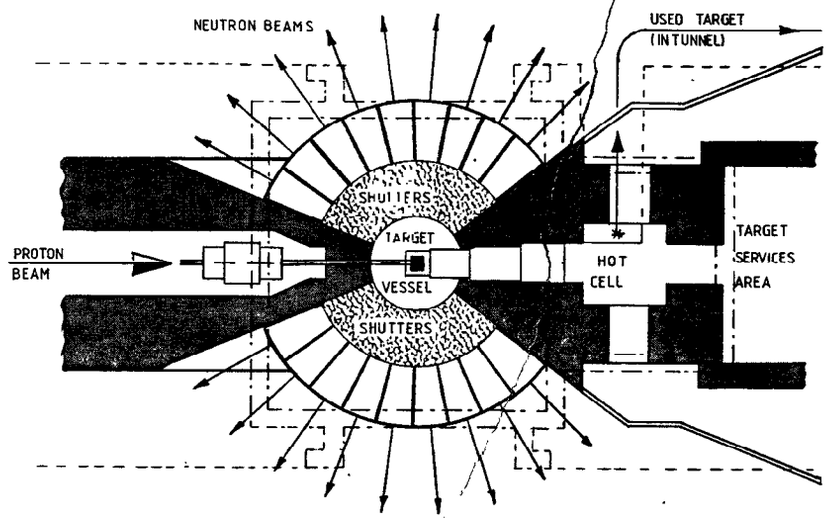

a) PLAN VIEW

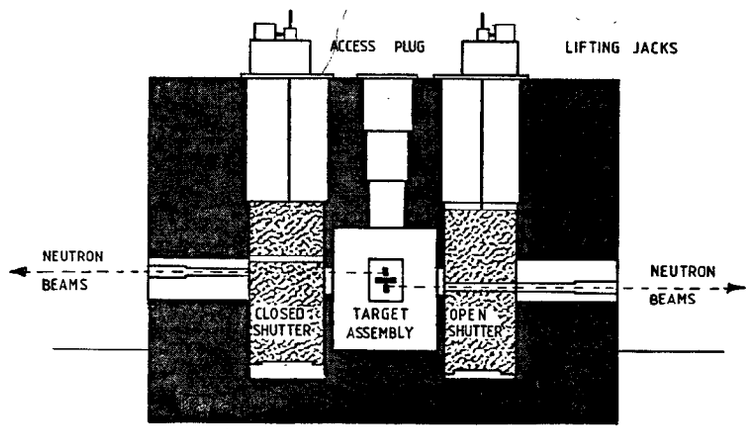

b) VERTICAL SECTION

Fig. 9 TARGET STATION BULK SHIELD SCHEMATICS.

Fig. 10 TARGET STATION PLINTH

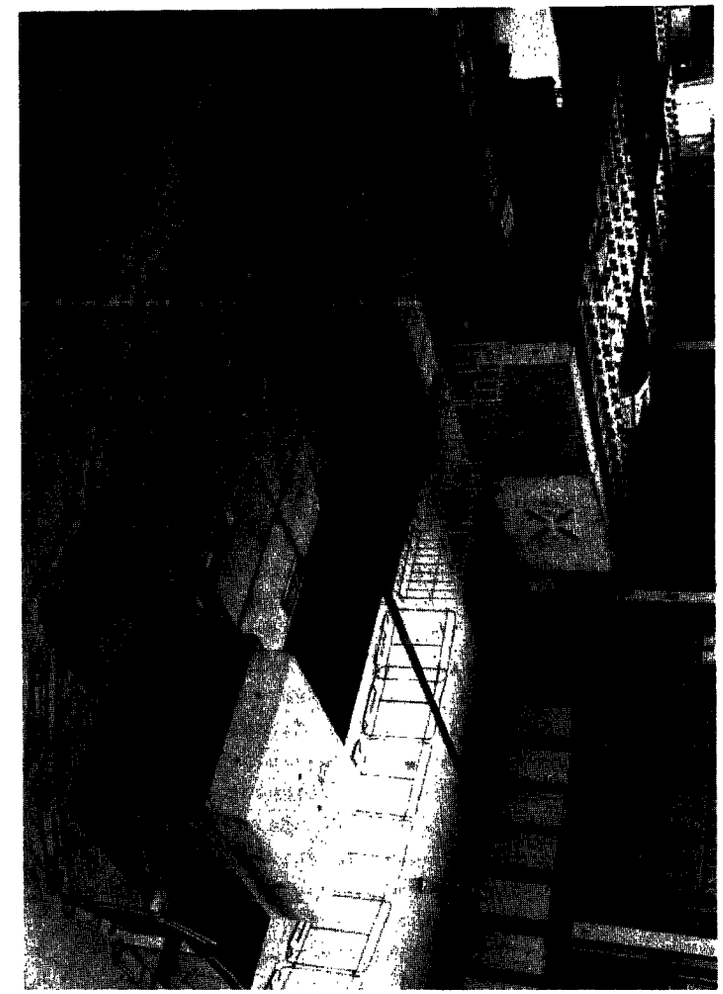

Layout of the Target Station for the German High Power Spallation Neutron Source Project

G.S. Bauer
Institut für Festkörperforschung
Kernforschungsanlage Jülich GmbH, Postfach 1913
D-5170 Jülich, West Germany

1. Introduction

The spallation neutron source presently under study in West Germany is designed to be competitive with a conventional high flux reactor in all fields of neutron scattering applications and to provide added flexibility not obtainable with a reactor in some respects. Since a fair number of well established experimental techniques with a high scientific potential such as triple axis spectroscopy essentially depend on the time average flux, the goal was reach $\phi_{av}^{th} = 6 \cdot 10^{14}\ cm^{-2}\ sec^{-1}$ to be within a factor of 2 of modern high flux reactors. Similarly, much emphasis was on the use of thermal and cold neutrons. The main reasons, why a neutron source, based on spallation rather than fission is considered are:

1.) The spallation neutron source, being driven by a linac /1/ can be operated with a time structure imposed on the neutron flux which gives a potential for significant advantages in its utilization /2/, /3/.
2.) In principle a proton compressor ring can be added which would even further shorten the proton pulses and allow a truly pulsed neutron source, opening up the epithermal neutron energy range.
3.) The spallation source will operate without a critical assembly and hence has an inherent safety potential which, in the case of a reactor, has to be provided for by a complex control system.
4.) There is no highly enriched uranium needed which may become more and more difficult to obtain in the future.
5.) There seems to be a potential to obtain significantly higher neutron fluxes with a spallation source relative to a reactor.

This paper describes the layout of the target station proposed for such a source. Separate papers will deal with the accelerator /1/, the scientific instrumentation /2/, /3/, the technical aspects /4/, specific materials problems /5/ and with the details of neutronics calculations /6/.

2. Time structure and neutron scattering experiments

For the experimentalist, a time structure imposed on the neutron flux is of interest for various reasons:

- Instruments traditionally using the average neutron flux can benefit by gating the detector to the time interval of interest and thereby suppress background and higher order contamination from the monochromator. For this purpose, the neutron pulses should be of the order of 0.5 ms long or less. (Since all of the useful intensity is compressed in this interval, instantaneous count rates may become very high and the pulse should not be made shorter than necessary).
- Instruments traditionally using time of flight for energy discrimination can be synchronized to the time structure of the source and thus benefit in full from the peak neutron flux. For this reason the peak flux should be as high as possible.

Considering also other aspects such as technical limits of accelerator components and flight path lengths resulting from the necessary thickness of the shield, the following parameters for the operation of the accelerator were chosen:

Pulse repetition rate	100 sec^{-1}
Pulse duration	0.5 ms
Maximum beam current	100 mA
Proton energy	1100 MeV

This results in a duty cycle of 1/20 and in an average beam power of 5.5 MW.

Both the high beam power and the time structure pose significant problems in the target design.

3. The target

3.1. Choice of target material

It is known from the literature (see e.g. /7/) that the neutron yield Y depends on the proton energy E, and the mass

number A, of the target nucleus according to

$$Y = a \cdot (A + b) \cdot (E - c)$$

For a target of 10 cm diameter and 60 cm length the constants are: $a = 0.1\ GeV^{-1}$ for non-actinides and $a = 0.2\ GeV^{-1}$ for depleted uranium; $b = 20$ and $c = 0.12$ GeV.

This shows that depleted uranium would be the best choice for a high neutron yield. Yet, building a uranium target is technically more complicated than building a target from e.g. Pb, due to the cladding requirements and the higher heat output in uranium. No uranium will therefore be foreseen in the initial design but the target concept should allow its later use if sufficient experience has been gained.

3.2. Choice of target geometry

It was assumed that the proton beam hitting the target would have a Gaussian intensity distribution with a FWHM of 4 cm and truncated at 4 cm radius. For a lead target, this results in a time average heat deposition at the hot spot of 6 kW/cm^3 or of 120 kW/cm^3 during the proton pulse /6/. The corresponding heating rate in an uncooled target is $4 \cdot 10^3$ K/sec. In order to cool such a target the only choice is to move the target through the proton beam and let it cool down elsewhere. An elegant way is to use a liquid target of Pb-Bi eutectic (melting point 123°C) and let the beam hit the flowing liquid, as originally proposed for the Canadian ING /8/. It is also investigated within the German study project /9/. Most likely, the beam would hit the vertically streaming liquid from above in order to avoid the need for a window under a mechanical load. The target geometry is essentially cylindrical, providing the possibility of building a neutron source which resembles closely that of a reactor: A large D_2O tank is used as a moderator with the beam tubes running tangentially to the target. While having a potential for a high time average neutron flux such a concept gives only moderately high peak fluxes and precludes the use of uranium.

A different target concept, which has been selected as the reference design is depicted in Fig. 1. It is a rotating disc of 2.5 m diameter with the target material mounted on its circumference and the proton beam coming in at right angles to the axis of rotation. In this case the target has essentially slab geometry, i.e. it is extended in two dimensions, with the upper and lower half space available for independent moderators. Experimentally it has been found that the leakage of fast neutrons from a slab target in the direction normal to the slab is increased by a factor of 1.4 relative to a cylindrical target of the same diameter. This is probably due to scattering of fast neutrons in the "wings". This enables a more efficient coupling of moderators into the target under otherwise similar circumstances. The distribution of fast leakage neutrons on the surface is shown in Fig. 2.

3.3. The target reference design

There is a large number of different possibilities to arrange the target material and cooling channels in a rotating target, which allows room for optimization. The approach to start with is chosen to minimize operational hazards. The target material is subdivided into 9128 individually canned pins, arranged in close packing. The coolant water is brought in through the shaft of the wheel and flows outward between the target pins. Channels are provided in the upper and lower support structure to return the coolant to the shaft.

The speed of rotation of the target is 0.5 rps which is adjusted such that consecutive proton pulses hit adjacent areas of the outer window whose centres are one FWHM apart. If a target pin is fully hit by the proton pulse, its mid-plane temperature distribution is as shown in Fig. 3a /10/. The peak temperature of 113°C is considered a safe temperature. The temperature of the Al can after the shot is 73°C. After a full revolution the peak temperature has fallen to 76°C and the temperature of the Al-can is 57°C. It is obvious that the temperature variation in the Al is fairly modest even for the most heavily loaded pins. The tensile stresses in the Al due to the higher thermal expansion coefficient of Pb superimpose on the compressive stress from water pressure.

Since each pin is exposed to the proton beam only once every two seconds, the radiation damage rate is reasonably low.

Also the operating temperature is a favourable one for Al with respect to void formation and helium mobility /5/. A minimum lifetime of 15000 to 20000 hours of actual operation at full power is expected. This holds also for the outer beam window.

The problem which might arise for an Al canning with a Pb-target is the production of mercury in the spallation process. A preliminary upper limit estimate yielded an average of 130 ppm of mercury over the whole target with the peak concentration being as high as 1300 ppm after one year of continuous operation /11/. The actual production should be lower than that. Nevertheless this might become a problem if significant diffusion takes place. On the other hand, up to 25% of mercury appears to be soluble in lead /12/. This means that small amounts would not tend to diffuse out of the solid target pins. This problem will be considered in more detail, in particular also for the case of an accidential melting of the lead in the Al-can. Of course, if necessary a different canning will have to be chosen or a suitable coating provided on the inside.

4. Moderators and Reflectors

With the average neutron flux of the proposed facility matching that of a reactor, uses other than neutron scattering are also being considered, such as fast and thermal neutron irradiation. For this reason it is desirable not only to have a high neutron flux but also a large volume of high flux. This is, at a first glance, a contradiction to the requirement of a short neutron pulse. However, with the two locations above and below the target being available for independent moderator design, a hybrid moderator concept has been conceived with a fast H_2O moderator with a reflector below the target (for good pulse structure) and a D_2O tank (for a large volume of high flux) above the target. Experiments on a mock-up of such a system at SIN /13/ showed that even in the case of a Pb-target very little cross talk will occur with respect to time structure between moderators, even if used without a decoupler.

4.1. The fast moderator for thermal neutrons

4.1.1 Geometry of the moderator

In order to obtain the above mentioned time structure of some 500 µs FWHM, an H_2O moderator is necessary. This pulse width does not require any decoupler or poison and the moderator geometry can therefore be trimmed for highest neutron leakage. It was found /14/ that adding fins to the moderator surface leads to a considerable increase of neutron leakage. The best results were obtained with a moderator as shown in Fig. 4a with 6 to 9 cm long fins (or, alternatively, 6 cm deep grooves) of 0.5 to 1 cm thickness /15/*. The experiments also showed that, in a well reflected geometry, H_2O and polyethylene are equivalent with respect to intensity. H_2O must be used because an estimated 20 kW of heat /11/ have to be removed from the moderator.

4.1.2 The reflector

The moderator will be surrounded by a reflector for fast neutrons which, as shown in Fig. 4b, is designed for minimum losses. It was found experimentally /18/ that, while giving nearly the same overall intensity**, a Pb-reflector produces less strong tails on the neutron pulses than a Be-reflector does. Therefore, the reflector will probably be of Pb, which is also a significant advantage from the point of view of shielding.

4.2. The D_2O-moderator

To facilitate the installation of cryogenic and irradiation equipment, it was decided to place the D_2O-moderator above the target. The dimensions of the tank would be 1 m radius by 1 m high.

---

* Such grooved moderators, although with less deep grooves have also been investigated with respect to their time structure at the CERN booster Synchrotron /16/ and at the ZING-P'-facility at Argonne /17/. It is found that there is some but little pulse broadening and such moderators may even be useful for pulsed sources. At the same time the neutron spectrum is considerably softer for the grooved moderator.

** This result has also been confirmed by computer simulation /19/.

Its main purpose is to serve as a reflector for the cold neutron source and as a volume to locate irradiation facilities.

The thermal neutron flux distribution measured in such a tank for 600 MeV protons on a Pb and a U-238 slab target with 10% polyethylene in the volume and with 6 mm polyethylene and 30 mm Al between the target and the D_2O is shown in Fig. 5 /20/. At 1100 MeV a somewhat flatter gradient along to the proton beam would be expected. The volume of high flux, although being smaller than in a reactor, is still sufficient to accomodate an efficient cold neutron source and a few irradiation thimbles.

The fast neutron flux above the target will be of the order of 10^{15} cm^{-2} sec^{-1}. Therefore it has been conceived to avoid the risk of a leak developing in the D_2O tank by a design as shown in Fig. 6, where the most heavily radiation loaded structural part does not serve as D_2O containment.

4.3. The cold neutron source

With the D_2O constituting a long-life time neutron reflector, the choice for the cold neutron source will probably be D_2 for maximum cold neutron leakage. However, no final decision has been made yet and other possibilities are being considered /21/. The cold source would be inserted into the D_2O tank in a separate pipe of aluminium or zircaloy (Fig. 6). The bottom part of this tube would contain a light water cooled plate of lead or bismuth for γ-shielding and pre-moderation to avoid excessive heat load on the cold source. It is believed that a detailed calculation will show that the cold neutron leakage from this source should almost match that of the HFR Grenoble where the cold source could not be placed at the peak flux position due to heating problems.

This design will also reduce the fast neutron load on the containment of the cold source considerably.

4.4. Expected performance of the moderators

Considerable experimental and computational work has gone into the assessment of the expected performance of the moderators with respect to thermal neutron leakage and time structure. A list of expected performance data is given in Table 1. Listed are the peak thermal neutron flux, the peak-to-average ratio, the

decay constants and the fractions of the flux decaying with the respective parameters. The data are inferred from measurements at SIN /13/ (600 MeV, scaled to 10 mA which is roughly equivalent to 5 mA, 1.1 GeV). Some allowance has been made for added losses in a real design.

For the case of a Pb-target the time-dependent thermal neutron flux is shown in Fig. 7. In the H_2O-moderator, which has a decay constant of 200 µs, 92% of the stationary flux is reached 500 µs after the proton pulse is switched on. This shows that the proton pulse of 500 µs is the maximum that should be chosen, because for longer pulses the neutron flux would not increase further. Although a pulse of 250 µs with twice the intensity would yield a higher neutron flux, 500 µs is considered a good choice for the reasons mentioned in section 2.

In the D_2O-tank - and likewise in the cold source - a FWHM of the neutron pulse of 850 µs is expected for a Pb-target with a significant tail at long times. Nevertheless this pulse structure is still sufficiently pronounced to be taken advantage of in some slow neutron applications /3/.

5. Shielding and beam holes

5.1. Bulk shielding

In order to be able to accept as large a solid angle as possible, and to avoid frame overlap with the background of the following pulse when working with relatively slow neutrons (e.g. 4 Å) the shield should be not too thick. For this reason an attempt will be made to provide as efficient a shield as possible. The moderators and reflectors will be surrounded by water cooled lead with possibly some dense metal shot embedded in it. The problem is particularly serious at the D_2O tank since the D_2O itself has practically no shielding effect for thigh energy neutrons. Fortunately the rotating target provides good lateral shielding itself and also the Pb-reflector would be helpful in this respect. It is foreseen that only two beam tubes penetrate the shield at the level of the D_2O tank in addition to the neutron guides. All thermal neutron beams ending in the target hall will view the lower moderator. The diameter of the beam tubes will be 10 cm at the moderator and increase to 20 cm at the out-

side of the shield. The exact composition of the shield has not yet been determined, but probably it will consist mostly of cast iron.

5.2. Neutron guides

Use of the cold neutrons will be mainly made by neutron guides leading into a separate neutron guide hall. Two bundles of 6 guides each will view the cold source in such a way that the reflector displacement is minimized (Fig. 8). The neutron guides will be tailored for different wavelengths by their curvature with the longest-wavelength guides ending close to the target hall. The guides will be shielded to twice the length of direct sight. A list of the characteristic parameters of the guides is given in Table 2. The cross section will be 20 x 3 cm^2 to allow multiple use by splitting the height.

5.3. The shutters

The shutters should provide sufficient protection when closed to allow at least temporary work on the neutron beam lines while the source is operating. It has been assumed (with proof still to be provided) that for a beam hole not looking directly at the target, some 3 m of shielding are sufficient. Since the shutters, when closed, should not weaken the nearby shielding unduely, a system has been chosen which consists of 3 m diameter discs with horizontal axes of rotation and with the beam hole running in the disc (Fig. 9). When rotated away from the open position, these discs close the beam hole very quickly, without opening up a new hole in the shield. When fully closed, the beam hole in the shield points vertically and beam hole inserts can be changed from above with the shutter safely closed. The beam hole does not run through the centre of the disc which, in principle, allows to put the hole at the level of the upper or the lower moderator without changing the disc's position in the shield *. It is even conceivable to use shutters with two beam

* This feature might become of interest if, upon addition of a proton compressor ring, the source should ever be converted into a pulsed source (see section 7.2).

holes to bring out two beams on top of one another. For the purpose of maintenance the shutters can be lifted out of the shield if required /4/.

Wells for the installation of choppers running in phase with the source are provided behind the shutters. The outer part of the shield is designed to be easily changable to retain maximum flexibility for the installation of monochromators etc.

The shutters for the neutron guides are designed differently, since the diameter of the disc shutters would force the front end of the neutron guides too far away from the cold neutron source. Since the neutron guides can be shut off individually for routine work on the experiments, the task of these shutters is mainly to shut off the whole bundle of guides when work on the neutron guides themselves is necessary. This will be done only when the source is not operating and therefore the shutters only have to suppress the decay radiation from the target. They are designed as lift- and lower shutters operated from above.

6. Experimental Areas and Facilities

6.1. The target hall

The target shield will be located in a 40 m diameter hall which will be occupied by the thermal neutron scattering instruments. There will be conventional instruments adopted to the intensity modulated source such as triple axes spectrometers, diffractometers and time-of-flight spectrometers (with a chopper) as well as newly conceived instruments especially designed to take advantage of the time structure /2/. The target hall will be equipped with a 20 t crane able to reach almost every point in the hall. Air conditioned cabins for the electronis are foreseen along the outer wall. The possibility will be provided to extract certain beams to locations outside the hall for long flight path instruments.

6.2. The neutron guide hall

The two bundles of 6 neutron guides are separated by an angle of 30°. In this way it becomes possible to make very efficient use of the space in the neutron guide hall (Fig. 10), because four lines of instruments can be installed. Preference

has been given to a larger number of neutron guides rather than a higher cross sections because the guides are easier to build and excessive length (resulting in higher losses) is avoided. Two parallel cranes with a capacity of 10 t each will serve the two halves of the neutron guide hall. Similar to the target hall, air conditioned cabins for the electronic equipment will be arranged along the walls.

6.3. The neutrino cavern

Since the spallation source provides an intense source of neutrinos it is conceived that a cavern for neutrino experiments should be located under the target station (Fig. 11). It should be shielded from the target by some 8 m of iron and subtend a solid angle of one steradian relative to the target.

6.4. Irradiation facilities

6.4.1 Low temperature irradiation facility

Low temperature irradiation of solids is an important method to obtain information on defects caused by energetic particles in solids. It is of particular interest to be able to select between a thermal neutron spectrum to produce radiation damage from recoil nuclei after neutron capture and a fast neutron spectrum to produce the damage by direct knock-on processes. It has been shown /22/ that the spectrum produced by a spallation target with a Pb-reflector is well suited to study the radiation damage by a fission spectrum. For this reason an attempt has been made to provide an irradiation thimble which allows selection of the type of spectrum by the irradiation position. As shown in Figs. 6 and 8 there is a tube running through the D_2O-tank which holds the low temperature irradiation thimble. A hole in the lateral Pb-shield of the target is foreseen under this tube such that samples to be irradiated can be pushed down into the Pb-shield for fast neutron irradiation. Thermal neutron irradiation is possible if the samples are lifted to a level inside the D_2O tank. The fast flux in the lead is estimated to be $1 \cdot 10^{14} cm^{-2} sec^{-1}$ the maximum thermal flux accessible will be $3 \cdot 10^{14} cm^{-2} sec^{-1}$.

6.4.2 Room temperature irradiation

A second irradiation position, mainly for chemical applications has been proposed. However, so far no detailed design has been worked out. A vertical tube of 10 cm$^{\emptyset}$ ending in the D_2O tank is foreseen for this purpose.

6.5. Ultra cold neutrons

The possibilities of building an efficient source of ultra cold neutrons, especially by taking advantage of the time structure of the fast neutron pulses are being considered in detail. So far no decision has been made as to the type of ultra cold neutron source. Extraction of suitable cold neutron beams through a horizontal beam tube or a vertical one looking directly on the cold neutron source are, in principle, possible. In the last case the beam tube would penetrate the Be-reflector above the cold source (see Fig. 6) and be equipped with a curved vertical neutron guide.

7. Options and extensions

The question, what could be done later to further improve the performance of the source, is obviously an important one in the process of decision making. Basicly three possibilities have been considered, which are outlined briefly in the following sections.

7.1. Increase of average proton current

Since the peak proton current is an important design feature of the accelerator /1/, the only realistic possibility would be to increase the duty factor by lengthening the proton pulses. This would have an adverse effect on the time structure of the source and might even be a disadvantage with respect to high energy neutron shielding. At the same time the load on the accelerator components would be increased.

7.2. Use of uranium as target material

Some experimental work has gone into the problem of a possible gain in neutron flux by using depleted uranium as target material. As can be seen from Fig. 5 and Table 1, the expected

gain is roughly a factor of 2 with no degradation of time performance. Therefore the possibility of changing to a uranium target later on remains very interesting. Although the design of the target would allow to use depleted uranium rather than lead, the larger heat output and different thermal expansion may make it necessary to provide means for an improved thermal contact ot the canning material and to compensate differential expansion, e.g. by immersing the U-238 in a Pb-Bi eutectic which would melt when the target is in operation. Whether Al could then still be used for canning will be investigated in detail, but also using stainless steel canning seems feasible. In this case it might be of advantage to fabricate also the wheel itself from stainless steel to avoid water corrosion problems. The extra heat output in the uranium could be handled by slightly increasing the water flow through the target. There would probably also result a higher γ-flux from the use of uranium but this could be handled in the case of the cold source by increasing the thickness of the Bi-shield, if necessary. Since the number of fast cascade particles produced is essentially the same for Pb and U-238, no significant effect on the background situation or bulk shielding is expected.

7.3. Pulsed source with a compressor ring

One unique feature of spallation neutron sources is the fact that the epithermal neutron energy range can be made accessible to experimental research, which is practically not possible on reactors. For this the proton pulses have to be considerably shorter than foreseen in the facility as described above. A conceptual design has been worked out for a compressor ring which could be added to the facility /23/. The idea is to accumulate protons on a circular orbit whose length is such that the time of revolution of the protons corresponds to the desired pulse length. When the accumulation is completed, all protons are extracted from the ring in one single turn and directed onto the target. The diameter of such a ring would be 65 m with 4/5 of the circumference filled with protons, allowing for a gap to activate the extraction magnet. Up to $3 \cdot 10^{14}$ protons can be accumulated circulating in the ring at the transition energy. This

mode of operation ensures isochronism which keeps the bunch together without rf-equipment. Instabilities occuring are slow enough to be of no importance during the short accumulation period of 500 µs. A pulse compression by a factor of 600 should thus be achievable.

Obviously, in order to utilize the shorter proton pulse, suitably designed moderator-reflector geometries are needed. The simplest way to provide these would be to replace only the H_2O moderator and retain the D_2O tank with the cold source for conventional use. With the fast moderator-reflector assembly mounted on the target trolly /4/ it is relatively easy to replace this part with a differently designed one with, say two smaller and decoupled moderators. These could be viewed by some of the beam tubes without changes, whereas others would perhaps have somewhat unfavourable glancing angles. These tubes might be shifted to the upper level for use with the D_2O tank. Suitable provisions will be made in the design of the shield, but the D_2O tank itself would probably have to be exchanged for a differently designed one. This solution would, of course, impose serious restrictions on the possibility of thermal neutron work. Therefore, the optimum solution would be to build a second target station for pulsed neutron work. This would make the facility an unprecedented tool for neutron scattering research.

References

/1/ J.E. Vetter: "Linear accelerator for the German spallation neutron source" (1980) this conference (talk presented orally only)

/2/ B. Alefeld: "Some new instruments designed to use the time structure of a quasi continuous spallation neutron source" (1980) this conference

/3/ N. Nücker and W. Schmatz: "Advantage of neutron sources with time structure for special neutron spectrometers" (1980) this conference

/4/ H. Stechemesser and G.S. Bauer: "Engineering, active handling and emergency considerations for a rotating high power target" (1980) this conference

/5/ W. Lohmann: "Materials problems in beam windows and structural components of the SNQ-target" (1980) this conference
/6/ D. Filges, T.W. Armstrong, P. Cloth, M. Kloda, R.D. Neef and G. Sterzenbach: "Theoretical studies related to spallation target physics" (1980) this conference
/7/ J.M. Carpenter: "Pulsed spallation neutron sources for slow neutron scattering" Nucl. Inst. Meth. 145 91-113 (1977)
/8/ G.A. Bartholomew and P.R. Tunnicliffe eds.: "The AECL study for an intense neutron Generator" (AECL 2600 (1966)
/9/ H.J. Hoffmann, P.E. Huber and M. Piesche: "Liquid metal target development for the German neutron source" (1980) this conference
/10/ F. Stelzer: (1980) private communication
/11/ T.W. Armstrong: (1980) private communication
/12/ M. Hansen: "The constitution of binary alloys" 2nd ed. Mc Grow Hill (1958)
/13/ G.S. Bauer, W.E. Fischer, F. Gompf, M. Küchle, W. Reichardt and H. Spitzer: "Thermal neutron leakage and time structure measured for various target- moderator- reflector configurations for a spallation neutron source" (1980) preprint
/14/ G.S. Bauer, K. Grünhagen and H. Spitzer: "Einige Voruntersuchungen zu wasserstoffhaltigen Moderatoren für eine Spallations-Neutronenquelle" (1980) preprint
/15/ G.S. Bauer, F. Gompf, W. Mannhart, W. Reichardt, R. Scherm and H. Spitzer: "Thermal neutron leakage from hydrogeneous Moderators for a spallation neutron source" (1980) preprint (in preparation)
/16/ G.S. Bauer, J.P. Delahaye, H. Spitzer, A.D. Taylor and K. Werner: "Relative intensities and time structure of thermal neutron leakage from various moderator-decoupler systems for a spallation neutron source" (1980) preprint
/17/ J.M. Carpenter: (1980) private communication
/18/ G.S. Bauer, H. Conrad, K. Friedrich, G. Mileret and H. Spitzer: work in progress
/19/ A.D. Taylor: (1980) private communication
/20/ V. Drüke: (1980) private communication
/21/ W. Reichardt: "Studies of cold neutron sources for spallation targets" (1980) this conference

/22/ M.A. Kirk, R.C. Bircher, T.H. Blewitt, L.P. Greenwood, R.J. Popek and R.R. Heinrich: "Measurements of neutron spectra and fluxes at spallation neutron sources and their application to radiation effects research" (1980) to appear in J. Nucl. Mat.
/23/ H. Willax: (1980) private communication

Target	Moderator	Reflector	$\hat{\phi}$ $10^{14} cm^{-2} sec^{-1}$	$\frac{\hat{\phi}}{\bar{\phi}}$	α_1 (μs^{-1})	α_2 $(\mu s)^{-1}$	$\frac{\phi(\alpha_1)}{\phi(\alpha_2)}$
Pb	H_2O	Pb	130	18.4	$(200)^{-1}$	-	-
	D_2O	D_2O	50	7.9	$(759)^{-1}$	$(3333)^{-1}$	13.3
U-238	H_2O	Pb	290	18.4	$(200)^{-1}$	-	-
	D_2O	D_2O	125	10.2	$(440)^{-1}$	$(5000)^{-1}$	32.3

Table 1 Flux data and decay parameters inferred from measured data /13/ for the hybrid moderator concept with targets of Pb and U-238. In the D_2O-tank a 15% depression due to structural parts and beam tubes has been allowed for. All values may be about 10% lower in the real design due to a larger coolant volume fraction.

guide	(m)	λ_{nom} (Å)	λ_{min} (Å)	L_{II} (m)
1	1151	6	4.2	33
2	2591	4	2.8	50
3	4606	3	2.1	67
4	2591	4	2.8	50
5	1658	5	3.5	40
6	414	10	7	20

Table 2 Characteristic data of the neutron guides.

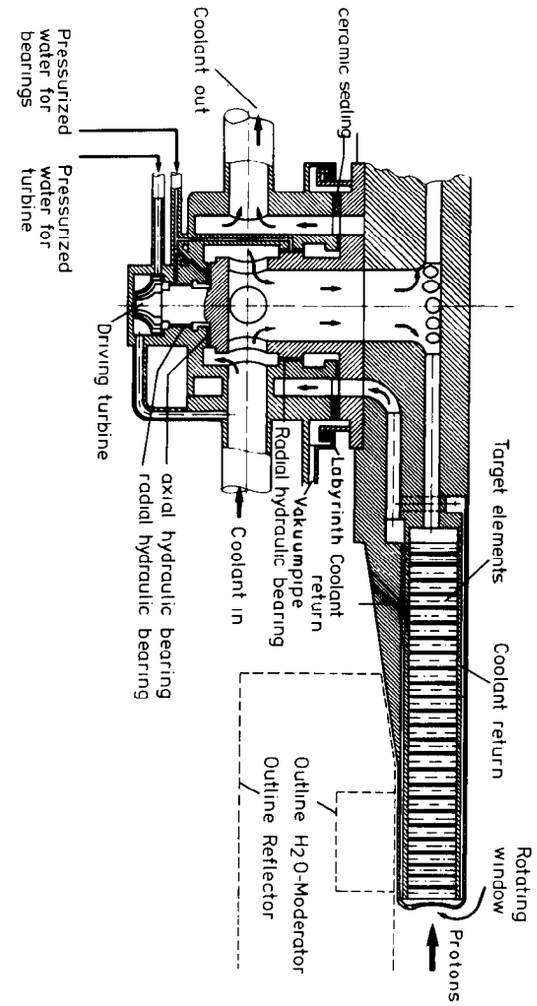

Fig. 1 Rotating target proposed for the German high power spallation neutron source. About 9000 Pb zylinders of 18 to 24 mm diameter and canned in aluminium are arranged on the circumference of a 2.5 m diameter wheel and cooled by water flowing between them. Only one half of a section through the wheel is shown.

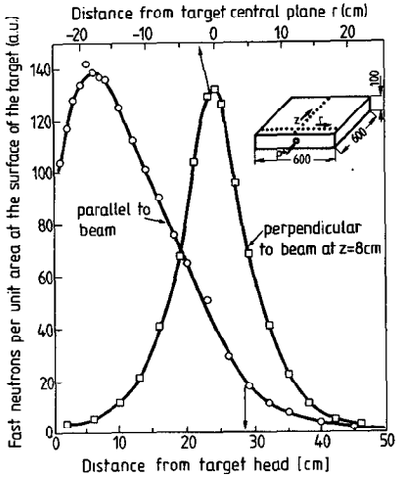

Fig. 2

Distribution of fast neutron leakage at the surface of a Pb-slab target as measured by Rh-activation for 600 MeV protons impinging on the target. The foils were arranged as indicated on the inset.

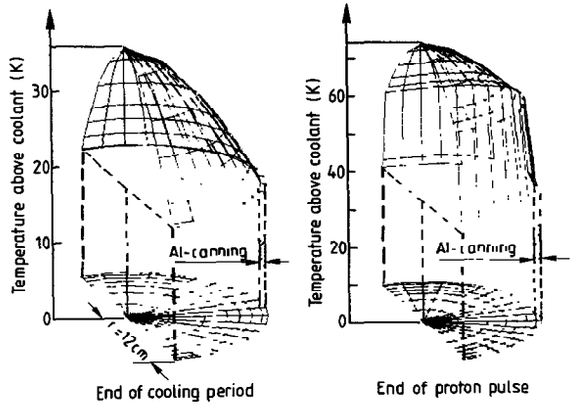

Fig. 3 Temperature distribution in the mid-plane of the most heavily loaded target pin of 24 mm diameter.

a) Temperature distribution directly before the proton pulse

b) Temperature distribution directly after the proton pulse

The network of finite elements used for the calculation is shown at the bottom of each Figure. Temperature scales are different in both graphs!

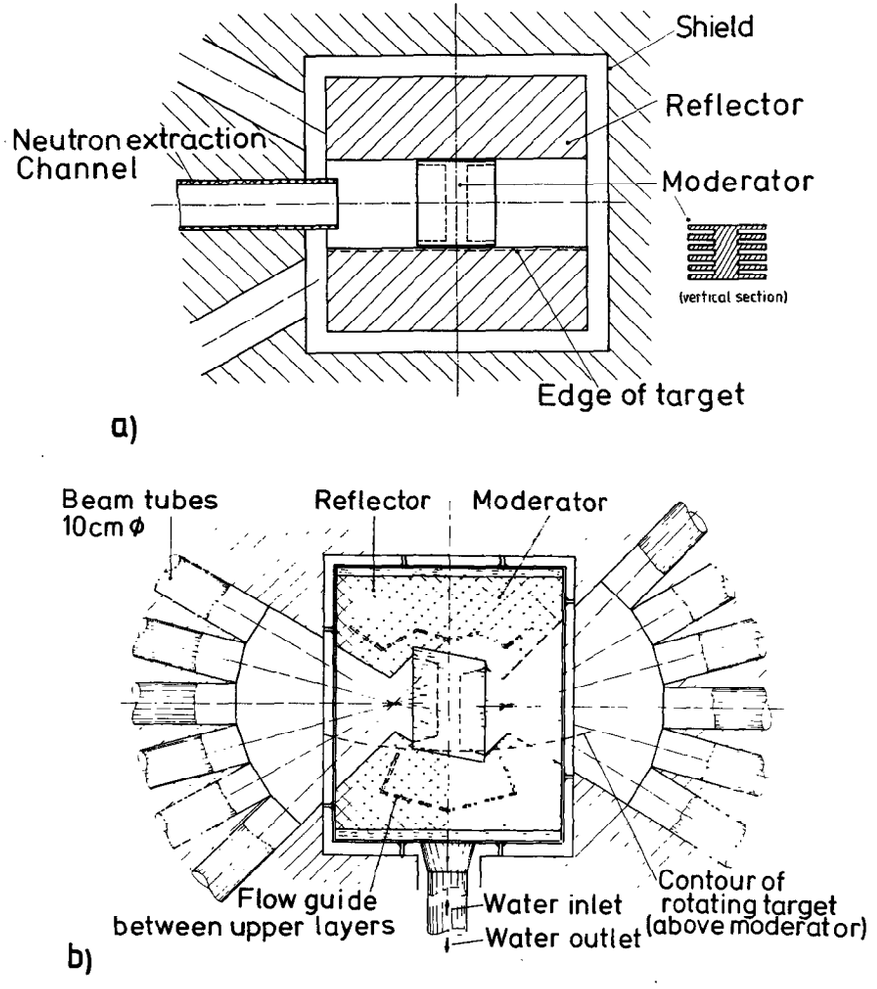

Fig. 4 Moderator-reflector arrangement for the spallation neutron source.

a) Polyethylene moderator used in a straight reflector tunnel in the measurements.

b) Proposed moderator-reflector arrangement for the reference design.

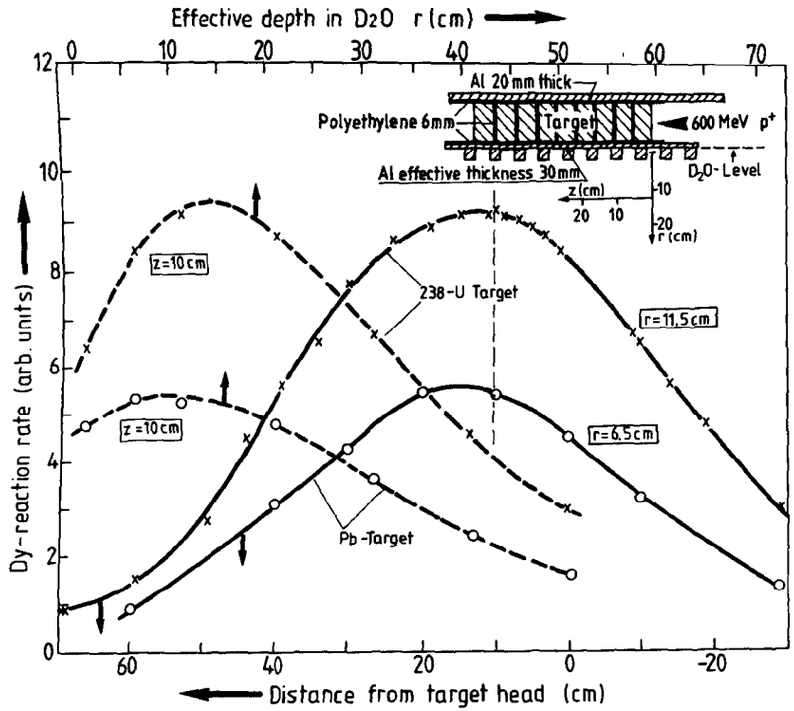

Fig. 5 Thermal neutron flux distributions measured in the D_2O of a hybrid moderator arrangement for slab targets of Pb and U-238. A schematic diagram of the arrangement used is given in the inset.

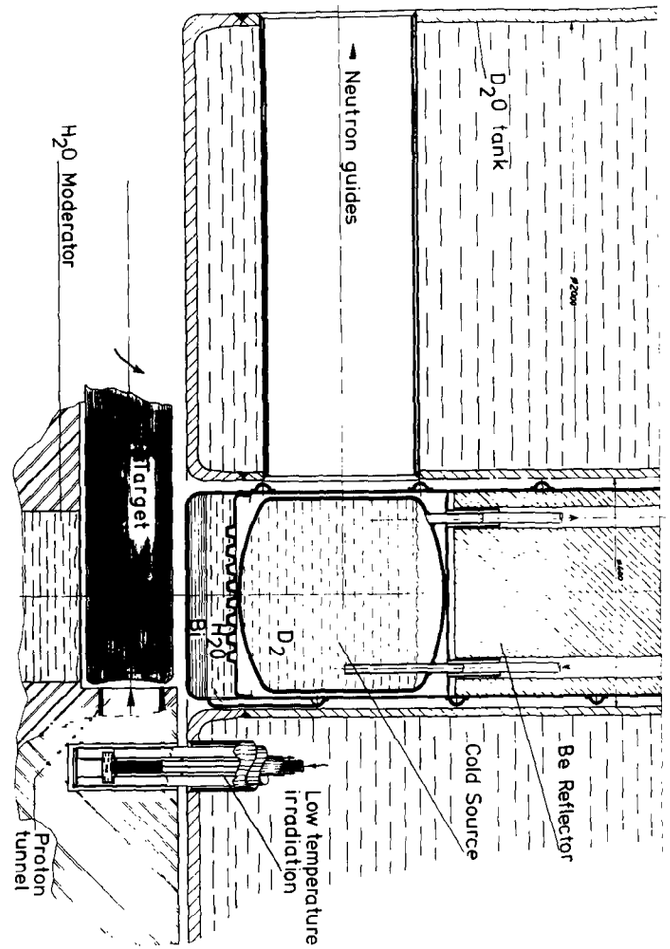

Fig. 6 Schematic representation of a possible design for a cold neutron source in conjunction with a rotating target.

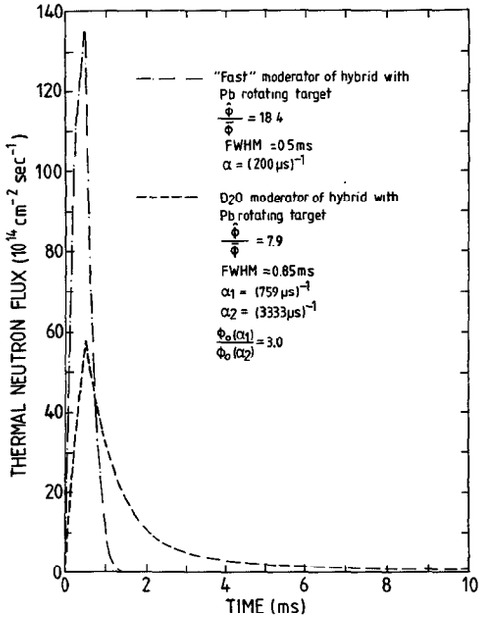

Fig. 7

Expected time dependent neutron flux for the moderators of the hybrid system (unperturbed in the case of the D_2O).

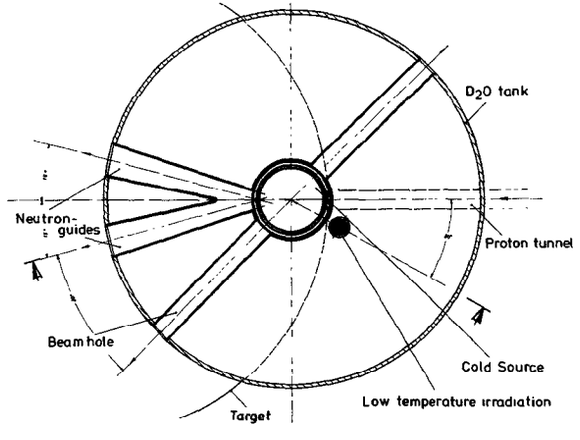

Fig. 8 Schematic horizontal cut through the D_2O tank at the level of the cold neutron source.

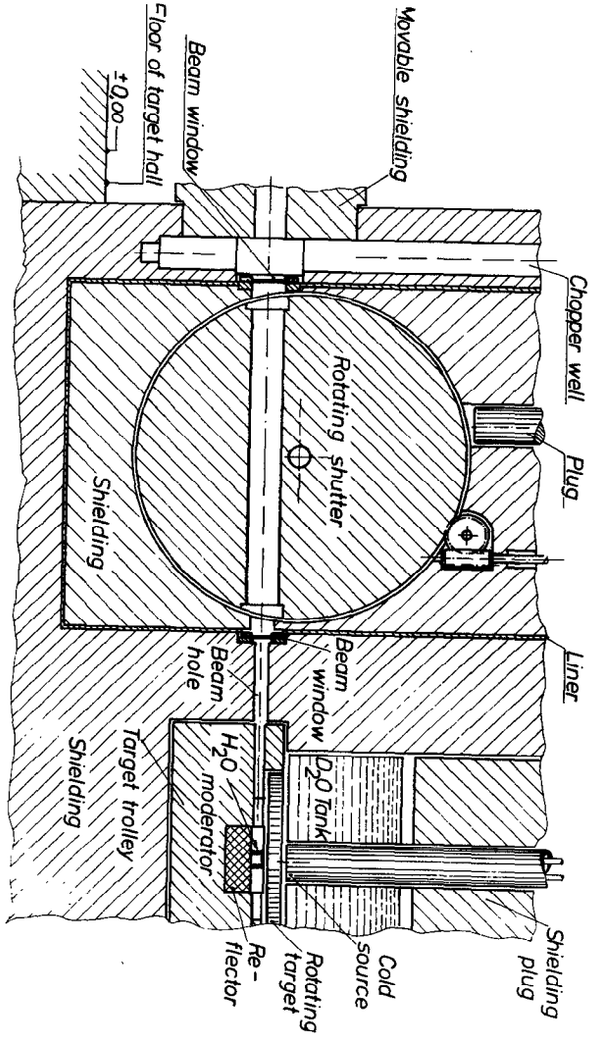

Fig. 9 Schematic of beam hole layout with disc shutter. Rotating the shutter through 90° will allow replacement of beam hole inserts (collimators) while the beam hole is closed. Rotating through 180° brings the beam hole to the level of the upper moderator (cold source).

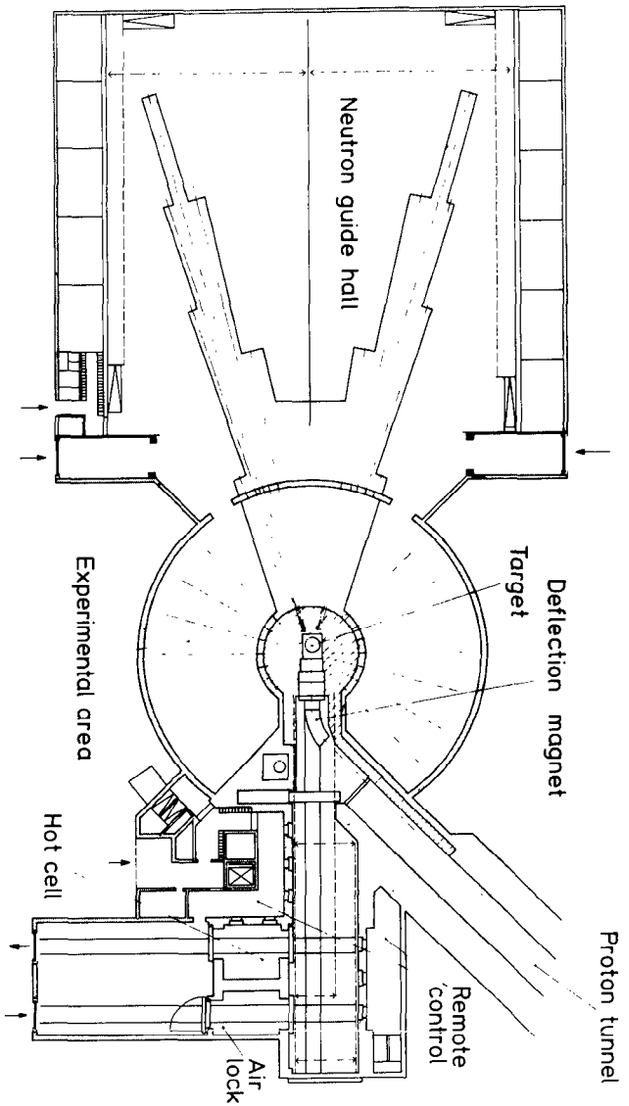

Fig. 10 Horizontal cut through the target complex showing the circular target hall with the adjacent target service area and the neutron guide hall. Two bundles of neutron guides separated by 30^0 are looking at the cold neutron source.

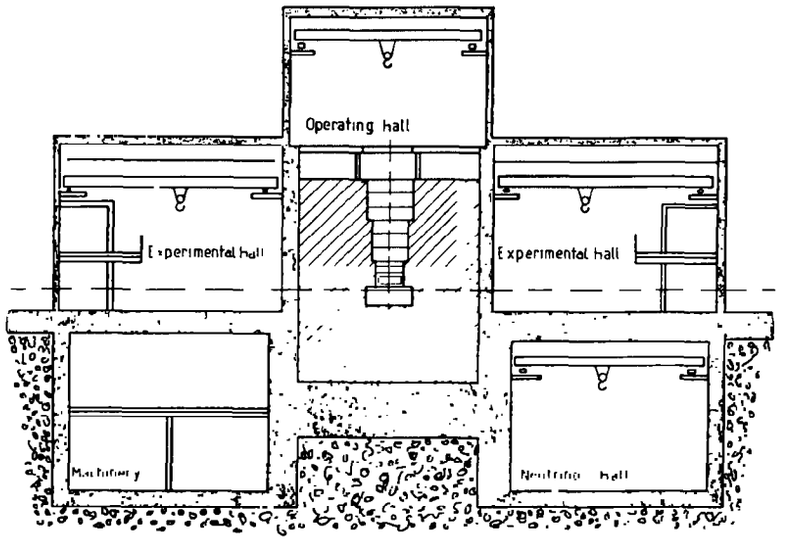

Fig. 11 Vertical cut through target building. Above the experimental area a service area is located which holds the cryogenic equipment for the cold neutron source and the low temperature irradiation facility and eventually the sample processing station for the room temperature irradiation facilities. Below the target and shielded by 8 m of iron there is, laterally displaced, the neutrino cavern.

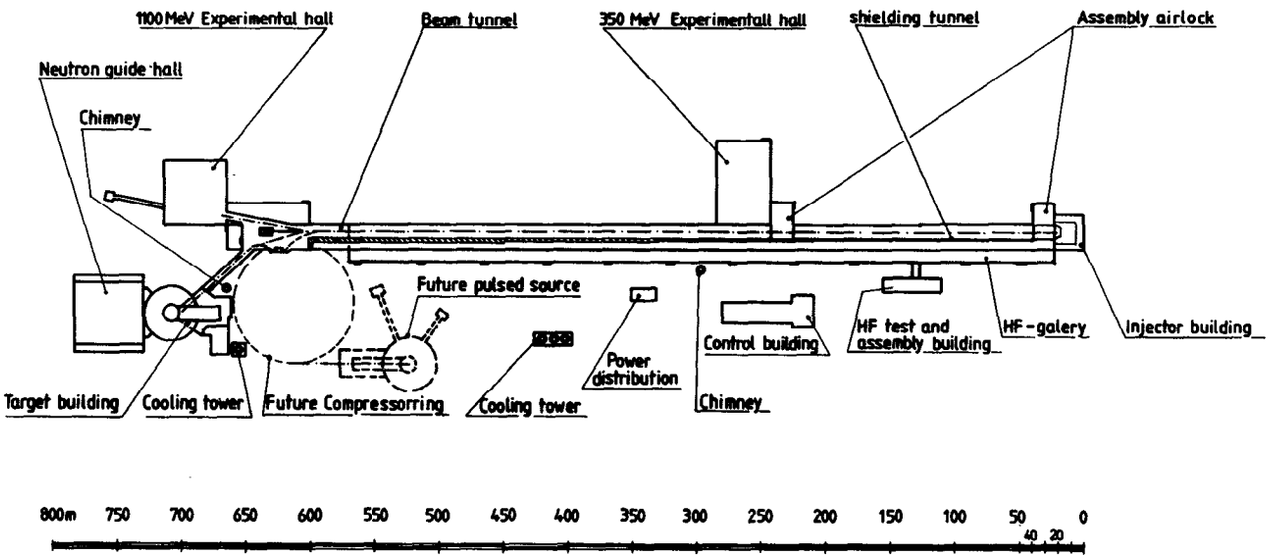

Fig. 12 Ensemble of buildings for the proposed spallation neutron source. The options of a compressor ring and a second (pulsed) target station are shown dashed to emphasize that the location of these buildings may change in the course of a detailed planing.

KENS TARGET STATION

N. Watanabe, S. Ikeda

National Laboratory for High Energy Physics

Oho-machi, Tsukuba-gun, Ibaraki 305 Japan

and

Y. Ishikawa

Department of Physics, Tohoku University, Sendai, 982 Japan

1. Description of the KENS Target Station

The complete KENS target assembly consists of the target, two kinds of moderator with decouplers and a neutron reflector. The present target element is composed of two blocks of tungsten 6 cm thick as shown in Fig. 1. The target is cooled by circulated light water. The cooling channels which are only 1.4 or 2 mm in width are positioned at both sides and ends, and between the two target blocks, although not on the top and the bottom.

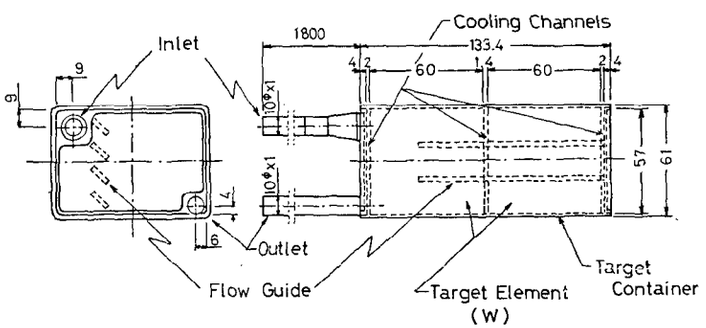

Fig. 1 KENS tungsten target

Several studies have been made in order to optimize the coupling efficiency of the target-moderator system. Figure 2 shows a cross sectional view of the KENS target-moderator-reflector assembly. A target of rectangular shape was adopted to increase the leakage of fast neutrons in the vertical direction towards the moderators. A target height of 5.7 cm was chosen on the basis of the size of the proton beam at the target and the stability of its position. The full width of the beam in the vertical sense was estimated to be about 2.7 cm and the maximum fluctuation of the beam spot position was assumed to be less than 1 cm. In addition, a small margin is necessary to limit the secondary escape particles to a tolerable level in the bottom of the cold moderator.

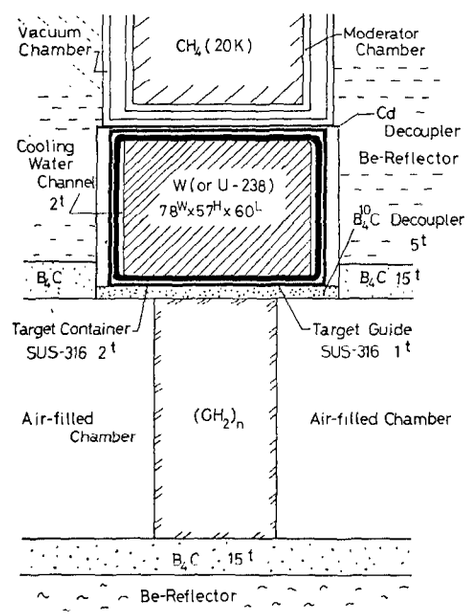

Fig. 2 Target-moderator configuration

A polyethylene moderator of dimensions 10 cm^W x 10 cm^H x 5 cm^T was located below the target. A sintered plate of $^{10}B_4C$ was adopted as a decoupler between the target and the polyethylene moderator and its thickness was limited to 0.35 cm in order to minimize the distance between them. In our design there are no cooling water channels between the target and the moderators and the distance between the center line of the target and the top of the polyethylene moderator is only 3.6 cm including the widths of the target container and a guide pipe used during target installation. A solid methane moderator of dimensions 12 cm^W x 15 cm^H x 5 cm^T is installed above the target, decoupled by a 0.5 mm thick cadmium sheet. The distance from the target center to the bottom of the solid methane is only 4.6 cm including the thickness of the walls and the vacuum gap required for thermal insulation.

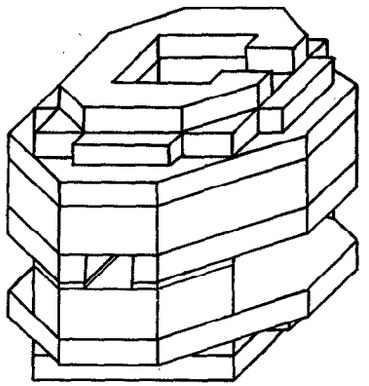

Fig. 3 Be reflector assembly

The target and the two moderators are enclosed within a reflector system composed mainly of beryllium but with graphite as an auxiliary. The beryllium reflector consists of approximately

120 beryllium blocks (about 220 Kg in total weight) which are assembled as shown in Fig. 3. More than 30 graphite blocks are added to the beryllium to complete an octagon and the reflector assembly is then haused within an aluminium vessel (see Fig. 4).

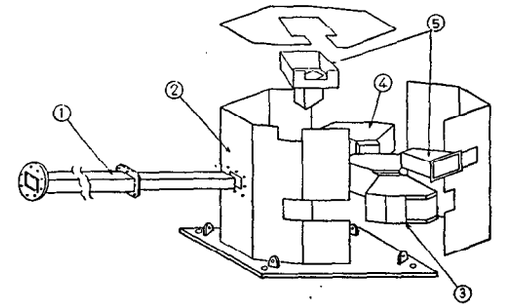

Fig. 4 Target-moderator-reflector assembly:
1) target guide/proton beam drift tube
2) assembly vessel made of aluminium
3) B_4C decoupler
4) polyethylene moderator at room temperature in a drawer
5) Cd decoupler for cold moderator

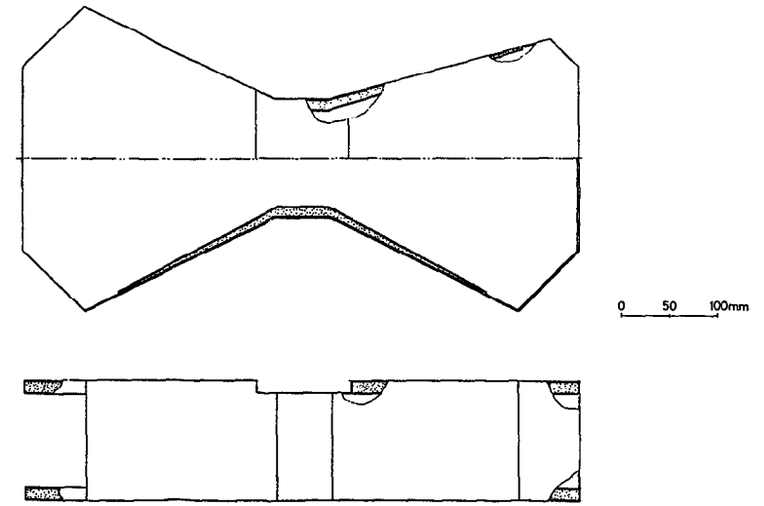

Fig. 5 B_4C decoupler for polyethylene moderator at ambient temperature

The ambient temperature polyethylene moderator is decoupled from the reflector by a B_4C plate as shown in Fig. 5. The moderator fits into an alminium drawer in the B_4C decoupler. The cryostat which accomodates the cold moderator is installed within a cadmium decoupler with an air gap of only 2 mm.

Finally the whole assembly is attached to a movable shield plug (see Fig. 6). The target station is inserted into the biological shield as illustrated in the photo picture. After the target station has been inserted in the center of the biological shield, the target itself is introduced through the proton beam tube (target guide), using the device described in section 5.

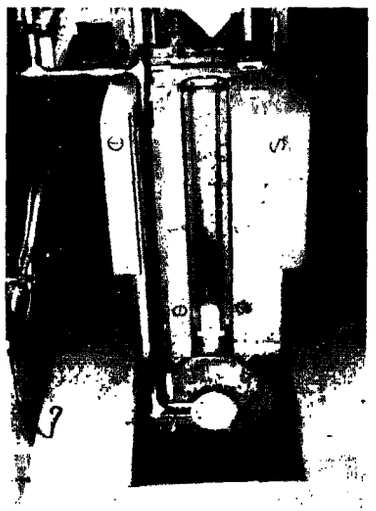

Fig. 6 Target-moderator-reflector assembly on movable shield plug

2. Proton Beam Profile

The first beam of 500 MeV protons from our booster accelerator was successfully delivered to the KENS target on June 18, 1980. The final position and profile of the proton beam at the front of the target were measured by an activation detector of sectioned paper which utilizes $^{12}C(P, P'n)\ ^{11}C$ reaction. After irradiation the paper was cut into small pre-determined sections and the beta activity of each piece was measured by a GM counter with aid of a sample changer. This method has been found to be both precise and convenient. The measured profiles of the proton beam at the target are illustrated in Fig. 7 (in this case, the horizontal position deviated somewhat from the center of the target). A contoured picture of the beam spot may also be seen in Fig. 6 of Ref 1. The beam spot is quite large due to emittance degradation at a beam window located at about 5 m up-stream from the target. The full width of the beam was 3.6 cm in horizontal direction and 3.1 cm in vertical direction, which is somewhat larger than expected.

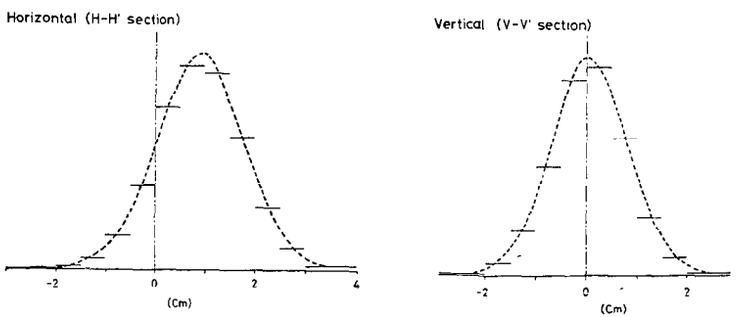

Fig. 7 Proton beam profile in front of neutron target

3. Performance of the KENS Target-moderator-reflector System

3.1 Energy Spectra

The energy spectra of neutrons emanating from both the ambient and cold moderators were measured at the exits of the beam tubes by means of the scattering from vanadium. Figure 8 shows the measured spectrum for neutrons from the polyethylene moderator at ambient temperature. The epithermal region exhibits $E^{-0.88}$ rather than 1/E behaviour because the moderator is heavily decoupled.

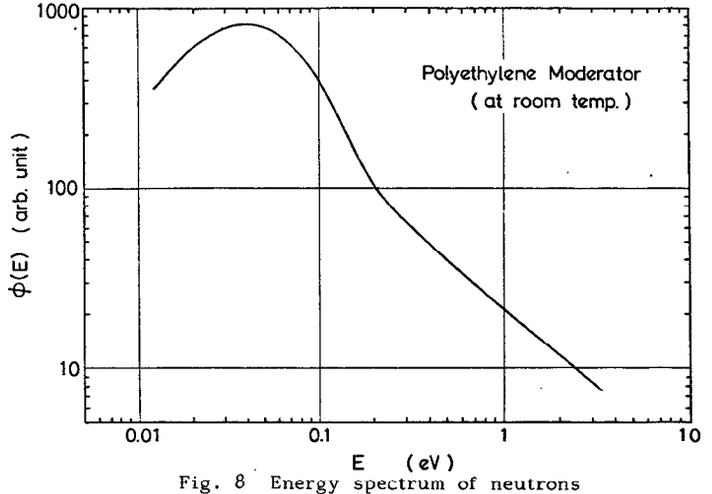

Fig. 8 Energy spectrum of neutrons from KENS polyethylene moderator at ambient temperature

The measured neutron spectrum from the solid methane moderator at 19.7 K is displayed in Fig. 9 in comparison with the results for a similar cold moderator at Hokkaido University[2]. The latter has dimensions 25 cm^W x 25 cm^H x 5 cm^T and is embedded in a graphite reflector decoupled by cadmium. The build-up of cold neutrons in our moderator is less than in that at Hokkaido by a factor of about 1.5 due to higher backling of our cold moderator.

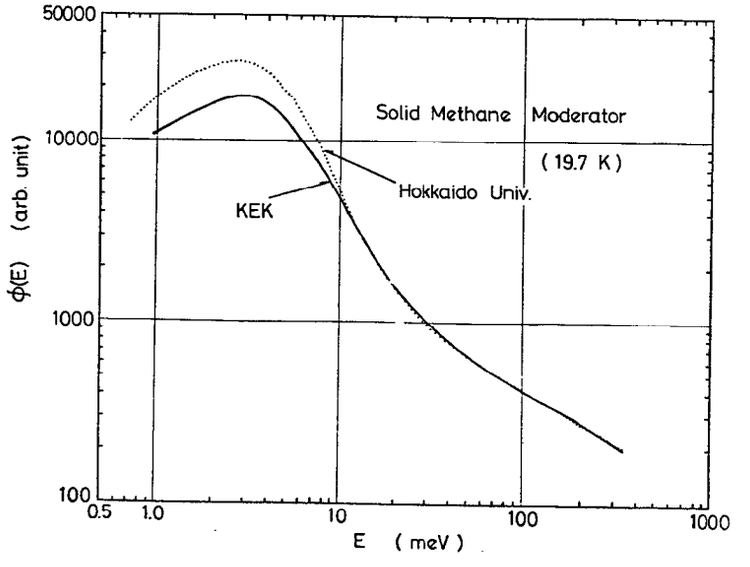

Fig. 9 Energy spectrum of neutrons from KENS cold moderator

3.2 Conversion Efficiency, Coupling Efficiency

The conversion efficiency of protons to thermal neutrons ($n_{th} \cdot str^{-1} \cdot p_f^{-1}$) and the coupling efficiency between target and moderator ($n_{th} \cdot str^{-1} \cdot n_f^{-1}$) in the target-moderator-reflector system are the two most important parameters of pulsed neutron source. The absolute intensities of the KENS neutron beams were measured by the activation of gold foils with and without cadmium covers[3]. The results are summarized in Table I in terms of the conversion and coupling efficiencies and in comparison with the results from other laboratories. The measured values for our compact system turned out to be fairly high. For example, the coupling efficiency of our 300 K polyethylene moderator is almost 2 times higher than that of a system of similar scale at ZING-P'[4]. The value of the

Table I Comparison of Conversion Efficiency and Coupling Efficiency of the Pulsed Spallation Sources

	Ep	Target/ Coolant	Reflector	Decoupler	Solid Methane (20 K)		Polyethylene Moderator (300 K)			
					I^{th}		I^{th}		$EI(E)\|_{1eV}$	
	MeV				$n \cdot str^{-1} \cdot p^{-1}$	$n \cdot str^{-1} \cdot n_f^{-1}$	$n \cdot str^{-1} \cdot p^{-1}$	$n \cdot str^{-1} \cdot n_f^{-1}$	$n \cdot str^{-1} \cdot p^{-1}$	$n \cdot str^{-1} \cdot n_f^{-1}$
KENS	500	W/H_2O	Be							
Cold				Cd	3.1×10^{-2}	3.9×10^{-3}				
Normal				B_4C			2.2×10^{-2}	2.7×10^{-3} *	5.26×10^{-3}	6.6×10^{-4} *
ZING-P' (ANL)	500	W/H_2O	Be	B_4C					2.62×10^{-3}	3.3×10^{-4} *
SNS Mock-up (Rutherford)	720	U/D_2O	Graphite	B_4C			1.74×10^{-2} **	7.4×10^{-4}	2.9×10^{-3} **	1.21×10^{-4}

* Assuming 8 neutrons per proton

** Assuming 23.5 neutrons per proton

coupling efficiency appears even more favourable when compared with larger systems such as the SNS Mock-up[5]. The coupling efficiency for our cold moderator is higher by a factor of 1.4 than that for the 300 K polyethylene moderator because the decoupler for the former is made of cadmium. The distance between the center line of the target and the bottom of the solid methane moderator is 4.8 cm, while the corresponding distance for the 300 K polyethylene moderator is 3.6 cm. The emanating surface of the solid methane moderator is only 87 cm^2 because the beam window of the beryllium reflector which views the brightest part of the moderator surface is 10 x 8.7 cm^2. The present value of the coupling efficiency was as expected from our mock-up test.

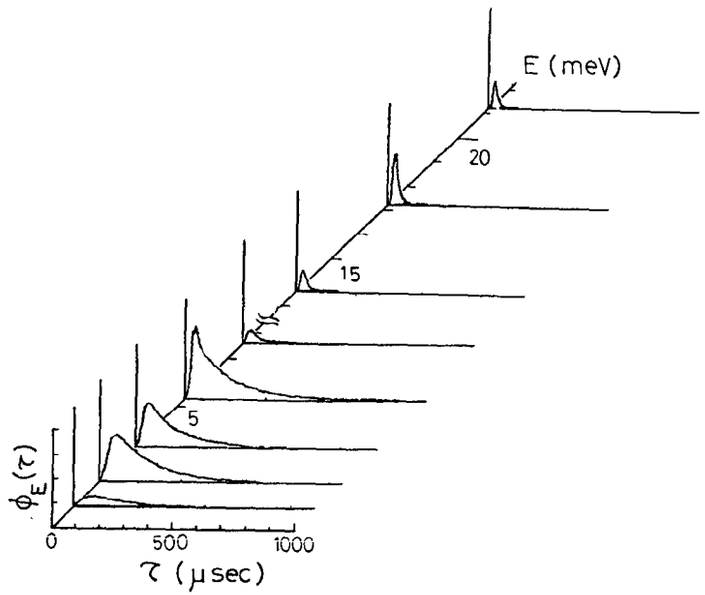

Fig. 10 Time distribution of neutrons from solid methane moderator at 19.7 K

3.3 Time Distribution of the Neutron Pulse

The time distributions of neutrons at various energies were monitored by Bragg diffraction from a mica single crystal in back scattering mode. A typical result obtained for the solid methane moderator at 19.7 K is displayed in Fig. 10. We found that the FWHM of the pulse is approximately given by 22 $\lambda(A)$ μsec. A preliminary measurement for the 300 K polyethylene moderator was also performed, but the accuracy of the data in the epithermal region were rather poor and an improved measurement is therefore required.

4. Biological Shield

The KENS biological shield was designed so as to satisfy the following two criteria

(1) The maximum dose equivalent rate at the surface of the bulk shield in the horizontal direction should be less than 0.8 mrem/hr.

(2) The annual dose equivalent at the nearest site boundary (about 350 m from the source) should be a small fraction of the natural background radiation, since existing facilities on the site has already produced an appreciable radiation intensity.

The design studies for the biological shield was reported in Ref. 6.

Horizontal and vertical cross-sectional views of the KENS shield as constructed are displayed in Fig's 11(a) and (b). It is composed of a fixed heavy concrete shield and several movable blocks made of iron and heavy concrete. The thicknesses of the bulk shield are 3.65 m (at least 1.25 m iron and 2.4 m heavy concrete (ρ = 3.5 g/cm^3))

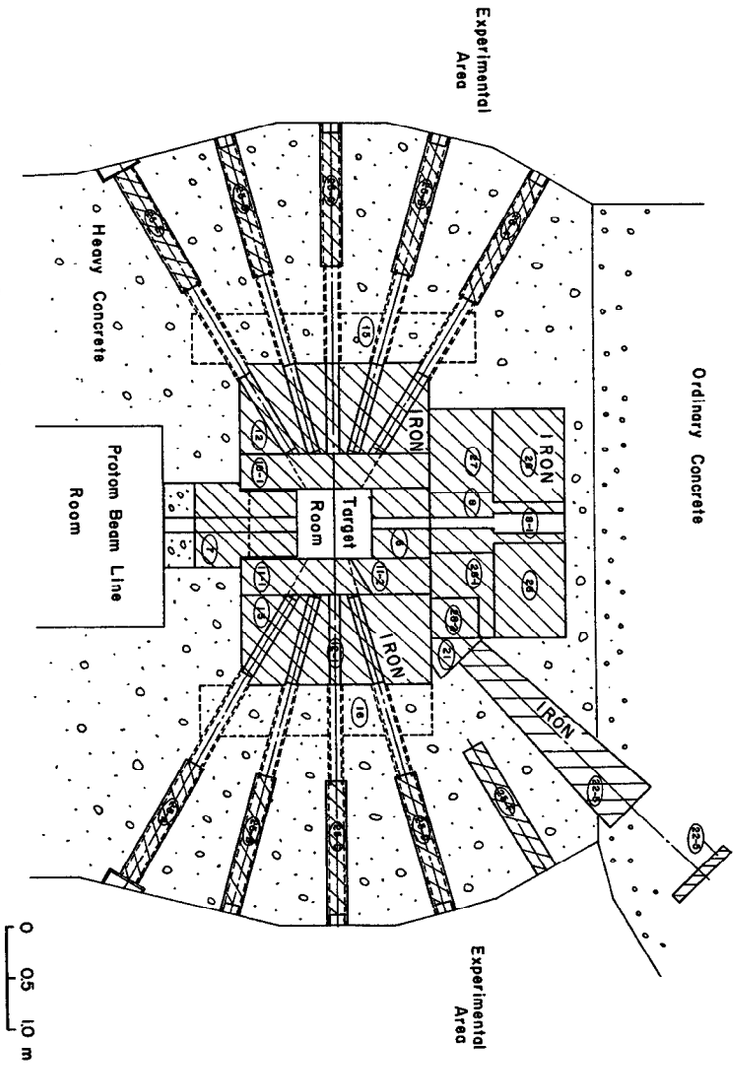

Fig. 11 (a) KENS biological shield (horizontal)
Iron blocks 12-1 are beam shutters

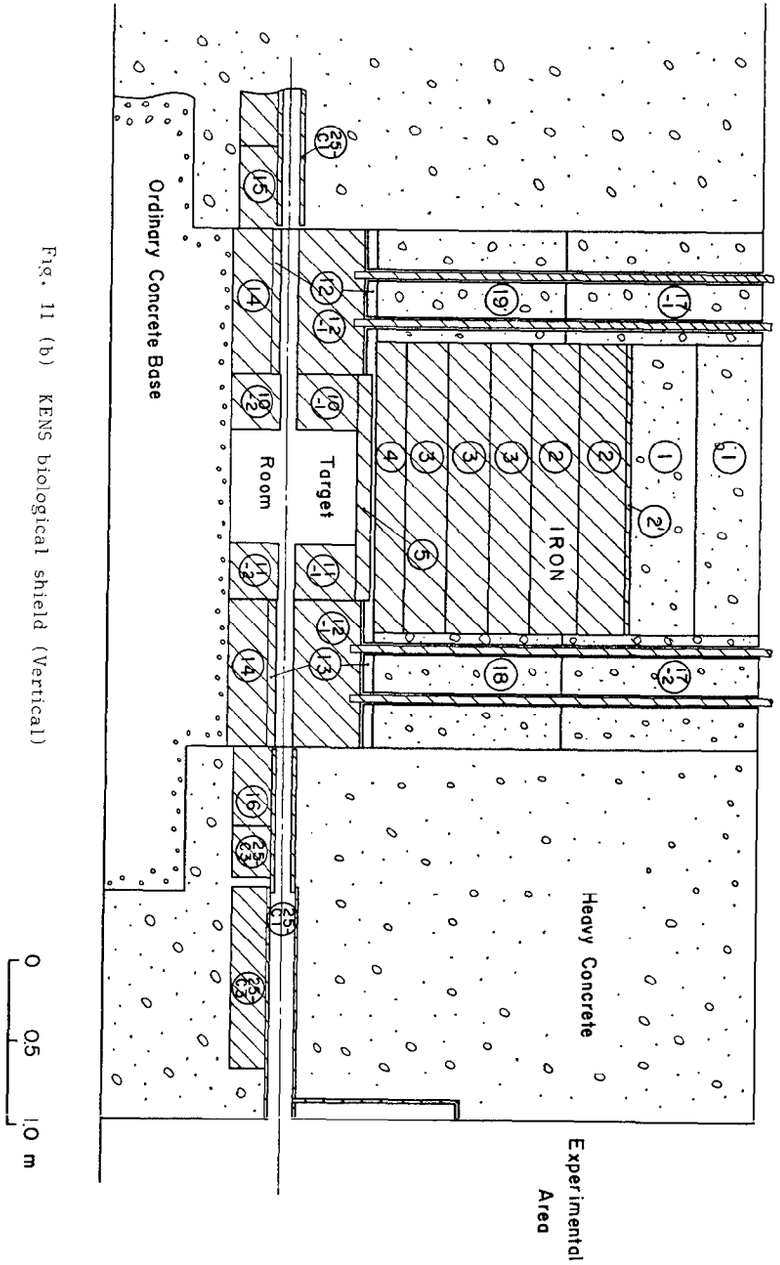

Fig. 11 (b) KENS biological shield (Vertical)

in the horizontal direction and 2.45 m vertically (inner 1.55 m of iron and outer 0.8 m of heavy concrete). These thicknesses correspond to 13 and 11 attenuation lengths for high energy neutrons respectively.

The neutron beam pipes which are square in section and made of iron are embedded in the bulk of the shield just above and below the target level. In this configuration, an appreciable portion of the shield thickness around the beam tube is missing. Additional iron blocks are therefore embedded above or below the beam tubes which view the upper (cold) and lower (ambient) moderators respectively (block number 15, 16 and 25-c-3 in Fig. 11(b)).

A beam shutter is installed in the inner section of each beam tube to prevent the neutron beam from entering the experimental area when the beam is not used or when experimenters need to approach the beam line. The shutter consists of an iron block of dimension 12 cm^W x 45 cm^H x 90 cm^L haused within a shutter casing. The height of the shutter block was chosen such that the height of the air gap necessary to allow shutter movement would not cause a serious short-fall in the shield for people working around the bulk shield.

Square alminium pipes are mounted within the beam pipes to form evacuated paths and inner iron collimators are then inserted into these pipes.

The performance of the KENS shield was monitored during actual operation and the radiation levels were found to be very close to the design values. Further details of the measured performance of the shielding are given elsewhere in this proceedings (Ref. 7).

5. Handling Devices for Active Target and its Surroundings

5.1 Target Cask

A lead cask for remote target handling is located in front of the movable shield plug which accomodates the target-moderator-reflector assembly. The proton beam is fed to the target through a large rectangular hole in the cask. Photographs of the cask are shown in Fig. 12. For target removal, a section of the beam transport tube is removed, and the couplers for the target coolant are released. The target and part of the water cooling system may then be withdrawn under motor drive towards the up-stream direction. The cask is equipped with motor-driven shutters at each end of the hole. A special mechanism is installed in the cask so that the position of the target can be adjusted with respect to both the hole in the cask and the target guide pipe of the target-moderator-reflector assembly.

5.2 Handling Device for Cold Neutron Source

A remote handling device for the installation and removal of the cryostat for the cold neutron source was constructed as illustrated in Fig. 13. By this device the cryostat together with part of the helium transfer tube can be mounted (or removed) on the target-moderator-reflector assembly within an accuracy of 2 mm with the aid of the guide pins shown in the photo. The device will be handled by a remote crane which is currently under construction.

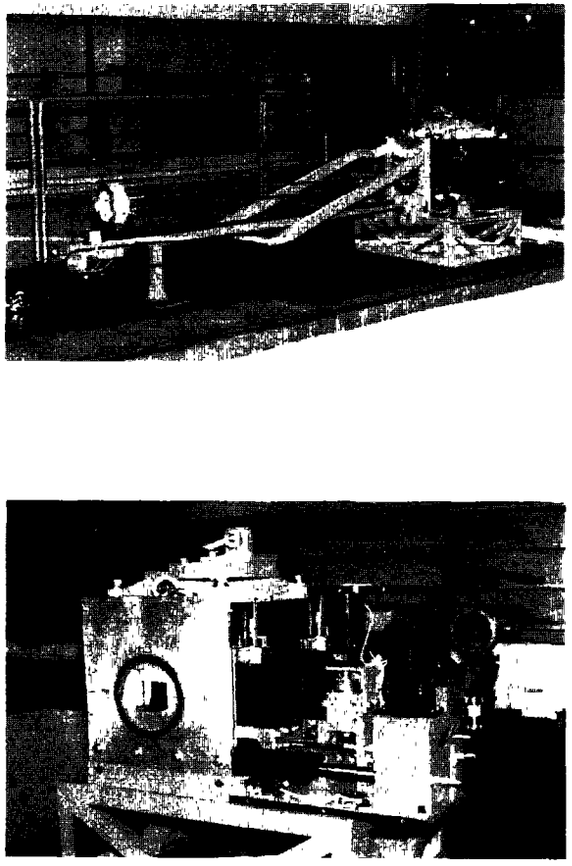

Fig. 12 KENS target cask

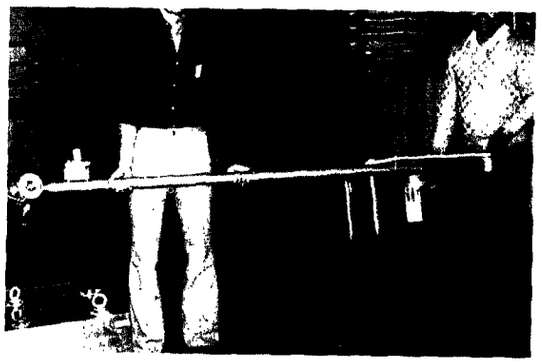

Fig. 13 Handling device for cold neutron source. Lower photograph shows the cryostat with guide pins and helium transfer tube.

5.3 Handling Device for the Assembly

A photograph of the device which has been constructed to allow the target-moderator-reflector assembly to be mounted or dismounted from the movable target shield plug is shown in Fig. 14. The remote crane will also be used to handle this device.

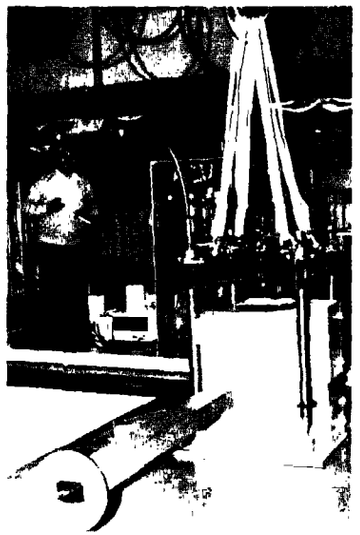

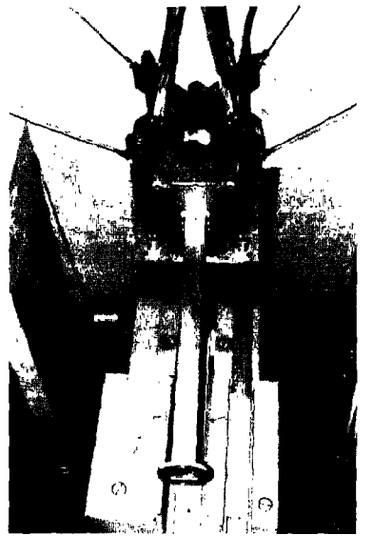

Fig. 14

Acknowledgments

KENS project required over three years to design and construct the target station and a large number of people made significant contribution to the project. The authors wish to acknowledge all the persons who contributed it. One of the author, N. Watanabe would like to express his sincere gratitude to Dr. M. Misawa,

Dr. N. Niimura and Dr. K. Yamada for assisting with design of the target station, and his deepest thanks to Prof. K. Katoh, Dr. H. Hirayama and Dr. S. Ban for their sincere advices concerning the shielding design.

The authors wish to acknowledge Prof. H. Sasaki and Prof. K. Inoue who discussed the various aspects of the work with authors. Thanks are also due to many colleagues, especially Prof. S. Yamaguchi, Prof. T. Mizoguchi, Dr. S. Tomiyoshi, Dr. Y. Fujino, Dr. K. Kai, Dr. Y. Kiyanagi, Dr. I. Kawada, Dr. F. Okamura, Dr. M. Isobe, Mr. H. Iwasa, Mr. M. Suzuki and Mr. M. Sato who contributed to the construction and alignment of the target station.

References

1) Y. Ishikawa : Present Status of the KENS Facility, Proc. ICANS-IV (1981).

2) K. Inoue : Private Communication

3) S. Ban and H. Hirayama : Private Communication (Measured data on the neutron beam by the activation of the gold foil)

4) J.M. Carpenter, D.L. Price and N.J. Swanson (Compiled) : IPNS, ANL-78-88 (1978) p-123.

5) B.C. Boland, A. Carne, G.C. Stirling and A.D. Taylor : Spallation Target-Moderator-Reflector Studies on Nimrod, Rutherford Laboratory Report RL-78-070 (1978).

6) N. Watanabe, K. Katoh and R.H. Thomas : Shielding Design for KENS, KEK Report, KEK-78-7, Note 6 (1978).

7) S. Ban : KENS Radiation Shield, Proc. ICANS-IV (1981).

KENS COLD NEUTRON SOURCE

S. Ikeda, Y. Ishikawa* and K. Inoue**

National Laboratory for High Energy Physics, Tsukuba,
*Department of Physics, Tohoku University, Sendai
and **Department of Nuclear Engyneering,
Hokkaido University, Sapporo.

§1. KENS Cold Neutron Source

This paper summarizes the experimental results obtained during stationary operation of the KENS cold neutron source over a period of about three months.

A side view of the cold neutron source as finally constructed is shown in Fig. 1. The moderator dimensions of $120^W \times 50^D \times 150^H mm^3$ were determined from the results of a mock-up experiment performed in 1978[1]. The moderator case of pure aluminum is 4 mm in thick except for the wall behind the surface from which the cold neutrons are extracted. This wall has a greater thickness of 7 mm in order to increase the moderator cooling efficiency. The separation between the bottom of the moderator case and the upper surface of the target is only 17 mm. The heat exchanger consists of a Cu block which is suspended from the top of the cryostat by a thin stainless steel rod. The total height of the cryostat is 290 mm and the moderator section is surrounded by Be reflectors decoupled by Cd sheets. The complete cold neutron source assembly consists of separate systems for cooling, methane gas circulation, vacuum pumping and safety

control. A PGH-105 cryo-generator with a cooling power of 40 W (at 15 K) is used to cool He gas which is then transferred to the heat exchanger through a 7 m long transfer tube. The temperature of the He gas can be controlled to some extent by a heater inserted in the cryo-generator. Details of the safety control system were already been described in a previous report[1].

§2. Moderator Cooling and Nuclear Radiation Heating

The temperature of cold moderator could be reduced from ambient to 16.8 K in about two hours. By this rapid cooling, however, all the methane gas in the reservoir tank could not be condensed into the moderator case. The moderator case temperature was controlled to be around 100 K by the heater until all the methane gas in the reservoir tank was liquified, followed by further cooling to the lowest temperature. The cooling process which is now usually followed is illustrated in Fig. 2. The temperature of the methane is monitored by a hydrogen pressure thermometer placed inside the moderator. At the lowest temperature of 16.8 K, the temperature of the moderator remains constant to within ±0.15 K as shown in Fig. 3.

The moderator temperature was found to rise by one degree, when the full proton beams (4.8×10^{11} ppp x 38 p/2.5 sec) is incident on the target, as illustrated in Fig. 3. The amount of heat deposited inside the moderator by nuclear radiation was estimated from the decrease in moderator temperature with time after the irradiation was ceased. Let us suppose that the constant heat q (watt) is generated inside the moderator by the irradiation and that, under equilibrium conditions, the created heat flows to the heat exchanger on the moderator case through a connecter with thermal conductance $\bar{K}$.

After cessation of an irradiation, the temperature variation of the methane moderator $\Delta T(t)$ is then given by the following differential equation

$$q = \bar{K} \cdot \Delta T + C \frac{d(\Delta T)}{dt} , \qquad (1)$$

where C is the heat capacity of the methane moderator. The variation of heat loss by thermal radiation can be neglected because it is less than 10^{-4} watt/K at 20 K. A solution of equation (1) is the relation

$$\Delta T = g(1-e^{-ht}) , \qquad (2)$$

with $g=q/\bar{K}$ and $h=\bar{K}/C$.

Values of g=1.0 K and $h=1.44 \times 10^{-3} s^{-1}$ were then determined by simple analysis of our experimental results as displayed in Fig. 4. The heat capacity C is given by $C=P_0 V C_0$ where P_0 and C_0 refer to the density and specific heat of solid methane at 20 K, respectively and V is the volume of the moderator.

Using the values of $P_0=0.522\ g \cdot cm^{-3}$, $V=900\ cm^3$ and $C_0=1.59\ J \cdot g^{-1} \cdot K^{-1}$ the heat capacity was estimated to be $747\ J \cdot K^{-1}$ and the heat q deposited by irradiation was therefore calculated as $q=g \cdot h \cdot C=$<u>1.2 watt</u> for 7.3×10^{12} proton/sec. This result is in good agreement with the value estimated from the mock-up experiment[1].

§3. Energy and Time Spectra of the Emitted Cold Neutrons

Cold neutron energy spectra for the two different moderator temperatures of 20 K and 30 K were determined by measuring the TOF

spectrum of the incoherent elastic scattering from a Vanadium metal sample. (Fig. 5) The spectra have maxima at 3.0 meV (35 K in neutron temperature) and at 3.5 meV (41 K) for the moderator temperatures of 20 K and 30 K respectively. The disagreement between the moderator and neutron temperatures suggests that the size of the KENS cold neutron source is insufficiently large to moderate completely the incoming spallation neutrons. The relationship between the size of the moderator and the descrepancy between the neutron and the moderator temperatures were examined using data from the cold neutron sources of KUR[2] and Hokkaido University[4] as well as that at KENS. (Fig. 6) The figure clearly indicates that the neutron temperatures from the thin moderators of KENS or Hokkaido Univ. are higher than those from the thicker moderator of KUR.

The time spectra of emitted cold neutron at selected neutron energies were also determined by measuring Bragg diffraction from a mica crystal. The crystal was placed at a distance of 7 m from the source and the detector was fixed at a angle $2\theta_B = 160°$. Five diffraction peaks with different indices were observed from which the time spectra corresponding to five different incident neutron wavelengths were determined. The observed pulse shape is characterized by three parameters α, β and γ as shown in Fig. 7. The rise time, β, is defined as the interval between the times at which $0.1(t_1)$ and $0.9(t_2)$ of the peak intensity is found. The decay time, α, is obtained from the exponential decay of the pulse after it passes the maximum. The third parameter, γ, is the full time width at half maximum. The values for these parameters which were determined at the five different incident neutron energies are plotted against neutron energy and wavelength in the lower part of the figure 7. The rise

time β is found to increase linearly with the wavelength λ. The pulse time width, γ, appears to be proportional to the neutron energy E, and it has an approximate value of 100 μsec for cold neutrons with E = 5.5 meV(5 Å). The value of the decay time, α, is nearly independent of neutron energy.

§4. Radiation Damage and Induced Activity

The radiation damage induced by the spallation neutrons is a crucial question for the methane moderator. The extent of methane decomposition after one week's operation (corresponding to 52 hours of full power operation) was determined using gas chromatograph by Kondoh[3]. The methane gas restored to the reservoir tank was found to contain about 0.14% of hydrogen after the moderation of about 1.4×10^{18} spallation neutrons. The concentration of hydrogen in the methane moderator of Hokkaido University was reported to be about 7% after the moderation of about 1.8×10^{18} fast neutrons[4]. This is some fifty times larger than that found at KENS suggesting that the decomposition in the Hokkaido cold neutron source mainly occurs through γ-ray irradiation, an inevitable consequence of using an electron LINAC. The presence of tritium H^3 was also detected at 9×10^{-6} μCi/cm^3. This level is reasonably low compared with H^3 natural abundance (2×10^{-6} μCi). About 60% of the produced H^3 occurs in the form of hydrogen molecules. No other radioactive nuclei could be detected.

The induced activity of the moderator cryostat was also measured with a survey meter after a cooling period of sixty days following stoppage of the proton beam. Prior to the cooling, the cryostat had been subjected to the irradiation by about 1.4×10^{18}

spallation neutrons. The measured radio activity levels are given in Fig. 8. A maximum radiation level of 60 mR/hr was detected on the bottom surface of the cryostat which lies closest to the tungsten target. It is not yet known which materials in the cryostat are responsible for this induced activity.

References

1) Y. Ishikawa and S. Ikeda, KENS Report I (1980) 19
2) K. Sumita, EURATOM Report EUR 4954 e (1971) 287
3) K. Kondo This proceedings
4) K. Inoue Private Communication

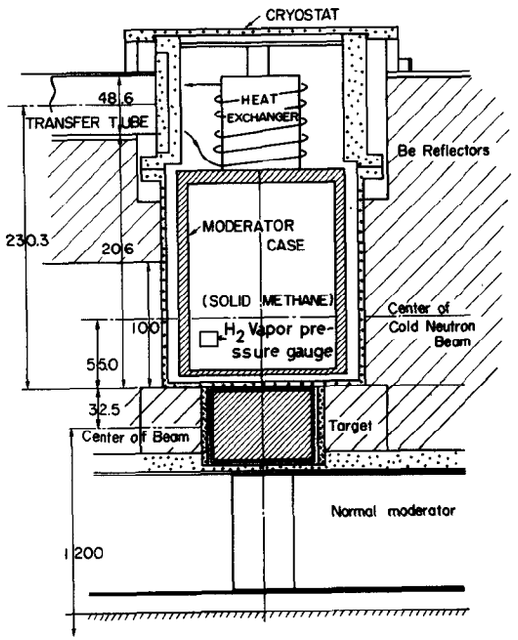

Fig. 1 Side View of KENS Cold Neutron System

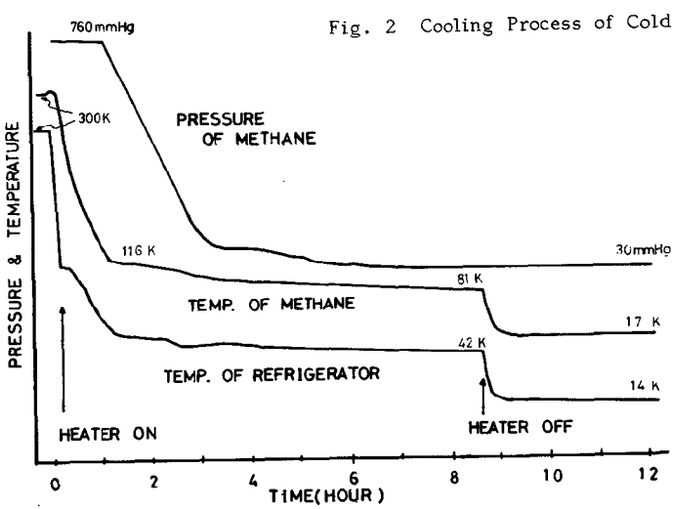

Fig. 2 Cooling Process of Cold Moderator

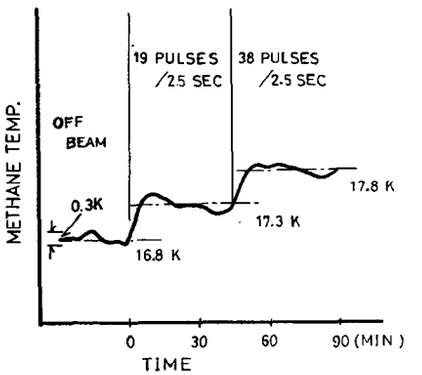

Fig. 3 Temperature Variation of Methane Moderator

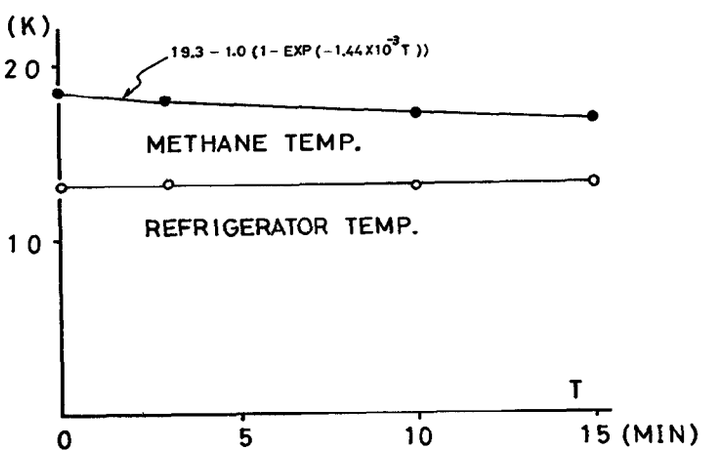

Fig. 4 Decrease in Moderator Temperature with time after Cessation of an Irradiation

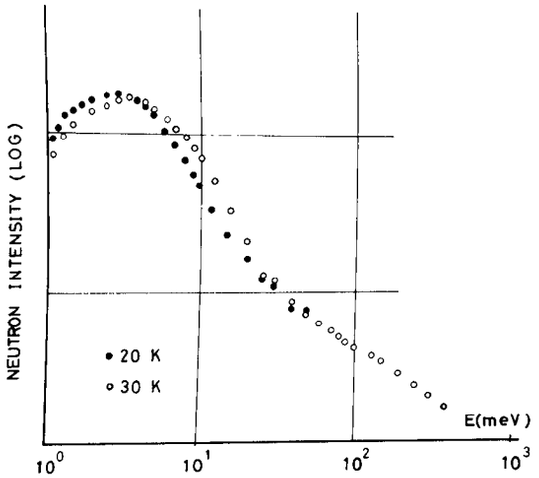

Fig. 5 Energy Spectra of Emitted Cold Neutrons

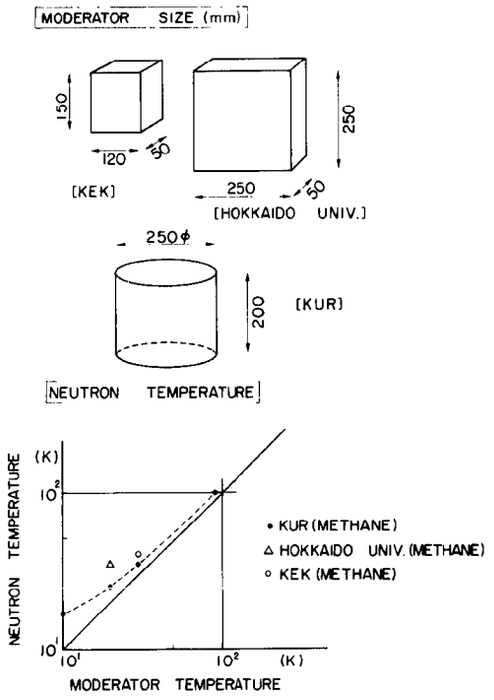

Fig. 6 Moderator Size and Neutron Temperature

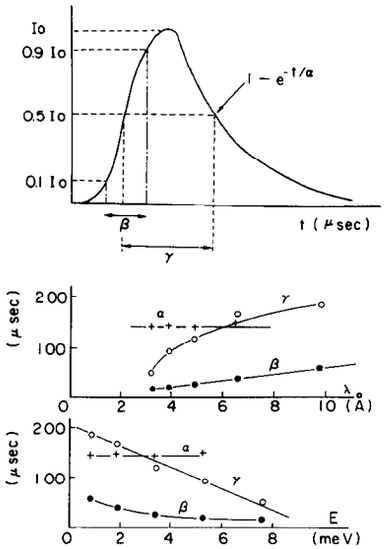

Fig. 7 Time Spectra of Emitted Cold Neutrons

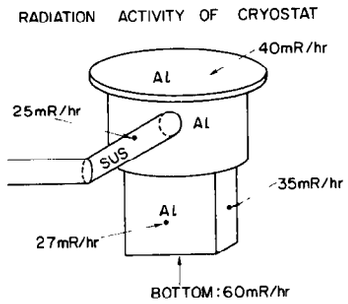

Fig. 8 Induced Activity of Moderator Cryostat

Measurements Of Spallation Target-Moderator-Reflector Neutronics At The Weapons Neutron Research Facility

G. J. Russell, M. M. Meier, J. S. Gilmore,
R. E. Prael, and H. Robinson

Los Alamos Scientific Laboratory
Los Alamos, New Mexico 87545, U.S.A.

A. D. Taylor

Rutherford and Appleton Laboratories
Chilton, Diocot, OXON OX11 OQX, U.K.

ABSTRACT

Basic neutronics data initiated by 800-MeV proton spallation reactions are important to spallation neutron source development, electronuclear fuel production, and computer code validation. We are measuring angle- and energy-dependent neutron production cross sections, neutron spectra and production from thick targets, thermal and epithermal neutron spectra and surface and beam fluxes from moderators, and fertile-to-fissile conversion yields inside thick targets. Other experiments are planned. The measurements are being done at the Weapons Neutron Research facility on a variety of targets and target-moderator-reflector configurations. The experiments are relevent to the above applications and provide data to validate computer codes.

INTRODUCTION

Several laboratories throughout the world are building and designing intense pulsed and steady-state thermal and epithermal spallation neutron sources.[1-5] There is also some interest in utilizing high-energy particle accelerators for converting fertile material to fissile material.[6] At the Los Alamos Scientific Laboratory (LASL), we have a self consistent experimental program (using 800-MeV protons) relevant to the above applications, and pertinent to validating computer codes used in these applications. The 800-MeV proton source is the Clinton P. Anderson Meson Physics Facility (LAMPF). We conduct the experiments at the Weapons Neutron Research facility (WNR)[1]--See Fig. 1.

Differential measurements provide data to test the fundamental processes and assumptions employed in the Monte Carlo computer codes used to calculate spallation reactions. Integral measurements inherently provide more complicated data because they include the effects of particle transport and secondary processes. We describe here our experimental program (see Table I for a summary) and show some preliminary results. Specific measurements underway or completed are:

- angular-dependent neutron production cross sections from 0.5-800 MeV for targets of Aℓ, Cu, In, Pb, and depleted U,
- neutron spectra (at 90°) from 0.5-400 MeV for thick Ta and W targets,
- neutron production from thick targets of W, Pb, Th, and depleted U,
- fertile-to-fissile conversion yields inside Th and depleted U targets, and
- thermal and epithermal neutron spectra, and surface and beam fluxes from moderators.

We will compare all experimental data with calculated predictions. The Monte Carlo computer codes used in our computations are the Oak Ridge National Laboratory (ORNL) code HETC[7] for particle transport $\gtrsim 20$ MeV, and the LASL code MCNP[8] for neutron transport $\lesssim 20$ MeV. Our present version of HETC does not include fission when predicting particle production from nucleon and pion collisions with a fissile nucleus. A version of HETC which accounts for the fission process in uranium will soon be released by ORNL.[9]

NEUTRON PRODUCTION AND CONVERSION MEASUREMENTS

The LASL Fertile-to-Fissile Conversion (FERFICON) program is a cooperative effort with the Canadians at the Chalk River Nuclear Laboratory. The LASL experiments provide an extension to 800 MeV of similar measurements (but more exhaustive in numbers) conducted using the TRIUMF cyclotron in Vancouver, B.C. The Canadian measurements were done at proton energies of 350 and 480 MeV. The LASL FERFICON program consists of two parts: a) the determination of neutron production from thick targets, and b) the measurement

of fertile-to-fissile conversion yields inside thick targets.

Neutron Production

To determine target neutron production, we place a target inside a 2-m-diam by 2-m-high water-bath (see Fig. 2) and measure, using an array of bare and cadmium-covered gold foils, the axial and radial neutron flux distributions in the water. We beta count the 0.0025-cm-thick foils (without chemical separation) to determine the $^{197}Au(n,\gamma)^{198}Au$ reactions, and use the cadmium ratio to correct the gold activation for resonance neutron capture. We integrate the measured flux distributions over the water-bath volume to obtain the total neutron captures in the water.

The number of protons striking the target are found by passing them through a three-foil aluminum packet located just upstream of the target. We count the central 0.025-cm-thick foil with a Ge-Li detector system and determine the number of $^{27}Al(p,3pn)^{24}Na$, $^{27}Al(p,x)^{22}Na$, and $^{27}Al(p,x)^{7}Be$ reactions. In general, the proton distributions are strongly peaked at the center and have "wings" which do not fall off as rapidly as a circular bivariate (Gaussian-type) distribution (see Ref. 10).

The targets used in the measurements (a combination of solid and clustered cylinders) are depicted in Fig. 3; details of the targets are given in Table II. All targets were stopping-length targets (long enough to range-out 800-MeV protons). The thorium and (larger) uranium targets were stopping targets since essentially no protons leaked from them.

In an applied sense, the most useful quantity is the neutron yield from the target per proton (and not the total neutron captures in the water-bath per proton). The water-bath affects target neutron production in several ways:

- There is an energy above which neutrons from the target are lost from the water-bath.
- Spallation reactions with oxygen nuclei by high-energy neutrons and protons escaping from the target produce a distributed neutron source throughout the water-bath.
- The water-bath reflects neutrons back into the target to be captured, that is, the target can act as a neutron sink.

- The water-bath reflects neutrons back into the target, and these neutrons may cause "secondary" (n,f) and (n,xn) source-type reactions, that is, the target can act as a "secondary" neutron source. These latter neutrons supplement the "primary" spallation neutrons and attendant "primary" (n,f) and (n,xn) source-type reactions which occur in the absence of the water-bath.

The first two items in the above list tend to compensate each other and are not too dependent on target material and size; the last two items can compensate each other, however, the net effect is complicated and depends on target material and size. Because of these complications, we will compare calculated neutron captures in the water-bath with measured values.

Calculated neutronics for the FERFICON bare-targets are shown in Table III. In the computations, we mocked-up the geometry of the clustered targets exactly. The low-energy, $\lesssim 20$ MeV, neutron-enhancement (ratio of low-energy leakage neutrons to low-energy spallation neutrons) is ~3% for tungsten, lead, and thorium, and ~21% for uranium. Note the number of low-energy neutron captures and fissions in the thorium and uranium targets.

We compare calculated neutronics of clustered targets with "equivalent" solid targets in Table IV. The heterogeneity effects in the clustered targets are not too great, ranging from ~1.7% for the thorium target to ~4.4% for the uranium target.

We show comparisons between our preliminary data and BNL Cosmotron results[11,12] in Table V. For comparable targets (except for the difference in target length), there is good agreement between experimental results. Our computations of water-bath neutron captures are underway; we will compute water-bath neutron captures using versions of HETC with and without fission competition during the evaporation process. As part of an effort to benchmark his new code, R. G. Alsmiller has recently computed the neutron captures in the water-bath for our uranium targets.[9] Alsmiller's results (which incorporate fission when predicting particle production for nucleon and pion collisions with a uranium nucleus) are shown in Table V. There is good agreement between our preliminary data and Alsmiller's computations.

Conversion Measurements

We will measure the axial distribution of fertile-to-fissile conversion yield (^{232}Th to ^{233}U or ^{238}U to ^{239}Pu) inside the 19-

rod thorium and 37-rod depleted uranium targets, and integrate this distribution over the target volume to obtain the total conversion yield. We will also measure the total number of fissions occuring in a target. We will determine fertile-to-fissile conversion using a Ge-Li detection system to observe the ^{233}Pa activity in the thorium target and the ^{239}Np activity in the depleted uranium target. The measured spatial conversion yield, integrated conversion yield, and total number of fissions will be compared with calculated predictions.

NEUTRON SPECTRA AND PRODUCTION CROSS SECTIONS

We have measured, at 90° to the proton beam, the neutron spectra from 0.5-400 MeV for the tantalum and tungsten production targets used in the WNR high-current target area. We have also measured angle- and energy-dependent (0.5-800 MeV) neutron production cross sections for aluminum, copper, indium, lead, and depleted uranium targets. These latter measurements were made at 0°, 30°, 45°, and 112° to the proton beam. The production cross section measurements were part of the Ph.D. thesis of S. D. Howe; he is preparing the data for publication. Preliminary results of the tantalum and tungsten neutron spectra measurements are given in Refs. 10 and 13.

Qualitatively, our neutron spectra and neutron production cross section measurements show reasonable agreement with calculations for energies $\lesssim 20$ MeV; however, the measurements are consistently higher than the calculations by factors of 2-4 for energies $\gtrsim 20$ MeV. The relatively good agreement between measured and calculated results at the lower energies is consistent with data described in Ref. 14. The underprediction of the calculations above ~ 20 MeV is consistent with other results obtained using 740-MeV protons[15], but disagree with 450-MeV proton data.[16,17] Since calculations are generally used to predict the neutron source incident on a shield, the underprediction of the neutron yields above ~ 50 MeV is relevant to shield design problems for spallation neutron sources.

THERMAL AND EPITHERMAL NEUTRON SPECTRA FROM MODERATORS

The research program utilizing the WNR high-current target

area requires thermal ($E \lesssim 1$ eV), epithermal (1 eV $\lesssim E \lesssim 100$ keV), and fast (100 keV $\lesssim E \lesssim 400$ MeV) neutrons. The tantalum (2.54-cm diam by 15.24-cm long) production target is water cooled and inside an aluminum canister. The tungsten (4.45-cm diam by 24.13-cm long) production target is water cooled and inside a stainless steel canister. The first 5 cm of the tungsten target has a tapered reentrant hole (2.54-cm diam to 1.42-cm diam). We use the water-cooled tantalum target by itself for fast neutron production, and polyethylene moderators around the tantalum target (in a hybrid slab geometry--see Fig. 4a) for epithermal neutron production. Optimum thermal neutron production is a more complicated issue.

For spallation neutron sources, a reflected moderator can increase thermal neutron beam fluxes by a factor of 2-4 over a bare moderator. There are also significant differences (factor of 2) in thermal neutron intensities between center-looking (where the field-of-view looks at the target) and offset geometry (where the target is not viewed directly). However, in center-looking geometry there can be substantial contamination of thermal neutron beams with higher-energy neutrons and charged particles; these beam-contaminants may cause unwanted background problems.

Total neutron production from a target is not necessarily a definitive indicator of resultant thermal neutron beam fluxes. A particular target-moderator-reflector configuration needs to be assessed as an integral unit relative to thermal neutron generation. We studied theoretically the neutronics of several unreflected target-moderator geometries (see Fig. 4b and Ref. 18), and will measure absolute thermal neutron production from a variety of target-moderator-reflector configurations. In addition to the unreflected hybrid slab-moderator (which was the initial target-moderator geometry installed in the WNR high-current target area[19]--see Figs. 4a and 5a), we are studying several reflected target-moderator configurations. The reflected geometries are depicted in Figs. 5b, 6a, and 6b.

The experiments are conducted in the WNR low-current target area. We measure, using bare and cadmium-covered gold foils, the absolute value of the thermal and epithermal neutron beam fluxes, and the spatial distribution of the thermal and epithermal neutron

fluxes at the surface of a moderator. We also use BF_3 and fission detectors to measure thermal and epithermal neutron spectra. Proton monitoring has been mainly done using aluminum foils. We are presently evaluating on-line methods of proton detection such as toroids and secondary emission monitors, and are calibrating these devices on an absolute basis. We present here some preliminary results from our target-moderator-reflector development program.

Reflected Wing-Moderator

The initial reflected wing-moderator studied is shown in Figs. 6a and 7. We placed the target (a cylinder of depleted uranium, 10.0-cm diam by 40.7-cm long) in a stainless steel canister. There was an air gap (~1 cm) between the uranium and the outside of the canister. The low-density polyethylene premoderator was 5.0-cm thick, poisoned with 0.076-cm of cadmium and backed with a 1.27-cm-thick high-density polyethylene moderator. The beryllium reflector was essentially a cube with ~66-cm-long sides, and was decoupled from the polyethylene by 0.076-cm of cadmium. The wing-moderator was located 2 cm from the front surface of the target.

We define the 2200 m/s neutron flux, φ_o, to be the activations in a gold foil by neutrons with energies < 0.5 eV divided by the 2200 m/s gold cross section. The Maxwellian thermal neutron flux, φ_m, is related to φ_o by Eq. (1)--Ref. 20,

$$\varphi_m = \frac{1}{g(T)} \frac{2}{\sqrt{\pi}} \left(\frac{T}{T_o}\right)^{\frac{1}{2}} \varphi_o, \qquad (1)$$

where g(T) is the non-1/v factor, T is the absolute temperature of the neutrons, and T_o = 293.6 ^oK. Some preliminary spatial distributions of φ_o at the moderator surface are shown in Figs. 8a and 8b. Note the rapid falloff of the neutron flux with distance from the target; the neutron flux in the direction of the target axis is fairly symmetric. An average $\bar{\varphi}_o$ (over ~78 cm^2 of moderator surface) is $\bar{\varphi}_o \approx 1.8\times10^{-3}$ $n/cm^2 \cdot p$.

We plan to make further measurements using the reflected wing

geometry, however, the number of moderators will be increased to four. We will study the effect, on thermal neutron beam fluxes, of varying the target material and diameter, and of altering the target-moderator-reflector decoupling. We will measure absolute thermal neutron beam fluxes, spectra, and pulse widths for both the "upstream" and "downstream" moderators.

Reflected 'T'-Shape Moderator

The layout of the flight paths in the WNR high-current target-area is shown in Fig. 9. The flight paths are clustered in groups of three, and there is a cluster in each quadrant. The reflected 'T'-shape moderator shown in Figs. 10a and 11 makes reasonable use of the existing flight path arrangement, and provides for a number of concurrent thermal neutron beam experiments. For similar moderators, the thermal neutron beam fluxes from the various "legs" of the 'T'-shape moderator are essentially the same. This is in contrast to the reflected-wing geometry with multiple moderators where factors of two in thermal neutron beam fluxes between the "upstream" and "downstream" moderators can be expected.[21] With the 'T'-shape configuration, the flight paths view the moderators in offset geometry. The premoderator-moderator concept allows each moderator to be optimized (as illustrated in Fig. 10b) for a particular class of instruments using thermal neutron beams.

We have recently installed a prototype reflected 'T'-shape moderator in the WNR high-current target area. The reflector is a composite of polyethylene and beryllium; cadmium is used as the neutron decoupler. We presently have a development program to optimize the reflected 'T'-shape moderator and reflector. We will replace the prototype 'T'-shape configuration with an "optimized" version when our studies are complete.

We have made some preliminary neutronic measurements with a reflected 'T'-shape moderator. The configuration studied is illustrated in Figs. 10a and 11. In the experiments, we are using three targets (lead, tungsten, and depleted uranium). Each target is 4.45-cm diam by 24.13-cm long. The first 5 cm of each target has a tapered reentrant hole (2.54-cm diam to 1.42-cm diam). With the exception of the reentrant hole, the targets are solid. For handling convenience, each target is encapsulated in a stainless steel tube. In addition, the depleted uranium target has a

0.076-cm-thick cadmium layer between the target and stainless steel canister. The purpose of the cadmium is to offer some neutronic decoupling between the moderator-reflector and the target. Calculated neutronics of the bare-targets are shown in Table VI. Note for the uranium target that the low-energy ($\lesssim 20$ MeV) neutron enhancement via (n,f)- and (n,xn)-type reactions is $\sim 14\%$.

The low-density polyethylene premoderator was poisoned with 0.076-cm of cadmium and backed with a 1.27-cm-thick high-density polyethylene moderator. The beryllium reflector was roughly cubic with ~ 61-cm-long sides, and was decoupled from the polyethylene by 0.076-cm of cadmium.

We constructed an experimental setup to specifically measure thermal and epithermal neutron beam fluxes and spectra; we will be adding the capability of measuring neutron pulse widths in the near future. We have made the following changes in experiment parameters and looked at the effects on thermal neutron beam fluxes and spectra:

- varied the target material (lead, tungsten, and depleted uranium),
- changed the premoderator material (polyethylene, water, and titanium hydride),
- altered the poison (cadmium and gadolinium) between the premoderator and moderator,
- varied the moderator thickness,
- used reentrant-type moderators,
- removed the moderator and its decoupler, and looked at the premoderator itself,
- changed the shadow-bar material (polyethylene, beryllium, copper, and tungsten), and
- varied the size of the reflector.

The data are being analyzed. Absolute thermal neutron beam fluxes and spectra will be reported. Results comparing the effects of using different types of targets are shown in Table VII. The calculated neutronic enhancement for depleted uranium (relative to lead and tungsten) is somewhat lower than that measured using thermal neutron beam fluxes. This may indicate a deficiency in the code package used (our present version of HETC does not

account for uranium fission), or illustrate that energy neutronic decoupling is needed between the uranium target and the moderator-reflector.

Results of moderator variation are presented in Table VIII. We found gadolinium (0.0025-cm-thick) to be superior to cadmium (0.076-cm thick) as a poison material at a given depth. A marked increase in moderation is found as the depth of poisoning is increased. However, thermal neutron beam fluxes alone are not sufficient to assess target-moderator-reflector performance; thermal neutron pulse widths are also important. The thermal and epithermal neutronic performance is degraded by increasing the premoderator thickness. (An optimization of material and thickness for the 'T'-shape premoderator and reflector will be the subject of a future study.) For the 'T'-geometry, mini-reentrant moderators produced no enhancement of the thermal neutron flux, although a significant lowering of the neutron temperature was observed. Our results for reentrant-type moderators disagree with measurements made by others.[22] However, the criteria used in all three measurements (geometric coupling, conservation of moderator thickness or mass, etc.) differed. In particular, our results may be very dependent upon which "leg" of the 'T'-shape moderator is viewed. We will continue to study thermal neutron beam fluxes, spectra, and pulse widths from reentrant-type moderators.

A sample of the raw time-of-flight data obtained with our BF_3 detector (nominally 13% efficient for neutrons of energy 0.025 eV) is shown in Fig. 12. The data are shown as neutron spectra, $\varphi(E)$, in Fig. 13. The Maxwellian temperature is ~ 380 ^{o}K. The data in Figs. 12 and 13 are for the tungsten target, a low-density polyethylene moderator, and a 1.27-cm-thick high-density polyethylene moderator decoupled by a 0.076-cm layer of cadmium, the beryllium reflector was a cube with sides ~ 61-cm long.

FUTURE PLANS

We will continue our measurements of neutron production and neutron production cross sections using other target materials and angles. Fertile-to-fissile conversion yields will be measured

this fiscal year. We will measure thermal neutron beam fluxes, spectra, and pulse widths in a continuing study of target-moderator-reflector configurations, these studies will include the effects of changing decoupler materials between the target-moderator-reflector. We will measure thin-target neutron production using bath techniques, and plan to measure neutron spectra from thick bare-targets. We will measure cold moderator neutron beam fluxes, spectra, and pulse widths. We could also measure neutron production and fertile-to-fissile conversion yields inside massive (~ 2000 kg) thorium and uranium targets. Energy deposition in spallation targets and cold moderators is another area where we could make relevent measurements.

ACKNOWLEDGEMENTS

This work was performed under the auspices of the U.S. Department of Energy. We would like to acknowledge the support and encouragement of R. Woods, and useful discussions with J. L. Yarnell, and J. S. Fraser. We appreciate the help of J. R. Baldonado and K. J. Hughes in setting up the experiments, and of P. R. Martinez for typing assistance. We acknowledge the cooperation of E. R. Whitaker, the WNR operations crew of R. D. Ryder (head), H. M. Howard, R. A. Johnson, and M. R. Lopez, and the help of the CNC-11 counting room personnel.

REFERENCES

1. G. J. Russell, P. W. Lisowski, and N. S. P. King, "The WNR Facility--A Pulsed Spallation Neutron Source at the Los Alamos Scientific Laboratory," Intl. Conf. on Neutron Physics and Nucl. Data for Reactors and Other Appl. Purposes, Harwell, England (1978).

2. L. C. W. Hobbis, G. H. Rees, and G. C. Stirling, eds., "A Pulsed Neutron Facility for Condensed Matter Research," Rutherford Laboratory report RL-77-064/C (1977).

3. J. M. Carpenter, D. L. Price, and N. J. Swanson, eds., "IPNS--A National Facility for Condensed Matter Research," Argonne National Laboratory report ANL-78-88 (1978).

4. Y. Ishikawa, ed., "KENS Report I," KEK Internal report 80-1 I/B (May 1980).

5. G. S. Bauer, ed., "Targets for Neutron Beam Spallation Sources," Jül-Conf-34, ISSN 0344-5798, Jülich (1980).

6. H. J. C. Kouts and M. Steinberg, eds., "Proc. of an Information Meeting on Accelerator-Breeding," ERDA Conf-770107, Brookhaven National Laboratory (1977).

7. K. C. Chandler and T. W. Armstrong, "Operating Instructions for the High Energy Nucleon Meson Transport Code HETC," Oak Ridge National Laboratory report ORNL-4744 (1972).

8. W. L. Thompson, ed., "MCNP - A General Monte Carlo Code for Neutron and Photon Transport," Los Alamos Scientific Laboratory report LA-7396-M (1979).

9. R. G. Alsmiller, Jr., et al., "Thermal Neutron Flux Generation by Medium-Energy (< 1.5 GeV) Protons in Thick Uranium Targets," Oak Ridge National Laboratory report ORNL/TM-7527 (1980).

10. G. J. Russell, et al., "Spallation Target-Moderator-Reflector Studies at the Weapons Neutron Research Facility," Proc. of Symposium on Neutron Cross-Sections from 10 to 50 MeV, BNL-NCS-51245, Vol. I, 169-191, Brookhaven National Laboratory (1980).

11. J. S. Fraser, et al., "Neutron Production by Thick Targets Bombarded by High-Energy Protons," Physics in Canada, Vol. 21 No. 2, 17-18 (1965).

12. P. M. Garvery, "Neutron Production by Spallation in Heavy Metal Targets," Proc. of Meeting on Targets for Neutron Beam Spallation Sources, Jül-Conf-34, ISSN 0344-5798, Jülich (1980).

13. S. D. Howe, et al., "Neutron Spectrum at 90° from 800-MeV (p,n) Reactions on a Ta Target," Proc. Conf. on Nuclear Cross Sections for Technology, Knoxville (1979) - to be published.

14. L. R. Veeser, et al., "Neutrons Produced by 740-MeV Protons on Uranium," Nucl. Inst. Meth., 17, 509-512 (1974).

15. R. Madey and F. M. Waterman, "High-Energy Neutrons Produced by 740-MeV Protons on Uranium," Phys. Rev. C, Vol. 8 No. 6, 2412-2418 (1973).

16. J. W. Wachter, W. A. Gibson, and W. R. Burrus, "Neutron and Proton Spectra From Targets Bombarded by 450-MeV protons," Phys. Rev. C, Vol. 6 No. 5, 1496-1508 (1972).

17. R. G. Alsmiller, Jr., "Calculation of the Neutron and Proton Spectra from Thick Targets Bombarded by 450-MeV Protons and Comparison with Experiment," Nucl. Sci. Engr., 36, 291-294 (1969).

18. G. J. Russell, P. A. Seeger, and R. G. Fluharty, "Parametric Studies of Target/Moderator Configurations for the Weapons Neutron Research (WNR) Facility," Los Alamos Scientific Laboratory report LA-6020 (March 1977).

19. G. J. Russell, "Initial Target/Moderator Configuration for the Weapons Neutron Research Facility," Trans. Am. Nucl. Soc., 27, 861-862 (1977).

20. K. H. Beckurts and K. Wirtz, Neutron Physics, Springler-Verglag, New York, Inc. (1964).

21. A. D. Taylor, "Neutron Transport from Targets to Moderators," Proc. of Meeting on Targets for Neutron Beam Spallation Sources, Jul-Conf-34, ISSN 0344-5798, Julich (1980).

22. G. S. Bauer and J. M. Carpenter, private communication at ICANS IV Conference (Oct. 1980).

TABLE I
PROGRAM FOR MEASURING SPALLATION TARGET-MODERATOR-REFLECTOR NEUTRONICS AT THE WEAPONS NEUTRON RESEARCH FACILITY

GENERAL GOALS

- Obtain basic data relevant to spallation neutron source development, accelerator breeder technology, and computer code validation
- 'Optimize' a target-moderator-reflector configuration for materials science research at the present WNR and any upgraded WNR
- Characterize WNR targets and moderators for nuclear physics applications

SPECIFIC OBJECTIVES

- Measure the effects of different targets, moderators, reflectors, and decouplers on thermal and epithermal neutron beam fluxes and thermal neutron pulse widths
- Ascertain the 'practical' gain of a uranium spallation target (versus lead, tantalum, tungsten, etc.) by measuring thermal neutron beam fluxes and pulse widths
- Measure the high-energy neutron and particle contamination in thermal neutron beams for offset and center-looking geometry
- Study neutron yields and pulse widths from cold moderators
- Measure neutron production and spectra from thin and thick targets
- Measure the fertile-to-fissile conversion yields inside thick targets of thorium and depleted uranium
- Measure energy deposition in spallation targets and cold moderators
- Compare all measurements with calculated predictions

TABLE II
PHYSICAL CHARACTERISTICS OF FERFICON TARGETS

TARGET MATERIAL	DENSITY (g/cm^3)	DIAMETER (cm)	LENGTH (cm)	^{235}U ENRICHMENT (wt%)
W[a]	18.26	4.45	24.13	----
Pb	11.31	9.85	40.65	----
U	18.4	10.01	40.65	0.198
Th	11.38	18.28[b]	40.65	---
U	19.04	20.09[c]	40.65	0.251

[a]The first 5 cm of the target had a tapered reentrant hole (2.54-cm diam. to 1.42-cm diam.)

[b]Effective diameter ($D = d\sqrt{n}$) for a 19 rod array with an individual rod diameter of 4.1928 cm.

[c]Effective diameter ($D = d\sqrt{n}$) for a 37 rod array with an individual rod diameter of 3.3035 cm.

TABLE IV
CALCULATED NEUTRONICS OF CLUSTERED AND SOLID BARE-TARGETS

	Th		U	
	Solid Target[a] 18.28-cm diam (n/p)	Clustered Target 19-Rod Array (n/p)	Solid Target[a] 20.09-cm diam (n/p)	Clustered Target 37-Rod Array (n/p)
LOW-ENERGY (< 20 MeV) SPALLATION NEUTRON PRODUCTION[b]	21.39±0.27	20.98±0.27	25.06±0.33	24.20±0.33
NEUTRON LEAKAGE (< 20 MeV)[c]	22.05±0.26	21.74±0.26	30.42±0.38	29.55±0.37
NEUTRON LEAKAGE (> 20 MeV)	0.97±0.02	1.05±0.02	0.71±0.02	0.79±0.02
TOTAL NEUTRON LEAKAGE	23.02±0.26	22.79±0.26	31.13±0.38	30.34±0.37
NEUTRON CAPTURE (< 20 MeV)[d]	1.51±0.02	1.32±0.02	4.44±0.06	3.72±0.06
TOTAL NEUTRON PRODUCTION	24.53±0.26	24.11±0.26	35.57±0.39	34.06±0.38
NEUTRON INDUCED FISSIONS [< 20 MeV] (fiss/p)	0.60±0.01	0.57±0.01	4.43±0.07	3.72±0.06

[a]Solid targets had an effective diameter $D = d\sqrt{n}$ where d is the diameter of an individual rod in a clustered target, and n is the number of clustered rods.

[b]Evaporation neutrons produced inside the target; fission competition with evaporation was not included in HETC.

[c]Includes net effects of (n,f)- and (n,xn)-type reactions occuring during the transport of low-energy spallation neutrons.

[d]Neutron capture occuring in a target during the transport of low-energy spallation neutrons.

TABLE III
CALCULATED NEUTRONICS FOR FERFICON BARE-TARGETS

	Solid Targets[a]			Clustered Targets[a]	
	W 4.45-cm diam (n/p)	Pb 9.85-cm diam (n/p)	U 10.01-cm diam (n/p)	Th 19-Rod Array[b] (n/p)	U 37-Rod Array[c] (n/p)
LOW-ENERGY (< 20 MeV) SPALLATION NEUTRON PRODUCTION[d]	13.15±0.16	16.12±0.20	21.37±0.27	20.98±0.27	24.20±0.33
NEUTRON LEAKAGE (< 20 MeV)[e]	13.47±0.17	16.55±0.20	25.84±0.32	21.74±0.26	29.55±0.37
NEUTRON LEAKAGE (> 20 MeV)	1.18±0.02	1.17±0.02	1.05±0.02	1.05±0.02	0.79±0.02
TOTAL NEUTRON LEAKAGE	14.65±0.17	17.72±0.20	26.89±0.32	22.79±0.26	30.34±0.37
NEUTRON CAPTURE (< 20 MeV)[f]	0.155±0.002	0.009±0.0002	1.05±0.02	1.32±0.02	3.72±0.06
TOTAL NEUTRON PRODUCTION	14.81±0.17	17.73±0.20	27.94±0.32	24.11±0.26	34.06±0.38
NEUTRON INDUCED FISSIONS [< 20 MeV] (fiss/p)	-------	-------	2.34±0.04	0.57±0.01	3.72±0.06

[a]Proton energy is 800 MeV; the W target was 24.13-cm long, and the first 5 cm had a tapered reentrant hole (2.54-cm diam to 1.42-cm diam); all other targets were 40.65-cm long.

[b]Individual rod diameter was 4.1928 cm.

[c]Individual rod diameter was 3.3035 cm.

[d]Evaporation neutrons produced inside the target; fission competition with evaporation was not included in HETC.

[e]Includes net effects of (n,f)- and (n,xn)-type reactions occuring during transport of low-energy spallation neutrons.

[f]Neutron capture occuring in a target during transport of the low-energy spallation neutrons.

TABLE V
PRELIMINARY LASL FERFICON RESULTS COMPARED TO BNL COSMOTRON DATA

	LASL FERFICON			BNL COSMOTRON[a]		
TARGET MATERIAL	LASL TARGET SIZE DIAMETER x LENGTH (cm x cm)	CALCULATED H_2O NEUTRON CAPTURES PER PROTON	MEASURED H_2O NEUTRON CAPTURES PER PROTON	BNL COSMOTRON TARGET SIZE DIAMETER x LENGTH (cm x cm)	CALCULATED H_2O NEUTRON CAPTURES PER PROTON[b]	MEASURED H_2O NEUTRON CAPTURES PER PROTON
W	4.45 x 24.13[c]		10.2	---	---	---
Pb	9.85 x 40.65		13.0	10.2 x 61.0	16.4	13.4
U	10.01 x 40.65	27.2±1.2[f]	25.3	10.2 x 61.0	23.3	26.3
Th	18.28 x 40.65[d]		17.1	---	---	---
U	20.09[e] x 40.65	28.6±0.8[f]	28.8	---	---	---

[a] Interpolated at 800 MeV (Ref. 10)

[b] Ref. 11

[c] The first 5 cm of the target had a tapered reentrant hole (2.54-cm diam to 1.42-cm diam)

[d] Effective diameter ($D = d\sqrt{\pi}$) for a 19-rod array with an individual rod diameter of 4.1928 cm.

[e] Effective diameter ($D = d\sqrt{\pi}$) for a 37-rod array with an individual rod diameter of 3.3035 cm.

[f] Ref. 9

TABLE VI
CALCULATED NEUTRONICS FOR BARE (REENTRANT) TARGETS[a]

	Pb (n/p)	W (n/p)	U (n/p)
LOW-ENERGY (< 20 MeV) SPALLATION NEUTRON PRODUCTION[b]	11.34±0.16	13.25±0.16	16.88±0.23
NEUTRON LEAKAGE (< 20 MeV)[c]	11.52±0.16	13.59±0.16	19.16±0.27
NEUTRON LEAKAGE (> 20 MeV)	1.10±0.02	1.18±0.02	1.21±0.02
TOTAL NEUTRON LEAKAGE	12.62±0.16	14.77±0.16	20.37±0.27
NEUTRON CAPTURE (< 20 MeV)[d]	0.002±0.00003	0.16±0.002	0.22±0.003
TOTAL NEUTRON PRODUCTION	12.62±0.16	14.93±0.16	20.59±0.27
NEUTRON INDUCED FISSIONS [< 20 MeV] (fiss/p)	-------	-------	1.01±0.02

[a] Targets were 24.13-cm long; the first 5 cm had a tapered reentrant hole (2.54-cm diam to 1.42-cm diam); uniform proton beam spot (1.5-cm diam).

[b] Evaporation neutrons produced inside the target; fission competition with evaporation was not included in HETC.

[c] Includes net effects of (n,f)- and (n,xn) -type reactions occuring during transport of low-energy spallation neutrons.

[d] Neutron capture occuring in a target during transport of the low-energy spallation neutrons.

TABLE VII
RELATIVE PERFORMANCE OF SPALLATION TARGETS

Target Material[a]	Ratio of Calculated Spallation Neutron Production[b]	Ratio of Calculated Low-Energy Neutron Leakage[c]	Ratio of Measured Thermal Neutron Beam Flux[d]
Pb	1.00	1.00	1.00
W	1.17	1.18	1.25
U	1.49	1.66	2.13

[a] Targets were 24.13-cm long; the first 5 cm had a tapered reentrant hole (2.54-cm diam to 1.42-cm diam); 1.5-cm-diam uniform proton beam spot assumed; 800-MeV incident protons.

[b] Low-energy (< 20 MeV) evaporation neutrons produced inside a bare target; fission competition with evaporation was not included in HETC.

[c] Leakage neutrons (< 20 MeV); includes net effects of (n,f)- and (n,xn)-type reactions occuring during transport of low-energy spallation neutrons.

[d] 'T'-shape polyethylene moderator reflected by beryllium; the uranium target was decoupled from the polyethylene moderator by 0.076 cm of cadmium.

TABLE VIII
SUMMARY OF MODERATOR SPECTRAL MEASUREMENTS

ALL DATA TAKEN WITH A TUNGSTEN TARGET AND A 'T' SHAPED PREMODERATOR SURROUNDED BY A 46 cm CUBE BERYLLIUM REFLECTOR AND DECOUPLED BY 0.076 cm OF CADMIUM.

A. 1.27 cm POLYETHYLENE MODERATOR: VARIATION OF POISON AND PREMODERATOR

MODERATOR	T[a] (meV)	J_{th}^{a}	$E\phi(E)|^{b}_{1eV}$	$J_{th}/E\phi(E)|_{1eV}$	SUB - Cd[c]
1,27 cm poisoned by Gd[d]	35	61	23	2.7	1.00
1 27 cm poisoned by Cd[e]	33	37	22	1.7	0.64
1.27 cm poisoned by Gd with additional 1.27 cm of premoderator	34	52	20	2.6	0.83

B. POLYETHYLENE MODERATORS 2.54 cm THICK AND POISONED BY Gd[d]: MINI-REENTRANT HOLE STUDY

MODERATOR	T (meV)	J_{th}	$E\phi(E)|_{1eV}$	$J_{th}/E\phi(E)|_{1eV}$	SUB - Cd
No holes	34	92	20	4.6	1.16
0.64 cm deep circular holes[f]	32	91	20	4.6	1.21
1.27 cm deep circular holes	30	81	21	3.9	1.20
1.91 cm deep circular holes	30	62	23	2.7	1.09
1.91 cm deep grooves[g]	30	76	21	3.6	1.16

C.. MODERATORS POISONED BY Gd[d] VARIATION OF POISON DEPTH

MODERATOR	T (meV)	J_{th}	$E\phi(E)|_{1eV}$	$J_{th}/E\phi(E)|_{1eV}$	SUB - Cd
0.64 cm polyethylene	42	45	25	1.8	0.89
1.27 cm polyethylene	35	61	23	2.7	1.00
1.91 cm polyethylene	34	84	21	4.0	1.13
2.54 cm polyethylene	34	92	20	4.6	1.16
Premoderator only No poison	33	237	26	9.1	2.59

[a]The apparent maxwellian temperature, T, and the maxwellian intensity, J_{th}, are determined by a fitting

$$\phi = J_{th} \frac{E}{T^2} \text{ EXP } [-E/T]$$

in the range 0 – 50 meV. See figure 20. Units are arbitrarily normalized to incident protons.

[b]The 1eV lethergy is obtained by fitting in the range 1 – 10 eV. See figure 19. Units are arbitrarily normalized to incident protons.

[c]Relative sub-cadmium fluxes normalized to the 1.27 cm, Gd poisoned moderator.

[d]0.0025 cm gadolinium foil

[e]0.076 cm cadmium sheet

[f]81 0.79 cm diameter, straight sided holes. 40% of area removed.

[g]Tapered grooves, 0.4 cm at base and top

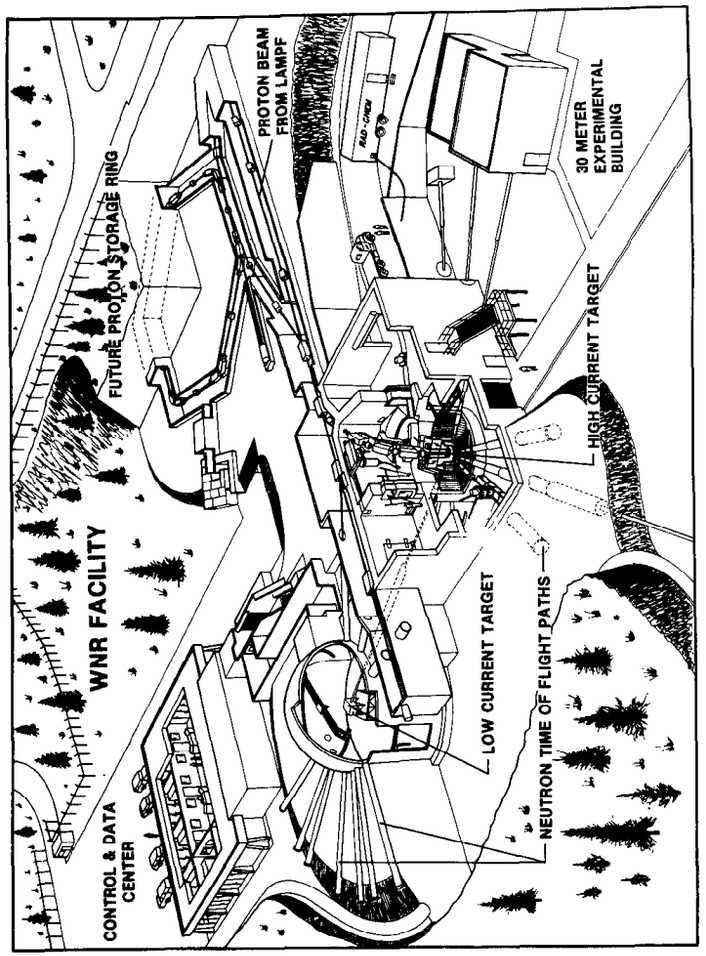

Fig. 1 General layout of the WNR showing the two target areas. The high-current target is located in a vertical proton beam and is viewed by 11 horizontal flight paths. The low-current target is located in a horizontal proton beam and viewed by 12 horizontal flight paths and one vertical flight path.

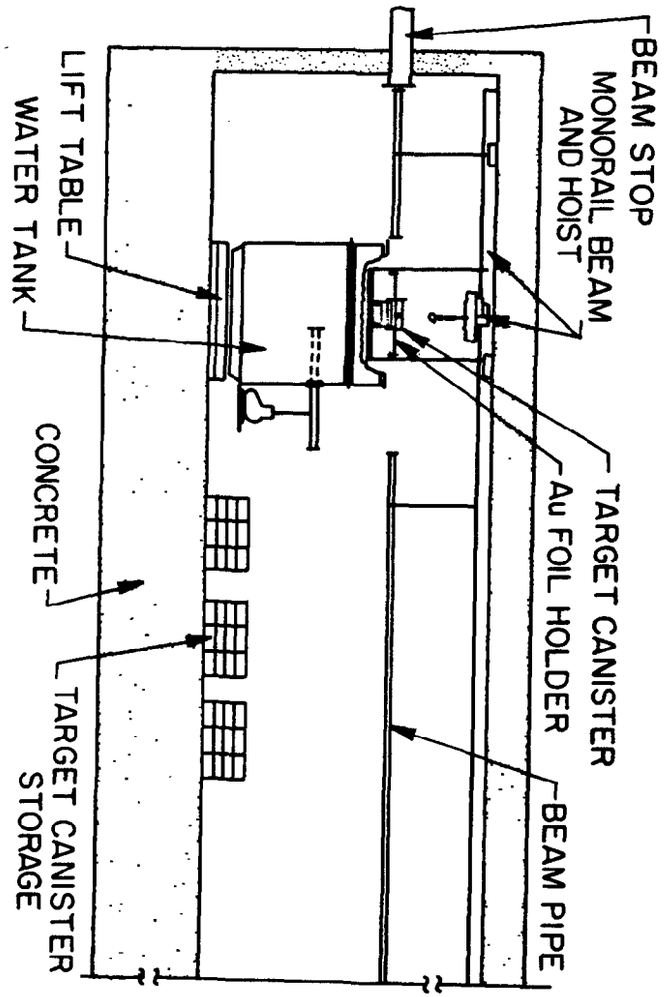

Fig. 2 Section through the WNR beam channel showing the location of the FERFICON experiment.

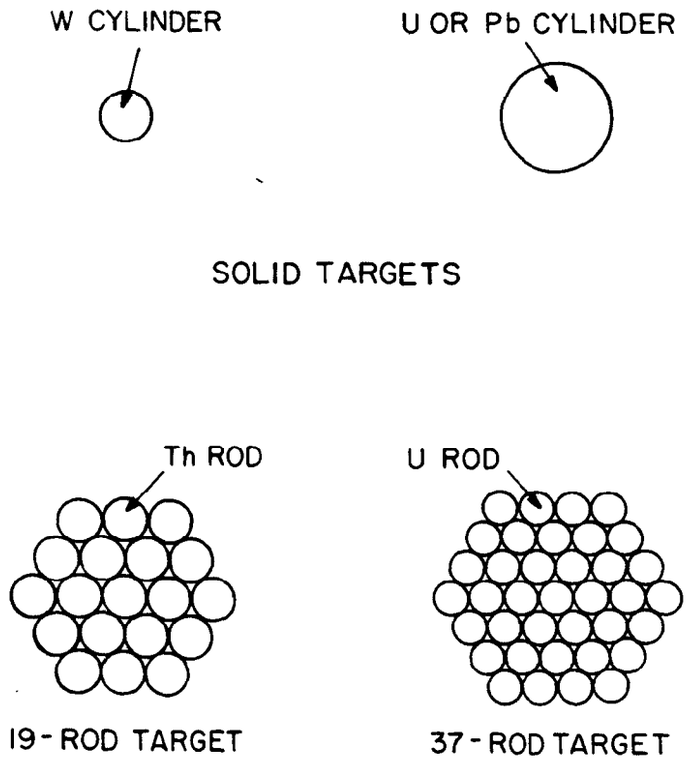

Fig. 3 Targets used in the LASL FERFICON experiments (relative sizes are as indicated).

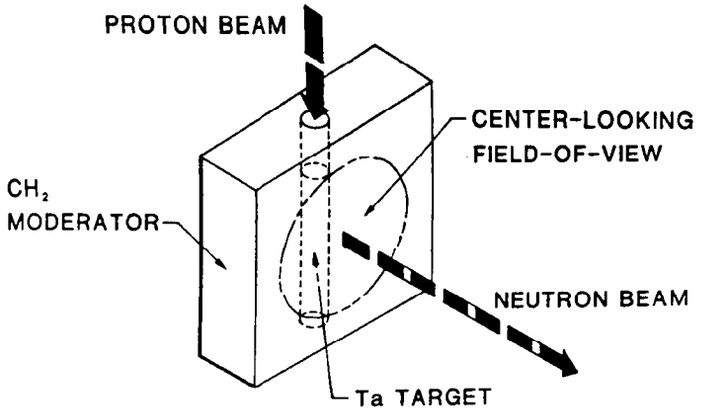

Fig. 4a Unreflected hybrid slab-moderator used at the WNR to produce neutrons with energies 1 eV $\lesssim$ E $\lesssim$ 100 keV.

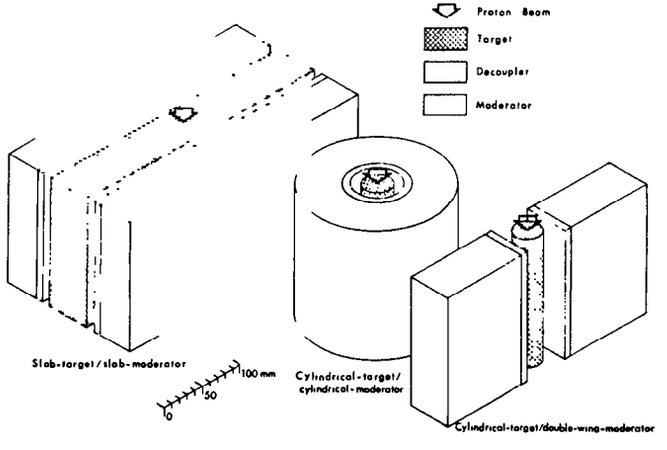

Fig. 4b Several unreflected target-moderator configurations studied theoretically.

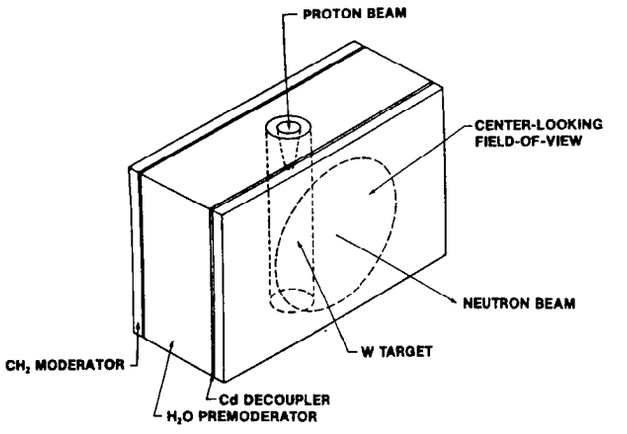

Fig. 5a Unreflected hybrid slab-moderator initially used at the WNR for thermal neutron production.

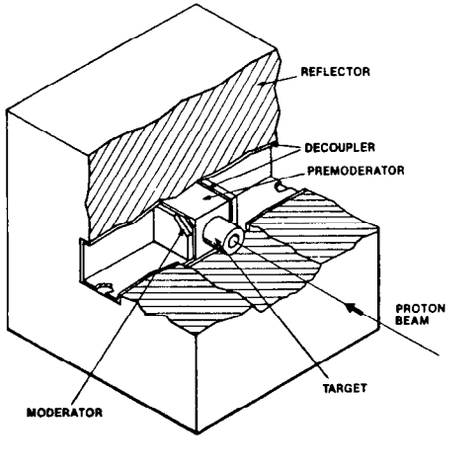

Fig. 5b This figure depicts a reflected hybrid slab-moderator; such a configuration is neutronically efficient.

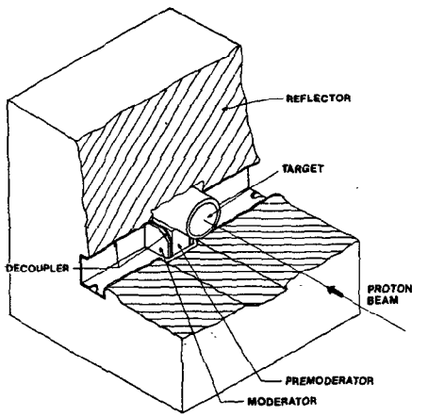

Fig. 6a This figure depicts a reflected wing-moderator. A variation of this configuration is being adopted at several pulsed spallation neutron sources around the world.

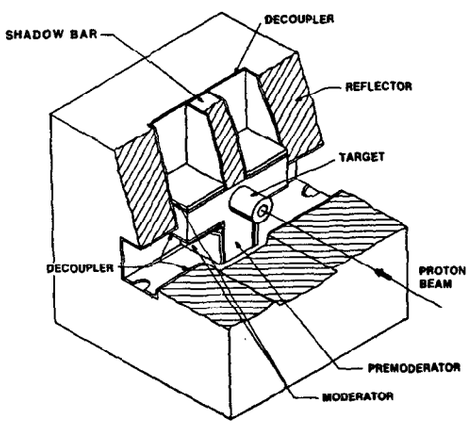

Fig. 6b This figure depicts a reflected 'T'-shape moderator. A prototype of this configuration has been installed in the WNR high-current target area.

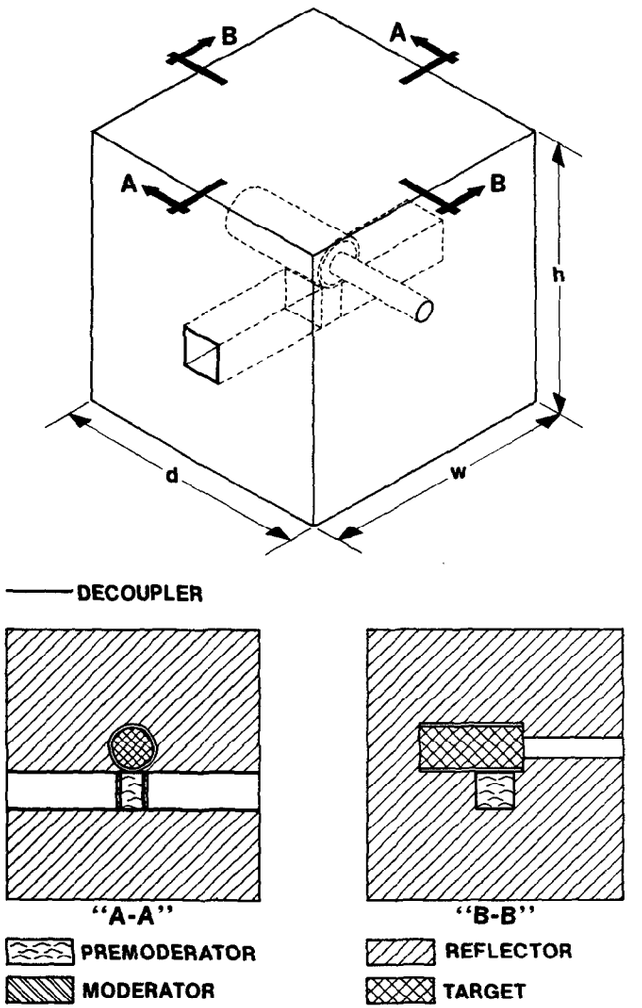

Fig. 7 Section through a reflected wing-moderator.

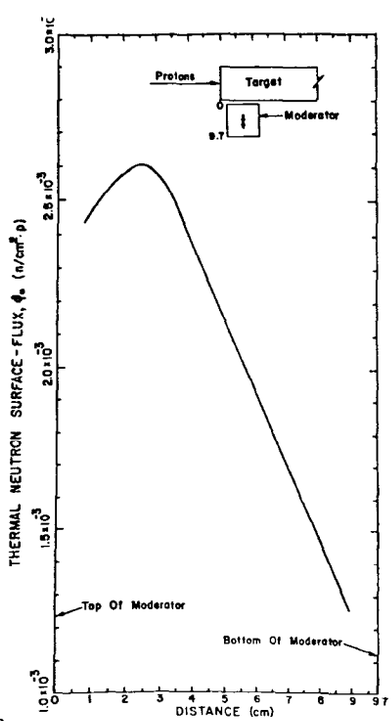

Fig. 8a

Preliminary measured 2200 m/s neutron surface flux distribution from a reflected wing-moderator (see Fig. 6a). The distribution shown lies along the vertical center of the 9.7-cm by 9.7-cm moderator surface.

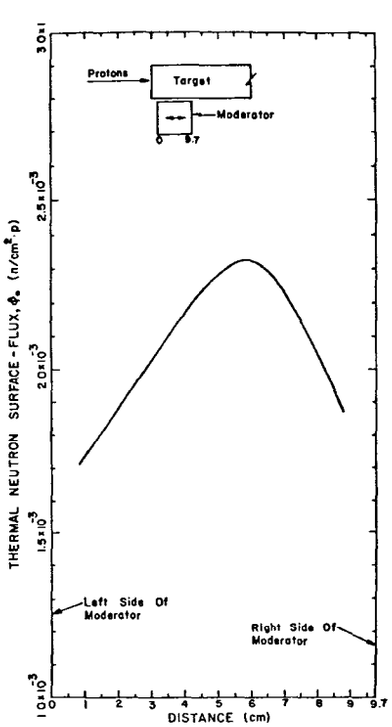

Fig. 8b

Preliminary measured 2200 m/s neutron surface flux distribution from a reflected wing-moderator (see Fig. 6a). The distribution shown lies along the horizontal center of the 9.7-cm by 9.7-cm moderator surface.

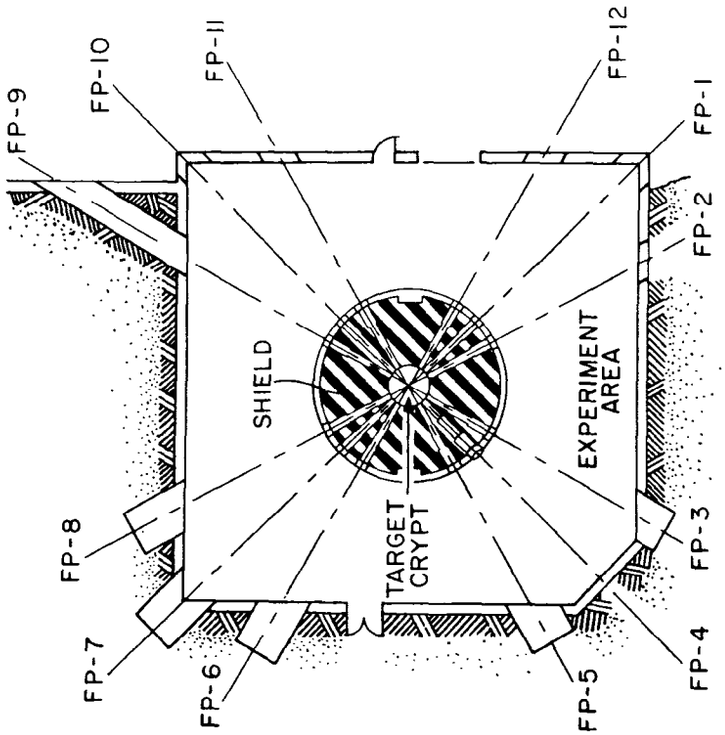

Fig. 9 Layout of the neutron flight paths in the WNR high-current target area.

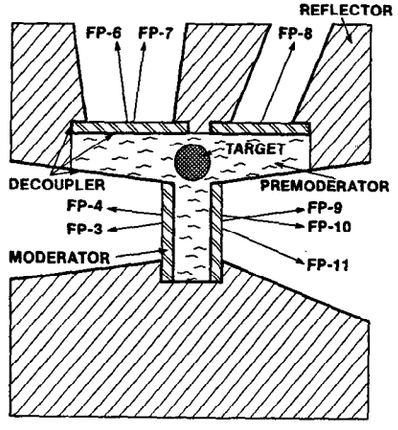

Fig. 10a Section through a reflected 'T'-shape moderator showing the location of various neutron flight paths (in the WNR high-current target area) relative to moderator surfaces.

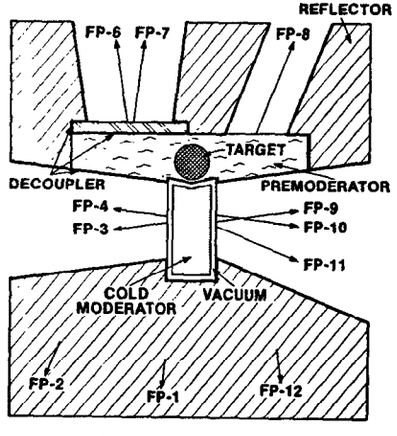

Fig. 10b Possible variation of a reflected 'T'-shape moderator which "optimizes" various moderators for each cluster of neutron flight paths.

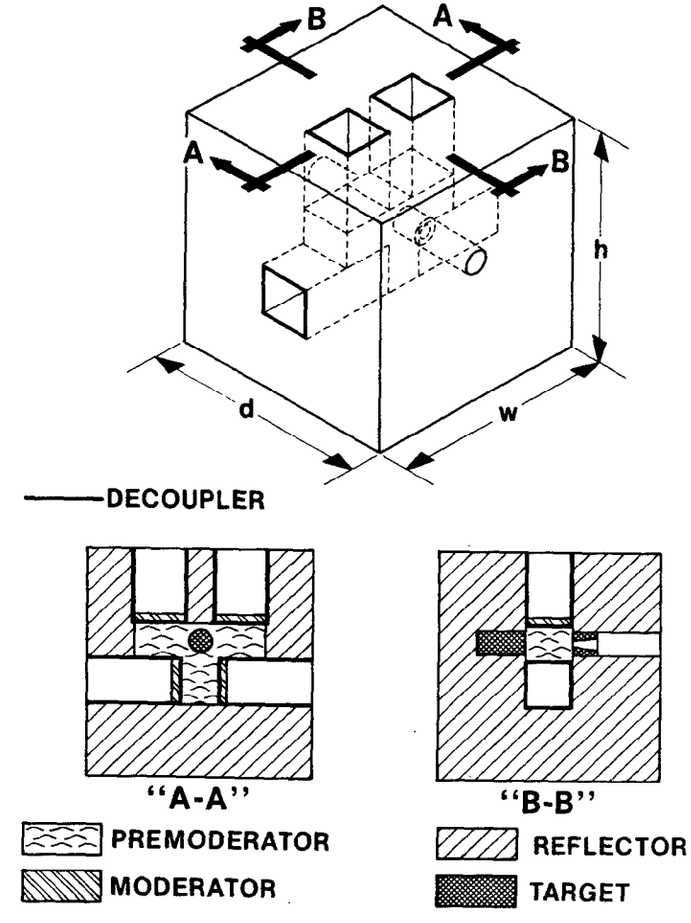

Fig. 11 Section through a reflected 'T'-shape moderator.

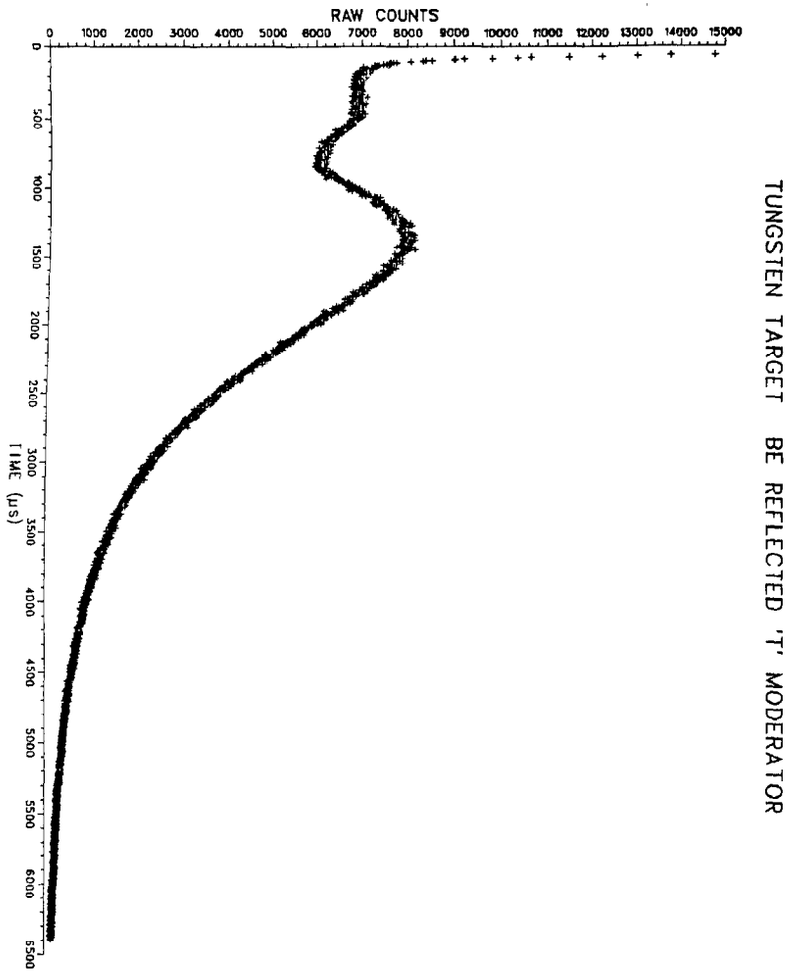

Fig. 12 Raw time-of-flight spectra obtained with a BF_3 detector.

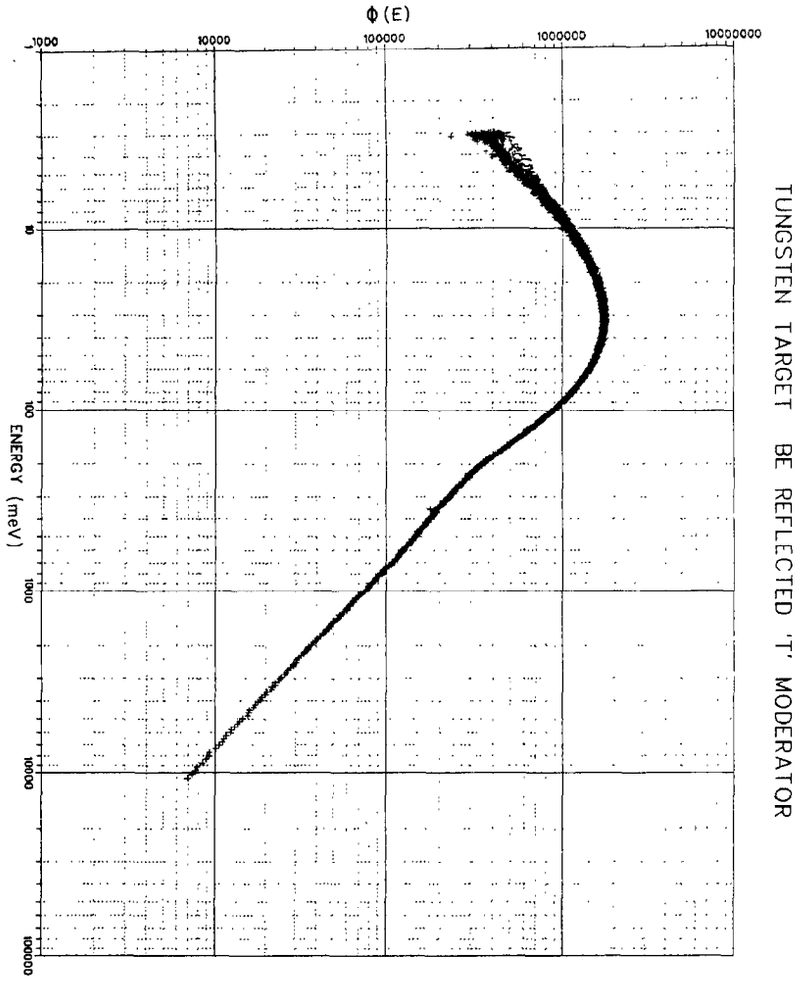

Fig. 13 Neutron spectra corrected for background and BF_3 detector efficiency.

Some General Results from a Calculation of a TRAM Assembly

F Atchison

Target Station Group, SNS Division, Rutherford & Appleton Laboratories, Chilton, Didcot, Oxon OX11 OQX, U.K.

1. INTRODUCTION

A calculation of the performance of a full target, reflector and moderator (TRAM) assembly corresponding closely to the current design to be installed, has recently been completed [1]. In this paper, a selection of some of the results of a more general nature are presented; those concerning the performance of SNS are included elsewhere in these proceedings [2].

2. THE EFFECT OF FISSION

The calculational model used for fission has been described elsewhere [3]; essentially it only makes a distinction of detail between fission induced by particles in the hundreds of MeV region compared to, for example, that induced by MeV neutrons. For this section we look at processes in the isolated target Uranium; numbers are normalised to per proton incident at the target.

2.1 Neutron Production. An approximate account of the energy interchange in the high energy cascade is shown in Table I; quantities underlined are 'known' from analysis of the particle transport whilst the rest are deduced; 'Particle' energies include a value of 7.5 MeV/nucleon for separation energy.

There are 21.4 neutrons of energy <15 MeV released, which account for ~30% of the incident proton's Kinetic energy. The entries on the second line show ~35 MeV of 239 MeV binding energy released by fission goes to create extra neutrons (~3 extra).

TABLE I: ENERGY INTERCHANGE DURING HIGH ENERGY CASCADE IN TARGET - UNITS ARE MEV/INCIDENT PROTON

	Energy Sources		Energy Sinks		
Process	Incident Protons' Kinetic Energy	Nuclear Binding Energy	Escape	Deposited as Heat	Nuclear Excitation
Ionisation loss for primary protons	230	-	-	230	-
1.3 Fissions	171	239	-	204	206
0.5 spallations	66	-	-	-	66
High Energy Escapes	315	-	145(a)	170	-
Low Energy Neutrons	-	-	237(b)	-	-237
Residual Excitation	-	-	-	18	-18
γ Production	18	-	-	18	-
Other Evaporations	-	-	7	10	-17
	800	239	389	650	0
	1039		1039		

Notes (a) Escapes from surface of target and includes 7.5 MeV/ nucleon separation energy.

(b) Escapes from nucleus and includes 7.5 MeV/nucleon separation energy.

Roughly 15 neutrons are evaporated from fission fragments due to the transfer of primary excitation energy from the intranuclear cascade. Evaporation from the lighter mass fission fragments leads to a harder neutron spectrum; Fig 1 shows the average Kinetic energy for neutrons evaporated as a function of excitation energy, from masses typical of Uranium interactions. The harder evaporation spectrum will lead to increased fissions induced by these neutrons in transport to the surface of the target; the neutron induced fission cross section for ^{238}U is shown in Fig 2.

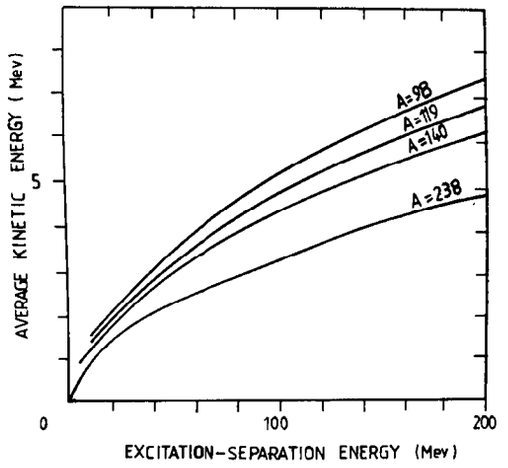

Fig 1 The average Kinetic Energy for neutrons evaporated from mass 238,140,119 and 98 AMU nuclei, as a function of excitation minus separation energy.

That is: High energy particle induced fissions increase neutron production by two distinct processes; (i) The transfer of binding to nuclear excitation energy and hence extra neutron evaporation (ii) an increase of evaporation-neutron induced fissions, because of the harder spectrum from the lighter mass of the fission fragments.

The mean energy for sub-15 MeV neutrons produced in the cascade is 3.6 MeV, whilst that of the neutrons escaping the surface of the target is ~2 MeV. The high energy end of the neutron spectrum will be responsible for inducing fissions and productive (n, xn) reactions, but will induce lower nuclear excitation energies than for instance high energy fissions and consequently (see Fig 1) have a lower average Kinetic energy.

The surface escape neutron intensity is 24.7: The extra 3.3 neutrons come from the balance of 5.5 neutrons created

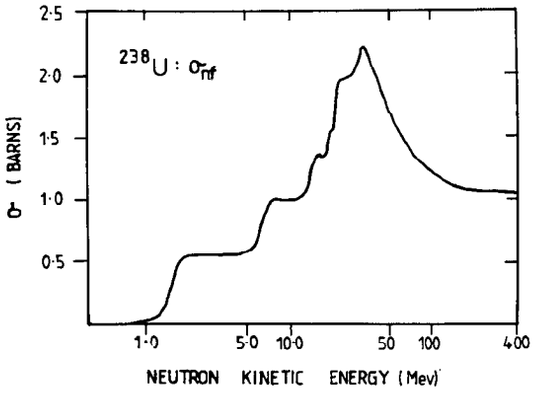

Fig 2 The cross-section for ^{238}U (n,xnf) as a function of incident neutron energy.

in 1.8 fissions, 0.7 neutrons created in (n, xn) reactions and 1.1 neutrons absorbed. It is estimated that 80% of these escape neutrons come from fission events.

2.2 Energy deposition. In table I roughly 2/3 of the energy deposition in the high energy cascade comes from ionisation loss (primary protons and secondary charged particles). The majority of the binding energy released in fission is taken by recoil of the fission fragments under their mutual couloub repulsion. The 21.4 neutrons released are accompanied by an energy deposition of 650 MeV (i.e. 30 MeV/neutron).

Neutron transport from production point to target surface leads to a further deposition of 330 MeV, almost all of which comes from fission fragment recoil. This energy is deposited in creating an extra 3.3 neutrons, that is, ~100 MeV/extra neutron. This component of the energy deposition leads to a strong variation of energy deposition with target size [e.g. a 10 x 10 x 30 cm^3 solid Uranium block gave 740 MeV in releasing 25.4 neutrons for the high energy cascade, and 590 MeV during neutron transport with the creation of an extra 5 neutrons].

2.3 Nuclide production in spallation. Fission leads to the production of two nuclei well displaced in mass from the parent. The spallation products from the calculation [1] are shown as a contour plot in the charge-mass plane in Fig 3.

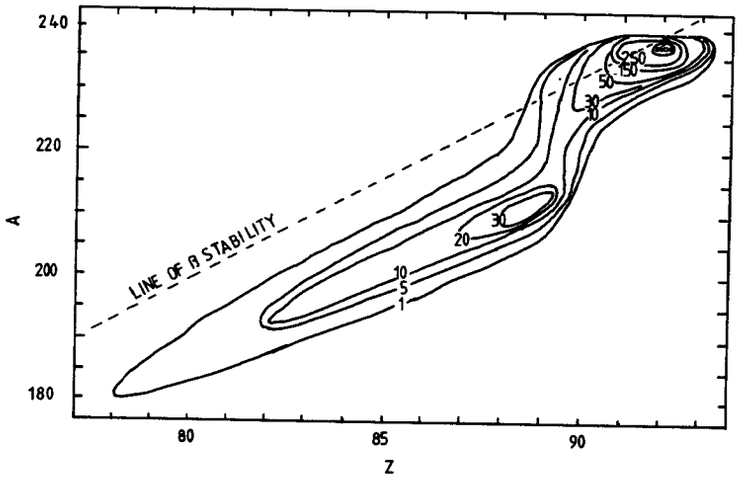

Fig 3 Products from ^{238}U high energy particle induced spallation reactions. Intensities are in arbitary units. The parent nucleus $[^{238}U_{92}]$ is marked with an X.

A feature of this plot is the lack of low mass Uranium, Protactinium and Thorium isotopes due to the competition of fission. Fission probabilities for isotopes in the actinide region are independent of nuclear excitation energy once above a threshold of ~6 MeV [3]; their values are also significantly less than 1. The fission probability for an element increases as the isotope mass decreases [i.e. on neutron emission], but will decrease with the evaporation of a proton. Evaporation is biased toward neutron emission, particularly for the early stages, and for heavy nuclei [4].

This means that nuclei de-exciting via the most probable evaporation path will also have an enhanced chance of fissioning due not only to multiple chances but also to the increasing probablity at each stage; this will lead to a loss of the low mass isotopes of, for example, U, Pa and Th as spallation products as may be seen in Fig 3. A second consequnce of fission competition is that the highly excited fragments which would be destined to evaporate many nucleons, will also preferentially fission due to having many more chances to fission during their evaporation chain. This leads to a supression of the continued widening of the mass range typical of non-fissioning systems under increased bombardment energy.

3. THE EFFECT OF THE PRESENCE OF THE REST OF THE ASSEMBLY

In section 2, the results are for an isolated target. In Fig 4 is shown a visual picture of the overall energy balance for the TRAM assembly.

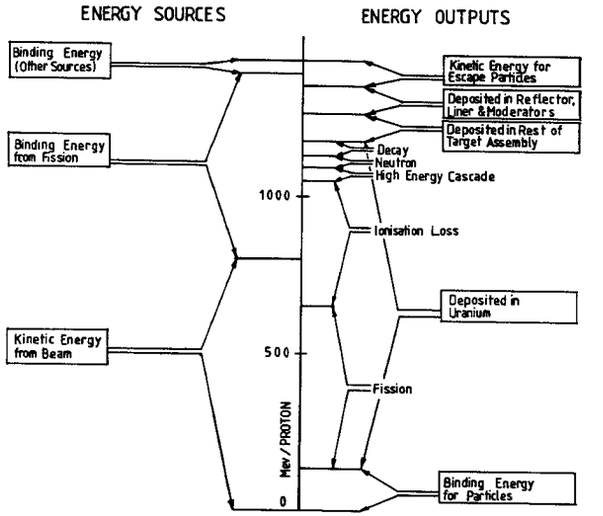

Fig 4 Energy balance for the Target, Reflector, Moderator assembly.

For energy sources, the contribution of "Binding Energy (other sources)" is from reactions like $^{10}B(n,\alpha)^{7}Li$ in the decoupler. The dominance of energy deposition in the target is clearly seen. The extension of the high energy cascade into the full system makes significant contributions to energy depositions in the components outside the target. e.g. Just over half the energy deposited in the reflector.

There is also some extra low energy neutron production [equivalent to 1.7 neutrons/proton]. The presence of material also causes neutrons to be reflected back to the target Uranium; these induce further ^{238}U fissions and lead to an ~4% increase in the prompt target energy deposition; these also cause a roughly 3-fold increase in radiative capture. Radiative capture is responsible for ~25% of the total target activity. Target activity varies with irradiation time but typically lies in the region 20 → 30 Bq/proton, with the associated decay power giving another 4% contribution to the total thermal load.

REFERENCES

[1] F Atchison — A theoretical study of a target, reflector and moderator assembly for SNS (In preparation).

[2] A Carne — These proceedings.

[3] F Atchison — Paper II — JUL-CONF-34(1980)

[4] K J le Couteur — Proc. Phys. Soc. A63, 259 (1950)

THEORETICAL STUDIES RELATED TO SPALLATION TARGET PHYSICS

D. Filges, T. Armstrong*, P. Cloth, R.D. Neef
M. Kloda, and G. Sterzenbach
Institut für Reaktorentwicklung
Kernforschungsanlage Jülich GmbH
Postfach 1913
D-5170 Jülich, Federal Republic of Germany
*Science Applications, Inc. 1200 Prospect St.
La Jolla, California, 92037, USA

1. Introduction

A calculational program is underway at KFA-IRE to investigate various aspects of the German spallation target station design. The major objectives of these theoretical studies are: (1) To assess expected performance of the present preliminary reference design target. This includes neutronics (e.g., predictions of neutron output spectra for continuous, pulsed, and hybrid operation); heating, and cooling requirements; radiation safety aspects (activation, shielding requirements, potential environmental hazards, etc.); and radiation damage levels for materials. (2) To investigate the effects, and possible design improvements, due to various parameter variations (target material alternatives, such as lead vs. uranium, moderator-reflector materials and arrangements, etc.);and, (3) to ascertain the accuracy of the theoretical models being used for such predictions, which includes performing benchmark physics experiments for simple target-moderator configurations.

The basic calculational methods and computer codes being used are summarized in Section 2, and the nature of several experiments that have been performed for code validation purposes are briefly discussed in Section 3. The main emphasis of our work at present is calculations related to evaluation of the preliminary target station design. These calculations are still in progress, but some interim results are presented in Section 4.

2. Calculational Methods

The main computer codes being used are the Monte Carlo codes HETC, for high-energy particle transport, and MORSE, for low-energy ($\leq$ 15 MeV) neutron and gamma-ray transport. The version of HETC operating at KFA has been interfaced with a combinatorial geometry module, so it is possible to use the same geometry description input for both HETC and MORSE.

A rather general HETC analysis code, called SIMPEL, has been written to compute, for example, flux and current spectra (over volumes or across surfaces), energy deposition, and residual nuclei distributions. One feature of SIMPEL is that a combinatorial geometry description can be input to define regions for computing spatial distributions within the material volumes used in the HETC calculation. Thus, analyses for different spatial grids can be performed without having to perform additional transport calculations.

For the MORSE calculations, two sets of cross sections have been used: (1) the coupled neutron/gamma-ray EPR Library, containing 100 neutron groups (one thermal group) and 21 gamma-ray groups and (2) a 53-group neutron set (26 groups below 1-ev, including up-scattering), generated from ENDF/B-IV using the KFA version of the code system RSYST. The EPR Library has been used mainly for energy deposition calculations. For MORSE energy deposition calculations, kerma-factors generated by the MACK code and cross section library were used.

3. Experiments for Model Validation

Several experiments have been performed at the SIN (600 MeV proton beam) and SACLAY (at 600 and 1100 MeV) accelerators to measure, by activation techniques, the neutron flux produced by proton bombardment of bare and moderated thick targets. Target materials of Pb, Pb-Bi, and depleted U and H_2O and D_2O moderators have been considered. For the bare target measurements, rhodium foils were used (threshold ~0.1 MeV) the thermal flux inside the moderators was measured using dysprosium

foils. Most of the data from these measurements have not yet been fully analyzed, and only preliminary experimental/theoretical comparisons have been made to date. For example, Fig. 1 shows the dysprosium reaction rate in a large H_2O moderator surrounding a cylindrical (15 cm dia x 60 cm long) Pb-Bi target bombarded by 590-MeV protons. The results are given as a function of radial distance from the target surface in a plane 10 cm from the front of the target. The values shown are calculated reaction rates, and, while the magnitude of the measured curve has been normalized to the calculation, the shapes of the two distributions are in rather good agreement. The peak radial reaction rate in Fig. 1 corresponds to a calculated thermal flux of about 1.6×10^{-2} $n.cm^{-2}$ s^{-1} per incident proton per second.

4. Theoretical predictions for reference design target

4.1 Configuration

A three-dimensional simulation of the target station configuration shown in Figure 2 has been used for initial radiation transport calculations. It should be emphasized that this model is for initial calculations only and based on preliminary design considerations; calculations for variations toward optimization have not yet been made, although several modifications for improved performance are believed possible.

The design of. Fig. 2 is of a "hybrid" type, with a D_2O moderator and "cold source" above the rotating target (for high continuous flux) and a fast moderator with reflector below the target (for high peak flux). The target region where most of the proton interactions take place consists of lead rods with aluminum cladding and water coolant. A homogeneous mixture of these constituents is used in the calculations.

Proton beam parameters assumed are: 1100 MeV, gaussian beam profile (FWHM = 4 cm), 5 mA average current, and 100 milliamperes peak current.

4.2 Neutronics

The spatial distribution of the low-energy ($\leq$ 15 MeV) neutron leakage current from the target wheel surface is shown in Fig. 3. A total of 29.4 n/p $\leq$ 15 MeV are produced, and the target wheel yield (neutron escapes without surrounding materials) is 25.3 n/p $\leq$ 15 MeV and 1.8 n/p > 15 MeV. The total neutron leakage from the target with surrounding materials (i.e., the integral of the curves of Fig. 3 over the target wheel surface, which includes neutrons that reflect back into the target and subsequently escape) is 69.5 n/p.

The neutron flux as a function of vertical distance in the D_2O tank (averaged over 20 cm diameter volume about the tank axis) is shown in Figure 4. (These calculations were made without the cold source, or beam tubes, in the D_2O tank.) The flux values shown have been normalized for an average beam current of 5 mA. The maximum thermal flux in the D_2O is $\overline{\Phi}_{th} = 7 \times 10^{14}$ n/cm^2-s and occurs at a height of about 15 cm, which is the location where the cold source would be placed.

For the H_2O moderator, we calculate an omnidirectional thermal flux of 6.6×10^{-3} $n.cm^{-2}s^{-1}$ per p ($\pm$ 15 % statistical error, one standard deviation) just outside the moderator (i.e., in a "detector volume" 0.5 cm thick placed in the void adjacent to the exit face of the moderator). For a peak current of $\hat{I}$=100 mA, this corresponds to a peak thermal flux of $\hat{\Phi}_{th} = 4.1 \times 10^{15}$ n/cm^2 sec, which is near (approximately within statistics) the nominal design objective of 5.5×10^{15} n/cm^2 s. (It should be noted that this calculated value is for a "solid" moderator. Under certain conditions, the thermal neutron output can be enhanced if there are "holes" near the surfaces; e.g., some measurements have shown a factor of two increase.)

The above flux values for both the D_2O and H_2O moderators are in agreement with measurements for similar configurations, as reported by G. Bauer in a separate paper.

4.3 Heating Calculations

The energy deposited in various components of the target station has been calculated to indicate general cooling requirements (Table 1). The energy deposited in the target is equivalent to about 50 % of the incident beam energy, with about 25 % to all other components and 25 % into binding energies associated with secondary particle production.

We have also computed the heating expected from the decay of radionuclides produced in the target should coolant flow be interrupted and the beam shut off. We calculate a maximum value for this "afterheat" with respect to irradiation conditions (infinite operating time, immediately after shutdown) to be about 38 kilowatts (compared to 2.9 megawatts during operation, Table 1) and a spatially maximum specific heating inside the target of only $\sim$ 1 watt/cm^3. Thus, this afterheat is not expected to be a problem should loss of coolant occur.

The calculated energy deposition inside the target (as a function of depth in the beam direction in various radial intervals about the beam axis) is shown in Figure 5. The spatially maximum deposition is about 1.2 MeV/cm^3 per incident proton, which, for a peak current of 100 mA, corresponds to a deposition rate of 120 kilowatts/cm^3 during the pulse.

4.4 Activation

Fig. 6 shows the residual nuclei distributions, calculated using HETC, from spallation collisions with the lead in the target. We find the total radionuclide production inside the target from Pb, O and Al spallations to be about 2.7 radionuclides per incident proton, corresponding to saturation activity (for 5 milliamperes average current) of 2.3 megacuries. Most of this activation is from interactions with the lead; for example, the saturation coolant water activity is 44.6 kilocuries.

In addition to spallation, radioactive products can be generated by high-energy fission interactions with the lead. For the calculated neutron and proton flux spectra over the target volume, the fission cross section is about 3.5 % of the spallation cross section, so fission is expected to contribute only about 7 % of the residual nuclei from lead, with fission product masses peaked at A $\sim$ 90.

5. Further calculations planned

The main theoretical work planned for the near future includes: (1) completion of calculations to assess the neutronics of the reference design configuration, including time dependence of the neutron output and neutron spectra produced by the cold source; (2) effects of different moderator materials (e.g., lead) and different target material (i.e., uranium); (3) calculations related to target station shielding and radiation safety; and (4) further experimental data analysis and theoretical comparisons for model validation.

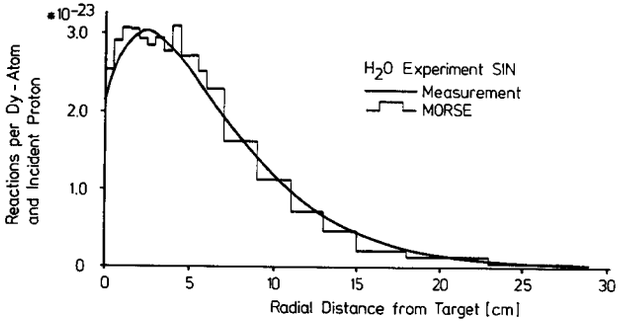

Fig. 1: Experimental/Theoretical Comparison for Neutron Reaction Rate in H_2O, 590-MeV Proton Bombardment of Pb-Bi Target.

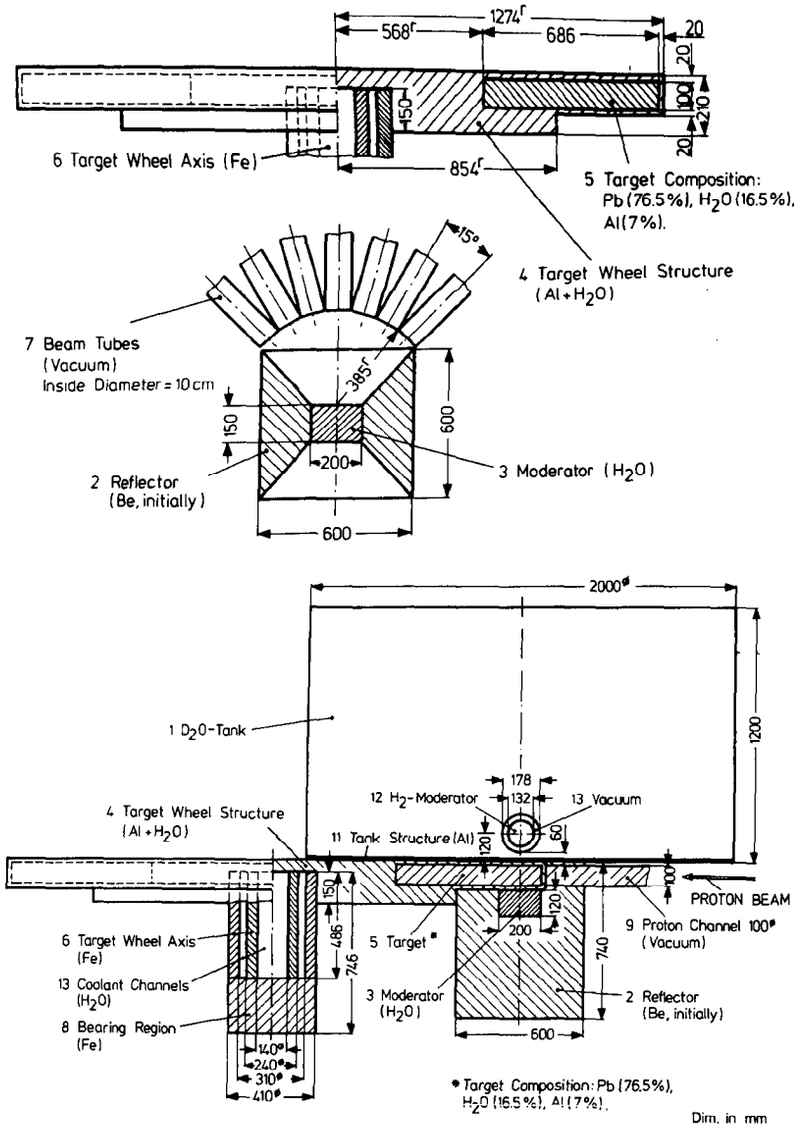

Fig. 2: Target Configuration Used for Calculations

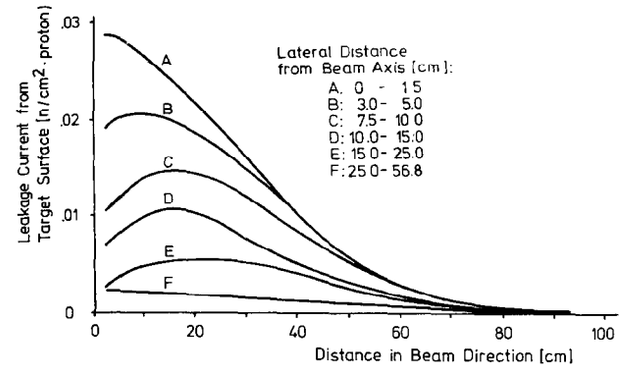

Fig. 3: Neutron Leakage from Target Wheel

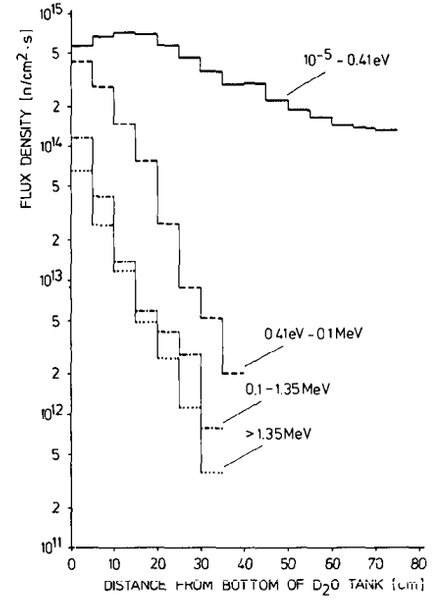

Fig. 4: Neutron Flux Distribution in D_2O Tank

TABLE 1 ENERGY DEPOSITION IN VARIOUS REGIONS OF TARGET STATION

Region Number(a)	Region Description	Material	ENERGY DEPOSITION: MeV per incident proton	Per cent of beam energy	Deposition rate (kilowatts) (c)
5	Target	Pb(76,5%), H_2O(16,5%),Al(7%)	571.0	51.9	2,854
(b)	Shield	Fe	81.8	7.4	407
4	Wheel: Structure	Al(92%),H_2O(8%)	61.9	5.6	308
1	Heavy Water	D_2O	58.3	5.3	292
2	Reflector	Be	29.1	2.6	143
11	D_2O Tank Bottom	Al	13.9	1.3	72
3	Moderator	H_2O	3.5	0.3	16
6	Wheel: Axis	Fe	1.6	0.15	8
12	Cold Source	H_2	0.5	0.05	3
13	Wheel: Coolant Channel	H_2O	0.3	0.03	2
8	Wheel: Bottom	Fe	~0.2	~0.02	~1
		Total Deposition:	822.1	74.8	4,106
		Nuclear Binding Energy (Inferred):	277.9	25.2	1,394
			1100.0	100.0	5,500

(a) See Figure 2
(b) Shield is assumed to completely surround target station
(c) For 5 milliamperes average current, 1100 MeV proton beam

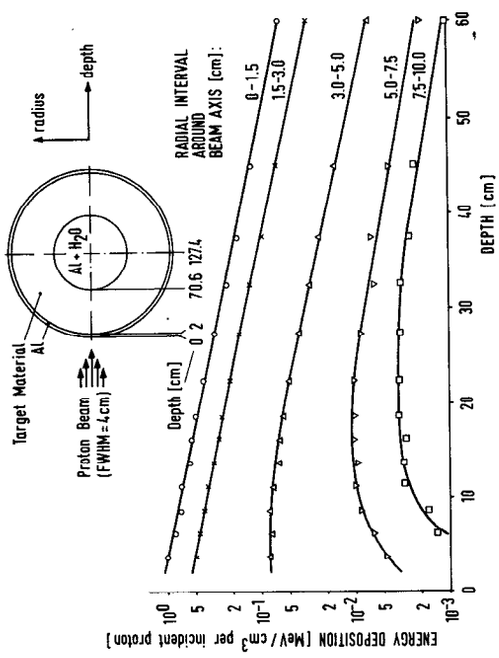

Fig. 5: Energy Deposition Inside Target Wheel

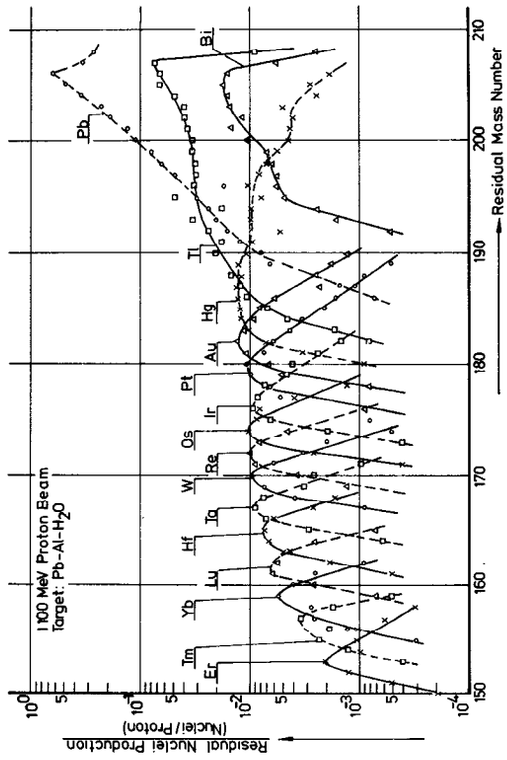

Fig. 6: Spallation Products from Lead in Target

Some Remarks on the Neutronics of Spallation Targets

W.E. Fischer
Swiss Institute for Nuclear Research, CH - 5234 Villigen, Switzerland

B. Sigg
Institute for Reactor Technology, CH - 5303 Würenlingen, Switzerland

Introduction

Target-reflector neutronics should provide us with energy and spatial distribution of the neutrons in the proximity of the spallation target. The time distribution is not essential for a continuous source and will not be considered in this paper. These investigations are usually performed with Monte-Carlo codes, e.g. HETC. A "black box" application of such codes may however be dangerous, involved and time consuming, especially for parametric studies. We therefore prefer some preparatory investigations preceding the application of the Monte-Carlo codes. This preparation consists of an educated guess as a first step, followed by a one-dimensional diffusion calculation furnishing physical insight into trends of parametric behaviour. In this paper we shall present a few typical examples related to the project of the SIN-spallation neutron source.

1) Inelastic Moderation of Evaporation Neutron Spectra in a Heavy Metal Target.

2) Neutron Multiplication due to (n, 2n)-Reactions in a Beryllium Reflector.

3) Neutron Multiplication due to Fast Fission in a Depleted Uranium Target.

The basic geometry in all these examples is quite simple: a cylinder-target embedded into cylindric moderators and reflectors. Where ever available, we use experimental data as input describing the nuclear physics in the target.

1) Inelastic Moderation of Evaporation Neutrons

a) Energy Loss of Evaporation Neutrons

Let $\Sigma(u)$ be the macroscopic inelastic cross section for neutron scattering depending on the lethargy u.
$\Delta u_1 = u_i - u_{i-1}$ are the group intervals
$f(u', u-u')$ is the scattering probability for an inelastic nuclear scattering, shifting the neutron lethargy from $u' \rightarrow u$. The group cross section $\Sigma^{k\rightarrow i}$ is then defined by

$$\Sigma^{k\rightarrow i} = \frac{1}{\Delta u_k} \int_{u_{k-1}}^{u_k} \Sigma(u')\, du' \int_{u_{i-1}}^{u_i} f(u', u-u')\, du \qquad (1)$$

The first integral represents the average inelastic cross section $\bar{\Sigma}$ (k) of neutrons in group k. The second one expresses the probability P $(k\rightarrow i)$ of scattering into group i. These data are available for several possible target and reflector materials[1]. In order to obtain an idea of the moderating power of different materials we have calculated the energy transfer

$$E^{k\rightarrow i} = (\bar{E}_k - \bar{E}_i)\ \bar{\Sigma}\ (k)\ P\ (k\rightarrow i) \qquad (2)$$

and particularly the average energy loss for neutrons from different relevant groups

$$\frac{d\bar{E}}{dx}\ (E_k) = \sum_{i=k+1}^{N} (\bar{E}_k - \bar{E}_i)\ \bar{\Sigma}\ (k)\ P\ (k\rightarrow i)\ [\mathrm{MeV/cm}] \qquad (3)$$

E_k or rather $dE/dx\ (E_n)$ is shown in Fig. 1 for Pb, Be, C and D_2 in the energy interval 1 to 15 MeV. For the light elements the energy loss due to elastic scattering alone is also indicated.

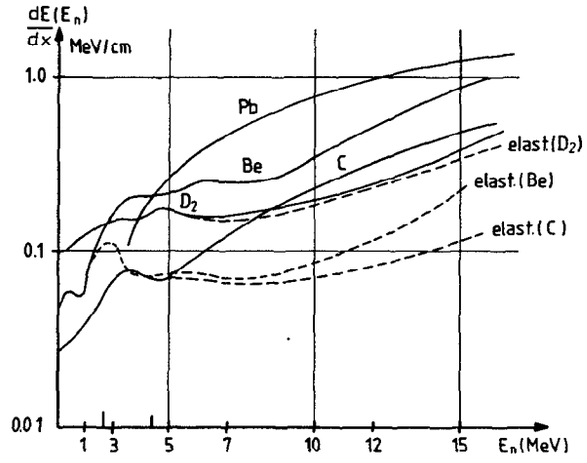

Fig. 1
Stopping power of evaporation neutrons in various target and reflector materials

We see that lead has the highest stopping power among all these moderators for neutrons with $E_n > 4$ MeV. Since the average energy of the primary spectrum of evaporation neutrons is somewhat larger than 4 MeV and the absorption cross section is low, even down to thermal energies, lead is a good moderator for such hard spectra. The same is certainly also true for bismuth. Furthermore the self-shielding property of lead and bismuth for γ-rays is obvious.

The moderation property of lead should be considered also in the interpretation of spectra measured at the bare target. Even if the primary evaporation spectrum is strictly isotropic, this isotropy will be destroyed in a thick target by inelastic moderation. Hence angular dependence of the evaporation part of the neutron spectra will be observed[2].

In order to obtain a quantitative idea on the distortion of the spectrum we carried out the following transport calculation. We start with an evaporation spectrum

$$W(E) = \frac{2}{\sqrt{\pi}} \frac{E^{1/2}}{T^{3/2}} e^{-E/T} \quad \text{with } T = 2.6 \text{ MeV} \qquad (4)$$

Transport of (4) through 1.3 cm of lead reproduces fairly well the leakage spectrum from a lead target with R = 1.3 cm obtained by Monte-Carlo method[3]. This spectrum is already deformed and cannot be described anymore by (4). With the one-dimensional ANISN-code we transport this spectrum through (infinitly long) lead cylinders of various radii. The calculation is done in S_8-approximation considering P_0, P_1-scattering and 15 energy groups. We assumed a rectangular beam profile with 5 cm diameter. The leakage spectra for targets with radii R_T = 5 and 10 cm are shown in Fig. 2. The moderation by the extra 5 cm-layer of lead is evident. The spectral content for energies E_n > 4 MeV is roughly halved. The average energy drops from 2.86 MeV to 2.06 MeV.

From Fig. 1 we realize that this softer spectrum is now most efficiently moderated further by beryllium. Since many neutrons are still above the (n,2n)-reaction threshold ($E \gtrsim 2.7$ MeV) we expect moreover some multiplication of neutrons in a Be-sleeve.

2) Neutron Multiplication in a Beryllium Reflector

In this chapter we would like to estimate the neutron multiplication due to (n,2n) reactions in a Be-sleeve.

a) Geometry - Average Chord Length

In Fig. 3 the geometry of the target-sleeve arrangement is shown. The chord length $S(\rho,\theta)$ averaged over target cross section and

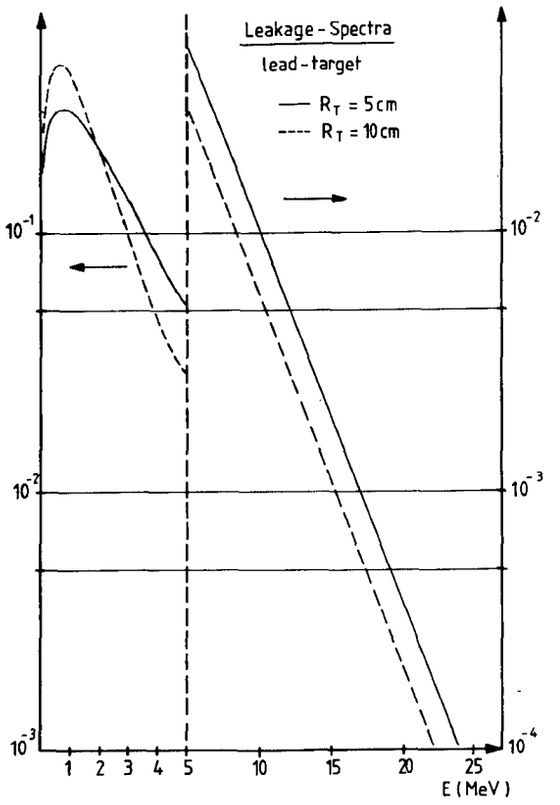

Fig. 2
Leakage spectra from a lead target with 5.0 and 10 cm radius

all plane directions θ is for r/R = 1/2

$$\bar{S} = 1.12\ r \qquad (5)$$

where r is the target radius and R the radius of the Be-sleeve.

For the estimate of the average path length in the beryllium we refer to Fig. 3b. For simplicity we assume a disk-source, 6 cm behind the target front face. From Rh-foil measurements on the surface of a lead target, we know that this is the

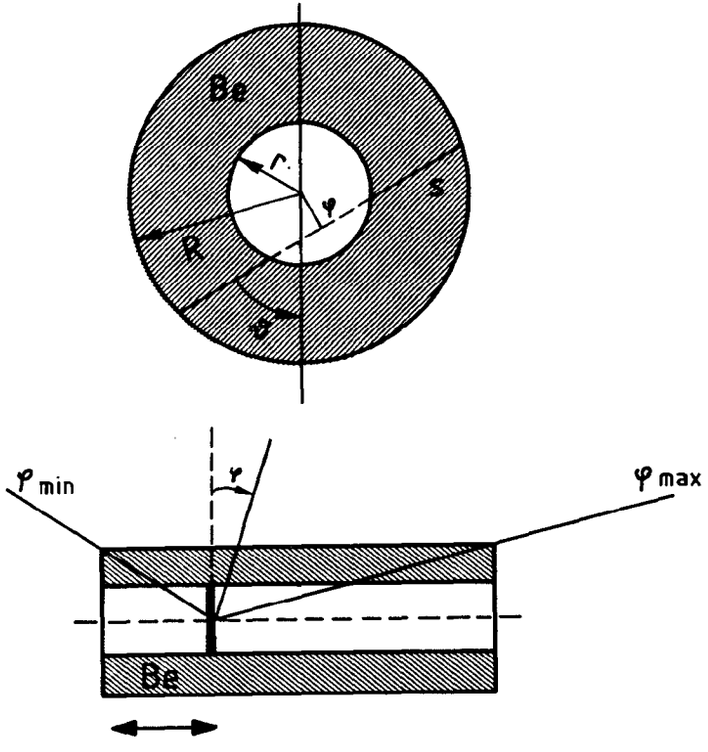

Fig. 3
Sketch of the target
beryllium sleeve geometry

position of maximal source strength for a 590 MeV proton beam. This is indeed a very rough approximation, but one may realize that the average path length is not very sensitive to this position and therefore also not to the exact source distribution.

With a macroscopic scattering cross-section Σ we obtain for the (no scattering) escape probability

$$P_o = \frac{\int_{\phi min}^{\phi max} \exp[-\bar{S}(\frac{R-r}{r}) \frac{\Sigma}{\cos\phi}] d(\sin\phi)}{\int_{\phi min}^{\phi max} d(\sin\phi)} \qquad (6)$$

The cross sections used in this formula should be averaged over the leakage spectrum from the corresponding target. We shall use here the spectrum from a 10 cm lead target (590 MeV protons) measured under 90° by time-of-flight technique at SIN[2] (Fig. 4).

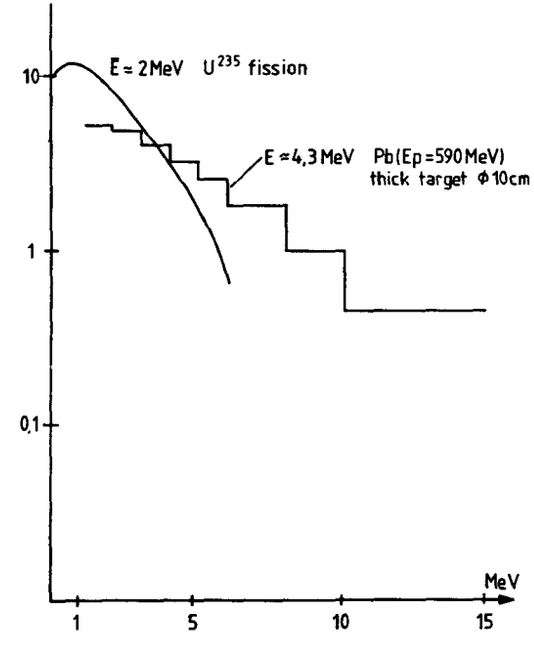

Fig. 4
Experimental TOF-spectrum of evaporation neutrons from a 10 cm diameter lead target, produced by a 590 MeV proton beam. For comparison a ^{235}U-fission spectrum is also shown.

According to chapter 1 this is the angular region with the hardest leakage spectrum. The multiplication figures we shall obtain, will therefore be somewhat overestimated.

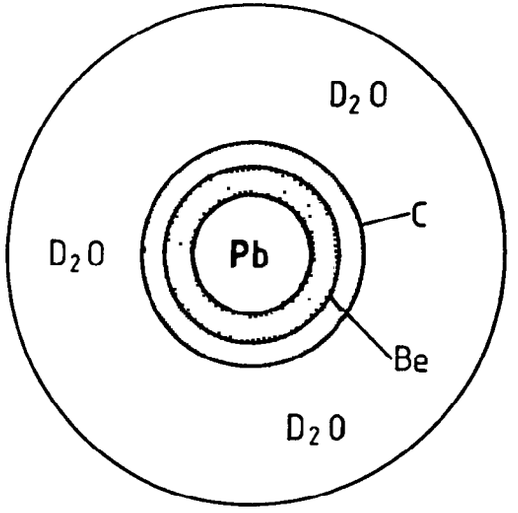

Fig. 5
Schematic target-containment-reflector arrangement for the proposed SIN-neutron source (we still believe in a carbon or beryllium containment for the lead-bismuth eutecticum).

The following values are obtained:

$\bar{\Sigma}_{tot} \approx 0.25\ cm^{-1}$ $\qquad$ $P_0 = 0.17$

$\frac{\bar{\Sigma}\ (n,2n)}{\bar{\Sigma}_{(tot)}} \approx 0.23$ $\qquad$ $\frac{\bar{\Sigma}(elast.)}{\bar{\Sigma}(tot)} \approx 0.77$

The collision probability is therefore 83 %.

b) Multiplication Tree

We follow now the neutrons a few collision generations through the Be-sleeve. We simplify this process with the help of two assumptions

i) First flight and first elastic collision lead to a homogeneous neutron distribution;

ii) After two elastic collisions the neutrons are scattered below the (n,2n) threshold.

The first assumption gives us the possibility to use, after the first collision the escape probabilities tabulated in Case et al.[4]. For r = 5 cm and R = 10 cm - P_c = 0.65. If assumption ii) is valid we can stop the procedure after the second generation. We obtain the following result: If a neutron leaves the target with an energy above (n,2n) threshold the probabilities of events in beryllium are

Escape (E > 2.7 MeV)	0.39
Escape degraded (E < 2.7 MeV)	0.32
(n,2n)	0.29

Since 60 % of all evaporation neutrons in our spectrum are above (n,2n)-threshold we obtain an increase of source strength by beryllium of 17 %.

We expect of course that the efficiency of a beryllium sleeve depends strongly on the hardness of the leakage neutron spectrum. Indeed if we consider the Monte-Carlo spectrum[3] of LA-4789 from lead, which is softer ($\bar{E} \approx 3.25$ MeV) we obtain the following situation

Escape (E > 2.7 MeV)	drops
Escape degraded (E < 2.7 MeV)	increases
(n,2n)	roughly the same

Since in this spectrum only 32 % of the source neutrons are above threshold the multiplication efficiency decreases to < 10 %. We therefore meet a competitive situation between target thickness and efficiency of neutrons multiplication in the beryllium sleeve. Let us analyze this situation with a corresponding diffusion calculation in the one-dimensional cylindrical geometry sketched in Fig. 5. The calculation starts

with a primary evaporation spectrum (4) with the same nuclear temperature (T = 2.6 MeV) and proceeds with nine energy groups. The results are shown in Table I.

Table I

Material, Thickness (cm)				Total Leakage of Thermal Neutrons per Source Neutron	Flux at Outer C-Surface
Pb	Be	C	D_2O		
10	0	6	90	0.634	0.172
7.5	2.5	6	90	0.704	0.204
5	5	6	90	0.776	0.239
10	5	6	85	0.651	0.172
7.5	5	6	87.5	0.712	0.203
5	5	6	90	0.776	0.239

In the first part of Table I we recognize a 11 % increase of the total leakage of thermal neutrons per source neutron for extra 2.5 cm layers of beryllium. The thermal flux at the outer carbon surface rises somewhat stronger, indicating the more efficient moderation by berylllium compared to lead. This would not necessarily be the case, if we had chosen a harder source spectrum.

In the second part of Table I we have just added 5 cm Be-layers to targets of various thicknesses. Compare now the flux at the outer carbon surface of the two parts in the Table, e.g. 10 cm target and 0 and 5 cm Be respectively. We recognize that the gain in source strength due to 5 cm beryllium approximately compensates the flux corresponding radial drop in the D_2O reflector. This is certainly only valid in the proximity of the source.

We have also verified a smaller gain due to the beryllium sleeve by interchanging the carbon with the beryllium layers in this geometry. Obviously the neutron spectrum entering into the beryllium becomes too soft in the carbon for an efficient (n,2n)-gain.

3) Neutron Multiplication Due to Fast Fission in a Depleted Uranium Target

Since we want to consider the finite length of the target in this subject, we should first obtain an idea on the longitudinal distribution of the source of primary spallation neutrons. Concerning these primary neutrons we do not distinguish between evaporation- and fission neutrons from spallation isotopes. We are interested here in the multiplication of the source neutrons by their internuclear cascade in a thick uranium target. We treat the longitudinal source distribution by a cascade model of Barbier et al.[5].

a) Longitudinal Cascade Model

Let $N_n(z)$ be the number of fast cascade nucleons produced in n^{th} generation at depth z. The total number of cascade nucleons is

$$N(z) = \sum_n N_n(z) \qquad z > 0 \tag{7}$$

The longitudinal cascade is ruled by the following equation:

$$dN_n(z) = \lambda^{-1} M_n N_{n-1}(z)dz - \lambda^{-1} N_n(z)dz \tag{8}$$

where

M_n : multiplicity for creation of fast cascade nucleons

λ : $A/N_0 \cdot \sigma \cdot \rho$(cm) relaxation length in the target material.

Using the relaxation length as length unit ($\zeta = z/\lambda$) we obtain for (8):

$$\frac{dN_u(\zeta)}{d\zeta} + N_n(\zeta) = M_n N_{n-1}(\zeta) \tag{9}$$

$N_0(\zeta) = e^{-\zeta}$ for an exponentially attenuated beam. The general solution is

$$N_n(\zeta) = \pi_n \frac{\zeta^n}{n!} e^{-\zeta} \quad \text{with} \quad \pi_n = \prod_{i=1}^{M} M_n \tag{10}$$

From experiments at thin heavy metal targets we know that 600 MeV protons produce ∿ 5 cascade nucleons. 10 % of them have an energy E > 300 MeV and are therefore still fertile for further cascade reactions. The multiplicity of fertile nucleon production in first generation is therefore $M_1 = 0.5$. We agree that the limit of 300 MeV for possible cascade mechanism is somewhat arbitrary.

For a beam energy of 600 MeV, consideration of 1 to 2 generations is presumably enough - let us for simplicity consider one generation only. Then

$$N(\zeta) = e^{-\zeta}(1+0.5\,\zeta) \approx e^{-z/\lambda_{eff}} \qquad \lambda_{eff} > \lambda \tag{11}$$

The definition of λ_{eff} follows from (11). Since the nuclei, suffering cascade reactions, are left with high excitation energy which is radiated off by evaporation neutrons, we consider λ_{eff} to be the parameters describing the longitudinal distribution of the primary neutron source. For lead and uranium we obtain

Pb : $\sigma^{in} \approx 1.7$ b $\lambda = 17.8$ cm $\lambda_{eff} \approx 28.5$ cm
U : $\sigma^{in} \approx 1.9$ b $\lambda = 11.0$ cm $\lambda_{eff} \approx 17.6$ cm

b) First Collision Density

We consider as primary neutron source an isotropic line source

$$Q = \frac{Q_o}{2\pi\rho} e^{-z/\lambda_{eff}} \delta(\rho) \tag{12}$$

The first collision density in a cylinder of radius R and length Z is

$$F(r,z) = \frac{1}{Q_o}\int_0^R d\rho\,\delta(\rho)\int_0^Z d\xi\, e^{-\xi/\lambda_{eff}} \frac{\Sigma}{4\pi[(r-\rho)^2+(z-\xi)^2]}$$

$$\exp(-\Sigma\sqrt{[r-\rho]^2+[z-\xi]^2}) = \frac{1}{4\pi Q_o}\int_0^Z d\xi e^{-\xi/\lambda_{eff}}$$

$$\frac{\Sigma}{r^2+(z-\xi)^2} \exp(-\Sigma\sqrt{r^2+[z-\xi]^2}) \tag{13}$$

The collision probability in the cylinder is

$$P = 2\pi\int_0^R r dr \int_0^Z dz F(r,z) \tag{14}$$

These expressions are very sensitive to the cross sections involved. We used spectrum averaged cross sections using the rather hard experimental spallation spectrum ($\bar{E} \approx 4$ MeV) already quoted[2].

$$\langle\sigma\rangle = \sum_i \left(\frac{dN}{dE}\right)_i \cdot \frac{\sigma(E_i)\Delta E_i}{N} \tag{15}$$

In Fig. 6 we show the spectrum weighted fission and (n,2n) cross section of ^{238}U. It is readily seen that the high-energy tail of the spectrum contributes strongly to further neutron production by fast fission and (n,2n) reactions. We have now to integrate (13) and (14) using an averaged transport cross section

$$\langle\sigma_{th}\rangle = 5.34 \text{ b}$$

leading to an average transport length $\lambda_{th} \approx 3.9$ cm. The ξ-integration in F (r,z) was obtained using an asymptotic expansion of the integrand. A closed approximate expression for F (r,z) followed.

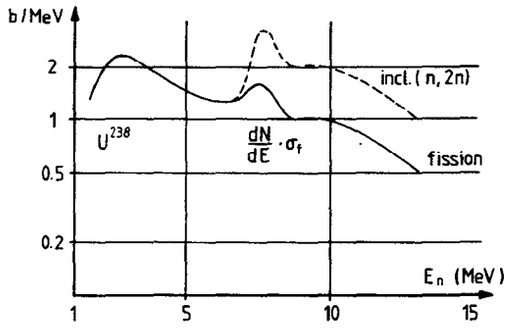

Fig. 6
Spectrum weighted fission and (n,2n) cross section of depleted uranium. The spectrum of Fig. 4 is used.

The collision probability P was obtained by evaluating the further integrals graphically. For an uranium target with a diameter of 15 cm the following first collision probability resulted:

$$P^{238U}_{\bar{E} = 4\ \mathrm{MeV}} \quad (R = 7.5\ \mathrm{cm}) = 0.8 \qquad (16)$$

c) Multiplication Tree

We use the terminology of reactor physics. The number of neutrons from one collision is

$$\eta = \frac{\nu\sigma_f + \sigma_e}{\sigma_{tr}} \qquad (17)$$

After n-collisions we have therefore (P_i : collision probability in i^{th} generation),

$$P_1 P_2 \ldots P_n \eta^n \qquad (18)$$

fast neutrons. Of these ($1 - P_{n+1} \frac{\sigma_i}{\sigma_{tr}}$ escape go below fission threshold

Hence after the nth generation

$$1 - P_{n+1} + P_{n+1}\, \sigma_i/\sigma_{tr} = 1 - \alpha P_{n+1} \qquad (19)$$

neutrons are not useful anymore for fission. Since the spallation neutrons with their hard spectrum are much more efficient for fission reactions than the fission neutrons themselfes, we have to distinguish these two species carefully in the averaging process. The relevant parameters are the following:

Average over Spallation Spectrum		Average over Fission Spectrum	
α_{sp}	= 0.59	α_f	= 0.43
η_{sp}	= 0.80	η_f	= 0.52
P_{2sp}	= 0.76	P_{2f}	= 0.70
P_1	= 0.8		

The first collision probability P_1 comes from the previous consideration. P_2 is the collision probability for all the further generations assuming, as in the case of the beryllium sleeve, a homogeneous distribution of the neutrons in the cylinder[4]. Following through three generations we obtain a multiplication factor

$$M = 1.45\ \text{Neutrons/Source Neutron} \qquad (20)$$

The yield of source neutrons (that is from a thin target) is by a factor of 1.4 higher from uranium than from lead[6]. Hence

$$\text{Yield}\ (^{238}U) \approx 2 \times \text{Yield}\ (Pb) \qquad (21)$$

The following critical remark is, however, appropriate. The high-energy tail of the spallation spectrum (E > 15 MeV) has not been considered. In view of the total cross sections at high-energy and the large neutron emission number ν a higher yield ratio than (21) is expected. Scaling with the total cross section suggests an increase of the yield ratio up to 2.5 to 3.0.

Conclusions

The task of these investigations is twofold. Firstly, we hope that we figured out a few useful numbers. Secondly, and hopefully more important indeed, it has been shown that these old fashioned methods are still a valuable tool to get some insight into the physics behind the neutronics of the system. This understanding, together with the certainly approximate quantitative results, gives us the confidence to tackle these problems - and more involved ones - with the powerful Monte-Carlo codes most efficiently.

References

1) С.М. Захарова и др.
Ядерная-физические константы для расчета реакторов
Госатомидат 1963

2) S. Cierjacks, M. Rainbow, M.T. Swinhoe, L. Buth,
Neutron Yield and Fast Neutron Spectra from Spallation Targets
(presented at this conferency by N. Nücker)

3) R.R. Fullwood, J.D. Cramer, R.A. Haarman, R.P. Forrest,
R.G. Schrandt, LA-4789, Los Alamos 1972

4) Introduction to Neutron Diffusion
K.M. Case, F. de Hoffmann, G. Placzek, Los Alamos 1953

5) M. Barbier, R. Hunter, CERN-71-13, 1971

6) M. Bercovitch et al. Phys.Rev. 119 (1960) 412, and
Р.Г. Васильков и др.
Ядерная физика 7, 88 (1967)

High Energy Neutrons from 500 MeV Protons on Lead

I.M. Thorson and L. Moritz
TRIUMF, Vancouver, British Columbia, Canada, V6T 2A3

1. Introduction

The angular distribution of high energy neutrons from a 10.2 cm diameter, 30.5 cm long lead target bombarded by 500 MeV protons was measured by the ^{11}C activation produced in plastic scintillators. The $^{12}C(n,2n)^{11}C$ reaction has an energy threshold of 20 MeV so that essentially only the high energy, direct interaction (cascade) neutron component is seen by these measurements. The number of protons incident in two bombardments, one with a bare target and the second with an 80 cm thick H_2O shield around the target were also measured, enabling the determination of effective, absolute neutron source strengths for 500 MeV protons stopping in a thick lead target.

Section 2 describes the experiment in more detail. Section 3 describes the parameters used to reduce the data to effective source strengths and Section 4 assesses the probable accuracy of the experiment.

2. Experimental Measurements

The angular distribution of secondary neutrons from a stopping thickness lead target bombarded by 500 MeV protons was measured using the $^{12}C(n,2n)^{11}C$ reactions in plastic scintillators. Two separate measurements were made, one with a bare 10.2 cm diameter, 30.5 cm long target and one with the same target surrounded by blanket of H_2O approximately 80 cm thick. In both measurements the 5.1 cm diameter, 5.1 cm high, NE-102 scintillators were mounted outside a 183 cm diameter, 1.3 cm thick wall aluminum tank at the positions indicated on Fig. 1. The target was contained in a 24 cm diameter, 32 cm long air-tight

aluminum can and the 10.2 cm diameter proton beam tube extension was evacuated in common with the rest of BL4A at TRIUMF, both shown dotted on Fig. 1.

The ^{11}C activity was assayed by placing the scintiallators on a photomultiplier and counting the pulses above a fixed discrimination level. The absolute detection sensitivity of 79% for the setting chosen was established in two ways. One was to count a scintillator at various discriminator settings and extrapolate the dependence to a zero discriminator setting. The second was by assaying a highly activated scintillator on an independently calibrated, low geometry Ge(Li) spectrometer. The deduced sensitivity factors agreed within ~5%.

The 500 MeV proton beam was delivered to the target for both bombardments at a current of 20 to 30 nA over periods of 20 to 30 min. The instantaneous beam current was determined by measuring the electron current on the foil used to strip the H^- for extraction from the cyclotron. The total number of protons incident on the target was estimated by numerical integration of the beam intensity as a function of time; these estimates for subsequent FERFICON bombardments generally yielded results within 20% of those deduced from $^{27}Al(p,3pn)^{24}Na$ monitor reactions. The recorded time profile of the bombardment was used to estimate the decay correction for the 20.38 min half-life ^{11}C activity to determine the effective, instantaneous integral proton beam current that would have produced the same activation at the end of the bombardment period.

3. Data Reduction and Analysis

The scintillators were recovered from the target assembly tank within 20 min of the end of the bombardment with the 80 cm H_2O blanket and counting was started immediately. The decay curves for the first 80 min after end-of-bombardment (EOB) for this run followed the 20.38 min half-life of the ^{11}C decays to within 0.5%; beyond this period longer lived and background

contributions started to become significant. The ^{11}C activity at EOB was deduced by back extrapolation of three assaying points taken on each scintillator during the initial period.

The counting rates for the scintillators used in the bare-target bombardment showed a significant contamination by a 35-40 min activity at the earliest times for which assaying was carried out—in that case between 30 and 80 min after EOB. The contribution from this contaminant amounted to between 5 and 20% of the gross count rate at the earliest assaying times and showed a nearly—within a factor of 2—isotropic angular distribution. Its identity was not established with certainty but ^{38}Cl from thermal neutron activation is suspected. The thermal neutron component was enhanced by the water inadvertently left in the tank at a level 15 cm below the target container during the target bombardment. Longer lived ^{122}Sb and ^{124}Sb components from neutrons capture were positively identified later by half-life and γ-spectroscopy and traced to black masking tape around the sides of the scintillators, used to improve their optical characteristics.

The ^{11}C decay rates for all of scintillators for both the bare target and water blanket bombardment runs are listed in Table 1, along with the estimated effective integral proton beam current, corrected for ^{11}C decay during bombardment. The results are also shown as effective secondary neutron source strengths in the various directions per incident 500 MeV proton reaching the scintillators at the outside of the water tank from the bare target and through the water shield. To obtain the effective source strengths the $^{12}C(n,2n)^{11}C$ reaction probability in the scintillators (110 g of ^{12}C) was estimated for a 1/E spectrum-weighted-average cross section of 10.7 mb in the energy range 20 to 400 MeV. This value is based on the published[1] data

between 20 and 40 MeV and an assumed constant cross section of 10 mb above 40 MeV. Specifically, the number ^{11}C species produced by a total fluence, $\emptyset$ cm^{-2}, of such neutrons on a scintillator would be

$$R = \emptyset \times 0.6023 \times 0.0107 \quad \frac{110}{12}$$

$$= 0.0590\emptyset$$

and the induced decay rate, D, would be

$$D = R \times \frac{\ln 2}{20.38 \times 60}$$

$$= 5.67 \times 10^{-4} \ R \ s^{-1}$$

$$= 3.34 \times 10^{-5} \ \emptyset \ s^{-1} \ .$$

For a counting efficiency of 79% the count rate, C, would be

$$C = 0.79 \ D$$

$$= 2.64 \times 10^{-5} \ \emptyset \ s^{-1}$$

Thus

$$\emptyset = \frac{C}{2.64 \times 10^{-5}} = 3.78 \times 10^{4} \ C \ .$$

Finally to obtain the effective source strength, S per steradian per incident proton the effective fluence $\emptyset$ is multiplied by the square of the distance (94 cm) from the centre of the target to the centre of the scintillators and divide by the number of protons incident

$$S = \frac{94^2 \ \emptyset}{P}$$

$$= 3.34 \times 10^{8} \ \frac{C}{P} \ \text{steradian}^{-1} \ .$$

The deduced effective source strengths are listed in Table 1 for the bare and

water shielded configurations; they are also plotted in Fig. 2 as a function of the cosine of the angle between the incident proton beam direction and the direction of the scintillator from the target centre.

4. Discussion of Results

The accuracy of the results in Table 1 and Fig. 2 are expected to be limited by the possible error on the measurement of the number of 500 MeV protons incident on the lead target during the bombardments. As cited above the integration of the cyclotron stripper foil current, renormalized by well established loss factors for the electron current, gave general agreement on other occasion with aluminum foil activation measurements within a limit of 20%. Although the sizes of the beam spots on the target were not as good as for subsequent FERFICON runs—fwhm $\sim$ 1 cm as compared to 0.3 cm for most bombardments—the beam transport loss were probably quite small.

The relative accuracy of the angular distribution for each bombardment is expected to be much better, more like 5%, limited by the extraction of the ^{11}C component from the scintillator decay curves. The cause of the apparent discrepancy at high angles through the water blanket is unknown; lacking any reproducibility check, transposition of the data points cannot be ruled out. The sharp drop in intensity in the forward direction for the bare target measurement is probably due to attenuation by the downstream end of the 25 cm long lead target. A smaller reduction in the water shielded case is expected because of the angular resolution broadening that such a blanket would produce.

The angular distribution shown in Fig. 2 presumes that the effective source is at the centre of the Pb target. The source is actually distributed

and the centre of the proton collision distribution is 6.5 cm ahead of the target centre. Thus the angular distribution as seen from large distances would be more anisotropic. In forward directions the intensity would be increased by the approximate factor

$$\left(\frac{94}{94 - 6.5}\right)^2 = 1.14$$

and decreased in the backward direction by the reciprocal, namely $1.14^{-1} = 0.88$.

Reference

1. D.I. Barber and R.R. Kinsey, Neutron Cross Sections, BNL 325, Third Edition, Vol. II, 1976.

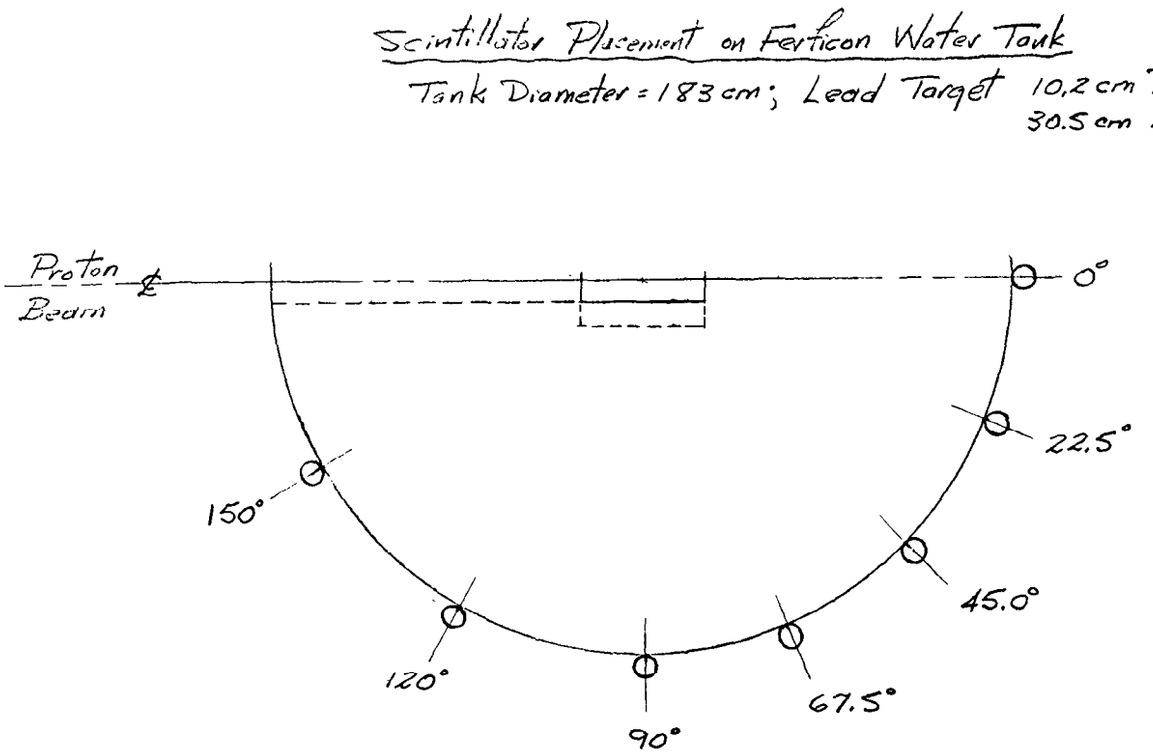

Fig. 1. Schematic plane view of geometry for $^{12}C(n,2n)^{11}C$ activation experiment.

Table 1

^{11}C Activation Results for Bare and Water Shielded Pb Targets Bombarded by 500 MeV Protons

		Bare Target		80 cm H_2O Shield	
Θ	μ	Scint. Decay Rate @ EOB s^{-1}	Effective Source Strength $(p \cdot steradian)^{-1}$	Scint. Decay Rate @ EOB s^{-1}	Effective Source Strength $(p \cdot steradian)^{-1}$
0°	1.000	19000	0.122	18530	0.032
22.5°	0.924	31000	0.200	19670	0.034
45°	0.707	27000	0.173	14370	0.025
67.5°	0.383	18500	0.119	7820	0.0133
90°	0	10000	0.064	3720	0.0064
120°	-0.500	5000	0.032	1570	0.0027
150°	-0.866	3600	0.023	1830	0.0031
Decay Corrected Integral Number of Protons P		0.52×10^{14}		2.0×10^{14}	

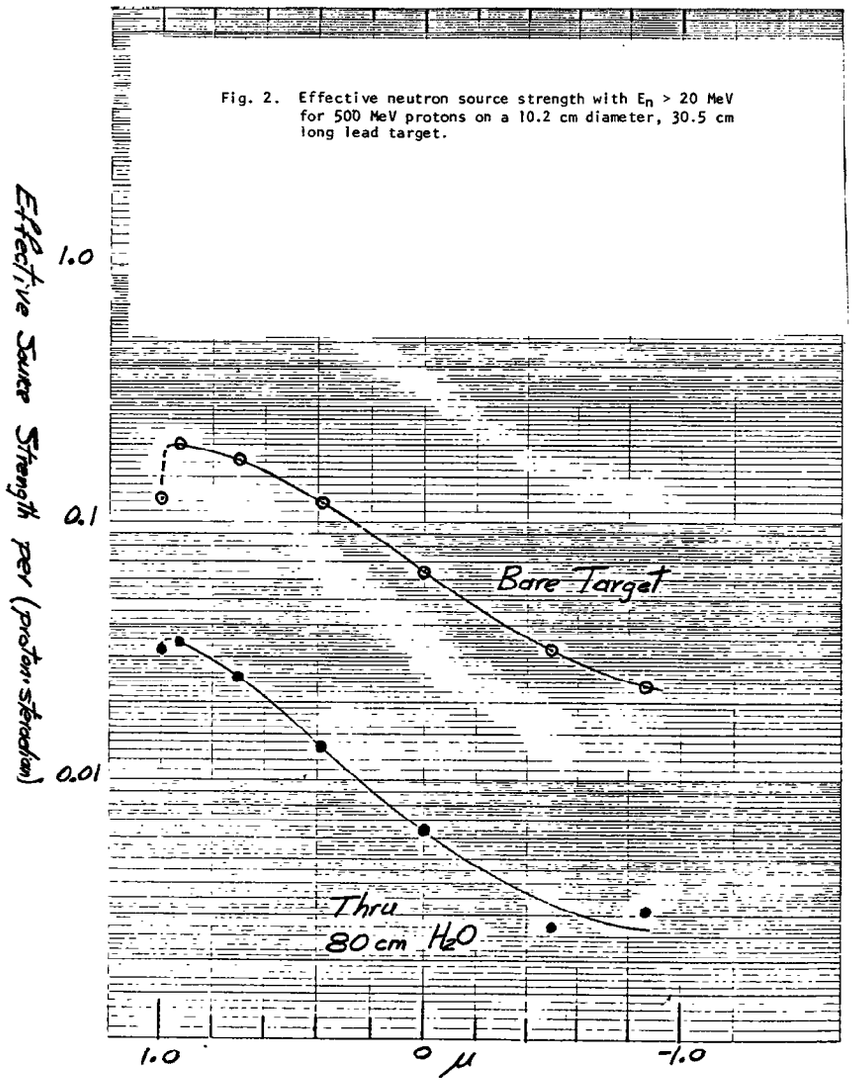

Fig. 2. Effective neutron source strength with E_n > 20 MeV for 500 MeV protons on a 10.2 cm diameter, 30.5 cm long lead target.

Studies on high energy spallation and fission reactions

Y. Nakahara

Division of Reactor Engineering,
Japan Atomic Energy Research Institute,
Tokai, Ibaraki, Japan

1. Introduction

In the feasibility studies of accelerator driven nuclear fuel breeders and the designs of intense spallation neutron sources, the first stage of nuclear reaction and nucleon transport processes, initiated by incident protons from a linear accelerator, has been simulated by the Monte Carlo method, generally by the use of the MMTC[1] or HETC[2] code. It is important to keep it in mind that these codes do not calculate the fission processes which would be caused by the nucleons in the high energy range above the cutoff for the nucleon cascades.

It was reported that these codes underestimate the average number of neutrons produced in a target/blanket system per incident proton by several tens % in comparison with experiments[4),5)]. In this regard, the importance to include the fission reactions in competition with the evaporation has been pointed out by several persons, for example, by Atchison[6] and Takahashi[7].

In the calculations by Barashenkov et al. the fission process in the high energy reaction has been included and their results show fairly good agreement with experiments[8].

Details of their computational scheme, however, have not been published. Atchison incorporated the fission process into the HETC code, employing a very practical treatment with the use of empirical formulas as far as available. He reported that a comparison at a very early stage indicated a 30% increase in neutrons as compared to the case with no fission and also found a 60% increase in the neutrons above 2 MeV. On the other hand, Takahashi has been trying to perform calculations not relying on the experimental formulas. He simplified the Fong's formulas for the statistical fission model[9] to make them adaptable to the Monte Carlo calculation by the NMTC code.

The approach employed by the present author to treat the fission process is close to the Atchison's, but more consistent with the Cameron's mass formula[10] used in the NMTC code, into which our scheme has been incorporated[11].

2. Incorporation of fission into the intranuclear cascade and evaporation processes

The fission occurs in competition with the evaporation after the high energy nucleon cascade through the nucleus. At the fission the nucleus splits into two fragments, from which particles would or would not evaporate further but no fission is assumed afterwards. The scheme similar to Atchison's is shown in Fig.1. White and black arrows show the computational flow for the particles and residual nuclei, respectively.

The judgement if the fission will occur is done randomly on the fission probability given by

$$P_f = (1 + \Gamma_n / \Gamma_f)^{-1} \quad , \qquad (1)$$

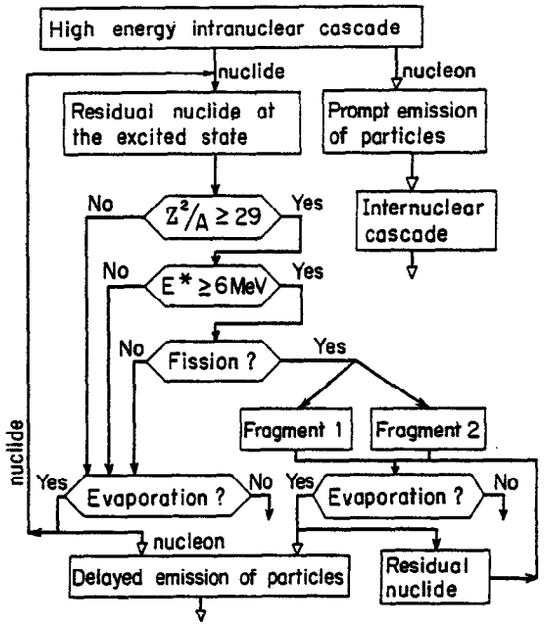

Fig.1 Competition of fission and evaporation processes

where Γ_n and Γ_f are neutron and fission width, respectively.

In our NMTC/JAERI code the following expression of the statistical theory[12] is used both for actinides and sub-actinides, i.e.,

$$\frac{\Gamma_n}{\Gamma_f} = \frac{4\ A^{2/3}\ a_f(E - Q_n)}{K_o a_n [2\ a_f^{1/2}(E - E_f)^{1/2} - 1]}$$

$$\times \exp[2\ a_n^{1/2}(E - Q_n)^{1/2} - 2\ a_f^{1/2}(E - E_f)^{1/2}] \ , \qquad (2)$$

where

A = mass of fissioning nuclei,

E = excitation energy,

Q_n = neutron binding energy,

E_f = fission barrier,

$K_o = h^2/(8\pi^2 m\ r_0^2)$, m = neutron mass,

r_0 = nuclear radius.

The level density parameter for the evaporating nucleus, a_n, is calculated from the LeCouteur's expression:

$$a_n = \frac{A}{8}\ [1 + 1.5\ (\frac{A - 2Z}{A})^2] \ . \qquad (3)$$

The level density parameter for the fissioning nucleus, a_f, is fitted to the experimental data compiled by Vandenbosh and Huizeng[12]. The fitting is given by the following simple equation linear in Z^2/A,

$$a_f/a_n = 1.0 + 0.1(Z^2/A - 29.0) \ . \qquad (4)$$

As for E_f, we use the simple liquid drop model prediction given by Cohen and Swiatecki as a function of the fissility parameter x[13];

$$E_f = \begin{cases} 0.38\ (0.75 - x)E_s^0, & 1/3 < x \le 2/3 \ , \\ 0.83\ (1 - x)^3\ E_s^0\ , & 2/3 < x \le 1 \ , \end{cases} \qquad (5)$$

where

$x = E_c^0/(2E_s^0)$,

E_c^0 = the Coulomb energy of undistorted sphere,

E_s^0 = the surface energy of undistorted sphere.

Eq.(5) with the approximate expressions for E_c^0 and E_s^0

derived experimentally by Green[14]:

$$E_C{}^0 = 0.7103\ Z^2/A^{1/3} \quad \text{(MeV)},$$
$$E_S{}^0 = 17.80\ A^{2/3} \quad \text{(MeV)}, \qquad (6)$$

gives a very good fit to the experimental barrier heights, as shown by Bandenbosh and Huizenga[12].

The neutron binding energy Q_n can be obtained in the same way as in EVAP, which is used as Subroutine DRESS in NMTC.

3. Sampling of masses and charges of fission fragments

If it has been decided that the fission will occur, masses, charges and other parameters have to be selected for the fission fragments.

If the most probable value $\bar{x}$ of a certain parameter x is known, the statistical theory provides the fluctuation probability[15]:

$$P_y\ (x) \propto \exp\ [\ -\ \frac{(x - \bar{x})^2}{<\Delta x>^2}\ ] \quad , \qquad (7)$$

where

$$<\Delta x>^2 = [\ \frac{T}{2} \frac{\partial^2 W}{\partial x^2}\Big|_{x=\bar{x}}\ ]^{-1} \quad , \qquad (8)$$

T = the temperature at the moment of rupture,

W = the total energy.

The index y in Eq.(7) denotes the distribution of x for a fixed value of y. The thermodynamic distribution of such quantity as the fragment charge can be determined for a given mass.

According to the statistical fission theory of Pik-Pichak

and Strutinskii's, when the mass A of a fission fragment has been determined for a fissioning nucleus of the mass A_0 and charge Z_0, the most probable charge of the fragment is given as follows,

$$\bar{Z} = -\ \frac{1}{10} \frac{e^2}{r_0\beta} \left(\frac{A_0}{2} \right)^{2/3} \left(1 - \frac{5}{8\rho}\right) \frac{Z_0}{2}$$
$$+\ A\frac{Z_0}{A_0}\ [\ 1 + \frac{1}{10} \frac{e^2}{r_0\beta} \left(\frac{A_0}{2} \right)^{2/3} \left(1 - \frac{5}{8\rho}\right)\ ]\ , \qquad (9)$$

which is consistent with the Cameron's mass formula. In Eq. (9) β is a parameter in the Cameron's mass formula, the value of which is given by him as $\beta = -31.4506$ MeV and 2ρ is the distance between the center of mass of each fragment.

The fluctuation relative to $\bar{Z}$ is given by the expression:

$$\frac{1}{<\Delta Z>^2} = -\ \frac{16\beta}{A_0 T}\ [\ 1 + \frac{\phi}{\beta} \left(\frac{2}{A_0}\right)^{1/3} - 0.055\ \frac{e^2}{r_0\beta}\ A_0{}^{2/3}\ ]\ , \qquad (10)$$

where $\phi = 44.2355$ MeV being also a parameter in the Cameron's mass formula. In deriving Eqs.(9) and (10), the pairing energy and symmetry energy correction terms in the mass formula have been neglected, because their contributions are $1 \sim 2$ MeV at most.

The most difficult and controversial problem in the computational procedures of the fission is how to select masses of fission fragments. Pik-Pichak and Strutinskii derived also the expressions of $\bar{A}$ and $1/<\Delta A>^2$ for subactinides. For actinides, however, it is well known that when the excitation energy of the fissioning nucleus is high, the fission is symmetric, but it changes gradually to asymmetric as the excitation energy decreases. The overall shape of the distribution

of this type may be expressed very well by a triply-folded normal distribution:

$$P(A) = \frac{2}{\sqrt{\pi}\, b \langle W_{1/2} \rangle [\, 2\alpha + \beta \,]}$$

$$\times \{ \alpha \exp [- \frac{(A - \bar{A}_1)^2}{b^2 \langle W_{1/2} \rangle^2}] + \beta \exp [- \frac{(A - \bar{A}_2)^2}{b^2 \langle W_{1/2} \rangle^2}]$$

$$+ \alpha \exp [- \frac{(A - \bar{A}_3)^2}{b^2 \langle W_{1/2} \rangle^2}] \} \quad . \qquad (11)$$

The same half width at half maximum is assumed for the three normal distributions in Eq.(11). The constant b is the normalization factor. The heights of the two side peaks α and the central peak β (or valley) have been fitted by us to the data of ^{239}Pu fission induced by a helium ion obtained by Grass[16];

$$\alpha(E) = \begin{cases} \exp(0.5991E - 13.1869), & 6 \text{ MeV} \le E \le 25 \text{ MeV}, \\ \exp(0.08026E - 0.2149), & 25 \text{ MeV} < E \le 40 \text{ MeV}, \\ \alpha(40 \text{ MeV}), & 40 \text{ MeV} < E \ , \end{cases} \qquad (12)$$

$$\beta(E) = \begin{cases} \exp(0.7013E - 17.5325), & 6 \text{ MeV} \le E \le 25 \text{ MeV}, \\ \exp(2.2672\sqrt{E} - 11.3431), & 25 \text{ MeV} < E \le 48 \text{ MeV}, \\ \beta(48 \text{ MeV}), & 48 \text{ MeV} < E \ , \end{cases} \qquad (13)$$

Since the binding energy of α particle is approximately 6 MeV, the relation between E and the excitation energy E^* of the fissioning compound neucleus is given as $E = E^* + 6$. For lack of experimental data and theoretical models sufficient enough to get general expressions of α and β for the wide range of nuclides, we assume that Eqs.(12) and (13) would be applied to all actinides.

Fitting parameters $\bar{A}_1$, $\bar{A}_2$ and $\bar{A}_3$ in Eq.(11) are chosen as

$$\bar{A}_1 = \frac{2}{5} A_0, \quad \bar{A}_2 = \frac{1}{2} A_0, \quad \bar{A}_3 = \frac{3}{5} \quad .$$

The width $\langle W_{1/2} \rangle$ is assumed to have the same expression[17]:

$$\langle W_{1/2} \rangle = E^* - E_f + 7 \qquad (14)$$

as for the subactinides, which is used in the Atchison's computational scheme in the subactinide region[12].

It is not obvious how to make a random sampling of A from the distribution given by Eq.(11). In order to avoid unsubstantial computational complicatedness, a simplified expedient procedure is employed in NMTC/JAERI.

If $\alpha > \beta$, β is taken to be equal to 0. In this approximation, the asymmetric fission is overestimated and the symmetric one is underestimated. In this case, we generate a random number x from the folded normal distribution:

$$f(X) = \frac{1}{\sigma\sqrt{2\pi}} \{ \exp [- \frac{(x - \mu)^2}{2\sigma^2}] + \exp [- \frac{(x + \mu)^2}{2\sigma^2}] \} \qquad (15)$$

where

$x > 0$,

$\mu = (\bar{A}_1 - \bar{A}_3)/2$, $\qquad \sigma = b \langle W_{1/2} \rangle / \sqrt{2}$.

Then masses of two fission fragments are obtained as

$$A_1 = x + \frac{1}{2} (\bar{A}_1 + \bar{A}_3) \ , \quad A_2 = A_0 - A_1 \quad . \qquad (16)$$

If $\alpha < \beta$, α is taken to be equal to zero and the normal distribution:

$$f(x) = \frac{1}{\sigma\sqrt{2\pi}} \exp\left[-\frac{(x-\mu)^2}{2\sigma^2}\right], \qquad x > 0 \qquad (17)$$

with

$$\mu = \bar{A}_2 \quad \text{and} \quad \sigma = b < W_{1/2} > / \sqrt{2}$$

is used to generate a random number and we get

$$\bar{A}_1 = x, \qquad \bar{A}_2 = A_0 - A_1 \quad . \qquad (18)$$

This time the asymmetric fission is underestimated and the symmetric one is overestimated.

We expect optimistically that the cancellation of errors due to over- and under-estimate will result in the reasonable value of number of neutrons produced. Once the masses of fragments have been determined, their charges can be obtained immediately by generating random number x from Eq.(17) with

$$\mu = \bar{Z}, \qquad \sigma = <\Delta Z> / \sqrt{2}$$

where $\bar{Z}$ and $<\Delta Z>$ can be calculated by the use of Eqs.(9) and (11). We have

$$Z_1 = x, \qquad Z_2 = Z_0 - Z_1 \qquad (19)$$

4. Kinetic and excitation energies of fission fragments

The total kinetic energy E_k of the fission fragments is determined by the Coulomb repulsion at the moment of splitting, i.e.,

$$E_k = \frac{Z_1 Z_1 e^2}{r_1 + r_2} \qquad (20)$$

where r_1 and r_2 are nuclear radius of fragments. Exactly speaking, E_k depends on the excitation energy and angular momentum of the fissioning nucleus.

In actual calculations it is convenient to use the experimental formula[12]:

$$E_k = 0.1071\ Z^2/A^{1/3} + 22.2 \quad . \quad (\text{MeV}) \qquad (21)$$

The recoil energies of fragments are determined by the relations:

$$E_{k_1} = \frac{A_2}{A_1 + A_2} E_k, \qquad E_{k_2} = \frac{A_1}{A_1 + A_2} E_k \quad . \qquad (22)$$

The total energy released at the moment of fission of a nucleus of the excitation energy E^* is given by the relation:

$$E_T = M(A_0, Z_0) + E^* - M(A_1, Z_1) - M(A_2, Z_2) \quad , \qquad (23)$$

where M(A, Z) is the Cameron's mass formula. The total excitation energy of two fragments is obtained from the conservation of energy as follows,

$$E^{*\prime} = E_T - E_k \qquad (25)$$

According to the statistical theory, the excitation energy of a nucleus is proportional to its mass[9].

Finally, the total excitation energy $E^{*\prime}$ can be distributed among fragments as

$$E_1^{*\prime} = \frac{A_1}{A_1 + A_2} E^{*\prime}, \qquad E_2^{*\prime} = \frac{A_2}{A_1 + A_2} E^{*\prime} \qquad (26)$$

5. Analysis of experiments by Vasil'kov et al.

The experimental results published by Vasil'kov et al.[18] are very interesting, since they give us still a few valuable means to check the applicability of our complicated computational scheme. Fig.2 shows the cut-away view of the target and shield in the Vasil'kov et al.'s experiments. Its cross-sectional view is shown in Fig.3 with a cylindricalized volume-equivalent target. Actually, the beam hole in the experiments was off-centered as shown by the dotted square in Fig.3. Vasil'kov et al. themselves, however, integrated the Np-activity measured by a series of foils located as shown in Figs.2 and 3 as if the target were a symmetrical cylinder. In our calculations the beam hole is assumed to be on the center as shown by the full square in Fig.3 and the target is replaced by the volume-equivalent cylinder. It is not clear, however, how the cylindricalization was done in the integration by Vasil'kov et al.

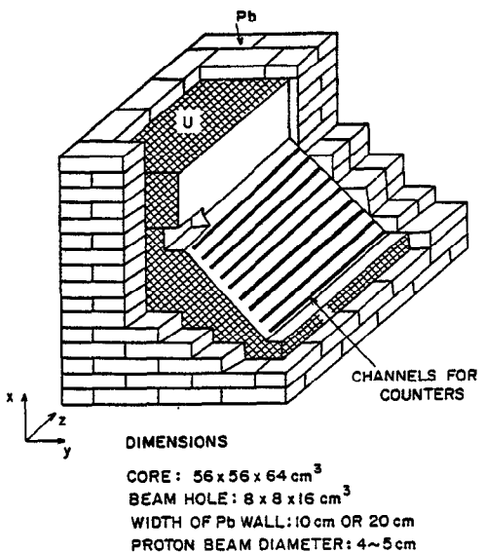

Fig.2 Target in Vasil'kov et al.'s experiment (cut-away view)

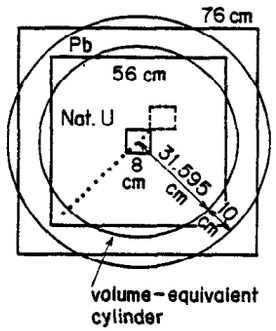

Fig.3 Target of Vasil'kov et al.'s experiment (cross-sectional structure)

The analysis of the experiments have been done already by Takahashi and Nakahara[4] and by Garvey[5]. Their calculations resulted in significant underestimates of the measurements. It may be said to be one of the main reasons of the discrepancy that their calculations do not include fissions which occur in competition with evaporation processes.

Now, it is quite interesting and worthwhile to make an analysis of the Vasil'kov et al.'s experiments by using the NMTC/JAERI code, into which the computational scheme of fissions has been incorporated. Preliminary results are summarized in Table 1. About 36% increase is seen in the values of number of neutrons N obtained by NMTC/JAERI in comparison with those by NMTC in the case of E_p = 660 MeV.

Table 1. Analysis of number of neutrons captured by ^{238}U per primary proton

Target	E_p	N	N_c	Exper. N_c
Nat. U	660 MeV	(a) 31.1 ± 3.5	44.9 ± 5.1	46. ± 4.
		(b) 22.9 ± 2.1	33.1 ± 3.0	
	400 MeV	(a) 11.81 ± 3.44	15.96 ± 4.65	22.1 ± 2.4
		(b) 9.95 ± 0.60	13.44 ± 0.81	

E_p = energy of proton beam,

N = average number of neutrons per one primary proton, produced by reactions in the nucleon energy range above 15 MeV.
(a) cascade·evaporation·fission (NMTC/JAERI),
(b) cascade·evaporation[4] (NMTC),

N_c = number of neutrons captured by ^{238}U per one primary proton (NMTC + TWOTRAN-II results),

Exper. N_c = experimental N_c due to Vasil'kov et al.[18]

The increase in N due to high energy fission is lower for the lower E_p. In the case of E_p = 400 MeV, the increase is only 19%. A fairly good agreement between computational and experimental values of number of neutrons captured by ^{238}U (production rate of ^{239}Pu) is seen for E_p = 660 MeV, but the discrepancy is still large for E_p = 400 MeV. We have not yeat reasonable explanations why the discrepancy occurs.

In Table 2 also is shown the effect of high energy fissions on the average number of neutrons produced by a 1 GeV proton in the molten salt, $LiF-UF_4$, in the nucleon energy range above 15 MeV. The 18% increase in N is observed in this case. Other results on various molten salt targets are to be reported by Furukawa et al. in this session.

A flow of computation and computer codes involved in the neutronic calculations are described in appendix.

Table 2. Effect of high energy fission on neutron production in a molten salt target

Target	E_p	N	
		without	with fissions
$LiF-UF_4$ (71 - 29)	1.0 GeV	28.1 ± 2.8	33.2 ± 2.6

(71 - 29) mole %

N = average number of neutrons per one primary proton, produced by reactions in the nucleon energy range above 15 MeV.

6. Conclusion

Although crude approximations are used especially in the sampling scheme of masses of fission fragments, the NMTC/JAERI code gives us a reasonable estimate of number of neutrons produced by protons with high energy. It can be said that the code system described in Appendix provides us a practical tool in design analysis of accelerator target/blanket systems for the purpose of nuclear fuel breeding or intense neutron sources.

Acknowledgments

The author would like to express his sincere thanks to Drs.H. Takahashi (BNL), K. Tsukada (Nihon Univ.) and K. Furukawa (JAERI) for valuable discussions. Acknowledgments are also due to T. Tsutsui for his speedy and trustworthy programming works and K. Horikami for his valuable advices in using the FACOM-M200 computer.

References

1) W.A. Coleman and T.W. Armstrong; "NMTC Monte Carlo Nucleon

Meson Transport Code System", RISC ORNL CCC-161.

2) K.C. Chandler and T.W. Armstrong; "Monte Carlo High Energy Nucleon Meson Transport Code", RSIC ORNL CCC-178.

3) H. Takahashi and Y. Nakahara; Bull. Americal Phys. Soc., 24, 874 (1979).

4) P. Garvey; "Neutron Production by Spallation in Heavy Metal Targets", in Targets for Neutron Beam Spallation Sources, Jül-Conf-34 (1980).

5) F. Atchison; "Spallation and Fission in Heavy Metal Nuclei under Medium Energy Proton Bombardment", ibid.

6) H. Takahashi; "Fission Reaction in High Energy Proton Cascade", presented at the Symposium on Neutron Cross Sections from 10 - 50 MeV, BNL, May, 1980.

7) V.C. Barashenkov, V.D. Toneev and S.E. Chigronov; "On the Calculations of the Electro-nuclear Method of Neutron Production", JINR-R2-7694 (1974) (in Russian).

8) P. Fong; "Statistical Theory of Nuclear Fission", Gordon and Breach Science Publisher, N.Y. (1969).

9) A.G.W. Cameron; Canad. J. Phys., 35, 1021 (1957).

10) Y. Nakahara and T. Tsutsui; the NMTC/JAERI code, to be published in the near future.

11) R. Vandenbosch and J.R. Huizenga; "Nuclear Fission", Academic Press (1973).

12) S. Cohen and W.J. Swiatecki; Ann. Phys., 22, 406 (1963).

13) A.E.S. Green; Phys. Rev., 95, 1006 (1954).

14) G.A. Pik-Pichak and V.M. Strutinskii; "Physics of Nuclear Fission", pp.8 - 18, (ed.) N.A. Perfilov and V.P. Eismont, Israel Program for Scientific Translation, Jerusalem (1964).

15) R.A. Grass et al.; Phys. Rev., 104, 404 (1956).

16) E.F. Neuzil and A.W. Fairhall; Phys. Rev., 129, 2705 (1963).

17) R.G. Vasil'kov et al.; Atomnaya Energiya, 44, 329 (1978).

Appendix : Computer code system for neutronics calculations of accelerator target/blanket

The computer code system prepared at JAERI to use on the FACOM-M200 computer for the neutronics analysis of accelerator driven nuclear fuel breeders and intense spallation neutron sources consist of many codes, interrelations between which are illustrated in Fig.A1 as well as the flow of computations.

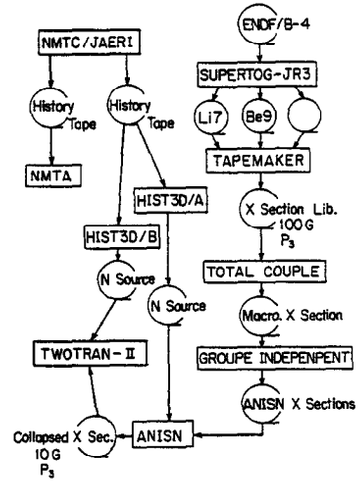

Fig.A1 Flow of neutronics calculations

Studies of Cold Neutron Sources for Spallation Targets.

W. Reichardt
Kernforschungszentrum Karlsruhe
Institut für Angewandte Kernphysik I
7500 Karlsruhe, Postfach 3640
Federal Republic of Germany

1. Introduction

According to our present knowledge the main region of interest for the application of cold neutron lies between 3 Å and 20 Å which corresponds to .2 meV<E<10 meV. For λ>100 Å we have the region of ultra cold neutrons whereas the intermediate region has not been used much up to now. The need for cold neutrons appears to be met optimally by a large deuterium source like the cold source installed at the HFR Grenoble. Fig. 1 shows the maximum possible neutron intensities obtained by shifting the Maxwellian distribution in a large non absorbing moderator towards lower temperatures (upper dashed line).

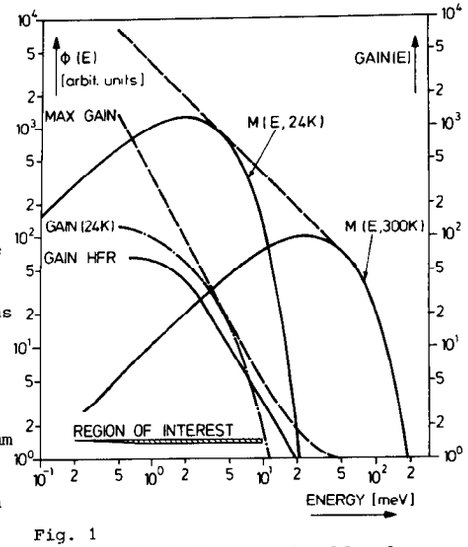

Fig. 1
Fluxes and gainfactors of cold moderators

The Maxwellian distribution for T=24 K, the boiling temperature of D_2, has its broad maximum right in the middle of the region of interest. The corresponding intensity gain is indicated by the dash-dotted curve. The actual gain achieved with the Grenoble source is somewhat smaller due to the following reasons:

1. finite size of the cold moderator
2. position of coldest spectrum in the center, not at the surface
3. flux depression by structural elements

4. absorption and scattering of the neutron beam in the walls
5. rethermalization of neutrons in the moderator layer between source and beam tube

The curve marked by MAX. GAIN gives the maximum possible gain if the source temperature is always adapted to the particular neutron energy used in the experiment. This curve is not very far from the actual D_2-result above about 2 meV. This demonstrates that there is no need for an intermediate source with a moderator temperature above that of liquid D_2. On the other hand it may be worth while to look into the performance of a solid D_2 source cooled with liquid helium by which higher intensities below 1 meV may be obtained. However, it can be foreseen, that serious cooling problems will arise for such a source.

The intensity emanating from a cold source is given by $I(E) \sim \phi_{th}(E,\vec{r}) \cdot GAIN(E)$ where $\phi_{th}(E,\vec{r})$ is the thermal flux in the moderator without the cold source. It is this quantity which has to be optimized. Fig. 2 shows a typical radial distribution of the thermal flux in a D_2O moderator.

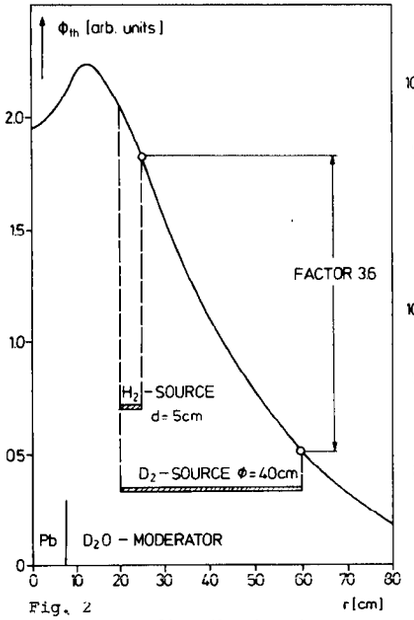

Fig. 2
Radial flux distribution in a cylindrical Pb target - D_2O moderator assembly

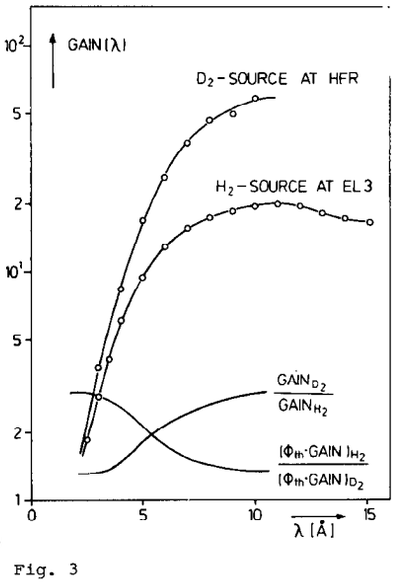

Fig. 3
Gainfactors of H_2 and D_2 sources

These calculations are based on the assumption that there are no gas bubbles in the liquid. The small difference between the two upper curves in Fig. 4 tells us that in a large vessel a considerable amount of gas bubbles (up to 50 volume %) can be tolerated without appreciable disadvantage for the efficiency of the source if these bubbles are distributed about uniformely in the liquid.

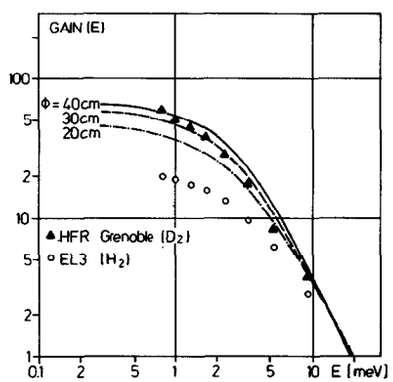

Fig. 4
Gainfactors for D_2 sources of various sizes

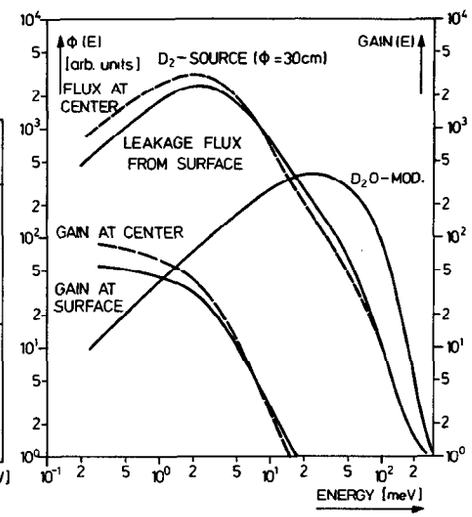

Fig. 5
Fluxes and gainfactors at the center and from the surface of a spherical D_2-source with 30 cm diameter

3.2 Reentrant Hole

The most efficient rethermalization of the neutrons occurs in the center of the cold source. Therefore, by using a reentrant hole reaching to the center of cold moderator a better performance of the cold source may be achieved. As the cross section of the reentrant hole has to be of the order at least of 200 cm^2 this can be done only in cases of a large D_2 vessels. Fig. 5 compares the leakage flux from the surface of a 30 cm Ø source with the flux at the center and shows the corresponding gain factors for a case where there is no gradient in the integrated

flux of the surrounding moderator. The small differences between the two spectra does not seem to justify the installation of a reentrant ho hole.

However, the use of a reentrant hole may be advantageous if the neutron beam is extracted in the direction of a strong flux gradient because it shifts the radiating surface to a position of higher integrated neutron flux. Plans on these lines are presently being discussed at the HFR in connection with the "deuxieme souffle". An improvement by a factor of two is expected /5/.

4 H_2-Cold Sources

4.1 General Aspects

Compared to the D_2 sources the problems in connection with H_2 sources are much more complex. We may distinguish between three cases according to the postulations put forward by the users as listed in Table 2.

case	postulations		mode of operation of accelerator	production of cold neutrons	position of the cold source
	ϕ_{av}	ϕ_{max}			
1	high	not of interest	steady state	rethermalization of thermal neutrons from surrounding moderator	maximum of thermal flux
2	not of interest	high	short proton pulses $\Delta t_p \approx 1\mu s$	moderation of fast neutrons in the source itself	as close to the target as possible
3	high	high	coarse pulsing $\Delta t_p \approx 500\mu s$	rethermalization of thermal neutrons + moderation of fast neutrons	intermediate between target and maximum of thermal flux (in reality: close to the target)

Table 2: Use of H_2-sources at proton accelerators

The problems in connection with case 1 are similar to those encountered with hydrogen sources in reactors with the main difference that the heating by fast neutrons is more severe. In order to obtain high peak currents (case 2) the cold source has to be placed very close to the proton target. Crude estimates lead to a nuclear heating of about 2 to 3 KW per liter H_2 and 1 MW of proton beam power for a Pb Bi target.

In the region of the large D_2 source with 40 cm diameter the thermal flux drops by a factor of 4. If the cold neutrons are extracted radially i.e. from the outer surface of the source, as is done at the HFR, the flux level is small. If we use a slab hydrogen source placed in such a way that the distance to the target (or core) is the same as that for the D_2 container this source will have a much better performance as is seen in Fig. 3. Although the gain factors obtainable are smaller than those for D_2 /1/ the intensity of cold neutrons is higher in the whole energy region.

2. Nuclear Heating

SOURCE OF HEATING	SOURCE DISTRIBUTION
1. γ's from (n,γ) reactions in the core or proton target 2. γ's from the fission and/or spallation process 3. high energy protons from the target	$I_\gamma \sim e^{-\frac{r}{25}}/r^2$
4. fast neutrons	$\phi_f \sim e^{-\frac{r}{9}}/r^2$
5. γ's from (n,γ) reactions in the surounding moderator and structural elements (beam tubes) 6. γ's from (n,γ) reactions in the cold moderator and structural elements of the cold source 7. β's from the β-decay after (n,γ) reactions in the structural elements of the cold source	$\sim\phi_{th}$

Table 1: Nuclear heating in a cold source

Table 1 shows the main processes responsible for the nuclear heating of a cold cource. For a Pb-Bi target the contributions due to the γ's from the target are considerably reduced compared to the core γ's in a reactor and may be neglected in the heating calculations. This is generally considered as a particular advantage of a spallation source. However, it should be mentioned that for the HFR source only one quarter of the total nuclear heating is due to the γ's from the core /2/. Little is known about the influence of high energy protons. A Bi layer of suitable thickness between the target and the source may eliminate this contribution. The heating due to items 5 to 7 is proportional to the thermal neutron flux and therefore a common problem for both the reactor and the spallation source.

A major problem seems to be caused by the fast neutrons due to the rather hard source spectrum. In a reactor the fission spectrum has a mean energy of $\bar{E}$=2.0 MeV. According to the measurements of Cierjacks et al./3/

the average energy of the source spectrum from a Pb target is 25 MeV, which is a factor 12.5 higher than for the fission spectrum. However, in the heating calculations a factor of 2.5 instead of 12.5 corresponding to $\bar{E}$=5 MeV, seems to be more adaequate. These values can be made plausible by the following considerations:

1. In liquid hydrogen and deuterium the scattering mean free path increases beyond 50 cm for energies above 30 MeV. Thus even a large D_2-source with linear dimension of 30 to 40 cm becomes transparent for neutrons above 30 MeV. With 30 MeV as a cutoff energy an average energy of $\bar{E}$=5.5 MeV is obtained using the data of Cierjacks et al.
2. Calculations on the energy deposition by fast neutrons in a H_2-source close to the spallation target taking into account the detailed source spectrum yield the same result as a simplified calculation based on a single group of fast neutrons with $\bar{E}$=4.5 MeV.
3. Measurements of the fast neutron yield from a Pb-Bi spallation target by Gompf and Reichardt /4/ using a modified long-counter yielded an average energy of about 4.5 MeV for those neutrons of the source spectrum which are moderated in the paraffine and afterwards recorded in the detector. Thus existing calculations for cold sources in reactors may be used also for spallation source problems if we increase the energy deposition caused by fast neutron collisions by a factor of 2.5.

3. D_2-Sources

3.1 Size Effects

Due to the large dimensions of a D_2-source the installation of such a source is only possible in a D_2O moderator where the thermal flux distribution is only slowly varying. However, we have seen before that also in D_2O the thermal flux changes by a factor of four along a distance of 40 cm which corresponds to the diameter of the Grenoble cold source. This rises the question about the efficiency of smaller D_2-sources. Fig. 4 shows calculated gainfactors for three diameters of spherical sources (d=40,30,20 cm). Even the small source with a diameter of 20 cm yields higher gains than the H_2 source. Compared to the large vessel with a diameter of 40 cm the intensity is reduced only by a factor of 1.5 below 1 meV. Above this energy the intensity losses are even smaller. Therefore it may be advantageous in specific cases to use a small D_2 source with a diameter of about 20 cm if this allows to install the source closer to the target where the flux in the moderator is higher. This, however, will increase the heating problems.

Most of this heating is caused by the fast neutrons. If the compressor ring of the German spallation source project can make use of the full beam current of the linac, there will be about 12 to 18 KW of heat production in a hydrogen cold source of volume 1 liter if it is placed close to the target. This means that there will be only vapour in the container. A layer of H_2O of suitable thickness between the target and the cold source will devrease the nuclear heating. However, it will decrease the cold flux in a similar way, as in hydrogeneous moderators the distribution of the thermal neutrons closely follows that of the fast neutron flux.

Case 3 represents the German spallation source project without compressor ring. It is hoped that stationary experiments can be performed under similar conditions as at the HFR whereas TOF experiments will profit considerably from the pulse structure. A suitable cold source seems to be a hydrogen source in a D_2O moderator. Peak intensities for the energy integrated neutron flux of about 10^{16} (n/cm^2 sec) are expected if the cold source is placed close to the proton target. This, of course, leads to the same unsolvable heating problems that have been mentioned in connection with case 2. However, in the present case, the fast flux and thus the nuclear heating decreases faster than the thermal flux if we remove the cold source from the target to a position where the technical problems caused by the nuclear heating become solvable.

The short mean free path of subthermal neutrons together with the postulations for large beam cross-sections, where the height should be larger than the width, lead to the plate shaped hydrogen cold sources. Typical dimensions are: 25 cm high, 12 cm wide, 5 cm thick. Due to this shape the position of the H_2-source will respect to the proton target is of considerable importance. Four cases have to be considered:

1. proton beam horizontal, source in WING-geometry
2. proton beam horizontal, source in SLAB-geometry
3. proton beam vertical, source in WING-geometry
4. proton beam vertical, source in SLAB-geometry.

As in general cold neutrons are extracted via neutron guides, the background problems are less severe than with thermal beam tubes. Therefore slab-geometry seems to be preferable as the target moderator coupling is better than for wing geometry. Obviously Nr. 1 is rather unfavourable configuration for in addition to the bad target-moderator coupling the cold neutrons flux decrease rapidly with increasing distance from the

target. Therefore the upper part of the cold source does not contribute much to the extracted neutron beam. Configuration 2 cannot be realized with a target wheel and those targets where the cooling circuits are lying in a horizontal plane. More satisfactory configurations are achieved if the proton beam hits the target vertically.

4.2 Parahydrogen

It has been shown by Würtz /6/ that for spallation neutron sources with short proton pulses (∿1μs) the use of para-hydrogen will offer considerable advantages as the lifetime of the subthermal neutrons is considerably smaller than in all other hydrogeneous moderators. This is caused by the peculiar behavior of the neutron cross-section which drops to a rather small value of 1.5 barn below 14 meV (see Fig. 6). The corresponding mean free path is 16 cm. Thus neutrons scattered down below 14 meV have a high probability to be emitted from the moderator without further collisions. Fig. 7 shows the mean emission time as function of energy for neutrons leaking out of a cylinder (15 cm Ø, 15 cm height) of almost pure para-hydrogen.

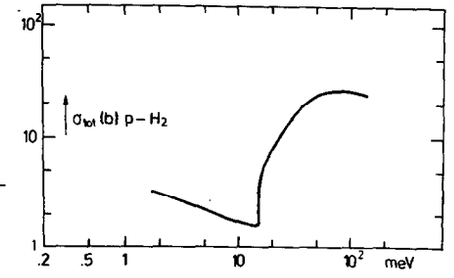

Fig. 6
Total slow neutron cross-section of para-hydrogen

The ordinate is the variance Δt which is defined by $\Delta t=\sqrt{\overline{t^2}-\overline{t}^2}$. For an exponential decay $\Delta t=1/\lambda$ where λ is the relaxation constant. Above 30 meV we find the typical $1/\sqrt{E}$ bahvior of the slowing down region. However, also below 10 meV the curve roughly follows an $1/\sqrt{E}$ dependence. This is caused by the fact that the time for emitting a neutron from the moderator surface is essentially determined by the time elapsed between the scattering process and the arrival of the neutron at the surface of the moderator. This time behavior is very useful for time of flight experiments as it leads to a constant energy resolution.

The other 77% para-23% ortho mixture also shown in the figure is somewhat arbitrary as it does not correspond to the usual high temperatur

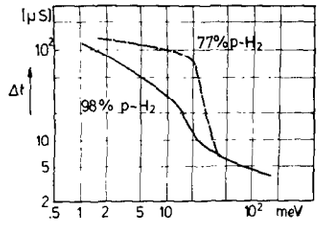

Fig. 7
Variance of the neutron emission time from liquid hydrogen

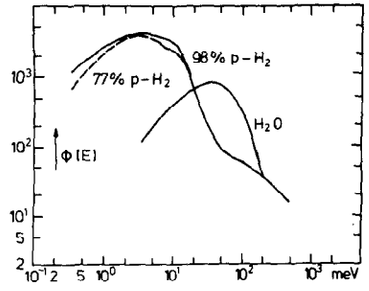

Fig. 8
Stationary leakage spectra from liquid hydrogen

equilibrium composition of 25% para-75% ortho, which is mostly conserved also in liquid hydrogen unless special efforts are undertaken using ortho-para converters. As the scattering by para-hydrogen is very small compared to that by ortho-hydrogen below 14 meV its presence can be largely neglected in this energy region. Thus the dashed curve will be representative also for the usual para-ortho composition. As can be seen from Fig. 8 the time integrated intensities $\bar{\Phi}(E)$ are nearly the same for the two cases. Therefore the peak intensity $\hat{\phi}$ in para-hydrogen is considerably higher than in ordinary hydrogen according to the relation $\hat{\phi}(E) \sim \frac{\bar{\Phi}(E)}{\Delta t(E)}$.

5. A D_2 Source for the German Spallation Source Project

Fig. 9 shows a possible arrangement for a D_2 source in the heavy water tank above the target wheel as proposed by G. Bauer /7/. The volume is about 30 l - similar to that of the HFR -, the midpoint is 36 cm from the midplane of the target wheel. Cold neutrons are extracted vertically at an average thermal flux level of about $3 \cdot 10^{14}$ n cm/sec.

Fig. 10 compares the thermal and fast flux distributions in the D_2O tank along the cylinder axis with those of the HFR. The later data were taken from the "Yellow Book" /8/ and represent the unperturbed thermal flux. The zero point for the abszissa is the surface of the fast neutron source (core, spallation target) for both cases. The curves for the spallation source were obtained from a two dimensional multigroup diffusion

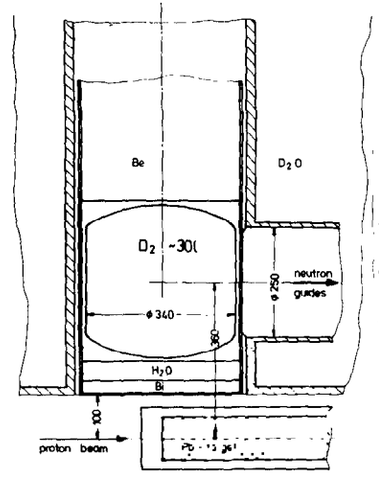

Fig. 9
D_2-source proposed for the German spallation source

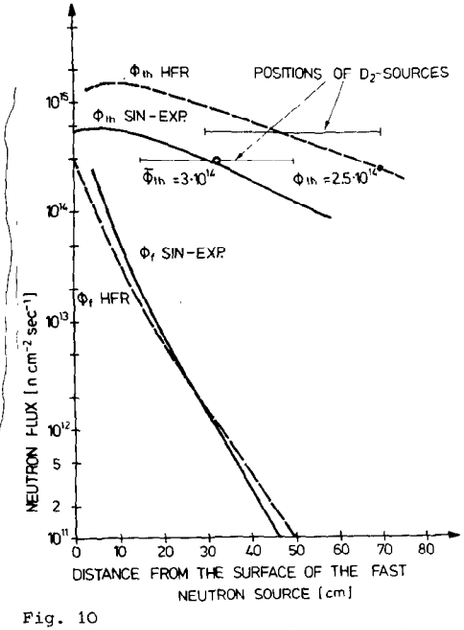

Fig. 10
Fast and thermal neutron fluxes in the D_2O moderator

calculation simulating a pilot experiment performed a SIN. The height of the thermal flux was adapted to the flux values measured in the SIN experiment. It decreases somewhat faster with increasing distance from the source than the HFR flux due to the smaller size of the heavy water tank compared to the vessel of the HFR. The fast fluxes do not differ much in the region of interest. (In the calculations the fast neutron spectrum was truncated at 10 MeV). Also indicated are the positions of the D_2 sources and the average thermal fluxes at the points of beam extraction. Based on the data for the HFR source we have estimated the heat production in the cold source under the assumption that the structural materials are the same for both cases (inner vessel 1.5 mm Al. outer vessel 8 mm zircaloy.) The results are shown in Table 3. The quoted figures can be considered only as very rough estimates due to the fact that detailed information about the

source	volume	$\bar{\Phi}_{therm}$ at position of beam extraction	heating [Watt] by			total [Watt]
			core γ's	fast neutrons	(n,γ) β	
HFR Grenoble	30 l	$2.5 \cdot 10^{14}$	1460	140	4200	5800
spallation source	30 l	$3 \cdot 10^{14}$	-	3000	2400	5400

Table 3: Nuclear heating of D_2-sources

amount of structural material in the environment of the cold source is not yet available. However, we learn from these figures that the nuclear heating in the source considered here has a similar magnitude as that in the HFR source. Therefore the cooling should not cause particular problems.

More serious problems may arise from the radiation damage caused by the fast neutrons in the Al-vessel. The side close to target views a fast neutron flux that is about 20 times larger than that impinging on the HFR source.

The time behavior of the cold neutron flux will closely follow that of the surrounding D_2O moderator. Therefore a peak intensity of the energy integrated flux of $2 \cdot 10^{15} n/cm^2$ sec is expected. A time of flight spectrometer placed at this source will have an intensity that is 8 times higher than at the IN5 in Grenoble.

References

/1/ P. Ageron, Progress Report 78 AG224T, ILL, Grenoble, 1978

/2/ P. Ageron et al., Note PCBT 223/70, C.E.A.-C.E.N.G., 1970

/3/ S. Cierjacks et al., "Neutron and Charged Particles Production Yields and Spectra from Thick Metal Targets by 590 MeV Protons", this conference.

/4/ F. Gompf, W. Reichardt, to be published

/5/ P. Ageron, private communication

/6/ H. Würtz, "Untersuchungen zur Neutronenthermalisierung an flüssigem Ortho- und Para-Wasserstoff", Thesis Karlsruhe 1972

/7/ G. Bauer, private communication

/8/ Neutron Beam Facilities at the HFR Available for Users

Engineering, Activity Handling and Emergency Considerations for a Rotating High Power Target

H. Stechemesser* and G.S. Bauer**

* Zentralabteilung für Allgemeine Technologie
** Institut für Festkörperforschung
Kernforschungsanlage Jülich GmbH, Postfach 1913, D-5170 Jülich, West Germany

1. Target Engineering

The target concept proposed for the German spallation source project (see also ref. /1/) is a disc or wheel-shaped target rotating about a vertical axis. It is mounted on a trolley and has moderators above and below the disc to provide the desired thermal and cold neutrons for extraction through beam holes or neutron guides.

For inspection, maintenance and certain repair operations on the target the trolley can be moved out of the shielding block where is located during operation into an inspection cell.

1.1 The target disc

The material to be used as spallation target is lead, although depleted uranium might be a candidate for a later version if sufficient experience has been accumulated. Four different possibilities for the internal structure of the target have been considered

I Target with evolvent-shaped segmentation of the material
II Target with arrangement of spheres
III Target with cylindrical elements
IV Massive ring target.

The heterogeneous arrangement in versions I to III allows very intense cooling and results in relatively low operating temperatures with the advantage of the material remaining solid and retaining good mechanical rigidity . The proton beam would enter the target through the outer periphery of the wheel, passing through a window which is part of the coolant-containment. The inner surface of this window is directly cooled by the target coolant (water). This, together with the fact that this window is hit by the proton beam only once per revolution, ensures low operating temperatures which are important for mechanical properties as well as radiation damage effects.

For the massive ring target (alternative IV) heat removal would occur only from the outer target surface. The resulting temperatures at the centre

plane would be high enough for the lead to melt. While this reliefs many of the thermal stresses, provisions are necessary to ensure proper containment of the material. Therefore the proton beam would hit the inner surface of the ring-shaped target with the outer, solid parts supporting the molten portion. To pass above the opposite part of the ring, the beam would be brought in, pointing slightly downwards. To confine evaporating target material a window with internal cooling was considered necessary.

The concept chosen for the reference proposal is alternative III (cylindrical target elements), with the Pb target cylinders clad in aluminium cans. The reasons are

- Well established manufacturing technique by electron beam welding
- Low temperature level (73K above coolant at hot spot /3/)
- Good thermal contact from target to cladding because of thermal expansion coefficients
- Easy handling of pins for disposal.

Some 9128 pins of 10 cm hight and diameters ranging from 18 to 24 cm are arranged on concentric circles in a close packed structure with 1 mm cooling gaps between neighbouring pins to form a target of 700 mm radial depth (Figs. 1a and b). The pins can expand individually without causing excessive thermal stresses on the support structure.

A static stress is caused on the target wheel structure (aluminium-magnesium alloy) by the pressure of the coolant (3 bars average) which drops by 0.5 bar from the inner to the outer target region. Finite element calculations are in progress to ensure adequate design throughout the structure.

1.2 Coolant supply, bearing and target drive system

The water needed to cool the target has to be brought in from the stationary support to the rotating target. The necessary rotating seals are integrated in a unit which at the same time provides for the support of the rotating wheel and encorporates also the drive system.

For the bearings, three possibilities have been considered

- Standard ball and roller bearing, oil lubricated positioned outside the high radiation field on an extended shaft /2/.
- Magnetic bearings using permanent magnets for the axial support and hydrostatic bearings for the radial guidance or magnets for both /4/.
- Hydrostatic water bearings.

Although the first two concepts are considered feasible and continue being examined, the last one was picked for the reference design because of

its low friction torque, its small structural dimensions, its short shaft allowing a small height of the transport trolley and because its spent water could be fed into the cooling circuit quite easily (Fig. 2).

The target disc is driven by a water turbine acting directly on the disc shaft. Nominal speed of 30 rpm is reached within 3 minutes and is measured by a contact free ceramic insulated inductive sensor. No high stability is necessary for the control of the target's rotation. The spent water from the turbine is also fed into the colling circuit.

The coolant flow as determined by the heat transfer coefficient on the pins is 250 $m^3 h^{-1}$, with a pressure of 3.5 bars when entering the target. The coolant flows from the centre of the wheel to the outer window and is returned through a large number of bores in the upper and lower support structure (Fig. 1). The sealing against the vacuum surrounding the wheel is on the low pressure side by a ceramic slide ring working against graphite and surrounded by a separately pumped vacuum space (10^{-1} bar) and an annular labyrinth gland towards the main vacuum (Fig. 2). Water seeping out of the seal can thus be pumped off separately and the conditions of the sealing can be checked via the water leakage. The expected leakages is about 10 g/h under routine conditions.

1.3 The target trolley

To enable the target to be moved into and out-of operating position, it is mounted on a trolley (Fig. 3) which is also part of the target shield during operation. All supplies to the target and the lower moderator are incorporated in this trolley with the connections arranged at the rear end. All feed-throughs on the trolley are arranged to minimize neutron streaming in them. Jumpers which can be placed by remote handling provide the connections to the stationary ducts. One common vacuum hood will cover all the feed-throughs. The total weight of the trolley is about $12 \cdot 10^5$ kg. It is supported by 32 wheels arranged in twin sets and running on two rails.

2. Active handling system

Active handling will have to be provided for (1) the target disc, (2) the bearing, driving and water sealing unit, (3) the target trolley, (4) the lower moderator, (5) the last proton beam deflection magnet, (6) the upper moderator tank and cold source, (7) the beam shutters and, (8) the beam tube windows. Items (1) through (5) which are the most likely ones to need servicing can be handled using the provisions in the inspection cell alone. Servicing or

replacing items 6 and 7 requires temporary use of the crane in the hall above the target block (see ref. /1/) to transport these parts through this hall before lowering them into the inspection cell through a hole which can be opened between them. If one of the beam windows has to be changed, this will be done with suitable equipment through the beam tube.

In order to retrace the target trolley into the inspection cell, part of the proton beam line will be removed and the heavy deflection magnet (see Fig. 4) will be moved to the far end of the cell on rails. After this the vacuum cover over the trolley's connecting pipes will be removed and the jumpers disconnected. For this purpose a heavy duty manipulator will be available which can use tools of up to 50 kg weight or lift parts up to 5000 kg. In addition, the cell will be equipped with a crane of 25000 kg lifting capacity and four directly operated manipulator units.

A special engine will be available to move the deflection magnet or the target trolley on their rails into a position where several non-destructive tests can be carried out such as visual inspection by television, microhardness measurements, collection of irradiated test probes, leak testing and examination and exchange of the transport wheels. The target disc, the support and driving unit and the lower moderator can be dismounted and replaced in this cell.

Parts which have to be put out of service, in particular spent target discs, will be transported to the adjacent hot cell where they are prepared for disposal. Here equipment for machining and cutting will be available to dismantle the target wheels and remove the target pins one by one to be safely packed for shipment.

3. Emergency considerations

The proposed design has been chosen largely to minimize hazards which might result from the target operation. As a primary precaution, the proton beam will be turned off whenever irregularities in the operating parameters are detected. Since the beam can be shut off in lees than one pulse's duration (i.e. in a few tens of microseconds) the emphasis has to be on the detecting systems for any fault that might occur.

3.1 Loss of proton beam

In the case of a loss of the proton beam along the beam transport line, increased radiation levels in the tunnel will lead to a shutdown of the accelerator. This will also be true if the vacuum in the beam line is lost.

These cases do not constitute a hazard to the target's operation.

3.2 Loss of target coolant

Loss of target coolant can occur due to rupture of the supply pipes or due to failure of the operating water pumps. The coolant flow will be monitored by redundant pressure and flow gages in the circuit and by the pumps' electrical data. The temperature of the coolant will also be measured. All joints are equipped with leakage detecting systems and the water vapour content in the vacuum system will be monitored.

If a complete loss of coolant occurs, each proton pulse will heat the most heavily loaded target pin by 70 degrees. Since each pin returns to the proton beam only after 2 seconds, and a temperature rise of 150 degrees is no problem, no specially fast detection systems are needed. It should be noted that it is foreseen to have always two coolant pumps with separated pipe systems and independent electrical supplies operating in parallel and that also the spent water from the turbine and the bearings contribute to the coolant flow. It is therefore extremely unlikely that any sudden complete loss of coolant will happen at all.

3.3 Afterheat

According to calculations /5/ the heat production in the target immediately after shutoff of the beam from full power will be 40 kW and will drop to 25 kW within ten seconds and to 12 kW within one hour. Assuming that all heat is stored in the target with heat exchange occurring only within the target, the target temperature would rise by 150 K within the first hour, which would still be below the melting point of lead. Although being very conservative, this estimate shows that minor cooling for 24 hours (100 ℓ of water per hour) after shutoff is sufficient to keep the target in safe conditions for later use. Even in an emergency case there would be ample time to start safety measures such as sprinkling the target from outside to avoid any damage.

3.4 Failure of target pin cladding

Should the aluminium containment of some of the target pins fail, e.g. due to burnout following a cooling gap closure or due to corrosion effects, this will eventually result in an increase of the coolant activity level. Since the amount of water in the circuit is fairly high, it will be necessary to monitor the water and the filters for specific radioactive nuclides

which can only be produced from the target and not from the structural material. Due to the large number of pins in use, the release of activity will always be small if one or a few of the pins become defective. The target will be put out of service if coolant contamination becomes intolerable.

3.5 Loss of water pressure in the bearings

If the water supply for the turbine is turned off routinely, the friction in the sealing will bring the target wheel to a standstill after two minutes if water lubrication and pressure for the bearings remain normal. Should the water pressure of the bearings and the turbine be lost simultaneously, the time needed for slowing down the wheel would be 35 seconds. Since the change in the wheel's speed of rotation as well as the pressure loss would lead to a shutdown of the proton beam, there is no risk of overheating due to the wheel's slowing down.

References

/1/ G.S. Bauer
Layout of the Target Station for the German Spallation Neutron Source Project
this conference

/2/ G.S. Bauer
Design Studies for a Rotating Target for a Spallation Neutron Source
Jül-Conf 35, p. 155-183

/3/ F. Stelzer
private communication

/4/ K. Boden and J.K. Fremerey
private communication

/5/ T.W. AMmstrong, P. Cloth, D. Filges, R.D. Neef, G. Sterzenbach and M. Kloda
"Studies Related to Spallation Target Physics"
this conference
and T.W. Armstrong, private communication

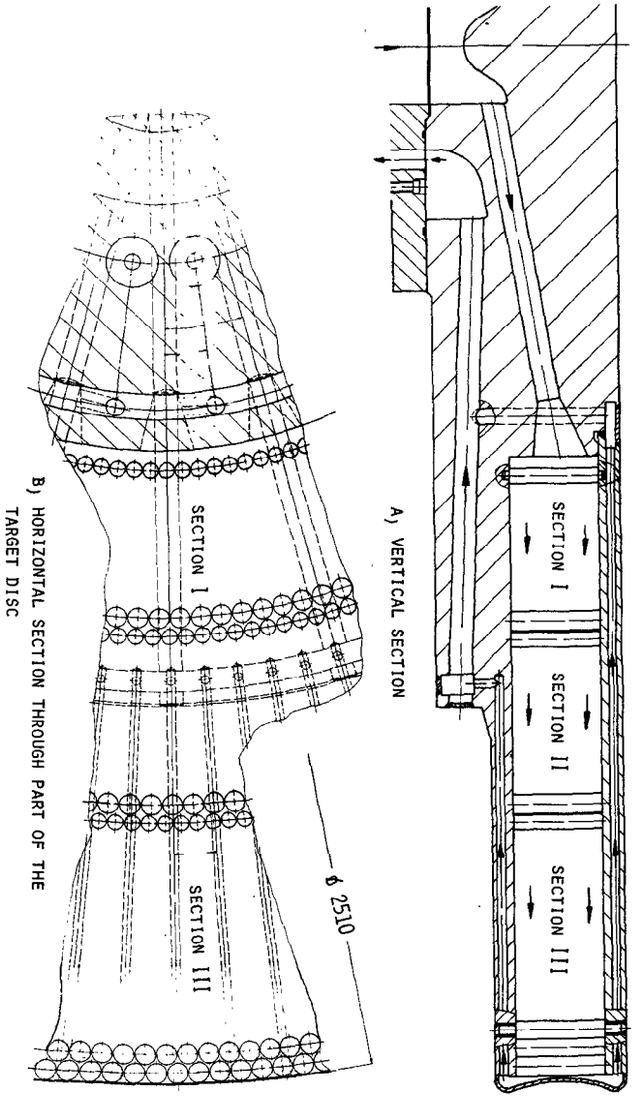

FIG.1 ARRANGEMENT OF TARGET PINS AND COOLANT CHANNELS IN THE TARGET DISC, CLOSELY PACKED PINS OF DIAMETERS VARYING FROM 24 TO 18 MM ARE ARRANGED IN THREE GROUPS OF CONCENTRIC CIRCLES.

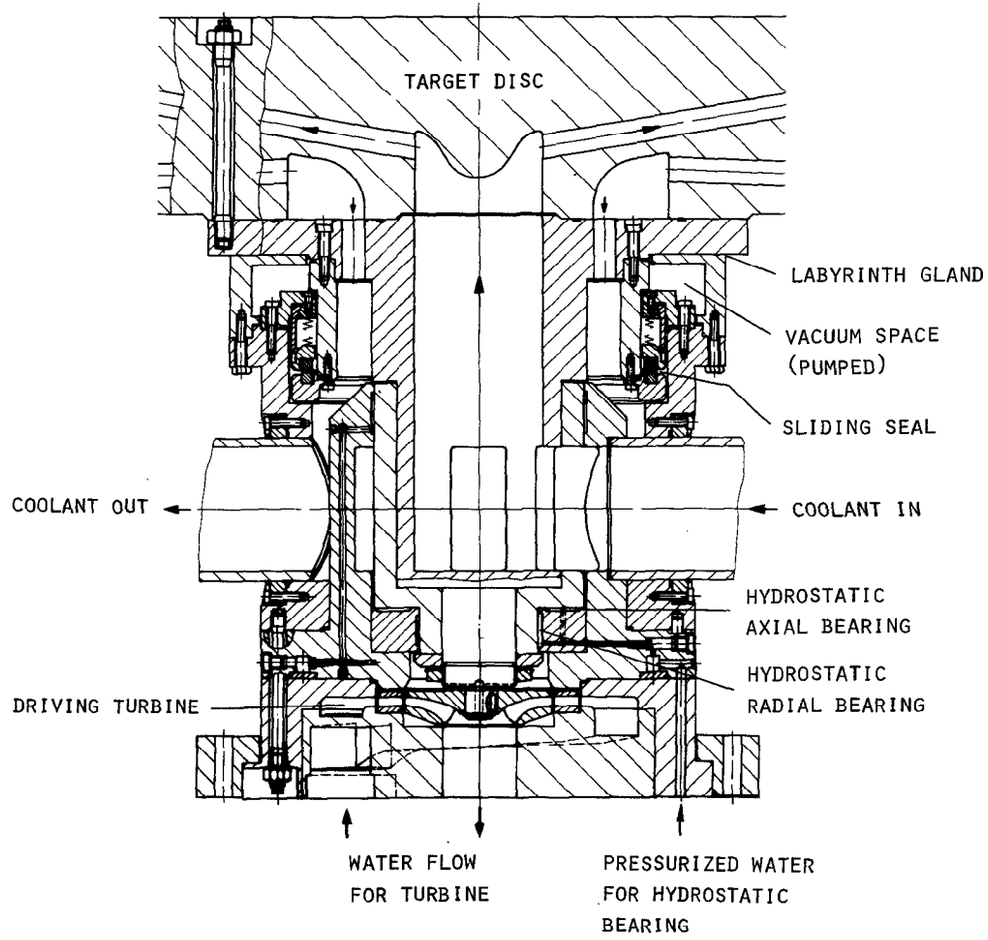

FIG.2 SECTION THROUGH TARGET SUPPORT AND DRIVE UNIT

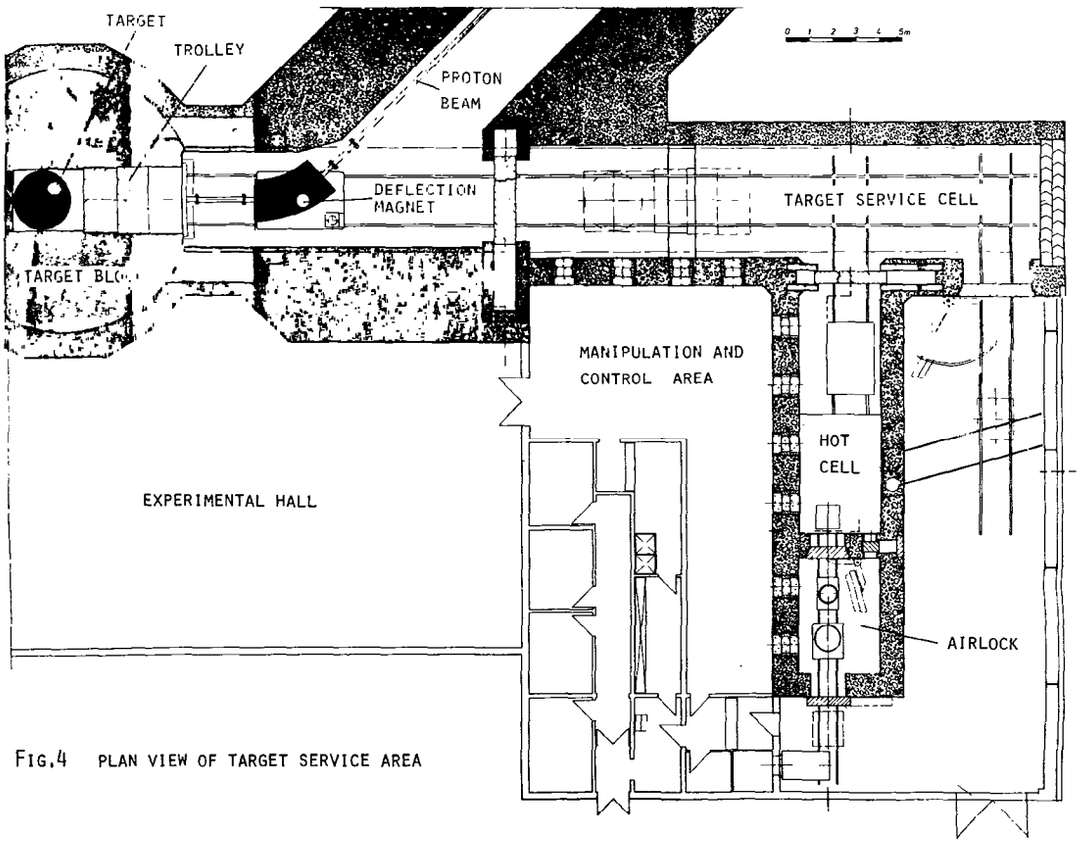

FIG.4 PLAN VIEW OF TARGET SERVICE AREA

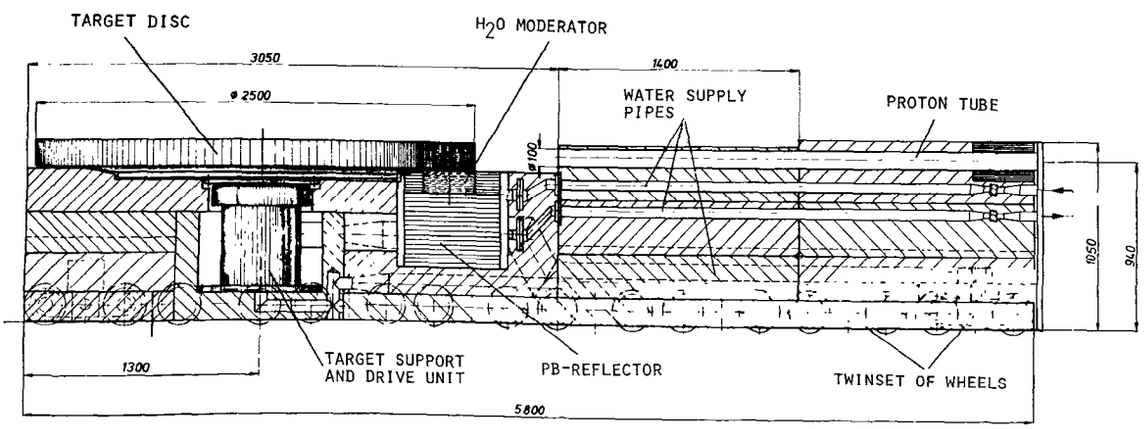

FIG.3 VERTICAL SECTION THROUGH TARGET TROLLEY WITH TARGET WHEEL AND WATER MODERATOR

Materials Problems in Beam Windows and Structural Components of the SNQ-Target

W. Lohmann
Institut für Festkörperforschung
Kernforschungsanlage Jülich GmbH, Postfach 1913
D-5170 Jülich, West Germany

1. Introduction

The materials performance of structural components must provide a reliable and economic operation of the SNQ target station. This means, that also critical parts should last for reasonably long times like two years, or have to be replaceable during shut-down periods easily. The load for these parts is strongly influenced by these LINAC reference data:

- E_p = 1.100 MeV
- $\bar{I}_p$ = 5 mA; $\hat{I}_p$ = 100 mA
- ν_p = 100 Hz
- FWHM = 4 cm

Apart from the lifetime question, there is another requirement: a change from the Pb- to a U-target with the connected higher thermal load has to be allowable. This implies a strength reserve of the material for higher temperatures as quoted for the reference design.

The information given in this paper is based on available irradiation, temperature-dependent strength and corrosion data. Results coming from the Fusion Reactor Materials R+D are of special importance. The considerations are valid for the present layout of a rotating target, being an essential part of the German high power spallation neutron source project (17, 18).

2. Thermal Load and Radiation Damage of Structural Material

The mean LINAC beam power of 5.5 MW will cause a high power density in parts hit by the proton beam. This is the case for the beam window, the cladding of the target rods and for the target material itself. Typical values of the mean power density

range from 2.7 $\frac{kW}{cm^3}$ for Mg up to 10.1 $\frac{kW}{cm^3}$ for Mo. Due to the heat deposition distribution, the highest temperatures are expected within the beam window on the centerline of the beam.

Further, these components suffer thermal fatigue out of different reasons, as treated in chapter 3 in more detail.

In addition to that, radiation damage is created by the high energetic protons, the produced neutrons and by secondary particles like spallation fragments. This leads e.g. to the following macroscopic effects, given in the order of decreasing importance:

- <u>embrittlement</u>, due to internal production of light gases or due to the shift of the ductile-brittle-transition temperature into the operations temperature range.
- <u>swelling</u>, due to voids or solid transmutation products.
- <u>radiation enhanced diffusion</u>, by which the release of undesirable spallation products is facilitated.
- <u>sputtering</u>, which could be a problem for thin foils (cf. 3.122)
- <u>corrosion</u>, e.g. by the radiolysis of the coolant and followed by an attack on the piping system.

The synergetic effects are of special importance and should be investigated carefully. So, fatigue under irradiation will have a strong influence on the lifetime, and the decrease of the thermal conductivity (irradiation leads to decohesion of the grain boundaries) should be taken into consideration.

The operations conditions are much less severe for material outside of the proton beam. They are similar to fission reactor conditions (Table 1). Therefore, mainly an analysis of the worst case is necessary. As an example, one can consider the beam window.

3. Problems of Beam Windows

One can define two different versions of a beam window:

a) A stationary window, separating the whole target station from the accelerator tube. It is necessary for the (back-up) liquid metal target design. Because of some advantages (avoidance of water leakage into the accelerator tube, further activity

barrier), it is a desirable component for the rotating target, too.

b) The target wheel circumference is called the rotating window. It is an essential part of the target wheel (17).

3.1 Stationary Window

3.11 Operations Conditions

Operations conditions like the following are expected:

- pressure differential over the window of about 3 bar,
- high temperature, dependent on the choice of material, thickness and cooling mode,
- high cycle thermal fatigue, caused by the accelerator time structure.

The latter two points are illustrated in Fig. 1. For Mo, one has a mean temperature of about 800°C with a ΔT of about 50°C and a repetition frequency of 100 Hz.

- high damage rate, mainly determined by the protons,
- high gas production rate, for which also the protons are decisive.

One can calculate by Monte Carlo Methods (NMTC, HETC) (1) values for some metals (Table 2). The range for displacement damage spreads from 0.05 up to 3.10 dpa/day. The He-production rate lies between 15 and 125 appm/day, and the H-production rates show about seven times higher numbers. The main problems, based on these data, are considered to be strength at high temperatures, high temperature embrittlement as a result of the huge He-quantity, and fatigue under irradiation. There is a fairly limited choice of materials, which are able to withstand these conditions.

3.12 Possible Candidate Materials

3.121 Refractory Metals (RM)

The RM show good mechanical strength, also at higher temperatures. For this class of materials, there is a favourable combination of thermal expansion, Young's modulus and thermal conductivity, which keeps thermal stresses small. The high T_m will facilitate the cooling. From the high solubility of H in RM and the high H-diffusitivity at higher temperatures one can

conclude, that the H-production should not be a problem here.

Looking at the irradiation properties, nearly only n-irradiation results are available. They indicate a very high resistance against void swelling, and a lot of adjustable parameters is known, too. For example, V-20 Ti shows no void swelling at all after 38 dpa at 650°C (2).

The RM of goup VI (like Mo) show a strong shift of the ductile-brittle-transition temperature (DBTT) under irradiation. For a n-irradiation of Mo at 425-1000°C and 11 dpa, a DBTT up to 700°C was found (3). As a further disadvantage, the effects of high He-concentrations are generally not known; due to the low thermal He-release, also for temperatures approaching T_m, severe detoriations are likely. By an appropriate choice of T/T_m, which can be kept small, unfavourable, thermally activated processes can perhaps be avoided.

3.122 Metallic Glasses (MG)

This new kind of materials offers several advantages, like very good strength/fatigue properties (4) and an excellent corrosion resistance, at least for Cr-containing MG (5).

As an unique feature due to the amorphous structure, a damage of dpa-type is not produced. Further, MG containing some crystalline phase may be reconverted to the glassy state under irradiation. This has been demonstrated e.g. for $Nb_{40}Ni_{60}$ (6).

Also the behaviour of He in MG might be different from crystalline metals. This is indicated by microhardness measurements (Fig. 2) (7), as well as by microstructure investigations (TEM) (8) of He-implanted samples. Further research within this field is under way in our institute.

Of course, there remain a lot of technological problems. The MG-production by methods like splat-cooling or roller-squeezing is connected with geometrical restrictions in diameter (~3 cm) respectively in width ($\leq$ 16 cm) and in thickness, which is about 50 µm typically. In principle, these limitations can be avoided by using the (very ambitious and expensive) high-rate sputtering method. To get bulky material, an explosive compaction technique has been shown to work for special MG (9). For the difficult task of welding and joining, only very few techniques like explosive

or ultrasonic welding seem to be applicable at all.

Because of the metastable state of the MG, the operations temperature has to be kept below the glass temperature T_g. MG with a T_g up to 900°C have already be found. A further increase of T_g by an appropriate choice of constituents for RM-based MG seems to be possible, although difficult, because these components do not belong to the easy glass formers. Nevertheless, a potential for R+D can be seen.

3.2 Rotating Window

Here are relaxed operations conditions:

- pressure differential of ~ 3 bar will exist,
- low mean temperature (~ 50°C) because of rotation and efficient cooling (16),
- low cycle thermal fatigue due to the wheel rotation frequency of 0.5 Hz and a ΔT of 15°C. These values hold for a Al-window, 5 mm thick,
- radiation damage reduced by a factor of at least about 200, given by the ratio of beam width versus wheel circumference.

For aluminium, this gives about 3.4 dpa/year, a He-production of 130 appm/year including (n,α) and T-decay, a H-production 302 appm/year including (n,p) and a Si-production of about 0.15%/year (1 year = 6.000 operation hours).

Problems remaining here are the still fairly high thermal stresses and particularly the fatigue under irradiation. For the case of Al under p-irradiation and operations conditions similar to those quoted above, an effect on the microstructure (bubble-like inclusions at the grain boundaries) has been detected after ~0.1 dpa, giving ~10 appm He (10). A more detailed study of this synergetic effect is under way at the KFA.

3.21 Candidate Materials

First choice in this case is Al. It shows good thermomechanic properties, a favourable behaviour with regard to neutronics and induced activity and offers a manageable technology.

3.221 Al-Mg-Si Alloys

In order to keep relative changes in the Si-content small,

it is proposed to use a Si-containing alloy from the very beginning. The material has an adequate strength for temperatures below ~ 150°C. Joining and welding can be practised by standard methods.

Being a reactor material, the n-irradiation response is fairly well known. Especially the alloys from the US-6000 Al series are very irradiation resistive; after 260 dpa at 328 K, a swelling of less than 1% was found (11). The ductility still remains acceptable (5-10%). Nearly no data are available for the fatigue under irradiation, so experiments are necessary.

3.222 SAP

The sintered aluminium product (SAP), consisting of an Al-matrix with Al_2O_3 as a second phase, presents good mechanical properties (strength, fatigue) also at higher temperatures (> 150°C), where conventional Al-alloys fail. These temperatures could occur, if one goes on from Pb to U as a target material.

On the other hand, the material is fairly brittle, and joining as well as welding is not well developped. But there seem some possibilities for materials preparation such, that a weldable border (Al) surrounds the rest of the component. This is under investigation in more detail.

A major advantage of SAP is the ability of allowing high amounts of light interstitial gases without drastic degradiation. This has been demonstrated for He/H-contents of up to 1700 appm each (12). The other radiation damage data are comparable with those of Al-alloys. Again, data for fatigue under irradiation are still missing.

4. Further Materials Problems

4.1 Cladding of the Target Rods

Apart from the lower heat production (wall thickness ~0.5 mm), the materials problems are equal to those of the rotating beam window. Therefore, Al is again the recommended material. A special point is the Hg-production by spallation events within the Pb-target. It is estimated to be 13o appm/year (13). Irradiation is known to enhance the thermal diffusion process, which is fortunately slow for Hg in Pb at the expected

temperature. Hg, once in contact with the Al cladding, will destroy the oxide layer and possibly cause corrosion or liquid metal embrittlement. A detailed investigation remains to be done.

4.2 Sealings and Bearings of the Target Wheel (18)

Out of engineering considerations, special sinter materials (Triballoy) for the bearings and a combination of carbides together with cold-pressed carbon for the slide ring sealing of the target wheel are proposed. A special requirement is a low swelling of the bearings material in order to maintain the very narrow water flow gaps ($\sim$ 40 µm). Because data on the behaviour under irradiation are very scare for the cited materials, the feasibility of this and other properties should be investigated by a n-irradiation experiment; a calculation of the expected neutron fluxes is under way.

4.3 Radiolysis of Cooling Water

The proton beam, penetrating the cooling water, will lead to the formation of e.g. H_2 gas and H_2O_2. This causes corrosion of the surrounding structural material. For Al, the problem should be manageable by a purification and pH-control of the cooling water. These and other remedies are known from high energy accelerator experience (14).

5. Summary

For the most part of the structural material, the operations conditions are similar to nuclear reactor conditions. Nevertheless, there are some distinct weak points:

A stationary beam window, which is the worst case of a SNQ component, shows some analogies with the first wall of a fusion reactor. Promising materials are refractory metals and metallic glasses. The expected lifetime - at least for the metals - will not exceed several days.

For a rotating beam window, suitable materials are Al-Mg-Si alloys and SAP. A lifetime of more than two years seems to be feasable.

If not defeated by the Hg-corrosion, this holds for a target rod cladding, too, when Al-Mg-Si alloys are used.

For the bearing of the wheel, which requires a low swelling material, special sinter materials are envisaged. As in the case of the sealings (material: ceramics), a lifetime estimate cannot be given yet.

References

(1) W. A. Coleman/T.W. Armstrong, Nucl. Sci. Eng. 43, 353 (1971) and W.V. Green, private communication (1979)

(2) J.A. Sprague/F.A. Smidt jr./J.R. Reed, J. Nucl. Mat. 85+86, 739 (1979)

(3) B.L. Cox/F.W. Wiffen, J. Nucl. Mat. 85+86, 901 (1979)

(4) T. Masumoto, Sci. Rep. RITU, A-26, 4-5 (1977)

(5) T. Masumoto/K. Hashimoto, Ann. Rev. Mater. Sci 8, 125 (1978)

(6) M.D. Rechtin/J. Vander Sande/P.M. Baldo, Scr. Metall 12, 639 (1978)

(7) R.V. Nandedkar/S. Panchapakesan/K. Varatharajan, conf. paper for the Madras Symp. (1979)

(8) W. Jäger/J. Roth, to be published in Nucl. Instr. Meth.(1980)

(9) D.G. Morris, to be published in Journal de Physique (1980)

(10) W.F. Sommer/W.V. Green, LASL-Report LA-UR-79-2818 (1979)

(11) K. Farrell/R.T. King, conf. paper for 9th ASTM meeting (1978)

(12) P.J. Maszíasz/K. Farrell, J. Nucl. Mat. 85+86, 913 (1979)

(13) T.W. Armstrong/G. Sterzenbach, internal report (1980)

(14) M.H. Van der Voorde, CERN-Report 70-5 (1970)

(15) H. Ullmaier/W. Schilling, Lectures on Radiation Damage on Metallic Reactor Materials (1980)

(16) F. Stelzer, internal report (1980)

(17) G.S. Bauer, this conference

(18) H. Stechemesser, this conference

Parameter	Fast Breeder	Fusion Reactor	SNQ
Number of thermal cycles [1/sec]	$3 \cdot 10^{-7}$	0.3 - 30 (inertially conf.)	0.5 rot. window 100 stat. window
Temperature [°C]	300 - 600	300-500 (steel) 500-1000 (refract.)	<100 structure rot. target >350 structure liquid metal target 800 stat. window
Average displacement damage [dpa/day]	0.1 - 0.2	0.02 - 0.1	<0.1 structure 0.05-3.1 stat. window
He-production [appm/day]	0.03	0.1 - 1.7	15-125 stat. window

Table 1: Comparison of important parameters for different nuclear facilities (15)

Material	Average displacement damage [dpa/day]	He-Production [appm/day]	H-production [appm/day]
Be	0.05	15	low
Al	0.15	45	190
316 SS	0.65	70	540
Cu	1.00	85	550
Mo	2.25	125	860
W	3.10	125	1100

Table 2: Expected values for radiation damage of a stationary window

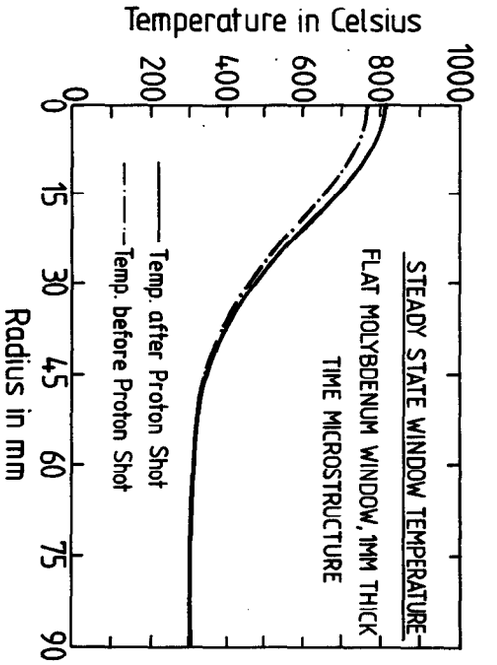

Fig. 1 Thermal operations conditions for a stationary, circular window. The proton shot has a length of 0.5 msec and a repetiton frequency of 100 Hz (16).

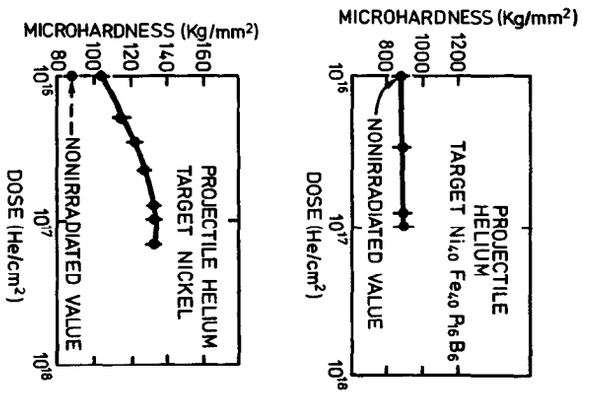

Fig. 2 Effect of He-implantation into a metallic glass and a metal (7).

LIQUID METAL TARGET DEVELOPMENT FOR THE GERMAN NEUTRON SOURCE (SNQ)

H. J. Hoffmann, P. E. Huber, M. Piesche*)

Kernforschungszentrum Karlsruhe
Institut für Reaktorbauelemente
Postfach 3640, 7500 Karlsruhe 1
Federal Republic of Germany

*)Technische Universität Karlsruhe
Institut für Strömungslehre und Strömungsmaschinen
Postfach 26, 7500 Karlsruhe, FRG

1. INTRODUCTION

The heat released in the target of the German neutron source (1100 MeV; 5 mA) amounts to several MW and must be continuously transported to a heat sink. Two different target systems are under consideration:

. A solid lead target system designed as rotating wheel with internal cooling passages /1/ and
. a liquid lead or lead bismuth target system provided with a flowing liquid metal circulated through a heat transport loop.

This contribution concentrates on the work performed for the liquid metal target system. The target system can be designed in different ways, for example:

. As a vertical cylinder with a free liquid surface at the top of the target (in analogy to /2/. The proton beam enters this target vertically.
. As horizontal curved channel of rectangular cross section in which the flowing metal forms a nearly free liquid surface at the inner curvature of the channel. The proton beam enters this target horizontally.

Most theoretical and experimental work was carried out for the vertical cylinder target, only theoretical investigations have been performed up to now for the horizontal arranged flat channel target. In the following the main results will be summarized subdivided in the topics:

. The liquid metal heat transport system.
. The liquid metal targets and their main fluid dynamic and thermodynamic characteristics.
. The proof of the operation of a liquid metal system.

2. THE LIQUID METAL HEAT TRANSPORT SYSTEM

An eutectic mixture of lead bismuth was chosen as target material. It is contained and circulated in a coolant circuit. The heat released in the target is transported from the primary coolant system via heat exchangers to a secondary alkali metal coolant circuit and finally to air. The primary system can be connected to a purification loop if necessary. The total PbBi inventory can be drained into a dump tank. The overall liquid metal target heat transport system is shown in Fig. 1. Both target versions can in general be connected to the heat transport loop.

Using lead bismuth as target material, two temperature limits must be taken into account due to corrossion effects /3,4/:

. The maximum temperature of structural materials should be $\leq 450^{o}C$ and
. the maximum temperature difference within the heat transport system should be $\leq 125^{o}C$.

For these conditions low alloy ferritic steels can be used as structural materials. In addition, the minimum fluid temperatures should be kept well about the liquid metal freezing point.

The basic thermodynamic and fluiddynamic data of the primary heat transport system were calculated for a variety of operational conditions /5,6/ assuming a maximum temperature of the structural materials of $450^{o}C$, which is identical to the averaged maximum fluid temperature. Fig. 1 shows the main characteristics of the heat transport system for a target power of 4.2 MW and fluid temperature increases of $125^{o}C/20^{o}C$ for the cylindrical/flat channel target respectively. The minimum temperatures of the primary circuit of $325^{o}C/430^{o}C$ then provide an excellent safety margin over the eutectic Pb Bi freezing point which is $125^{o}C$. The mean temperature level of the primary system is large enough to allow a good heat transport from the primary via the secondary circuit to air without requiring too large dimensions of the circuit components /6/. Instead of lead bismuth pure lead could be chosen as target material. In this case the overall operation conditions of the primary and alkali metal heat transport circuit must be increased at last by $50^{o}C$ for the cylinder target due to the Pb freezing point of $327^{o}C$. The corrosion determined temperature limits however are less stringent in comparison to PbBi as target material.

From these considerations it follows that the heat transport from the target to the heat sink is feasible and that the components of the heat transport system (pumps, heat exchangers, etc.) seem manufacturable.

3. THE LIQUID METAL TARGET AND ITS MAIN FLUID DYNAMIC AND THERMODYNAMIC CHARACTERISTICS

3.1 The Vertical Cylinder Target

This target consists of two coaxial tubes connected by a hollow jet nozzle at the top of the target (Fig.1). In this case the cooled liquid from the heat exchanger flows upward through the annulus. At the top of the annulus the flow is reversed and forms a rotational symmetric hollow jet which at an appropriate axial level coalesces forming the beginning of the free falling cylindrical target (Fig. 2b). The proton beam enters the hollow jet nozzle and reaches the target surface at the point of coalescence. The heat is released along the cylindrical target and transported by circulating back the liquid target material via a pump to the heat exchanger. This target design is characterized by:

- a vertical arrangement,
- a free liquid surface (without fluid guiding walls within the proton beam),
- a flow direction where the lowest fluid temperatures prevail at the target, section with the highest thermal load,
- an axisymmetric temperature distribution with maximum values in the axial center and minimum values at the periphery of the flow,
- high flow velocities (several m/s) and small target diameters.

Essential parameters determining the flow and heat transport characteristics of the jet nozzle and the target were investigat theoretically /7/ - /9/. Experiments were performed in water and are in preparation for liquid metal flow to support the theoretical calculations.

The main fluid dynamic results are:

- The flow characteristic of the hollow jet is determined by the nozzle contour. The point of coalescence is mainly a function of the Froude-Number ($Fr = u_0/\sqrt{g \cdot r_0}$, where u_0 is the flow velocity at and r_0 the radius of the nozzle entrance, and g the gravity). In addition the Euler- as well as the Weber-Numbers are of influence. Fig. 2a shows the axial position of the

point of coalescence for various Froude-Numbers plottet versus the x/r_0-ratio of a typical nozzle geometry. Theoretical and experimental data are in good agreement. In addition a photograph of a typical hollow jet contour measured in a water flow is reproduced (Fig. 2b).

Measured velocity profiles in front of and behind the point of coalescence lead to the conclusion that a small velocity decrease together with high turbulence may prevail at the point of coalescence. The first effect stimulates the existence of a possible hot spot, the second diminishes this possibility. To describe these effects quantitatively the velocity profiles will be determined at the point of coalescence in detail by us of a Laser-Doppler-Anemometer.

Thermodynamic characteristics of the vertical cylinder target were determined. Due to the global calculations of the basic fluid dynamic and thermodynamic characteristics of the primary heat transport system the liquid metal mass flow rates are known. Demands of target neutronics call for a target diameter of about 10 cm. Both magnitudes determine the flow velocity of the target and the hollow jet nozzle contour. For the characteristics shown in Fig. 1 the point of coalescence is reached approximately 35 cm downstream of the nozzle inlet. the target velocity being about 3 m/s.
For these flow parameters the temperature fields were calculated assuming an exponential power decrease in axial target direction and a radial Gaussian (variance σ = 2.5 cm) power distribution. Based on these power distributions, Fig. 2c indicates the calculated radial temperature distributions at different axial target positions. These calculations assume slug flow, steady state conditions and neglect turbulent heat conduction within the fluid. It can be seen that

- the radial temperature variations across different axial target sections (Z) take a Gaussian curve, and that
- the maximum temperature increase ΔT is calculated to be 440 ^{o}C at the end of the target axis while the target periphery remains at inlet temperature.

These main fluid dynamic and thermodynamic design data are extreme values. The calculations result in a high local temperature at the end of the target axis. Despite this high temperature, a flow instability must not be expected. Evaporation at the axis of a free falling liquid metal jet can be excluded taking notice of surface tension effects, by guiding the flow in a liner or by reducing the temperature level of the primary coolant circuit (in case of PbBi). In addition future calculations must be based on more realistic power

distributions, taking into account turbulence effected radial heat exchange (measurements are in progress).

3.2 The Horizontal, Rectangular, Curved Channel Target

This target consists of a horizontal channel curved about 180 degree. The liquid enters the channel and is forced to flow at right angle to the proton beam which penetrates the liquid horizontally at the inner curvature of the channel. Here the fluid is enclosed only on three sides. A free liquid metal surface can be stabilized by the centrifugal forces acting in direction to the outer curvature of the channel. After passing the proton beam the liquid reaches a diffuser and a dump tank. The heat released by the proton beam across the longer aspect of the flow channel is transported by circulating back the liquid target material via a pump to the heat exchanger (Fig. 1).
This target features

- a horizontal arrangement,
- a free liquid surface (without fluid guiding walls at the proton entrance to the target),
- high flow velocities and small target diameters.

Essential parameters determining the flow and heat transport characteristics of the target were investigated theoretically /11/, and experiments are in preparation to support the calculations.

The main fluid dynamic results are:

- A minimum flow velocity must be generated to get centrifugal forces able to realize a free surface contour in the vacuum approximately vertical to the proton beam. Calculated results (not taking into account wall friction) are shown in Fig. 3a. It can be seen that the flow velocities must reach approximately 2 m/s to keep the fluid well stabilized at the outer curved channel wall. This does also impose that at the beam entrance a valve must be forseen to avoid voiding of the flow channel in cases of flow reduction and start ups.
- This flow velocity must be sufficiently high to support the axial fluid transport. Due to the fact that there exists no pressure gradient in flow direction between the vacuum system at the free liquid surface and the dump tank the driving forces for the fluid flow can only be achieved by the kinetic energy of the fluid. Calculations taking into account wall friction show that a velocity reduction of approximately 10 % is needed to avoid flow reversal and to maintain the fluid motion along a proper designed diffuser of about 2 m length before it flows vertically into the dump.

The main thermodynamic results are:

- The flow velocity should be high enough to avoid local temperature increases within the fluid which are too large. Fig. 3b shows as example the calculated temperature increases in flow direction for a fluid velocity of 2 m/s for different axial proton beam sections. It can be seen that about 150 ^{o}C temperature increase are to be expected along the free flow surface center line (z = 0).
- A minimum flow velocity - acceptable from the thermodynamic and fluiddynamic points of view - should be realized to avoid large mass flow rates ($\dot{m}$) and to keep the operational and design parameters of the heat transport circuit in a realistic range (heat exchanger, pumps etc.). In comparison to the cylinder target, an increase in mass flow rate must be taken into account due to the enlarged flow area of the flat channel and the necessary flow stabilizing velocities. An increase in mass flow rate by a factor of 3 to 5 seems reasonable, yielding flow velocities in the range of working liquid metal systems i. e. between 2 and 4 m/s, dependent mainly on the axial energy released by the proton beam, the target length, and the target thickness /11/.

These fluid dynamic and thermodynamic design data are assumed conservative. The main facts must be supported by model experiments in water flow which are in preparation.

4. OPERATION OF A LIQUID METAL SYSTEM

The manufacturing and handling of the liquid PbBi system must be investigated. In this respect great advantage can be drawn from liquid alkali metal circuits, where experience with loops of up to 100.000 hours of individual operation time is available. It seems that all components (instruments, pumps heat exchangers) may be manufactured satisfactorily in low-alloy ferritic steel in a temperature range up to 450 ^{o}C without raising too severe problems.

To get the special know how of a liquid PbBi system a small model circuit (mass flow rate 5 m^3/h) was built and a large one (mass flow rate 100 m^3/h; target scale 1:1) is under construction. These loops mainly serve to investigate the different liquid metal targets in PbBi flow, to support the results gained in water flow and to investigate the influence of a vacuum on the flow behavior. In addition the design, manufacturing, construction and operation of

these loops will be of great use to collect experiences of a PbBi system and to define additional needs.

5. SUMMARY

From the fluid dynamic and thermodynamic point of view liquid metal can be used as target for a spallation neutron source. The heat generated in the target can be transfered to a heat exchanger and via an intermediate heat circuit to a heat sink. Vertically as well as horizontally arranged liquid metal targets seem possible. To support the design calculations for these targets model experiments in water and lead bismuth circuits were and are carried out. The operation of PbBi circuits should demonstrate that liquid metals can be reliably and safely used as targets for an advanced spallation neutron source.

REFERENCES

/1/ G.S. Bauer: "Layout of the Target Station for the German Project", this Conference.

/2/ G.A. Bartholomew, P.R. Thunicliffe: "Intense Neutron Generator"; AECL 2600, (1966).

/3/ J. R. Weeks: "Lead, Bismuth, Tin and their Alloys as Nuclear Coolants", Nucl. Eng. Design 15 (1971) - and Pers. Communication (1979).

/4/ H.U. Borgstedt. C. Politis: "Bleiwismuthkorrosion von Werkstoffen für das Target der Spallationsquelle"; unpublished report (1979).

/5/ H.J.Hoffmann: "Prospects of a Liquid Metal Target Source", in JOL-Conf. 34, pp. 127-153, (1980).

/6/ P.E. Huber: "Untersuchungen zur Kühlmöglichkeit eines Flüssigmetalltargets für eine Spallationsneutronenquelle" unpublished report (1980).

/7/ K.O. Felsch, M. Piesche, W. Veith: "Vorläufige Strömungsuntersuchungen zur Auslegung eines Flüssigmetalltargets mit freier Oberfläche für eine Spallationsneutronenquelle", unpublished report (1980).

/8/ M. Piesche: "Drallbehaftete Flüssigkeitshohlstrahlen bei Einwirkung von Massen- und Oberflächenkräften", unpublished report (1980).

/9/ K.O. Felsch, M. Piesche, W. Veith: "Theoretische Untersuchung der reibungsbehafteten Strömung in rotationssymmetrischen Düsen zur Auslegung eines Flüssigmetalltargets für eine Spallationsquelle", unpublished report (1980).

/10/ Cl. Günther, H.J. Hoffmann: "Stand der Temperaturfeldmessungen zur Auslegung eines Flüssigmetalltargets für eine Spallationsneutronenquelle", unpublished report (1980).

/11/ P.E. Huber: "Thermo- und fluiddynamische Untersuchungen am horizontal gekrümmten Rechteckkanal-Target", unpublished report (1980).

/12/ E. Wild, K.J. Mack, M. Gegenheimer: "Blei-Wismut-Kreislauf I - Beschreibung der Versuchseinrichtung", unpublished report (1980).

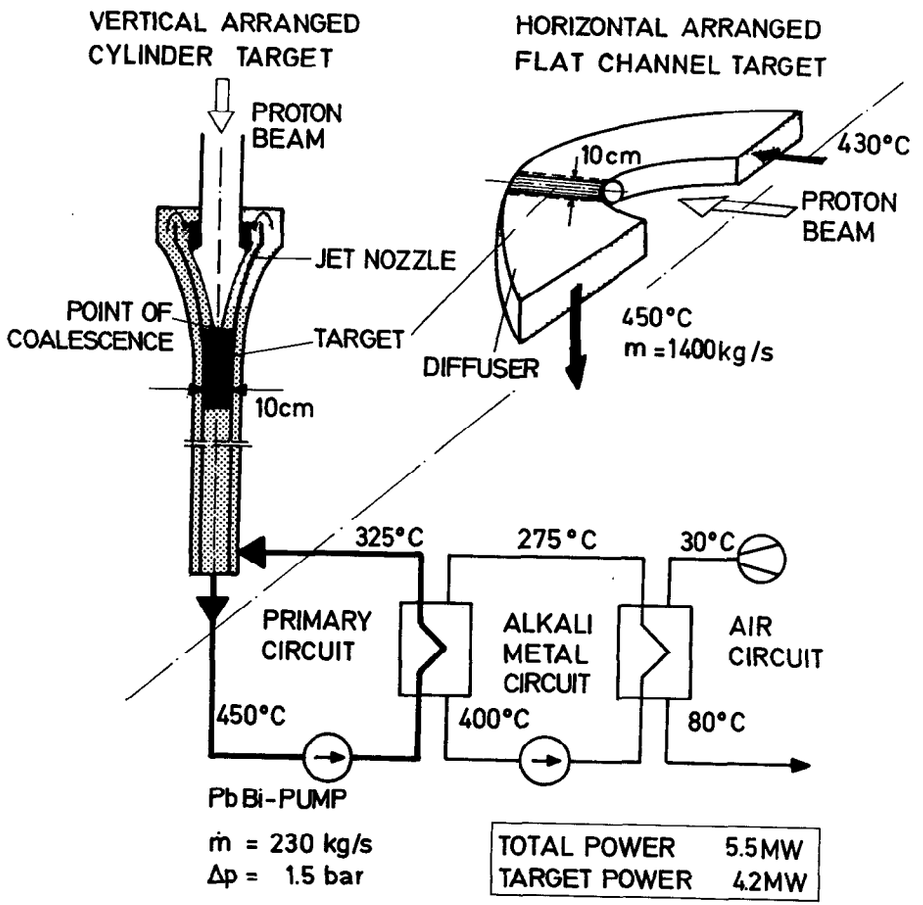

Fig. 1 HEAT TRANSPORT LOOP AND TARGET ARRANGEMENTS

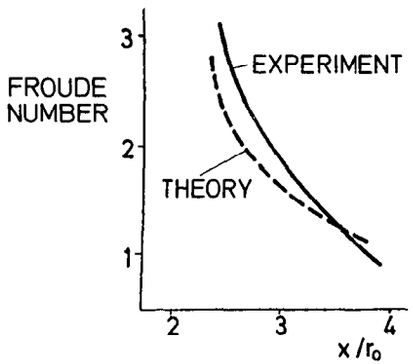

(2a) POINT OF COALESCENCE VS. FROUDE NUMBER

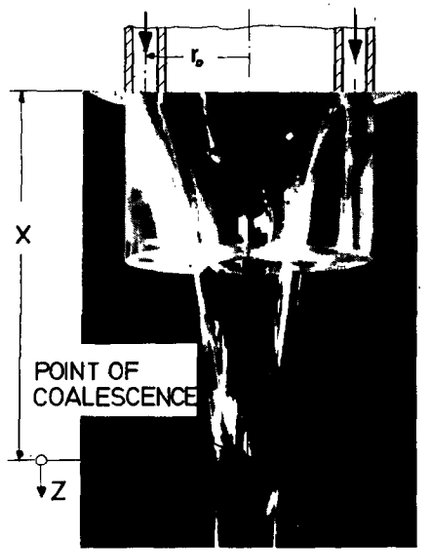

(2b) HOLLOW JET

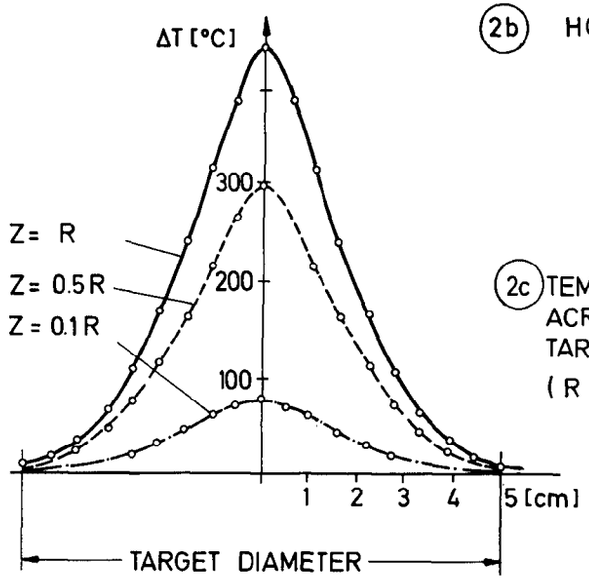

(2c) TEMPERATURE INCREASE ACROSS DIFFERENT TARGET SECTIONS Z (R = BEAM PENETRATION)

Fig. 2 FLOW CONTOURS AND FLUID TEMPERATURES

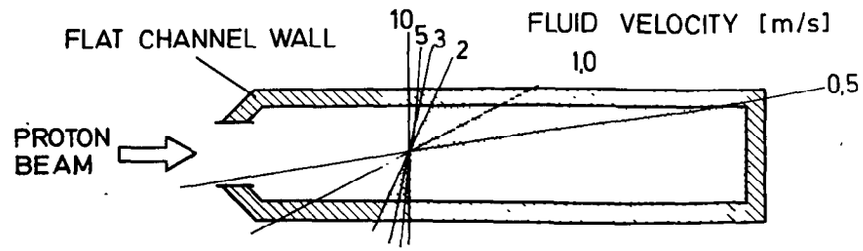

(3a) FREE TARGET SURFACE CONTOURS FOR DIFFERENT FLOW VELOCITIES

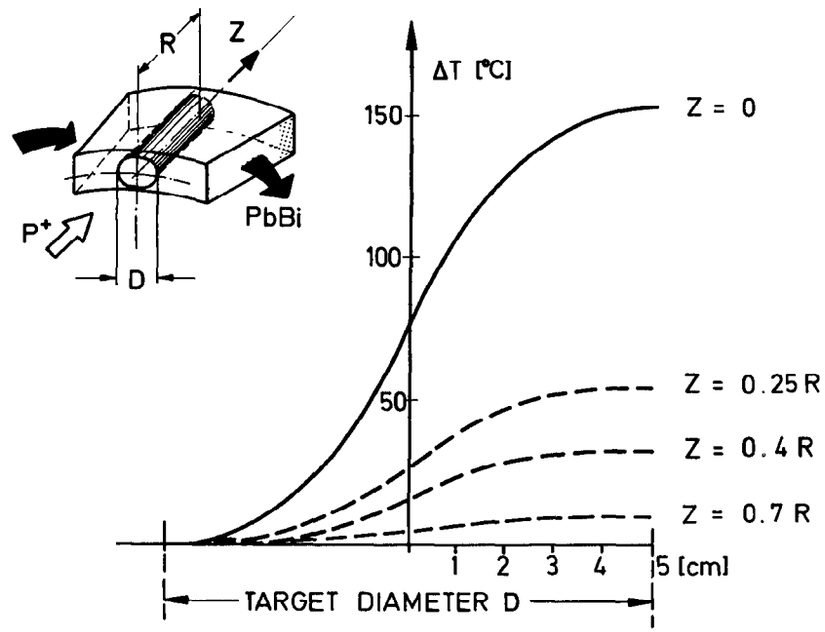

(3b) TEMPERATURE INCREASE ACROSS DIFFERENT TARGET SECTIONS Z (R = BEAM PENETRATION)

Fig. 3 FLOW CONTOURS AND FLUID TEMPERATURES

Free Convection Liquid Metal Target

C.Tschalär, SIN

As an alternative to the present forced convection liquid lead-bismuth (LBE) target concept, the possibility of a sealed LBE target has been looked into as was mentioned in the survey talk. The target consists essentially of a cylindrical vessel of about 4 to 6 m length and a diameter of 20 to 25 cm filled with LBE (see Fig. 1). It is centered on the axis of the proton beam which enters the target through a conical graphite window at the lower face of the target vessel. In the upper half of the vessel, a cylindrical array of cooling pipes near the wall of the vessel serves as a heat exchanger. In order to guide the resulting free convection flow of the LBE, especially at start-up, a concentrical tube is inserted which separates the upward and downward LBE streams.

In order to study the feasibility of such a source concept, the characteristics of the stationary flow can be obtained by assuming an uniform turbulent flow pattern (Kolbenströmung) where the buoyancy of the hot LBE is balanced by the frictional flow forces on the flow surfaces and in particular on the cooling pipes and the resulting pressure drop Δp is quadratically dependent on the flow rate $\dot{V}$ =

$$\Delta p = k \cdot \dot{V}^2$$

Energy balance between buoyancy and friction yields

$$\frac{dE_b}{dt} = \frac{dE_f}{dt}$$

$$h \cdot g \; \frac{d(\rho V)}{dt} = \Delta p \cdot \dot{V}$$

$$hg \; \rho \beta T_\infty \; \dot{V} = K \dot{V}^3$$

where h = mean vertical rise of hot LBE

ρ = mean density of LBE

β = thermal volume expansion coefficient of LBE

g = acceleration of gravity

T_∞ = temperature difference between hot and cold LBE stream

The problem is simplified by the fact that the heating power P is deposited independent of the flow pattern:

$$P = c_p \; \dot{V} \; T_\infty$$

we therefore find

$$T_\infty = \left[\frac{kP^2}{h} \Big/ \left(c_p^{\,2} \rho g \beta \right) \right]^{1/3}$$

$$\dot{V} = \left[\left(\frac{Ph}{k} \right) \cdot \left(\frac{\rho g \beta}{c_p} \right) \right]^{1/3}$$

For a beam power P of 1 MW, a reasonable friction factor k of $3 \cdot 10^{-3}$ bar /(l/s)^2 and a rise h of 2 m we obtain a temperature rise of 200 ^{o}C and a flow rate $\dot{V}$ of about 3,6 l/s which is comparable to the assumed values for the forced convection case. As the expressions for T_{∞} and $\dot{V}$ show, beam profile and stopping distribution do not enter the overall flow characteristics but only influence local convection currents near the stopping region.

As further important aspect of free convection flows is the start-up phase. The flow element closest to the beam entrance window is overheated the most because it takes longest to move out of the beam heating region. To calculate the temperature rise in this element we can neglect frictional forces compared to inertial forces in the flow. If as a further approximation the heating is assumed to be uniform over a finite length of the inner tube of the target vessel, then the temperature rise ΔT_{max} of the critical flow element and it is velocity w when leaving the heating zone can be calculated analytically,

$$\Delta T_{max} = \left(\frac{Q^2 L}{\gamma} \cdot \frac{6}{c_p^{\,2}\, g\beta} \right)^{1/3}$$

$$w = 3 \cdot 1 \left(\frac{Q \gamma}{L} \cdot \frac{g\beta}{6\, c_p} \right)^{1/3}$$

where Q is the heating power density, γ the sine of the angle ε

of inclination of the target axis, L the total length of the average flow path in the target, and l the length of the heating zone.

For a vertical target (γ=1) of an inner diameter of 16 cm and a length of 3 m (L=600 cm). ΔT_{max} is about 1200 ^{o}C and w=10 cm/s or about half the stationary velocity. Distribution of the heating power over the cross section of the inner tube is effected by local convection currents. Local overheating is to be expected but estimates show that due to the large latent heat of evaporation vapor bubble formation is quite unlikely. More detailed calculations of the time dependent convective flow are in progress.

From the technical point of view a free convection target described above would eliminate the need for a LBE circuit. In case of a target change, only the secondary cooling circuit whose activation is minimal would have to be disconnected and the highly radioactive LBE would remain sealed in the target container. Although somewhat larger than the forced convection target, the free convection target is a relatively inexpensive unit which could be discarded if it failed thus eliminating the need for expensive hot-cell repairs. A disadvantage is the relatively large amount of LBE (150 to 200 l) which would escape into the containment in case of a window failure. A drainage pipe would have to be connected to the proton beam vacuum pipe which would collect and slow down the leaking LBE and feed it into a shielded dump. Preheating and melting of the LBE content

of the target at start-up could be achieved by circulating hot gas through the last part of the beam vacuum pipe.

A particularly attractive neutron source concept is the combination of a vertical free convection target incorporated in a vertical beam source allowing thermal neutron ports distribution over the full circumference of the source as described in the summary table. A more detailed technical study on this version is in progress.

Fig 1: Free Convection LBE Target

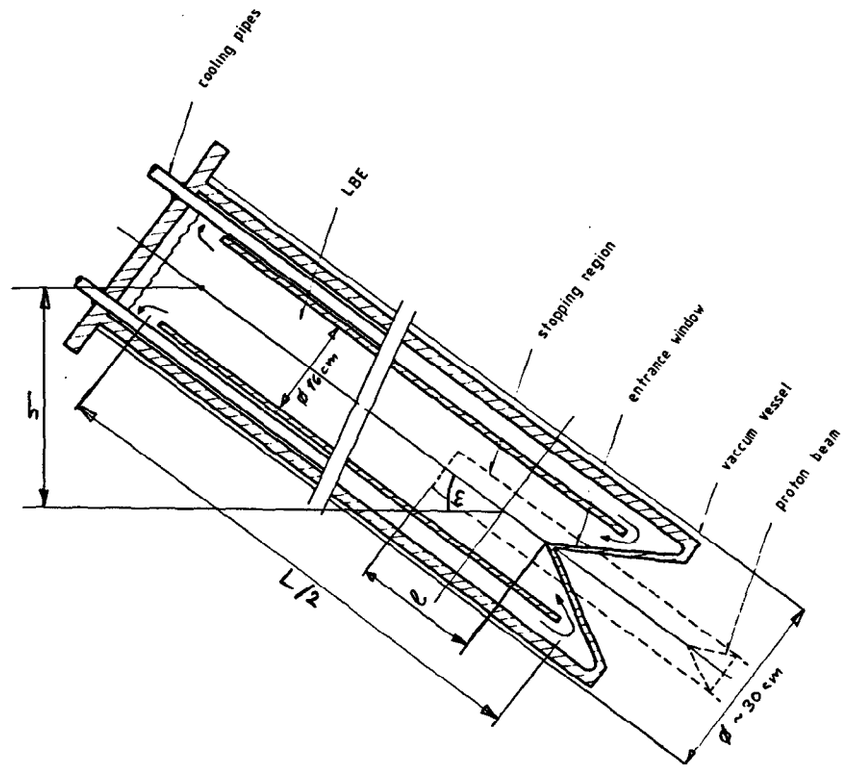

"MOLTEN-SALT TARGET AND BLANKET CONCEPT"

[Application of the Molten-Salt Technology on the Spallation Neutron Facilities]

Kazuo FURUKAWA*, Kineo TSUKADA**, and Yasuaki NAKAHARA*

* Japan Atomic Energy Research Institute, Tokai-mura, Ibaraki-ken 319-11 JAPAN

* Atomic Energy Research Institute, Nihon University, Kanda-Surugadai, Chiyoda-ku, Tokyo, 101 JAPAN

SUMMARY

The applications of molten-salt target and blanket to the Molten-Salt Intense Neutron Source (MSINS) and the Accelerator Molten-Salt Breeder (AMSB) are discussed, where the molten fluorides including ThF_4 or UF_4 in high concentration are utilized as shown in Table 1.

This concept naturally has several significant benefits relating to the target fabrication, design, radiation damage, heat removal, safety, economy, etc. So far, however, it was thought to have a poor spallation neutron yield as a severe fault. According to the results of neutronic calculation carried on the molten-salt system such as $LiF-BeF_2-ThF_4$, $LiF-NaF-ThF_4$, $LiF-BeF_2-UF_4$ etc., their neutron yields have been found comparable or superior to the values for heavy metal targets such as Bi and Pb, assuring the high performance of MSINS and AMSB.(1)

The schematic figures of MSINS and AMSB are shown in Figs.1 and 4, together with the several tables and figures of their neutronic calculation models, neutron yields, predicted performances, etc.(1) Neutronic calculations have been performed

with the use of NMTC/JAERI modified to include fission processes, TWOTRAN-II and other auxiliary codes. The spatial and energy distributions of neutrons are also calculated, though an effect of Be(n,2n) reaction is not included. The chemical aspect of spallation products in these facilities are examined and estimated that they are practically manageable in processing.

One of the most useful applications of MSINS may be the material irradiation facility for engineering test because of the larger irradiation volume than that in the other metal targets.

Reference

(1) K.Furukawa, K.Tsukada, and Y.Nakahara, "Single-fluid-type Accelerator Molten-Salt Breeder Concept", J. Nucl. Sci. Tech. 18 (1981). in press

Table 3. Neutron Yield per 1GeV Proton at the Window of the Intense Neutron Source (MSINS)

molten salt	cascade + evaporation + fision (≥15 MeV)	whole energy range (1000 ~ 0 MeV)
$^{7}LiF-BeF_2-UF_4$ (61−21−18)	14.5 ± 2.2	16.9 ± 2.6

Table 4. Example of Predicted Performances of the Molten-Salt Intense Neutron Source (MSINS)

poton beam	1 GeV 10 mA
salt example	$^{7}LiF-RbF-UF_4$ (57-10-33 mol %)
melting point (Tm)	470 °C
density at Tm+100°C	3.57 g/cm^3
viscosity coefficient	17~19 cpoise (600°C)
salt temperature	inlet 520°C outlet 600°C
salt volume	3 m^3
salt weight	10.7 ton (Th 6.5 ton)
salt flow	150 l/min
heat generation	~ 50 MW th
fissile material generation	~ 5 kg/year
spallation reaction products	~ 0.7 kg/year

Table 5. Example of Predicted Performances of Single-fluid-type Accelerator Molten-Salt Breeder (AMSB)

proton beam	1 GeV, 300 mA
salt example	$^{7}LiF-NaF-ThF_4$ 54.5−13.5−32 m/o
melting point (Tm)	525 °C
density at Tm+100°C	3.31 g/cm^3
viscosity coefficient	19~22 c poise (600°C)
	11~13 〃 (700°C)
salt temperature	inlet 560°C outlet 650°C
salt volume	100 m^3
salt weight	331 ton (Th 208 ton)
salt flow	6 m 3/sec
thermal output	~2500 MW th
elec. power generation	~1100 MWe
elec. power consumption	750 ~ 900 MWe
fissile material production*	800~1000 kg/year
	640~ 800 kg/year (80% load)
spallation products	~40 kg/year
fission products	~40 kg/year

* Except for the continuous removal, this will be increased to about twice.

Table 1 Candidate Target Salts and Their Predicted Properties

	mol %	melting point Tm (°C)	density at Tm+100°C (g/cm^3)	viscosity coeff (cpoise) 600°C	viscosity coeff (cpoise) 700°C
$LiF-BeF_2-ThF_4$	72−16−12	500	3.35	12	7
〃	71−9−20	540	2.97	16~18	7~9
〃	67−18−15	500	2.70	13~15	6~7
〃	64−18−18	540	2.7	12~14	6~7
$LiF-ThF_4$	71−29	568	3.36	20~22	12~14
$LiF-NaF-ThF_4$	54.5-13.5-32	525	3.31	19~22	11~13
$NaF-KF-ThF_4$	11−67−22	535	2.54	14~16	8~10
$LiF-BeF_2-UF_4$	61−21−18	550	2.87	13~15	6~7
$LiF-UF_4$	71−29	525	3.41	20~22	12~14
$LiF-NaF-UF_4$	43.5-24.3-32.2	445	3.09	20~22	12~14
$LiF-RbF-UF_4$	60−10−30	460	3.62	16~18	10~12
〃	57−10−33	470	3.57	17~19	11~13
$NaF-RbF-UF_4$	45−27−28	500	2.99	15~17	9~11
$NaF-KF-UF_4$	47−20−33	550	2.89	18~20	11~13

Table 2. Comparison of Neutron Yields per 1GeV Proton for Some of Target Salts including Th and U

Case	molten salt	cascade + evaporation (≥15 MeV)	cascade + evaporation + fission (15≥MeV)	whole energy range (1000 ~ 0 MeV)*
1	$^{7}LiF-BeF_2^{**}-ThF_4$ (72−16−12)	22.3 ± 2.3	25.1 ± 3.0	
2	〃 (71−9−20)	26.1 ± 2.1	29.6 ± 2.1	
3	〃 (67−18−15)		28.6 ± 3.3	29.5 ± 3.4
4	〃 (64−18−18)			
5	$^{7}LiF-ThF_4$ (71−29)	27.3 ± 2.2	33.04 ± 1.9	
6	$^{7}LiF-NaF-ThF_4$ (54.5-13.5-32)		32.4 ± 2.1	34.0 ± 2.2
7	$NaF-KF-ThF_4$ (11−67−22)		25.9 ± 3.0	
8	$^{7}LiF-BeF_2-UF_4$ (61−21−18)		31.2 ± 2.4	38.4 ± 3.0
9	$^{7}LiF-UF_4$ (71−29)	28.1 ± 2.8	33.2 ± 2.6	
10	$^{7}LiF-RbF-UF_4$ (60−10−30)	27.7 ± 1.7		
11	〃 (57−10−33)		36.0 ± 4.0	
12	$NaF-RbF-UF_4$ (45−27−28)	28.0 ± 1.8		

(*) Including fission in the energy range both above and below 15 MeV.

(**) The effect of Be(n,2n) reaction is not enoughly included yet.

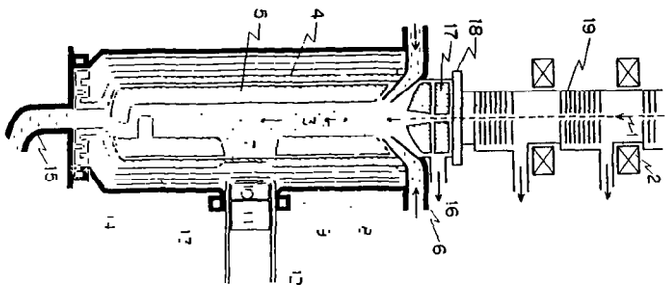

Fig. 1. Schematic Figure of MSINS (Molten-Salt Intense Neutron Source)
1 proton beam, 2 quadrupole magnet, 3 molten salt, 4 graphite vessel, 5 graphite inner cylinder, 6 inlet nozzle, 7 holes, 8 metallic container, 9 BN (decoupler), 10 polyethylene, 11 Be (BeO), 12 B_4C, 13 thermal shield, 14 freeze seal, 15 outlet, 16 vacuum line, 17 neutron shield, 18 beam shutter, 19 differential pumping system.

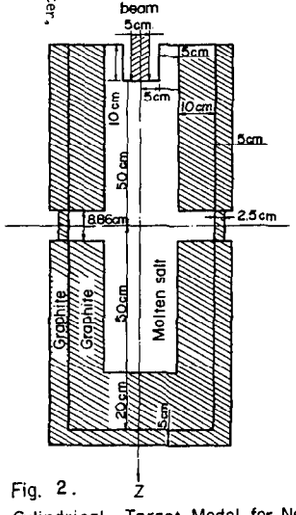

Fig. 2.
Cylindrical Target Model for Neutronic Calculations of MSINS (Molten-Salt Intense Neutron Source)

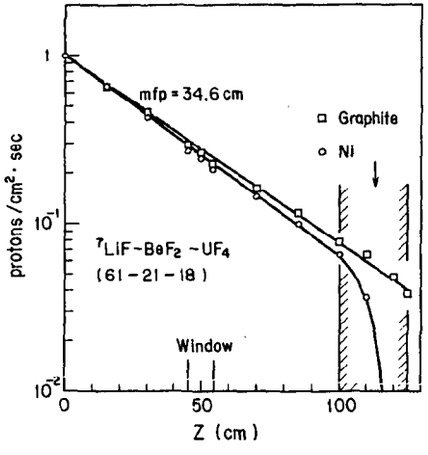

Fig.3 Axial distribution of primary protons

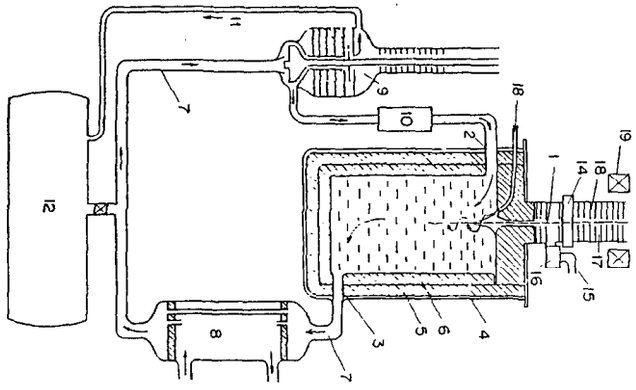

Fig. 4 Schematic Figure of Single-fluid-type Accelerator Molten-Salt Breeder
1 proton beam, 2 salt inlet, 3 salt outlet, 4 reactor vessel, 5&6 graphite, 7 primary loop, 8 heat exchanger, 9 main salt pump, 10 throttle valve, 11 overflow line, 12 storage tank, 13 high-pressure salt outlet, 14 gate valve, 15 vacuum line, 16 vapor trap, 17 duct, 18 orifice, 19 focussing magnet.

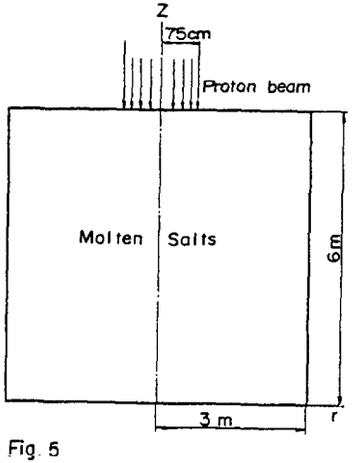

Fig. 5
Cylindrical target model for neutronic calculations of AMSB (Accelerator Molten-Salt Breeder)

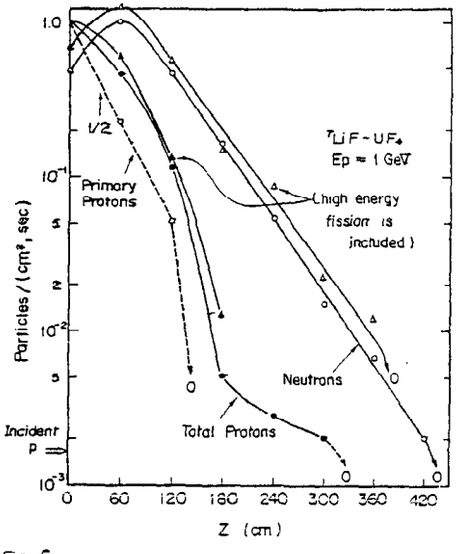

Fig. 6.
Flux Distributions of Protons and Neutrons in the Direction of Incident Proton Beam. [>15MeV] (Cascade-Evaporation Only)

KENS Radiation Shield

S. Ban and H. Hirayama

National Laboratory for High Energy Physics
Oho-machi, Tsukuba-gun, Ibaraki, 305, Japan

1. Introduction

To prove the adequacy of the KENS radiation shield, several preliminary experiments were performed. Fast neutron yield from the target bombarded by 500 MeV protons was measured using activation detectors. Attenuation lengths of fast neutrons were evaluated for iron and concrete shields. And dose rates outside the KENS shields were estimated using these parameters. After that, KENS began to be operating and dose rates above the KENS overhead shield were measured. They were rather in agreement with above estimation.

2. Preliminary experiments

KENS neutron production target[1] is made of tungsten and 7.8 cm(W)×5.7(H)×12(L). Secondary fast neutron yields were measured using several activation detectors. Saturated activities of these detectors for 0° and 90° directions are shown in table 1. They are expressed as follows,

$$A = \int_{E_t} \sigma(E)\ \phi(E)\ dE = \bar{\sigma} \int_{E_t} \phi(E)\ dE$$

where σ is the microscopic reaction cross section, E_t is threshold energy and ϕ is neutron flux. For $C(n,2n)^{11}C$ reaction, the average cross section ($\bar{\sigma}$) is 22mb and E_t is 20 MeV. Then, integral flux above 20 MeV was determined.

Neutron flux outside the shield is expressed as follows,

$$N_o = N_i \cdot \exp(-d/\lambda) \cdot r_o^{-2} \qquad (2)$$

So first N_i and N_o were measured then, the attenuation length (λ) is determined as follows,

$$\lambda = d/\ln\ (r_i^2/r_o^2 \cdot N_i/N_o) \qquad (3)$$

where N_i and N_o is the neutron flux inside and outside the shield, r_i and r_o are the distance from target to each measurement points and d is the thickness of the shield.

To determine the attenuation length of iron for 90° direction, KENS target was put in the iron beam stop and bombarded by 500 MeV protons. The beam stop is 30 cm thick for the transverse direction. Neutron leakage fluxes were measured by activation detectors using C(n,2n) reaction. Then using eq. 3, the value of λ turned out to be 116g/cm^2.

Next to know the attenuation length of concrete for various directions, the iron beam stop was put in the beam dump room and irradiated by 500 MeV protons. Both inside and outside the concrete shield surrounding the beam stop, neutron fluxes were measured for 0° - 100° directions as shown in fig. 1. Measurements were done using activation detectors ($Al(n,spal.)^{18}F$, $C(n,2n)^{11}C$ and $Al(n,\alpha)^{24}Na$).

Then λ was determined using eq. 3 for various angles and is about 123g/cm^2 for the forward direction and 90g/cm^2 for the transverse direction.[2]

3. Results

The vertical view of KENS shield is shown in fig. 2. Its overhead shield is made of iron and heavy concrete. The former is 165 cm thick and the latter 80 cm thick. Dose equivalent rates outside the shield is expressed as follows,

$$H = H_0 \cdot \exp(-d/\lambda) \cdot r^{-2} \qquad (4)$$

and these shielding parameters estimated from above preliminary experiments are shown in table 2. There was not additional information for heavy concrete, it is assumed that it is the mixture of iron and concrete so its attenuation length was obtained by interpolation. These design values[1] are also shown. Next neutron flux was measured using C(n,2n) activation detectors on the top of the overhead shield. It is assumed that the conversion number, 3 neutron (>20 MeV) cm^{-2}s^{-1}/mrem h^{-1} would give the total dose equivalent rates due to neutrons. This results is also shown in table 2. Design values and estimated ones are different with each other, but the calculated dose equivalent rates using eq. 4 are in agreement with the measured value within factor 2 or 3.

References

(1) R.H. Thomas et al., KEK-78-7 (1978)

(2) S. Ban et al., to be published

Table 1. Neutron yield from tungsten target measured using activation detectors.

Reaction	Threshold Energy	0°	90°
S(n,p)^{32}P	3 (MeV)	1.7E-26	/sr/p
Al(n,α)^{24}Na	6	3.7E-27	2.0E-27
C(n,2n)^{11}C	20	1.6E-27	5.4E-28
Al(n,spal)^{22}Na	30	8.8E-28	
C(n,spal)^{7}Be	40	5.5E-28	
Al(n,spal)^{18}F	50	3.7E-28	4.1E-29

Table 2. Vertical shielding paramaters.

	Evaluated Value	Design Value
H_0 (rem/h)m^2/(p/s)	8.2E-10	3.1E-10
λ(Iron) g/cm^2	116	145
λ(Heavy Concrete)	96	129
H (rem/h)/(p/s)	8.6E-17	6.2E-16
H(Measured Value)	1.8E-16	

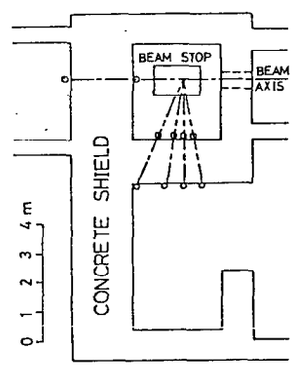

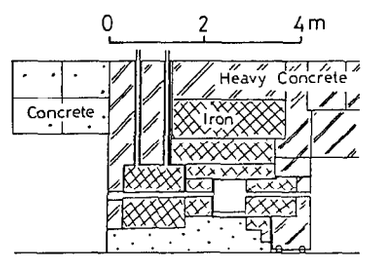

Fig. 2. Vertical view of KENS shield. Right hand side is upstream.

Fig. 1. Plane view of beam dump room. Open circles denote measurement points.

Beam hole design

W S Howells
Neutron Division, Rutherford and Appleton Laboratories

The main problem in collimating the primary neutron beam is that the neutrons of interest for the instruments are of high energy (∿ eV) compared with reactors and the normal absorbing materials used in reactor instruments are ineffective in absorbing these higher energy neutrons and may even have a substantial scattering contribution. A scheme has therefore been devised, based on ray diagrams, to minimise the scattering from the collimating surfaces. The system involves a series of apertures separated by longer regions of wider aperture in which surfaces viewed by the moderator are not seen by the sample and vice versa. This scheme is also useful in determining how a collimating system interacts with other constraints, such as beam shutters and choppers, and can indicate possible problem areas such as insufficient shielding of the target in wing moderator arrangements for high energy (MeV) neutrons.

A fuller account of the scheme may be found in the Rutherford Laboratory Report RL-80-054, 'Primary Neutron Beam Collimation on a Pulsed Source' by W S Howells.

Some Comments on Beam-tube Shielding

C. G. Windsor, AERE Harwell and Tohoku University, Sendai

Both for radiation protection and for spectrometer background reduction we must shield against both fast (> 1 ev) and slow neutrons. Figure 1 shows some of the causes of biological and spectrometer background in a typical beam-tube spectrometer.

To clarify the discussion let us define two types of surface. "Bright" surfaces are those which see the moderator directly. "Visible" surfaces are those which are seen by the counter, either directly or by scattering from the sample or crystal analyser.

1. Neutrons transmitted by the bulk shield are relatively easy to calculate. $\phi = \phi_o e^{-\lambda t}/L^2$ gives a fair answer. They are usually not a problem. For example our spectrometer background gives us a fair monitor of the local fast neutron intensity. As the measurements on page 607 indicate, this usually drops to negligible levels on closing off the beam.

2. How much should we shield an external beam tube? A simple model as in figure 2 gives an estimate for a conical beam tube with "reflecting" surface. The difference in the neutron flux at distance r and r + δr must equal the flux to be shielded over the length δr. The loss of flux per unit area is

$$\frac{\delta\phi}{\delta A} = \frac{\phi_o}{32}\left(\frac{W_m}{r}\right)^3$$

For a moderator of width 15 cm the tube brightness at 5 m works out at $\sim 10^{-6}$ of the source brightness. Thus the shielding required is certainly not negligible compared with the main shield attenuation.

3. How can we minimise "bright" surfaces? Figure 1 illustrated the converging/diverging lines which define the ideal spectrometer whose "bright" surfaces are never "visible". Figure 3 shows the typical arrangement of stepped irisis which attempts to approximate to this ideal arrangement. The thin irisis should be a few scattering lengths thick. Much discussion at ICANS IV centred over what energy range the various parts of this collimator will function. There is no problem for < 1 eV neutrons, but for the fast neutrons there will be some penetration of the irises - one on its own is insufficient to attenuate the beam to negligible values. Thus there will be a penumbra of fast neutrons present outside the geometric penumbra of the beam tube irisis.

4. Where should the final collimator go?

It is obvious that the final beam umbra should match the sample size. Should the final collimator be near the sample where penumbra effects are reduced? Alternatively should it be reasonably remote from the sample where it can be well shielded? How thick should it be? What energy range of neutrons are we trying to stop with the final collimator? Probably the best solution is to divide all these functions - first a rough fast neutron final collimator placed well back in the beam tube shield, then a thick main collimator in a position well away from the sample, finally near the sample, a final "thin" collimator to clean up the penumbra.

5. How do we reduce visible surfaces.

It is clear that we must never let visible surfaces be anywhere near bright ones! All visible surfaces should be cadmium or borated. They should never be extensive in area. For example a simple "nose" or collimator in front of a counter reduces its visible surface by a large factor. We usually remember "first order" visible surfaces seen by the counter but forget "second order" ones seen by say a crystal analyser or by the sample. All these surfaces should be cadmium or borated. Every iron, concrete, wax or even paint surface is a nice neutron moderator and reflector.

6. How big should the centre hole of a spectrometer be?

Obviously it should be a little larger than the geometric penumbra of our beam, but by how much? Experiment and calculation are needed here. We need to know the extent of the fast neutron penumbra to the beam. We must expect it to be there and ensure that these penumbra fast neutrons are moderated and absorbed before they can get near a visible surface.

7. What material should we put where the beam hits inside the beam stop?

For spectrometer background reasons we should try to absorb rather than scatter all the neutrons we can in the beam stop. This means fast neturon absorbers like boron carbide powder are best. More moderating materials like borated resin reflect a percentage of the faster neutrons, and so are not so good. An iron or concrete surface here gives a fast neutron source with comparable intensity to that of the beam itself!

8. What shape should the beam stop be?

A "bottle" shape as in figure 4 ensures that reflected neutrons are mostly absorbed before they can reach the spectrometer environment. From solid angle considerations the bottle should be as long as possible. Thus the beam stop should be as far away from the spectrometer as possible.

Really fast MeV neutrons will penetrate the boron carbide area. They must be moderated and stopped in hydrogenous borated material which should therefore surround the actual beam stop.

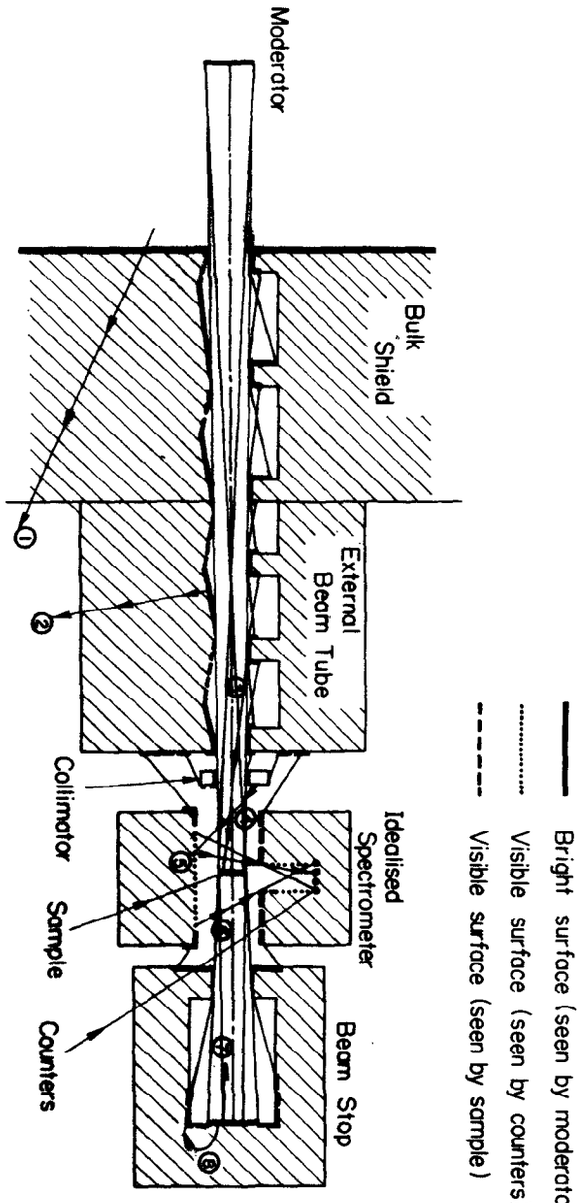

Fig. 1. Some sources of background in an idealised pulsed neutron spectrometer.

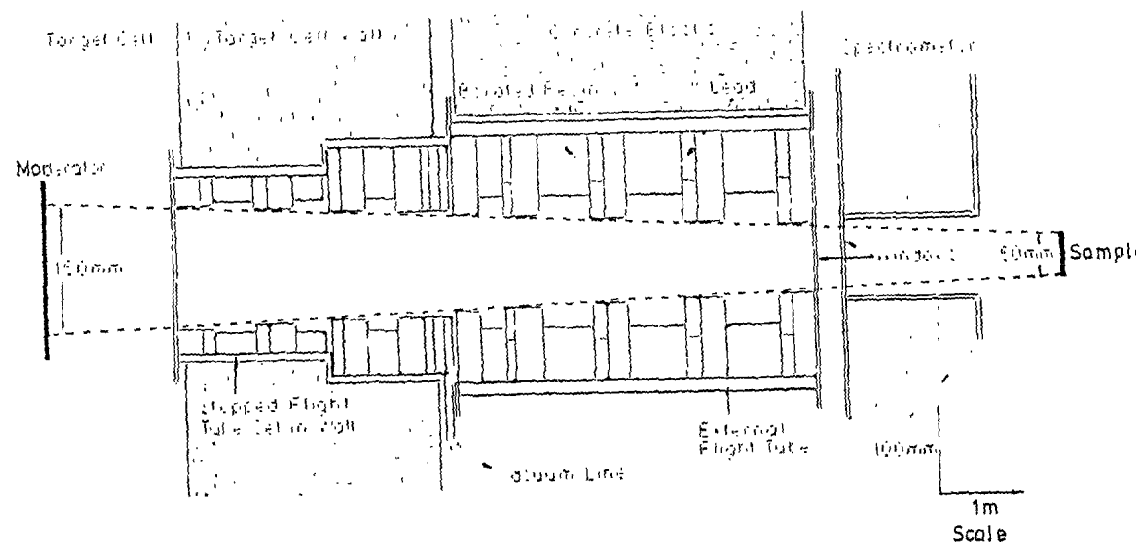

Figure 3 . An expanded view of a typical beam tube on the Harwell linac. The absorber sections converge from a 150 mm diameter moderator area to a 50 mm diameter sample.

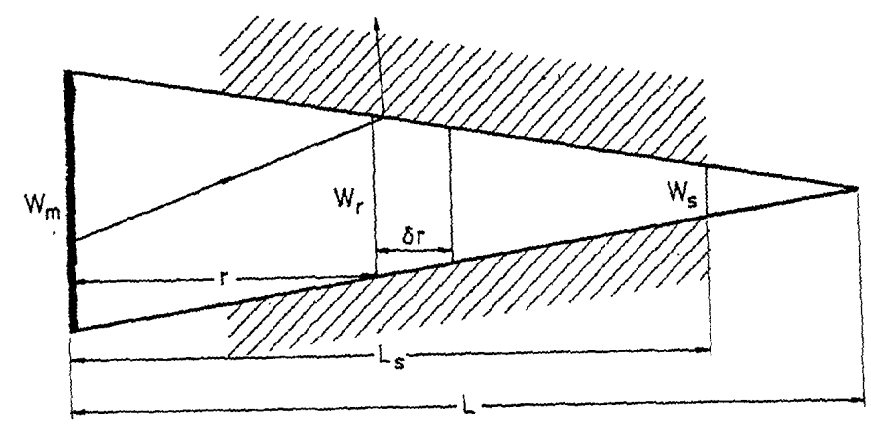

Figure 2 Neutrons incident on a beam tube wall are generally scattered outwards and must be shielded. A uniform conical tube is assumed. The effective source brightness of the conical segment δr, is equal to loss of flux between r and $r+\delta r$ divided by its area $\pi W_r \delta r$.

COST OF RADIATION SHIELDING.

M. M. BARBIER.

Marcel M. Barbier, Inc.
3003 Rayjohn Lane Herndon, Va. 22071 U.S.A.

SUMMARY.

Characteristic cost factors are defined depending on material, shield geometry and attenuation properties for a particular radiation.

These cost factors are calculated for a series of materials, geometries and types of radiation.

Dimensions and cost of a typical pulsed neutron source shield are estimated for various materials.

INTRODUCTION.

In view of the increasing number of materials that have been proposed for radiation shielding, the need arises for cost calculations based on shield volume as dictated by the material's radiation attenuation characteristics.

1. SHIELD VOLUME CALCULATION BASED ON ATTENUATION LENGTH.

Let us assume the material's shielding properties with respect to a given type of radiation can simply be described by a characteristic attenuation length (or mean free path) L, after which the radiation intensity is decreased by a factor e. This attenuation length will of course vary with the type and energy of the radiation. In some cases, when the energy of the radiation varies with penetration, the attenuation is not purely exponential; however the exponential approach can be used in most cases as a first step for volume and cost determination.

Let us therefore assume that the number N of mean free paths required is given to start with. The shield thickness is then NL in the direction of propagation of the radiation. The volume is determined by the geometry of the shield, which depends on the directions the radiation is coming from and the objects to be shielded.

Basically one can distinguish between three shield geometries: plane, cylindrical and spherical. In a first pass one can consider the case where the plane wall has a thickness equal to NL, the cylinder has a radius NL and the sphere a radius NL. As characteristic shield volumes, one is naturally led to take the volume per unit surface NL of the plane shield, the volume per unit axial length 3.14 N^2L^2 of the cylindrical shield, and the total volume of the spherical shield (4/3) 3.14 N^3L^3.

Let p be the price of the shielding material per unit volume in $\$/m^3$. The shield cost figures to be used for comparisons between materials will then be the above typical volumes multiplied by p.

One sees that, N being given in advance, the costs for these geometries are proportional to ρL, ρL^2, ρL^3, which we call the "cost factors" and depend on the type of material for each geometry. The cost factor is thus a function of the price of the material per unit volume and the attenuation length (or mean free path) that the particular type of material can achieve for the particular radiation. It therefore only depends on the material itself and is a figure of merit for the material (given the geometry), the lowest cost factor being the best.

The cost of the shield can easily be derived once the cost factor of the particular material for the relevant geometry is known (table 1).

In the case of cylindrical and spherical shells of thickness NL the volume and cost formulae are more complicated and the cost factors become dependent on the shield efficiency N. They are given in table 1 for completeness sake.

2. COST COMPARISON FOR VARIOUS RADIATIONS AND MATERIALS.

What will be compared will be the cost factors defined in the previous section for plane, cylindrical, spherical geometries, i.e. ρL, ρL^2, ρL^3. This will be done for various materials, such as concrete, steel, iron oxide mortar (including 50% by weight elemental iron), tungsten, lead, and for various kinds of radiation, including high energy neutrons (above 60 MeV), fusion neutrons (14.5 MeV), reactor neutrons (from 8.3 MeV to thermal) and gamma rays of 1 MeV. The properties of each material with respect to these kinds of radiation are different and, combined with the price, lead to a different choice of material for minimum cost for each kind of radiation (assuming space considerations do not dictate the choice of the material).

Table 2 gives the cost factors for the various kinds of radiation and materials considered.

For neutrons above 60 MeV, regular concrete is less expensive than the other materials for all geometries. If space is a consideration, the iron oxide mortar attenuation length lies half way between regular concrete and steel and the material is much less expensive than steel. Tungsten and lead seem prohibitive from the cost point of view.

For 14.5 MeV neutrons, the same observations as above apply.

For reactor neutrons, especially at 1.5 MeV and down to thermal energies, iron oxide mortar beats both regular concrete and steel by a large margin, both in cylindrical and spherical geometries. It is therefore the ideal material for all nuclear reactors and fission devices. Iron oxide mortar should also be preferred for all installation where the shielding is dominated by evaporation neutrons i.e. for accelerators of protons up to 60 MeV, deuterons, alphas and heavy ions, and for electron accelerators whose shielding is dominated by giant resonance neutrons, i.e. all medical or industrial electron accelerators.

For 1 MeV gamma rays, the least expensive material is regular concrete, then come iron oxide mortar, steel and lead, if space has to be saved.

Table 1: Calculation of Radiation Shield Costs for Various Geometries.

	Shield Volume	Shield Price	Cost Factor
Plane Geometry	NL m^3/m^2	$NL\rho$ $\$/m^2$	$L\rho$ $\$/m^2$
Cylindrical Geometry	$3.14\ N^2L^2$ m^3/m	$3.14\ N^2L^2\rho$ $\$/m$	$L^2\rho$ $\$/m$
Spherical Geometry	$(4/3)\ 3.14\ N^3L^3$ m^3	$(4/3)\ 3.14\ N^3L^3\rho$ $\$$	$L^3\rho$ $\$$
Cylindrical Geometry with Coaxial Void of Radius R_o	$3.14\ N^2L^2\ [1 + 2(R_o/NL)]$ m^3/m	$3.14\ N^2L^2\rho\ [1 + 2(R_o/NL)]$ $\$/m$	$L^2\rho\ [1 + 2(R_o/NL)]$ $\$/m^2$
Spherical Geometry with Centered Void of	$(4/3)\ 3.14\ N^3L^3\ x$ $[1 + 3(R_o/NL) + 3(R_o/NL)^2]$	$(4/3)\ 3.14\ N^3L^3\rho\ x$ $[1 + 3(R_o/NL) + 3(R_o/NL)^2]$	$L^3\rho\ x$ $[1 + 3(R_o/NL) + 3(R_o/NL)^2]$

Symbols:

L: Mean Free Path (Attenuation Length), meter
N: Number of Mean Free Paths Required
NL: Shield Thickness, meter
ρ: Price of Material per Unit Volume, $\$/m^3$
R_o: Void Radius.

3. COST COMPARISON FOR PULSED NEUTRON SOURCE.

A typical pulsed neutron source case will be calculated for a proton beam intensity of $I = 1.5\ 10^{14}$ protons per second (Carpenter, 1978) and a permissible high energy neutron flux outside the shield of $F = 2.5$ n/sec.cm^2 (corresponding to a radiation level better than or approximately 0.5 mrem/h). Let us assume this permissible flux is attained at $R = 6$ m from the source. The product of permissible flux and square of distance per incoming proton is then

$$R^2\ F/I = 36\ 10^4 \times 2.5/1.5\ 10^{14} = 6\ 10^{-9}$$

For this value one derives (Barbier 1980) the number of mean free paths required in various direction as presented in table 3, which also includes the resulting thicknesses for shields made of regular concrete, iron oxide mortar and steel.

The schematics of the neutron shield design are shown in fig. 1. The cavity at the center has been neglected. The proton beam level above ground is assumed to be $h = 1.5$ m. The shield is assumed not to go below ground level. The height above the proton beam is assumed to be equal to the shield thickness at 90° in the horizontal plane, to ensure permanent access to the top of the shield also.

Table 4 presents the resulting parameters and cost of the shield for the various materials. The cheapest shield is regular concrete. The iron oxide mortar shield offers an appreciable reduction in dimensions with respect to the concrete shield at half the price of the steel shield. It should be considered that, due to the propagation of the "iron window" neutrons through steel, a steel shield requires an additional 2 to 3 feet of regular concrete on the outside or distributed within. This circumstance partially offsets the gain in space achieved when using steel.

CONCLUSION.

The choice of the shielding material offers an additional degree of freedom in shield design and an opportunity of substantially reducing shielding costs depending on the radiation to be attenuated.

BIBLIOGRAPHY.

J. M. Carpenter, D. L. Price, N. J. Swanson, IPNS— A National Facility for Condensed Matter Research, Argonne National Laboratory, 9700 South Cass Avenue, Argonne, Illinois 60439, U.S.A., November 1978.

M. M. Barbier, Shield Calculation Taking into Account Neutron Spectra and Variation of Nuclear Cross-section with Energy, Marcel M. Barbier Inc. 3003 Rayjohn Lane, Herndon VA 22071, U.S.A., July 29th, 1980.

Table 2: Comparison of Material Cost Factors for Radiation Shields of Various Geometries (continued).

4. Gamma Rays	Regular Concrete	Iron Oxide Mortar	Iron	Tungsten	Lead
Attenuation Length* at 1 MeV L m	0.086957	0.0625	0.0256	0.01111	0.0177
Plane Cost Factor ρL \$ /m^2	6.52	24.00	122.15	8,799.1	264.08
Cylindrical Cost Factor ρL^2 \$/m	0.57	1.50	3.13	97.76	4.67
Spherical Cost Factor ρL^3 \$	0.049	0.0925	0.08	1.08	0.083

* Attenuation Length is 1/ (Narrow Beam Mass Absorption Coefficient x Specific Gravity).

Table 2: Comparison of Material Cost Factors for Radiation Shields of Various Geometries.

	Regular Concrete	Iron Oxide Mortar	Iron	Tungsten	Lead
Price p $\$/m^3$	75	384	4,764	792,000	14,920
1. Very High Energy Neutrons (above 60 MeV).					
Nuclear Interaction Mean Free Path L m	0.461	0.329	0.1734	0.101	0.178
Plane Cost Factor Lp $\$/m^2$	34.58	126.36	826.08	79,992.00	2,665.76
Cylindrical Cost Factor L^2p \$/m	15.94	41.17	143.24	8,079.19	472.73
Spherical Cost Factor L^3p \$	7.35	13.67	24.84	816.00	84.15
2. Fusion Reactor Neutrons					
Attenuation Length* at 14.5 MeV L m	0.091	0.0735	0.056		
Plane Cost Factor pL $\$/m^2$	6.82	28.24	264.69		
Cylindrical Cost Factor pL^2 \$/m	0.62	2.08	14.71		
Spherical Cost Factor pL^3	0.056	0.15	0.82		

* Attenuation Length is $1/\sqrt{3\, S_{scattering}\, S_{absorption}}$, when S refers to the macroscopic cross-section.

Table 2: Comparison of Material Cost Factors for Radiation Shields of Various Geometries (continued).

3. Fission Reactor Neutrons	Regular Concrete	Iron Oxide Mortar	Iron
3.1 Attenuation Length* at 8.3 MeV	0.11236	0.081967	0.040816
Plane Cost Factor	8.42	31.36	194.45
Cylindrical Cost Factor	0.95	2.57	7.93
Spherical Cost Factor	0.11	0.21	0.33
3.2 Attenuation Length* at 1.5 MeV	0.49261	0.1046	0.05814
Plane Cost Factor	36.95	40.17	276.98
Cylindrical Cost Factor	18.20	4.20†	16.10
Spherical Cost Factor	8.97	0.437†	0.94
3.3 Attenuation Length* at 0.25 MeV	2.9851	1.2077	0.56497
Plane Cost Factor	223.88	463.86	2,691.5
Cylindrical Cost Factor	668.31	560.21†	1,520.6
Spherical Cost Factor	1,995.5	676.6†	859.11
3.4 Attenuation Length* at thermal energy	0.081301	0.02907	0.013089
Plane Cost Factor	6.0976	11.165	62.356
Cylindrical Cost Factor	0.49574	0.3246†	0.81618
Sherical Cost Factor	0.0403	0.0094†	0.010683

* Attenuation Length is $1/\sqrt{3\, S_{scattering}\, S_{absorption}}$, where S refers to the macroscopic cross-section.

† beats regular concrete.

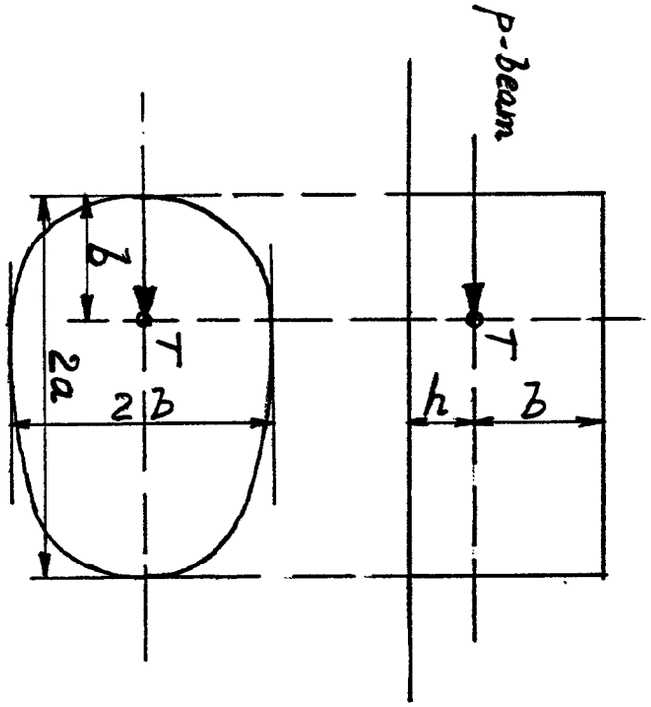

Figure 1: Schematics of Neutron Source Shield Design.

Table 3: Neutron Source Shield Calculation for 1.5 10^{14} protons/sec.

Emission Angle (Degree)	Number N Mean Free Path	Thickness Regular Concrete (m)	Thickness Iron Oxide Mortar (m)	Thickness Steel (m)
7	18.5	8.53	6.09	3.21
28	17.5	8.07	5.76	3.04
53	16.6	7.65	5.46	2.88
90	15	6.92	4.94	2.60
140-180	13.7	6.32	4.51	2.38

Table 4: Parameters and Cost of Neutron Source Shield for 1.5 10^{14} protons/sec.

	Regular Concrete	Iron Oxide Mortar	Steel
Long Half Axis a (m)	7.43	5.30	2.80
Short Half Axis b (m)	6.92	4.94	2.60
Height above ground H (m)	8.42	6.44	4.1
Ground Surface S (m^2)	161.53	82.25	22.87
Volume V (m^3)	1,360.1	529.7	93.77
Material Cost ($/$m^3$)	75	384	4,764
Shield Cost ($)	102,000	203,400	446,720

KENS Radiation Activity : Structural Materials

H. Hirayama and S. Ban

National Laboratory for High Energy Physics
Oho-machi, Tsukuba-gun, Ibaraki, 305, Japan

1. Introduction

Studies of residual radiation leveles concerning to KENS are reported. The saturated activities of produced nuclide in samples (of materials exposed to either the direct or the scattered beam of 500-MeV protons from the KEK Booster Synchrotron) were obtained by analyzing a pulse height distribution measured with a Ge(Li) spectrometer. The residual radiation levels were calculated with using the obtained saturated activities.

γ-ray spectrum measurements near accelerator structure were also done by using a pure germanium detectors and the decay cureves of residual activities were calculated with the same method used in the sample exposure.

2. Measurement of Nuclides Induced in Various Materials

0.1 cm thick samples of Al, Fe, stainless steel and Cu are placed at the beam dump entrance and the surface of the extraction septum magnet of the KEK Booster Synchrotron. At the sureface of the extraction septum magnet, the samples

were irradiated with the secondary particles produced by 500 MeV protons. (secondary particle irradiation). The gamma-ray activities of the samples were detected with a Ge(Li) detector having a detection efficiency of 10% compared to a 3"ϕ × 3" NaI(Tl) detector coupled to a multichannel pulse height analyzer. Fig. 1 shows the saturated activities per incident high energy particles (≥30 MeV) for the Al and Fe samples. The incident beam intensity for the direct exposure was obtained using the reaction $^{27}Al(p, spal.)^{18}F$. In the case of the secondary particle irradiation, it is very difficults to known the total particle flux. So the high-energy particle flux above 30 MeV was calculated with the saturated activities of $^{27}Al(n, x)^{22}Na$ and the average cross section is 20 m barn. From Fig. 1, neutron contributions were clearly seen in the secondary particle irradiation.

The exposure dose rate after irradiation time t_{ir} and cooling time t_c is given by

$$D(d) = I_0 \sum_{i=1}^{j} Q_i \cdot \Gamma_i \cdot [1 - \exp(\lambda_i t_{ir})] \exp(-\lambda_i \cdot t_c)/d^2, \quad R/h/cm^3 \qquad (1)$$

where

I_0= incident high energy particles (≥30 MeV)/sec,

Q_i= saturated activity of i-th nuclide, Ci/cm^3 per high particle

Γ_i= specific gamma-ray constant, R/h/Ci at 1 m,

λ_i= decay constant of i-th nuclids

d = distance from the material, m

The residual radiation levels for thin samples irradiated for 100 day is shown in Fig. 2. The material dependence of the residual radiation levels is nearly same with the published data. The saturated activities obtained in the measurement cannot be directly applied to the thick sample. It may be useful for the study of residual radiation level to measure the saturated activities both for the direct and the secondary particle irradiation as the function of the sample thickness.

3. Measurements of Gamma-ray Spectrum Inside the Accelerator Room.

Radionuclides induced in accelerator structures were measured by using a pure Ge detector having a detection efficiency of 3% compared to a 3"ϕ × 3" NaI(Tl) scintillator and a portable multichannel pulse height analyzer. Fig. 3 shows the measured pulse-height spectrum 2 hours after the beam-off near the extraction septum magnet of the Booster Synchrotron. (Booster M3) Identfied nuclides except ^{24}Na in Fig. 3 mainly produced in the vacuum chamber or the magnet. ^{24}Na may be produced in the concrete walls via the spallation reaction of Si or the thermal capture reaction of ^{23}Na.

The relative activities of identified nuclide were obtained from the photo-peak area and their relative detection efficiencies.

The decay of the exposure dose rate can be calculated with eq. (1) by using the relative activities instead of the saturated activities. In Fig. 4, the decay of the total exposure dose rats at the Booster M3 is shown with that of the exposure dose rate due to each individual nuclide. The shape of the decay curve is similar to that of stainless steel by 500 MeV protons in Fig. 3 after 100 hours. This shows that the residual radiations in the accelerator tunnel are caused from the nuclides produced in the vacuum chamber by the direct reaction of 500 MeV protons except ^{24}Na in the concrete wall.

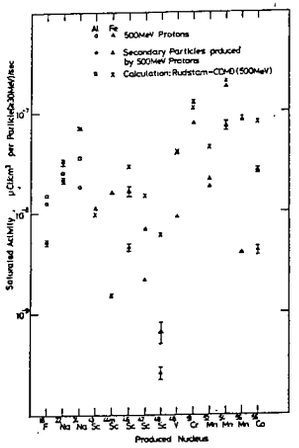

Fig. 1 Saturated activities induced in Al and Fe.

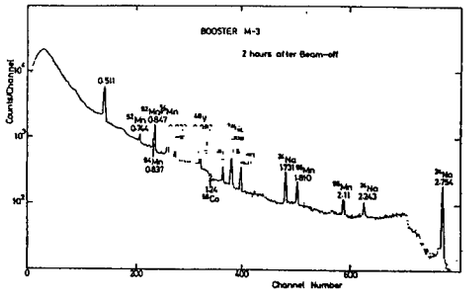

Fig.3 Pulse height distribution of gamma-rays in the Booster room.

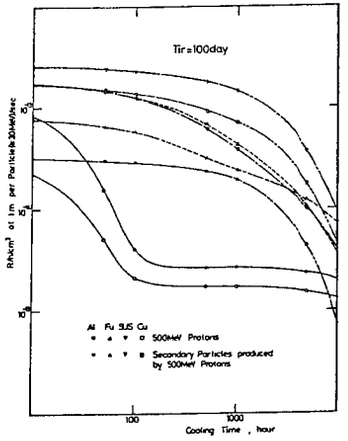

Fig.2 Residual radiation decay curves for thin samples for 100 days.

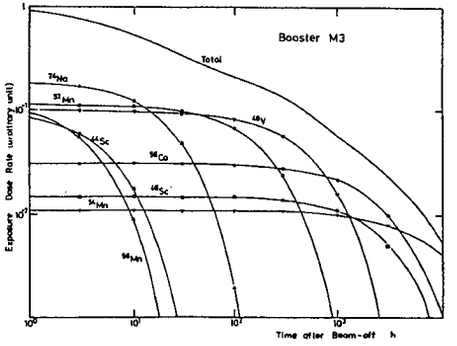

Fig.4 Residual radiation decay curve in the Booster room.

Radioactivity and Radiolysis of the Solid Methane used as a Cold Neutron Moderator in the KENS Target Assembly

K. Kondo and K. Hozumi

National Laboratory for High Energy Physics
Oho-machi, Tsukuba-gun, Ibaraki, 305, Japan

Abstract

The radioactivity and radiolysis of the solid methane used as a cold neutron moderator in the KENS target assembly were studied extensively. $H_2^{\cdot}$, C_2H_4 and C_2H_6 were identified as radiation decomposition products using a gaschromatograph and their concentrations were less than 1 % for the bombardment of 500 MeV protons on the W target at an average beam intensity of 1.2 μA for 52.7 hrs. Only ^3H and ^7Be were detected as radioactive nuclides in the irradiated CH_4 gas. The concentrations were of the order of 10^{-10} μCi/cm^3 for ^7Be and 8.5×10^{-6} μCi/cm^3 for ^3H. About 60 % of ^3H atoms produced was in the chemical form of ^3HH and the rest 40 % in tritiated - CH_4, C_2H_4 and C_2H_6. Further the ^3H concentrations in the cooling waters for the target assembly and the magnets for beam transport were 0.73×10^{-4} μCi/cm^3 and ~ 10^{-6} μCi/cm^3 respectively.

1. Introduction

The cold neutron moderator installed in the KENS target assembly consists of a solid methane of $13^W \times 5^D \times 15^H$ in size, which is placed just upon the tungsten target[1]. Fig. 1 shows the details of target assembly. The moderator is cooled down to 20°K by circulation of He gas using a small cryogenerator. When a cycle of two weeks experiments was finished, the methane is evaporated and transferred to a reservoir tank of 0.5 m^3, from which the gas is purged into air through a stack every two weeks.

While the W target is bombarded with 500 MeV protons from the booster synchrotron, the solid methane moderator is exposed to high radiations of secondary particles and photons for a relative long period. The informations on the radiation decomposition and the radioactivites of this methane moderator are therefore ~~are~~ required prior to the use at a full power operation.

Recently a short term test was conducted on July 7 to 25 of 1980 to examine the various performances of the KENS facilities. The radioactivity measurement and chemical analysis of the irradiated methane were performed at the same time. Their experimental results are presented in this paper. In addition, the radioactivities of cooling water for the target assembly and the magnets for beam transport are reported.

2. Radiation decomposition of the solid methane

The W target was bombarded at an average beam intensity

of 1.2 μA for 52.7 hrs in the test run. The solid CH_4 exposed to high radiations was transfered to a reservoir tank of 0.5 m^3 after the run. The sample gases to be assayed was taken from this reservoir tank.

The sample was analysed by gaschromatography under the following conditions;
Column: stainless steel 3 mm diameter, 1.5 m long,
Column packing: molecular seive 5 A, 80 ~ 100 mesh,
Column temperature: temperature programmed at the rate of 10°C/min. from 35°C to 200°C, Carrier gas: N_2, TCD filament current and temperature: 100 mA, 150°C.

Fig. 2 shows the block diagram of the gaschromatograph used in the present experiment.

The retention times of H_2, CH_4, C_2H_4 and C_2H_6 gases and their sensitivities to TCD were determined in advance using the standard gases, which were prepared by mixing these gases at various ratios of concentration with a vacuum line. Fig. 3 is the gas chromatogram obtained for the above sample. H_2, C_2H_4 and C_2H_6 were identified as radiation decomposed products, and their relative concentrations were calculated from the peak area in the gaschromatograms and the sensitivity of each gas to TCD, being presented in Table 1 (CH_4=100%).

The major product was H_2, however its concentration was of small quantity less than 1 %. The production ratios of C_2H_4 and C_2H_6 to H_2 in the gas phase radiolysis of CH_4[2)] were lower than the present results. This is indicative that the reactions concerning radicals and/or excited species

containing C atoms take place in the spur more frequently in the solid.

3. Radioactivity of the solid methane moderator

The high energy secondary particles from the W-target interacts with C atoms of the moderator to give spallation reaction products of ^3H (half life: 12.3y) and ^7Be (53 days).

The sample gas taken from a reservoir tank was introduced to a CuO-Oxidation furnace as shown in Fig. 4, and all hydrogen atoms were oxidized and converted to H_2O. The tritiated H_2O collected by a Dry Ice-ethanal trap was measured with a liquid scintillation counter. 2ml of the above water was mixed with 13ml of a Insta-Gel scintillation cocktail, and ^3H-radioactivity was determined by an external standard method. The chemical forms of tritium atoms in the CH_4 moderator were also examined with the apparatus shown in Fig. 4. Tritiated compounds are divided into two fractions of H_2 and organic one (CH_2, C_2H_4 and C_2H_6) by the use of the liquid N_2 trap placed between the sample gas container and the CuO-oxidation furnace.

The results were presented in Table 2. The ^3H activity in the CH_4 gas reservoir was 8.5×10^{-6} μCi/cm^3 on an average and 40 % of ^3H atoms was in the chemical form of H_2 and the rest 60 % in CH_4, C_2H_4 and C_2H_6. The tritium atom produced by spallation reactions has very high translational energy and loses gradually its energy in collisions with surroundings. These hot tritium atom enter the chemical combinations in the energy region less than a few tens of electron volts.

The main reactions of ^3H with CH_4 are H-substitution (1) and H-abstraction (2) reactions[3)]

$$^3H + CH_4 \longrightarrow CH_3{}^3H + H \text{ ----- } (1)$$

$$^3H + CH_4 \longrightarrow {}^3HH + CH_3 \text{ --- } (2)$$

On the other hand, C_2H_4 and C_2H_6 are considered to be formed in the hot zone, in which a large amount of energy are dissipated and the reactions concerning radicals and excited species take place. The ^3H concentration of the CH_4 gas was greater than the $(MPC)_a$ for ^3H (2×10^{-6} μCi/cm^3). However the concentrations at the boundaries of site and controlled area can be kept less than the values of KEK radiation rule, 2×10^{-4} μCi/cm^3 and 2×10^{-6} μCi/cm^3 at each position, by releasing the gas through the stack of 20 m in height. Whereas ^7Be by the reaction of ^{12}C (n, spallation) ^7Be ($E_{th} \approx 30$ MeV, $\sigma \approx 10$ mb) is expected to be produced in the same extent to the ^3H activity. However its concentration in the CH_4 gas was of the order of 10^{-10} μCi/cm^3, being extreamly small compared with the ^3H activity of 8.5×10^{-6} μCi/cm^3. This indicates that the most ^7Be reacts with CH_4 and/or O_2 present as an impurity to form non-volatile compounds and are adsorbed on the walls of the container and pipes.

The ^3H concentration in the cooling water of the target assembly and the magnets for beam transport were further examined. In order to eliminate ^7Be and other radioactivities, the sample was distilled, and then the water collected at the trap was measured with a liquid scintillation counter in a similar manner as above mentioned. Their concentrations

were 0.73×10^{-4} μCi/cm^3 for the target cooling water and 2×10^{-6} μCi/cm^3 for the magnet cooling water respectively.

References

1) "KENS Report-I" ed. by Y. Ishikawa, P.32, (1980).

2) K. Yang and P.J. Manno, J. Am. Chem. Soc., 81, 3507 (1959).

3) E.A. El-Sayed, P.J. Estrup and R. Wolfgang, J. Phys. Chem., 62, 1356 (1958).

Table 1. Product yields due to the radiation decomposition of the solid CH_4 (CH_4=100%)

Sample No.	H_2	CH_4	$CH_2=CH_2$	CH_3CH_3	O_2
1	0.13 %	100 %	0.03 %	0.05 %	<0.005
2	0.15	100	—	—	<0.003
3	0.15	100	0.04	0.07	<0.003

Table 2 Radioactivity of tritium and chemical forms of tritiated compounds

A) Radioactivity of Tritium

Sample No.	concentration ($\mu Ci/cm^3$)
1	8.7×10^{-6}
2	7.9×10^{-6}
3	8.9×10^{-6}

av. $8.5 \times 10^{-6} \mu Ci/cm^3$

B) Chemical Forms of Tritiated Compounds

sample No.	H_2-fraction	oraganic fraction*
1	60.8 %	39.2 %
2	60.9 %	39.1 %
3	59.7 %	40.3 %

* including CH_4, C_2H_4 and C_2H_6

Fig. 1 Side View of KENS Cold Neutron System

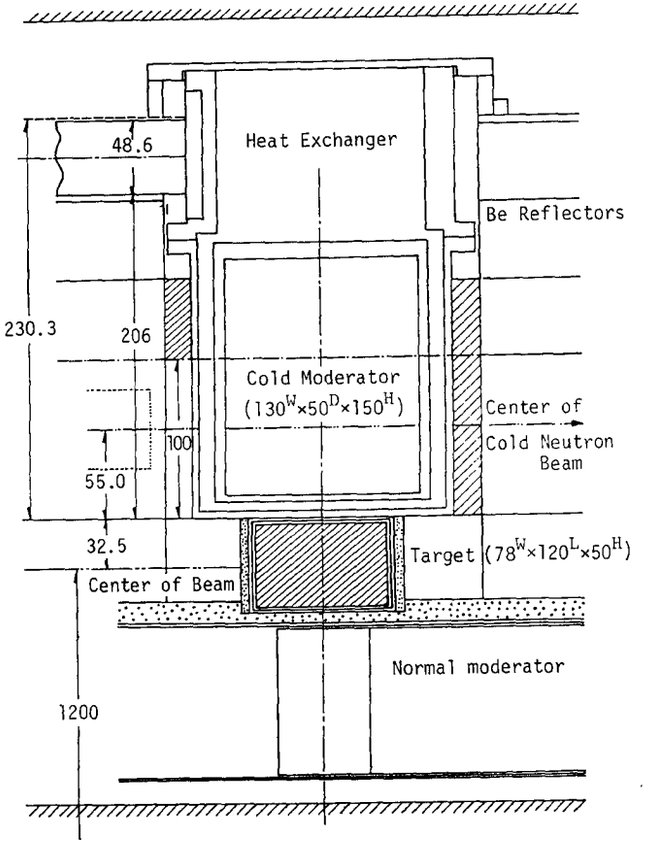

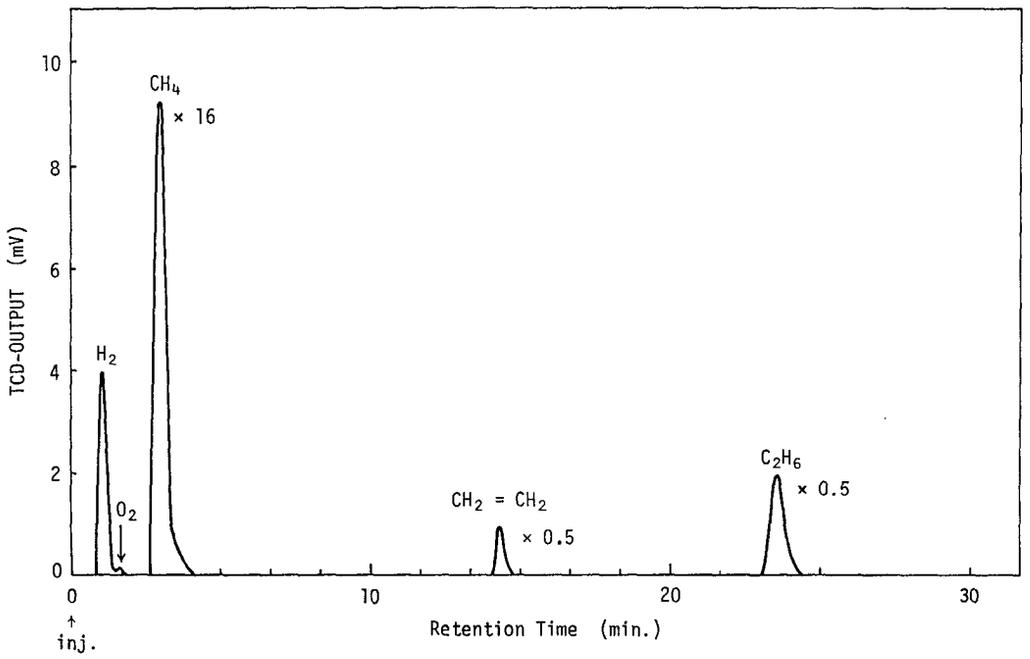

Fig.3 Gas-chromatogram of the irradiated CH_4 moderator

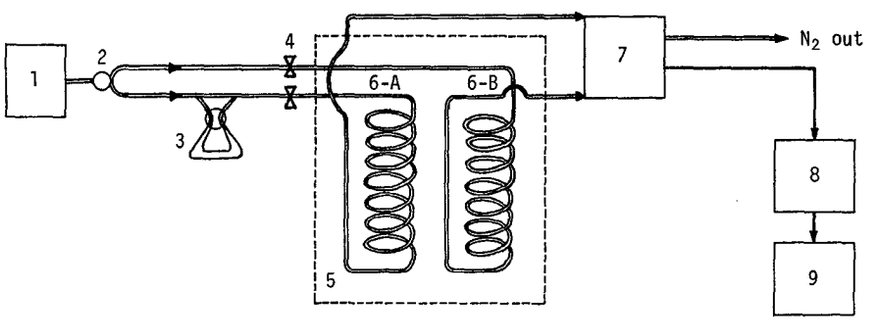

Fig.2 Block diagram of the gaschromatogroph

1. N_2 gas container (carrier gas)
2. three-way stopcock
3. sample gas container (10ml) with a four-way stopcock
4. carrier gas flow regulator
5. oven (temperature programmed)
6. 6-A : sample column, 6-B : reference column
7. TCD (thermal conductive detector)
8. amplifier
9. recorder

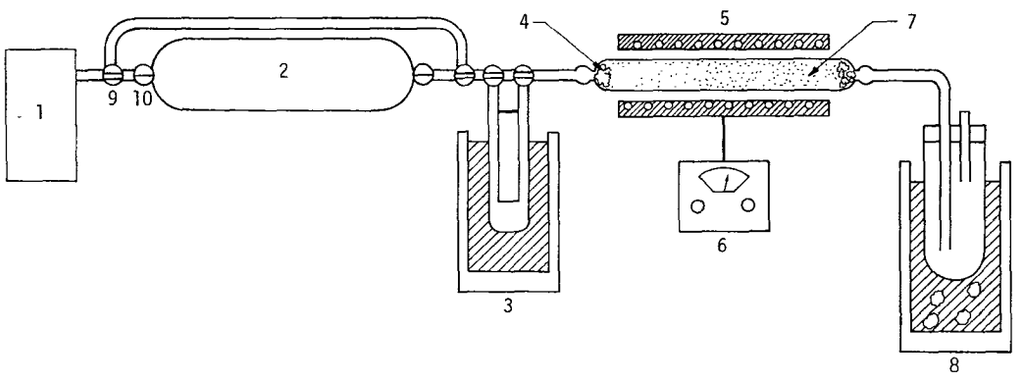

Fig.4 Oxidation apparatus of the sample gas

1. He gas
2. sample gas container
3. lig. N_2 trap
4. glass wool
5. electric furnace
6. temperature controller
7. copper oxide
8. Dry Ice ethanol trap
9. three-way stopcock
10. straight stopcock

Experimental Studies of the Induced Radioactivities in a Uranium Target

K. Katoh, S. Ban, H. Hirayama, S. Ikeda, K. Irie, K. Kondo, M. Miyajima, S. Satoh, N. Watanabe and S. Yamaguchi*

National Laboratory for High Energy Physics
Oho-machi, Tsukuba-gun, Ibaraki, 305, Japan

and

* Department of Nuclear Engineering, Tohoku University
Aramaki, Sendai, Miyagi-ken 980, Japan

1. Introduction

Uranium is attractive as a spallation target material for producing intense neutron beams owing to its high expected neutron yield and its high density. However, from a safety point of view, special attention must be paid to the level of induced radioactivity as this will be greater than that experienced with other common target materials such as iron, copper or tungsten.

In Japan uranium is designated legally as a nuclear fuel material and before it can be used as a spallation target material, the potential hazards must be analysed so that the

safety of the source can be guaranteed.

This paper deals with the results of a preliminary study on this subject.

2. Experiment

Blocks of depleted uranium coated with polyurethane sheet of 15 μm thickness were assembled together with sealed powder specimens of yellow cake for the activity measurement as shown in Fig. 1. The target was exposed to 6.1×10^{13} protons of 500 MeV at the beam dump of the Booster Synchrotron at KEK. Profiles of the proton beam as monitored by a carbon (paper) detector[1] just before the target are shown in Fig. 2. The exposure time was 239 seconds.

3. Radiation Levels due to the Induced Activities

The radiation levels on and around the assembly were measured with GM survey meters, an ionization chamber and a NaI(Tl) gamma-ray detector. Table 1 lists the results of the measurements made immediately after and also 1 hour after the irradiation. Fig. 3 shows the decrease in the radiation level from the 0.5 cm thick block (#1) for cooling times between 1 and 1,000 hours. For comparison, the similar curve for 600 MeV protons as measured by Barbier[2] is also displayed in the figure after normalisation to the same number of protons and quantity of U-238. The exposure rate at 1 m for a cooling time of 1 hour is exactly the same as that given by Barbier. A predicted decay curve as computed from the levels of the identified dominant nuclides at the cooling time of 644 hours

is also plotted in the figure. For the latter, the longer the cooling time the steeper the curve, although at these extended cooling times there might be possible compensations from longer lived radionuclides which are buried in the γ-ray spectra obtained in earlier measurements.

4. Induced Beta-Activities

Fig. 4 shows the absorption characteristics of the induced β-rays from the yellow cake specimens inserted between the uranium blocks. The appearances of the five curves are very similar, which implies that the energies of the β-rays are almost the same and hence independent of the position in the target. Fig. 5 displays the spatial distributions of the β-ray yield at various cooling times. Absorption characteristics are also independent of the cooling time.

Examples of the γ-ray spectra from the yellow cake No. 2 measured with a Ge(Li) detector are shown in Fig. 6. They are rather complicated and identification of radionuclides is therefore not an easy task. The identifications given in the figure are incomplete but the dominant nuclides seem to originate from fission, in contrast to the case of a tungsten target where the dominant nuclides derive from spallation.[3)]

Estimated absolute values of the saturated activities for the nuclides of Te-132, Sr-91 and Ru-105 were calculated. The results are shown in Fig. 7.

The sample for the γ-ray spectroscopic measurements were prepared from the yellow cake specimen by dissolution in nitric acid. The concentration of U-238 in the sample was 1.34×10^{19} $^{238}U/2.5 \times 2.5$ cm^2.

5. Induced Alpha-Activities

The energy spectra of α-particles emitted from the irradiated specimens were measured with a gridded-ionisation chamber.[4)] A typical energy spectrum obtained from specimen No. 1 which had been placed on the front face of the block (Fig.1) is shown in Fig. 8. The increased emission rates of α-particles are listed in Table 2.

The concentration of U-238 in the sample for the α-ray measurements was 1.33×10^{18} $U/2.5 \times 2.5$ cm^2. The backing material was stainless-steel.

The increased emission rate at the front surface of the target was found to be much higher than those at different depths, although why is not yet clear.

6. Conclusion

The radiation levels produced around the irradiated U-target block were measured and their decay behaviours monitored.

Most of the induced activity was found to be due to the fission products.

However, this experiment was a preliminary one and for more complete information further work is required.

Nevertheless, we hope that the outcome of the present study will be useful in assisting the design of future experiments utilising U-targets.

References

1) N. Watanabe, S. Ikeda and Y. Ishikawa: KENS Target Station, Proc. ICANS-IV (1981).

2) Marcel Barbier: Induced Radioactivity, North-Holland Publishing Company, Amsterdam-London (1969), p.209.

3) H. Hirayama: to be published.

4) M. Miyajima: "Two Stage Single Gridded Ionisation Chamber", to be published.

Tables

Table 1. Radiation levels on and around the assembly after the irradiation

Table 2. Summary of the measurements of alpha-activities

Figure Captions

Fig. 1 Layout of the assembly subjected to irradiation by the proton beam

Fig. 2 Incident proton beam profiles

Fig. 3 Decay of the level of the induced radioactivity at 1 m from the front surface of the 5 mm-thick block (——— : present, —·—·—: by Barbier, - - - - - -: predicted)

Fig. 4 Absorption characteristics of the induced beta-rays in the yellow cake specimens

Fig. 5 Spatial distribution of the beta-ray yield at various cooling times

Fig. 6 Gamma-ray spectra and trial identification of radio-nuclides (Specimen No. 2)

Fig. 7 Saturated activities of Te-132, Sr-91 and Ru-105 as typical decay products

Fig. 8 Typical measured α-particle energy spectrum (Depth 0 mm)

Fig. 1

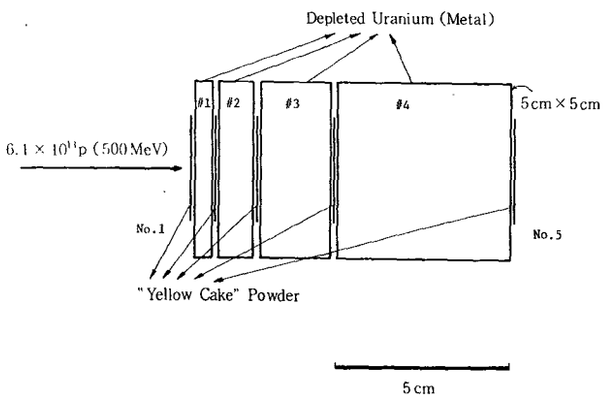

Fig. 2

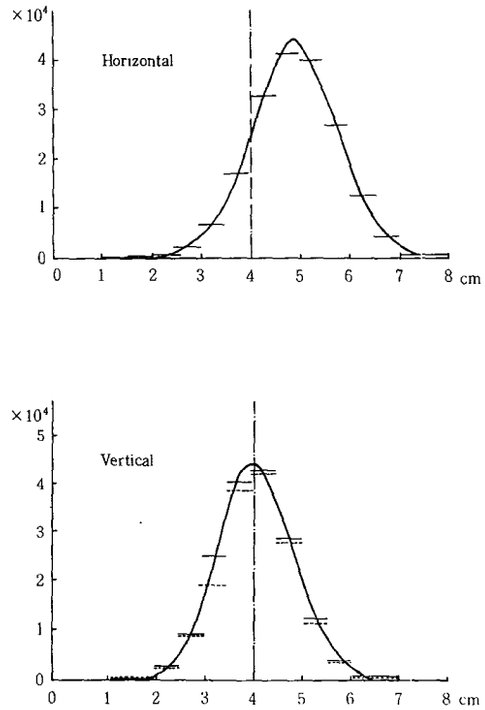

Table 1

Exposure Rate

Immediately after the irradiation (as whole)

Front surface	25 R/h
Rear surface	12 〃

after 1 hour cooling (blocks)

	at 30 cm	at 1 m	at surface
5 mm F	28 mR/h	3 mR/h	1.7 R/h
R	20	3	1.4
10 mm F	50	7	0.9
R	50	6	0.9
20 mm F	80	9	1.1
R	80	9	1.1
50 mm F	—	14	1.2
	100	8	1.1

F : front surface

R : rear surface

Table 2

α-Activity

Increased Emission Rates of α-Particles
(Relative to that of Natural U-238 in Equilibrium)

Depth (mm)	I.E.R. (%)	Cooling Time (days)	Measuring Time (sec)
0	19.0	5	4×10^4
5	3.1	2	1×10^4
15	2.0	4.4	4×10^4
35	4.6	0.3	1.6×10^4
85	1.4	1.3	4×10^3

Irradiation: 6.1×10^{13} protons of 500 MeV
(100 pulses, 239 sec)
1980. 7. 16 (12:46 ~ 12:50)

Samples : For Irradiation 4.46×10^{18}U/2.5cm × 2.5 cm
For Measurement 1.33×10^{18}U/

Measurement: Gridded Ionisation Chamber

Fig.3

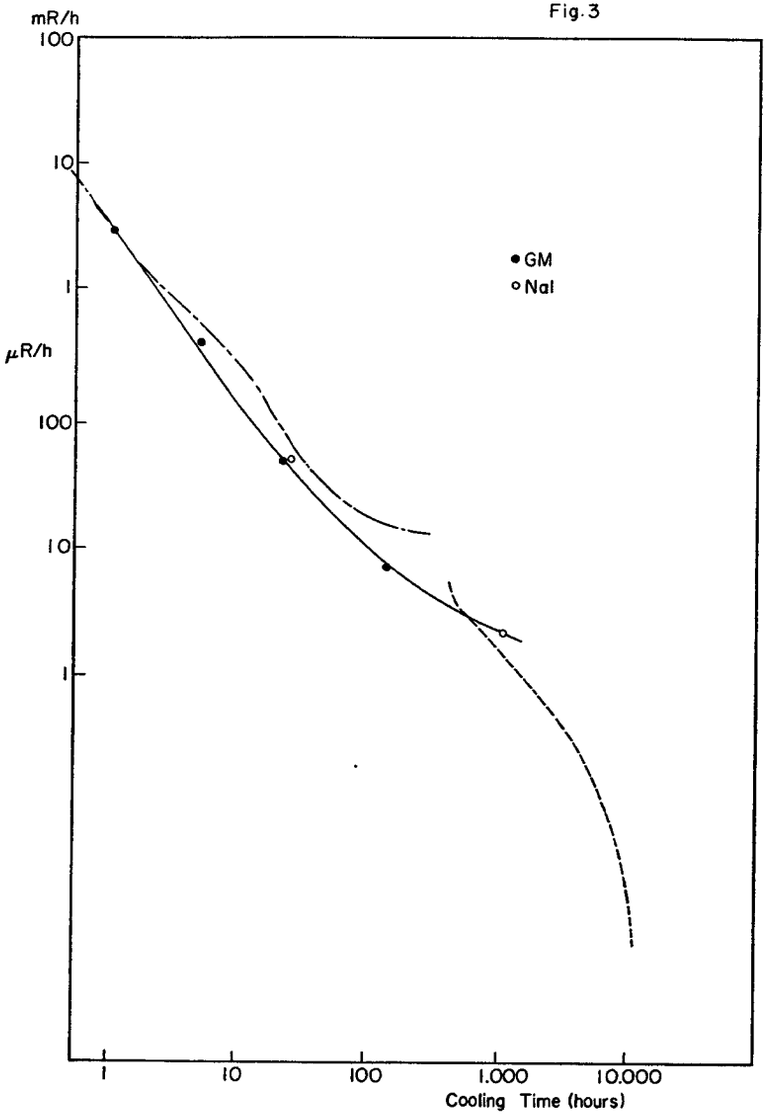
mR/h
100
10
1
μR/h
100
10
1
• GM
○ NaI
1
10
100
1.000
10.000
Cooling Time (hours)

Fig.4

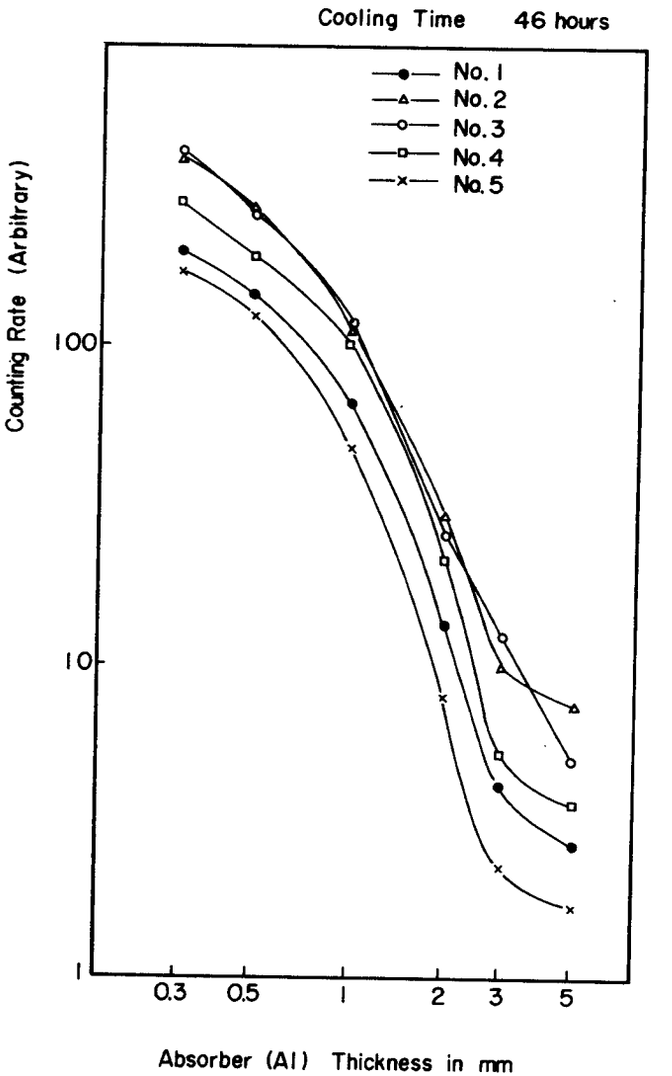
Cooling Time 46 hours
No. 1
No. 2
No. 3
No. 4
No. 5
Counting Rate (Arbitrary)
100
10
1
0.3
0.5
1
2
3
5
Absorber (Al) Thickness in mm

Fig. 6

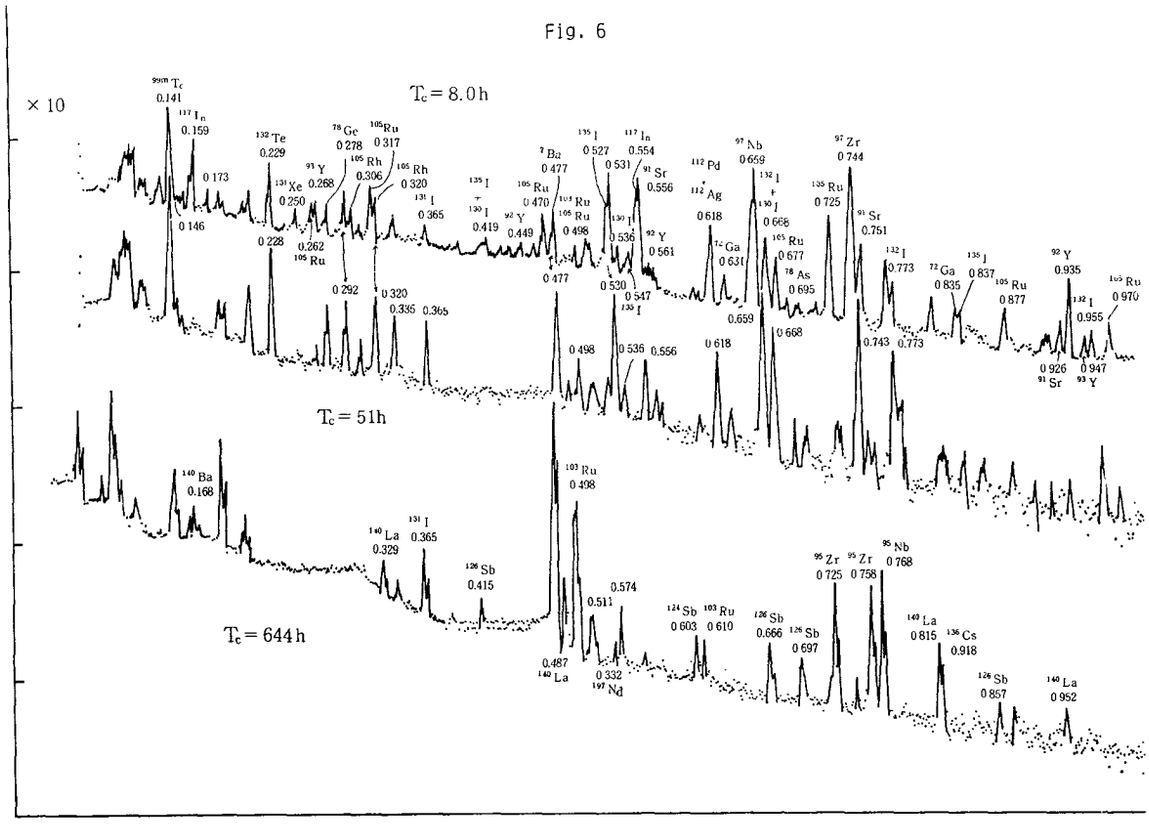
× 10
Tc = 8.0h
Tc = 51h
Tc = 644h

Fig. 5

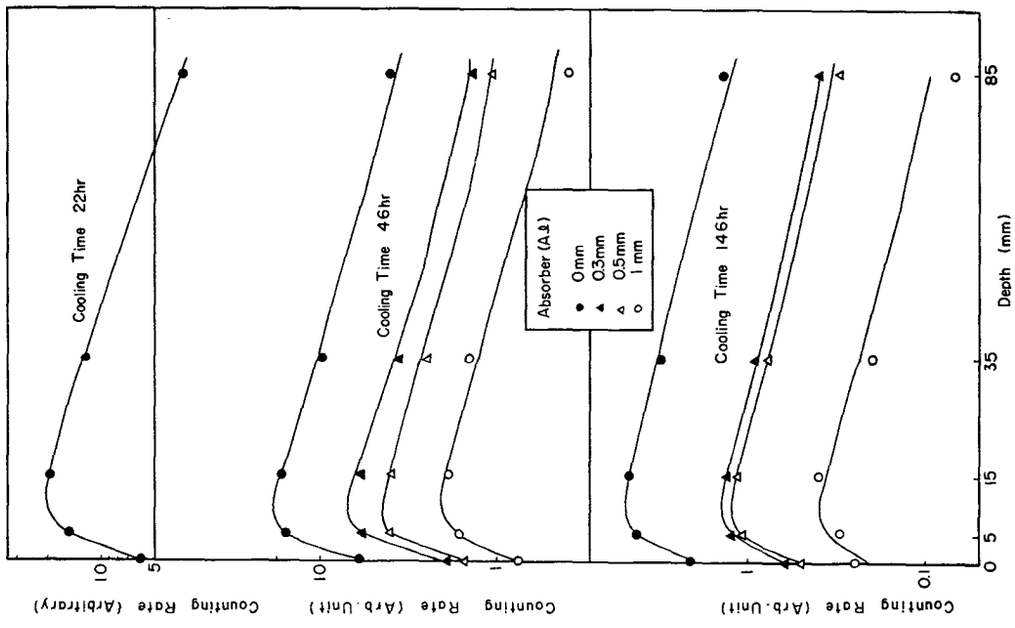
Cooling Time 22hr
Cooling Time 46hr
Cooling Time 146hr
Absorber (Al)
0mm
0.3mm
0.5mm
1 mm
Counting Rate (Arbitrary)
Counting Rate (Arb. Unit)
Counting Rate (Arb. Unit)
Depth (mm)
0
5
15
35
85

Fig. 7

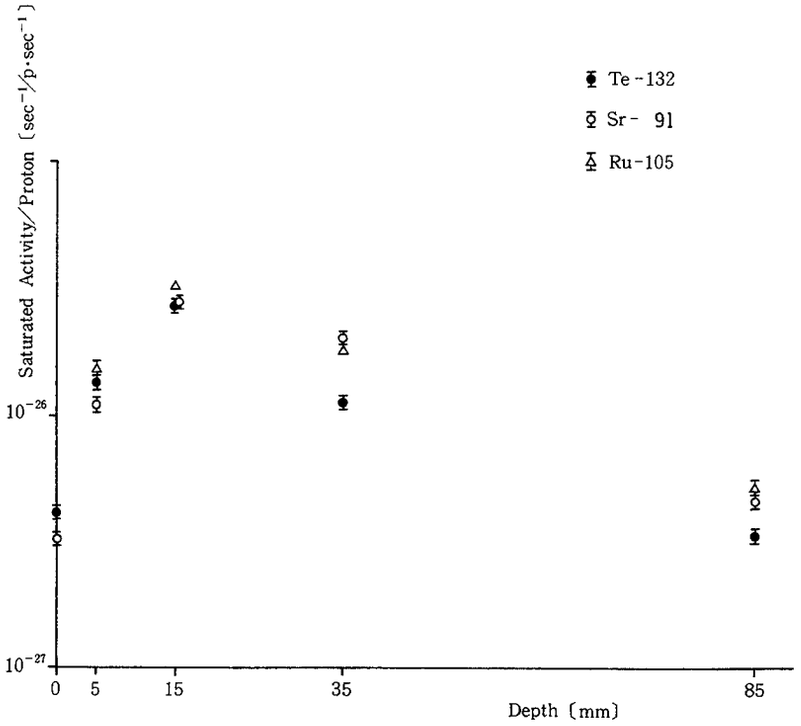
Te-132
Sr- 91
Ru-105
Saturated Activity/Proton [sec⁻¹/p·sec⁻¹]
10⁻²⁶
10⁻²⁷
0
5
15
35
85
Depth [mm]

Fig. 8

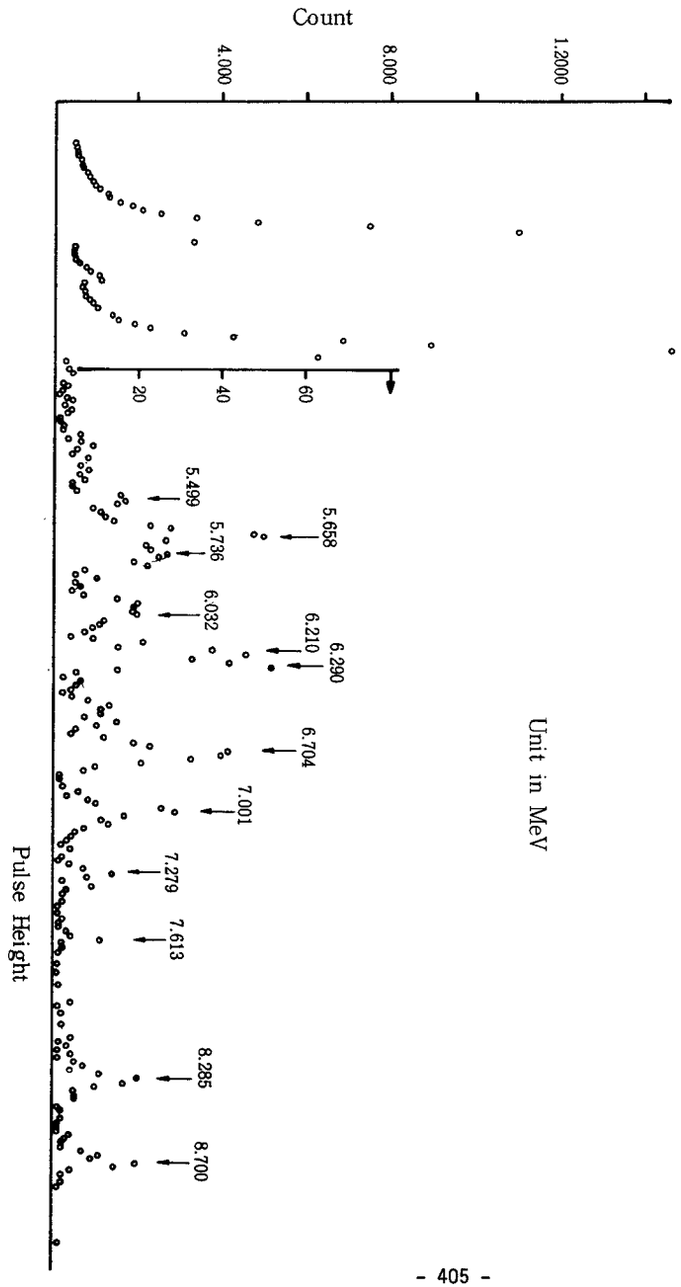
(U-238)
4.195
(U-234)
4.768
Count
1.2000
8.000
4.000
20
40
60
5.499
5.736
6.032
5.658
6.210
6.290
6.704
7.001
7.279
7.613
8.285
8.700
Pulse Height
Unit in MeV

BSF Beam Control System

Y. Irie

Booster Synchrotron Utilization Facility,

National Laboratory for High Energy Physics

Components of the control system can be divided into:

(1) control desk

(2) programmable sequence controller

(3) timing system

(4) computer

(5) television system

(6) access control system

(7) gate monitor

Fig. 1 shows the schematic diagram of the hardware interconnections.

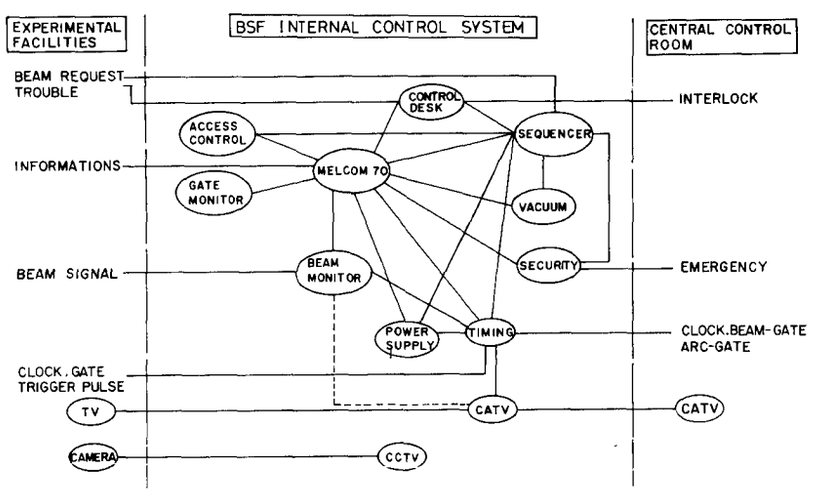

Fig.1 Simplified schematic diagram of the hardware interconnections

1. Control Desk

A BSF operation mode such as NORMAL, DUMP and MAIN RING INJECTION is selected at the control desk. Each operation mode means the following case:

(1) "NORMAL", where the booster beam is injected into the BSF beam channel.

(2) "DUMP", where a power supply B-2 is turned off and the beam goes down to the beam dump.

(3) "MAIN RING INJECTION", where power supplies B-2 and PB-1 are turned off and the booster beam is used for main ring injection only.

In the NORMAL mode, the beam switch of the control desk plays the most important role of the beam ON/OFF control. The conditions for beam injection directly interlock the beam switch by hardwiring (relay logic). If the interlock chain is broken the beam switch turns off and the beam is inhibited at the ion source of the preinjector.

2. Programmable Sequence Controller

5TI-1023 programmable sequence controller (TEXAS INSTRUMENTS INC., hereafter called a sequencer) is used for sequence control. The response of the sequencer is within 30.5 msec in a 50 Hz operation. According to the BSF operation mode the sequencer selects the doors which are allowed to be opened and signals the choices to an access control system. Beam request status from users is READY/PRESET/PAUSE/REJECT and each facility sends one of these requests. The sequencer accepts these requests and decides the beam delivery mode. After checking all conditions for the beam delivery it sends

"BSF ready" signal to the control desk if all conditions are satisfied. The "BSF ready" signal interlocks the beam switches on the control desks both in the BSF control room and the central control room (CCR).

3. Timing System

A beam-gate, clocks and trigger pulses are transmitted from the CCR. The beam-gate is a gate pulse of about 1.9 sec in width which corresponds to an excess of the booster beam pulses over the main ring injection. In this gate we can choose the beam pulses in any form of a pulse sequence by using a "BSF-programmer". Beam selection is made following the beam dilivery signal from the sequencer. The selected beam gate signal (arc-gate) is sent to the CCR and fed into the arc-triggering system for the preinjector. Timing clocks, trigger pulses are used for synchronizing pulsed operating devices to the booster cycle. Triggering a pulsed switching magnet, taking beam profile data, rotating a neutron chopper etc. should be in synchronization. These clocks and pulses are distributed to each facility.

4. Computer

The computer to be used is a MELCOM-70 mini-computer (M-70) made by MITSUBISHI ELECTRIC CORPORATION. Fig. 2 shows the constitution of the M-70 system. The software system is based on the real-time disc operating system RDOS and batch disc operating system BDOS. In the present system RDOS supervises 14 levels of tasks in the foreground and does not include a background job because of a limitation of the core memory size. The batch processing program is executed under the supervision of BDOS.

All the magnet power supplies are controlled by the M-70.

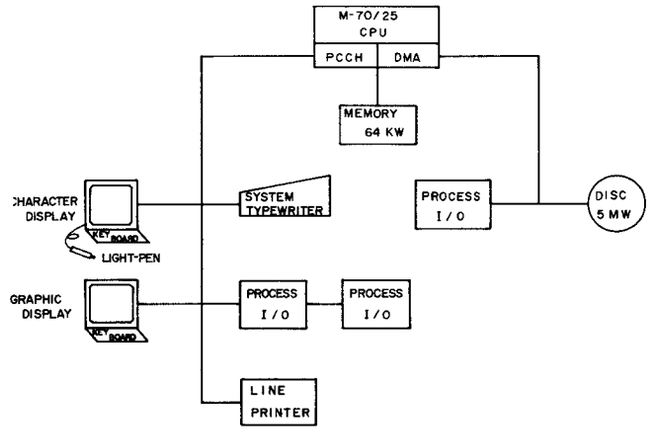

Fig.2 Constitution of the MELCOM-70 system

The control of ON/OFF, UP/DOWN and switching of polarity is performed. Beam profile data are taken through DMA synchronizing to the beam injection and are shown on a graphic terminal. Fig. 3 shows beam profiles on a graphic display. The beam line tuning is made by watching the screen and controlling the magnet power supplies.

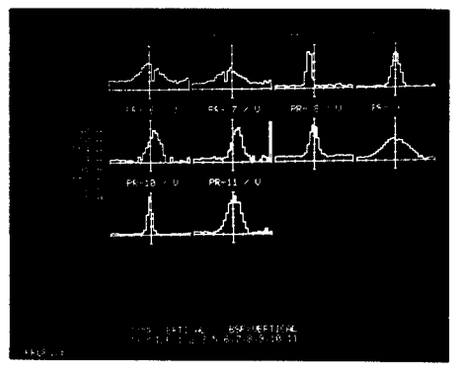

Fig.3 Beam profiles along the BSF beam line in a vertical direction. Each horizontal step corresponds to 2.5 mm in width. Beam profiles in a horizontal direction are the similar ones.

Beam current monitor output is fed into a sample/hold module and integrated with an ADC and counter module. The M-70 takes these integrated values by an external synchronizing signal and displays on the character terminal or the control desk in units of protons per pulse or counts per second.

Any other informations on the beam channel, experimental facilities and the safety status are gathered and displayed on the character terminal. Surveillance program checks these data. When it finds an incorrect status or a value out of tolerance, an alarm bit is generated. According to the alarm bit, the character on the screen which shows the item concerned changes its color so as to inform an operator of the accident. The alarm message is also printed out on a system typewriter for recording. Operation, access and contamination records are accumulated in a disc file of the M-70 and these data can be always read out and printed out in an arranged form.

5. Television System

Closed-circuit television CCTV is required for the purpose of surveillance of the access points, the beam channel and experimental areas especially around the neutron and the meson target. Video signals are connected to a multiplexer and displayed on the access and control consoles. Video informations on the BSF operation and the beam delivery mode are transmitted to the CCR. The signal is modulated and distributed anywhere in KEK by means of cable television (CATV) system. It is scheduled to transmit the beam profile data together with the informations described above.

6. Access Control System

Beam lines, a cable pit, experimental areas and a transfer tunnel are all controlled areas for radiation safety. Access to these areas is restricted and it depends upon the BSF operation mode which is selected at the control desk. According to each mode, access to the following areas is possible.

(1) NORMAL : neutron scattering experimental area and meson experimental area

(2) DUMP : all areas except for a primary beam line

(3) MAIN RING INJECTION : all areas

All doors of these controlled areas are electrically locked. One who wants to open the door has to, for the first time, contact the control room by means of an interphone placed inside/outside the door. On condition that the door is allowed to be opened, the power of the door control panel placed inside/outside the door can be switched on from the control room. The electric lock is released by performing a key operation on the door control panel. Entering or leaving is made under TV surveillance from the control room. For the access to the primary beam line, it is necessary to use a particular key which is reserved on a personal keyboard. When these kies are removed from the keyboard it becomes impossible to turn on the beam switch and the relevant magnet power supplies such as PB-1 and B-2. Removing or replacing the key is recorded by the M-70 as the personnel entering or leaving the primary beam line.

7. Gate Monitor

The radioactive contamination of whole human body surface

and equipments is checked by a gate monitor which is located at the entry gate to the primary beam line. Gas flow counters (helium + isobutane) and NaI scintillation counters are used for checking human body surface and equipments respectively. A detection sensitivity for body surface is within 7×10^{-6} $\mu Ci/cm^2$ calibrated by U_3O_8 β-ray and for equipments within 10 nCi calibrated by C_s γ-ray. If the contamination is found at either some portions of body surface or equipments, the personnel can not pass through the gate. In the case it is required to cool down the radioactivity of the equipments in the beam line tunnel and/or to clean the body surface. The contamination data are recorded by both the M-70 and a recorder provided for the gate monitor.

This work is made by the collaboration with the staff in the KEK accelerator department, the BSF and the radiation and safety control division with outside help.

SUMMARY OF TARGET PHYSICS DISCUSSIONS AT ICANS-IV

Gary J. Russell

Target physics (the basic processes governing spallation reactions which occur inside a target bombarded by energetic particles such as protons) affects the overall design of a spallation neutron source. For example, the total number, energy, and angular distribution of neutrons emitted during the spallation process determine the amount of shielding for the source, and (together with the target-moderator-reflector configuration) the ultimate source intensity. Also, energy deposition mechanisms inside the target affect target and target-cooling-system design. Energy deposition by particles and gamma-rays emmitted from the target affect premoderator, moderator, decoupler, and reflector design (including their cooling systems), and may influence the design of the inner part of the massive neutron shield. Target handling, disposal and the need to cool the target (when there is no incident proton beam) depend on the progeny produced in the spallation reactions. Whether or not a target will fission is important in target design and can affect facility safety considerations. The performance and design of spallation neutron sources have (in general) been calculated using a variety of computer code packages. Experimental data relevant to the design and performance of both pulsed and steady-state spallation neutron sources are just recently becoming available. The details of present computational capabilities and current experimental data relevant to spallation neutron sources are contained in the various papers presented at ICANS-IV. Overviews of these topics are given below.

Most computations relevant to spallation neutron sources begin with the High Energy Neutron Transport Code (HETC) developed at the Oak Ridge National Laboratory. This code uses Monte Carlo methods and includes the intranuclear-cascade-evaporation model as a series of subroutines; the code calculates (as needed) particle production data from nucleon-nucleus and pion-nucleus collisions. In general, HETC is used to transport neutrons with energies $\gtrsim$15-20 MeV. Below these energies, evaluated differential neutron cross-sections exist, and these "low-energy" neutrons are transported using more conventional Monte Carlo and reactor codes. Until (relatively) recently, HETC did not include fission reactions in competition with the evaporation process. This so called "high-energy" fission should be important for spallation neutron sources using depleted uranium as a target (similar arguements hold for thorium and uranium targets and/or blankets in the Accelerator Breeder application). Several laboratories (including the Oak Ridge and Brookhaven National Laboratories in the United States, the Japan Atomic Energy Research Institute, and the Rutherford and Appleton Laboratories in the United Kingdom) have independently modified HETC to include high-energy fission effects. Depending on the quantity of interest, the output of HETC and the low-energy neutron transport code are analyzed in a variety of ways. The application of these code-packages for facility

design and comparison with experimental data are detailed in several ICANS-IV papers. Because of the variety of computer code packages used at the various ICANS laboratories, it may be useful to intercompare computed results between laboratories. Within the framework of the ICANS, relevant benchmark experiments could be identified, and the various code packages intercompared with the experiments.

Until the last couple of years, experimental data relevant to spallation neutron sources have been relatively scarce for incident proton energies of 500-1100 MeV. Neutronics, energy deposition, radiation damage, neutron shielding, spallation progeny production, target fission, and neutron beam quality data are important in spallation neutron source design and performance. Details of experiments performed at existing spallation neutron sources and data being gathered for more intense spallation neutron sorces are given in several ICANS-IV papers. In some of these experiments, basic data were measured such as:

- angular- and energy-dependent neutron production cross-sections for a variety of materials,
- angular-dependent neutron and proton spectra from thick targets of lead and uranium,
- angular-dependent high-energy ($\gtrsim$20 MeV) neutron yield from a thick lead target,
- total neutron production from a variety of thick targets,
- delayed neutron fraction in a thick uranium target, and
- radionuclide production inside a thick uranium target.

Such experiments are valuable in testing the fundamental processes and assumptions employed in the computer codes used to calculate spallation reactions and neutron transport. Other experiments have measured the effectiveness of neutron shields, total power produced in tungsten and uranium targets, local power density in a uranium target, and nuclear heating in cold moderators and other materials. Still other experiments deal with measuring thermal neutron beam intensities, spectra, and pulse widths from moderators. These latter measurements depend on the particular target-moderator-reflector configuration used, and depend upon whether the spallation neutron source is pulsed or steady-state. Specific details of target-moderator-reflector design and the presence or absence of neutron decouplers (used in the configuration) determine the ultimate performance of the system as a thermal or epithermal neutron source. Significant gains (factors of 2) can be attained in some moderator designs. Beam quality (the amount of gamma-ray, charge particle, and high-energy neutron contamination in thermal and epithermal neutron beams) is important. Once a target-moderator-reflector configuration is chosen for a spallation neutron source, absolute thermal and epithermal neutron beam intensities, spectra, thermal neutron pulse widths (where applicable), and beam quality should be measured, and the experimental results compared with calculated predictions.

G.S. Bauer

ICANS-IV Summary on target engineering

During the five years following the first experiments with a proton-beam driven spallation source performed at ANL in 1974 and 1975, a rapid and wide-ranged development has taken place. Today a point has been reached, where the first production targets have already been put out of operation after a substantial time of service, thus providing an opportunity not only for theoretical studies but also for practical checks. New assemblies are under construction for more powerful sources requiring more sophistication in design and operating conditions, and proposals have been forwarded to go to even higher beam powers, which makes special measures necessary such as moving the target to deal with the heat dissipation. Table 1 gives a summary of spallation source projects worldwide.

	Target	Proton beam power (maximum)	Proton energy	Mode of operation
Facilities shut down				
ZING-P'	U-238	3.6 kW	500 MeV	pulsed, 30 Hz
Facilities in operation				
KENS	W	0.7 kW	500 MeV	pulsed, 15 Hz
WNR	W	4.8 kW	800 MeV	pulsed, 120 Hz
TRIUMF	Pb	50 kW	500 MeV	continuous
Facilities under construction				
IPNS-1	U-238	12 kW	500 MeV	pulsed, 30 Hz
SNS	U-238	160 kW	800 MeV	pulsed, 60 Hz
Proposed Facilities				
IPNS-2	U-238	380 kW	800 MeV	pulsed, 60 Hz
LAMPF + PSR	?	800 kW	800 MeV	pulsed
Swiss project	Pb-Bi	500 kW	500 MeV	continuous
German project	Pb	5500 kW	1100 MeV	intensity modulated

Table 1 Target parameters of spallation sources worldwide

The overwhelming majority of the projects listed in Table 1 are pulsed neutron sources with their characteristics frequently dictated by existing accelerators or other constraints. Notable exceptions are the cyclotron-driven sources at TRIUMF and the one proposed at SIN. With a continuously operating accelerator those sources will, from the point of view of the user, resemble much more a reactor than the pulsed sources do. Consequently the design objectives are also different, aiming at a high time average neutron flux rather than a good time structure. The German proposal, characterized as 'intensity modulated' is intermediate between the two extremes in that its proton pulse duration of 0.5 ms at 100 Hz still allows to take advantage of such nice features as background suppression by detector gating and a good peak-to-average flux ratio, but does not allow to use the neutron pulse as primary resolution element in the experiments. The layout considerations are therefore again different in this case.

Thus, the ICANS-IV meeting was a timely point to get together and exchange information and promote new efforts.

Experience has been reported with targets of various designs. Surface cooled tungsten targets are or have been in use at WNR, ZING-P' and KENS, all of which are relatively low power facilities. It has been demonstrated especially at the KENS-facility that extremely good target-to-moderator coupling is possible if the target is not diluted by cooling channels and engineering constraints are relaxed due to the low power dissipation. These smaller spallation neutron

sources therefore have a potential to be not only precursor to the more powerful ones but are likely to become valuable research tools in their own right.

An interesting target design has been in use at TRIUMF for some time now, where a lead target encased in a stainless steel container is allowed to melt and transport its heat to the water cooled container by natural convection during operation. Experience has shown that such a repetitively melting target can be operated reliably. It, too, has the advantage of not being diluted by cooling channels and because of the phase change involved it is very flexible with respect to changes in beam power. It has been noted that most of the mercury produced in the spallation process tends to evaporate and be pumped off the surface of the target.

For the more powerful pulsed sources now under construction at Argonne (IPNS-1) and Rutherford Lab. (SNS) heterogeneously cooled targets of depleted uranium are being developed. Here the target is composed of a series of discs individually clad in zircaloy with the coolant flowing between these discs. For the IPNS-1 target, the zircaloy-2 cladding cans are fabricated in two halfs and electron beam welded to hold the depleted uranium discs. High temperature isostatic pressure bonding is applied to diffusion weld the cladding to the disc for optimum thermal contact. A target of this type has been in use at ZING-P' before its final shutdown and has exceeded its predicted fatigue life time without any obvious signs of damage. The target has now been removed and is ready for detailed examination. Since fatigue is the

most likely damage to limit the life time of these targets it will be interesting to see the results of this examination. At SNS, where circular uranium discs will be embedded in rectangular circaloy frames, development work is still going on to avoid fracturing of the cladding along the edge of the target discs.

Operating facilities, especially ZING-P' have made possible a number of measurements relevant to future target design and engineering. Among them are measurements, as reported by J.M. Carpenter, of power density and power distribution, neutron beam currents, radiation fields in the beam holes and target radioactivity. Some of these results, such as the total thermal power dissipated in the target, which was found to be considerably higher than predicted by calculations, are of great importance for the design o future facilities. Systematic studies relating to the design of high power spallation neutron sources have also been carried out by a joint Swiss-German study group at various European proton accelerators. Most of these experiments so far (as partially reported by W. Fischer) were conceived to assess the neutronic performance of high power spallation sources, but future efforts will be directed more and more at producing relevant engineering data. Such data are indispensable with, if the limits of possible heat and radiation loads on materials are approached. At the SNS target concept this is more or less the case already. In this target with its discs of variing thickness and elaborate water flow guidance a fair amount of engineering effort manifests itself. Plates of six different thicknesses ranging from 0.65 cm to 2.45 cm and clad with 0.025 cm zircaloy will be used with 0.175 cm

cooling gap between them. This means that in the front part of the target the volume fraction of uranium is 74% as imposed by heat removal requirements. This is at a total beam power of 170 kW.

For future spallation sources operating in the multimegawatt beam power range it will not be possible to retain the concept of a target which is stationary in the proton beam. Power densities of the order of 5 - 10 kW/cm^3 time average will make it mandatory to move the target through the proton beam and allow it to cool down elsewhere. Another major concern in high power targets is radiation damage caused by the intense proton beam as well as by the high flux of fast neutrons. A very elegant way to handle some of these difficulties is the liquid metal target concept as proposed as early as in the late 1960's for the Canadian ING concept. The eutectic of lead and bismuth, both of which are good spallation targets materials, has a melting point of only 123°C and can therefore quite conveniently serve as a liquid target. Work on such a concept has been resumed recently in the context of the Swiss and German high power target proposals, as reported by C. Tschalär and J.E. Vetter (see paper by Hoffman et al.). Forced convection loops are considered with the proton beam hiting the target flowing parallel to the proton beam. For a horizontal proton beam - as in the Swiss proposal - this requires a beam entrance window. This is considered the most critical part because it is subject to radiation damage from both proton and fast neutron irradiation and to a mechanical load as well as thermal stresses. Although a suitable choice of the window's shape may relieve some of these problems, it is not yet

clear whether such a window can withstand the thermal stresses set up in it and in particular the thermal shocks occurring in the case of sudden short term beam breakdowns. A concept in which such a window is avoided by taking advantage of centrifugal forces has been outlined, but no detailed layout has been attempted so far. Another possibility to avoid a beam window is the vertically streaming target as described in the paper by Hoffmann et al.. Some development work on this concept is continuing at the Kernforschungszentrum Karlsruhe. However, it is well understood that a beam line to bring a 5 mA 1.1 GeV proton beam in from above is a complex and expensive thing to build. Another concern is the fact that in such a target the walls of the flow tube would be subject to high radiation doses at temperatures which are quite unfavourable with respect to swelling and helium embrittlement for many materials. The choice of materials is further limited by corrosion problems, mechanical strength and neutronic considerations. Graphite has been envisaged for the Swiss concept because of its good neutronic properties, high temperature resistance and good compatibility with Pb-Bi. Although some successful development in joining graphite to copper has been reported recently in Los Alamos, fabrication of a complete target containment out of graphite seems to require some more development work. Concern has also been expressed about radiation damage which, in particular in the case of pyrolytic graphite leads to anisotropic swelling and contraction.

Since liquid metal target systems are more or less confined to the Pb-Bi eutectic as target material, a different concept has been selected for the German project which will in principle also allow

to use uranium as target material. Here the disc-shaped and internally cooled target is rotated around a vertical axis with the proton beam entering through the outer circumference of the disc. Apart from enabling the heat removal over a time period 200 times longer than the time interval between two proton pulses, this concept will reduce the radiation load on the target and its structural components by the same ratio. Several ways of arranging the target material in the disc have been considered. In the concept finally selected the target consists of a large number of individually canned vertical pins directly cooled by the water flowing between them. For a lead target with Al canning the higher thermal expansion and higher temperature rise in the lead will ensure good thermal contact between the lead and the canning. Fabrication of these pins is easily accomplished by electron beam welding. Under the envisaged operating conditions, thermal cycling will be 50 K at the hot spot in the lead and 12 K in the aluminium once every two seconds. Should depleted uranium be used in a later stage, the possibility of establishing thermal contact to the cans by means of a molten metal will be investigated. Although the weight of such a target amounts to 5000 kg, its mechanics is very conservative. Nevertheless some development has to go into the rotating coolant sealing and radiation resistant bearings. It is quite clear that with beam powers in the multi-megawatt range, spallation neutron sources will become a good deal more sophisticated machines than those presently in operation. However, performance data derived from mockup experiments are very promising and seem to justify the efforts going into this development.

Apart from concepts reported as frozen in or proposed, interesting new ideas were forwarded which animated the discussion and showed that, in a field which is developping as rapidly as the design of spallation targets a lot of immagination is active. This is a very positive situation because the discussion of such apparently out-of-the-way concepts may often produce spinoffs which are very useful in solving existing problems.

Finally, it should not remain unmentioned that with all the optimism about the neutron flux that can be obtained from suitably designed moderators, there is also some concern regarding the contamination of the neutron beams with high energy neutrons and the possibility of working on the experiments while the source is operating. Some measurements along this line have been reported from the ZING-P' facility and WNR and more data will soon become available from the new KENS facility. However, looking at the beam power levels given in Table 1, it is obvious that this problem is much more serious in projects proposed for the future. Along with extensive studies related to moderator-target-reflector performance an effort has therefore been made by the German study group to obtain information on this questions from mockup experiments. Evaluation of these data is still under ways but it is clear that it is very difficult to obtain significant results from relatively poorly shielded low power arrangements which can be used to predict the situation in a high power system. Here, more experience from sources to become operational in the near future will certainly fill a gap in our knowledge and possibly give important information for a suitable choice of design and operating parameters.

G.S. Bauer

Summary on a discussion on moderators with grooved surface

Results were presented by G.S. Bauer on experiments performed by the German study group at SIN and SATURNE* to increase the neutron leakage from hydrogeneous moderators by rearranging part of the moderator material near the surface in such a way that grooves of 1 cm width and up to 9 cm depth were obtained with a 50% ratio of void and material (Fig. 1).

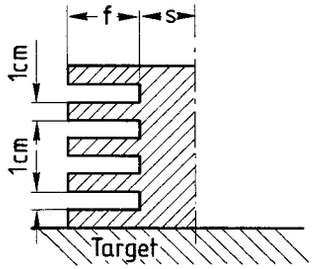

Fig. 1 Section through one half of a grooved moderator

The moderators were placed on a slab target of Pb 10 cm high 50 cm wide and 60 cm deep. The proton beam hit the target below the moderator centre plane. Table 1 summarizes results obtained for different moderator geometries with and without a reflector or lead shielding. The moderators were 20 cm long and 11 cm high. The thickness of the reflector, if in place, was 20 cm and the lead shield was 50 to 80 cm thick with a cavity to accept the reflector.

The gain obtained for a bare moderator due to the grooves is 1.8 (measurement 4 relative to 2) and in a well reflected geometry it is 1.35 (measurement 12 relative to 10).

Similar gains were also found in experiments performed at the CERN booster** for decoupled arrangements (Fig. 2).

The neutron current emerging from a moderator surface is determined by the neutron flux level ϕ_λ at a distance of one transport length (λ_{tr}) below the surface. The flux distribution inside the moderator has roughly the form of a cosine distribution going to zero at a distance $d = 0.7 \cdot \lambda_{tr}$ outside the moderator (Fig. 3a). A higher flux level than ϕ_λ could in principle be reached by a reentrant hole reaching inside the moderator. However, this hole's diameter should be only of the order of λ_{tr} in order to avoid creating a new outer surface. For H_2O λ_{tr} is only 4.5 mm and therefore such a reentrant

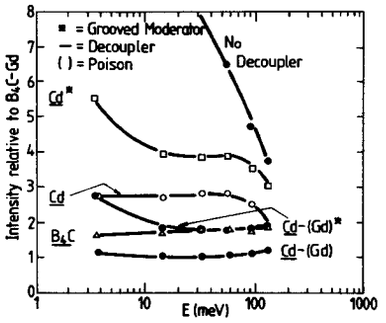

Fig. 2 Integrated intensities of reflections obtained from a pyrolytic graphite crystal as a function of neutron energy for various moderators with decouplers and heterogeneous poison. Moderator material was polyethylene. The systems are characterized by the symbol for the decoupler used with the poison set in parenthes. N stands for no decoupler, an asterix marks a moderator with 15 mm deep grooves on the surface.

hole can only be very small. In the experiments performed at the SIN by the German study group the leakage from the moderator surface could be considerably increased, if a large number of holes were introduced in the moderator surface. In order to avoid the collimating effect of these holes, horizontal grooves running over the moderator surface were used in later measurements. They were found to yield a similar increase in neutron leakage without the undesired collimating effect in the horizontal plane. Qualitatively the effect of these grooves which were arranged such as to yield a 50% material-to-void ratio can be understood as follows (Fig. 3b). Starting from a moderator of thickness L with a neutron flux distribution as indicated in Fig.3a the material contained in a surface layer of thickness F is rearranged thus as to yield a layer of thickness 2F with a macroscopic scattering cross

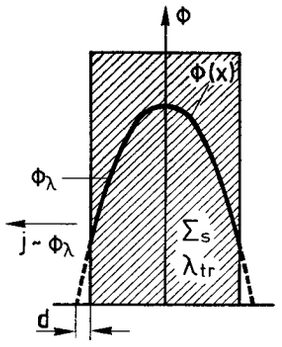

Fig. 3a

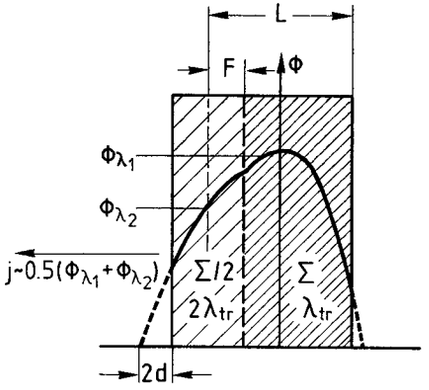

Fig. 3b

section $\Sigma_s/2$ and hence a transport length $2\lambda_{tr}$. The flux distribution then goes to zero at a distance $2d = 1.4\ \lambda_{tr}$ from the new moderator surface as indicated in Fig. 3b. Due to the fact that the material is distributed heterogeneously in the layer of thickness 2F, two flux levels will be significant for the neutron leakage perpendicular to the surface: $\phi_{eff}=0.5\cdot\phi_{\lambda_1}+0.5\cdot\phi_{\lambda_2}$. This value is obviously higher than the value ϕ_λ which determines the leakage from a solid moderator of the some amount of moderating material.

Experiments of this type have also been performed at ZING-P' with the goal of establishing the effect of the grooves on time structure. It was found that there was a slower rise and a faster decay of the neutron pulses resulting in an overall increase of the FWHM by 5%. In these experiments the grooves were running at right angles to the target surface which results in a decrease of the solid angle subtended by the moderator and hence a poorer target-moderator coupling. Correspondingly the intensity gain was only less than 20% yielding no change in the figure of merit $I/(\Delta t)^2$. However, since an arrangement of the grooves parallel to the surface of the target will not alter the time behaviour while improving the coupling, it was concluded that grooved moderators are also beneficial for pulsed sources as well as quasi-continuous ones.

#	Moderator	Dimension	Reflector	Shield	Gain
1	CH_2	37.5s	-	-	1
2	CH_2	50 s	-	-	1.06
3	CH_2	10s+60f	-	-	1.83
4	CH_2	22.5s+60f	-	-	1.91
5	CH_2	22.5s+60f	-	Pb	3.31
6	CH_2	"	CH_2	Pb	3.21
7	CH_2	"	Be	Pb	5.43
8	H_2O	30s	Be	Pb	4.42
9	H_2O	45s	Be	Pb	4.25
10	H_2O	55s	Be	Pb	4.22
11	H_2O	15s + 60f	Be	Pb	5.66
12	H_2O	7.5s+90f	Be	Pb	5.72
13	H_2O	22.5s+90f	Be	Pb	5.50

Table 1 Relative thermal neutron leakage from the moderator surface for various configurations with fins and with and without reflector and shielding

* G.S. Bauer, F. Gompf, W. Mannhart, W. Reichardt, R. Scherm and H. Spitzer "Thermal Neutron Leakage from hydrogeneous Moderators for a Spallation Neutron Source"

** G.S. Bauer, J.P. Delahaye, H. Spitzer, A.D. Taylor and K. Werner: "Relative Intensities and Time Structure of Thermal Neutron Leakage from Various Moderator-Decoupler Systems for a Spallation Neutron Source" report under preparation.

A. Carne

SUMMARY OF MEETINGS ON

a) Energy Deposition in Moderators
b) Shielding
c) Activation
d) Safety

a) Energy Deposition in Moderators

Early papers in the meeting gave the performance of the KENS cold moderator, the ZING-P' cold moderators and estimates of powers in the SIN and SNQ cold moderators. These examples of the pulsed and continuous sources posed for us two problems:-

i) How the pulsed moderator energy depositions compared, especially when extrapolated to the SNS.

ii) How well the energy deposition in the C.W. liquid H_2 or D_2 moderators could be estimated, where at kW levels a factor 2 represents very large quantities of money.

A number of participants met to collect the information on existing and proposed moderators. This is shown in Table 1 and contains, we believe, all the relevant information for making reasonable comparisons. The left hand columns show the input conditions; the right hand ones show the moderator characteristics and information on material, decoupler and reflector. Table 2 compares measured powers extrapolated roughly to SNS moderators and also the SNS estimates. The SNS estimates agree well with the extrapolated ANL values but not with the KENS value.

It is hoped further measurements will be done on the KENS moderator to help resolve the differences. We look forward to early measurements on the IPNS-1 cold moderator when that facility starts up in April 1981.

Of the continuous source cold moderators, the SIN 30ℓ D_2 moderator has power depositions of 600 W due to capture γ's and 1.2 kW due to neutron slowing down. Such estimates are very difficult to make and it is clear that with such large powers errors can be very costly. It is hoped that TRIUMF might be able to mount an isolated moderator in the TNF. SIN and TRIUMF will explore this possibility.

b) Shielding

i) General Problems

The session opened with a discussion on the problems of shielding against

fast and slow neutrons, both for radiation protection and reduction of spectrometer background. Whereas neutrons transmitted by the bulk shield were "easy" to calculate, shielding of external beam tubes is much less easy, but just as important. Bright surfaces, ie those seen by the moderator, must be minimised in area and preferably be absorbing; visible surfaces, ie those seen by the sample, should also be minimised and absorbing. Visible surfaces should never be bright ones!

There is a clear need to provide good thermal neutron shielding around choppers to reduce the area of visible surfaces. Gadolinium oxide paint is an excellent material for making surfaces black to thermal neutrons.

The location of the final collimator is important but not easy to decide. The beam stop must be effective in absorbing fast neutrons and in preventing moderated neutrons reaching the spectrometer. There were severe background problems at WNR, especially due to the beam stops.

Many ad-hoc solutions have been obtained to shielding problems, but few written up and reported. Solutions to some of the problems are probably more easily obtained from communication of hard-won experience than by large scale use of Monte-Carlo codes.

ii) Particular Topics

The meeting heard of measurements taken on the newest of the spallation source target stations - that of KENS. Measurements were made using 500 MeV protons on the neutron production target, using several activation detectors. From measurements of saturation activity in both forward and transverse directions the effective attenuation lengths of iron were obtained. In particular the value at 90^0 was 116 g/cm^2. Similarly, by adding heavy concrete around the target within the iron surround attenuation values at 0^0 (130 g/cm^2) and 90^0 (96 g/cm^2) were obtained. Radiation measurements were made at the top of the KENS, and some of the longitudinal beam holes were open (we recall the KENS vertical shield is 4 m high containing 1.65 m of iron and 0.8 m of heavy concrete). The levels measured fell nicely between the value expected from the original design figures for attenuation length and that based on the newly evaluated figures. In the discussion on comparative shielding assemblies it was felt there is a need for care in defining the input beam intensity and how it was measured.

In a discussion on shielding materials themselves, cost proportional factors were presented for basic geometries, material and allowing for the dependence

of attenuation length on neutron energy. It was found that in the basic geometries considered that over the fission-to-thermal energy range, iron oxide mortar (Fe 50 w/o) was the cheapest material. In a practical target station with several functions to perform a combination of materials was considered more effective. Iron shot is a cheap and convenient material to use in providing packing for holes and gaps. However great care must be taken to avoid severe problems later if dismantling becomes necessary, due to rust, activation and contamination.

The problems of the design of primary beam collimators were considered. The aim is to reduce the amount of scattering from the collimating system whilst keeping good beam definition. This is obtained by a series of defining apertures and absorbers, based on the use of ray diagrams. However the beams contain both high and low energy neutrons and the collimators must have materials and geometry to take both into account.

c) Activation and Component Materials Irradiation

Activation and component materials irradiation are major problem areas in the operation of neutron sources and solutions are required which:

i) Maximise safe operating conditions and component longevity.
ii) Minimise initial construction costs and operating costs.
iii) Simplify maintenance and handling requirements.

A number of papers were presented at the meeting, also participants met to discuss some particular problems, as indicated below.

Irradiation of Coolants

Under irradiation radiolysis and activation of component cooling water occur, particularly in the target. Radiolysis requires special handling for recombination and venting, whilst activation (primarily from spallation of oxygen) requires positive containment for biological safety purposes. Corrosion can also present problems. Tests on the KENS target and magnet cooling water for a 2.4 μA-day irradiation were described, giving respectively 10^{-4} μCi/cm^3 and 10^{-6} μCi/cm^3 of ^{7}Be. Experience with ZING-P′ at the ANL showed the target cooling water blanket gas (He) to be rich in hydrogen and deficient in oxygen for no identifiable reason.

Irradiation of hydrocarbons in moderators (eg CH_4) can be expected to cause hydrogen displacement and associated polymerisation. Total radiolysis products in the KENS cold CH_4 moderator were found to be about 1% (including initial impurities).

Tritium and ^{7}Be as spallation products of carbon have also been seen. The moderator is frequently replaced. Some neutronic changes have been observed as the concentration of radiolysis products increases. The ANL reported that for a total 1.8 x 10^{18} n/cm^2 (ie about 1 year's irradiation) about 4 μCi/gm of ^{7}Be was found in CH_4. Provisions have been made at IPNS-I to allow a continuous purge of fresh methane for its two methane moderators.

Fission/Spallation Products in Targets

The SNS and IPNS-I will use segmented uranium targets, clad in Zircaloy-2 to prevent corrosion and to contain the fission/spallation products. Much effort has gone into the enumeration of these products, where, for example, some 1200 nuclides were surveyed to determine total activity and decay of the SNS target. The effects of high irradiation and nuclides on the cladding is not well known. A report was presented of a preliminary study made at KENS on the induced activities in a uranium target. A segmented target, overall length 9.5 cm, of "Yellow Cake" uranium was irradiated with a total of 6 x 10^{13} 500 MeV protons. Exposure rates, decay characteristics including radioacive nuclide analysis, spatial and temporal changes in the β-ray distribution of the target were studied. Preliminary measurements of α-decay were also made. Such quantitative measurements are of great importance for the proposed uranium targets, not least as independent tests on the HETC code packages.

With the proposed SNQ source considerable effort is being devoted to the study of proton and fast neutron radiation damage. Mercury, a spallation product of lead, will cause corrosion and high temperature embrittlement problems. Much effort is going into the selection of materials and there will be several complex technological problems with fabrication.

Target Window Materials

A number of different window materials are being considered for the spallation source targets, as can be seen in Table 3. The material selections have been made based on experiences in similar but not identical environments. Little is known about high radiation damage effects due to protons: much is yet to be learned and documented. The results of future tests and post-irradiation inspections are of great interest to all source designers.

Thermal Cycling Effects in Targets

Inherent instabilities associated with some accelerator operations impose severe

operating conditions to target materials due to cycling of induced thermal stresses. This cycling is expected to be the governing factor in the life of most targets. The anticipated materials fatigue may be exaggerated by the effects of irradiation. Normally applied codes to depict the effects of thermal cycling will require refinement to allow for irradiation effects. A report is in preparation at the ANL to define the effects of thermal cycling in the IPNS-I targets. Dissemination of experience in these areas will be of considerable value.

d) Safety

For effective and efficient operation of a facility it must be easy to maintain. Similarly, easy dismantling, whether for change of scope or even final disposal, is a basic engineering requirement. Design must reflect these requirements at the outset of a project and experience is to be gained from related fields, eg reactor technology and remote handling.

A fundamental requirement is that the facility must be safe to operate. The facility must have a full hazard assessment, show safe operation and proper emergency procedures.

Though many of the papers and discussions contained safety needs implicitly, and all of the proposed designs reflected their in-built safety requirements, only one paper addressed the problems of safety as such. There remains the need to compare hazard assessments, safety and emergency procedures. Much benefit is to be obtained by the mutual discussion of problems. It remains our duty to show we can operate properly these exciting new facilities.

Conclusions on the Summaries

During many of the discussions, as typified above, many of the solutions were clear or available from hard won experience. The cost and time burdens can be reduced by mutual exchange of information at ICANS meetings but also through continued interchange of ideas through open communication. The ICANS IV was very successful meeting in the development of the art of neutron sources. Much work remains to be done and many problems still require detailed study: in fine shielding and backgrounds, activation and component material irradiation, target limitations and safety. Future ICANS meetings will derive great benefit from the close study of these topics.

Footnote: During the final session it was announced that the ANL has produced its safety assessment document (October 80). This is available to participants.

SITE	I_p	E_p	n_f	ENERGY DEPOSITION	MODERATOR	MOD. r	COMMENTS MATERIAL DECL. CONTS REFL.
KENS	2μA	500	0.8×10^{14} (W)	≯ 10 W TOTAL EXCL. CRYOSTAT	w 12 h 15 d 5 T 20°K	17m W→CH_4	CH_4 Cd AL Be
ANL	22	500	2×10^{15} n_f/SEC.	MEAS. 11.6 mW/cm³ } LH₂ CAL. 17.4 mW/cm³ } MEAS. 29.7 mW/cm³ } CH_2 CAL. 36.8 mW/cm³ } (or CH_4) MEASURED AT ~ 11.5 cm FROM SOURCE	A 824 cm³ } LH₂ B 727 cm³ } C 524 cm³ } LCH_4 D 524 cm³ } AT ~ 12 cm FROM SOURCE	≈ 12 cm FROM UP ℄ TO MOD. ℄	A NONE B Gd C Cd D Gd
SIN	1mA	590	6×10^{16}	600 W CAPTURED 8's 1.2 KW NEUTRONS ?	SPHERE 30 LITRES 20°K	40cms	AL, Zr D_2
SNQ	5mA	1100 meV		H_2 2.3 kW D_2 1.5 KW	d = 13 cms 15 cms DISTANCE FROM TARGET		
RL	2.5×10^{13} 50Hz 200 μA	800	3×10^{16}	283 + CRYOSTAT LOSSES	w = 11.5 cm h = 11.5 cm d = 5.0 cm T = 20–77°K	3.2 9.7	CH_4 D B_4C C AL+ R Be+D_2O

TABLE 1. MODERATOR ENERGY DEPOSITION

KENS. EXTRAPOLATION TO SNS	SNS ESTIMATED VALUE
(10w) ⟶ 3-4 kW	283w (CH_4)
ANL EXTRAPOLATION TO SNS	
(11.6 mW/cm³) ⟶ 200 w FOR 2×10^{15} n_f/s	240w (LH_2)
FOR (30 mW/cm³) ⟶ 330 w	~ 283W (CH_4)

TABLE 2. MODERATOR ENERGY DEPOSITIONS : EXTRAPOLATIONS TO SNS

PLACE, DATE	MATERIAL	DIMENSION	TEMP. °C	ENERGY MeV	INTENSITY mAh	SPOT cm^2	RESULT
SIN 7-80	GRAPHITE	3 mm ø20 mm	1000-1200	600	20	0·2	OK ON INSPECTION
SIN 8-80	PYRO-GRAPHITE	6 mm ø20 mm	1500-2000	600	80	0·2	UNKNOWN
LAMPF 11·80	SUPER-PYRO	6 mm	~1500	800	~200?	1	TEST IN PROGRESS
LAMPF 81	AL, Fe REFR. MATL. METALLIC GLASS		200 1500 800	800 800 800		1? 1? 1?	PLANNED
TRIUMF	AL 6000 AL 6000 AL 6000	3 mm 3 mm 3 mm	100 100 100	450 450 450	50 100 350	30 30 30	OK ON INSPECTION WINDOW WORKS PLANNED

TABLE 3 WINDOWS, RADIATION DAMAGE TESTS

N. Watanabe

A Comment on Energy Deposition in the KENS Cold Moderator

We would like to revise the estimate that was reported at ICANS-IV of the energy deposition in the KENS solid methane moderator, as we have found our earlier measurements to be somewhat misleading. On checking these measurements we found that the position of the electrical heater used to simulate the nuclear heating was quite different from that anticipated and we have therefore since performed a new measurement without using this heater.

In this new measurement, the temperature of the moderator was monitored as a function of time after a sudden halt of the proton beam. The temperature was measured by a hydrogen vapour-pressure thermometer installed inside the moderator chamber. The thermal energy deposited by radiation was calculated from the measured rate of temperature decrease using known values for the heat capacity of the solid methane and the moderator vessel. The new value was found to be 1.2 Watt for a proton beam current of 1.3 μA. The moderator volume was 900 cm^3 (12 cm^W x 5 cm^T x 15 cm^H), and the distance between the target center and bottom of the moderator was 4.55 cm, Cd decoupled. The tungsten target was irradiated by 500 MeV protons. The average value of the nuclear heating is therefore 1 m Watt/cm^3,μA. The present result is thus in reasonable agreement with that of ANL if the differences in the target and moderator materials and the different coupling efficiencies of target-moderator systems are taken into account.

The Welcoming Party

S. Komura, D. Filges, B. Alefeld

The Welcoming Party

III INSTRUMENTATION

The contributions on instrumentation span a complete range of development from the novelty of the conceptual stage to the statistics of results. The variations in the stages of development and the different styles of the presentations have made it somewhat difficult to organise the separate contributions into a coherent whole. However, in keeping with the spirit of international collaboration, we have attempted to group together papers on similar topics from different sources. We hope that our arrangement will prove acceptable, but firstly, perhaps for those less familiar with instrumentation, we include some pointers towards the content of the subsequent papers and to relate them to the sessions at which they were presented (Appendix I).

Two sessions (I-1) were dedicated to discussions on the concept, design and performance of scattering instruments. The papers of Eckert et al. and Borso et al. provide overviews of the instrumentation at the spallation sources of LASL and ANL. Suzuki et al. and Windsor outline recent developments at the electron LINACS of Tohoku University and A.E.R.E. Harwell. These general presentations precede the contributions from KENS and the Rutherford Lab. which are somewhat more detailed and comprise a selection of separate papers on individual spectrometers. Most of the instruments for the SNS are still at a design or pre-test stage,while the papers from KENS describe spectrometer installation and some results which have been obtained in the few months between completion of the facility and the time of this report.

The order in which these papers are arranged is such that, following the papers on neutron guides and choppers, the emphasis proceeds from the simplest, total scattering machines — low resolution total scattering, high resolution powder diffractometers and small angle or low Q spectrometers — to the inelastic scattering instruments. The papers on the latter are grouped in the order of direct geometry, beryllium filter, quasielastic and crystal analyser machines. Contributions on polarised beams, data acquisition and detectors then follow, with, finally, the presentations of Nucker and Schmatz and Alefeld containing new ideas for instrumentation at long-pulse sources.

The outcome of the two sessions on instrument design (I-1) is well summarised by Windsor and Endoh. Their Table 1 lists the numbers and types of spectrometers which are at a constructed or design stage at each facility. This table thus provides a useful means of cross-referencing between the general accounts from ANL, WNR (LASL), Harwell and Tohoku and the individual papers from the Rutherford Lab. and KENS. The Data Acquisition and Detector session (I-2) which contained contributions on computer configurations and on developments in position-sensitive detector (PSD) research is summarised by Newsam and Niimura. The last session on instruments was concerned with Neutron Guides, Choppers and Polarised Beams and a summary of this final session is given by Newsam and Williams.

INSTRUMENT DEVELOPMENT FOR MATERIALS SCIENCE RESEARCH AT WNR

J. Eckert, R. N. Silver,
A. Soper, P. J. Vergamini, J. Goldstone
A. Larson, P. A. Seeger, J. Yarnell
University of California
Los Alamos Scientific Laboratory
P. O. Box 1663, MS-805
Los Alamos, New Mexico 87545 USA

I. INTRODUCTION

The neutron scattering program at the Los Alamos spallation neutron source is based on the operational WNR facility which provides up to 11 μA of 800 MeV protons to a target in pulse widths up to 8 μs at 120 Hz. The immediate goals of the program are:

- to gain experience with neutron instrumentation at spallation neutron sources;
- to explore the scientific potential for condensed matter research at these sources.

The proton storage ring (PSR) funded for construction will provide 100 μA in 0.27 μs pulses at 12 Hz, therefore greatly improving intensity, time-of-flight (TOF) resolution, and repetition rate. The longer term program goal is to develop a condensed matter research and instrument capability to make optimal use of the PSR when it becomes operational in 1985.

The initial emphasis, given limited manpower and resources, has been placed on developing a set of prototype instruments which are relatively easy to implement and which take advantage of the unique characteristics of the present WNR when compared with reactor neutron sources. Given the advantage of a working spallation source, we can test instrument developments as we proceed. In instrument development we have addressed problems common to all spallation sources, e.g. shielding against fast neutrons, chopper phasing to the variable line frequency, electronics for multidetector arrays, megaword memories for position sensitive detectors, and slab vs wing geometry moderators. These developments are closely coupled to the experimental optimization of targets and moderators reported by G. Russell at this meeting.

The instruments currently being developed at the WNR (see Fig. 1) are:

- a crystal analyzer spectrometer and a filter detector spectrometer on the same beamline for inelastic scattering
- a chopper spectrometer
- an electronic time and resolution focused general purpose diffractometer for powder, liquid, and amorphous samples
- a geometrically time focused special environment diffractometer for powder diffraction
- a single crystal diffractrometer based on the LAUE TOF technique

II. FACILITY DEVELOPMENTS

The WNR has a vertical injection target with 12 neutron beam tubes viewing the target/moderator assembly. All the experiments reported below used Cd poisoned 1/2" polyethylene moderators. The initial experiments used a hybrid slab water moderator with some beam tubes viewing the target and some offset. For the most recent experiments, a new reflected T-shaped target/moderator assembly is used with all neutron beam tubes in offset geometry. This has greatly improved signal-to-noise as illustrated below.

We have also constructed new liquid Hg beam shutters. These use lead inner collimation to block the view of the target, a Hg vessel in the center operated by a He pressure system, and interchangeable outer collimators adapted to the individual instruments. These shutters have proven to be effective and to be inexpensive ($12 K/each) to construct. For the present experiments background caused by the scattering of neutrons from the inner surfaces of the shutter has not been a problem.

Behind each instrument an evacuated get-lost-pipe carries neutrons to a beam dump placed in the recesses in the walls of the experimental hall, or outside the hall where possible. In a beam dump, fast neutrons reflected back from the walls will see first Pb bricks, then polyethylene, Cd sheet, and finally concrete bricks. The radiation levels at the beam dumps have been high, indicating that a future optimization is required.

All the experiments described below were carried out with ~ 3 μs proton pulse widths and less than 3μA on target. We have not realized the

WNR potential for neutron flux-hours due to various difficulties. Among these are fast kicker magnet reliability, the splitting of available beam time with nuclear physics research, LAMPF operation in a variable energy mode in the most recent cycles, and the use of nonoptimized target/moderator assemblies. We expect significant improvements in these operational problems in the near future.

III. INELASTIC NEUTRON SCATTERING SPECTROMETERS

A. Crystal Analyzer Spectrometer (CAS)

A prototype crystal analyzer was installed at flight path 5 in July 1979 at which time the target was viewed directly by the beam tube. The instrument utilized a set of nonoptimal pyrolytic graphite crystals with a mosaic spread of 0.4^{o}. Four of those crystals of dimension 5 cm wide by 7.5 cm high were mounted in a time-focused geometry with a mean scattering angle $2\theta_A = 90^{o}$ at an angle of 90° and a distance of 50 cm from the sample. A Monte Carlo computer code due to Sköld (Crawford, private communication) was used to optimize the crystal and detector geometries. Two blocks of beryllium, each with a cross-sectional area of 10 x 10 cm^2 and length of 20 cm, separated by a cadmium sheet, were placed between the analyzer crystals and the detectors for elimination of higher orders. Thus the instrument had a final flight path of 1 m with a source-sample distance of 5.65 m. The incident beam was approximately 7.5 cm high and 4 cm wide.

Spectra obtained with the prototype instrument included those of TiH_2, ZrH_2, and $NaHF_2$. The noteworthy points of these trial runs were:

- the good energy resolution of the instrument: e.g. the splitting of the TiH_2 fundamental optic peak was easily observed
- the background at early times (energy transfer greater than 100 meV) was large and rising steeply but was low in the thermal region
- cooling the filter was necessary

The crystal analyzer was then moved to the tangential flight path 6 as well as improved in several other ways. The analyzer crystal array was enlarged to include six of the 0.4^{o} mosaic graphite crystals, more suitable ^3He counters were used in the counter bank, and a liquid nitrogen cryostat was installed to cool the beryllium filter. The present graphite analyzer

incorporates further improvements, primarily in shielding. A view of the crystal analyzer combined with the separate prototype beryllium filter detector (see below) is shown in Fig. 2. The large improvement in background, which we attribute to the move to a tangential flight path, is demonstrated by the TiH_2 spectra shown in Fig. 3. In the present configuration the background counting rate in the crystal analyzer is approximately 1/4 count per 3.2 μs channel per hour in the thermal neutron region, and approximately twice that amount in the epithermal range.

At present the graphite crystal analyzer is considered to be operating in a production mode even though the instrument is not quite optimized. Installation of graphite crystals of approximately 1.2^{o} mosaic of a size large enough (10 cm high) to accept the total beam would almost double the count rate with no deterioration of the energy resolution. This modification is being considered for the near future since in the present configuration a typical metal hydride spectrum takes approximately 24 hrs. to acquire with satisfactory counting statistics.

Extensive data has been collected on $NbH_{.87}$ at four different temperatures between 10 and 300 K. Some of the results are shown in Fig. 4 from which it was founded that the hydrogen local mode peaks become split at temperatures somewhere below 200 K. At 78 K the magnitude of the splitting obtained by fitting Lorentzians convoluted with a Gaussian for the instrumental resolution is 8.4 meV at an energy transfer of 120 meV for which the calculated energy resolution is 5.5 meV FWHM. The intrinsic width of the peaks was found to be 1.5 meV, thereby indicating that the energy resolution of the instrument is known quite accurately. Additional evidence to support this conclusion is given by the fact that the results at 300 K agree very well with those of Richter and Shapiro as obtained at a Brookhaven High Flux Beam Reactor. The deuterides did not show the same effect.

A principal aim of the work on NbH is to gain information on anharmonic effects on the local hydrogen potential. To this end efforts were made to discern the higher harmonics of the local modes. However, because of the additional complication of the splitting in the low-temperature spectra, the weak peaks at higher energy transfers cannot be unambiguously identified, while in the high-temperature spectra the peaks are broadened too much. A sample with a concentration of 78% H which in a previous measurement was found not to have undergone the same transformation as in the 87% sample is currently being investigated for the purpose of measuring the higher harmonics.

Several options are being considered for the future development of the crystal analyzer. Initially, we would like to improve energy resolution at large energy transfers. For this purpose the construction of a time-focused Ge(111) arm is being studied with a final energy of about 50 meV (Fig. 5). A trial setup for the investigation of count rates and background problems will use a Ge(111) crystal of large mosaic (~ 1°) previously used by Day and Sinclair. In preparation for the much higher intensity neutron beams available when the PSR comes on line, crystal analyzers for single crystal work such as the "constant Q" and "high symmetry" instruments will be investigated.

B. Filter Detector Spectrometers (FDS)

As part of the initial crystal analyzer trials a simple beryllium filter instrument was first set up at the target-center-looking flight path 5,5.65 m from the source, with a sample to detector distance of 45 cm. Two 10 x 10 cm^2 x 20 cm long Be blocks were used uncooled. After the move to flight path 6 the filter detector was mounted opposite the crystal analyzer (Fig. 2) for a more direct comparison between the two instruments. The principal trade-off between the two instruments was a count rate more than a factor of 50 greater for the FDS than the crystal analyzer but a factor of three degradation in resolution. Experience with these prototypes indicates that both may be of use.

Since for large energy transfer the resolution of the FDS depends crucially on the ratio of final to initial flight paths, the present instrument was installed at a second sample position 11.42 m from the source and "downstream" from the crystal analyzer. In addition, five new Be pie sections were fabricated, each 10 cm high with an inner radius of about 9 cm radial length of 15 cm and subtending 18° of scattering angle. The individual wedges are separated by Cadmium foil and each section is individually time-analyzed by six 1/2" diam, 10 atm ^{3}He counters. The final flight path is 28 cm and its dimensions were largely determined by requirements for sample cryostat and future filter cryostat dimensions along with a minimum thickness of filter material.

The much improved resolution and background characteristics of this new filter instrument became quite obvious in the comparison shown in Fig. 6 which shows raw data on ZrH_2. The spectrum from the present FDS is that of one of the pie sections only. The energy resolution of this instrument has improved to about 10% ($\Delta E/E$, FWHM) with data rates still higher than the crystal

analyzer in spite of the fact that the filter is not yet cooled. A more recent set of data is shown in Fig. 7 on the temperature dependence of the $FeTiH_{1.14}$ (β-phase) local mode spectrum.

Since the inelastic neutron scattering program at WNR includes studies where sample size may become a problem, the FDS will be retained. A liquid-nitrogen cooled Be/BeO difference filter as shown in Fig. 8 is under construction. The final flight path will remain about 28 cm while the initial flight path (currently 11.42 m) may be increased to about 15 m by moving the instrument to a flight path of its own (flight path 7).

C. Chopper Spectrometer (CS)

The initial effort on inelastic neutron scattering at the WNR centered on a high energy transfer, small-Q chopper spectrometer. The 240 Hz Fermi chopper with Cd slits, a low-angle detector bank, and associated shielding were acquired from the MTR in Idaho. The chopper was installed 5 m from the source and 50 cm in front of the sample. The evacuated final flight path was 2 m and contained 24 1" ^{3}He counters at an average scattering angle of 5°. No additional shielding or collimation were constructed.

The primary purpose of these experiments was to learn how to phase the neutron chopper with the LAMPF proton pulses. Since the proton pulses are fired at the crossing, t_o, of the line voltage from the power grid, the frequency and phase of the proton pulses are variable. The period can vary by as much as 2 μs on a 10 s time scale resulting in phase errors of several milliseconds. We have developed a technique to define the phase to within + 1 μs, for a range of 16 values spaced 64 μs apart, but the method is limited as we shall discuss. The importance of the ability to control the timing of beam extraction cannot be overemphasized. This will be possible at the WNR when the proton storage ring becomes operational.

The WNR chopper operates by: (1) controlling the period and phase of the chopper using a microprocessor based active damping system, and (2) by selecting the time of firing the LAMPF proton pulse within an allowed window of 64 μs about the LAMPF t_o. The microprocessor averages the period error over a full libration period, and makes a correction of 80% of the computed value of the maximum acceleration. This simple feedback system is adequate to maintain the long term average rotor period within a fraction of 1 μs of the accelerator.

The phase of the chopper cannot be tightly defined because of the rotor stability, and the time required for feedback control. As a result the control system can only achieve a distribution of phase errors, typically with a FWHM at 400 μs centered about the correct phase, i.e., the desired incident neutron energy. To fire the LAMPF proton beam, a train of 16 pulses, produced 64 μs apart, is sent to LAMPF and a measurement of the chopper phase relative to the succeeding t_0 tells which (if any) of the pulses fell into the allowed window, and therefore fired the proton beam. Data collected from that neutron pulse is sorted into one of 16 different spectra each corresponding to a different incident energy. In the most recent operation of the chopper spectrometer, typically about 90% of the data fell into eight different spectra with about 30% of neutrons at the nominal incident energy. A schematic of the control system is shown in Fig. 9. Fig. 10 shows the spectra of TiH_2 taken at two incident energies with this method. The peak at ~ 140 meV is apparent in both spectra.

While this control scheme is adequate, data collection is for several incident energies simultaneously so that the signal-to-noise at any given spectrum is reduced. Also, this method will work for only one chopper at a time. Recently, LAMPF operations has agreed to widen the window to 128 μs which will improve signal-to-noise somewhat. The data in Fig. 10 also show a large background due to inadequate shielding against neutrons scattered by the chopper. The MTR chopper is unsuitable for scientific research at the WNR because of its poor mechanical reliability, and because it has a Cd slit package which is ineffective for epithermal neutrons. The next step is to acquire a chopper with a boron slit package, to build proper shielding and collimation, and to optimize further the control system. At present, this has been postponed because of budgetary and manpower limitations. Chopper development will have high priority in the planning for instruments to be available when the PSR becomes operational, at which time phasing will not be a problem.

IV. DIFFRACTION INSTRUMENTS

A. The General Purpose Neutron Diffractometer (GPD)

A time-of-flight neutron diffractometer has been built at the WNR pulsed source with a capability for liquid, amorphous, and medium resolution powder diffraction (0.5% Δd/d) experiments. The instrument tests the concepts of electronic time and geometric resolution focusing. The instrument consists of

62 ^3He proportional counters arranged in four banks at scattering angles 150°, 90°, 40°, and 10°, and two ^{235}U fission beam monitors. Each bank of detectors is mounted inside a borated polyethylene box and nose cone, designed to eliminate as much background scattering as possible. The whole detector array and sample position are housed in a shielded room constructed from large slabs of borated wax 30 cm thick contained in steel plate. This modular design will facilitate future modifications. See Fig. 11.

The sample is located 10 m from the target and the detectors are located 1 m from the sample, except for the low-angle bank where the flight path varies from 1 m to 2 m. The detector banks are angled relative to the scattered beam: this is the so-called resolution focussed configuration, where each detector in a bank has approximately the same resolution. The nominal specifications for each bank are shown in Table I.

TABLE I

Scattering Angle (2θ)	No. of Detector	Detector Height (cm)	Sample-Detector Path Length (m)	Resolution [Δd/d(%)]*
10	14	15 and 30	1-2	8-12
40	16	15	1.0	2
90	16	30	1.0	0.8
150	16	30	1.0	0.5

*at λ ~ 1.3 A

The incident collimator consists of an evacuated aluminum pipe with poly-boron inserts (5% boron) throughout its length. The area of the moderator viewed is 10 cm high by 5 cm wide and the collimator tapers this in five stages to a beam 5 cm high and 1.3 cm wide at the sample position. The walls of the collimator are smooth and uncoated. This configuration has produced a cleanly defined beam at the sample position with little spreading.

After the sample the beam passes through a box filled with argon, to reduce air scattering into the low-angle bank, and then into an evacuated get-lost-pipe which carries the beam a further 10 m to a beam dump outside the experimental room. The well-defined character of the beam can be seen from the fact that an "Albatross" neutron monitor placed on the get-lost-pipe

registered about 3 mR/hr but when placed near the beam dump recorded 120 mR/hr. So far we have not been able to test for beam carried background (i.e., neutrons down-scattered by the collimator and arriving at the sample at later times.)

A schematic for the electronics to accumulate neutron counts is shown in Fig. 12. The output from each detector is fed into a Le Croy charge sensitive pre-amp TRA510. The output of the pre-amp is pulse shaped to have a width of ~ 250 ns and this narrow width is partly responsible for its low amplitude (~ 4 mV). The outputs from all the pre-amps are fed into a multiplexer by co-axial cables which vary in length from 0.5 m to 2 m. The signals are amplified and discriminated using a Le Croy Model PC 700 hybrid, and then multiplexed for subsequent computer processing. The discriminator level is set for 32 detectors by one control.

We have found this system susceptible to the r.f. noise present in an accelerator environment. We believe we are susceptible to this noise primarily because of the low level signal from the preamplifier. Other problems have arisen from having one discriminator control for many detectors. We are presently considering both a reconfiguration, which should overcome the major problems, and alternative preamp/amplifier/discriminator systems which can be purchased at reasonable cost. There have been no problems with multiplexing 64 detectors into the CAMAC crate.

Experimental Data: Preliminary samples have been run to characterize the instrument. Figure 13 shows the raw data from 16 detectors combined as they would be for a powder diffraction experiment, for a vanadium rod 0.635 cm in diameter and 5 cm high, together with the air scatter over an equivalent counting period. The vanadium count rate suggests a thermal flux at the sample of ~ 1×10^5 n/cm^2-s. The relatively low background is a source for encouragement. Fig. 14 shows part of a MgO powder pattern for the 150° bank of detectors, taken in about seven hours. In Fig. 15 we show a preliminary analysis of a diffraction experiment on D_2O, compared to a typical reactor spectrum. No absorption, multiple scattering or Placzek corrections have been made, but the measured spectra have been divided by the incident beam monitor and then normalized to the vanadium data to remove the counter efficiencies. It will be seen that the structure factor possesses all the usual features for D_2O. The Placzek 'droop' which appears in reactor data has largely disappeared, even for a material for which $S(Q,\omega)$ is quite broad in ω relative to thermal energies.

Future Program: Initially we expect to use the instrument on a variety of simple experiments: crystalline powders particularly to look at magnetic structures at large d-spacings; molecular liquids and gases, to determine the variation of bond lengths as a function of pressure and temperature, and also determine inter-molecular orientations; structures of amorphous materials, where a broad range of momentum transfers are required. For accurate work it will probably prove necessary to incorporate a frame overlap chopper which is at a design stage.

B. Single Crystal Diffractometer (SXD)

A diffractometer is under development at the WNR for single-crystal structure determinations and the study of diffuse and incoherent scattering. The design is similar to an instrument being developed at ANL, but it has some unique features such as a novel megaword memory data acquisition system.

The heart of the single crystal instrument is a 2 atm ^{3}He filled multiwire Borkowski-Kopp type position sensitive area detector with dimensions 25 cm x 25 cm procured from Technology for Energy Corporation in Knoxville, Tennessee. This detector is designed to acquire data from a volume element consisting of x-y spatial information with a resolution of 2mm and time-of-flight information with a wavelength dependent resolution. This detector is mounted on a portable frame and is positionable at several distances and orientations from the crystal. A schematic of the instrument is shown in Fig. 16. The crystal is positioned in the beam with a quarter circle goniostat. The Hg filled shutter collimation system views a 10 cm x 10 cm area of the moderator and a 0.5 cm x 0.5 cm area of the sample. The moderator to sample distance has been chosen to be 5.8 m, just outside the biological shield, to attain the maximum neutron flux.

We have attempted to keep the geometrical features of the instrument as simple as possible in the initial design to maintain flexibility. Among the features which we plan to develop and include in the instrument are a more sophisticated automated goniostat, continuously variable detector positioning, and variable temperature and pressure sample environments.

Data Acquisition: The area detector design includes two orthogonal cathode grids strung continuously from single wires. The current pulse generated in the cathode circuits by the neutron reaction with ^{3}He gas

within the detector reaches the two ends at different times. The difference in rise times of the pulse is used to locate the x-y coordinates of the event. The analog signal produced by the total energy discrimination and risetime circuitry is digitized by a fast analog to digital converter and passed to a fast time-of-flight clock which latches timing information to the position information. The data is passed on to a high speed digital data acquisition system designed through a LASL-ORNL collaboration for use with two-dimensional position-sensitive detectors when a third parameter, such as time-of-flight, must be monitored. This data acquisition system presently includes a half megaword of MOSTEK memory and a unidirectional 24 bit data bus with two control lines. The data can thus be stored in memory very quickly and can be accessed via a standard CAMAC dataway for computer processing. A block diagram of the acquisition and analysis system is shown in Fig. 18. The system is fully described in a joint ORNL/LASL report, ORNL/TM-7325 or LASL-8260-MS by R. Hendricks, P. A. Seeger, J. Scheer, and S. Suehiro.

Data Reduction: The principal software problem involves the processing of the time-of-flight data from megaword sized histograms to simple reciprocal lattice intensities which can be analyzed with existing structural analysis software. A software package has been created for this purpose as a part of a continuing collaborative effort between ANL and LASL staff. It is anticipated that with an instrument of this complexity problems may arise which will require modeling corrections in the data reduction and processing. The reduced data will be analyzed with the LASL Crystal Structure Program Library.

Experimental Data: Preliminary data has been collected on several single crystals of inorganic and organometallic compounds. Histograms collected from a postassium sulfate crystal, covering almost a complete independent unit, are being used primarily for characterization of instrument parameters. Fig. 17a shows a raw data contour plot from one three dimensional K_2SO_4 histogram which has been compacted in the direction perpendicular to the incident beam and is displayed as 2θ vs. time (or wavelength) in four resolution segments. The (011) lattice line is indicated with the dotted line. Figure 17b shows the raw intensity of a single resolution element on the detector face (corresponding to the same (011) lattice line) plotted vs direct wavelength in Å. The signal-to-noise

for the K_2SO_4 data is remarkable and much better than what we saw for hydrogeneous samples.

C. Special Environment Diffractometer SED

A geometrical time focused special environment diffractometer has been in operation for the last two years at the WNR facility. This has been used for powder diffraction by the profile refinement method at high pressures and temperatures. The primary object of study has been the phase diagram of Pu.

Recently, the instrument has been rebuilt to improve the data rate. The new instrument has a source to sample distance of 6 m, a sample to detector distance of about 1 m, and two banks of 12, 1/4", 40 atm ^3He detectors geometrically time focused at an angle of 90°. The shutter-collimation system views a 3" x 4" moderator area time focused at 22.5^o and produces a beam size at the sample of 3/16" x 1 1/2". The geometry is such that incident and scattered neutron paths cross inside the sample, so that there are no Bragg peaks from the sample vessel. With this new design we anticipate that it will take about one hour to obtain a good powder pattern at current neutron fluxes. The sample vessel in use can currently study pressures up to 5 kbar and temperatures up to 350 ^oC. The instrument is shown in Fig. 19. Tests with the new instrument are about to begin.

ACKNOWLEDGMENT

This is a report on work carried out by many people connected with the neutron scattering group, P-8, at the WNR facility of the Los Alamos Scientific Laboratory. We thank R. Von Dreele of Arizona State University for his contribution to the general purpose diffractometer, D. Cromer for his work on the special environment diffractometer, and T. A. Kitchens for contributions to the chopper spectrometer. We acknowledge the engineering support of J. Scheer, and the technical assistance of H. Bowen, R. Hardee, R. Hawel, and L. Wagner. We also acknowledge a helpful collaboration with the IPNS program at the Argonne National Laboratory. We thank A. D. Taylor of the Rutherford Laboratory for his comments on the manuscript.

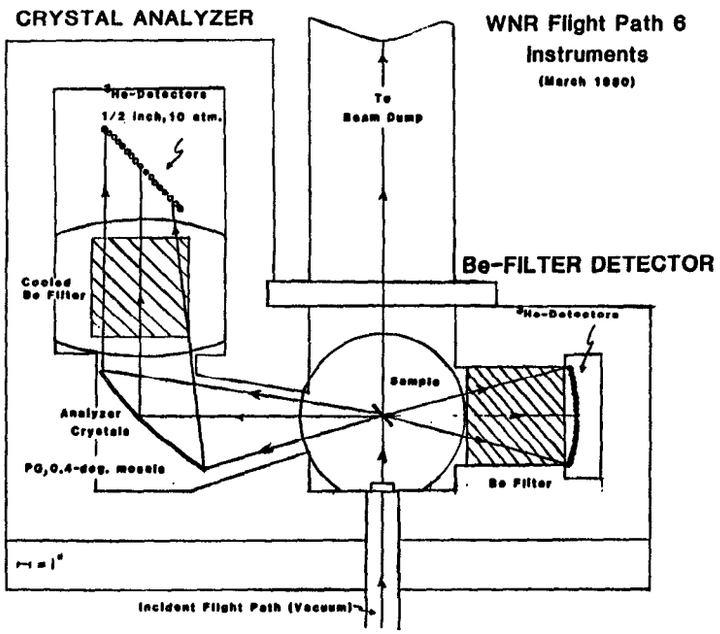

Fig. 2. Inelastic neutron scattering spectrometers at flight path 6 of WNR as of March 1980. Source-to-sample distance is 6.33 m, sample-to-detector distance 1 m for the crystal analyzer, 0.45 m for the Be filter.

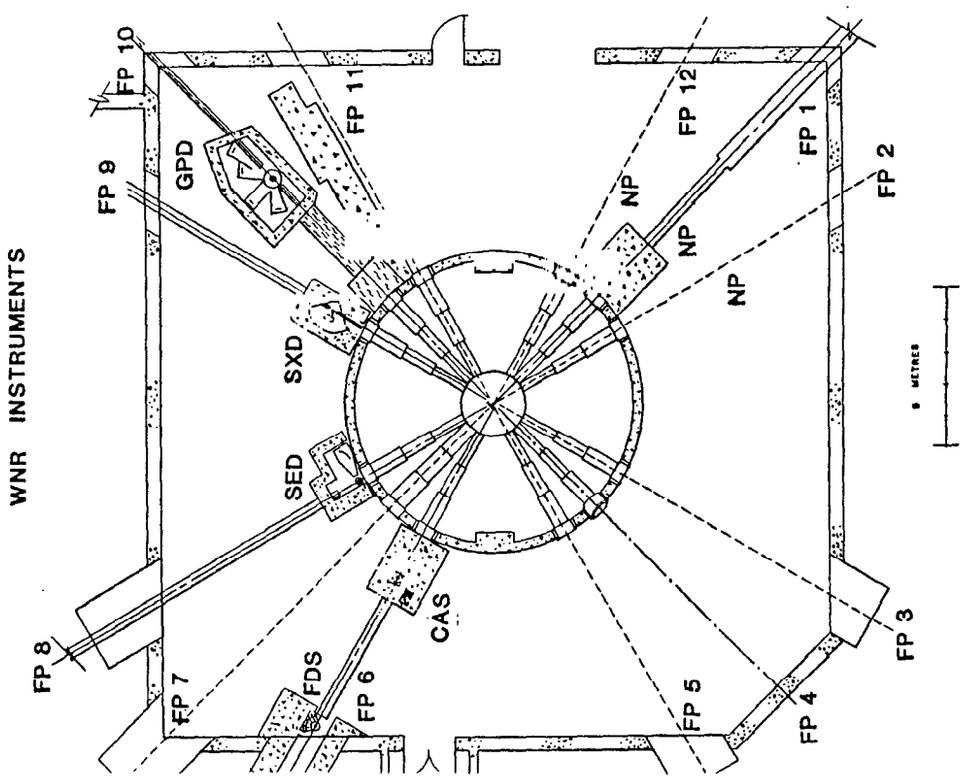

Fig. 1. Schematic layout of instruments in the experimental hall of the WNR.

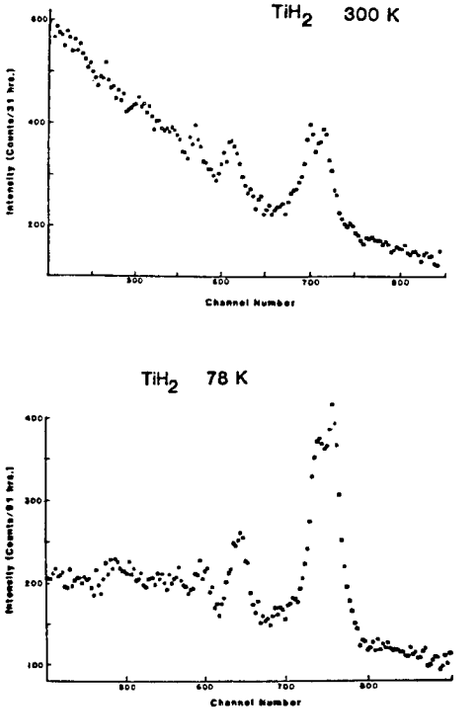

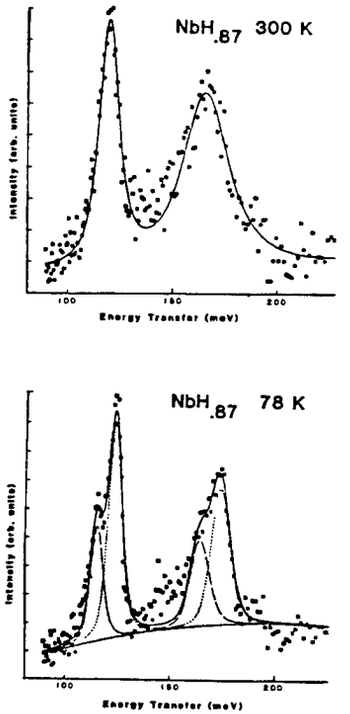

Fig. 3. (Left) Raw inelastic neutron scattering spectra of TiH_2 taken with the crystal analyzer of the radial flight path 5 (top) and the tangential flight path 6 (bottom). The beam area was four times larger at flight path 5. The Be filter was not cooled in either case. Each data point represents an average of three 3.2 μs channels.

Fig. 4. (Right) Hydrogen local mode spectra in NbH.87 at two temperatures. The data has been corrected for background and the incident spectrum. Each data set required approximately 24 hrs. of beam time at 120 Hz and 3 μA.

CRYSTAL ANALYZER SPECTROMETER

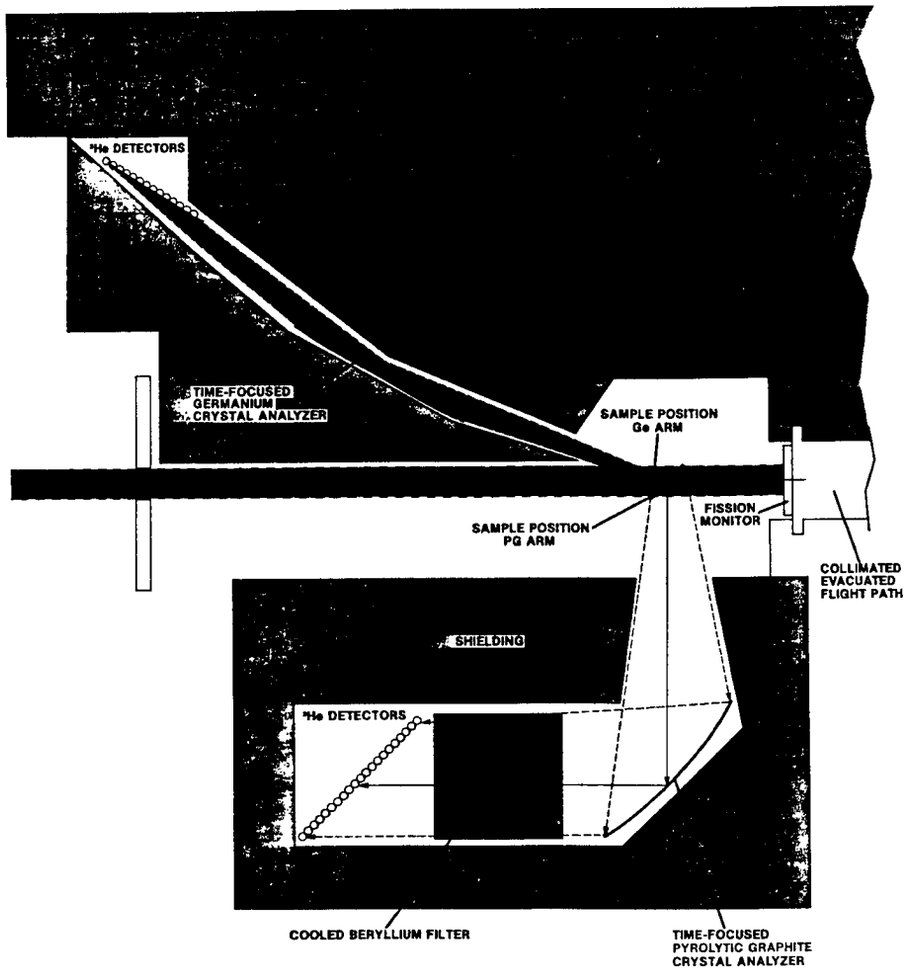

Fig. 5. Crystal analyzer with second, Ge-analyzer (E_f = 50 meV) planned for early 1981.

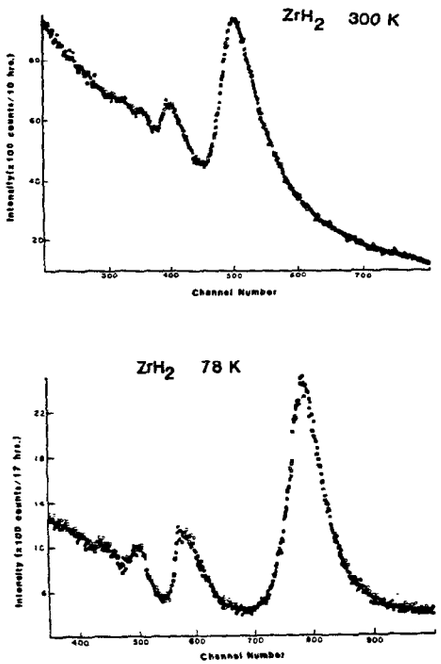

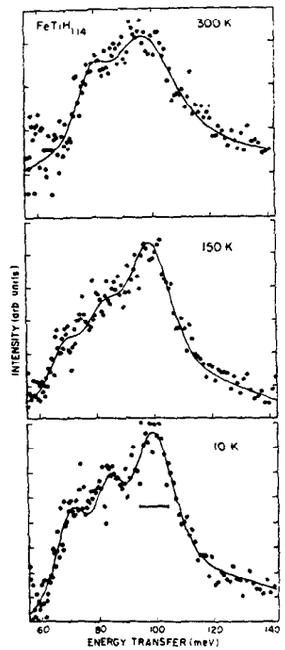

Fig. 6. (Left) Raw inelastic neutron scattering spectra of ZrH_2 taken with the Be filter detector spectrometer at flight path 5 (top) and flight path 6 (bottom). The ratio of final over initial flight path length improved by a factor of four from top to bottom.

Fig. 7. (Right) Corrected inelastic neutron scattering spectra of $FeTiH_{1.14}$ (β-phase) as a function of temperature obtained on the FDS. The contributions of three filter sections were added after correcting each data set.

BERYLLIUM - BERYLLIUM OXIDE DIFFERENCE SPECTROMETER

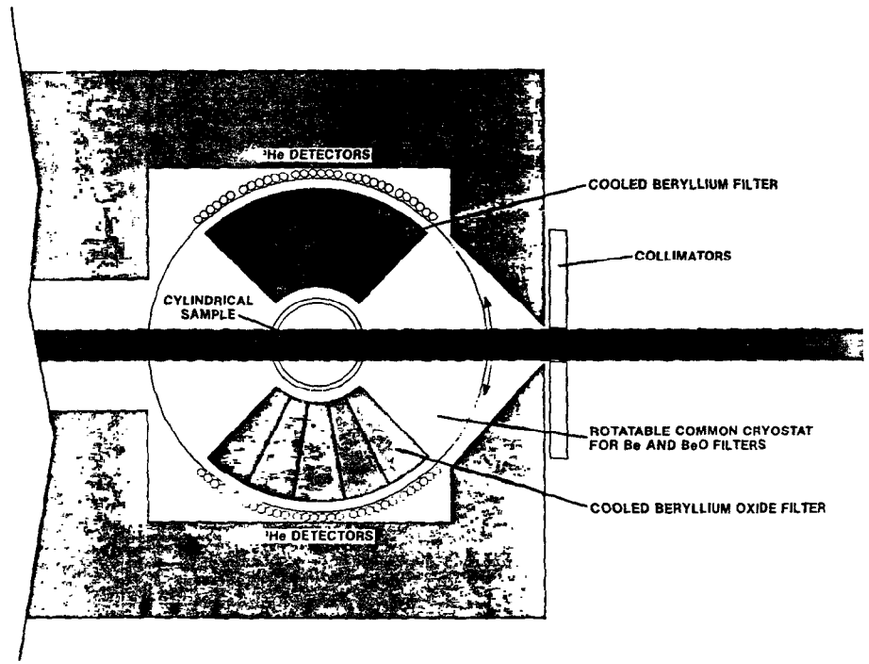

Fig. 8. Be/BeO difference filter instrument presently under construction.

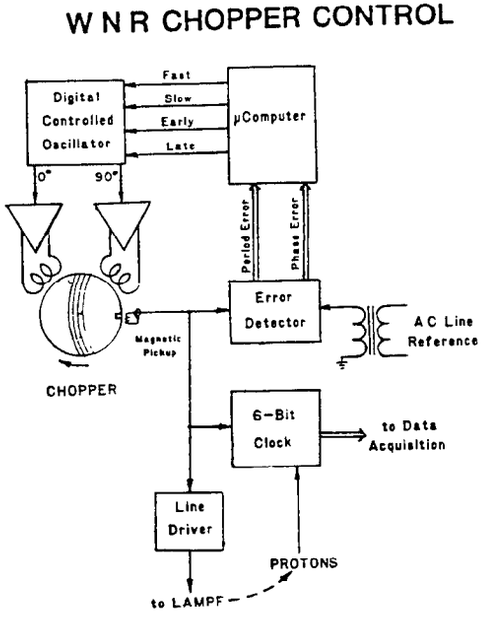

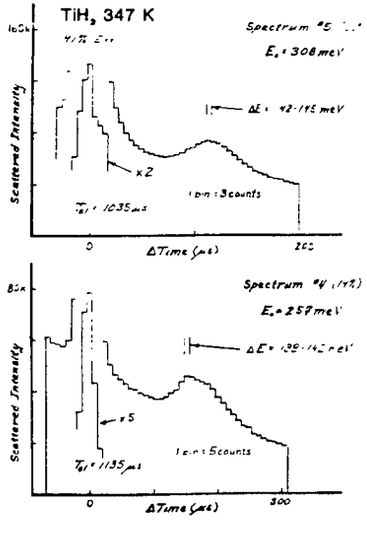

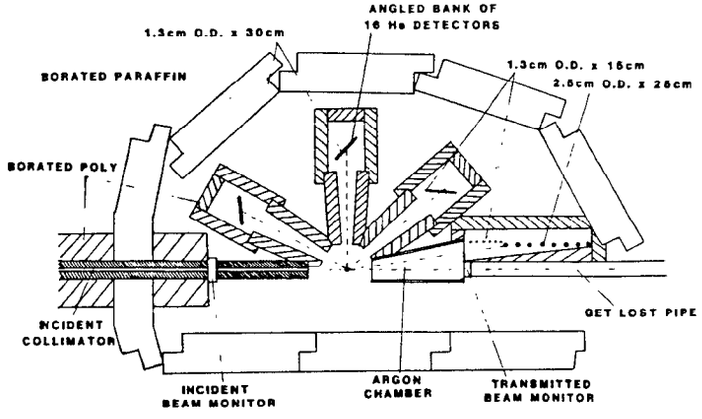

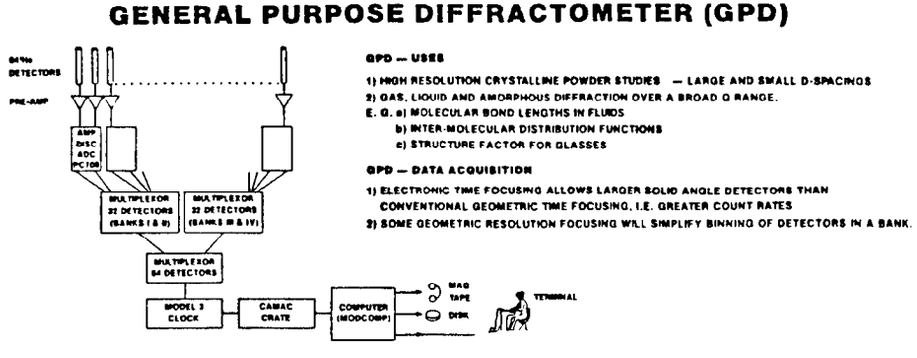

Fig. 9 (Left) Schematic of the chopper control system.

Fig. 10. (Right) TiH_2 spectra obtained with the chopper spectrometer. The overall efficiency for 8 spectra corresponding to eight different incident energies was 91%, with 30% of the scattered neutrons falling into spectrum 5 (E_0 = 308 meV).

Fig. 11. (Top) Schematic Layout of the General Purpose Diffractometer The sample is located 10m from the target.

Fig. 12. (Bottom) Data acquisition system for the GPD. The present preamplifier is a LeCroy TRA 510.

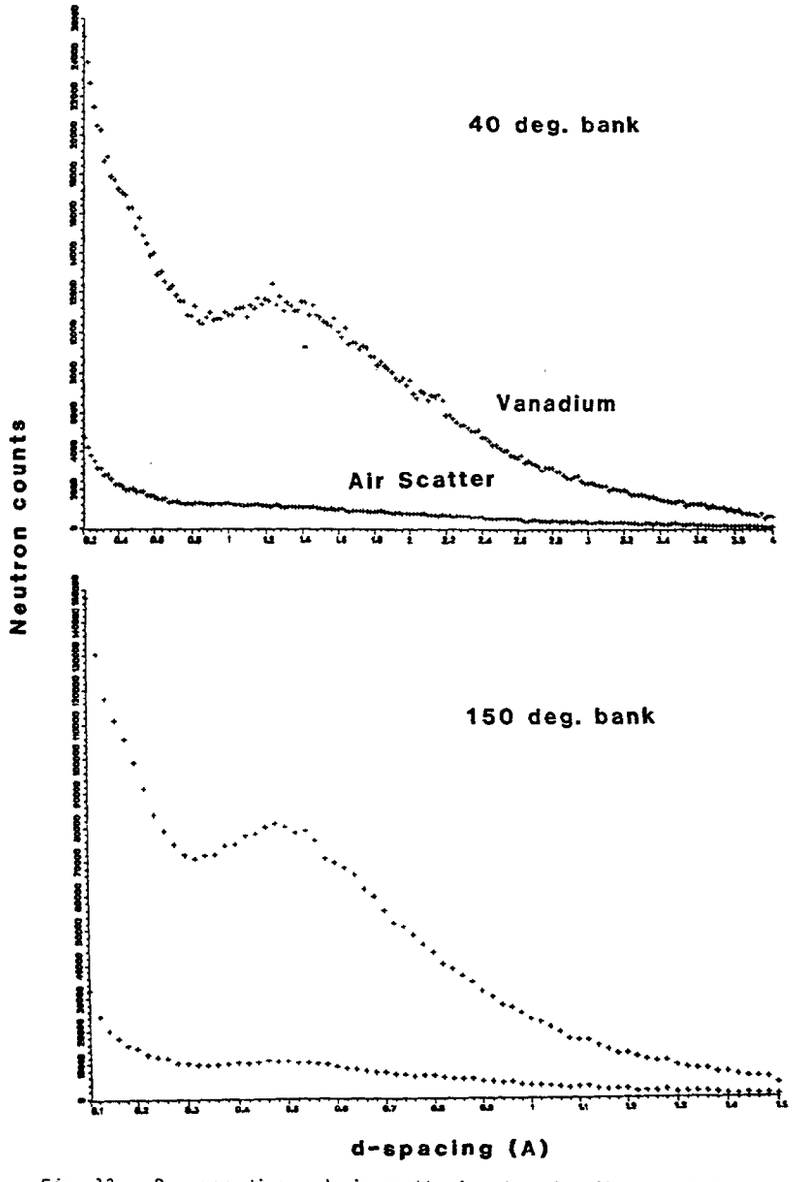

Fig. 13. Raw vanadium and air scattering data for 40° and 150° banks. The detectors are combined in 'd'-spacing bins of width 0.025 A. These data were obtained in about 12 hrs., running at 2.3 μA.

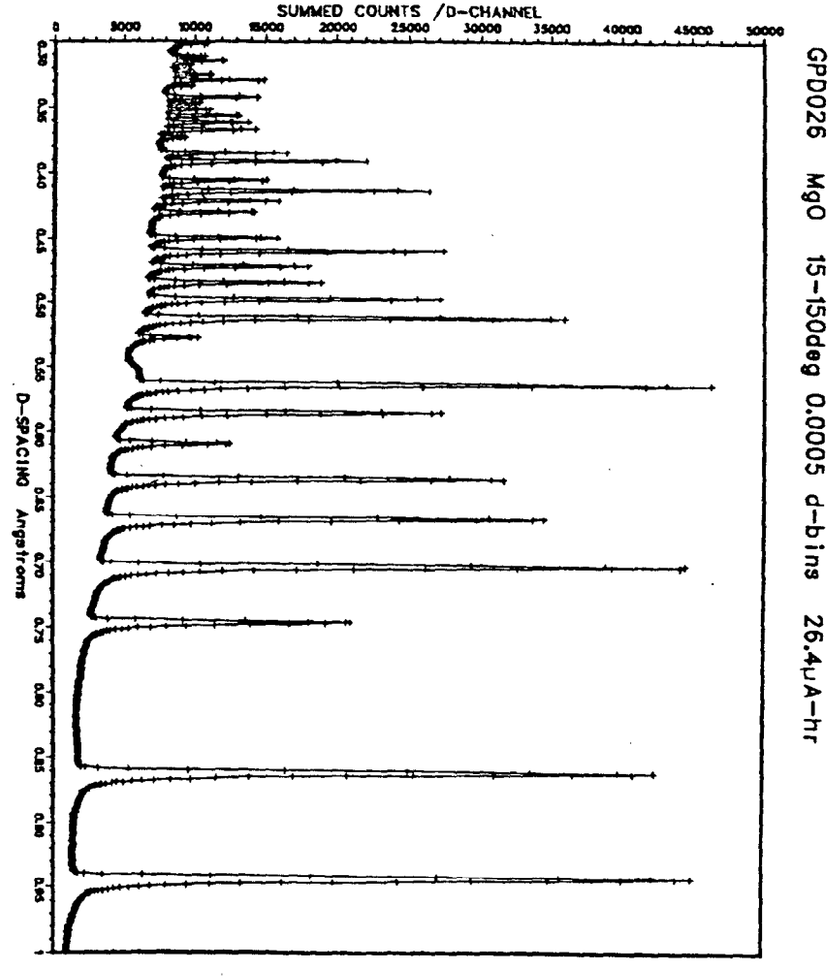

Fig. 14. Raw powder pattern from MgO. 15 detectors in the 150° bank have been grouped into the appropriate d-bins by software.

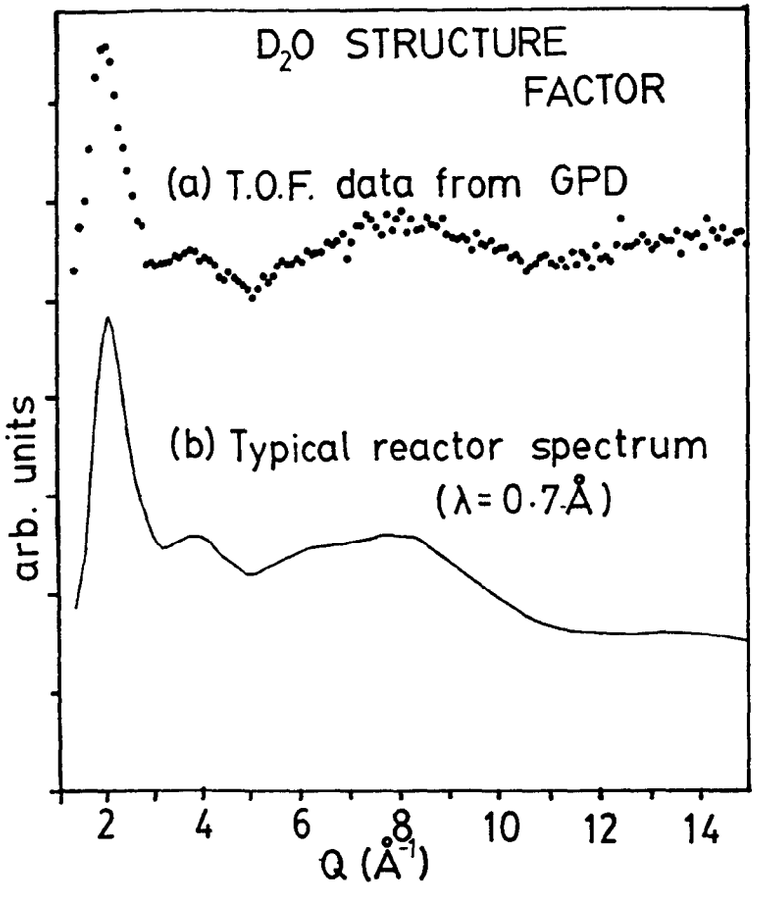

Fig. 15. Neutron time-of-flight spectrum from D_2O at 40° scattering angle. The data were normalized as in Fig. 14. They are compared with a spectrum for D_2O obtained at the I.L.L. All the features at the reactor spectrum are observed, and the Placzek effects are much less noticeable.

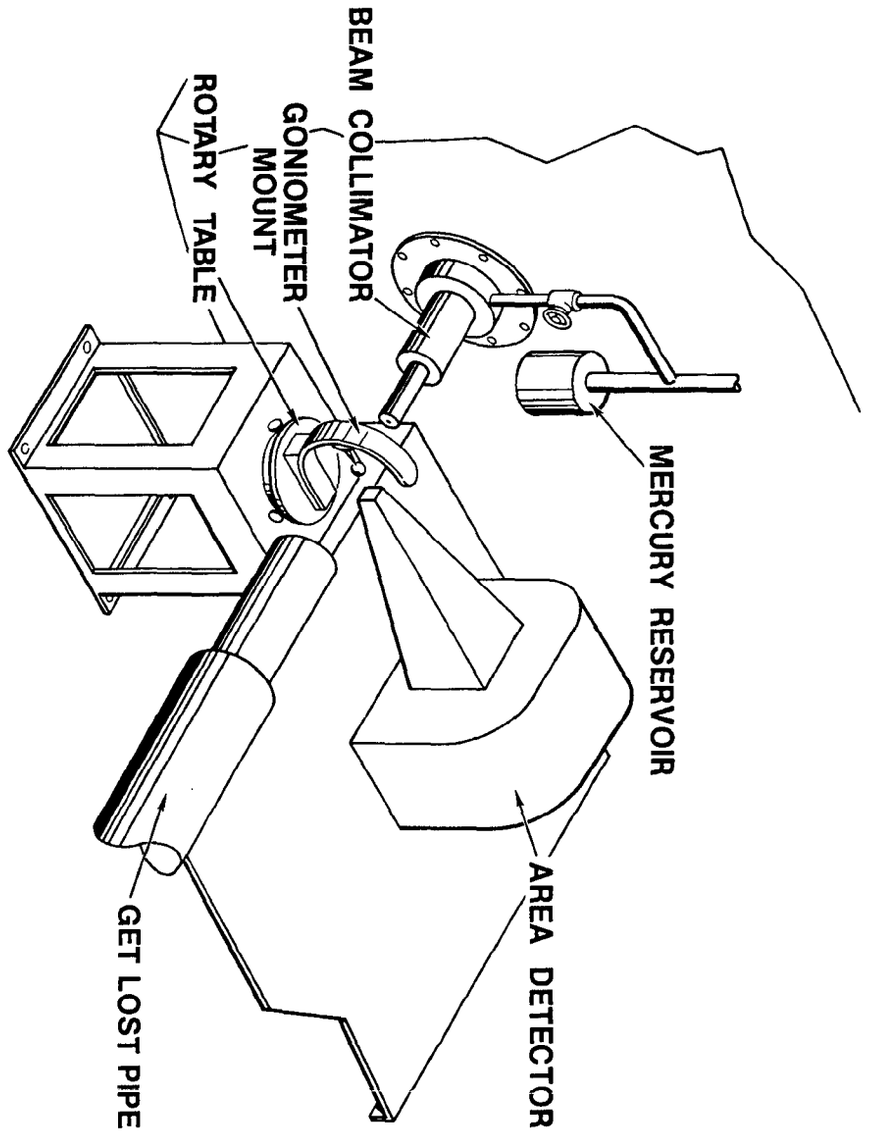

Fig. 16. The single crystal diffractometer of flight path 9. Source-to-sample distance is 5.8 m.

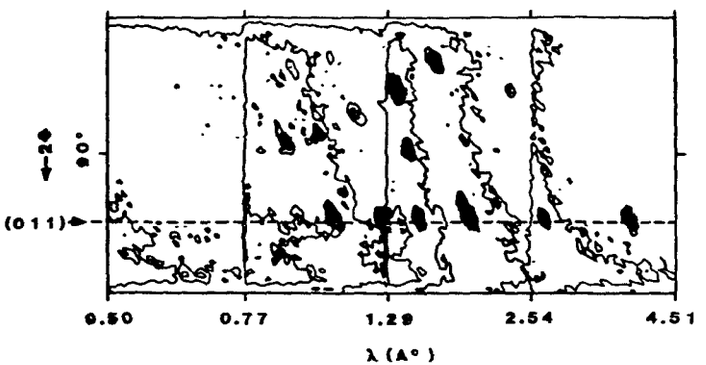

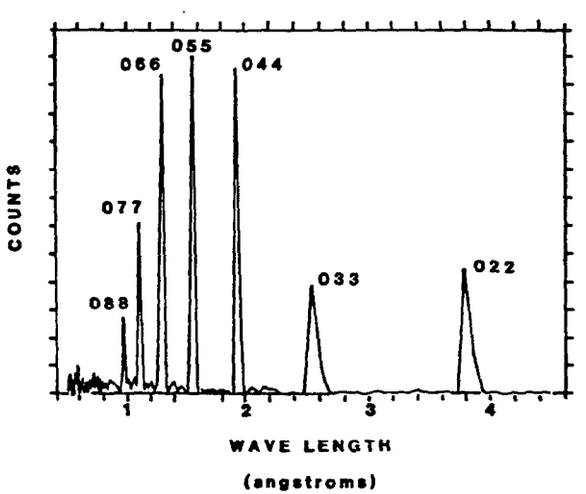

Fig. 17a (Top) Contour plot of a typical K_2SO_4 histogram containing the (011) lattice line.

Fig. 17b (Bottom) Intensity vs wavelength for one resolution element containing the (011) line.

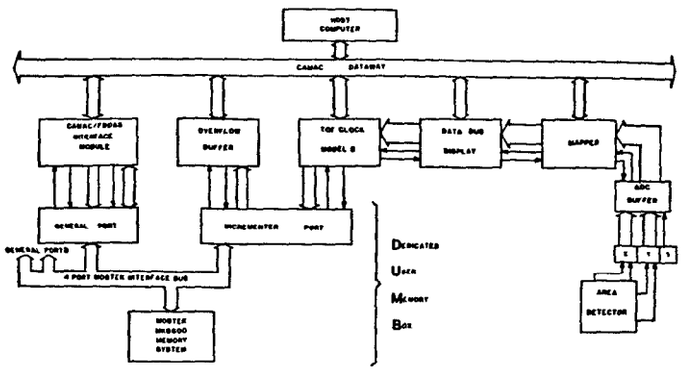

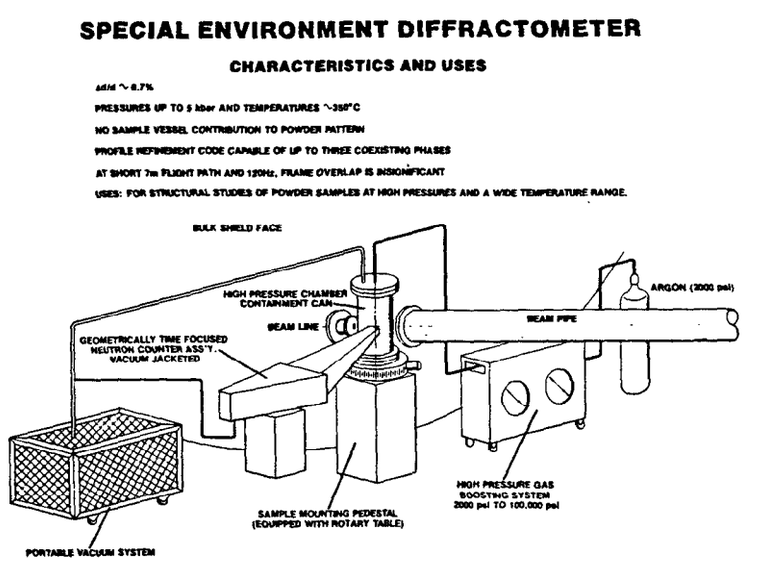

Fig. 18 (Top) Block diagram of the data acquisition system for the position-sensitive detector at the single crystal diffractometer.

Fig. 19 (Bottom) View of the special environment diffractometer at flight path 8.

IPNS Neutron Scattering Instrument Development

C.S. Borso, R. Brenner, T.O. Brun, J.M. Carpenter, R.K. Crawford, J.E. Epperson, G.P. Felcher, D.G. Hinks, G. Holmblad, J.D. Jorgensen, R. Kleb, G.A. Lander, M.H. Mueller, G.E. Ostrowski, C.A. Pelizzari, F.J. Rotella, A.J. Schultz, M.G. Strauss, R.G. Teller, F. Williamson, T.G. Worlton.

Argonne National Laboratory
9700 South Cass Avenue
Argonne, Illinois 60439

The ZING-P' Prototype has been used for the development of five types of instrument: (a) crystal analyzer spectrometer (b) chopper spectrometer (c) single crystal diffractometer (d) small-angle diffractometer and (e) high-resolution powder diffractometer. These five types comprise the initial group of seven IPNS-I instruments, the chopper spectrometers existing in high-resolution and high-intensity forms and the powder diffractometers in special-environment and general-purpose forms. In addition, we have also worked on (f) the development of resonance-neutron radiography (which, although not a scattering instrument, is convenient to discuss here), (g) area neutron-position detectors, and (h) polarized neutron instrumentation, as well as (i) the data acquisition system for IPNS-I. We will briefly summarize some of these developments.

A. Crystal Analyzer Spectrometer

The crystal analyzer spectrometer at ZING-P' was very active during the last operating cycle, partly because of the high neutron flux available during that period. Approximately 75% of the available beam time was spent on problems generated by outside users. The experiments performed include studies of:

1. Phonondensity of states of HCOOH at 25 K and 235 K with C. V. Berney and S. H. Chen (M.I.T.).
2. Phonon density of the water of hydration in RNA with G. Ascarelli, and G. Nucifora (Purdue).

3. Phonons in pyrolytic graphite with W. Kamitakahara (Iowa State Univ.).
4. Hydrogen vibrations in $LaH_x(D_x)$ and $CeH_x(D_x)$ with W. Kamitakahara (Iowa State Univ.).
5. Hydrogen vibrations in $VH_{0.75}$ with K. Ross (Univ. of Birmingham, England).
6. Tunneling modes in CsH_2PO_4 with R. Youngblood (Brookhaven National Laboratory).
7. Vibrational frequency spectrum of H in VH_x as a function of temperature. Fig. 1 shows a spectrum obtained with $VH_{0.02}$ at 30 K.

B. Chopper Spectrometer

Inelastic scattering spectra were taken at the Chopper Spectrometer for a sample of UN at room temperature using two incident energies, E_0 = 130 meV and 307 meV. The new Fermi chopper designed by Robert Kleb was used in both cases. This chopper, which will be used in Low-Resolution Medium-Energy Chopper Spectrometer (LRMECS) at IPNS-I, performed as predicted at these neutron energies and is expected to prove satisfactory for neutrons of energy 1 eV or higher. One of the spectra is shown in Fig. 2. The large-Q spectra (taken at a scattering angle of 85°) show well-defined peaks from the nitrogen vibration mode, including at least the second harmonic at 90 meV in the E_0 = 307 meV run. At small Q (7.5° scattering angle) the nigrogen mode is much weaker, as expected.

Information obtained in the operation of the Chopper Spectrometer is now being used to optimize the design of choppers and shielding for the IPNS-I chopper spectrometers.

C. Single Crystal Diffractometer

For the last 6 weeks of ZING-P', data were measured continuously on the time-of-flight single crystal diffractometer. Nearly 50 histograms were obtained

on a disk-shaped NaCl crystal (3 mm high x 4 mm diameter). These data cover a complete hemisphere in reciprocal space and will be used for developing software for converting raw integrated intensities into structure factors. Although the data were collected with a 20 x 20 cm position sensitive ^3He gas-filled detector, Figs. 3 and 4 are typical histograms and peak profiles. Other data were also collected on a crystal of $LiNH_4SO_4$.

One of our major efforts in the past few months has been the development of software which will permit fast and efficient data collection. A flow diagram for data collection is shown in Fig. 5. A crystal with an unknown unit cell is mounted on the difframtometer in an arbitrary orientation. Counts are accumulated for a histogram, which is then searched for Bragg peaks. The interpolated positions of the Bragg peaks are used in an auto-indexing program written by R. Jacobson (Iowa State University) which provides an orientation matrix and cell parameters. The positions of any number of Bragg reflections can be used in a least-squares procedure to obtain highly accurate cell parameters.

A table of diffractometer χ and ϕ setting angles are calculated using a program written by H. Levy (Oak Ridge National Laboratory). The settings provide coverage of a hemisphere of reciprocal space with minimum overlap. Each histogram is counted for a preset monitor count at which point the crystal is reoriented by driving χ and ϕ and a new histogram is started. Integrated intensities are obtained by calculating the location of reflections in each histogram and integrating in three dimensions. These data are then reduced and normalized to obtain structure factors for the structure solution and refinement.

D. Small Angle Diffractometer

The Small Angle Diffractometer at ZING-P' incroporated a multiple-converging-aperture collimator constructed of tapered stainless steel tubes. Gd_2O_3-epoxy

paint on the inside and outside prevented internal reflections and "cross talk" between tubes which were enclosed in a 10 cm diameter pipe filled with boric acid solution. The same detector and data acquisition system were used as for the Single Crystal Diffractometer. The diffractometer was used for two test measure ments, on cetylpyridinium chloride (described below) and on an irradiated single crystal of aluminum.

Cetylpyridinium chloride is a lipophilic compound which is known to form micellar structures in a variety of polar solvents. It thus serves as an excellent model system for the study of the aggregation and transport properties of these structures. The molecular structure

consists of a long hydrocarbon chain connected to a polar head group consisting of an aromatic ring.

The electron density of these structures is closely matched to that of water and thus X-ray studies have been difficult to perform. Several similar molecules have been studied with X-ray small angle scattering using various solutes to enhance the contrast of the molecule. Using these same X-ray techniques with CPC yields a classical small angle scattering curve characteristic of micelles. Using neutron scattering in 100% D_2O, however, as shown by our results at ZING-P' (Fig. 6), quite a different structure occurs at the same CPC concentration. We are continuing this study with further neutron experiments at University of Missouri and with SAXS and NMR at Argonne to fully characterize the structural properties of CPC.

E. High Resolution Powder Diffractometer

We first began collecting data on the High Resolution Powder Diffractometer (HRPD) at ZING-P' in July 1978. From that time until the final shutdown of ZING-P' in August 1980, 104 sets of time-of-flight diffraction data were collected on the HRPD, which represents work on 54 separate samples. Of the 54 experiments performed, 37% were proposed by collaborators from outside of Argonne, 15% were experiments on standard samples for instrumental characterization and calibration, and the remaining 50% were suggested by scientists here at Argonne.

The types of experiments performed on the HRPD were scientifically quite diverse. The utility of powder techniques as a structural tool was investigated by comparison of powder and single crystal neutron diffraction results on well-characterized samples. A study of the effect of the temperature on solid state structure, especially atomic thermal motion, was undertaken by comparing diffraction results on samples at room temperature and near the temperature of liquid helium. Samples which exhibit phase transitions induced at either above (to 1000°K) or below (to 10°K) room temperature were studied. Structural studies were carried out on electrical conductors -- ternary superconductors, fast-ion conductors and one-dimensional conductors and battery materials (see Fig. 7). Powder data were taken on samples of metal deuteride compounds in order to locate deuterium positions in the structure via Fourier synthesis. The structure of substances which are known to be active in the catalysis of certain types of chemical reactions were investigated.

Work done on the HRPD over the last two years has given a much better indication of the limits of the time-of-flight neutron powder techniques and the analysis of data therefrom, which will be invaluable in the design and operation of the powder diffractometers at IPNS-I. The ability to collect data on samples

in special environments -- at temperatures to 10° K in a closed-cycle DISPLEX refrigerator, at temperatures in excess of 900° K in a specially designed furnace and with a powder sample in an in situ liquid electrochemical cell -- was demonstrated. Strains as low as 0.2% were measured on the HRPD, and the extremely high-resolution of the HRPD also made evident inhomogeneities and impurities in some samples seen as homogeneous by other analytical tools. HRPD powder data have been analyzed using a time-of-flight version of the Rietveld profile refinement program, written by R. B. vonDreele at Arizona State University and modified and augmented here at Argonne. To date, 48% of all data taken on the HRPD have been analyzed, with many of our collaborators taking an active role in the actual analyses. This time-of-flight Rietveld code will be used as a prototype for the future data analysis software package that will be operative at IPNS-I. A standard Fourier synthesis program has been adapted to this Rietveld code, and with it, we have demonstrated the ability to generate maps of the nuclear density distribution in a solid from powder data.

F. Resonance Neutron Radiography

Radiography has been for many years one of the important applications of neutron beams. A pulsed source offers a unique advantage for certain applications of radiography because the various energies can be readily separated by time-of-flight techniques. Many nuclei exhibit neutron resonances in the epithermal region and our aim is to identify these nuclei in a target material by their absorption of neutrons at a specific resonant energy. The basic requirements for such a technique are a source of pulsed epithermal neutrons and a position-sensitive detector capable of high data rates and accumulation of data into x, y and t ($\propto E^{-1/2}$) channels. The NPSD described below is just such a detector.

To demonstrate the method, we describe briefly the test experiment at the ZING-P' facility in July 1980. The target, consisting of foils of Au and In, is shown in Fig. 8. In Fig. 9(a) we show the transmission profile from 1-7.5 eV, i.e., the intensity of neutrons summed over all the detector as a function of time-of-flight from the time t_0 when the proton pulse hits the target. Here we identify three resonance energies, two associated with In and one with Au. In Fig. 8 we examine the spatial dependence of these resonances by looking at the response of the detector at a given time channel. In the top view the 5.7 eV neutrons essentially give the beam profile as the target is transparent at this energy, the center and lower views show the In and Au positions, respectively. Note the overlap from channel 125-135 corresponding to the fact that in the center the target is opaque to both 1.46 eV (In) and 4.91 eV (Au) neutrons. Finally, we attempted a very rapid test on two fuel pellets. A transmission profile is shown in Fig. 9(b). This is more complex than Fig. 9(a) but we can readily identify ^{239}Pu, ^{235}U, ^{238}U, and ^{241}Am from the Pu decay.

These tests have proved that the method can work at IPNS-I and efforts are now underway to identify specific applications.

We appreciate the help of J. Reddy and R. L. Hitterman (MSD).

G. New Neutron-position Scintillation Detector

A new, two-dimensional, neutron-position scintillation detector (NPSD) is being developed at Argonne to meet the growing needs of scattering experiments at IPNS-I. The NPSD is based on the well-proven principle of the Anger γ-ray camera and has a number of important advantages over the conventional gas detectors. In particular, because there is no need for high pressure gas, the detector can be made much more efficient in the epithermal regime and, compared to the gas detector, the parallax of the NPSD is appreciably less and the construction is easier and therefore cheaper.

The NPSD was evaluated at ZING-P' in scattering experiments and resonance radiography.

Figure 10 shows on the left a perforated Cd mask with 2.75 mm holes spaced 10 mm apart along the X and Y axes. The mask was attached to the face of the detector which was at 90° with respect to the beam. A vanadium rod was placed in the beam 20 cm away from the detector to produce isotropic scattering. The scattered neutrons incident on the Cd mask produced the image on the right in Fig. 10. The image clearly shows all the holes.

Figure 3 shows a Laue pattern of a NaCl crystal containing all reflections between 0.7-4 A. The detector was at 90° with respect to the beam and 20 cm away from the crystal. The peak in the middle, right of center, is a superposition of four reflections. The second (right) and the third (left) order reflections are shown on the bottom.

Figure 4 shows the X and Y profiles of the Bragg peak in the lower left of Fig. 3. The peak widths reflect the intrinsic resolution of the detector (2-3 mm) and the broadening effects due to the crystal size (3 mm diameter), mosaic structure, and beam collimation and divergence.

The potential of the detector as an imaging device for resonance neutron radiography was evaluated by flooding a 3 mm thick $^{10}BC_4$ test pattern, placed on the face of the detector, with thermalized neutrons from a Pu-Be source located 2.5 m away. A photograph of the test pattern is shown on the left of Fig. 11. Its center section is comprised of 2 mm wide slits on the right and 4 mm wide bars on the left with disks and holes above and below. The image produced by the detector as observed on the CRT, after correction for nonuniformity by the computer, is shown on the right. Note that even with this first detector all the features are clearly visible. The high stability of this detector is reflected

in the good delineation seen in this image which was obtained over an 18 h period. The use of this detector in a resonance radiography experiment is described above.

H. Polarized Neutron Instrumentation

The availability of a "white" beam of polarized neutrons at IPNS would make possible novel experiments, such as the study of high-energy electron excitations in metals. Polarization of the beam can be obtained by passing it through a suitable filter, most typically a target material that contains a high concentration of polarized hydrogen nuclei. We have chosen as target a crystal of yttrium ethyl sulfate doped with ytterbium. Here high proton polarization is attained due to coupling of the proton spins with the magnetic impurity ytterbium (kept polarized by an external magnetic field) by a method called "spin refrigeration". We are presently assembling a prototype spin refrigerator, and in the near future we will test the achieved proton polarization by SQUID magnetometry. Subsequently, the efficiency of the device as a neutron spin filter will be tested in collaboration with C. Olsen at the WNR facility at Los Alamos. The device has the potential of eventually achieving ~75% proton polarization in an easily reachable sample environment (temperature ~1.1 K; applied magnetic field ~14 kG). This may also proved to be an attractive way to filter neutron spins well above the epithermal range of energy used in Solid State research; hence it might be useful for nuclear physics programs.

A study of the best utilization of the polarized beam of neutrons at IPNS has generated the concept of a novel kind of instrument, the "spin precession resonance spectrometer". Its function is the detection of medium and high energy excitations in solids at small momentum transfer. For these processes the energy and momentum conservation laws require not only a high energy E_i for the incident

neutrons but a high energy E_f for the scattered neutrons. The instrument is basically a resonance spectrometer. The detector consists of a target that absorbs neutrons only in an energy window $E_R \pm \Delta E_R$ surrounded by photomulitpliers which detect the ensuing burst of gamma rays. The machine in this simple form provides a resolution of E_f defined by the width of the resonance line, but this is too wide for a large number of experiments. The compression of ΔE_f is achieved in the following way: The initial beam is fully polarized, and the detector contains a target having a spin-dependent resonance. If the target is also fully polarized, it will analyze both the energy and the spin of the scattered neutrons. The compression of ΔE_f is achieved by inserting a short-spin precession unit, similar in form and function to that developed at I.L.L. in the spin-echo spectrometer, along the path of the scattered neutrons. In this way, ΔE_f is controlled by the maximum magnetic field available in the precessing unit. As an added bonus spin-flip processes (such as the scattering from magnetic excitations and nuclear spin incoherent scattering) can be separated from non-spin-flip processes. The first estimates of the luminosity and resolution attainable by this machine are promising. Further research and the acquisition of state of the art technology is required before its realization.

I. Data Acquisition System

Hardware and software procurement and development for the Data Acqusition System (DAS) for IPNS Neutron Beam Instruments is proceeding under the direction of the IPNS DAS Development Team, which includes hardware and software specialists and neutron scattering scientists.

The DAS will be in a "star" configuration as shown in Fig. 12 with a minicomputer and data collection system for each instrument connected to a central "Host" computer through independent data lines. The Host computer will be a

32-bit VAX 11/780 with a Floating Point Accelerator and 0.5 MB of memory. It will have an RM03 67 MB Disk Drive and a TU77 125 ips dual density magnetic tape unit. It will also have hard copy terminals, video terminals, graphics terminals, a Versatec Printer/Plotter and modems for remote communications. The star configuration has the advantage of independent data collection and centralized processing power and allows the more expensive peripherals to be concentrated on one machine. Most Host computer software will be in FORTRAN and will be run under the VAX VMS operating system.

Each Minicomputer System will have a 16 bit DEC PDP 11/34A minicomputer for experiment control and for communication with its Data Collection System and with the Host. The Minicomputer System software will also be mostly in FORTRAN and programs will execute under the RSX11M operating system. Programs and data will be stored on an RL02 10 MB capacity disk. Each Minicomputer System will include an LA120 180 character per second hard-copy terminal and a VS11 graphics terminal. A typical Minicomputer System is shown in Fig. 13.

Each Data Collection System will include a CAMAC System containing a Time-Digitizer Module, a Master Clock Module, Polling Modules for the Time-Digitizers, a CAMAC Crate Controller, and optionally, a Clock Prescaler Module. The Time-Digitizer Modules have 125 nsec time resolution and have eight input channels per single-width CAMAC module. The single channel analyzers in these modules have a software controllable lower discriminator level and each module has a common software-controllable upper discriminator level.

Each Data Collection System will also include a Central Data Corporation Z8001 single board microcomputer and bulk memory dedicated to data collection, transformation and storage. The microcomputer will accept the digitized data from the CAMAC System and will make the real-time transformations necessary to determine which memory location in the bulk memory should be incremented for a given detected neutron. A typical Data Collection System is also shown in Fig. 13.

Computers for the DAS have now been ordered and software development has begun on already available machines. Design and/or prototype testing is underway for the various hardware modules required. Construction has begun on a building to house the Host Computer System and some of the Minicomputer and Data Collection Systems. This building, scheduled to be completed this fall, will be located directly west of the main IPNS experiment hall (Building 375) and will also house data acquisition and control systems associated with the Radiation Effects Facility.

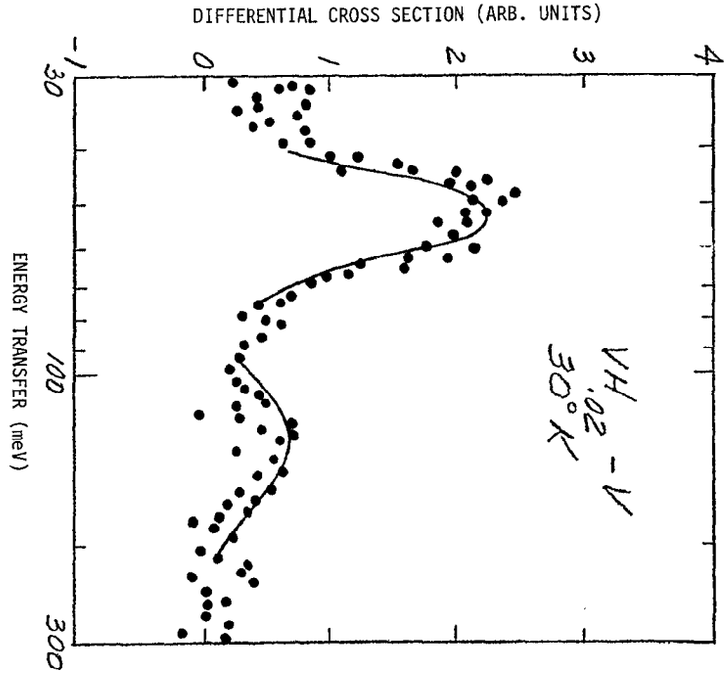

Fig. 1 Inelastic Neutron Scattering from $VH_{0.02}$, with V Scattering Subtracted

Time-of-flight spectra for UN under different conditons. Note the observation of the 1st, 2nd, and possibly even 3rd harmonic of the optic phonon mode with $E_0 = 307$ meV. At low angle ($\phi = 7.5°$) the phonon scattering is too weak to be seen.

FIG. 2

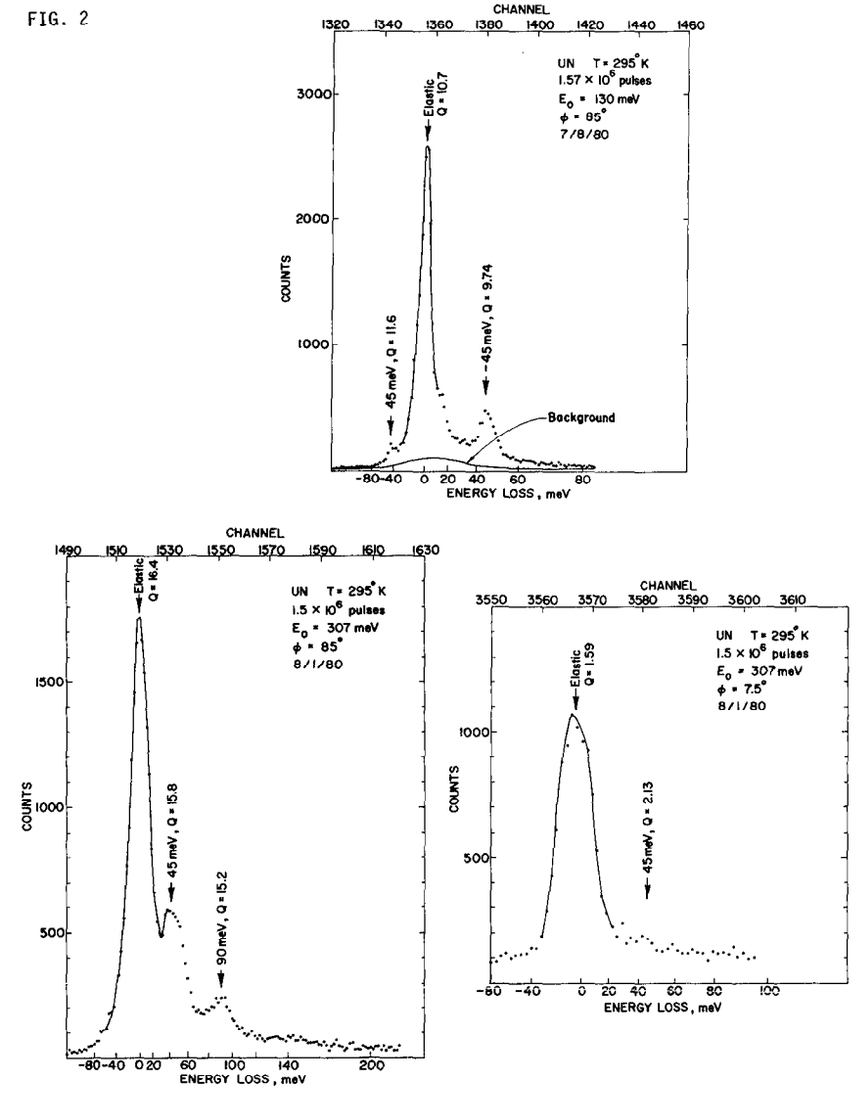

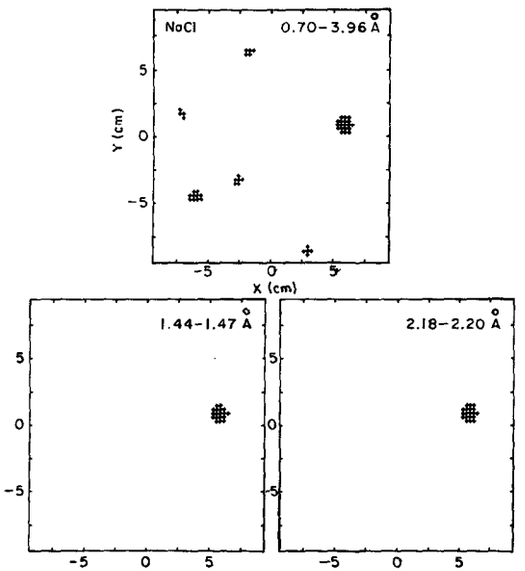

Fig. 3. Laue pattern from a NaCl crystal taken at ZING-P' with the NPSD. Upper section is summed over all energies (wavelengths) whereas lower sections show particular reflections.

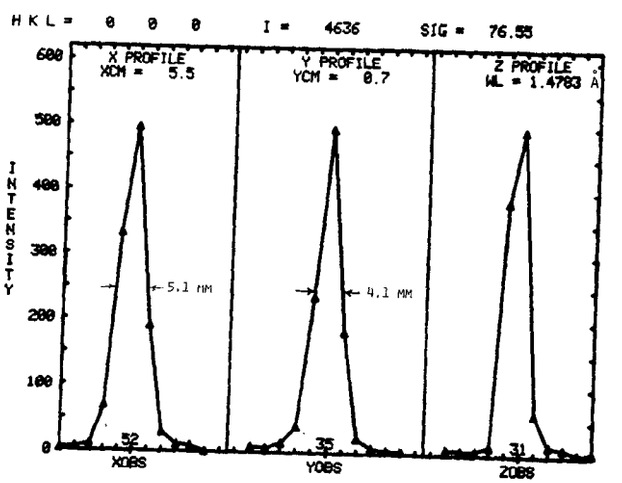

Fig. 4. Detail of Bragg peak in lower left of Fig. 3. Note the extremely good peak to background ratio in all three dimensions.

DATA COLLECTION FLOW DIAGRAM FOR IPNS SINGLE CRYSTAL DIFFRACTOMETER

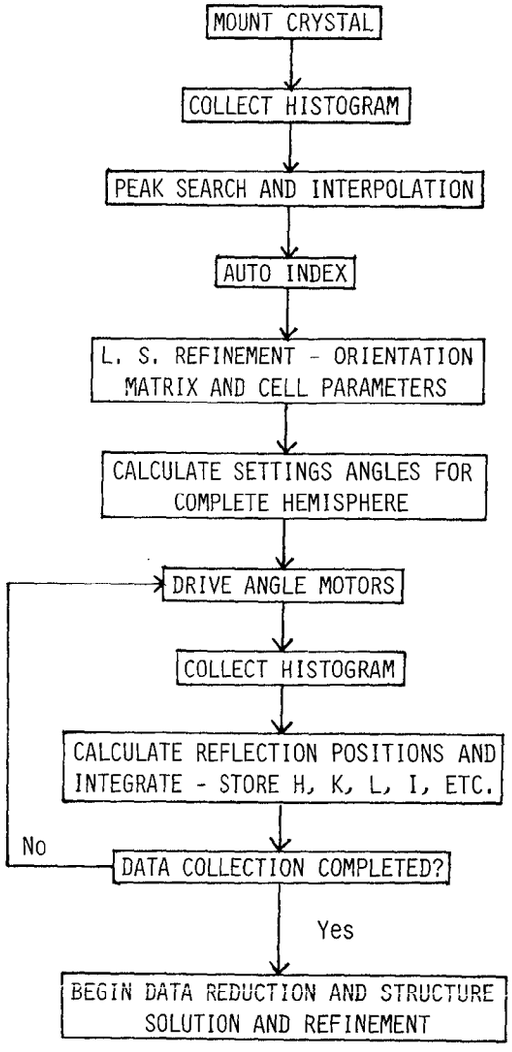

Fig. 5 Single Crystal Diffractometer Data Collection Flow Diagram

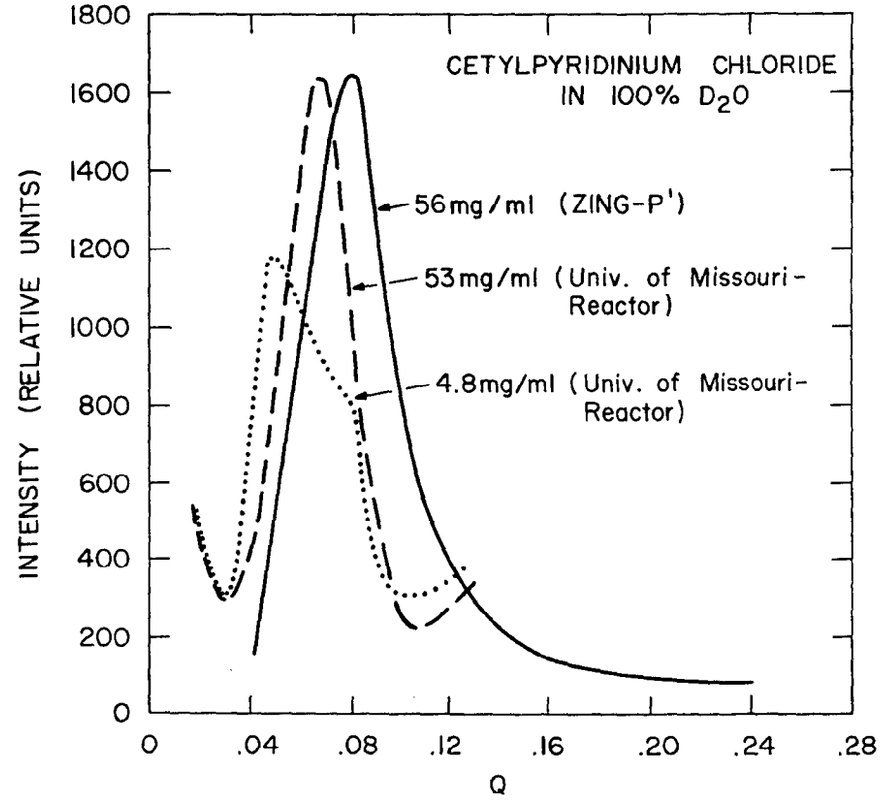

Fig. 6 Small-Angle Neutron Scattering from Cetylpyridinium Chloride

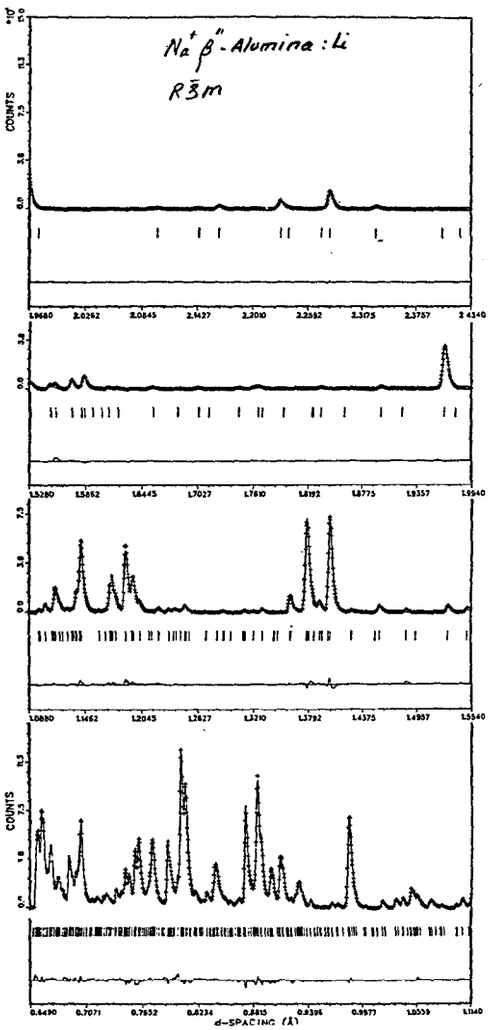

Fig. 7 Powder Diffraction Pattern from Li-Substituted Na-β"-alumina

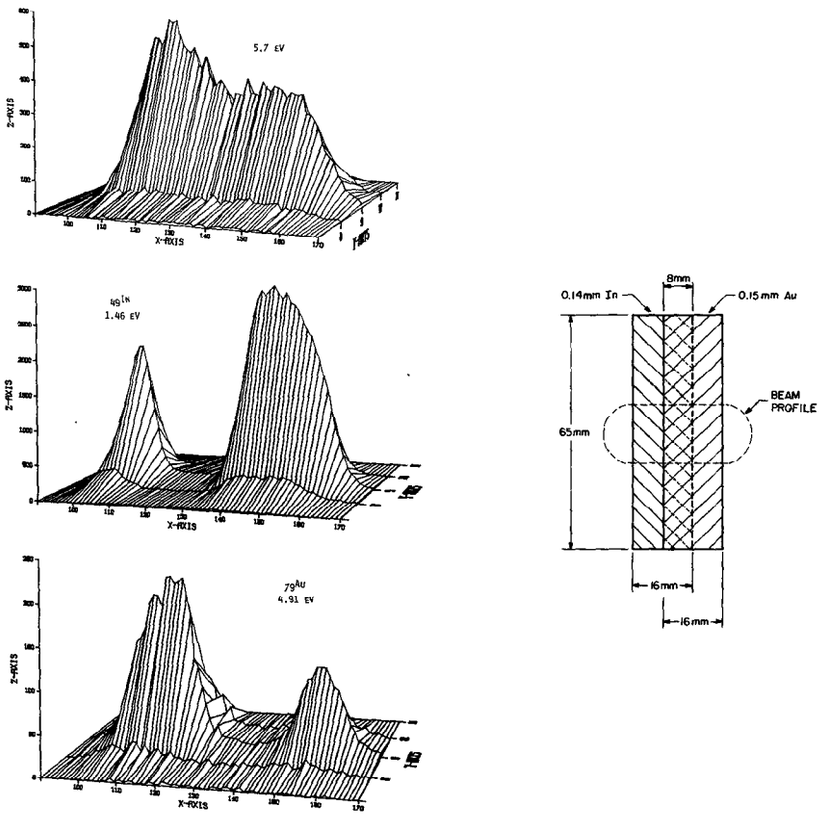

Fig. 8 The target is shown on the right. At the top is the spatial response at 5.7 eV, at which energy the target is almost transparent (see Fig. 9(a)). The center and lower sections are the spatial responses at the In and Au resonances, respectively, and clearly show the position of the foils.

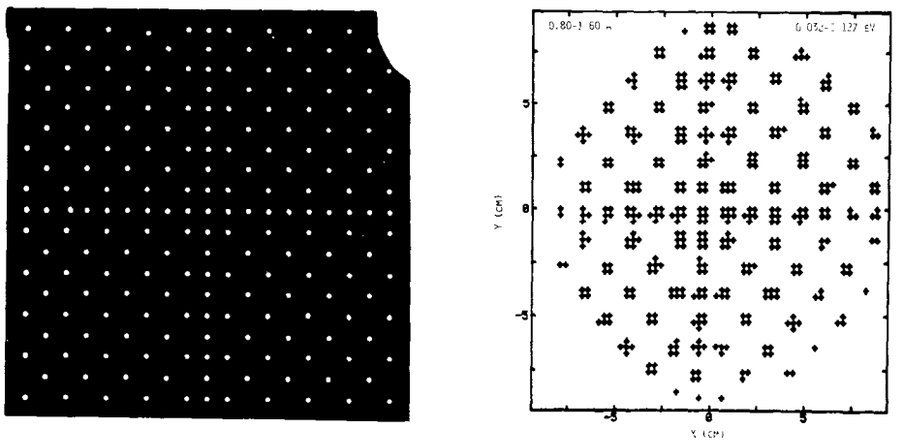

Fig. 10 Photograph (left) and output of NPSD on display screen (right) of cadmium mask. For the neutron pattern the mask was illuminated by scattering from a vanadium rod at ZING-P'.

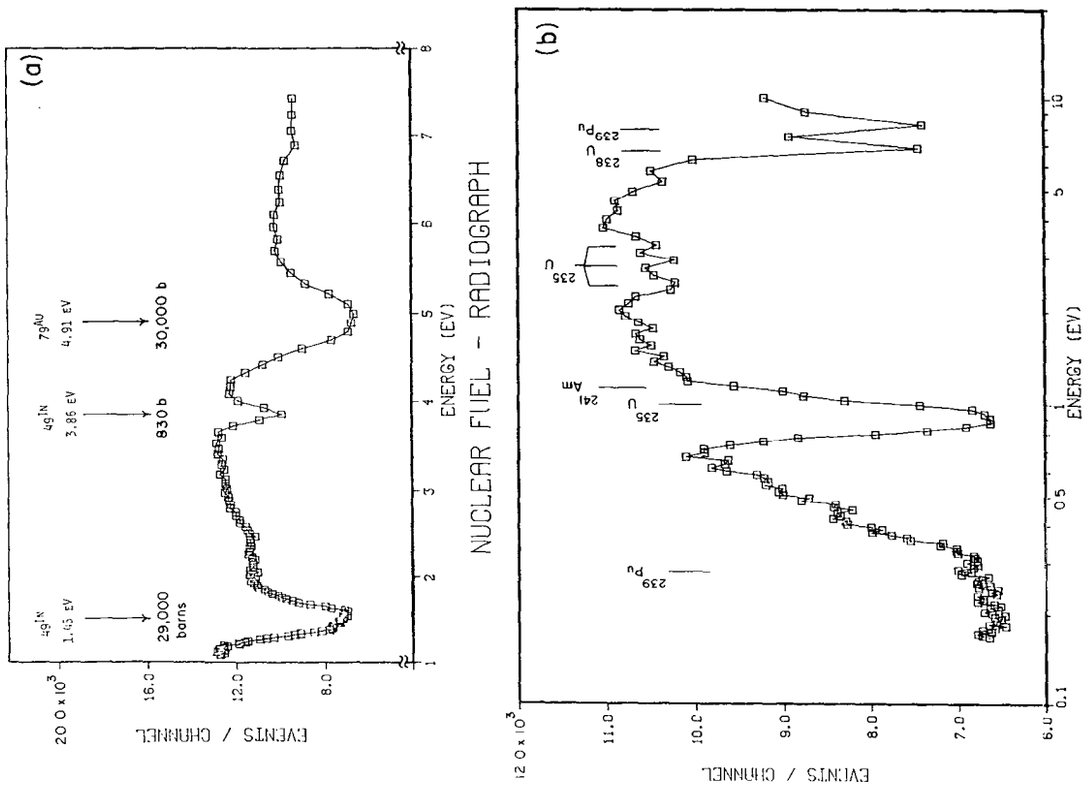

Fig. 9 Transmission Profile for (a) the Au-In Foil Target (see Fig. 8) and (b) the Nuclear Fuel Pellet

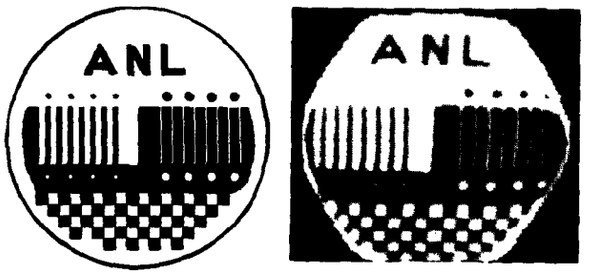

Fig. 11 Photograph (left) and output of NPSD on the display screen (right) of a BC_4 test pattern. See text for details of test pattern.

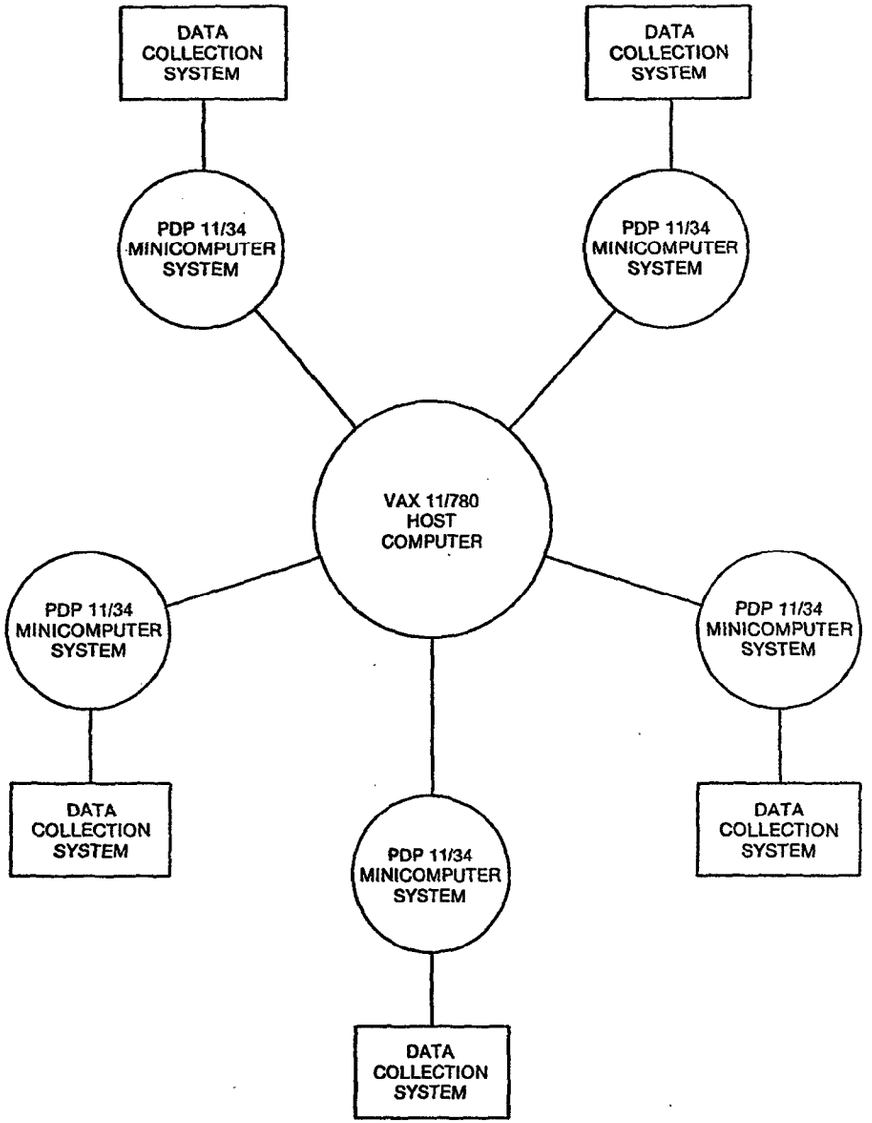

Fig. 12 The "star" configuration for the IPNS-I Data Acquisition System

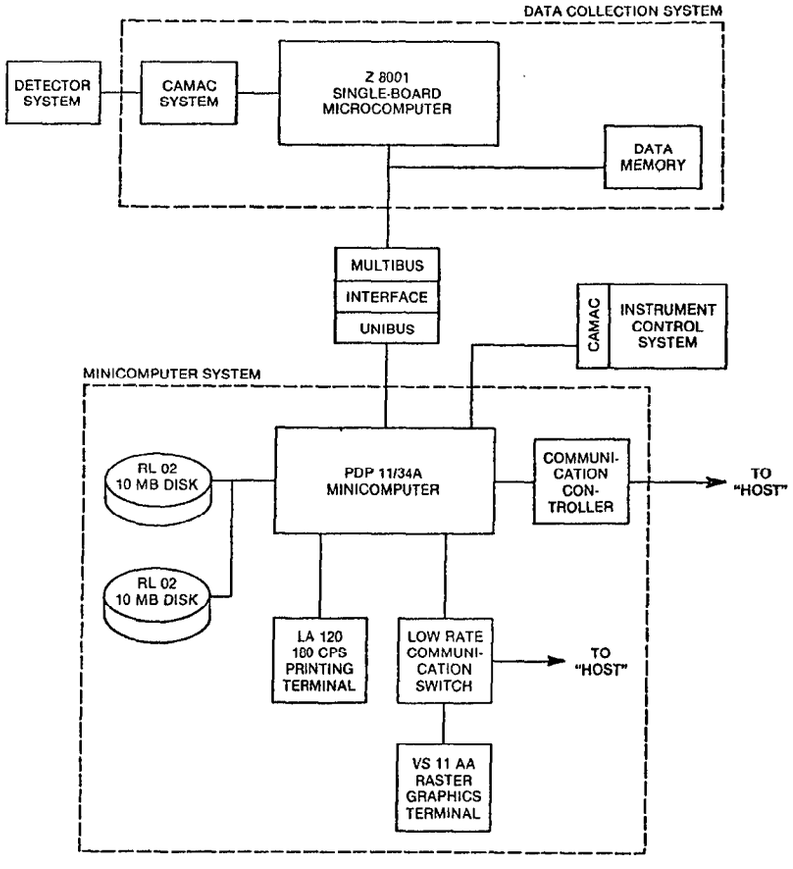

Fig. 13 Typical Minicomputer and Data-collection System for IPNS-I

NEUTRON SCATTERING FACILITIES AT THE TOHOKU UNIVERSITY ELECTRON LINAC

K.Suzuki*, N.Niimura**, T.Kajitani*, K.Kai*, Y.Endoh***, S.Tomiyoshi*, K.Yamada** and S.Yamaguchi****

* : The Research Institute for Iron, Steel and Other Metals Tohoku University
** : Laboratory of Nuclear Science, Tohoku University
*** : Department of Physics, Faculty of Science, Tohoku University
****: Department of Nuclear Technology, Faculty of Engineering, Tohoku University

In 1967 the Tohoku University 300 MeV electron linear accelerator was constructed. Since 1971 available pulsed neutrons have been supplied through nine horizontal and one vertical neutron beam tubes installed in the 2.5 m thick biological concrete shield. The length and cross section of the beam tubes are shown in Table 1.

The electron linear accelerator is usually operated at the acceleration energy of 250 MeV with the peak beam current of 60 mA and at the pulse duration of 3 μs with the repetition frequency of 115 pps. Therefore an electron beam of 5 kW mean power is irradiated to the multiplate tungsten target to provide the thermal neutron peak flux of 1×10^{12} $n/cm^2/s$ at the surface of the moderator. The specification of the target and moderator assembly is summarized in Table 2 and its arrangement is shown in Figure 1.

At the moment the nine neutron beam holes are occupied by various types of spectrometers and the one by a television monitor camera. The schematic layout of the neutron facilities in Tohoku electron LINAC is illustrated in Figure 1.

A medium size computer OKITAC-4500 plays the central function in the on-line data acquisition from the nine spectrometers. Each raw data collected is independently displayed and monitored on CRT. Necessary data can be recorded by a line-printer, paper-tape puncher and graphic copier. The whole system of data acquisition used is shown in Figure 2. The software and interface were totally developed by neutron users themselves.

Time Focusing Crystal Analyser Spectrometer

A time focusing energy-loss spectrometer with a reasonably good energy transfer resolution is installed at the H-1 beam hole to measure local modes of the hydrogen atom motion in transition metal hydrides in the crystalline and glassy state. The pyrolytic graphite crystal is used as an analyser in the inverted geometry at the expense of momentum transfer resolution. The beryllium filter of 15 cm in thickness is located in front of He-3 counters (1/2" diameter) without cooling it. The energy resolution achieved is 2.2 to 3.6 % over the energy transfer range of 50 to 600 MeV.

Rotating Crystal Inelastic Scattering Spectrometer

An inelastic scattering spectrometer with a pair of stationary and rotating pyrolytic graphite crystal plates is installed at the H-2 beam hole. Monochromatic pulsed neutrons with a desired wavelength from 1.5 to 4.5 are effectively chosen by adjusting the Bragg angle of the stationary crystal and tuning the delay of the firing time of the electron LINAC relative to the angular position of the rotating crystal. The neutron path is evacuated to avoid air scattering. Eight He-3 counter banks are arranged over the scattering angle from $2\theta = 10$ to $90°$ at the

position of 1.8 m apart from the sample. The momentum resolution is 20-7 % over the range of the momentum transfer from 0.2 to 4.5 A^{-1}, and the average energy resolution is 0.3 MeV over the range of the energy transfer from 0.3 to 100 MeV, respectively. The spectrometer has been used so far to measure the quasielastic neutron scattering due to the concentration fluctuation in Tl_2Te-Tl liquid, the diffusional motion of hydrogen atoms in $NbH_{0.32}$ single crystal and the Brownian motion in polystylene polymer-CH_2Cl_2 solution.

Magnetic Mirror Diffractometer

A magnetic mirror diffractometer is installed at the H-3 beam hole as an application of polarised pulsed neutrons to the structure study of magnetic substances. The magnetic mirror used is $Fe_{45}Co_{55}$ alloy evaporated on the OPP polymer film surface in 1 kOe magnetic field. The performance of the mirror shows the high polarisability of 90 % with the reflectivity of more than 85 % for the neutron of its wavelength longer than 2.5 A. This diffractometer is a prototype of the TOP spectrometer in KENS.

Liquid Total Scattering Spectrometer

The liquid total scattering spectrometer is installed at the H-4 beam hole to measure the structure factors of liquids and amorphous solids over a wide range of the scattering vector from 0.1 to 50 A^{-1}. The incident neutron beam size is defined to 10 mm wide × 50 mm high by a B_4C window and inner-beam tube collimator. Scattered neutrons are detected at six scattering angles (2θ = 3, 15, 30, 60, 90 and 150°) by He-3 detector (1/2" diameter × 20" length) banks placed symmetrically on each side of the incident beam. He-3 counters at the 60, 90 and 150°

scattering angles are arranged in the time-focusing geometry with large apertures. Therefore B_4C nose cones coated with Gd_2O_3 paint are located between the He-3 counter box apertures and a sample chamber to prevent the He-3 counters from finding neutrons scattered from anything except for the sample. The sample chamber is evacuated to avoid air scattering and has the collimators extended from the nose cones in it. Incident neutron flight path length is fixed at 4.359 m, while scattered ones are variable from 0.40 to 0.50 m for 2θ = 15 to 150° and fixed at 1.509 for 2θ = 3°. The resolution of the scattering vector varies from 20 to 1 % according to the change in the scattering angle from 2θ = 5 to 150°.

Single Crystal Diffractometer

A single crystal diffractometer with a goniometer is installed at the H-5 beam hole. The goniometer has simultaneously four He-3 counters at different four scattering angles. The sample can be tilted within ± 10° on the goniometer. The sample and scattering angle are stepped with the accuracy of 0.05°. Using this diffractometer, it has been so far found that the magnetic spin in cubic Mn_3Si single crystal has the double helical structure along the <111> direction and the solid solution of Mn_3Si and Fe_3Si (simple ferromagnetic) shows the magnetic phase transition of double helical → simple antiferro → canted ferro → simple ferro with increasing Fe_3Si content.

Glass Scintillator Total Spectrometer

A new total scattering spectrometer with glass scintillation detectors is scheduled at the H-6 beam hole with a 6.0 m incident neutron flight path length. Li-6 enriched glass scintillation counters are

arranged at the scattering angle $2\theta = 4$ to $10°$. At the moment the four scattering angles of $2\theta = 150$, 90, 45 and 26 ~ 22° have He-3 counter banks. In near future the He-3 counters will be replaced with the glass scintillation detectors to obtain much higher counting efficiency for epithermal neutrons. Furthermore all counters take the geometric and electric focusing arrangement. The estimated resolution of the scattering vector is between 0.1 and 1.0 A^{-1} over the range of the scattering vector from 0.2 to 60 A^{-1}. Several different samples are simultaneously mounted in the vaccum chamber which has high temperature furnace and helium cryostat.

Time-of-Flight Position Sensitive Detector Diffractometer

This diffractometer installed at the H-7 beam hole is a time-of-flight(TOF) single crystal diffractometer combined with a position sensitive detector(PSD). The one-dimensional PSD can provide the two-dimensional representation of the reciprocal lattice space when the TOF detection is used. Therefore the TOFPSD diffractometer is a quite promising and powerful instrument to measure the complicated intensity distribution in the reciprocal space. This diffractometer has been so far used for the observation of the thermal diffuse scattering and the rapid collection of many Bragg reflections from Cu_3Mn and NaCl single crystals. The positional resolution of the PSD used is 1.4 cm at 1.3 kV bias voltage. The scattering angle is set between $2\theta = 15$ and 120° by the goniometer, which mounts the PSD with the accessible aperture angle of about 30°. The two-dimensional data size is a 64 ch(position) × 250 ch (time). The channel width is variable from 2 to 32 μsec. The data collecting rate of the TOFPSD diffractometer is improved 100 times better than that of a conventional single counter diffractometer.

Vertical Beam Tube Diffractometer

A time-of-flight neutron diffractometer using the vertical incident beam tube (V-1) has been constructed to observe the medium resolution powder diffraction pattern ($\Delta d/d = 3\%$) as well as liquid and amorphous solid ones. This diffractometer consists of eight He-3 counters arranged at the scattering angles $2\theta = 160$, 130, 110, 90, 70, 50, 30 and 15°. Each detector is mounted inside a can filled with B_4C powder. The whole assembly of the detector array and sample are housed in a shielded box constructed from slabs of borated wax 10 cm thick. The sample is located at the position of 300 cm apart from the target and the detectors 25 cm from the sample. It is expected to use the diffractometer for a variety of simple experiments: crystalline powder patterns, determination of the Debye-Waller factor as well as the static displacement of lattice atoms and short-range structure of amorphous solids such as fluoride glasses.

Table 1 Distance between moderator and exit of beam tube, and its cross sections

Beam tube	Distance (cm)	Entrance cross section (cm)	Exit cross section (cm)
H-1	524.4	$10^W \times 10^H$	$20^W \times 7^H$
H-2	378.1	$10^W \times 10^H$	$8^W \times 8^H$
H-3	314.5	$8^W \times 8^H$	$5^W \times 5^H$
H-4	348.9	$6^W \times 6^H$	$6^W \times 6^H$
H-5	478.5	$10^W \times 10^H$	$5^W \times 10^H$
H-6	470.0	5.2 ϕ	5.2 ϕ
H-7	319.5	$5^W \times 5^H$	$5^W \times 5^H$
V-1	240.0	15 ϕ	20 ϕ

Table 2 Specification of target and moderator assembly

Target	Tungsten
	$30\times30\times2^{mm^3}$ (5 pieces)
	$30\times30\times5^{mm^3}$ (3 pieces)
	$30\times30\times9^{mm^3}$ (1 piece)
Moderator	water
	$115^{mm}\phi\times115^{mm}$
	height cylinder

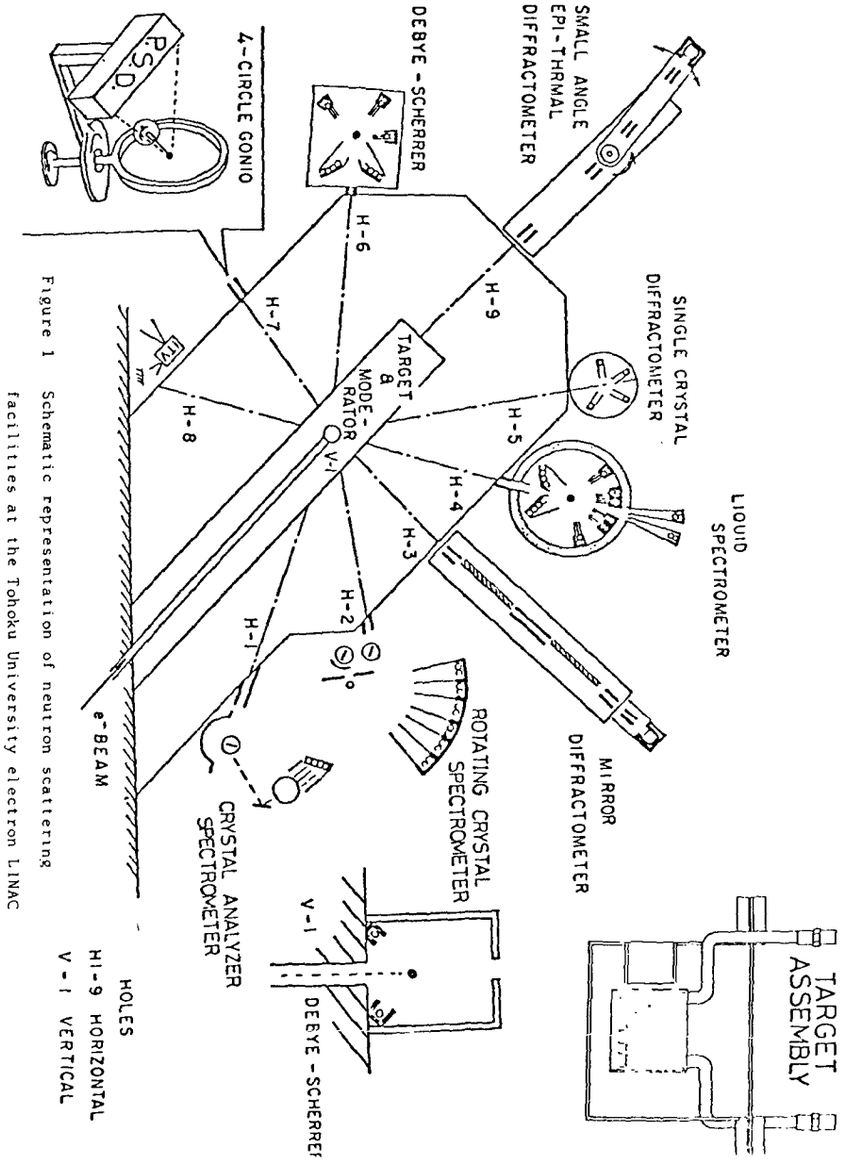

Figure 1 Schematic representation of neutron scattering facilities at the Tohoku University electron LINAC

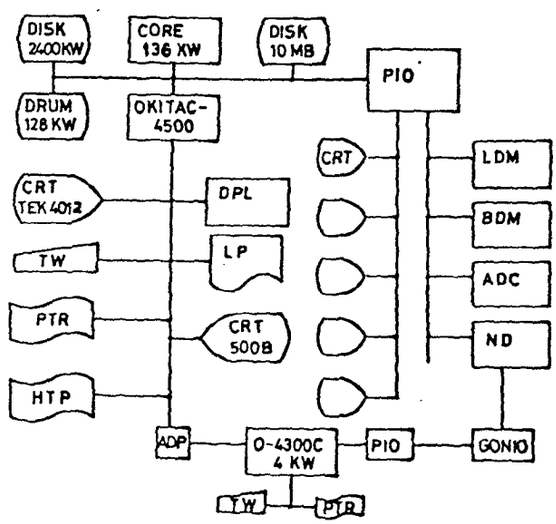

Figure 2 Block diagram of data acqusition system

Instrument Development at the Harwell Linac

Colin Windsor, Materials Physics Division,
AERE, Harwell, OX11 ORA, U.K.

The philosophy of the choice of spectrometers has been to concentrate on spectrometers able to use the epithermal range of neutron energies. The first seven spectrometers on the following list are ready, the others are in construction and will be installed during 1981. They are arranged on the two sides of the target shield as shown in the figure.

1) Total Scattering Spectrometer (TSS). A standard fixed angle diffractometer with a time focussed counter bank near 150°, of 0.12 steradian solid angle, and single counters in pairs at 90°, 58°, 35°, 20° and 10° which view curved boron carbide slits following the Debye-Scherrer cones. It has an incident flight path of 5.5 m and a scattered flight path of 0.46 m. The Q resolution $\Delta Q/Q = 0.01$; the useful Q range is from 0.6 to 60 $Å^{-1}$. The instrument is used to measure structure factors from ordinary and metallic glasses, molecular liquids, and liquids under pressure, and for phase diagram and time-dependent studies of diffraction patterns.

2) Back Scattering Spectrometer (BSS). A longer flight path of 12 m and a time focussed counter bank 2 m from the sample at 170° gives resolution $\Delta Q/Q = 0.003$, with solid angle of 0.056 steradians. The Q range available without frame overlap is from 5 $Å^{-1}$ to 100 $Å^{-1}$. The instrument is for powder diffraction to high spatial resolution, for Debye-Waller factor determinations, and for particle size and strain broadening measurements.

3) Active Sample Diffractometer (ASD). This simple diffractometer has a short incident flight path of 1.6 m so that the sample lies within the target cell inside the biological shield. The scattering angle is 155° to give a Q resolution $\Delta Q/Q \sim 0.02$. Active samples can be lowered into position through the shield from the target services room above the cell. It will be used for irradiated samples, samples containing unstable isotopes, and high fission cross-section samples.

4) Inelastic Rotor Spectrometer (IRS). This has a single nimonic rotor giving incident energy monochromatic neutrons in the 200 to 400 meV range. It has a large scattering angle range from 4° to 140° but its major counter bank is from 4° to 11° so as to reach energy transfers in the 50 to 150 meV range with low scattering vectors Q below 5 $Å^{-1}$ with $\Delta\hbar\omega/\hbar\omega = 5\%$ resolution. This enables vibrational spectrometry to be done with low multiphonon broadening and vibrational harmonic contamination. It also enables magnetic inelastic studies to be done within the limitation imposed by the form factor.

5) Constant Q Spectrometer (CQS). This crystal analyser spectrometer is for coherent inelastic studies using single crystal samples. It works with relaxed vertical collimation (60 x 10 mm^2 at the sample), and uses the MARX principle to obtain the energy scan. The germanium analyser is in transmission geometry so that the reflecting planes may be readily changed. The counter is a 50 element glass scintillator bank. At $|Q| = 4$ $Å^{-1}$, energy scans at a specified $\underline{Q}$ value are possible from 10 to 140 meV using Ge(511) planes. It will be suitable for high energy transfer phonon and magnetic excitation studies because of the good intensity and resolution of its incident neutrons.

6) Single Crystal Spectrometer (SCS). This is a development instrument constructed by the Rutherford Laboratory under Dr. Forsyth. Its basic counter array is a 32 element glass scintillator array covering scattering angles from 20° to 148° in the scattering plane. Later versions will include a secondary counter on the opposite side of the specimen which will test out two-dimensional position-sensitive detectors. It will be used for refinements of single crystal structures to high spatial resolution.

7) Resonance Detector Spectrometer (RDS). This development instrument has been constructed within a long vacuum pipe so as to allow low angle forward scattering with a total flight path of about 10 m. With a scattering angle of around 1° and a ^{238}U foil, neutrons are detected at 6.67 eV allowing energy transfers up to 1.2 eV with scattering vector $|Q| \sim 5$ Å^{-1}. γ rays from the foil will be detected by an intrinsic germanium detector with facility for γ ray energy discrimination. Initial studies will be on magnetic excitations.

8) Transmission Cross-section Spectrometer (TCS). This simple spectrometer is being operated in collaboration with Harwell's Nuclear Physics Division. It measures removal cross-sections over the range from 1 meV to 1000 eV. It uses converging-diverging geometry to allow good statistics with small samples. It will be used for basic nuclear data studies, for correction factors to diffraction studies, and also for test experiments on structure factor, vibrational spectra, and defect studies.

9) Liquids and Amorphous Diffractometer (LAD). This is a spectrometer for the Spallation Neutron Source (SNS) which will be installed on the Harwell Linac to relieve the load on total scattering studies until the SNS is operating.

10) High throughput Chemical Spectrometer (BFS). This is also an SNS instrument which will eventually be transferred to the SNS. It is a simple beryllium filter design with a long 12 m incident flight path and short 250 mm scattered flight path so as to allow reasonable incident energy resolution without precise definition of the scattered neutron energy. It will be used for vibrational spectroscopy studies.

11) Polarisation Filter Spectrometer (PFS). This is a total scattering spectrometer with full polarisation analysis constructed by the Rutherford Laboratory. Polarisation analysis will be done by two samarium absorption filters. At a fixed scattering angle of say 10° this will be used for the separation of magnetic from nuclear structure factors, and the separation of coherent from spin-incoherent diffraction patterns.

12) Small Angle Spectrometer (SAS). This is a development instrument. It has a velocity selector to give a $\Delta\lambda/\lambda \sim 10\%$ wavelength band over a 1 cm^2 beam area. A flexible scattered flight path area allows a 400 element position sensitive scintillator array with 1 cm^2 mesh to be placed up to 4 m away. Position analysis within a fixed time gate then allows small angle scattering with inelastic discrimination.

Data Collection

The data collection system is essentially complete. Each spectrometer has its own time-of-flight scaler and front-end computer (DEC 11V03 running on RT11) containing identical data collection programmes written in assembler code. These are linked by a relatively slow serial link to the hub computer containing the hard-copy, display and magnetic tape facilities. (DEC 11/40 with 112K core running on RSX). Communication with any experiment is through any of several terminals located in the computer rooms, experimental halls or offices. Each run is archived into a data-base system together with a header block of 256 words containing all information thought relevant to subsequent analysis. These are mostly stored on a large 60 M Byte disk. For each spectrometer, suites of FORTRAN programmes are being written to perform instant analysis of data. For example, automatic location of diffraction peaks, together with their widths and intensities, is already possible. Also the computation of the constant Q scan from the Constant Q Spectrometer can already be done automatically.

Figure 1. The Harwell Linac Condensed Matter Cell

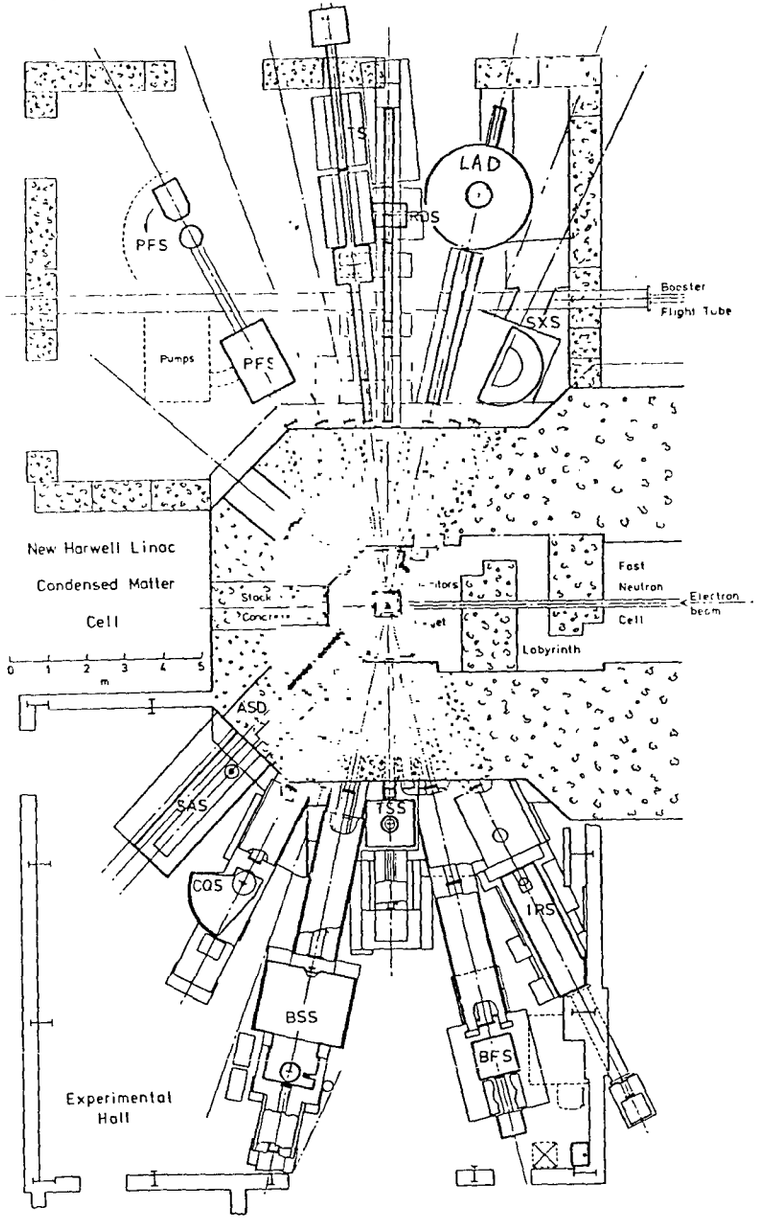

The Phasing of Fast Mechanical Neutron Beam Choppers to the SNS

T J L Jones and J H Parker
Neutron Division, Rutherford and Appleton Laboratories

1 Introduction

The need to produce a 1 μS (FWHM) pulse of 1 eV neutrons over a beam aperture of 50 mm x 50 mm with a phase stability of ± 0.3 μs with respect to the SNS neutron pulse on the High Energy Inelastic Spectrometer (HET) is the most demanding requirement for any of the SNS choppers. Our chopper development and testing programme has therefore been largely directed towards satisfying this specification.

A Fermi-type fast chopper spun at 36000 rpm on a modified Harwell Mk VIII spinning head and controlled by a new digital electronic control and drive system designed at the Rutherford Laboratory has been developed for this purpose. In order to monitor the phase stability, an optical transducer (OPTO) which senses the actual motion of the top of the chopper rotor body, was mounted within the vacuum spinning tank. Whereas normally chopper spinning systems are synchronised to crystal clocks, one of the proposed SNS operating modes ("locked to the mains") required that an investigation be made into the possibility of operating synchronised to the machine at ∿ 50 Hz.

2 Chopper Development

Two prototype chopper rotors have so far been produced. These consist of a 120 mm dia cylindrical body machined from a solid block of aluminium alloy and are pierced diametrically by a 56 mm x 52 mm aperture which contains the slit package. The slit package is an assembly of ∿ 50 neutron opaque 'slats' cut from a sheet of a matrix of boron fibres diffusion-bonded into aluminium; the slats are interleaved with neutron transmitting 'window frame' slits etched from 0.4 mm thick aluminium alloy foil. The two rotors differ in that one set of slats is of a single ply boron/aluminium matrix whilst the other is a triple ply boron/aluminium alloy matrix with a 90° lay up. Profiled cheek plates are used to curve the slit package to a cylindrical radius of 1.84 m which at 36000 rpm optimises the transmission of the rotor

for 1 eV neutrons. Both these rotors have been successfully spun for several weeks at their design speed and have been spun at speeds producing up to 25% overstress for short periods without any measureable change of parameters. An experimental programme to test their neutron transmissions and pulsing properties will commence when the new Harwell electron linac comes into operation.

Mechanical aspects influencing the Phase Stability of the Rotor when operated from a Fixed Frequency Source

It was decided at the outset of our chopper development programme to use the Harwell Mk VIII spinning head as the drive for our chopper rotors. Consequently much of the experience and procedures developed at Harwell were transfered directly into our programme. In general this has proved to be entirely satisfactory however a much more precise phase stability is needed for the HET application (± 0.3 μs) than has been customary and this has necessitated making several modifications. These are as follows:

i) Modifications to the Damper Mechanism

The drive from the spinning head is coupled to the chopper rotor by a flexible steel shaft 2 mm diameter and 200 mm long. This shaft traverses a dynamic oil vacuum seal and a sliding-plate damper mechanism. The function of the latter is to limit shaft whirls which develop due to imbalances and resonances of the shaft and chopper drive during the spin-up to its operating speed.

The Harwell damper, which is essentially a brass disc frictionally constrained between two rubber 'O' rings, did not give a consistent action over its lifetime and tended to stick and become non-central when the rotor was at its operating speed. This caused a residual bend in the shaft and led to precession of the rotor. These shortcomings have now been rectified by a) having a more precise tolerance in the hole linking the disc to the shaft, b) the substitution of PTFE for rubber in the 'O' rings and, c) by adding a wave-spring washer to provide compression.

ii) Dynamic Balancing of the Chopper Rotors

Although some Harwell chopper rotors were dynamically balanced during manufacture it was generally found adequate simply to check their balance

statically by rolling them on precisely levelled knife edges. However, the replacement of the Harwell magnetic pick-up coil at the top of the spinning head by OPTO sensors, which measured directly the actual motion and phasing of the chopper rotors revealed that, although grossly stable, statically-balanced rotors still had small imbalances which caused precessional and sometimes also vibrational motions to occur at the end of the flexible drive shaft. These sometimes resulted in phase variations of several microseconds with a periodicity ranging from less than one second to several tens of seconds.

To eliminate these precessional motions our chopper rotors are now dynamically balanced on specially adapted machines to a precision 5 times better than that used in the Harwell procedure. We believe that by refining our mounting and driving techniques the balancing will be further improved.

iii) Coupling of the Chopper Rotors to the Spinning Head

Zero precession can only be achieved when the axis of rotation of the rotor in its assembled spinning configuration is concentric with the axis of balance as established in ii) above. This requires that each of the mating surfaces between the flexible shaft, split collet, conical seating, threaded boss and oil-thrower nut which join the chopper rotor to the spinning head should be manufactured to close squareness and concentricity tolerances.

The Harwell specified tolerances were not sufficiently stringent to ensure that this condition was adequately fulfilled for our needs. We are currently modifying the collet design and retolerancing to meet the upgraded phase stability requirement for the HET spectrometer.

4 Results from Fixed Frequency Operation

When the above conditions are satisfied and the rotors are driven at a fixed frequency derived from a crystal clock using the electronics described in the following paragraphs, it has been possible to achieve long and short term phase stabilities better than ± 0.3 μs.

5 Drive and Control Electronics

The spinning head consists of a hysteresis motor mounted vertically running in air bearings and supported by a magnetic thrust bearing. Electronic circuits are therefore necessary to produce a three phase supply of the correct frequency together with some means of rotating the phase of the drive to align the rotors to the required angle. In general several rotors systems are needed and each must be capable of retaining a fixed phase relationship with a primary master timing pulse (50 Hz) to ± 0.3 μs at spin speeds of 600 Hz. This requirement even at fixed operating frequencies needed careful design to eliminate, as far as possible, all the static errors present and a servo loop was used to maintain its positional accuracy over long periods. Figure 1 shows a block diagram of the angular reference required for the digital system. A primary pulse frequency multiplier and time-of-flight programmable delay is also included in the diagram. The delay sets the time from beam extraction to the rotor open instant. The angular reference is a high speed phase locked loop which in effect divides each rotation of the chopper into 10,000 parts. The output is then a scalar in BCD which is used as anangular positional reference for a circulating store in the digital control loop. The Voltage Controlled Oscillator (VCO) output of 10,000 pulses per master pulse is used to develop reset pulses for a ROM based three phase static alternator to drive the hysteresis motor.

The rotor phase controller (Figure 2) is a phase locked servo loop. The demand position is developed from the scaler and in this system can be selected from 1 of 1000 points by switches. The demand is therefore both a velocity and position reference. A pulse developed by an optical transducer on the chopper is then compared to the demand position in a phase comparator and the error is converted to a pulse train which clocks a counter either up or down for an advance or retard error. The up/down counter is compared to the scalar and the coincident pulse modifies the phase of the drive in the static alternator to the hysteresis motor in the direction necessary to eliminate any error. The increments of correction are 1/10,000 of a chopper rotation period at an adjustable rate dependent on the system requirements. In order to make the system operate to the high limits of accuracy required all switching circuits are designed for synchronous operation. The phase characteristics of the motor load

combination are that of a second order system with almost zero damping, compensation networks are therefore included to damp out unwanted torsional oscillations. An analogue signal proportional to the low frequency instabilities of the rotor is developed and, after compensation, is fed back to the digital control loop via a voltage controlled phase shift circuit. The compensation networks required depend on the system characteristics ie chopper, drive power, gain etc.

The static alternator has sine wave programmed read only memories, one set per phase, clocked by resetable counters. The rotor controller provides the necessary pulses to form three phases, 120 degrees apart. Rotation of the phase of the drive is also controlled by the timing of the ROM counter reset pulses. The digital output from each ROM is changed to an analogue signal in an 8 bit digital to analogue conveter which is then fed to conventional power amplifiers and transformed to the correct operating voltage for the hysteresis motor. Using 100 steps per cycle with the amplitude set by 8 bits produces an adequate sine wave.

6 Operation with a Variable Input Frequency

In order to assess the performance as a 50 Hz mains synchronised system a phase locked loop with a long low pass filter time constant was connected to raw mains, effectively removing all rapid frequency changes. The maximum phase error was checked and generally found to be within ± 100 μs with occasional errors of ± 300 μs. The system was then operated from the output of the phase locked loop and the result shown on the chart recording (Figure 3) was obtained. Counters were also used to check the stability of the system and indicated that the chopper remained within ± 0.5 μs of a desired positon for 90% of the total time of the test and approximately 100% of the counts were within a ± 1 μs error. These tests were carried out using a 3.7 kg Fermi chopper which will normally be used on the SNS High Energy Inelastic Spectrometer.

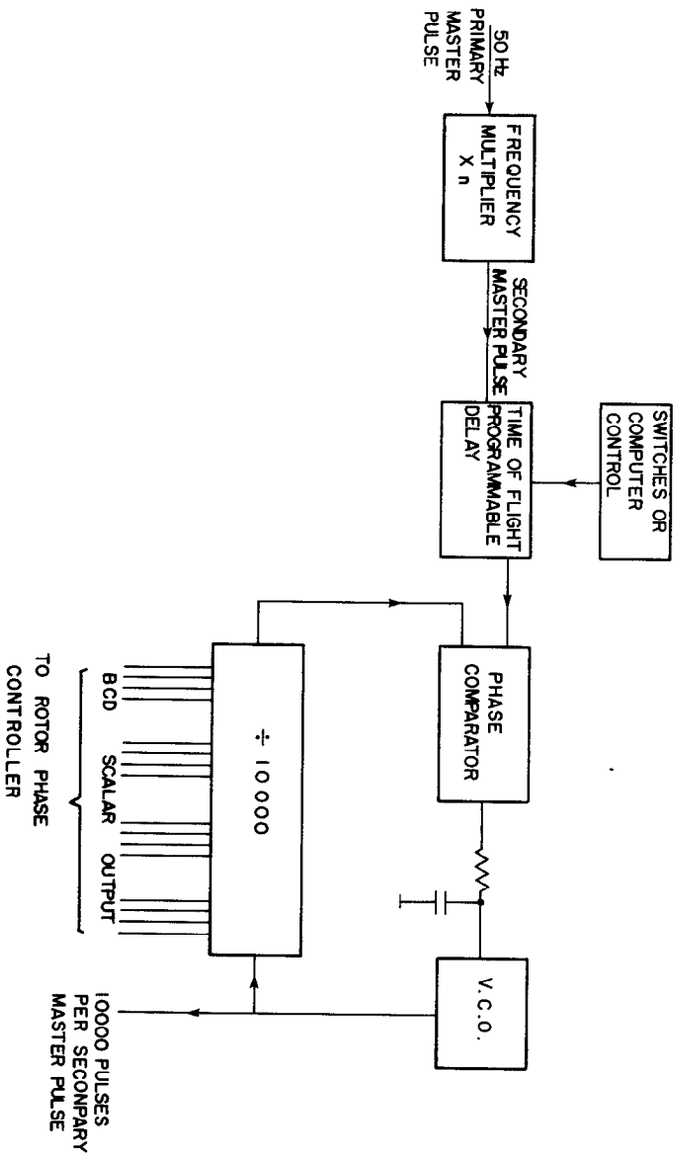

FIG. 1. SCALAR

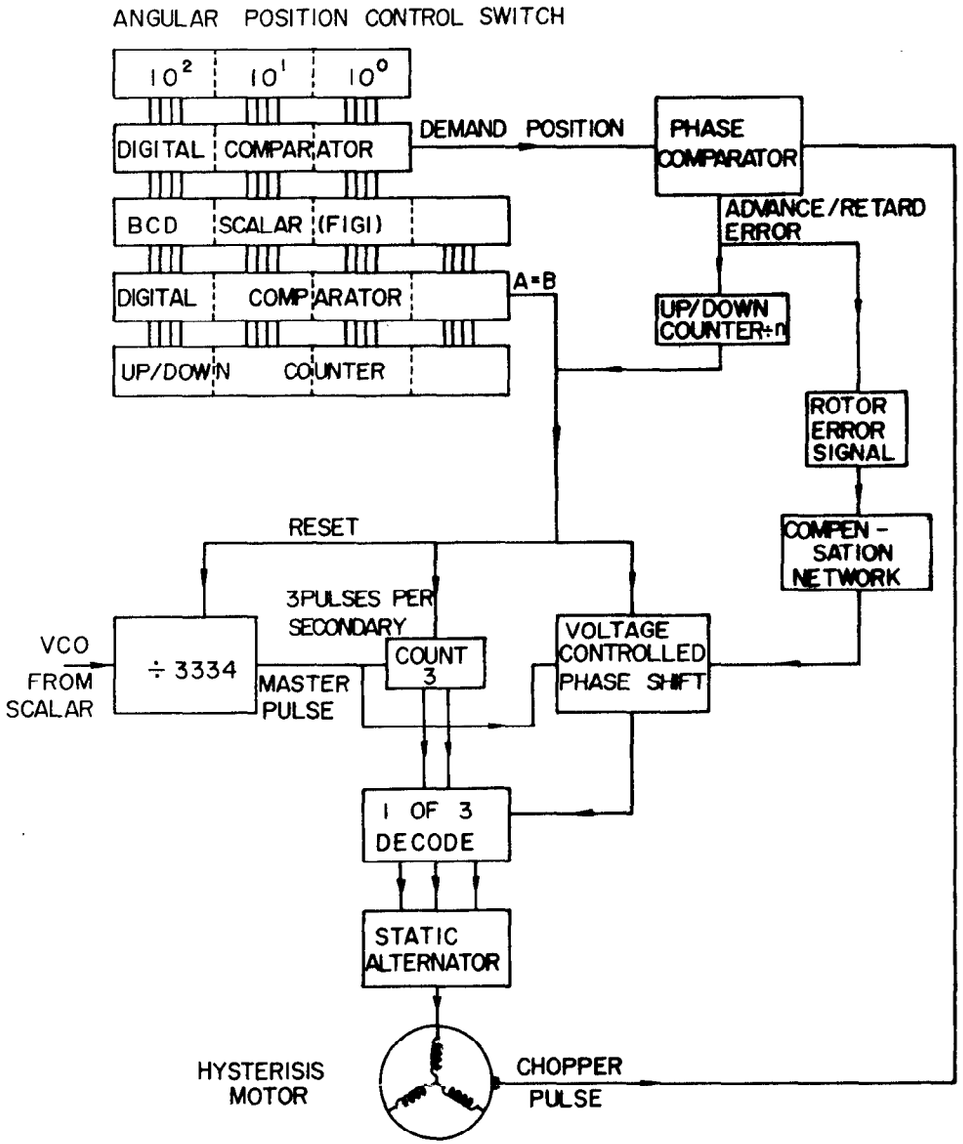

FIG. 2. ROTOR PHASE CONTROLLER

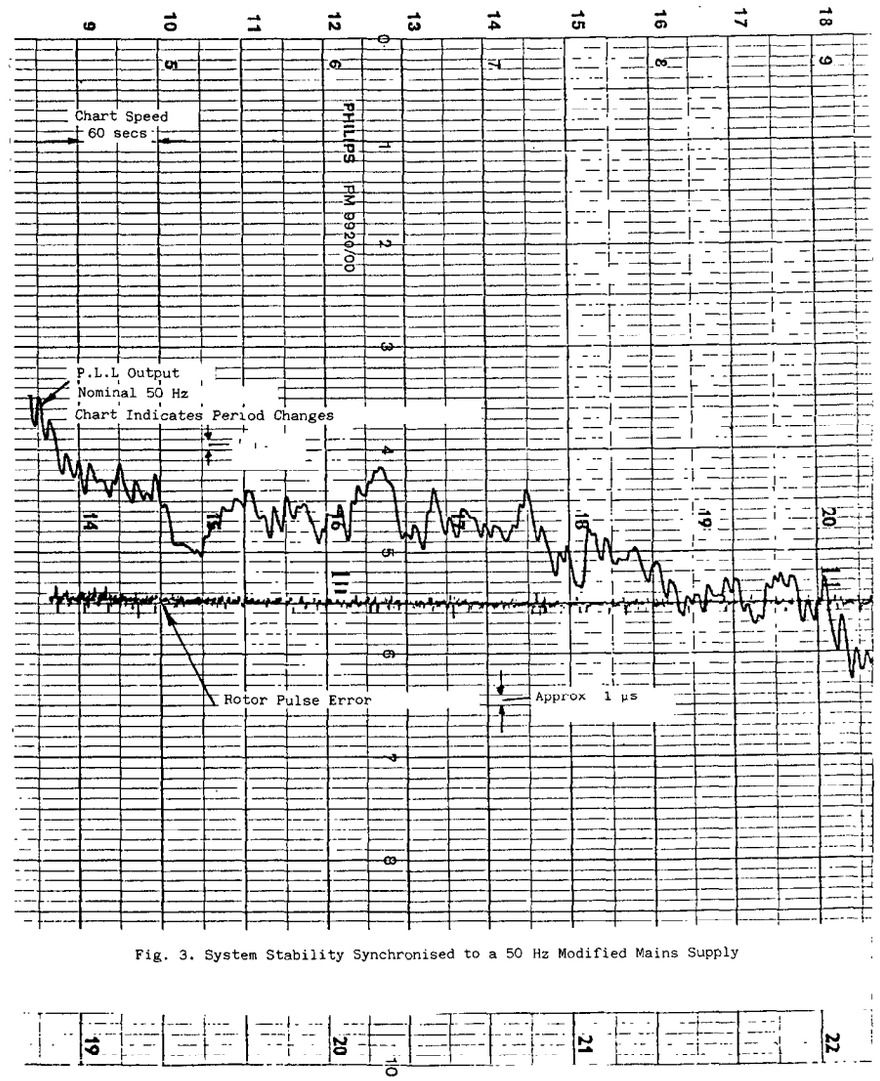

Fig. 3. System Stability Synchronised to a 50 Hz Modified Mains Supply

Neutron Guides

W G Williams and J Penfold
Neutron Division, Rutherford and Appleton Laboratories

1 Introduction

A Working Group was set up to investigate the implications of using guides on the Rutherford Laboratory SNS in July 1978; its first report was published in November 1979[1]. The main differences between steady state and pulsed source neutron instruments are that the latter necessarily view smaller moderator areas, and also that their lengths are primarily determined by time-of-flight resolution requirements. Both these factors affect the design of guides. Our study to date has concentrated on optimising the design of guides for two typical pulsed source instruments viz

(a) a 100 m long high resolution backscattering powder diffractometer (HRPD) which uses both thermal and cold neutrons, and

(b) a 40 m long high resolution backscattering inelastic spectrometer ('IRIS) which uses cold neutrons.

The properties of the various guide arrangements possible for these instruments were predicted using a new Monte Carlo code[2]. This paper summarises some of the most important conclusions of the Working Group up to the present.

2 Computer Simulation - MCGUIDE

It is only in the case of continuous straight guides that analytical expressions give an adequate description of real (ie imperfect) three-dimensional guides. All SNS guides are circularly curved and of length greater than the direct line-of-sight and the Monte Carlo code MCGUIDE[2] was written to simulate their behaviour. The code is very versatile and includes the following features:

a) the simulation of combinations of straight, curved, and tapered guide sections,

b) the provision of spaces between guide sections for other instrument components, and

c) allowance to be made for reflectivity losses due to surface waviness.

It has proved particularly valuable in predicting the spatial asymmetry in beams from curved guides and the effects of guide losses. The code has been extensively tested and it has been used to obtain most of the results presented in this paper.

3 Guide and Sample Illumination

The moderator areas at reactor sources (eg ILL) are generally large in comparison with guide dimensions and relatively little attention has been paid in the past to matching the source and guide areas so as to ensure complete illumination. Source-guide entrance matching is however very important for longer wavelength neutrons where the guide's solid angle of acceptance is large, and for cold sources which have relatively small source areas it is apparent that complete illumination is not always achieved at reactor installations. At accelerator based neutron sources, where the moderator areas are even smaller, incomplete illumination can occur even in the thermal neutron range unless the guide entrance is placed sufficiently close to the source.

The problem can be treated geometrically in one plane with the aid of the ray diagram shown in Figure 1a. The moderator (dimension m) illuminates a straight guide (dimension g) which transports the neutrons to the scattering sample (dimension s). The moderator to guide entrance distance is L_i, and the exit to sample distance is L_e. In most cases of practical importance for pulsed sources the condition $m > g > s$ applies.

We shall be concerned with nickel guides in which we assume that total reflection occurs at all glancing angles γ less than the critical glancing angle $\gamma_c = 0.0017\lambda$ rad; λ is the neutron wavelength in Å. Complete guide illumination occurs if the λ-dependent maximum guide solid angle $4\gamma_c^2$, when projected from any point on the guide entrance to the plane or the source, is completely covered by the source area. Complete sample

illumination occurs if the maximum guide solid angle $4\gamma_c^2$, when projected from any point on the sample to the guide exit plane, is completely covered by the guide exit aperture.

Illumination matching of the guide at a particular wavelength λ occurs when the rays joining the extreme edges of the moderator and the guide entrance are inclined to the guide axis at the critical glancing angle γ_c for that wavelength. Illumination matching of the sample follows the same behaviour (see Figure 1a). For nickel guides the matching conditions are expressed as follows:

$$0.0017\lambda_M = \frac{(m-g)}{2L_i}, \text{ and} \quad (1)$$

$$0.0017\lambda_M = \frac{(g-s)}{2L_e}. \quad (2)$$

These equations may be combined to give the complete matching condition for nickel guides:

$$\lambda_M = 294 \frac{(m-s)}{(L_i+L_e)} \quad (3)$$

This matched condition is conveniently represented by the ray diagram shown in Figure 1b. In any practical situation m is fixed by the source (eg m $\sim$ 10 cm for a moderator on the Rutherford Laboratory spallation neutron source), s is fixed by instrument resolution requirements and λ_M is selected to correspond to the critical glancing angle at the longest wavelength at which complete illumination is required. A selection of these three parameters fixes (L_i+L_e), the combined moderator-guide entrance and guide exit-sample distances. The value of the guide dimension g can be selected according to the limiting rays in Figure 1b for either fixed L_i or fixed L_e.

Table 1 shows calculated values for L_i and L_e for different values of the guide dimension g and at different wavelengths, but at constant (m-s) = 7 cm.

λ_M (Å)	(L_e+L_i) (m)	g = 4 cm		g = 5 cm		g = 6 cm	
		L_i(m)	L_e(m)	L_i(m)	L_e(m)	L_i(m)	L_e(m)
1	20.6	17.65	2.94	14.70	5.89	11.77	8.82
2	10.3	8.83	1.47	7.35	2.94	5.88	4.41
3	6.86	5.88	0.98	4.90	1.96	3.92	2.94
4	5.15	4.41	0.74	3.68	1.47	2.94	2.21
5	4.12	3.53	0.59	2.94	1.18	2.36	1.76
6	3.43	2.94	0.49	2.45	0.98	1.96	1.47
8	2.58	2.21	0.37	1.84	0.74	1.48	1.10
10	2.06	1.77	0.29	1.47	0.59	1.18	0.88

Table 1 Calculated L_i and L_e values at the matched condition for different guide dimensions and wavelengths but fixed moderator and sample dimensions.

For $\lambda<\lambda_M$ the gain factor G in the neutron flux transported by a straight guide over that observed at the end of a non-reflecting collimator is simply the ratio of the 'conducting' solid angle of the guide to the solid angle subtended by the source at the exit of the guide. This is given (for nickel guides) by:

$$G = 1.15 \times 10^{-5} \left[\frac{\lambda L}{m}\right]^2, \quad (4)$$

ie the gain at wavelengths $<\lambda_M$ is proportional to λ^2.

For $\lambda>\lambda_M$ the gain factor G continues to increase up to a saturation wavelength λ_s which is the longest wavelength that can be reflected by the guide at the extreme reflection angles connecting the bottom (or top) of the moderator to the top (or bottom) of the guide. λ_s defines the wavelength at which no further gains ensue. This effect is demonstrated in curve B of Figure 2 where the results were obtained using the Monte Carlo simulation code MCGUIDE.

4 Beam Asymmetry in Curved Guides

One of the problems associated with curved guides is the non-uniform radial intensity distribution at their exits. This non-uniformity is wavelength

dependent, and is particularly pronounced at wavelengths less than the characteristic wavelength λ^*[†] where the only mode of neutron transport is by garland reflections on the outer wall of the guide.

For a perfect rectangular cross-section curved guide which is uniformly illuminated, the radial distribution at a distance greater than the 'line-of-sight' may be derived analytically:

$$T = \cos^{-1}\left\{\frac{1 - \gamma_c^2/2}{1 - (f\gamma^{*2})/2}\right\} / \gamma_c = \left[1 - f\left(\frac{\gamma^*}{\gamma_c}\right)^2\right]^{\frac{1}{2}}, \qquad (5)$$

where T = transmission relative to that of a single straight guide, and
f = fractional distance across the guide exit aperture measured from the outer wall.

The variation of T with f at various values of λ/λ^* (= γ/γ^*) is shown in Figure 3.

It is possible to reduce this asymmetry by adding a straight guide section as the last component in a curved guide system. However, there are no analytic descriptions of curved-straight systems, and to investigate the length of the straight section required for a uniform distribution the computer code MCGUIDE was employed to study a number of curved/straight guide systems. This exercise revealed an interesting effect in curved/straight guide combinations which, while qualitatively predictable from simple guide theory, would be difficult to quantify. This effect may be described as a transverse wave which arises in the following way:

For neutrons with wavelengths $\lambda < \lambda^*$, the radial distribution at the end of the curved section is asymmetric and bunched at the outer guide wall. The resulting angular/space correlation gives a dispersing transverse wave which travels down the guide. Neutrons thus appear to 'wash' from one side

[†]The properties of a circularly curved guide are determined by a characteristic angle γ^* - the angle between a line-of-sight and the tangents at the start or finish of the line-of-sight. To good approximation $\gamma^* = (2a/R)^{\frac{1}{2}}$ where 'a' is the guide width in the plane of curvature and R is the radius of curvature. λ^* is the critical wavelength at the characteristic angle ie $\lambda^* = \gamma^*/0.0017$ for nickel.

of the guide to the other. The important fact to emerge is that, for a particular wavelength, there are points along the straight sections of the guide at which the transverse distribution is more uniform than at other points further down the guide. Furthermore, although increasing the straight section at the end of a curved guide generally results in an improvement in beam uniformity, there are also positions along the straight section which give rise to a high non-uniformity at particular wavelengths. These points are illustrated in Figure 4 where the transverse distribution of neutrons with λ = 1.0 Å in a 8 cm x 2.5 cm guide have been plotted at 70 m, 80 m, 90 m and 100 m along curved/straight guide systems. In this example the guide is curved (with R = 18 km) from 1 m to 60 m, the line-of-sight distance.

However, in deciding the 'best' straight section length for a particular instrument it is the uniformity at the sample position which is important. This can be quite different from that at the guide exit since, for example, neutrons could be uniformly distributed across the guide exit while having a non-uniform angular distribution. This effect has been studied for the HRPD instrument (Figure 5) for different aperture widths w and straight section lengths using MCGUIDE. Three guide widths were chosen (w = 2.0, 2.5 and 3.0 cm) and for each width a radius was chosen so that line-of-sight occured at the end of a 60 cm curved section. The guide parameters were as follows:

w(cm)	R(km)	λ^*(Å)	L_o(m)
2.0	22.5	0.78	60
2.5	18.0	0.98	60
3.0	15.0	1.18	60

A series of 10 m straight sections were then added, and the intensities on two halves of a 2 cm wide sample (at 2 m from the guide exit) were simulated for total guide lengths of 70, 80, 90 and 100 m. The results for a guide width w = 2.5 cm are shown in Figure 6 for λ = 0.6, 0.8, 1.0, 1.2, 1.4 and 1.6 Å. This illustrates that 'nodes' occur in the intensity distributions and that as λ decreases, the straight section must be longer for equalisation of the beam. From these results it would appear that a

final straight section of length 35 - 40 m would prove adequate at all the wavelengths for the HRPD guide.

5 Guide Losses

Principal loss mechanisms that we have considered are those due to abutment errors and surface waviness. Analytic calculations for both these losses have been performed; the MCGUIDE simulations were consistent with these calculations.

A detailed treatment of abutment errors has been reported[3]. Figure 7 shows the magnitude of the transmission losses calculated for the HRPD guide as a function of wavelength at three values of the abutment error σ. These losses are tolerable for $\sigma < 0.0025$ cm - a value which is technically feasible.

The other loss which has been thoroughly investigated is that due to surface waviness[4], particularly in the context of relaxing the surface quality of the guide sections nearest the source. Following reports of radiation damage in the ILL neutron guides[5], it was decided to study the effect of using more radiation-resistant mirror materials with a more inferior surface quality than glass (eg polished metals) as the early guide sections.

Any losses incurred this way are more crucial for the 'IRIS guide (Figure 8) which uses long wavelength neutrons and needs to start at approximately 2 m from the source to ensure complete illumination. Figure 9 shows the % loss in intensity computed as a function of wavelength for different values of surface waviness in guide section 1 (in-shutter) of 'IRIS (see Figure 8), where a 0.0005 rad waviness is assumed to give zero loss[6]. Surface waviness is treated in MCGUIDE by randomising the local shape at each reflection point about an angle $\pm \beta$ in two dimensions. Further calculations showed that a relaxation of the surface waviness of all the "in-shield" sections of the 'IRIS guide from 10^{-4} to 10^{-3} radians causes intensity losses < 5%. It was concluded that inferior surface quality guide sections could certainly be used in the shutter without significant losses in flux.

6 Guide Bunching

A study has been made of the implications of multiplexing neutron guides on the SNS[7]. The obvious advantage of multiplexing beam holes or guides

in what is normally a single neutron beam sector around the source is one of neutron economy. The main disadvantages are i) a weakening of the shielding, ii) instrument crowding and iii) the need for additional beam shutters per sector, so that the instruments can be used independently.

A major constraint on the design of pulsed source neutron scattering instruments arises from the need to utilise disc choppers both to prevent frame overlap and to define the incident energy window. Since the efficiency of a disc chopper increases with its diameter it is desirable that these are made as large as possible. The disc chopper design consequently leads to a minimum separation of adjacent neutron beams. The use of disc choppers close to the source (5 - 12 m) is particularly important for instruments situated on long guides (25 - 100 m). It was originally believed that a guide bunch of three could be incorporated into a SNS instrument sector (nominally $\sim 13^{\circ}$) without undue congestion[1]. Further detailed design work has shown that this is not advisable. The present policy being adopted on the SNS is that the multiplexing of guides should be limited to guide pairs.

7 Current Development Work

Several 1 metre long prototype guide sections are now being commercially produced in the UK. These are due to be delivered at the Rutherford Laboratory early in 1981 and will be tested optically[8]. A survey is being made of the commercially available glasses that can be used in neutron guides. The final choice of the glass will depend on the results of neutron irradiation tests carried out under conditions designed to simulate $\sim$ 5 years of SNS use.

References

[1] "Neutron Guides on Pulsed Sources" - C J Carlile, M W Johnson and W G Williams, Rutherford Laboratory Report RL-79-084.

[2] "MCGUIDE: A Thermal Neutron Guide Simulation Program" - M W Johnson, Rutherford Laboratory Report RL-80-065.

[3] M W Johnson - Rutherford Laboratory Guides Working Party, GWP/4/80, "Losses in neutron guies due to abutment errors".

[4] M W Johnson - Rutherford Laboratory Guides Working Party, GWP/3/80, "Transmission losses in initial neutron guide sections: some analytic results".

[5] P Ageron, P Blum - ILL, private communication.

[6] J Penfold - Rutherford Laboratory Guides Working Party, GWP/5/80, "Futher calculations of the neutron flux dependence on the surface quality of the "in-shield" sections of the 'IRIS guide".

[7] W G Williams, C J Carlile - Rutherford Laboratory Guides Working Party, GWP/1/80, "Beam hole multiplexing and possible uses for restricted access neutron beams on the SNS".

[8] C J Carlile, J Penfold - Rutherford Laboratory Guides Working Party, GWP/6/80, "Proposal for testing neutron guides".

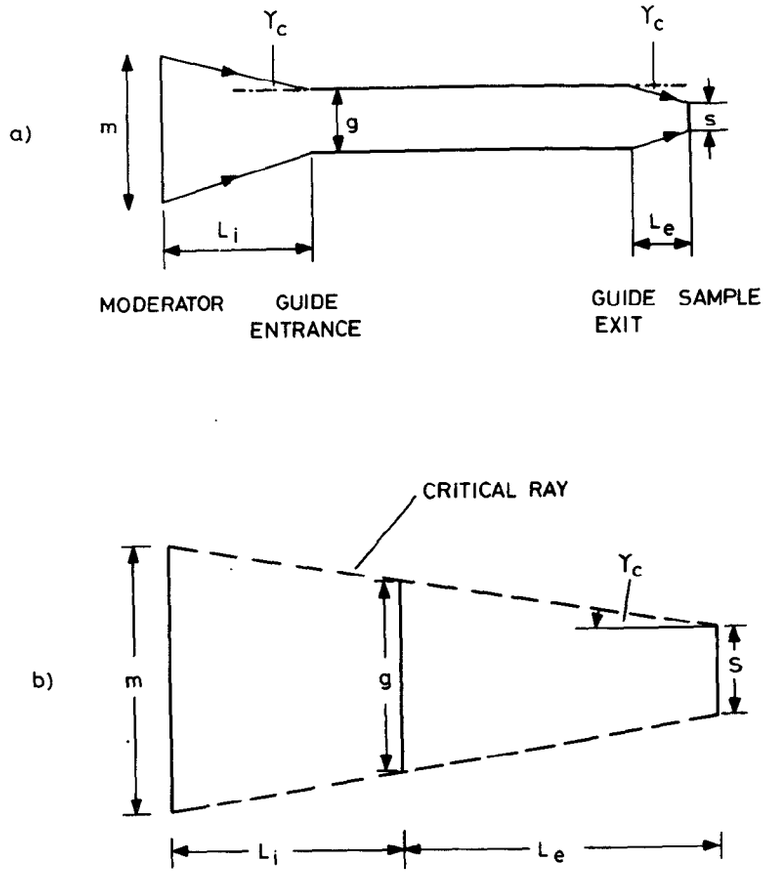

FIGURE 1. ILLUMINATION MATCHING OF GUIDE WITH MODERATOR AND SAMPLE

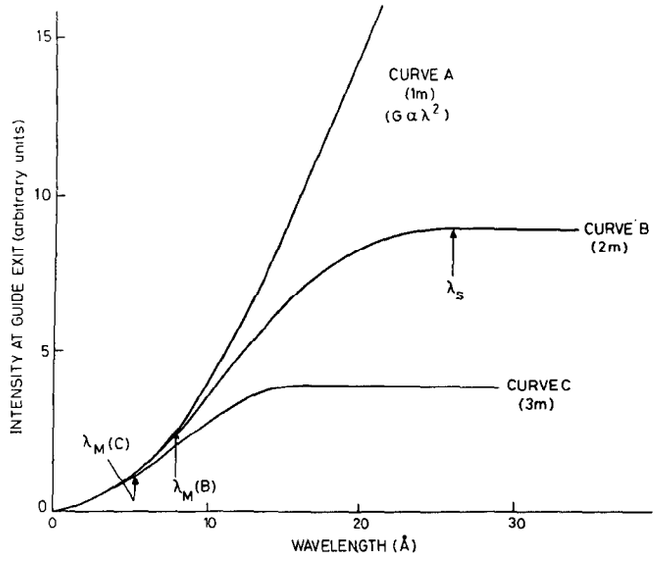

FIGURE 2. INTENSITIES AT EXIT OF STRAIGHT GUIDE AT 12m FROM SOURCE FOR DIFFERENT MODERATOR - GUIDE ENTRANCE DISTANCES

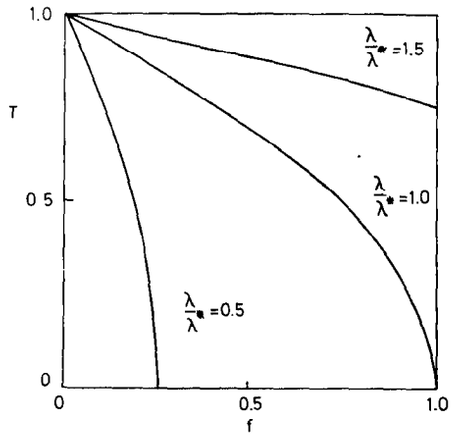

FIGURE 3. CURVED GUIDE TRANSMITTANCES (T) AS A FUNCTION OF FRACTIONAL DISTANCE ACROSS THE GUIDE APERTURE (f) FOR DIFFERENT λ/λ^*

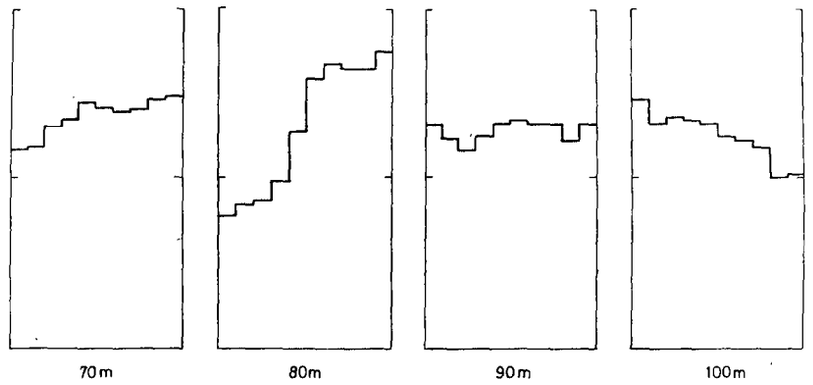

FIGURE 4. TRANSVERSE NEUTRON DISTRIBUTIONS AT $\lambda = 1$Å IN A (2.5cm x 8cm) CURVED - STRAIGHT GUIDE WITH A CURVED SECTION LENGTH $L_c = 60$m AT DIFFERENT POINTS ALONG THE STRAIGHT SECTION

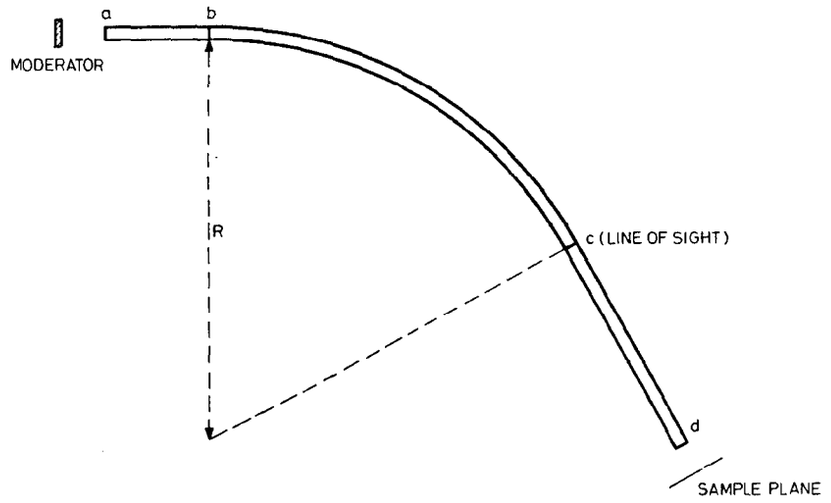

FIGURE 5. ELEMENTS IN GUIDE SYSTEM FOR HRPD INSTRUMENT

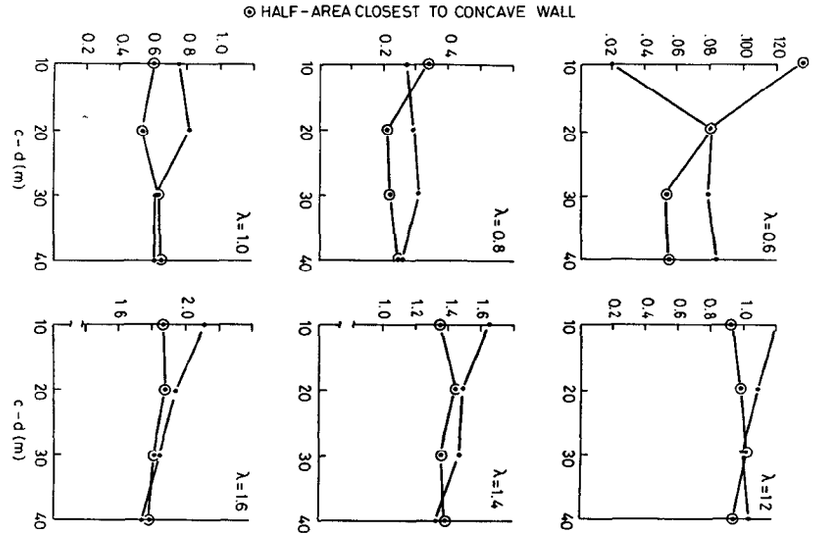

FIGURE 6. INTEGRATED INTENSITIES ON TWO HALVES OF SAMPLE AREA FOR 10m, 20m, 30m AND 40m STRAIGHT SECTIONS ON THE HRPD GUIDE; $0.6 < \lambda(\text{Å}) < 1.6$

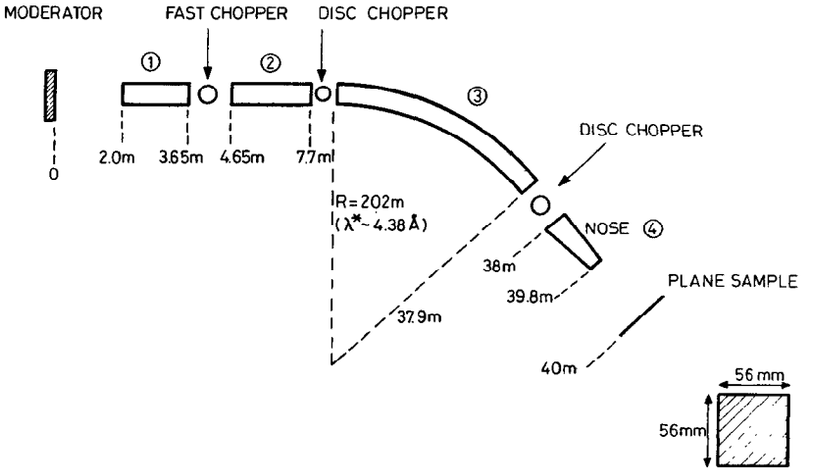

FIGURE 8. SCHEMATIC OF GUIDE SYSTEM FOR THE HIGH RESOLUTION QUASIELASTIC SPECTROMETER 'IRIS

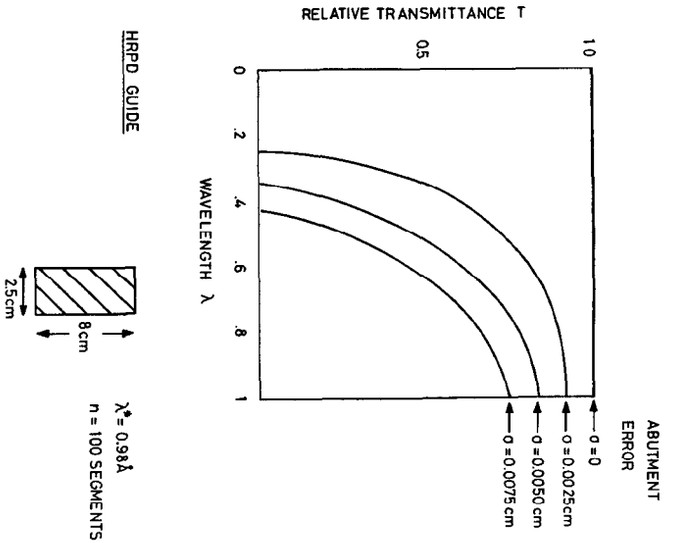

FIGURE 7. EFFECT OF ABUTMENT ERROR ON TRANSMITTANCE OF HRPD GUIDE.

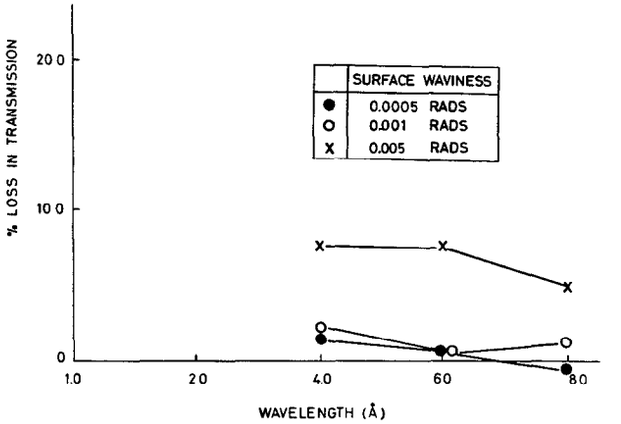

FIGURE 9. % LOSS OF INTENSITY IN IRIS GUIDE THROUGH VARYING THE SURFACE QUALITY IN THE FIRST 1.65m SECTION

Characteristics of KENS Cold Neutron Guide Tube

J. Mizuki, Y. Endoh, Y. Ishikawa and S. Ikeda*

Tohoku University

Sendai, Japan

* National Laboratory for High Energy Physics

Tsukuba, Japan

In the KENS facility three guide tubes view the cold neutron source and transport cold neutrons to the cold neutron experimental area. The spectrometers SAN and TOP have been positioned at the end of guides C_1 and C_3 and a high resolution spectrometer will be soon installed at the exit of guide C_2.

As has been previously noted in KENS Report I[1], these guide tubes consist of two parts. A straight section, 3.5 m long and with a cross section of 3×5 cm^2 is installed inside the biological shield. There is then a long curved section of radius of 830 m and cross section 2×5 cm^2 which is followed by a straight tube with about 0.4 m gap. The curved sections of guides C_1 and C_3 are 11 m long, while that of C_2 is 18 m. The curvature corresponds to a cut-off wavelength of 4 Å. The direct view distance is 14.47 m for each guide tube. A tail cutter is situated in the gap between the straight and curved sections of each guide tube in order to prevent the passage of neutrons with wavelengths longer than 12 Å. A film of Ni metal about 2000 Å thick evaporated onto 3 mm thick float glass was used as the neutron reflector.

The spatial distribution and the energy dependence of the flux of cold neutrons at the guide exits were directly measured. The

transmittance of the guide tube was also determined and the results of these measurements are briefly outlined below.

§2. Measurement of I(λ)

The neutron spectrum or the wavelength dependence of the neutron intensity, I(λ), was determined at the exit of guide tube C_3 by measuring the incoherent scattering from vanadium metal. The result is shown in Fig. 1. A two dimensional Monte-Carlo calculation had suggested that the wavelength dependence of the neutron intensity, I(λ), would be given by $\frac{1}{\lambda^4} \exp\left(-(\lambda_T/\lambda)^2\right)$ as shown by the broken line in the figure. The observed intensity distribution, however, is significantly lower than that calculated over whole wavelength range, suggesting that the two dimensional calculation is an oversimplification.

The intensity distribution, $I^0(\lambda)$ at the cold neutron source was measured at the exit of the beam tube C_4 which views the cold moderator source directly, and the result is plotted as a dotted line in Fig. 1. The triangles in the figure represent the intensity distribution at the exit of the straight guide tube estimated from $I^0(\lambda)$ by taking into account only the geometrical configuration of the guide tube. The estimated values agree approximately with the experimental value despite the simplified nature of the calculation.

The spatial distribution of the neutron intensity along the horizontal axis was also measured at the exit of the C_3 guide tube using a small (0.5×60 mm^2) slit in a Cd metal shied before a He^3 counter The results measured at four different position are displayed in Fig. 2. Our results show that the spatial distribution is practically uniform

for wavelengths longer than 6 Å, but the intensity of neutrons at shorter wavelengths is significantly reduced at the inner side of the curved guide. These results are in accord with our previous calculation.

§3. Absolute neutron intensity at the guide exits

3-1. Measurement by the activation of Au foils

The absolute intensity of cold neutrons at both the entrances and exits of the guides were determined by the activation of Au foils. The size of these foils was 10×10×0.1 mm^3. The Au foils were exposed for ten minutes, and absolute incident neutron intensity was then given by the saturation activity of Au divided by the absorption cross section, σ_a. The average absorption cross section $\langle\sigma_a\rangle$ was estimated from the experimental result of $I(\lambda)$, according to

$$\langle\sigma_a\rangle = \frac{\int_2^{16} \sigma_a(\lambda) I(\lambda) d\lambda}{\int_2^{16} I(\lambda) d\lambda}.$$

The value $\langle\sigma_a\rangle$ thus calculated was 317×10^{-24} cm^2. The derived value for the absolute neutron intensities are given in Table 1.

Table 1 Absolute Neutron Intensities I_0

Guide tube	I_0 (n/cm^2·sec)
C_1	0.78×10^5
C_2	0.91×10^5
C_3	0.91×10^5

These values correspond, in the case of a repetition rate of 16 pulses per second, to a neutron intensity per pulse of 5×10^{11} n.

3-2. Measurement of vanadium incoherent scattering

The absolute neutron intensities were also determined by the measurement of the vanadium incoherent scattering. Vanadium samples of three different shapes were employed; a cylinder 10 mm in diameter and 110 mm long, and two plates of respective dimensions 100×6.5×1 mm^3 (Plate 1), and 110×38×1 mm^3 (Plate 2). The measured intensities were corrected for absorption by the sample and by air, and the final derived intensities are summarized in Table 2.

Table 2 Absolute Neutron Intensities I_0'

	Plate 1	Plate 2	Cylinder (n/cm^2·sec)
C_1		7.3×10^4	5.5×10^4
C_2	(1.2×10^4 2.6×10^4	(4.8×10^4 5.1×10^4	4.6×10^4
C_3	(1.5×10^5 0.95×10^5	0.99×10^5	0.65×10^5

Although the values in the table are somewhat scattered, those obtained for plate 2 are probably the most reliable because, as this plate has large width, missetting errors could be minimized. From the values given in the table, the relative ratios of the intensities at the exits of the three guide tubes are calculated as 0.7:0.5:1 for $C_1:C_2:C_3$.

4. Measurement of transmittance

4-1. Direct measurement

The transmittances of the guide tubes were estimated by two different methods; (i) direct comparison of the measured neutron intensities the entrances and exits of the curved guides and (ii)

measurement of the transmittance a single section of the curved guide tubes.

In the former method, the neutron intensities in the C_1 and C_3 guide tubes were measured using a He^3 counter with a thin slit. The transmittance, T, is obtained from the ratio, I_{out}/I_{in}, of the intensities measured at the exit and entrance of the guide according to $T=C(\lambda)\cdot I_{out}/I_{in}$, where $C(\lambda)$ is a wavelength dependent correction factor arising from the different solid angles spanned by the counter. The calculation values are presented in Table 3. The average transmittances computed by assigning a weight of $I(\lambda)$ to each wavelength are 0.35 and 0.47 for guides C_1 and C_3 respectively.

Table 3 Transmittance of Guide Tubes C_1 and C_3

		4.5	5.3	6.0	6.7	7.4	8.0	8.9	9.6
C_1	I_{out}/I_{in}	.022	.022	.023	.025	.026	.032	.026	.026
	T	0.4	0.36	0.35	0.35	0.34	0.4	0.3	0.28

		4.5	5.3	6.0	6.7	7.4	8.0	8.9	9.6
C_3	I_{out}/I_{in}	.026	.029	.030	.033	.036	.046	.038	.039
	T	0.48	0.48	0.46	0.47	0.47	0.57	0.43	0.42

The ratio between that for C_1 and C_3 is about 0.75 which is in good agreement with that estimated from the absolute neutron intensities. The transmittance of guide C_2 was measured in a slightly different way. The incident neutron beams were collimated by inserting a 10" Soller collimator in front of the curved guide (This procedure is not possible for other guide tube.) in order to minimize the angular correction due to the beam divergence.

An average transmittance of 0.21 was obtained suggesting that the transmittance of guide C_2 is only 0.45 of that of C_1 which is also in good agreement with the results obtained from the absolute intensity measurement.

In order to determine the cause of the poor performance the transmittance of the 1 m long sections comprising the guide was estimated by monitoring the increase in intensity when the last two such sections were sequentially removed.

The ratio of the neutron intensity at the exit, A, to that at B (or C) which corresponds to the position of the end of the guide after the removal of one (or two) sections is plotted in Fig. 3. The measured average transmittance of a single 1 m section is approximately 92%. This gives rise to a transmittance of 0.2 ($=(0.92)^{18}$) for a guide composed of 18 similar sections, which is in good agreement with the aforementioned.

4-2. Estimation of the transmittance by absolute intensity measurement

The transmittance of guide tube C_2 was also estimated by comparing the total neutron intensities at the exit of the initial straight section with that at the exit of the curved section. The neutron intensity at the exit of the straight section was estimated by the Au foil method to be 4.4×10^5 n/cm^2·sec. After correction for the divergence of the beam in the air gap between the straight and curved sections, the intensity at the entrance of the later section becomes 3.2×10^5 n/cm^2·sec. This may be compared with the observed intensity at the exit of the curved section of 5×10^4 n/cm^2·sec, yielding a transmittance of 15.6%. Allowing for the ambiguities in the absolute

measurement this value agrees reasonably with the values estimated by other methods.

In conclusion, the KENS guide tubes have a maximum transmittance of about 50%. This low value is apparently due to low reflectivity in the mirror plates composing the guides, and to improve the guide performance further work should be directed towards increasing this reflecting.

Reference

1) S. Ikeda, Y. Ishikawa, and Y. Endoh : KENS REPORT I 45-72 (1980)

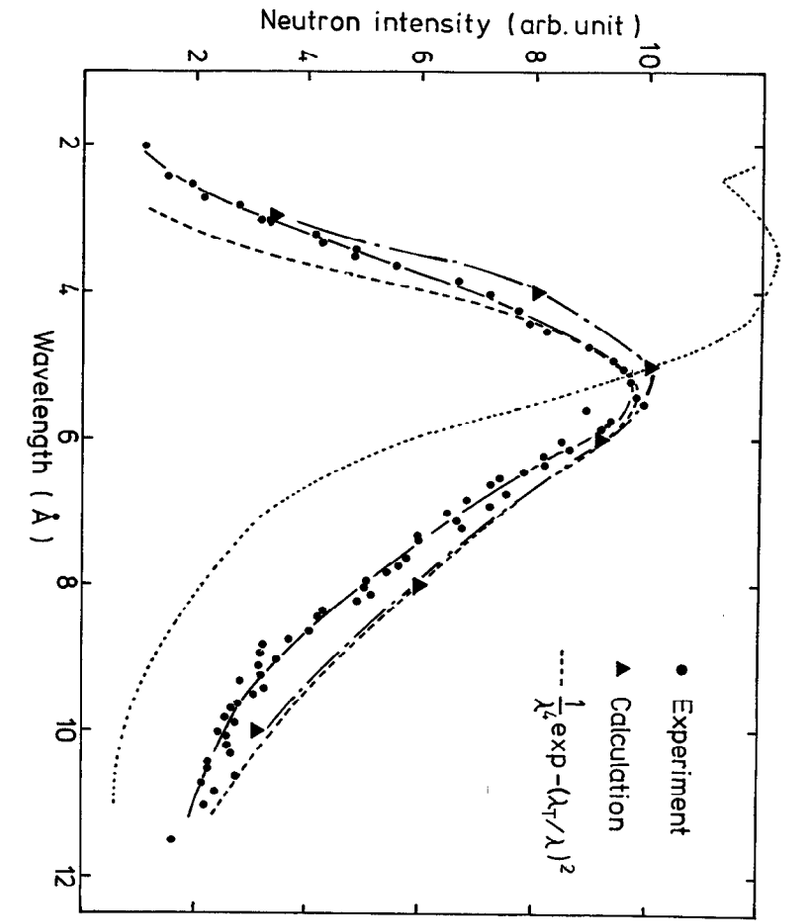

Fig.1 : I(λ) of guide tube, C_3.

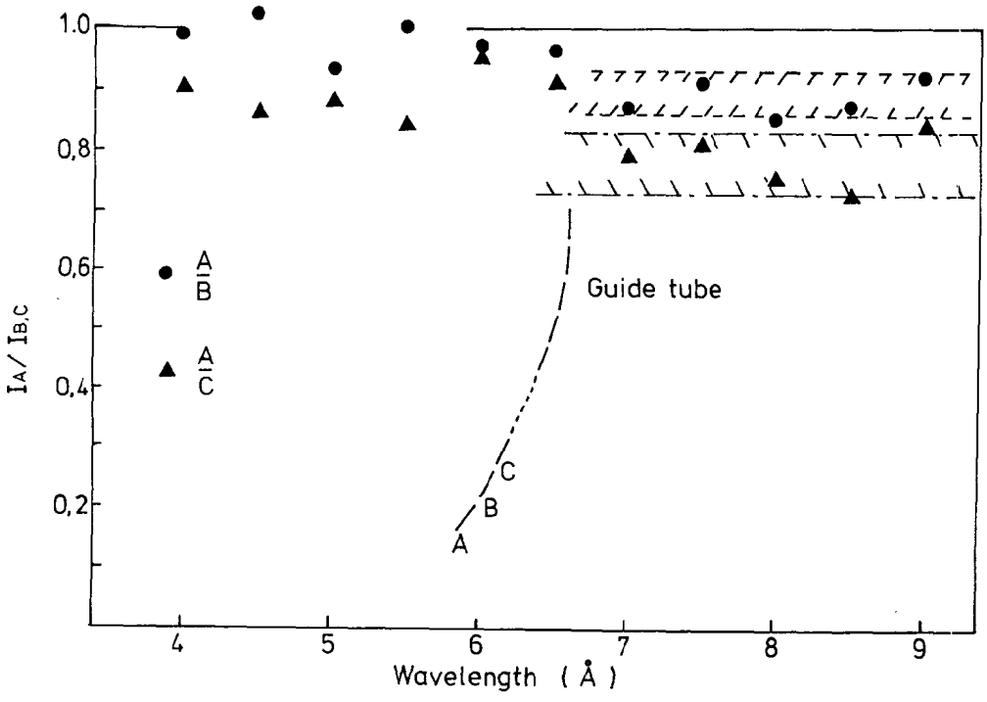

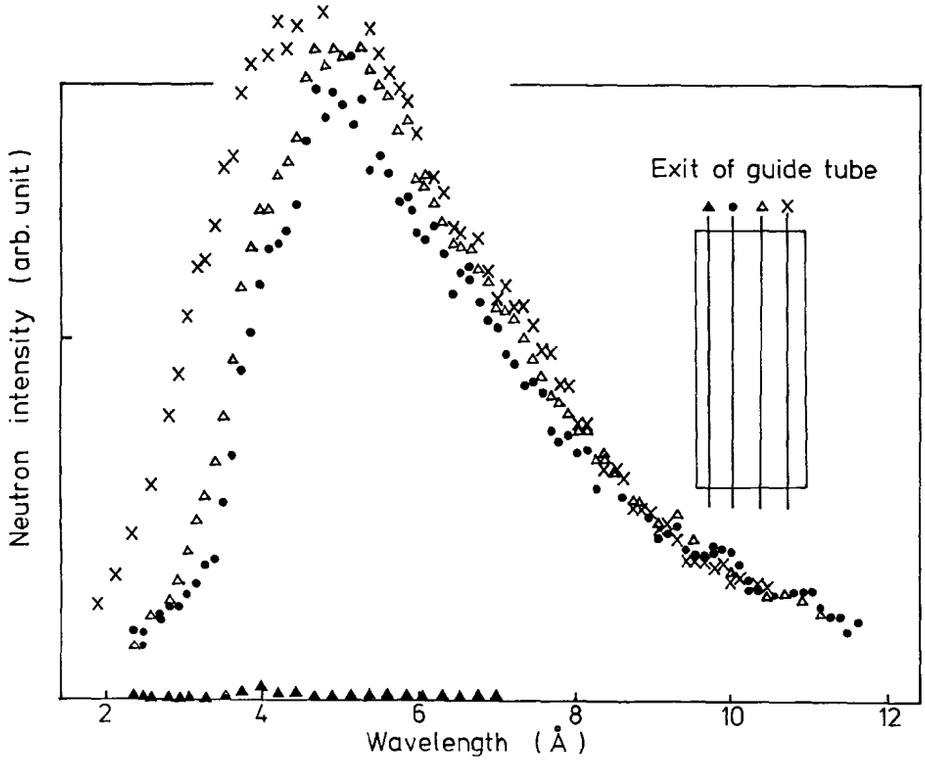

Fig.2 : The spatial distribution of the neutron intensity along the horisontal axis.

Liquid Diffraction

W S Howells
Neutron Division, Rutherford and Appleton Laboratories

1 Introduction

Neutron diffraction as a technique for structural studies of liquid and amorphous materials is now well established and one of the major advances in recent years has been the availability of instruments using short wavelengths whether on a reactor hot source, such as D4 at ILL, or a pulsed source, such as the Total Scattering Spectrometer (TSS) at the Harwell linac. For the SNS, two instruments for liquid studies have been proposed. The first, the Liquid and Amorphous Diffractometer (LAD) is a standard general purpose diffractometer based on the experience of TSS on the linac and so concentrates on the high Q region. The existing short wavelength instruments have extended the Q range to higher Q but there has been no corresponding improvement in the low Q region - D4 has a minimum Q of $\sim$ 0.2 $Å^{-1}$. This low Q region is accessible using existing low Q or small angle instruments, but it requires the use of long wavelengths ($\lambda > 6$ Å) neutrons. Furthermore, the small angle instrument may not be able to measure in the Q range corresponding to the main peak in the structure factor and so several instruments need to be used to obtain the full Q range. The second proposed instrument, the Small Angle Diffractometer for Amorphous and Liquid Studies (SANDALS) aims to fill this gap in the available Q range.

The LAD spectrometer will be built during 1981 and installed on the Harwell linac. Operating experience will then be gained before it is transferred to the SNS.

2 Inelastic Corrections

The accurate determination of the structure of liquids and amorphous solids depends on the understanding of the inelasticity or Placzek corrections. The corrections for time-of-flight diffraction have been discussed by several authors[2 - 5] and the conclusion has been that the corrections are easier to calculate and the useful range of neutron wavelengths is increased if the moderator is cooled rather than at ambient temperature.

Mildner et al[6] have measured the spectrum of three types of moderator - ambient temperature (300K), poisoned ambient, cold (77K) - and have fitted simple functions to the spectra. These results have now been combined with the formalism of Powles[5] to give a more versatile method of calculating the Placzek corrections[7].

The magnitude of the correction depends on the flight path ratio R, defined as $\ell_2/(\ell_1 + \ell_2)$ where ℓ_1 and ℓ_2 are the primary and secondary flight paths respectively. Powles showed that for the self-scattering term for a molecular fluid a small ($\sim$ 0.1) value of R is necessary whereas for the interference scattering a value of R = 1 is required. Other criteria, such as resolution, intensity and space available for the instrument will also influence the choice of R.

Using a cold moderator, the 1/E region is extended and the useful range of Q (ie the region where the correction is almost linear) is increased. Figure 1 shows the self-scattering correction for nitrogen gas at 77K for 2 types of moderator and the gain in Q for the cold moderator is obvious. The overlap of the useful Q range between angles is also improved and, as an extra bonus, the neutron pulse wddth on a cold moderator is narrower, thus improving the Q resolution.

3 LAD

The proposed instrument[8] (Figure 2) has path lengths ℓ_1 = 9 m and ℓ_2 = 1 m, thus giving R = 0.1. A cold (eg 77K) moderator has been specified, so for most use an energy range of 0.082 eV < E < 2.0 eV corresponding to 0.2 Å < λ < 1.0 Å is presently considered suitable. The maximum wavelength that can be used is determined by the frame overlap condition and is $\sim$ 8 Å. A maximum of 1.0 Å is considered more suitable because of the corrections. The minimum wavelength depends on the efficiency of the detectors; for example a 4 atm He^3 counter has an efficiency of only 15% at 0.2 Å compared with 50% at 1 Å. Thus while we refer to the range 0.2 Å < λ < 1 Å, the instrument could use wavelength less than 0.2 Å and up to 8 Å.

In order to obtain a large range of Q, a series of angles is chosen so that there is overlap in Q-range between adjacent detectors. The values chosen are 5°, 10°, 20°, 25°, 58°, 90° and 150°. At 150° there is a bank of detectors in the Q-focussing position[9], while all other angles have single detectors. The detector aperture for the 90° and 150° angles is 0.025 m wide by 0.3 m high whereas all the other angles have apertures 0.005 m wide lying on the Debye Scherrer cone.

The area of moderator viewed will be 0.1 m x 0.1 m and the maximum sample size 0.05 m x 0.05 m. The Q range and resolution for the various angles are given in table 1, where the resolution has been calculated for a sample 0.005 m in diameter and 0.025 m high. The detectors are 5 atm, 25 mm diameter He^3 counters and the count rates have been estimated as $7 \times 10^4\ s^{-1}$ at $\theta = 150^o$ decreasing to $5 \times 10^3\ s^{-1}$ at $\theta = 5^o$.

4 SANDALS

The proposed instrument is designed for structural studies in the Q range from 0.05 $Å^{-1}$ to 10 $Å^{-1}$ with the possibility of limited data up to 50 $Å^{-1}$. The instrument characteristics are similar to those of a conventional small angle instrument but with a different wavelength range. The maximum wavelength is restricted to 2 Å because inelasticity is difficult to correct for at longer wavelengths. The longer wavelengths will be removed with a gadolinium foil filter. With this maximum wavelength, the maximum possible length of the instrument, defined by the frame overlap condition, is 40 m.

The layout of the proposed instrument is shown in Figure 3. The main detector is a one metre diameter scintillation detector positioned 7 m from the sample. A series of rings 1 cm wide allow scattering angles in the range 0.5^o to 4°. Two more sets of rings are positioned at 4 m and 1.6 m from the sample to give scattering angles of 5° and 10° respectively. All these detectors are contained in an evacuated vessel and it is proposed to utilise vacuum tanks from the Nimrod particle physics programme. A further set of detectors, 5 mm wide by 30 cm high, is situated at 1 m from the sample at angles of 30°, 60° and 90°. The flight paths for these detectors and the sample area are in one vacuum tank which is connected to the main detector tank via a large vacuum valve so that the sample tank can be let up to air independently of the detector tank. The detectors will be of Li^6 glass - a 2 mm thick scintillator has an efficiency comparable to that of an 8 mm diam 40 atm He counter. The rings will be segmented - the lowest angles with four segments, higher angles in mulitiples of four with 64 at 4° to enable measurements of antisotropic scattering.

The sample position will be at 14 m from a cooled (eg 77 K) moderator and collimation of the incident beam will be by two variable apertures, the first in the bulk shielding after the beam shutter and the second at the entrance to the sample tank. Sample sizes will depend on the resolution required, but will be of the order of 1 cm square.

The resolution has been chosen so that it is comparable with liquids diffractometers such as LAD in the region of the main peak of the structure factor; it becomes progressively worse at lower Q values. The Q ranges and resolutions for the detectors are given in Table 2. Estimates of the count rate for a whole ring range from $\sim 10^3\ s^{-1}$ at $\theta = 4^o$ to $\sim 10^2\ s^{-1}$ at $\theta = 0.5^o$. The count rate for this 4° ring is comparable to that of the 5° detector on LAD.

References

[1] J C Dore and J H Clark - Nucl Instr and Meth, 136 (1976) 79.

[2] J M Carpenter and J D Sutton - Nucl Instr and Meth, 99 (1972) 453.

[3] J G Powles - Molec Phys, 26 (1973) 1325.

[4] R N Sinclair and A C Wright - Nucl Instr and Meth, 114 (1974) 451.

[5] J G Powles - Molec Phys, 36 (1978) 1181.

[6] D R F Mildner, B C Boland, R N Sinclair, C G Windsor, L J Bunce and J H Clarke - Nucl Instr and Meth, 152 (1978) 437.

[7] W S Howells - Rutherford Laboratory Report (1980) RL-80-084

[8] W S Howells - Rutherford Laboratory Report (1980) RL-80-017.

[9] J M Carpenter - Nucl Instr and Meth, 47 (1967) 179.

TABLE 1

The Q ranges and resolution ($0.2 < \lambda < 1.0$ Å) for LAD

θ (o)	ΔQ/Q	Q_{min} ($Å^{-1}$)	Q_{max} ($Å^{-1}$)	Detector Aperture
5	0.12	0.5	2.7	) 5 mm
10	0.06	1.1	5	) on
20	0.03	2.2	11	) Debye-Scherrer
35	0.017	3.8	19	) cone
58	0.010	6.1	30	
90	0.006	8.9	44	) 25 mm x 300 mm
150	0.004	12.1	61	

TABLE 2

The Q ranges and resolution for SANDALS

θ	Q_{min} ($\lambda = 2.0$)	Q_{max} ($\lambda = 0.1$)	ΔQ/Q
0.5	0.025	0.55	0.11
4	0.22	4.4	0.015
5	0.28	5.5	0.015
10	0.55	11.1	0.015
30	1.6	32	0.012
60	3.1	63	0.010
90	4.4	89	0.006

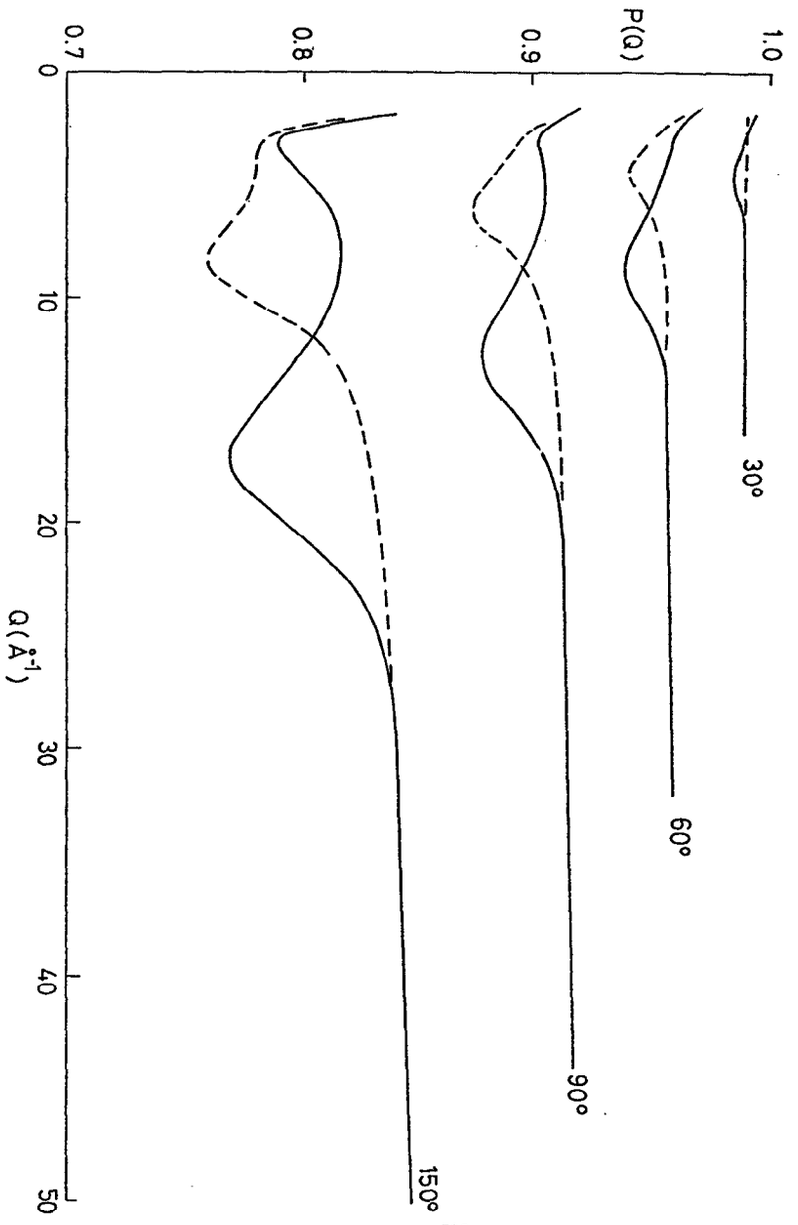

FIGURE 1 Placzek corrections for various detector angles and 2 types of moderator. (—— ambient (300K), --- cold (77K)).

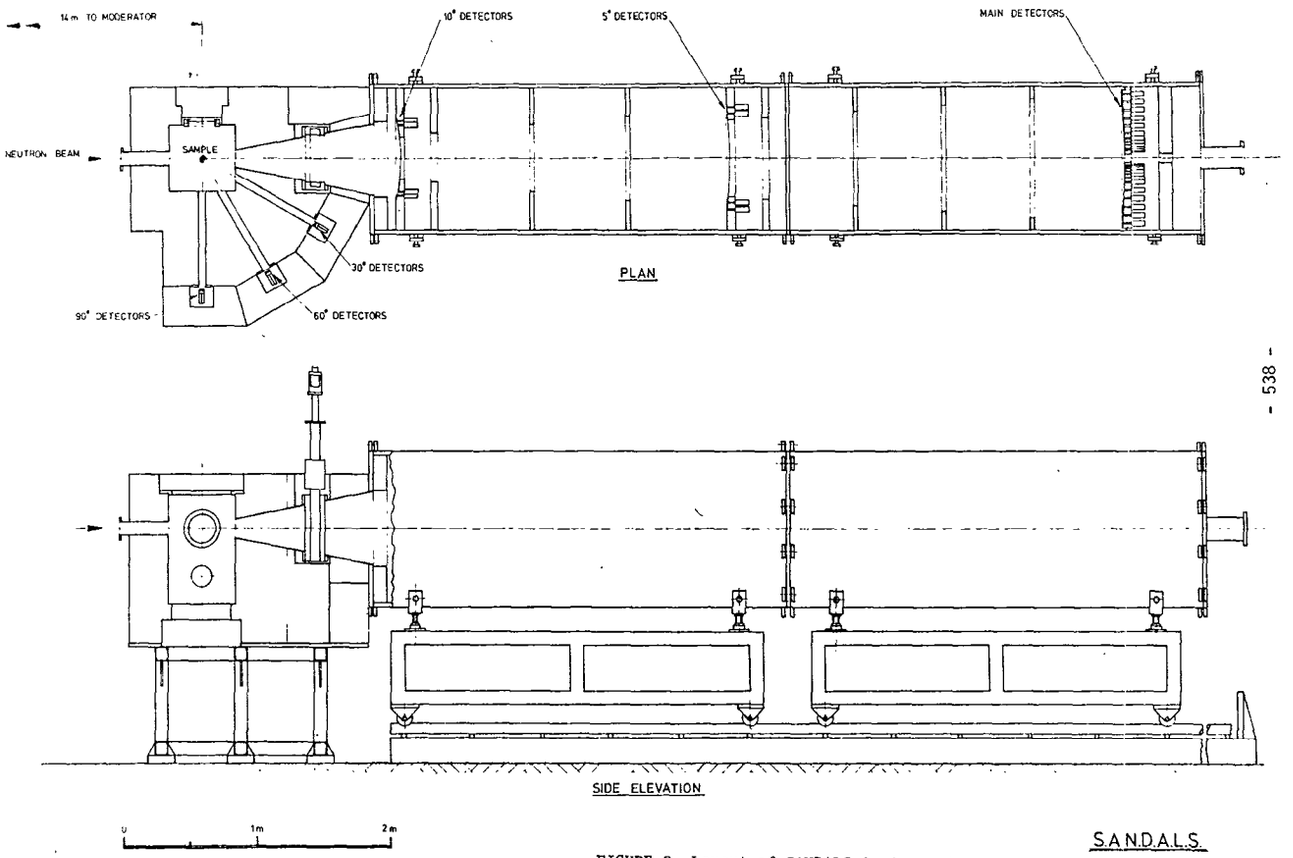

FIGURE 3 Layout of SANDALS instrument.

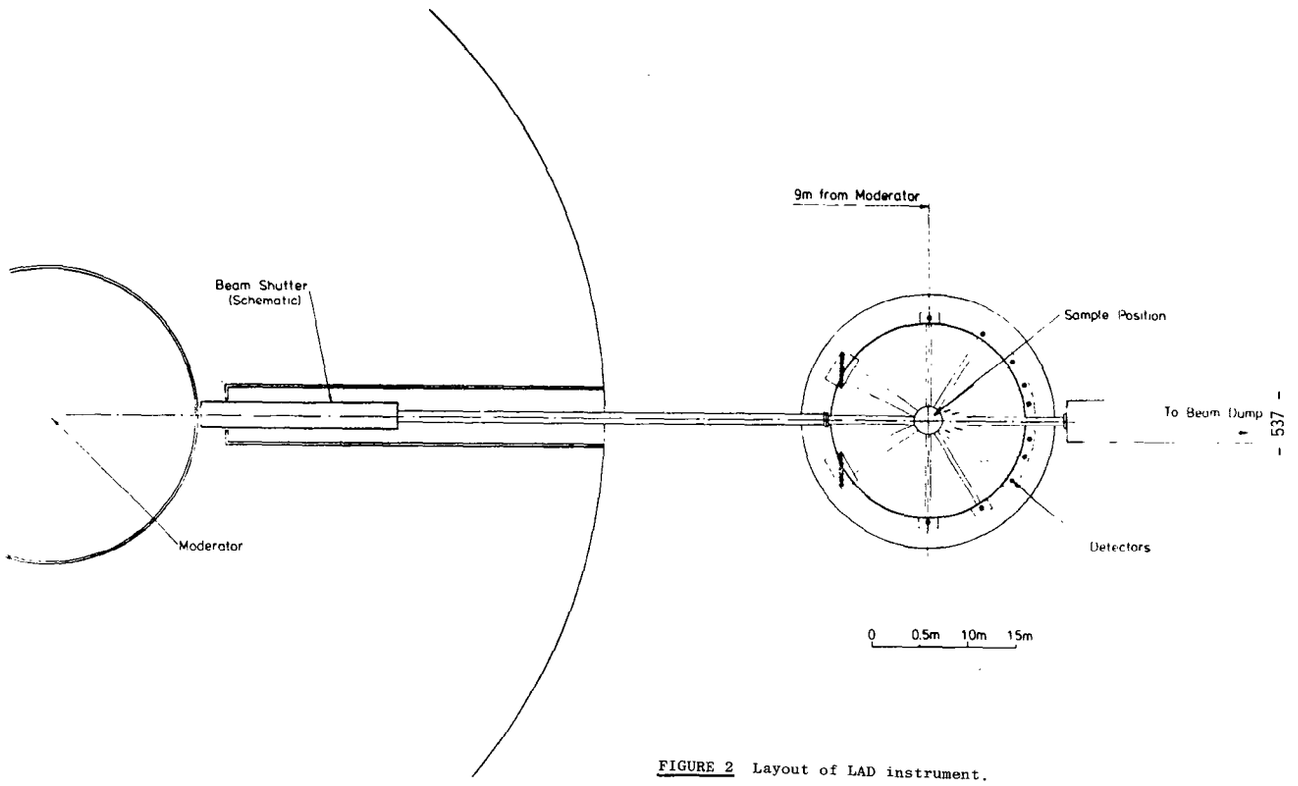

FIGURE 2 Layout of LAD instrument.

The High Intensity Total Scattering Spectrometer (HIT)

N. Watanabe

National Laboratory for High Energy Physics

Oho-machi, Tsukuba-gun, Ibaraki 305 Japan

T. Fukunaga, T. Shinohe*, K. Yamada**

Institute for Iron, Steel and Other Metals, Physics Department*

and Laboratory of Nuclear Science**, Tohoku University, Sendai, Japan

and

T. Mizoguchi

Department of Physics, Gakushuin University, Tokyo 171 Japan

Abstract

The High Intensity Total scattering spectrometer (HIT) has been constructed and installed according to the previously reported design.[1] Preliminary results indicate that the performance of the spectrometer meets the design specifications.

1. Introduction

HIT is a total scattering spectrometer designed to measure the structure factor, S(Q), of liquids and amorphous solids at a high rate of data collection. The scientific program for which this spectrometer will be used includes the precise determination of S(Q) over a wide range of momentum transfer ($Q \leq 50\text{-}100\ A^{-1}$), systematic measurements

from many samples covering perhaps a wide range of compositions, measurements on small or absorbing samples and real time studies of structural changes in nonequilibrium states. The machine was therefore designed to have the capability of handling high rates of data collection but with reasonable momentum resolution and with good SN characteristics.

2. Summary of the Spectrometer Configuration

A layout of the spectrometer as installed at the H-3 beam hole of the KENS facility is depicted in Fig.1.

Figure 2 is a photograph of the machine in position.

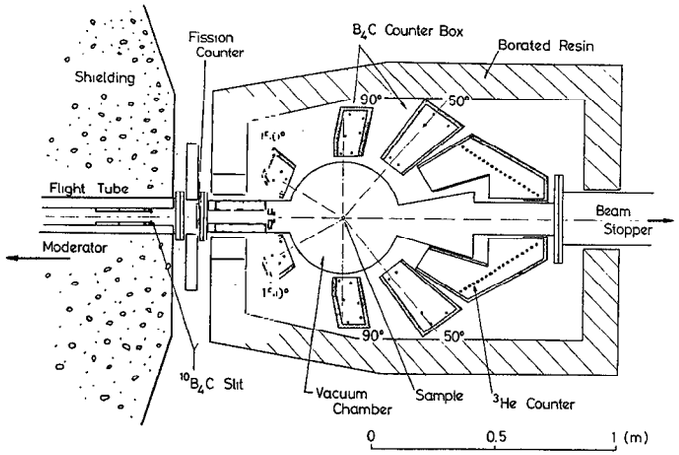

Fig. 1 Schematic diagram of HIT

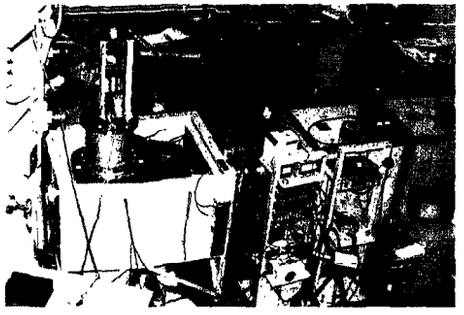

Fig. 2 Photograph of HIT

The machine has fifty He-3 counters (1/2" in diam., 12" long and filled to 20 atmospheric pressure) around the sample. Focussing geometries were adopted for the higher angle counters ($2\theta \geq 50°$), while those at lower angles were arranged to give approximately the same momentum resolution ΔQ. At higher angles there are two counter banks at slightly differing scattering angles and data from the respective counter banks are combined in order to obtain better counting statistics. The lower angle counters have apertures which limit their active hight in order to maintain the momentum resolution at the required value. The spectra recorded by each counter is accumulated independently and the data in Q space is collated after the necessary corrections. The present counter configuration at lower angles is useful for time-dependent structural studies where relaxation times are of the order of 100 μsec.[1)]

The spectrometer has a 4.7 m long incident flight path with slits made from sintered plates of $^{10}B_4C$. The sample is mounted in a large scattering chamber which may be evacuated in order to avoid air scattering. The spectrometer is equipped with a sample changer which can accomodate up to six different samples (see Fig.3).

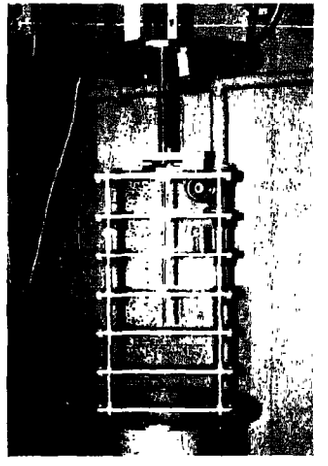

Fig. 3 Photograph of sample changer

The neutron signal from each detector passes through a pre-amplifier, a main (shaping) amplifier and a discriminator in slow NIM mode. It is then converted to a fast logic signal before being fed into a high speed time analyser[1)]. The spectrometer has 16 separate time analysers, each of which has 1 k 20 bit channels. The maximum data aquisition rate for each channel is several counts per μsec[1)].

3. Performance

3.1 Background

HIT has no Soller slit between the sample and the detector so that the solid angle of the detection can be large. This configuration, however, is more susceptible to background caused by air scattering around the sample. It is for this reason that HIT has been equipped with an evacuable scattering chamber.

Figure 4 displays scattered neutron TOF spectra measured with and without air in the scattering chamber. The strong air scattering signal is completely eliminated on evacuation, but an appreciable background persists at lower channels. This is probably due to epithermal neutrons

emerging from the beam exit of the biological shield and additional shielding is currently under construction to minimise this source of background.

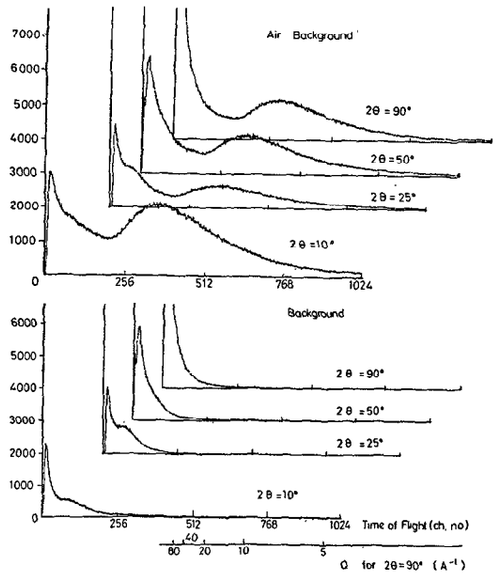

Fig. 4 Background with (upper figure) and without (lower figure) air scattering

3.2 Counting Rate

The capability for recording data at high counting rates is one of the most important characteristics of HIT and to examine its actual performance the following test measurements were carried out.

(1) Vitreous SiO_2

A sample of vitreous silica (1 cm in diameter, 5 cm long and about 9 grams in weight) was measured as a standard. Figure 5 shows typical spectra obtained with short measurement times. The actual counting time was only 90 sec, but although the counting statistics of the raw data are still rather poor (upper figure), the derived S(Q) (lower figure) is well defined, at least up to medium Q (~ $15A^{-1}$). For non-repetitive phenomena, therefore, our early results indicate that HIT will be useful for the measurement of time-varing S(Q) with relaxation times greater than 1 min.

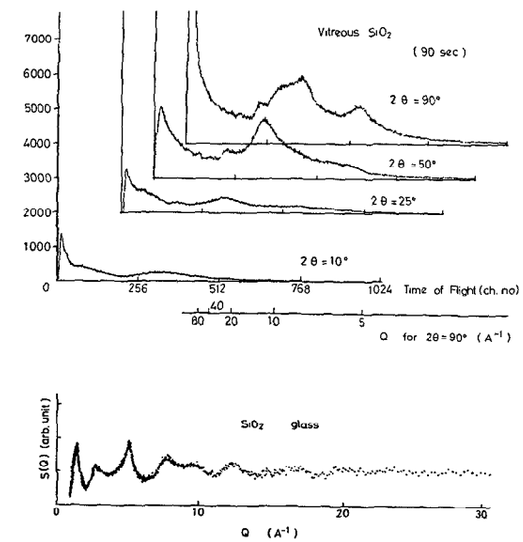

Fig. 5 Some TOF spectra (upper figure) and derived S(Q) (lower figure) for vitreous SiO_2 measured with 90 sec. The channel width is 4 μsec.

The counting statistics may, of course, be improved by extending the measurement time. Figure 6 shows some TOF spectra obtained from the same sample with a measuring time of 0.5 hours. The oscillation of S(Q) at high Q is very nicely defined up to about Q ~ 50A^{-1}.

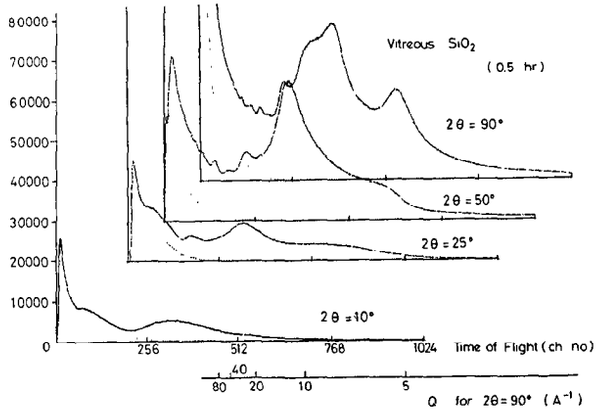

Fig. 6 Some TOF spectra for vitreous SiO_2 with a measuring time of 0.5 hours. The channel width is 4 μsec.

(2) Measurement on Small or Absorbing Samples

We anticipate that measurements on small or absorbing samples will be an important area of utilization of the machine, and, as an example of this kind, we have measured a sample of amorphous $Fe_{0.25}Ni_{0.55}Si_{0.1}B_{0.1}$. This was about 0.4 grams in weight and contained natural boron by 10 per cent. It was loaded into a vanadium cell of wall thickness 25 μm. A typical spectrum corresponding to a measuring time of 0.5 hours is shown in Fig.7. In spite of the relatively short measuring time the counting statistics and the

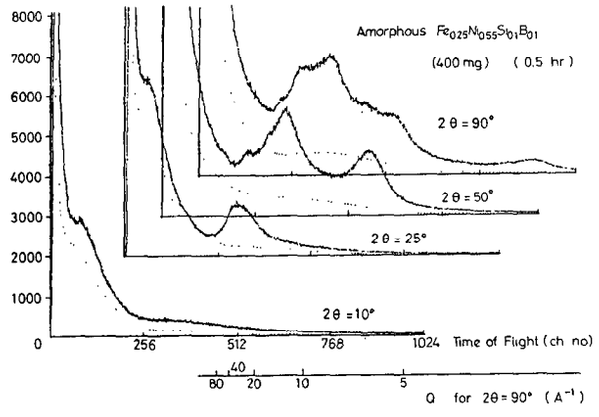

Fig. 7 Some TOF spectra obtained from a small and absorbing sample with a measuring time of 0.5 hours. The channel width is 4 μsec. The dotted lines indicate the pattern from the vanadium cell and instrumental background.

signal to background ratio are unexpectedly good. We have also measured another sample containing 40% natural boron (amorphous $Ni_{0.6}B_{0.4}$) and we found that even such a highly absorbing material was well within the range of practicable experiments. These early results encourage us to consider measuring amorphous semiconductors which exhibit photo-induced structural changes. For such measurements to be feasible, the sample must be thin enough for the bulk to be subjected to photon irradiation so that the total weight of the sample will be limited to ~0.1 g. Measurements on small samples containing expensive isotopes which provide information on partial structure factors provide another promising area of research.

3.3 Momentum Resolution

The momentum resolution of the spectrometer was monitored by using Bragg diffraction from a powder Si sample. The measured resolution which are close to the design values were about 0.6% at high Q for the back scattering counters, 1~3% for the medium angle counters and about 10% for forward counters. The resolution can be improved, if necessary, by using only data from the outside counters for higher angles, and by limiting the vertical length of the forward angle counters, although, of course, at the expense of a reduction in the counting rate.

3.4 Response of the Electronics

The maximum counting rate was found to be limited by the response time of the electronics, especially the main (pulse shaping) amplifier, rather than that of the gas proportional counter. In an attempt to increase the maximum counting rate, therefore, we tested a delay line clipping amplifier (Camberra Model 1411) and an active filtered amplifier (Camberra Model 2015/A). Typical dead times for 2015/A were found to be 2.3 μsec and about 6 μsec for shaping times of 0.5 μsec and 2 μsec respectively. The dead time of the 1411 with shaping time of 0.4 μsec was as short as 1.2 μsec. In Fig.6 the spectrum labelled $2\theta = 90°$ was processed through the 1411 while the other spectra were obtained using the 2015/A with shaping time of 0.5 μsec. In the former spectrum no saturation effect exists, but in the latter saturation clearly occurs in the epithermal region (at low channel number). These results demonstrate that the choice of amplifier is very important and for a high data rate capability delay line clipping amplifier is preferred to active filtered amplifier.

Acknowledgements

The authors express their sincere gratitude to Dr. Misawa who made significant contributions to the spectrometer design at the initial stage and also to Dr. N. Niimura and Mr. T. Kubota for design of the high speed time analyser. Thanks are also due to many colleagues, especially Dr. S. Hatta, Mr. J. Nishioka, Mr. T. Suemasa and Mr. S. Yamada for assisting in the spectrometer construction.

Reference

1) N. Watanabe, K. Yamada, M. Misawa and T. Mizoguchi : High Intensity Total Scattering Spectrometer (HIT), KEK Report KEK Int. 80-1, KENS Report I (1980) p-73.

The Powder Diffractometers

M W Johnson
Neutron Divison, Rutherford and Appleton Laboratories

HIPD

The high intensity instrument has been designed to provide the highest practical intensity consistent with a resolution in the range $3.10^{-3} < \Delta d/d < 10^{-2}$.

The design of the detector tank is shown in Figure 1 and a list of the instrument design parameters is given in Table 1. The principle design aims are set out below:

Moderator

Although the prime aim of HIPD is to provide a high intensity facility some thought must also be given to the effective resolution. A figure of merit

$$M(\lambda) = I(\lambda)/\Delta t(\lambda)^2$$

may be used to assess the relative performance of possible moderators. However, for powder diffraction there are two values of Δt which are of interest:

- A width (Δt at $\frac{1}{2}$ height, say) which may be used as a measure of the peak resolution.
- A width (Δt at 1/10 height, say) which may be used to determine the ability to gauge the 'background' spectrum beneath Bragg peaks.

Using $\Delta t_{\frac{1}{2}}$, the values of $M(\lambda)$ for Gd-poisoned or cooled moderators are only slightly higher than those for an unpoisoned ambient moderator. However, when $\Delta t_{1/10}$ is used the values of $M(\lambda)$ for Gd-poisoned or cooled moderators are much higher than those for an unpoisoned ambient moderator.

Detector tank

In a situation in which the detection rate is limited by the detector/data acquisition system it is imporant to eliminate extraneous background counts since each one, while adding to the statistical uncertainty, also eliminates a possible sample count. For this reason the sample tank will be evacuated and secondary collimation will be provided to reduce the detection of background counts from cryostat tails etc.

Detectors

The detectors are of the ^{6}Li glass scintillator type. The large, focussed 150° detector is the primary detector which has been optimised for intensity at good resolution ($\sim 3 \times 10^{-3} - 10^{-2}$). It is divided circumferentially into 100 x 5 cm segments. This fulfills two functions:

- The 100 detector elements and their parallel data acquisition paths permit an instantaneous count rate of 100 n/μs with only a 10% dead-time correction.
- The 2° segmentation permits anisotropic scattering to be detected.

In addition, two other detectors are provided. The 30° detector has a moderate resolution ($\sim$ 2%) and is segmented. It is provided to extend the d-range of the 150° detector.

The 10° detector has a poor resolution ($\sim$ 6%) and is not segmented. It is not intended to provide accurate data for refinement but to ensure that large d-spacing reflections are detected. A knowledge of these reflections is essential to index new patterns.

Data Acquisition

In typical diffraction patterns (eg $A\ell_2O_3$) the largest peak accounts for a few per cent of the entire diffracted intensity. Thus if total count rates of 10^6 n/s are to be maintained the system must be able to cope with $\sim$ 800 n within a particular Bragg peak (assuming ν = 50Hz). This corresponds to a peak detection rate of $\sim$ 40 n/μs. By using 100 sectors in the detector, each with its own data acquisition chain (with a $\tau_d \sim$ 100ns) the worst dead-time correction is kept down to $\sim$ 4%. For powder diffraction patterns recorded over time scales $\sim$ 20 ms it is found that a large fraction of the neutrons ($\sim$ 80%) is detected over a small fraction ($\sim$ 12%) of the total time available for detection. This means that some intermediate memory should be provided to store all events within a particular frame (ie within the 20 ms period). Currently it is envisaged that this intermediate memory will be provided in the form of 100 x 256 wd. dual-memory buffers - one for each detector segment.

The final descriptor has a maximum length of 18 bits. This may be built up from combinations of a space descriptor (n_s <8), time descriptor (n_t <13) and period descriptor (n_p <6). The latter is a tag applied to longer periods of time (ms - s) which is required in studying relaxation phenomena.

HRPD

The high resolution instrument (HRPD) has been designed to provide the highest practicable resolution consistent with reasonable counting times. Using the time-of-flight method it appears that resolutions in the region of $\Delta d/d = 3.10^{-4}$ may be reached, an improvement of a factor ~ 7 over existing high resolution neutron diffractometers. Such an improvement is important in two areas, structure determination and phase transitions.

The proposed design of the detector tank is shown in Figure 2 and a list of the main design parameters is given in Table 2. Some explanations of the choices are given below:

Guide

The guide cross-section, curvature and straight-section length have been optimised using the program MCGUIDE [1]. The details of the optimisation have been given elsewhere [2]. The aim of the optimisation has been to maximise the intensity of the wavelength range 0.8 - 4 Å while maintaining a uniform beam profile at the guide exit.

Disc Choppers

Disc choppers are provided at 6 m and 10 m to prevent frame overlap. Three apertures are provided to enable 1, 2 or 3 frame superposition.

Detectors

The two detector system (back scattering and low angle) are located inside the evacuated detector tank. The prime (back scattering) detector consists of 20 concentric rings lying in a plane perpendicular to the neutron beam. Time focussing is not achieved geometrically, but electronically before the event is registered. The provision of the low angle detector is for the same reason outlined in the HIPD description. It will be noticed that by having two sample positions and two detectors, four detector angles are effectively provided.

Data Acquisition

This follows the same scheme as that for the HIPD instrument. The major difference is in the larger number of time channels (32K) that must be provided.

References

[1] "MCGUIDE: A Thermal Neutron Guide Simulation Program" - M W Johnson, Rutherford Laboratory Report RL-80-065.

[2] "Neutron Guides on Pulsed Sources" - C J Carlile, M W Johnson and W G Williams, Rutherford Laboratory Report RL-79-084.

TABLE 1 HIPD parameters

MODERATOR	10 x 10 cm cooled or Gd poisoned
PRIMARY FLIGHT-PATH	9 m evacuated. Normal to moderator
PRIMARY COLLIMATION	Up to 5 x 5 cm at sample position. Collimator contains baffles to prevent multiple scattering.
DETECTOR TANK	Evacuated 10^{-1} torr for normal running (10^{-6} torr available). $\geqslant$ 20 cm boron/wax shielding.
DETECTORS	All Li glass scintillator. 150° - focussed array of 100 x 2° elements solid angle $\Omega = 0.3$ sr $L_2 = 1$ m. 30° - Unfocussed ring of 100 x 2° elements $\Omega = 0.017$ sr $L_2 = 1$ m r = 50 cm. 10° - Unfocussed ring of 1 element $\Omega = 0.005$ sr $L_2 = 87$ cm r = 15 cm
MONITORS	2 monitors at - 40 cm and + 100 cm from the sample position.
DATA ACQUISITION	150° - 100 x 256 wd (20 MHz) dual-memory buffer 30° - 25 x 256 wd (20 MHz) dual-memory buffer 10° - 1 x 256 wd (20 MHz) dual-memory buffer Overall limit of 10^6 events/s set by memory incrementation speed. Bulk memory = 0.25 M wd_6 ie $n_t.n_p.n_s \leqslant 0.25 \times 10^6$.
TIME SORTING	$n_t \leqslant 8192$ chan. Time boundaries may be software set.

TABLE 2 HRPD parameters

MODERATOR	10 x 10 mm cooled or Gd poisoned.
PRIMARY FLIGHT-PATH	100 m evacuated curved neutron guide.
GUIDE PARAMETERS	width 2.5 cm height 8.0 cm length of sections = 1 m 4 m - 6.5 m straight 6.5 m - 60 m curved: r = 18 km 60 m - 100 m straight $\lambda^* = 0.98$ Å
DISC CHOPPERS	At 6 m and 10 m. 3 apertures corresponding to 1, 2 or 3 frame supperposition. Variable speed at ν, $\nu/2$, $\nu/3$ etc.
DETECTOR TANK	Evacuated (10^{-1} torr normal, 10^{-6} available) light shielding. 2 sample positions at 1 m and 2 m from back-scattering detector.
DETECTORS	1 Back-scattering: 200 elements, 20 rings. $r_{min} = 7$ cm, $r_{max} = 37$ cm.

	1 m	2 m
Ω	0.37	0.1
$2\theta_{min}$	160°	170°
$2\theta_{max}$	176°	178°

2 Low-angle: 1 element r = 18.5 cm.

	1 m	2 m
Ω	.005	.04
2θ	7°	20°

MONITORS	2 monitors at - 275.5 cm and 75 cm from 2 m position.
DATA ACQUISITION	1 100 x 128 (20 MHz) dual-memory buffers 2 1 x 128 (20 MHz) dual-memory buffers Bulk memory = 0.25 M wd.
TIME SORTING	n_t < 32 K channel time boundaries s/w set.

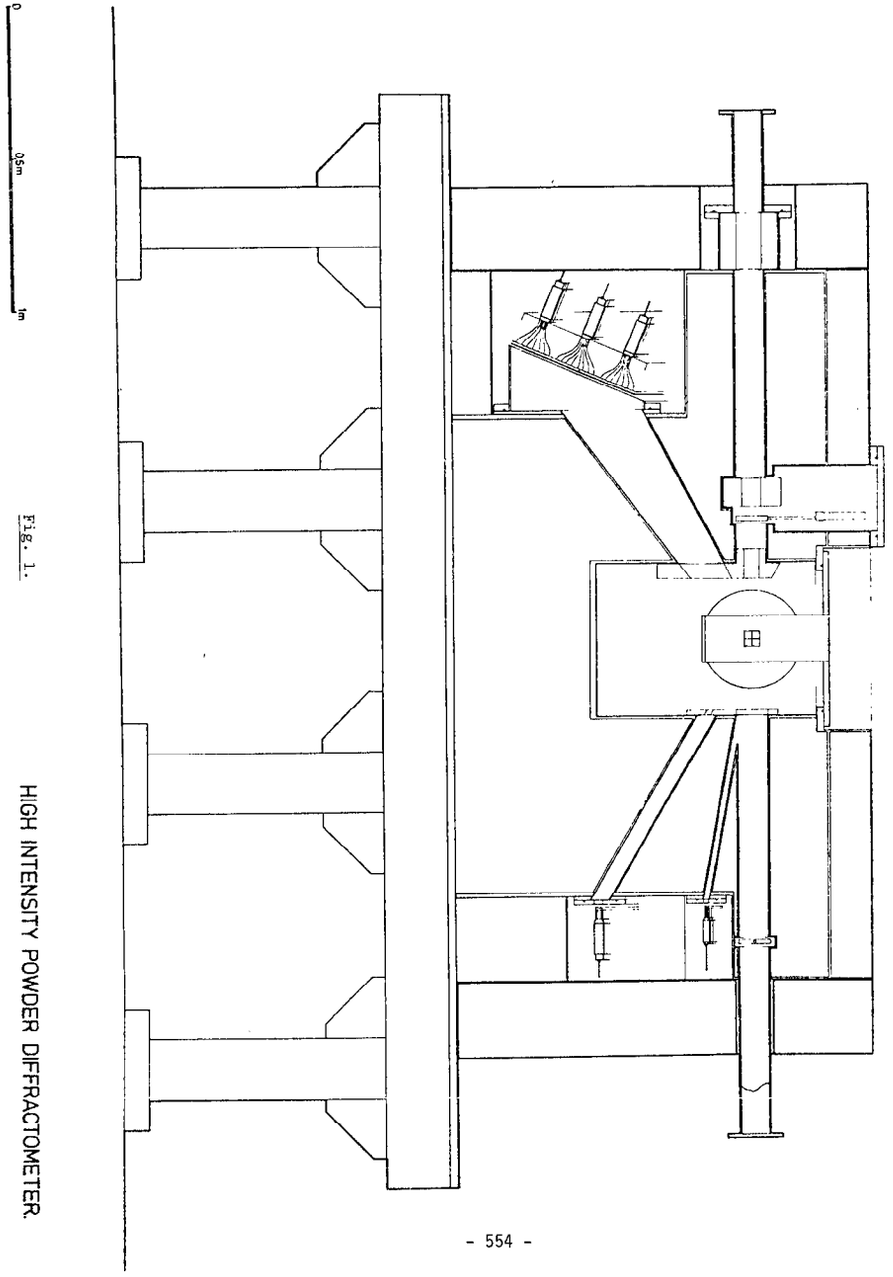

Fig. 1. HIGH INTENSITY POWDER DIFFRACTOMETER.

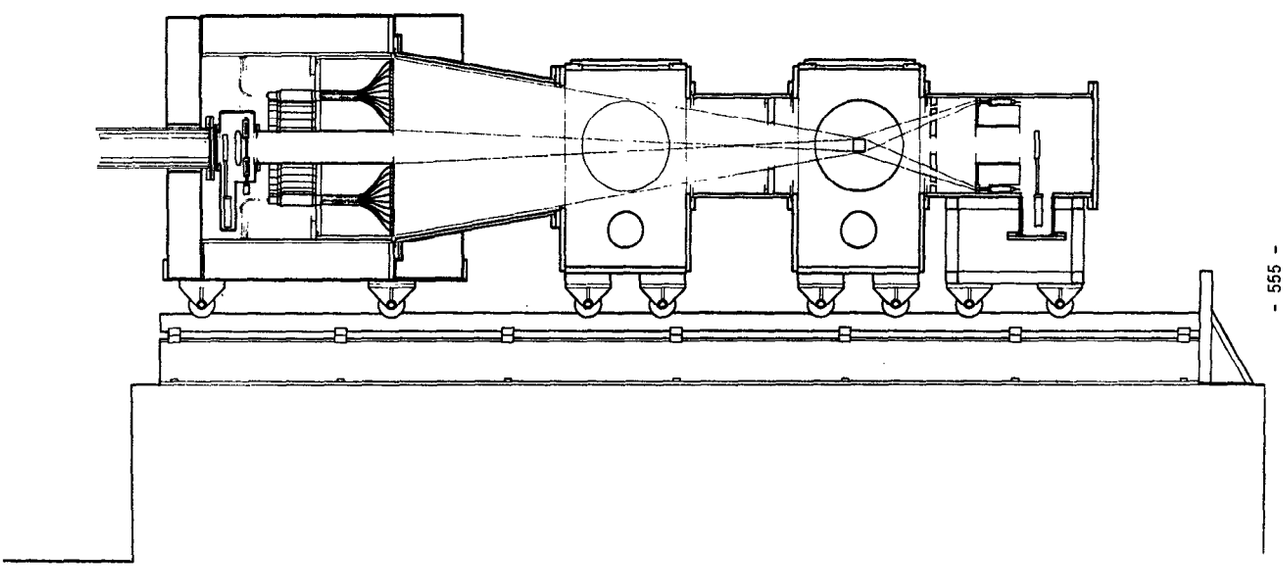

0 0.5m 1m

Fig. 2. HIGH RESOLUTION POWDER DIFFRACTOMETER

The Low Q Spectrometer for the Rutherford Laboratory Spallation Neutron Source

R J Stewart
J J Thompson Physical Laboratory, University of Reading

1 Introduction

Small angle neutron scattering (SANS) is used to study a wide variety of phenomena in many different disciplines (eg biology, polymer science, metallurgy; materials physics etc). The terminus technicus SANS does not only apply to small scattering angles but to small values of the magnitude Q of the scattering vector $\underline{Q} = \underline{k} - \underline{k_o}$ (where $\underline{k_o}$ and $\underline{k}$ are the wave vectors of the incident and scattered neutrons). For elastic scattering $|\underline{Q}| = 4\pi \mathrm{Sin}\theta/\lambda$ where 2θ is the scattering angle and λ the neutron wavelength. In materials studies the SANS range is usually defined by $0 < Q < \pi/d$ where d is the interatomic distance in the sample, typically $\sim 3\mathring{A}$ in condensed matter, giving an upper limit for $Q \sim 1\mathring{A}^{-1}$. The observed small angle scattering is produced by inhomogeneities of different scattering length density to their immediate environment. In biology the range $0 < Q < 1\mathring{A}^{-1}$ is also an important area but with even higher Q values also being of interest.

A typical small angle scattering curve is shown in Figure 1. This curve was obtained using three different sample-detector distances on the D11 spectrometer at the Institut Laue Langevin. Many experiments necessitate measurements on D11 using several different detector positions in order to cover a large enough Q range to enable a complete analysis of the data to be accomplished. Hence beam time is lost in moving the detector. In many experiments where the scattering from the sample changes as a function of time, experiments have to be restricted to a single detector position and thus limited Q range with the consequent loss of experimental information. The wide wavelength range available from the cold moderator of the SNS when coupled with a suitable multidetector will permit a large Q range to be simultaneously accessible in one experiment.

In addition to the possibility of simultaneously accessing a large continuous Q range the use of a pulsed beam has two other advantages compared to a continuous beam experiment:

a) Separation of elastic and inelastic scattering if the wavelength spread is limited. This is particularly important if one is interested in the elastic scattering from samples at high temperatures when the separation of the inelastic contribution is important. For example, if one is studying some temperature dependent transition at high temperatures one has to be able to discriminate the origin of changes observed as the temperature is varied (eg elastic or inelastic).

b) Possibility of synchronising a perturbation of a sample with the neutron pulse and thus investigating the response of the sample by collecting the scattered neutrons from many such cycles. In cases where the sample response is slower than the pulse repetition rate, the response over several neutron pulses could be studied, for example, the response of a rubber to stretching, a muscle to stretching, or cyclic deformation of a metal (fatigue, internal friction). In some experiments the pulse width at the sample may have to be limited by selection of a smaller band of wavelength in order to match the response time of the sample.

2 Specification

The low Q spectometer will use the 20K moderator in order to give a good intensity of neutrons up to $10\mathring{A}$. In order to obtain a large continuous and yet easily variable Q range a one meter diameter area telescopic detector has been designed. (Figure 2). The detector will be based on the Rutherford type of design (See P Davidson and H Wroe report at this meeting) and will be made of lithium glass scintillator. It will consist of 6048 individual cells arranged in annuli about the beam centre at radii between 5 cm and 50 cm. The spatial resolution in the radial direction will be 3.5% for radii from 10 to 50 cm. The annuli between 5 and 38 cm will be arranged as one miltidetector which can be positioned as a whole at any distance between 2.5 m and 20 m from the sample position. (Figure 3). If the outer rings are positioned at sample-detector distances of 70, 200, 500 and 1000 cm with the main detector at 2000 cm, a Q range of 0.003 to $1\mathring{A}^{-1}$

would be continuously accessible using a band of incident neutrons between 4 and 10A°, assuming that the 10 cm ring is the minimum used. If the wavelength range were extended to 1A° the maximum Q would increase to $4A^{o-1}$ and there would be considerable overlap of the Q ranges of the various sectors with a consequent increase in the statistical accuracy of the data obtained.

The entire detector will be housed in an evacuated square tube (1.1 m x 1.1 m by 20 m long). The detector will be capable of movement without letting the housing up to air. The lowest achievable vacuum will be 10^{-5} torr so that furnaces and liquid nitrogen cryostats can be used without problems of small angle scattering from window materials when measurements at low Q are required. Usually the vacuum will be $\sim 10^{-2}$ torr. A low efficiency two dimensional detector consisting of 137 elements, arranged in a rectangle 6 cm high by 5 cm wide will be mounted at the centre of the main detector but 10 cm behind it. This will be used to determine the gravity corrected beam centre for each wavelength, when large sample detector distances coupled with large wavelengths spreads need to be used.

3 Beam Limiting Choppers

These will be described briefly in their beam order. A more detailed description is in preparation (Dusic and Stewart, unpublished).

a) Chopper to produce a band of neutrons 1 to 10A°. This chopper is situated within the biological shield 4.3 m from the cold moderator. The frequency of revolution of the chopper will be phase locked with source. It will be manufactured from a nickel superalloy with 30 cm of the alloy in the beam path when in the closed position. The transmission for neutrons of wavelengths less than 0.5A° will be $\sim 10^{-7}$. On the input and output sides of the nickel chopper, simple MgCd alloy disc choppers will be mounted to limit the longest wavelength transmitted to 10A°. The removal of neutrons with wavelength shorter than 0.5A° is important since all choppers downstream use cadmium as the neutron absorbing medium; this elimination is particularly important when submultiples of the pulse repetition frequency of the source are used in the experiment. The lowest harmonic wavelength to be transmitted is 18.5A° which can be removed by suitable phasing of the subsequent choppers.

b) Tail cutting chopper

This is a simple MgCd disc chopper situated 4.8 m from the cold moderator. It is used to limit the lowest or highest wavelength transmitted. For example a beam spread from xÅ to 10Å can be obtained with x chosen to exceed the Bragg cut off of the sample under study. Thus contamination of the observed SANS pattern with single and multiple Bragg events can be avoided. In addition when run at a submultiple of the source frequency a beam from the first chopper of 1-10A neutrons, can be obtained at a pulse repetition rate of 25 or 16.6c/s by suitable adjustments of the frequency and phase of the chopper.

c) Velocity selecting choppers

These are again two simple MgCd disc choppers, rotating in opposite directions which enable a band of wavelengths of variable width ($\Delta\lambda$) to be selected. A pseudo monochromatic pulse beam of down to at least 5% ($\Delta\lambda/\lambda$) can also be obtained by suitable phasing of these choppers when the separation of elastic and inelastic scattering is necessary. These choppers are situated outside the biological shield at 7 m and 8 m from the cold moderator. When not in use they can be stopped in the open position. In addition a chopper for reducing the pulse repetition rate by ½, ⅓, ¼, ⅕, and ⅙ when necessary will be situated outside the biological shield.

4 Collimation

The initial collimation will be flexible with the possibilities of

(a) apertures at a fixed distance (as used on D11 at the ILL)
(b) soller collimators of the Rutherford type,
(c) and possibly eventually focussing collimators

5 Sample Area

The sample area will be housed in a cubic aluminium alloy box separated from the main detector vessel by a large vacuum valve. There will be sufficient space to mount a multiposition sample changer, cryostat or furnace and/or a magnet within the sample box. The maximum beam size at the specimen will be 3 x 3 cm, but usually a beam size of $\sim 1\ cm^2$ will be used.

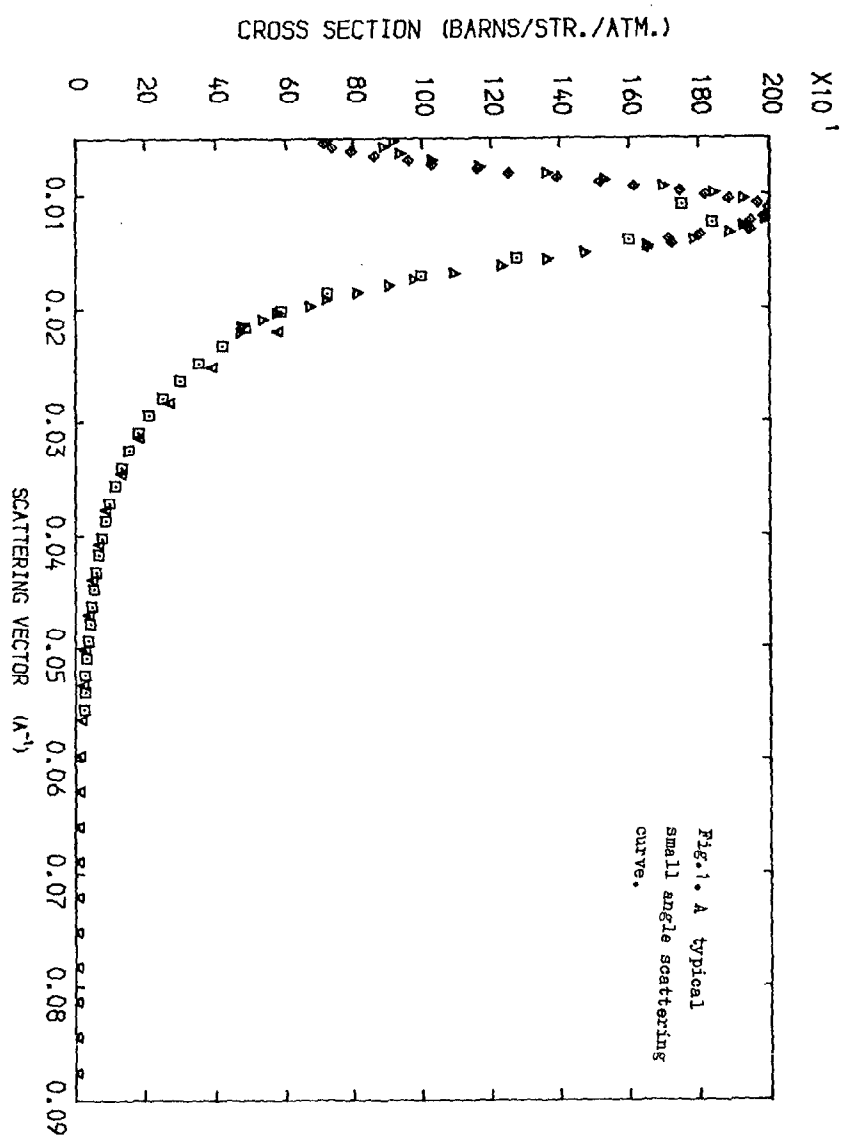

Fig.1. A typical small angle scattering curve.

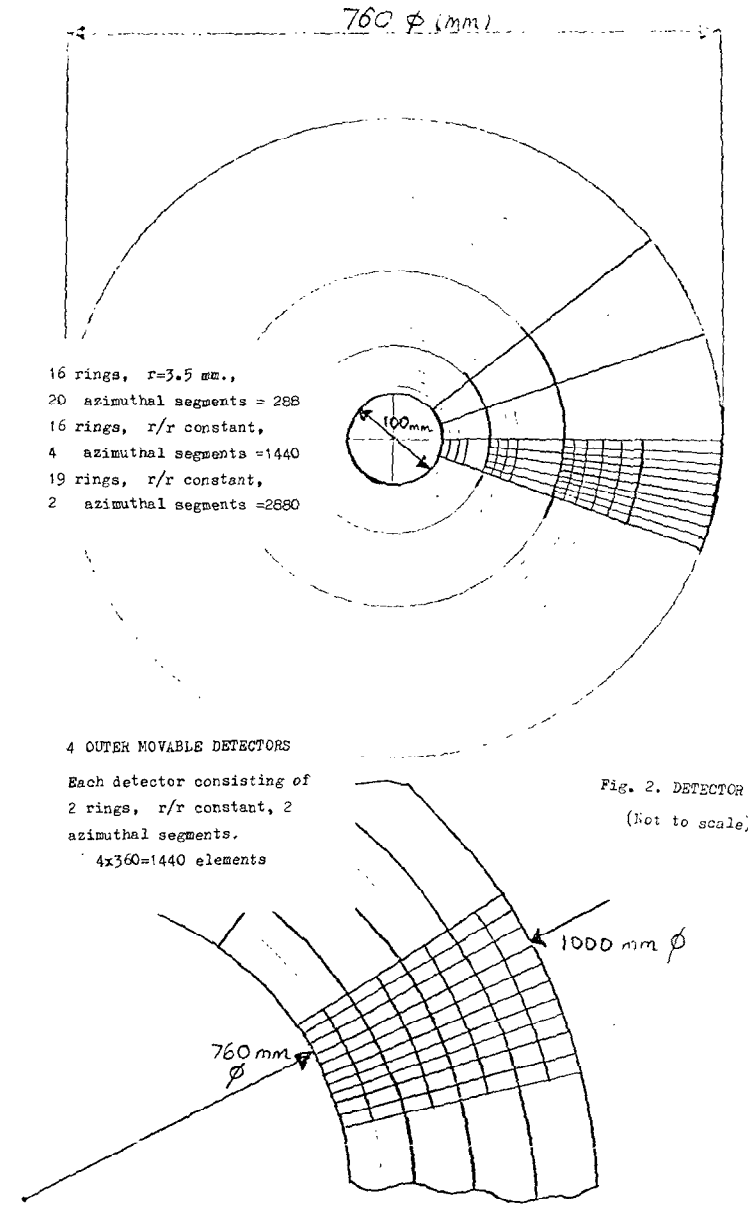

Fig. 2. DETECTOR
(Not to scale)

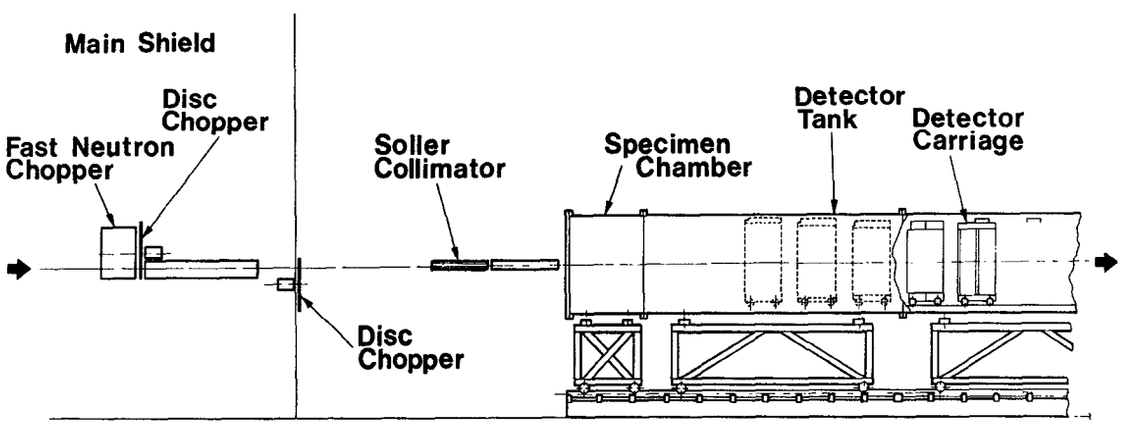

Fig.3. Low Q Spect.

SMALL ANGLE SCATTERING SPECTROMETER (KENS-SAN)

Y. Ishikawa, M. Furusaka, M. Arai, N. Niimura*,
S. Ikeda** and K. Hasegawa***

Physics Department, Tohoku University
*Laboratory of Nuclear Science, Tohoku University
**National Laboratory for High Energy Physics
***Department of Nuclear Engineering, Tokyo University

1. Spectrometer Characteristics

KENS-SAN is the first TOF small angle scattering spectrometer to be enstalled at a pulsed cold neutron source. The configuration of the constructed spectrometer is shown in the upper part of Fig. 1. The spectrometer was designed so as to benefit from the characteristics of the pulsed cold neutron source. This paper discusses the preliminary results that have been obtained with this spectrometer during the two months initial operation. The principles of the design have already been described in a previous paper[1)] and so that we present only a summary of the spectrometer characteristics.

1.1 Measurement of a Wide Range of Momentum Transfer

KENS-SAN is equipped with a two dimensional position sensitive He^3 counter bank (2D-PSD). This can be displaced inside a large vacuum detector chamber so that the distance between the sample and the detector can be altered between 1 m and 5 m without breaking vacuum. In addition, six sets of fixed 1" diameter single He^3

counters (Labelled A to F in Fig. 1) are installed at the scattering angles of 150, 90, 45, 26.6, 14.0 and 5.7 degrees. With this configuration and by utilizing all neutron wave lengths in the range 3 Å - 11 Å (or 4 Å - 12 Å), the spectrometer can be used to measure momentum transfers, Q, from 3×10^{-3} $Å^{-1}$ to 4 $Å^{-1}$ without changing the configuration as indicated in the lower part of Fig. 1.

1.2 Improvement of the S/N Ratio

KENS-SAN is installed at the exit of a bent guide tube whose length is longer than the direct view distance. The level of background radiation is therefore quite low and a thin 0.5 mm Cd plate is sufficient to protect the detectors against background noise.

1.3 Increase of the Effective Scattered Neutron Intensity

By inserting a converging Soller slit between the exit of the guide tube and the sample chamber, the sample size can be increased to 33 x 13 mm^2 (in case of focussing at 5 m from the sample). The statistics of the accumulated data may also be further improved by combining the data obtained at different wavelengths.

1.4 Quick Display of 2D-PSD Data

The quantity of data generated by the 2D-PSD using TOF scans is extremely large (43 detectors x 64 position channels x 32 time channels = 88,000 discrete data points) and so direct correction and display of the results is not possible. The three following simple on-line display systems were therefore developed.

i) Display of data obtained by integrating over one parameter (time or position).

ii) One dimensional display of the data in Q space obtained by integrating the data from all directions.

iii) Two dimensional display of the data in Q space obtained by integrating data from a limited range of wavelengths.

1.5 Use of a Second Chopper (cf. Figs. 1 and 6)

When a tooth chopper is positioned before the converging Soller slit (cf. Fig. 1), the inelastic scattering contribution can easily be removed. Conversely use of a convensional one window chopper enables the inelastic scattering to be measured.

2. Experimental Results

2.1 Fixed Single Counter Sets

The TOF spectra from an Al-10%Zn alloy measured by the fixed counter sets at an early stage of instrument development are displayed in a lower part of Fig. 2. The small angle scattering data obtained by the F counter set placed at 5 m from the sample is shown in the inset. The data has been corrected for the incident neutron intensity distribution. The agreement between data and that of Komura et al.[2] is satisfactory for Q values greater than 0.08 $Å^{-1}$, indicating that the fixed single counter sets themselves are quite useful for measurements of the high Q range. In this experiment we also found that the TOF spectra were contaminated by the fast neutrons which are seen as a spike in each spectrum in Fig. 2. This high energy neutron component, however, was spread over only ten time channels which could be omitted without introducing problems in the analysis. The level of the fast neutron background was later

substantially reduced on improving the shielding around three guides and this background is now completely absent when all the beam tubes in experimental hall B are closed.

2.2 Converging Soller Slit

The two dimensional converging Soller slit was made by combining 1 m long horizontal and vertical converging Soller slits in the manner shown in Fig. 3. Each of these components is composed of two separate 50 cm long sections so that the angular divergence may be alterned. The complete slit is designed so as to focus at a distance of 5 m from the sample. The sample size can then be as large as 33 x 13 mm^2. The measured spot size of the direct beam deriving from the finite angular divergence of the slit is 18.7 x 18.5 mm^2 and 35.4 x 17.1 mm^2 at respective distance of 5 m (focus) and 1 m from the sample. The direct beam could be stopped completely by a 1 mm thick Cd plate of dimensions 20 x 50 mm^2 even at the 5 m position. Use of this converging Soller slit, however, reduces the incident neutron intensity to 3% of that at the exit of the guide as expected from the design value of its angular divergence.

2.3 2D-PSD and Data Display

The 2D-PSD is composed of an array of 43 one dimensional PSD 1/2" in diameter and 24" in active length (RS-P4-0810-204) originally developed by Missouri University[3]. The preamplifiers which are attatched to each end of each PSD were specially designed for the low impedance of the PSD (R_c = 3.6 kΩ) and were installed inside the vacuum chamber with 2D-PSD. A high voltage of 1900 V can be safely applied to the PSD in the vacuum pressure of 8 x 10^{-3} mmHg

enabling a distance resolution of about 10 mm to be achieved. An actual resolution test was performed under atmospheric condition using a neutron source of Pu placed at 50 cm from the detector. In this case the maximum voltage that could be applied was 1800 V and a distance resolution of 19 mm was achieved. The interface between the 2D-PSD detector and the central computer was manufactured Oki-Electric Co based on the design described in the previous report[4].

Fig. 4 shows a typical example of the display of data from 2D-PSD. Fig. 4 (a) (top) is a measurement of the direct beam after collimation by the converging Soller slits when the beam stopper had been removed from the center of the detector by means of a small servo-moter. Each line in the figure depicts the data from a single PSD after integrating the separate time channels at each position. The results indicate the size of beam at a position 3 m from the sample. For the data shown in Fig. 4 (b) a 4 x 5 cm^2 beam stop was placed at the central position. The direct beam was found to be completely shielded by this stopper. The lowest figure (Fig. 4 (c)) is the result of the small angle scattering from a Al-10%Zn-0.1%Mg sample. Although the displayed data are the result of the integration of data of all the wavelengths, they retains the characteristics of the conventional small angle scattering; a distinct dip can be observable at the center of each PSD. These results were converted on-line to a one dimensional |Q| display by computing the Q value of each channel, adding the data for different channels with the same |Q| value, and then dividing the sum by the numbers of contributing channels. The output from this process, as it appeared on the graphic display, is shown in Fig. 5. The total computing time necessary for this process was about 3 min. The open circles

in the figure represent the results obtained after correction for the sensitivity of the counters, the incident neutron intensity distribution (as monitored using the result of incoherent scattering from pure water) and the absorption were made by an off-line computer. The agreement between the on-line display and the corrected data is fairly satisfactory, suggesting that the simple on-line display may be quite helpful in understanding the general characteristics of the small angle scattering.

2.4 Operation of the Second Chopper

The lower part of Fig. 6 shows a typical simple example of the operation of the toothed second chopper illustrated in Fig. 6 (a). By rotating the chopper in coincidence with the neutron pulse, the intensity of the TOF spectra recorded by the fixed counters is modulated to produce a comb-like pattern and the level of the troughs in these comb-like spectra provides information on the contribution from inelastic scattering. This is the most simple method by which to separate the inelastic component from the total small angle scattering. The energy resolution is about $\Delta\lambda/\lambda = 0.05$ ($\sim$50 μeV). This technique will thus be quite helpful in, for example, separating the magnon contributions in small angle scattering.

3. Conclusion

KENS-SAN is found to function according to design specification for measuring and it proves quite useful even conventional small angle scattering. It will take some time, however, to establish measuring techniques for this new type of small angle spectrometer

and to identify for which problems it will be most suitable.

References

1) Y. Ishikawa, S. Ikeda, M. Furusaka and N. Niimura: KENS Report 1 (1980) 101

2) S. Komura, K. Osamura, H. Fujii, T. Takeda and Y. Murakami: Proc. International Conf. SMAS(Berlin) (1980) 183

3) R. Berliner, R.M. Brugger, J.S. King, D.F.R. Mildner, O.A. Pringle, S.A. Werner and W.B. Yelon: Final Report on A Small Angle Neutron Scattering Spectrometer at MURR (1979) April

4) N. Niimura, M. Kohgi and N. Watanabe: KENS Report 1 (1980) 163

(a) KENS-SAN Arrangement

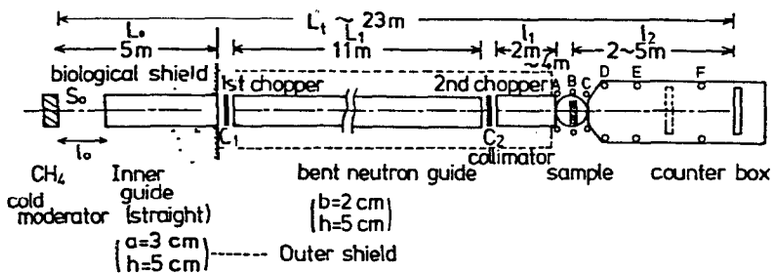

(b) Range of Q Covered by KENS-SAN

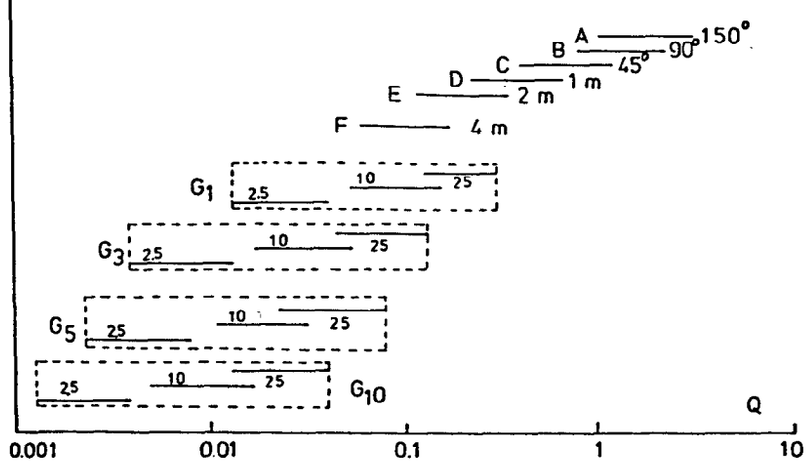

Fig. 1 Layout of KENS-SAN (a) and range of momentum transfers Q covered by this spectrometer

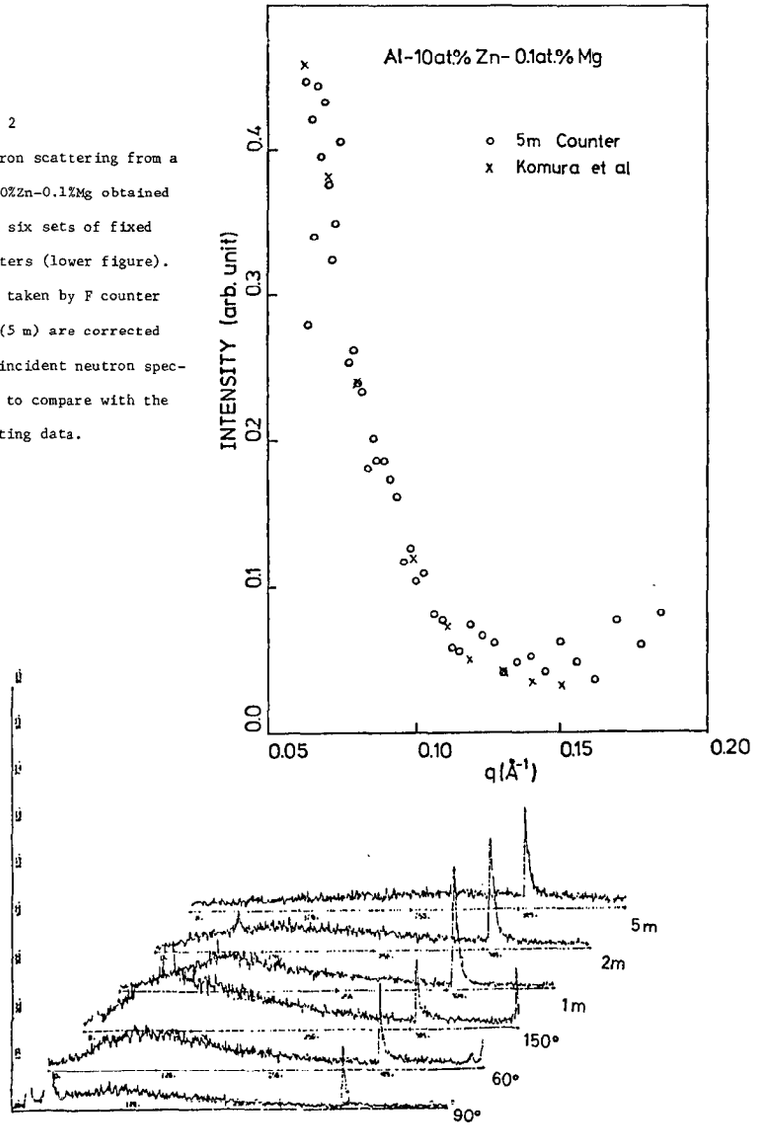

Fig. 2

Neutron scattering from a Al-10%Zn-0.1%Mg obtained with six sets of fixed counters (lower figure). Data taken by F counter set (5 m) are corrected for incident neutron spectrum to compare with the existing data.

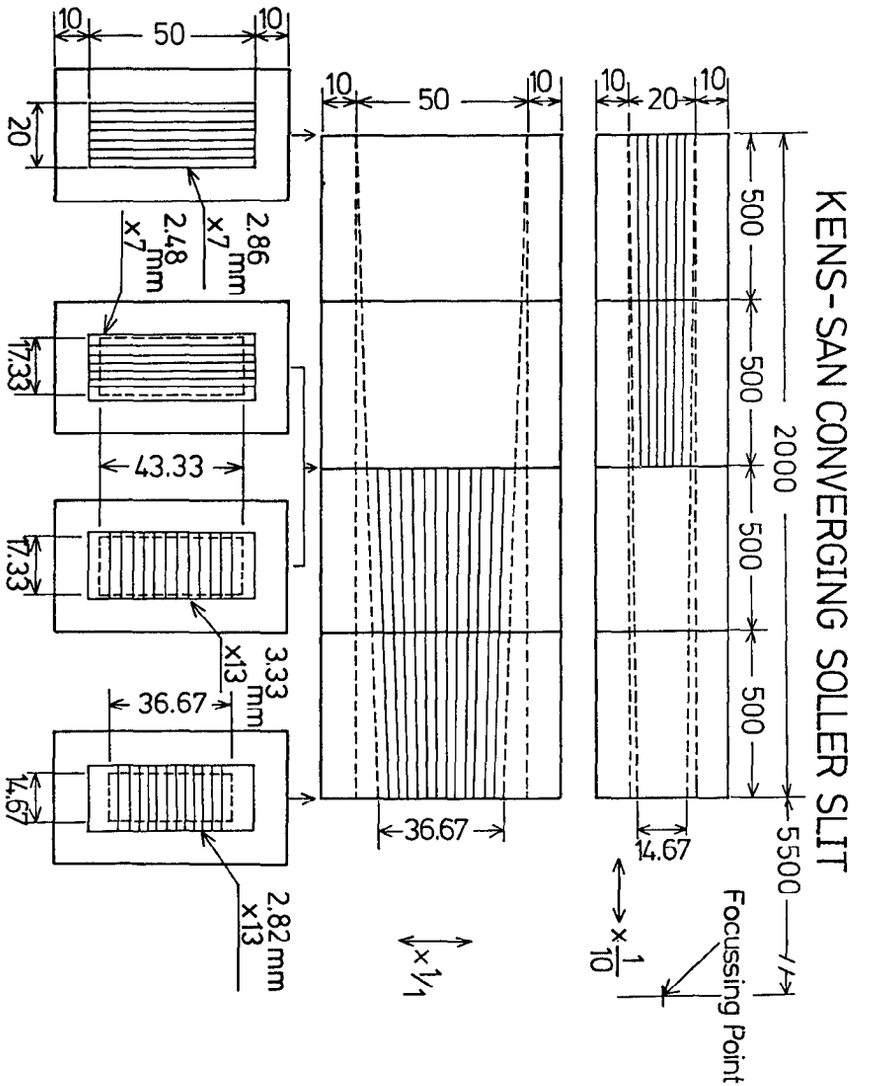

Fig. 3 Converging Soller slit

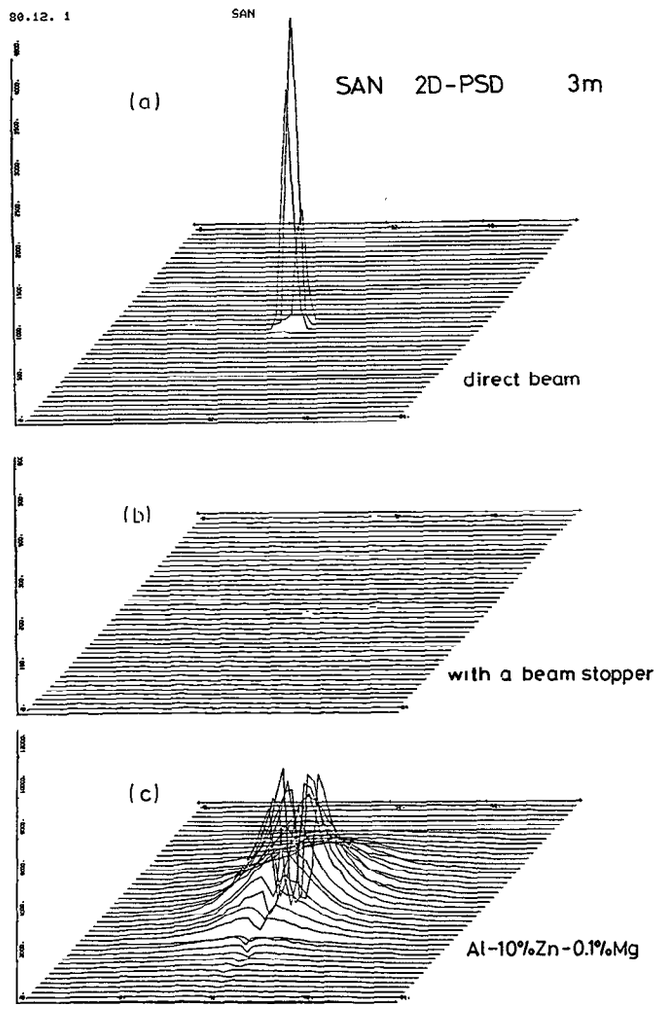

Fig. 4 A typical example of display of the 2D-PSD data. The data are integrated over all time channels. (a) profile of direct beam without a beam stopper (b) that with the stopper (c) small angle scattering from Al-10%Zn-0.1%Mg

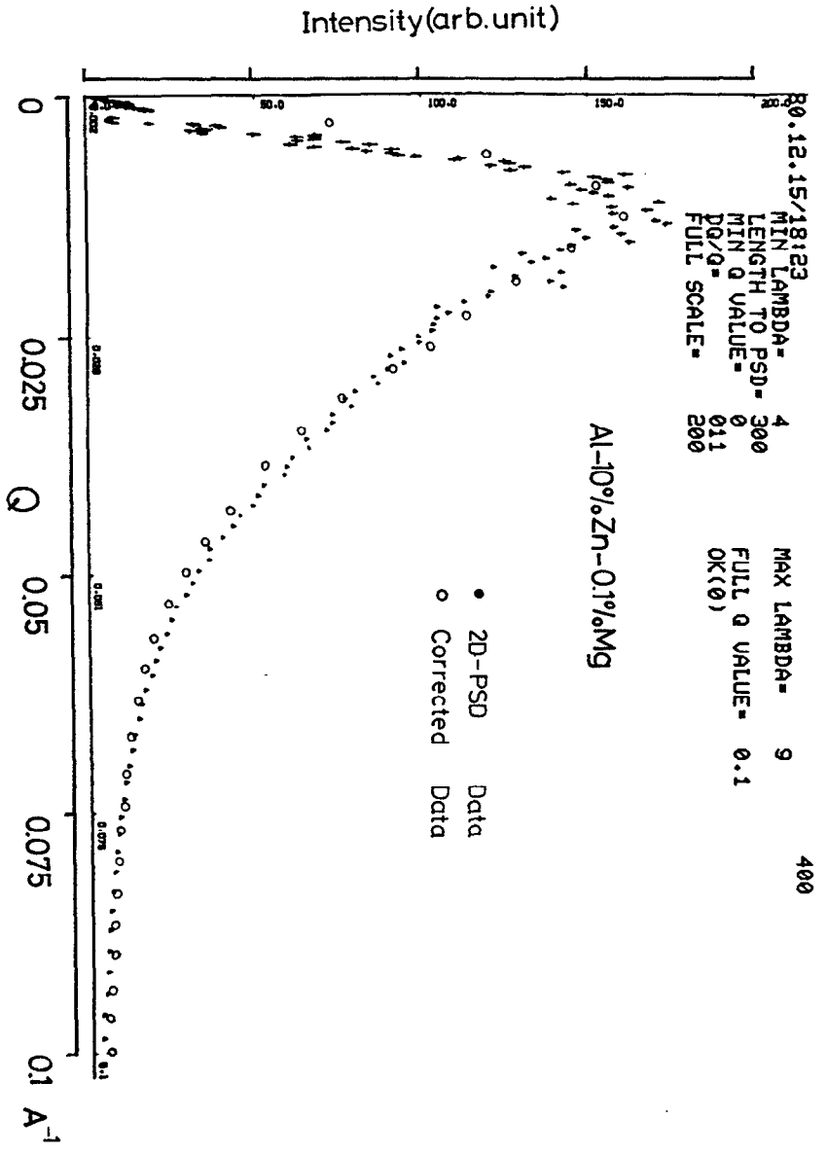

Fig. 5 On-line one dimensional display of small angle scattering (Fig. 4 (c)) against |Q| and comparison with the data corrected for incident neutron spectrum by V incoherent scattering

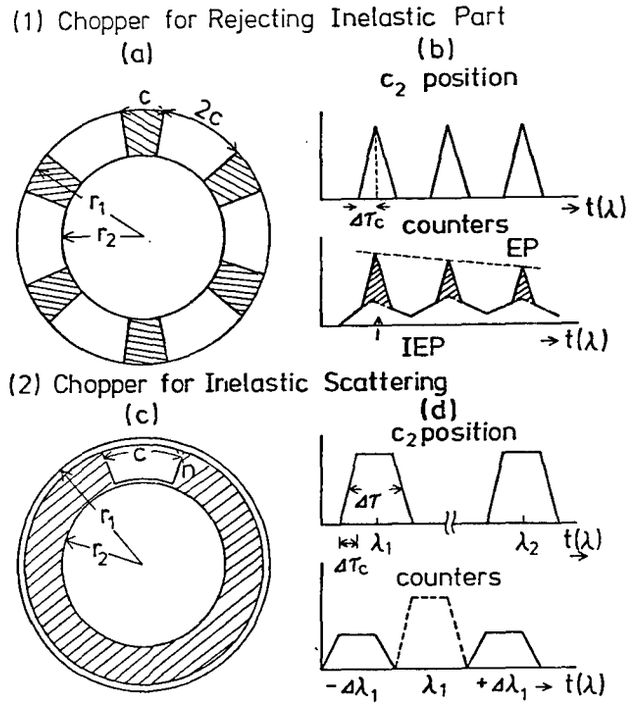

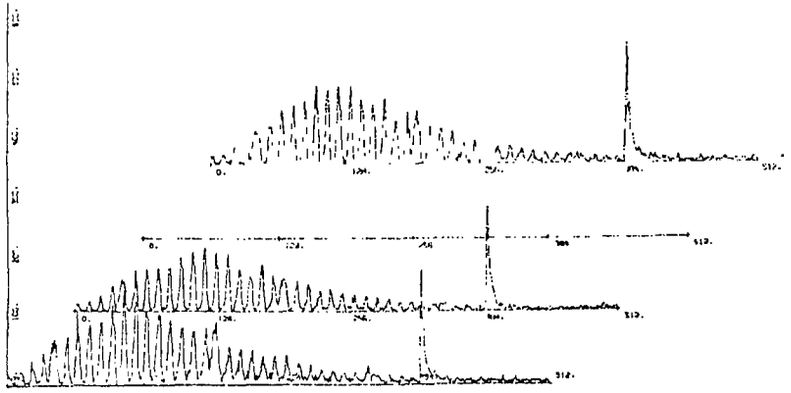

Fig. 6 Two types of second choppers (upper figure) and a result of opperation of a gear type chopper (a), (lower figure)

A Medium Energy Inelastic Spectrometer for SNS

A D Taylor
Neutron Division, Rutherford and Appleton Laboratories

1 Introduction

This paper identifies several active fields of inelastic neutron scattering which require a medium energy inelastic spectrometer covering a wide and variable region of Q and ω space with good resolution. A direct geometry spectrometer is envisaged. A suite of choppers, phased to the pulsed source, will provide incident energies in the range 20 meV < Eo < 140 meV. The secondary spectrometer will cover a wide angular range $-10^{o} < \phi < 135^{o}$. The spectrometer's performance characteristics will be optimised to achieve a resolution $\Delta E_o/E_o$ of $\sim 2\frac{1}{2}\%$ in the energy range 20 meV < E_o < 60 meV. Intensity at the sample will be some 10^3 - 10^4 n cm^{-2} s^{-1}. A dense net in Q space of, typically, 0.1 $\mathring{A}^{-1}$ steps over the large angular range will facilitate the interpolation of constant ϕ scans to constant $|Q|$. Such a specification represents a significant improvement over what is currently available on steady state sources.

2 Scientific Background

Excitations

Time-of-flight is particularly well suited to the study of polycrystalline and amorphous systems. (The study of the amorphous state may be identified as a 'growth area' as progress is made from the relatively simple ordered state to disordered problems, eg amorphous metals). Requirements for coherent density of states measurements are:

- Dense coverage at low Q so that all coherent features are observed.
- Large Q range so that a proper averaging of $\underline{Q}.\underline{U}$ over the Brillouin Zones is achieved.
- Incident energies in the range 20 meV < E_o < 60 meV with $\Delta E_o/E_o \sim 4$-5% at $2\frac{1}{2}\%$ at 60 meV.

S(Q,ω) Studies of Liquid Systems

A dense net in Q space over a wide Q range is required for these studies, typically 100 ϕ scans at Q increments of 0.1 $\mathring{A}^{-1}$. Resolution requirements are similar to those for density of states measurements ($\Delta E_o/E_o \sim 4$-5% at 20 meV; $\Delta E_o/E_o \sim 2$-3% at 60 meV) but incident energies up to $\sim$ 140 meV will be needed to increase the kinematic region probed.

Magnetic Scattering Laws

The form factors of magnetic systems place an upper bound of ~ 5 $\mathring{A}^{-1}$ on Q. The energy of excitations in ionic magnetic systems lies in the range 0-40 meV. Thus the specification of this spectrometer is ideally suited to study these inelastic magnetic systems.

A wide range of Q and ω is needed to study the paramagnetic or critical temperature region where the relatively smoothly varying scattering law gives information on the interaction constants of magnetic systems. There is also much interest in measuring the spin-spin correlation function for disordered systems such as magnetic metal glasses and spin glasses.

Molecular Spectroscopy

In molecular spectroscopy, the resolution requirements for this spectrometer are at their most severe, for there is always the unfavourable comparison with optical techniques. The need to separate peaks is at its greatest for energy transfers, $\hbar\omega$, < 20 meV. For example, $\Delta E_o/E_o$ = 2.5% (0.5 meV at 20 meV) would allow a peak separation of $\sim$ 0.2-0.3 meV at $\hbar\omega \sim 10$ meV. E_o of 60 meV with $\Delta E_o \sim 1.5$ meV would adequately cover the range 15 meV < $\hbar\omega$ < 50 meV, and $\Delta E_o/E_o$ of 5% is more than sufficient at E_o = 140 meV to study hydrogenous modes. If required an improvement in the 20 meV resolution may be achieved at a severe intensity cost by mismatching the chopper with the source.

Assignments in more complex systems, and the fitting of more precise models for the potential in simple systems, will be facilitated by studying intensity variations of a peak with both temperature and Q. The latter requirement can only be achieved if a wide range of scattering angles is available. Studies of a possible weak dispersion with Q of some modes require both this angular range and good resolution.

3 Choice of Design

Only a direct geometry instrument with a wide angled secondary spectrometer, allowing large and variable regions of Q, ω space to be probed, can satisfy the requirements of section 2. In a matched instrument the moderator pulse width dictates the chopper characteristics, leaving only the geometry of the primary and secondary flight paths, L_o and L_1, and the chopper to sample distance, D, as variables. (D may be chosen to be ∿ 1 m without much loss in generality). The specification of $\Delta E_o/E_o = 2\frac{1}{2}\%$ then limits the geometry to specific (L_o, L_1) pairs, differing in performance only in intensity which is proportional to $1/L_o\ (L_o + D)^2$. The physical size of the secondary spectrometer imposes further constraints: the minimum distance for a spectrometer with a horizontal scattering plane is L_o = 12 m (L_1 = 4 m); the minimum approach if the scattering plane is vertically downwards is L_o = 9 m (L_1 = 5 m). The intensity at the sample of these spectrometers favours the vertical geometry by a factor 2.3.

4 Instrumental Description

The instrument will be located on a "high resolution" moderator. A monochromatic incident beam will be provided by a family of choppers (typically at 20 meV intervals), each matched to the moderator pulse at a specific energy. Demands on chopper technology are not severe, the moderator pulse varying from 24 μs at 20 meV to 5.3 μs at 140 meV. The chopper will be located 9 m from the moderator and will spin at a frequency of 300 Hz (6 ν_{SNS}). In addition a crude chopper before the main device will be required to reduce fast neutron background and prevent 'order' contamination.

The layout of the spectrometer and the proposed detector pattern is shown in figure 1. The 2 mm thick Li^6 scintillator elements are arranged at low angles on Debye Scherrer cones. In the intermediate angular range, a central strip is retained offering tighter Q resolution for single crystal experiments. The 4.5 m secondary flight path is evacuated in two regions. The neighbourhood of the sample may be reduced quickly to a cryogenic vacuum and may be let up to atmosphere independent of the secondary spectrometer box, which is maintained at a rough vacuum to minimise scatter. Internal collimation in the secondary spectrometer provides mechanical strength and limits the volume viewed by the large detector array.

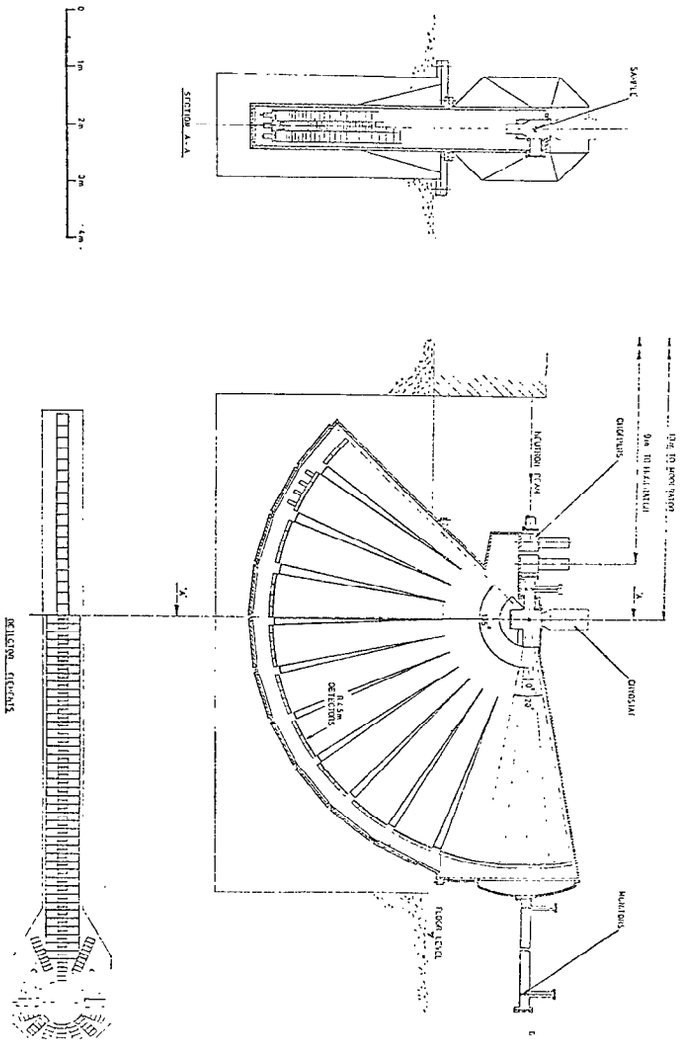

FIGURE 1 MEDIUM ENERGY INELASTIC SPECTROMETER

High Energy Inelastic Spectrometer

B C Boland
Neutron Division, Rutherford and Appleton Laboratories

1 Scientific Background

A spectrometer is proposed than can be used for inelastic neutron scattering experiments at high energy transfers, $\hbar\omega$, and at low momentum transfers $\hbar Q$, which is an important requirement in several areas of science.

(a) In Liquids and gaseous samples, measurements of the high frequency molecular vibrations require small Q vectors to minimise diffusional broadening of the features of the spectrum which increase as Q^2.

(b) In solids, the study of high energy internal vibrational modes require small Q vectors to reduce the effect of multi-excitations of low energy modes. The effect can be to broaden each mode by an amount which increases very rapidly with Q.

(c) The observation of high frequency magnetic excitations requires small Q vectors because the magnetic scattering is modulated by the square of the form factor F(Q) describing the spatial distribution of the spin density around the magnetic ions.

2 In addition the instrument will have the capability of making measurements of high momentum transfer $\hbar Q$, an important region for experiments on quantum liquids for example.

3 Instrument Description

The instrument is designed to measure energy transfers $\hbar\omega$ in the range 100 - 500 meV with momentum transfers $\hbar Q < 6$ Å^{-1} but it can be used outside this range. Figure 1 shows the layout. Incident energies from 200 - 1000 meV are used and selected by a fast neutron chopper placed 10 m from an ambient temperature moderator. The chopper operating at 600 Hz (12 times the SNS frequency) is accurately phased to the SNS pulse to ± ½ μ us and a range of incident energies chosen by varying the chopper phasing. In order to cover the whole energy range a set of four choppers will be required. Neutrons selected by the chopper fall on the sample placed 2 m downstream. This distance, containing collimation, is needed to ensure that low angle counters do not have a direct view of the chopper or chopper tank. Neutrons scattered from the sample are detected by annular Li-glass scintillator detectors at 4 m (3° - 7°) and 2 m (8° - 30°) from the sample. In addition to the horizontal plane there is a set of scintillator detectors from 3°-30° in ½^{o}steps ∿ 5 cm high for vector Q experiments. The main beam passes through the centre of the counter array to a beam stop 4 m downstream. Scatter from windows and air in the main beam is eliminated by evacuating the sample chamber and detector box which are connected by a vacuum gate valve. Single samples can be mounted in the vacuum at temperatures between 77K and 1200K. A 4 position sample changer can be fitted operating down to 77K. An insert with thin windows fitted to the sample box enable liquid helium crystats to be placed in the beam. The cryostat is supported from below by an automated goniometer. A small bank of counters is also placed at 4 metres from the sample at a scattering angle of 140° for measurements at large values of momentum transfer. In addition space is available for this bank to be extended in the future to a scattering angle of 70°. The high angle banks will be filled with helium gas. The neutrons detected are time-sorted into 2000 time channels whose widths can be chosen to be between ½ μs - 10 μs.

4 Instrument Performance

The energy resolution has been estimated assuming the instrument views the moderator normally. There is an advantage in viewing the moderator at an angle due to time focussing, the optimum angle being between 20° and 30°. At angles greater than 30°, the moderator flux is reduced in value. Figure 2 shows the energy resolution plotted against energy transfer for two values of incident energy, for a scattering angle of 3° and a counter bank at 4 m, together with the corresponding momentum transfers. Figure 3 shows similar curves for a 2 m bank. The low angle counter banks 3° - 30° give momentum transfers of ∿ 2 Å^{-1} - 10 Å^{-1} and the 140 bank ∿ 34 Å^{-1}. The counter bank for vector Q experiments subtending an angle of ½^o at the sample gives ΔQ ∿ 0.1 Å^{-1}. The intensity at the sample is estimated to be 1×10^4 cm^{-2} s^{-1} at 1.0 eV.

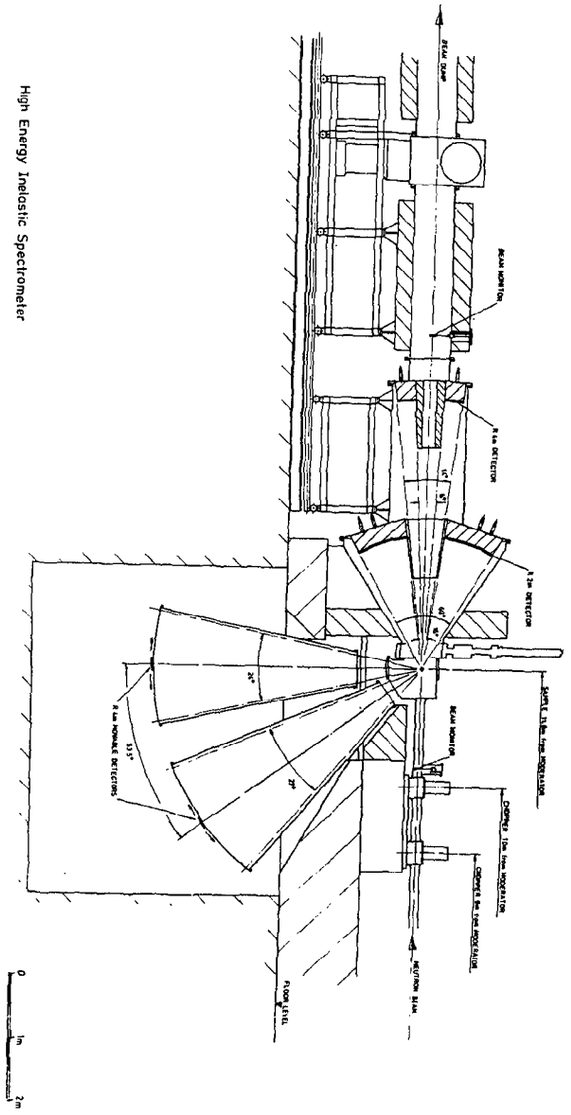

High Energy Inelastic Spectrometer

FIG 1

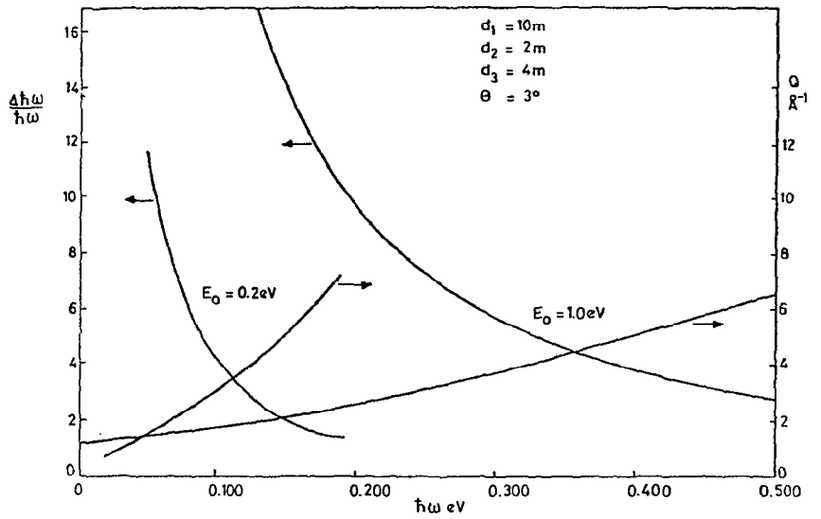

FIG 2

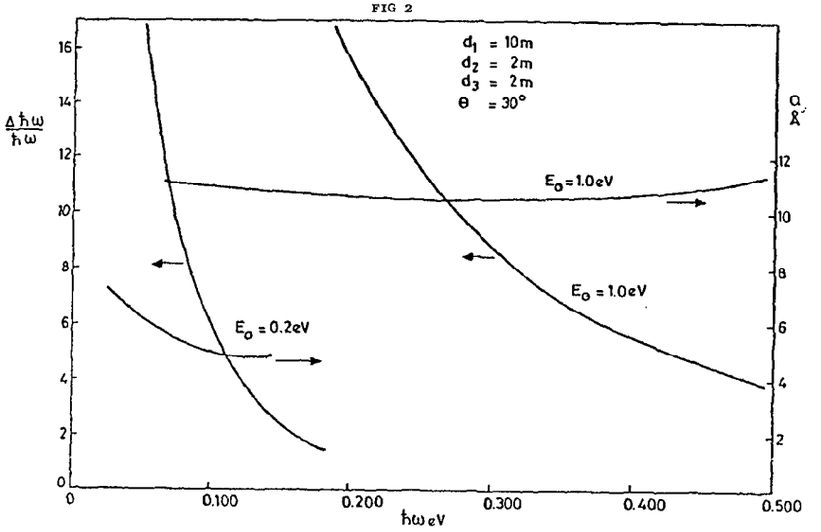

FIG 3

High Throughput Inelastic Spectrometer

R M Richardson
Neutron Division, Rutherford and Appleton Laboratories

1 Introduction

The "High Throughput Inelastic Spectrometer" is intended to provide the neutron scattering equivalent of infra-red spectroscopy for studying molecular vibrations. It is expected to find applications in vibrational spectroscopy of the solid phase, adsorbed species, and hydrogen in metals and alloys. It will be installed initially at the Harwell linac as soon as possible and eventually moved to the SNS. Most of the specification given below apply equally to installation on either neutron source but a few apply specifically to installation at the Harwell linac. In particular, it will be noted in Figure 1 that there is space for two energy analysers (either side of the sample). On the linac, the beryllium filter will occupy one side while the other is used for developing a high resolution analyser system which will be incorporated into the machine when it is moved to SNS. Only the beryllium filter analyser will be discussed here.

2 Principle

A wide range of observable energy transfers can be obtained by detecting down scattered neutrons with a band pass filter-detector. If the energy of the detected neutrons is low compared with the incident energy, their scattering vector Q is practically independent of scattering angle. A high count rate can therefore be obtained by detecting neutrons over a large solid angle without losing the Q resoltuion.

$$Q = 0.7 \sqrt{E_o + E - 2\sqrt{E_o E}\cos 2\theta}\ \text{Å}^{-1} \qquad 0.7\sqrt{E_o}\ \text{Å}^{-1} \text{ for } E \ll E_o$$

where E_o (E) is the incident (final neutron energy in meV and 2θ is the scattering angle. The main limitation of this technique is that there is no possibility of varying Q independently of the energy transfer ($\hbar\omega = E_o - E$) but this is unimportant for many applications.

3 Construction

The primary spectrometer consists of a 12 m initial flight path with associated collimation, supports and vacuum system. A special sample cryostat would allow cooling of the sample to 10K to minimise the loss of intensity from the Debye-Waller factor and multiphonon effects but would permit rapid sample changes if required. The sample would typically be a cylinder 25 mm x 100 mm.

The analyser will consist of a nitrogen cooled beryllium filter which only transmits neutrons with less than 5 meV energy to an array of 25 mm 2 atm boron trifluoride counters. The filter will be 0.15 m thick and cover a solid angle of 1.1 str and will be divided into 24 sections separated by 1 mm thick B_4C loaded resin sheets. This arrangement provides adequate fast neutron discrimination without degrading the time resolution. The output from 3 groups of 4 detectors will be separately time sorted to allow for different background conditions and the spectral distribution of the incident beam will be obtained by time-of-flight analysis on the output of a U^{235} monitor before the sample.

A 0.025 mm gadolinium foil will be placed before the monitor in order to absorb neutrons of 5 meV and less which would be elastically scattered by the sample and cause a high background. Figure 3 shows a spectrum with (solid line) and without (dashed lines) the gadolinium. For a source with a pulse repetition period of 6.7 ms, it is clear that the gadolinium must be used.

4 Resolution

The energy transfer resolution of the instrument is dominated by the effect of the pass band (ΔE_2) of the filter with smaller contribution from the pulse width (Δt) from the ambient temperature moderator and the distribution of secondary flight-paths (ΔL_2). The three terms are:

$$T_1 = \frac{\Delta E_2}{\hbar\omega}\left[\left(\frac{E_1}{E_2}\right)^{3/2}\frac{L_2}{L_1} + 1\right]$$

$$T_2 = \frac{\Delta t}{\hbar\omega} \cdot \frac{2\,E_1^{\ 3/2}}{2286\,L_1}$$

$$T_3 = \frac{\Delta L_2}{\hbar\omega} \cdot \frac{2\,E_1^{\ 3/2}}{L_1\,E_2^{\ 1/2}}$$

where $\hbar\omega = E_2 - E_1$ meV is the energy transfer. The contribution from the distribution in initial flight-paths is negligibly small. The total energy transfer resolution is

$$\frac{\Delta\hbar\omega}{\hbar\omega} = \sqrt{T_1^2 + T_2^2 + T_3^2}$$

Using the design parameters (L_1 = 12.0 m L_2 = 0.24 m) the above expression has been evaluated for various values of $\hbar\omega$ and shown in Figure 2. It should be noted that ΔE_2 is not 5 meV but typically 1.7 meV FWHM because the long time side of the peak (eg in Figure 3) decays rapidly (approximately τ^{-4}).

5 Intensity

Figure 2 also shows the total counts in an inelastic peak from a 10% scattering sample. The inelastic peak is assumed to result from down scattering from the fundamental mode of an isotropic Einstein oscillator with unit effective mass (eg hydrogen in a metal). Figure 3 shows the time-of-flight spectrum that would be expected from such a sample with a fundamental frequency equivalent to 100 meV. The shape of the spectrum has been determined by the pass band of the filter only. Incorporating the effect of the moderator pulse width and the distribution of secondary flight paths would round the corners of the peaks considerably but would not change the total intensities.

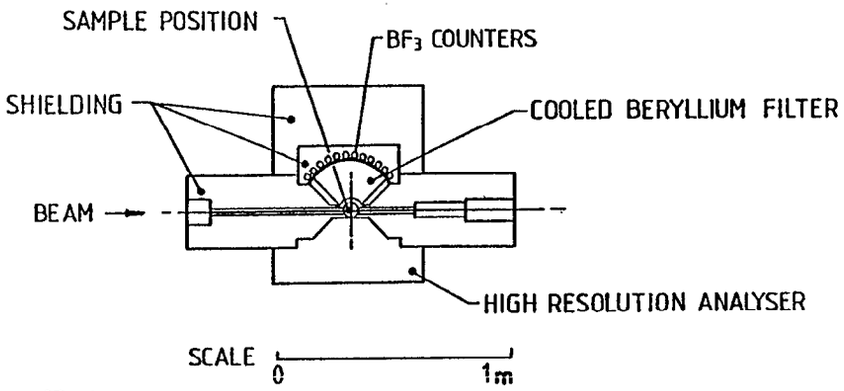

FIGURE 1

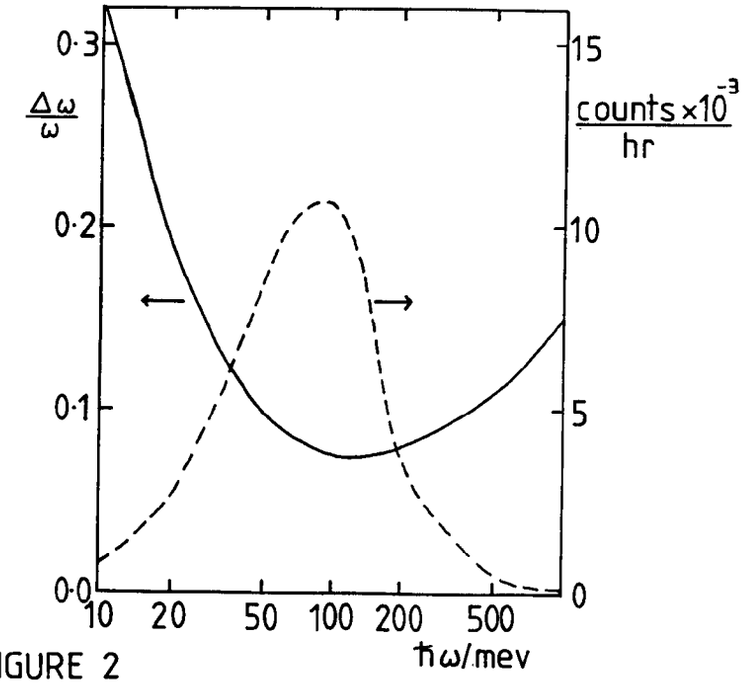

FIGURE 2

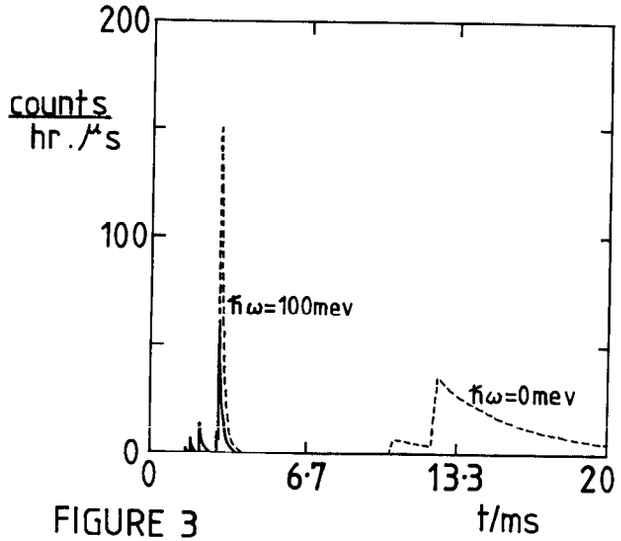

FIGURE 3

High Resolution Inelastic Spectrometer

C J Carlile
Neutron Division, Rutherford and Appleton Laboratories

1 Introduction

A high resolution inelastic spectrometer is at the stage of detailed design prior to installation on the SNS viewing the 20K moderator. It is the time-of-flight analogue of the backscattering spectrometer IN10 at ILL, Grenoble. By changing the neutron energy selector/analyser combination resolutions of ∿ 1 μeV and ∿ 13 μeV can be selected. The incident energy window is wider than that obtainable on IN10 and can be continuously extended by modulating the phase of the neutron energy band selector thus permitting inelastic measurements to be carried out with high resolution at energy transfers previously unattainable.

2 Scientific Background

The availability of a spectrometer which can measure energy transfers ∿ 3 meV with high resolutions will greatly extend the science carried out at present. It is expected that the study of diffusive motions in aqueous solutions, metal hydrides, superionic conductors, liquid and molecular crystals, intercalated compounds, and layered minerals will benefit from the ability to study the precise shape of the quasielastic peak out to higher energy transfers and, by changing the resolution during an experiment, to make precise measurements of the elastic incoherent structure factor. This latter point is particularly important when it is required to study the sample in an accurately known environment (temperature, pressure, concentration, humidity for example). At the present time such measurements in general require separate experiments on different spectrometers.

The measurement of tunnelling processes in molecular systems and the study of hyperfine splittings are fields which will benefit from the wider inelastic capabilities afforded by the the spectrometer. The

separation and assignment of nearly degenerate crystal field levels should also be facilitated.

3 Instrument Description

A schematic diagram of the spectrometer is shown in the figure. It operates in two modes both employing the same principle of mechanically selecting, close to the moderator, a band of neutron energies ΔE having a time width $\delta t(E)$ and allowing this band to disperse over a 40 metre drift distance along a neutron guide to provide the required incident energy resolution within the constraints of the frame overlap condition. Neutrons scattered from the sample whose energy is changed by an interaction with the sample to exactly the analyser energy (∿ 2 meV in both cases) are detected after backscattering from the crystal analyser system. Neutrons scattered directly into the detectors are discriminated against by the use of an asynchronous beam modulation chopper close to the analyser section.

By the use of a disc chopper as the neutron energy selector and graphite analysers a resolution ∿ 13 μeV is attainable over a window of ∿ 1 meV. Changing to the high resolution mode a fast Fermi chopper located 4.4 m from the moderator reduces the intrinsic time burst of the SNS pulse and in combination with a set of silicon analysers will provide a resolution ∿ 1 μeV within a window of ∿ 100 μeV. The intensity at the sample position is predicted to be ∿ 3×10^4 n cm^{-2} s^{-1} for the high resolution option and ∿ 5×10^5 n cm^{-2} s^{-1} for the low resolution option. A fuller list of instrument performance figures is given in Table 1.

In both modes it is possible to offset the phase of the first band selector with respect to the neutron pulse such that the window is centred around a discrete energy transfer to study a particular region more closely. It is also possible to modulate the phase of this chopper, for example sinusoidally, to cover a much wider range of energy transfers, possibly beyond 3 meV, in one measurement.

The neutron detector will comprise a position sensitive scintillator detector with ∿ 1500 elements set on a spherical surface precisely and permanently positioned in backscattering geometry with respect to both analyser banks (the graphite analysers being retractable). The centres of curvature of both sets of analysers and the detector will coincide at the sample position.

Table 1

Instrumental Parameter		Option	
		C(002)	Si(111)
Energy Resolution		13 μeV	1.2 μeV
Energy Window		960 μeV	100 μeV
Final Energy		2.07 meV	1.82 meV
Intensity at Sample		3×10^4 cm^{-2} s^{-1}	5×10^5 cm^{-2} s^{-1}
Scattering Angles		15°-165°	5°-165°
Q Range		0.25 Å^{-1} - 1.86 Å^{-1}	0.09 Å^{-1} - 1.98 Å^{-1}
Q Resolution at	15°	5.7%	5.7%
	90°	0.86%	0.75%
	165°	0.61%	0.11%
δQ at	15°	0.014 Å^{-1}	0.015 Å^{-1}
	90°	0.011 Å^{-1}	0.011 Å^{-1}
	165°	0.011 Å^{-1}	0.002 Å^{-1}
Solid Angle Detected		0.22 ster	0.85 ster

Quasielastic Scattering Spectrometer

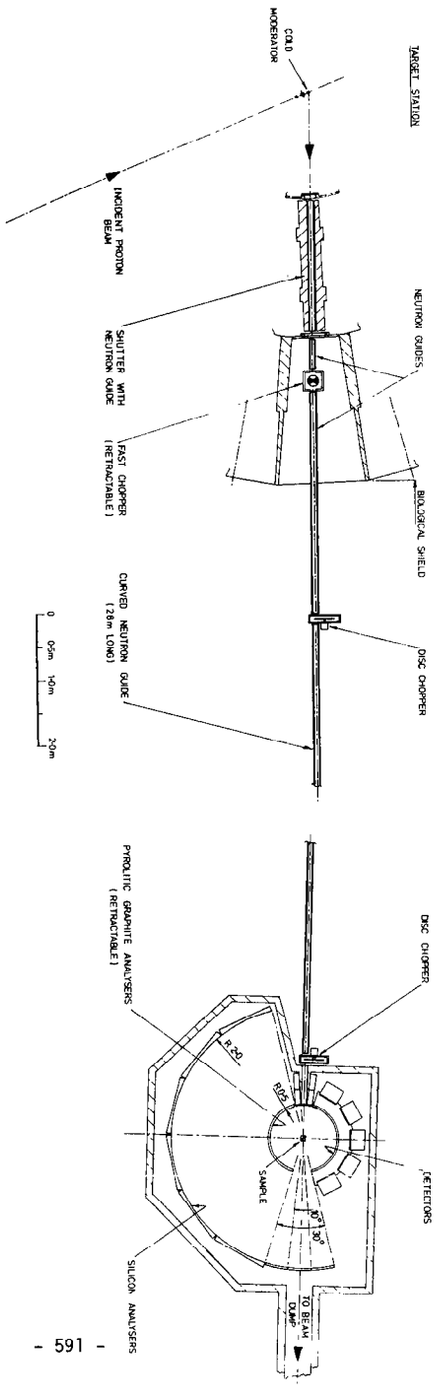

Large Analyser Mirror Low-Energy Spectrometers, LAM(KEK) and LANDAM(HU), and Electron Linac Cold Source

K. Inoue*, Y. Kiyanagi*, M. Kohgi†, Y. Ishikawa†, N. Watanabe††, H. Iwasa*, Y. Sakamoto* and K. Jinguji*

* Department of Nuclear Engineering, Faculty of Engineering, Hokkaido University, Sapporo

† Physics Department, Faculty of Science, Tohoku University, Sendai

†† National Laboratory for High Energy Physics, Tsukuba

The spectrometers, the LAM(KEK) and its prototype LANDAM(Hokkaido University), are suitable to measure the low energy transfer neutron scattering. They were planned mainly to be used in the studies of diffusive motion in condensed matter with conventional energy resolution. The accelerator-based cold neutron source was chosen for the features; its nearly flat distribution of the time-of-flight spectra and its ability to achieve a very low background level. These features are particularly advantageous in quasielastic experiments using a conventional energy resolution in which analyses of the quasielastic peak shape, and not only the peak width, are required. Figure 1 shows the cold neutron time-of-flight spectrum emanating from the 20 K methane cold source and the spectrum from ambient temperature water. The same size moderator chamber was used. The spectrum from methane exhibits enhancement and a nearly flat distribution of around 5 meV. Figure 2 shows the time-energy distribution, the typical time constants of the pulse; the rise time, half-width and decay time. The rise time is about 20 μsec and it does not vary appreciably as a function of energy.

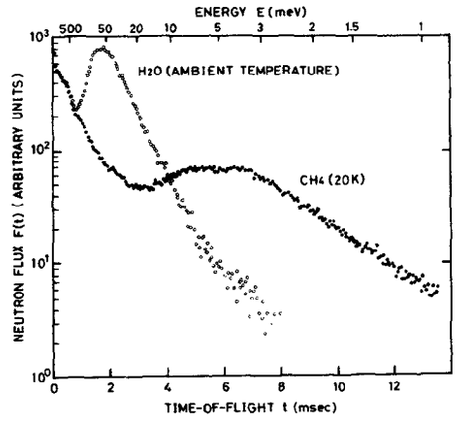

Fig. 1. Measured neutron time-of-flight spectra from a 20 K methane moderator and an ambient temperature water moderator.

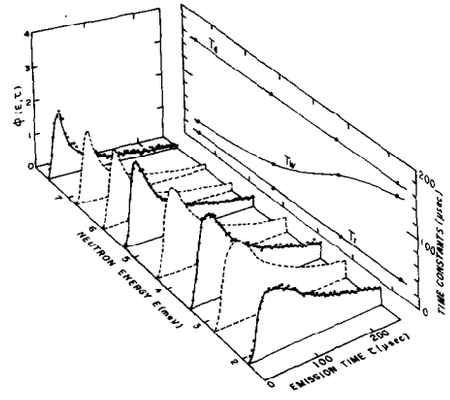

Fig. 2. Time dependent neutron flux emanating from a 20 K methane moderator. The experimental results are shown by the dots, and the synthesized curves are indicated by the smooth curves.

Figures 3 and 4 are the plane view of the LAM and the LANDAM, which are inverted geometry tof spectrometers. As illustrated in Fig. 5 the spectrometer consists of the cold source at distance ℓ_1 from the specimen and a set of four assemblies of large area crystal analyser mirrors, beryllium filters,

and counters. The spectrometer operates as follows: neutrons are scattered through the second flight distance ℓ_2, they are reflected by the analyser mirrors, impinge on the beryllium filters, and subsequently are detected by the counters as monochromated neutrons.

Untill now, many quasielastic investigations have been dominated by measurements of energy-gain scattering, and the scattered neutron spectra observed by time-of-flight spectrometers have been considerably distorted by the time factor t^{-3} weighting factor in the time-of-flight which inevitalby appears in ordinary direct geometry facilities. When inverted geometry is employed, this large spectral distortion is eliminated because of the nearly flat distribution of the cold neutron time-of-flight spectrum as shown in Fig. 1.

We were able to estimate the resolution of the spectrometer in an

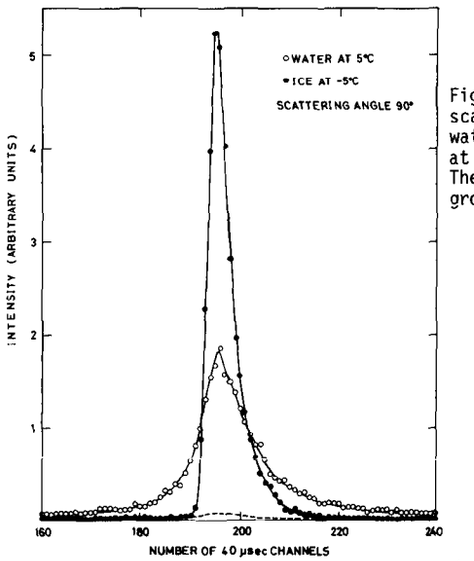

Fig. 6. Raw data of normalized scattered intensities from water at 5°C and ice at -5°C at 90° scattering angle. The dashes indicate the background counts.

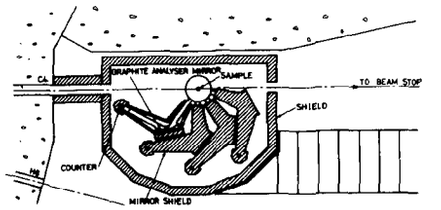

Fig. 3. Plane view of the LAM spectrometer

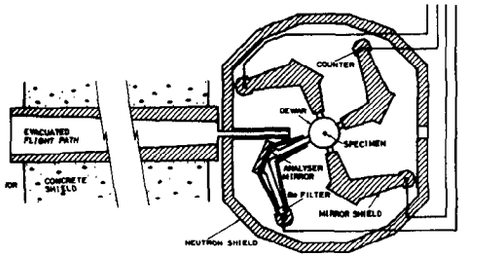

Fig. 4. Plane view of the LANDAM spectrometer

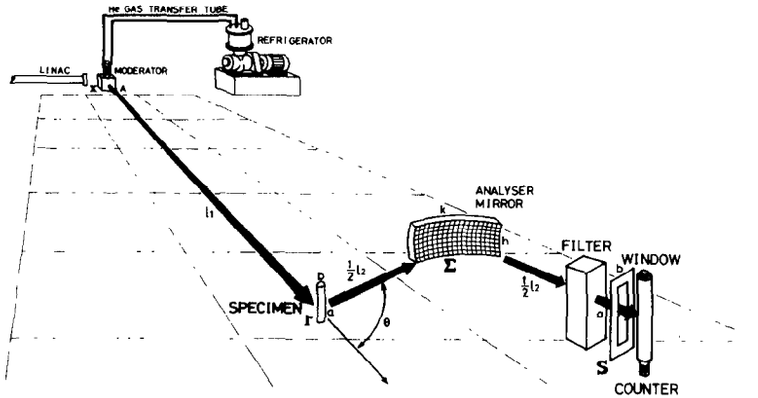

Fig. 5. General layout of the quasielastic spectrometer using an accelerator cold neutron source. Cold neutrons are produced by a methane slab moderator at 20 K.

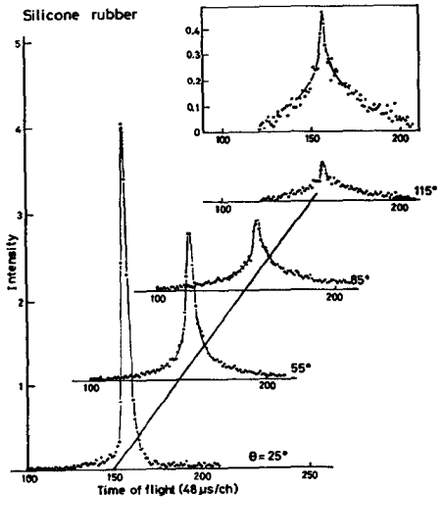

Fig. 7. Quasielastic peaks of silicone rubber at four angles at ambient temperature by LAM.

experiment on the scattered intensity of ice (Fig. 6). The rise time of the peak for the pure elastically scattered neutrons was short, and its shape, which appeared on the rising side, was nearly the same as that of the resolution function of the analyser mirrors. The decay time was relatively long, owing to the properties of the incident neutrons.

These spectrometers show high efficiency. One paint in fact is that for the count rate of the same sample, the LAM is almost exactly 10 times more efficient than the LANDAM. However, in comparing their cold neutron yields per one pulse, the KENS cold source yield is about 500 times higher than the LANDAM's.

Figure 7 is the scattered spectra from silicone rubber obtained from the LAM during its initial operation period. The sharp peak is caused from the stationary part in the correlation function which corresponds to the presense of the bridge in rubber polymer and indicates the oscillatory tendency as a

function of Q. This tendency may relate to the dynamical structure of the micro-Brownian motion of the polymer segments between the bridges. In another experiment by using the LANDAM we measured the spectrum of deuterium substituting methanole and its aqueous solution at ambient temperature. Although Fig. 8 is only the raw data, two components due to translational and localized motion were observed. From our data we concluded the localized diffusive motion of hydrogen in hydroxyl becomes restricted. We are continuing our investigations in this area.

The pulsed cold neutron source quasielastic spectrometers described herein have performed effectively under the experimental conditions we have imposed, and it has shown much promise as reliable instruments for application in quasielastic studies where conventional energy resolution is involved.

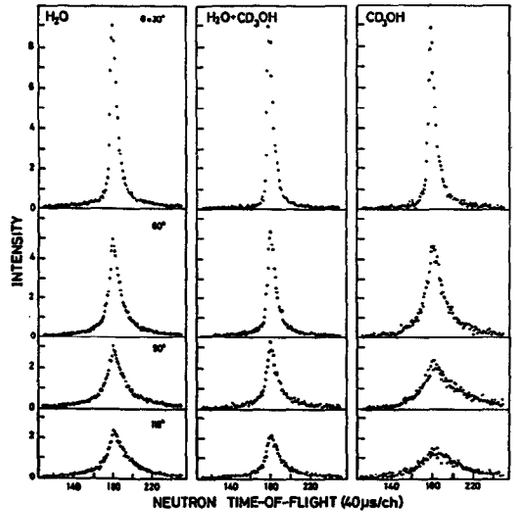

Fig. 8. Quasielastic spectra from water, deuterium substituting methanol and its aqueous solution.

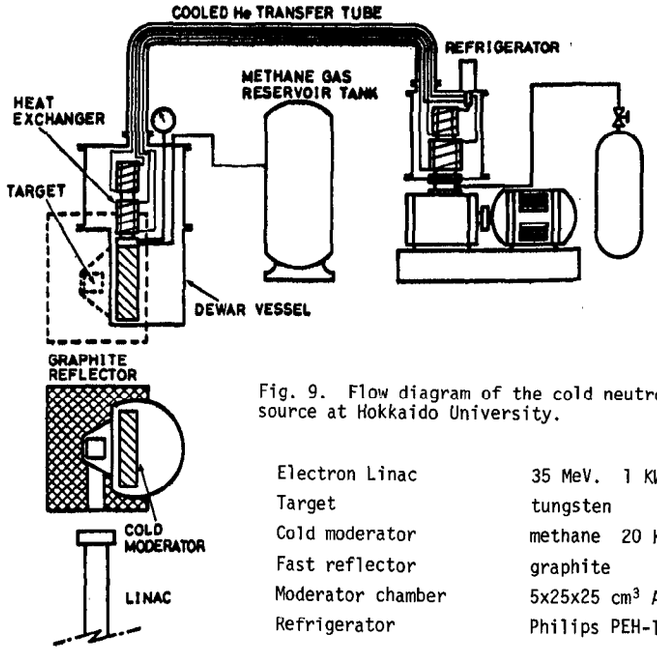

Fig. 9. Flow diagram of the cold neutron source at Hokkaido University.

Electron Linac	35 MeV. 1 KW
Target	tungsten
Cold moderator	methane 20 K
Fast reflector	graphite
Moderator chamber	5x25x25 cm^3 Al
Refrigerator	Philips PEH-100

The signal-to-background ratio is extremely good due to the pulsed source, and the spectral distortion is very small due to the inverted geometry and the cold source spectra. The energy resolution of about 100 ∿ 200 μeV is attainable with reasonable count rates; and the Q ranges are between 0.5 ∿ 2.5 $Å^{-1}$. These spectrometers may also be of value in the performance of peak profile analyses in quasielastic studies.

The cold source at Hokkaido University was developed to be used in a modest capacity electron linac of 35 MeV and 1 KW beam power under operational conditions. In order to accommodate the modest fast neutron source, we had

to develop an efficient cold source. According to several preliminary experiments we chose 20 K methane for the cold moderator. Finally it was demonstrated that the methane was very suitable as a cold moderator for the accelerator-based cold source. The flow diagram (Fig. 9) shows the cold source at Hokkaido University. The simplicity of design and our use of methane render the cold source fail-safe and fail-operative. Decomposition of methane occures during irradiation and the hydrogen production rate is 3.5 % per 1000 hr irradiation. This facility is effectively used as the cold source of the LANDAM spectrometer.

Multi-Analyser Crystals Spectrometer at KENS

K. Tajima, K. Kanai, Y. Ishikawa, S. Tomiyoshi*
and C.G. Windsor

Department of Physics, Tohoku University

* Research Institute for Iron, Steel and Other Metals, Tohoku University

§ Introduction

In order to investigate the neutron inelastic scattering a new type of spectrometer in which a crystal analyser is combined with the TOF method has been proposed by several authors[1~4]. If many analysers and detectors are used in this type of spectrometer, a wide range of $\hbar\omega$-Q space can be explored efficiently and it was based on this principle that we designed the MAX(Multi Analyser Crystal) spectrometer[4]. As described previously[4], the MAX has 15 analyser crystals whose scattering angle can be adjusted independently. In this way scan along the principal direction in reciprocal space can be performed efficiently. The MAX was recently installed at the H5 experimental hole at KENS and we outline below the initial alignment procedure and demonstrate some of our early results.

§ Spectrometer Alignment

As with all crystal analyser spectrometers, it is important that the various zero angles for the scattering angle $2\theta_s$, the analyser angle $2\theta_A$ and the analyser crystal axis ω_A are determined. In Figure 1 we show the definitions of the 3 zero angles which must be defined; $2\theta_s°$, $2\theta_A°$ and $\omega_A°$.

a) Scattering zero angle $2\theta_s°$

Because of the mechanical limitation it is generally

impracticable to rotate the $2\theta_s$ to the straight through position. Each angle can be calibrated independently by elastic diffraction from a powder sample of known lattice spacing. The total flight path L needs to be accurately known since the scattering angle is deduced from the flight time $t_{hk\ell}$ of a reflection of spacing $d_{hk\ell}$. The $2\theta_s°$ can be determined from a equation

$$2\theta_s - 2\theta_s° = 2 \sin^{-1} \left(\frac{\hbar}{m} \frac{t_{hk\ell}}{L} \cdot \frac{\pi}{d_{hk\ell}} \right).$$

b) Analyser arm zero angle $2\theta_A°$

The analyser arem zero angle, $2\theta_A°$, may be determined by measuring the incoherent elastic scattering from vanadium. The above expression becomes

$$2\theta_A - 2\theta_A° = 2 \sin^{-1} \left(\frac{\hbar}{m} \frac{t}{L} \cdot \frac{\pi}{d_A} \right),$$

where d_A is the analyser interplaner spacing and t is the flight time.

c) Analyser crystal zero angle $\omega_A°$

$\omega_A°$ can be accurately determined by using a sample reflection of equal d-spacing to that of analyser. This corresponds to the focussing condition and the width of the reflection from the analyser is a minimum.

§ Measurements

1) Vanadium

The incoherent elastic scattering from a polycrystalline vanadium rod was measured and some typical results are shown in Figure 2. These measurements were used for spectrometer alignment as above and to provide on the information on the analyser reflectivity, detector efficiency and instrumental resolution.

2) Phonons in b.c.c. Fe

A series of phonon spectra along the [100] direction in

Fe-4%Si were measured around the (110), (112) etc. reciprocal lattice points. The scattering diagram and the range of the measurement for some of the analysers is shown in Figure 3. The dotted lines represent the longitudinal and transverse phonon dispersion curves which were measured on a triple axis spectrometer[5]. Some examples of the spectra measured on MAX are shown in Figure 4. The arrows indicate the central position of the (002) reflection and the arrows marked with the letters 'L' or 'T' indicate the positions of the phonons as anticipated on the basis of Figure 3. The other peaks at lower channels are from higher order reflections of the analyser.

The spin wave peak is discernible in the spectra corresponding to $2\theta_s = 47°$, as indicated by the arrow marked with 'M'. This peak corresponds to 'up scattering' spin wave around the (110) reciprocal lattice point. However, mainly because of the low value of the magnetic form factor at higher Q values, no appreciable magnetic peak is observed in the vicinity of the (112) reciprocal lattice point.

Thus we found that the MAX spectrometer could measure the phonon spectra with a good signal to noise ratio. The magnetic excitations would also be detected in a wide range if the measurement would be done around an appropriate reciprocal lattice point, which is now in progress.

References

1) E. Maliszowski et al., "Inelastic Scattering of Neutrons", Vol. II, p. 313, IAEA, 1968.

2) C.G. Windsor et al., Nuc. Inst. Method, 151 (1978) 477.

3) C.G. Windsor, unpublished,

4) K. Tajima et al., KENS report I, KEK Internal. 80-1 p.86(1980).

5) B. Brockhouse et al., Solid State Commun. 5 (1967) 211.

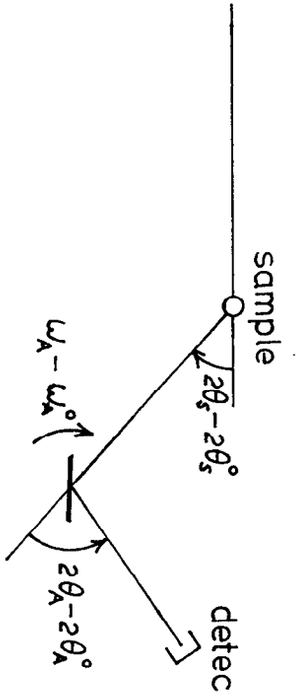

Fig. 1. The definitions of the three angles and their zero angles used in alignment of the spectrometer.

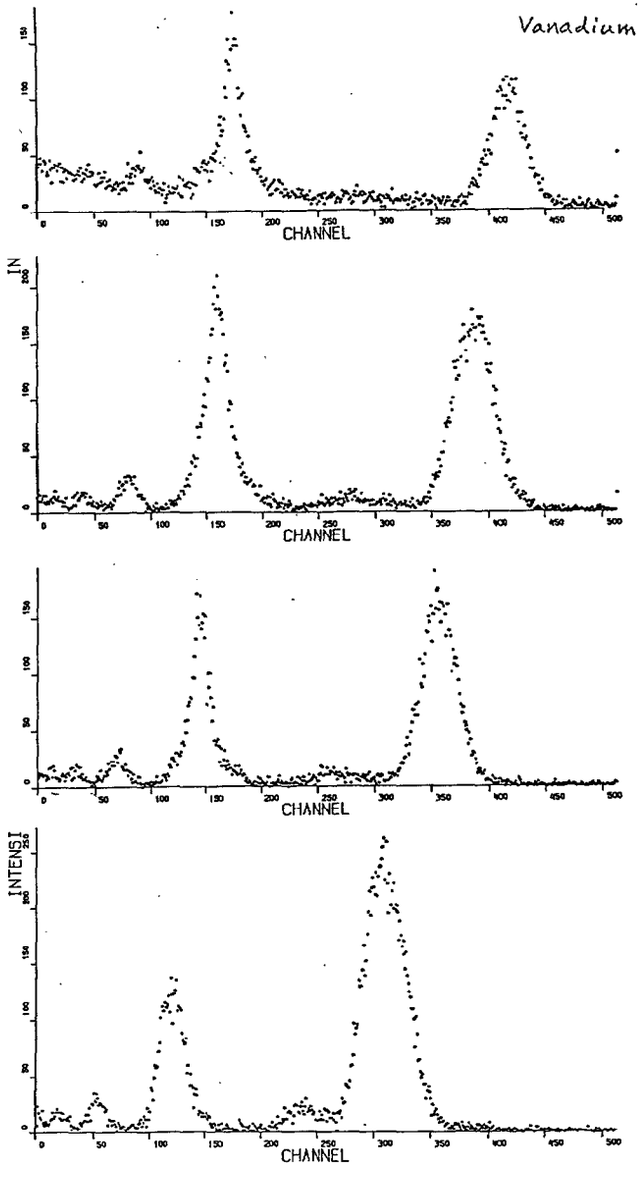

Fig. 2. The incoherent elastic scattering from vanadium.

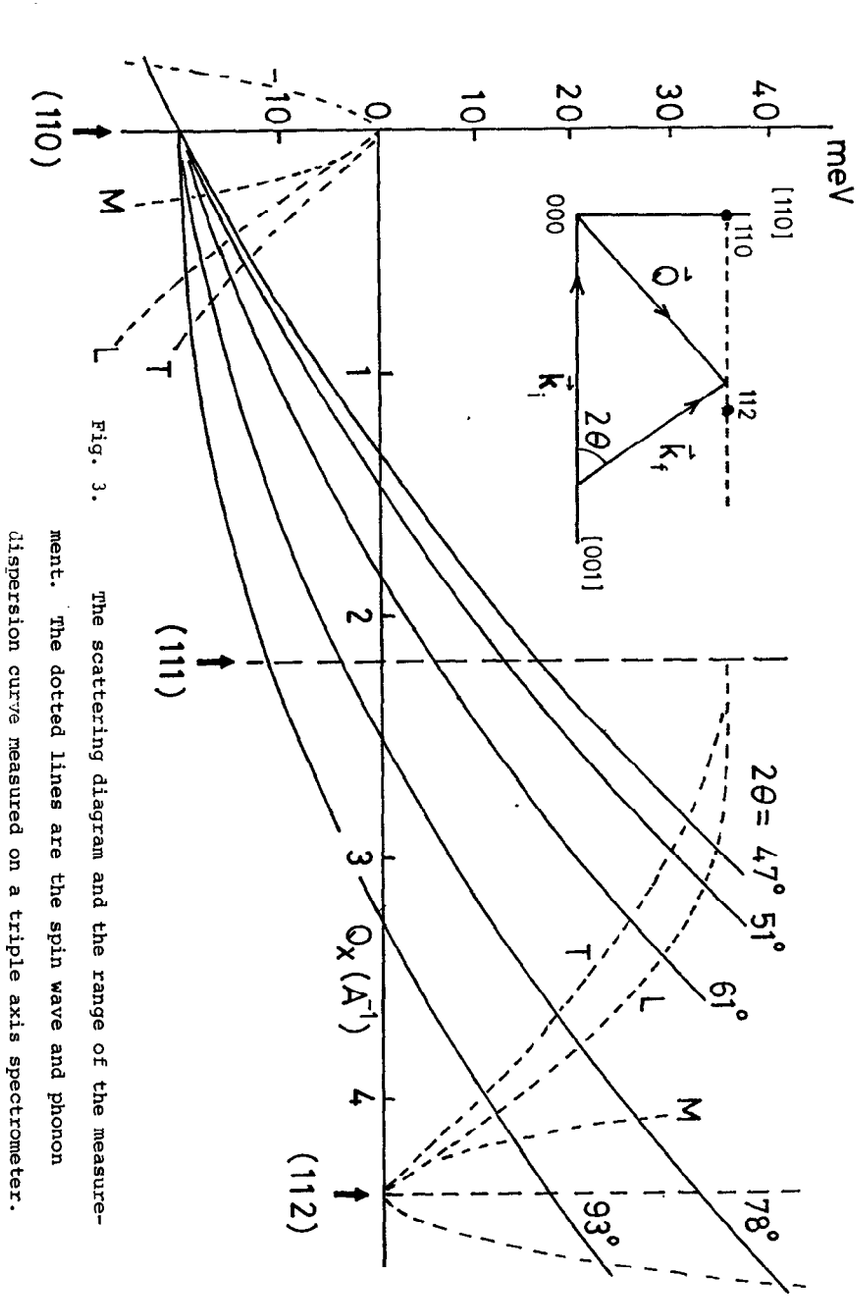

Fig. 3. The scattering diagram and the range of the measurement. The dotted lines are the spin wave and phonon dispersion curve measured on a triple axis spectrometer.

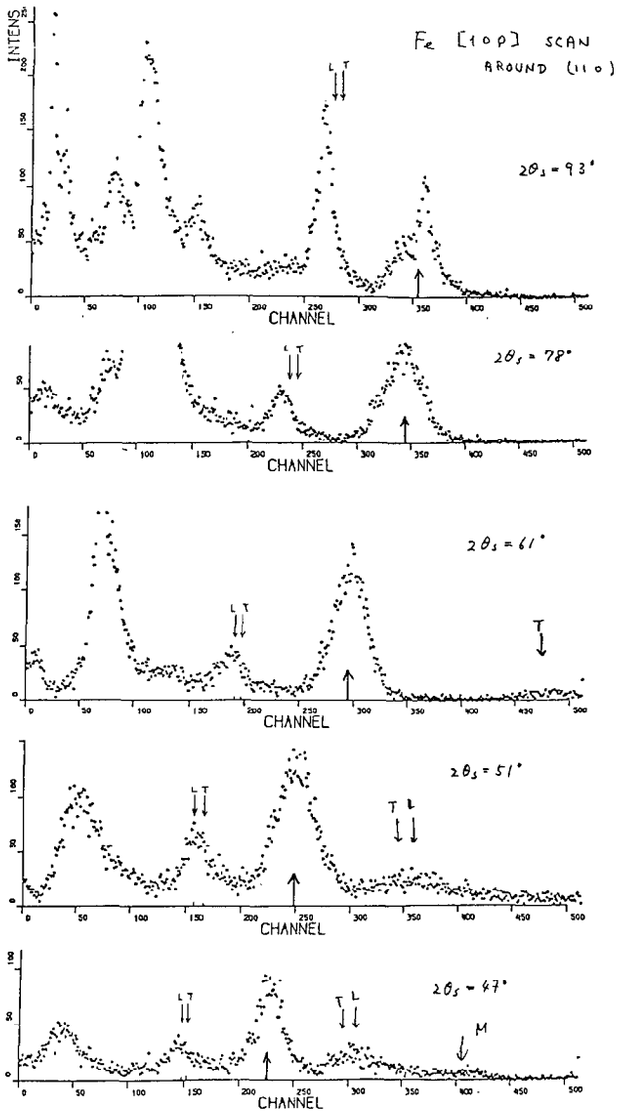

Fig. 4. Some examples of the measured T.O.F. spectra measured on MAX. The measuring time is 40 hours. For details, see text.

Some Background Measurements on the MAX spectrometer at KENS

C.G. Windsor

AERE Harwell, and Tohoku University, Sendai

The figure shows some data taken in October 1980 on the background level from the 3 counters on MAX at 16°, 22° and 28° while they were set to analyse neutrons at the graphite 002 reflection with $\theta_A = 2\theta_s$. Generally the background is seen to be extremely low with only around 1 count per 1000 μs in 10 minutes. However at low flight times the background rises to appreciable values as shown.

1) The full circles show the normal operating background.
2) Open circles show the background with the beam shutter closed. Clearly all our background is generated by our own beam.
3) Crosses show the background with the graphite analysers offset by 5°. There is little change. We are clearly not seeing air scattering.
4) Cadmium either before our sample or before our collimators had negligible effect. We are seeing the effect of fast epi-cadmium neutrons.
5) Removing the upper shield and side shield reduced the > 1 eV background (squares). Thus we are seeing the effect of shielding moderating and emitting fast neutrons. Boron or cadmium lining of all shield surfaces is therefore suggested.

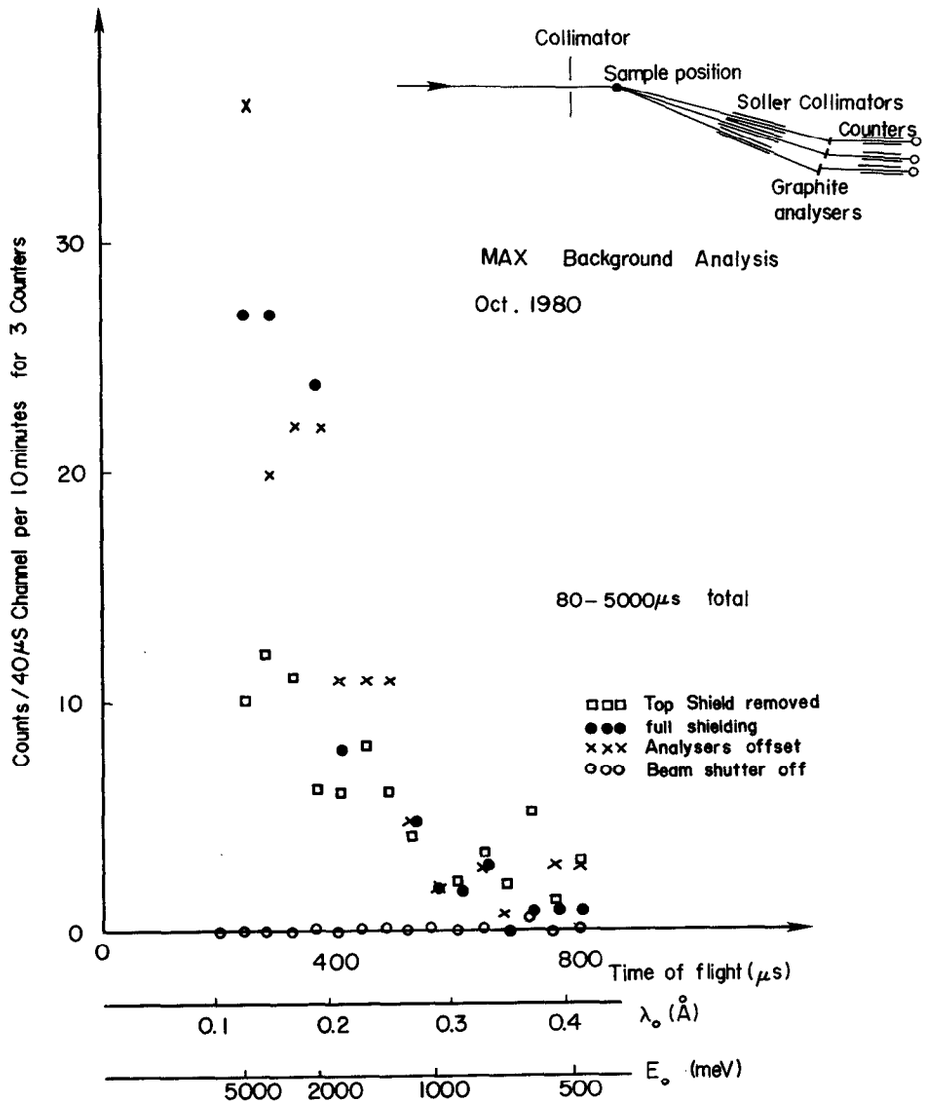

TIME OF FLIGHT SPECTROMETER WITH OPTICAL POLARISER

Y. Endoh, J. Mizuki, Y. Sasaki, H. Ono

Department of Physics, Tohoku University, Sendai 980

§1. Introduction

The optical technique for neutron polarisation has the advantage of combining relatively high polarisability with high reflectivity. In ideal cases, nearly 100% polarisability and 50% reflectivity with respect to the incident unpolarised neutron beam can be achieved. This technique is particularly appropriate for pulsed cold neutrons.

Firstly, for cold neutrons the glancing angle of the polariser magnetic mirrors with respect to the incident neutron beam can be large. The critical angle for total reflection by a $Fe_{45}Co_{55}$ magnetic mirror is, for example, approximately 25 minutes for 4 Å neutrons. Technical difficulties associated with accomodating small take of angles are therefore reduced. Secondly, polychromatic neutrons avail themselves to study by time of flight techniques. For the TOP spectrometer, cold neutron beams in the range of 4 Å - 12 Å are accepted from the neutron guide tube C_3.

Thirdly, applications of the Larmor precession of the neutron spin around an applied magnetic field may open new fields in low energy neutron spectroscopy. The spin rotation provides a probe, additional to that afforded by the neutron velocity, for monitaring energy changes on scattering by samples.[1]

We have recently completed construction of an time of flight

spectrometer with Optical Polariser (TOP).[2] The design concept of this TOP spectrometer has already been outlined in the previous KENS Report[2]. We describe here the performance of the completed spectrometer and, in the last section, we show some preliminary experimental results.

§2. Performance of the Spectrometer

A schematic diagram of the TOP spectrometer is shown in Fig. 1. The instrument consists of a neutron polarising system, a magnetic guide channel with a neutron spin flipper and a diffractometer with two independently-movable detector arms. The present arrangement is that designed for polarised neutron diffraction experiments, but the instrument can also accomodate inelastic TOF measurements[3] if additional components such as a precession magnet, polarisation analysers etc. are used. These latter components are, at present, at the design stage.

The neutron polariser consists of Soller-type $Fe_{1-x}Co_x$ magnetic mirrors inserted in an electromagnet which produces a maximum field of about 0.25 Tesla. Efficient polarisers are still being developed and the spectrometer was therefore designed such that the reflected (polarised) beam direction can be varied by $\leqslant 5°$ with respect to the incident neutron beam. The magnetic channel is composed firstly of a permanent magnet producing a vertical field of 100 Oe which is at a separation of 100 mm from the polarising magnet. This guide is followed by a Drabkin-type spin flipper[4]. The flipper consists of two coils which produce a variable magnetic field along the beam direction. The coupling between the guide and the flipper, therefore, should be arranged such that outside the two systems all changes

in the polarisation direction are adiabatic. Following the flipper there is a further coil producing a field along the beam direction which serves to maintain the neutron polarisation to the sample position. An electromagnet producing a variable field of up to 1.2 Tesla in a 50 mm air gap is mounted on the sample table. This magnet is designed to be rotatable around the horizontal axis by 360° and, as the sample table may also be rotated through 360° about the vertical axis, the field can be applied in any chosen direction. The sample table drive is controlled by a dedicated micro computer NEC-PC8001 to within 1/100° accuracy. Scattered beams within the range $-20° \leqslant 2\theta \leqslant 110°$ can be detected by two independently movable detector tables which are connected to the sample table.

The total flight path from the moderator to the detectors is 21.0 m. The guide tube section ends at 16.40 m from the source face. The central medium size computer is responsible for data acquisition and handling, but the dedicated micro computer is used to control the spin-flipper system. If required, the neutron polarisation may be flipped by π every pulse and, eventually polarisation dependent scattered signals will be easily obtainable. A block diagram of the operating system and a time chart are illustrated in Fig. 2. An overall view of the TOP spectrometer is given in Fig. 3.

§3. Polarisation of Neutrons

The attainment of high neutron polarisability over the entire wavelength range from 4 Å to 12 Å depends on the balance between the effective nuclear and magnetic scattering amplitudes in the polarising magnetic mirror[5]. Among the best polarising mirror materials are magnetized thin films of $Fe_{45}Co_{55}$ evaporated onto polymer substrates.

These substrates which are comprised mainly of $-(CH_2)_n^2-$ units have small, negative coherent scattering amplitudes. Further, when such plastic films are uniformly stretched their surface quality is relatively good.[6]

Although such curved Soller-type magnetic mirrors can provide polarised neutron beams with cross-section areas as large as 10 cm^2, the production process for high quality mirrors is laborious. In our case at least 40 sheets of evaporated $Fe_{1-x}Co_x$ films are required for polarisation of the 20 x 50 mm^2 neutron beam. The first such polariser is currently being manufactured although, in the meantime, we have made neasurements of polarising efficiencies and transmissions using prototypes of somewhat smaller dimensions[2]. The polarising efficiency was determined by measuring the flipping ratio from the 111 reflection of a Heusler analyser crystal[7] placed at the sample position. Up until the time of this report we have obtained results for the wavelength region 4 Å-6.5 Å. A typical time of flight scan is depicted in Fig. 4. The measurements for $Fe_{25}Co_{75}$ on Myler and $Fe_{25}Co_{75}$ on another commercial polymer film, OPP, gave maximum flipping ratios of 6.5 and 12.5 respectively for 4 Å. For the latter, the flipping ratio was almost independent of the wavelength within the range 4 Å-6.5 Å, although within this range the former showed some variation. Our results indicate that $Fe_{25}Co_{75}$ on OPP has a polarising efficiency of about 93%. The flipping efficiency of the Drabkin-type flipper system was also proved by inserting a tunable Mezei-type π-flipper[8] between the paired coils. Our results indicated that the flipper system works satisfactorily.

These recent measurements have confirmed that the present configuration of the TOP spectrometer meets the design performance

as a polarised neutron diffractometer. After completion of the fun-size polarising mirrors we will commence full operation.

Finally, as an indication of the type of initial measurement that is being made, we shown in Figure 5 polarisation dependent diffraction patterns from Fe-Pd bilayer films. These bilayers are currently being studied to probe interfacial magnetic properties.[9]

References

1) F. Mezei; Z. Phys. 255 (1972) 146

2) Y. Endoh and Y. Ishikawa; KENS Report I (1980) 149

3) F. Mezei; Nu. Inst. Met. 164 (1979) 153

4) G.M. Drabkin et al.; Sov. Phys. JETP 29 (1969) 261

5) J.B. Hayter, J. Penfold and W.G. Williams; J. Phys. E 11 (1978) 454

6) Y. Sasaki and Y. Endoh; Res. Rept. Lab. Nucl. Sci. Tohoku Univ. 13 (1980) 92

7) The crystal was kindly loaned from Prof. Y. Ito, ISSP, Univ. of Tokyo

8) J.B. Hayter; Z. Phys. B 31 (1978) 117

9) M. Sato, K. Abe, Y. Endoh and J.B. Hayter; J. Physl C 13 (1980) 3563

T. Shinjo, S. Hine and T. Takada; 1977 Proc. 7th Int. Conf. Vac. Congr. and 3rd Int. Conf. Solid Surfaces. Vienna ed R. Dobrozemsky (Ham. Austria: Berger & Söhne) 2655

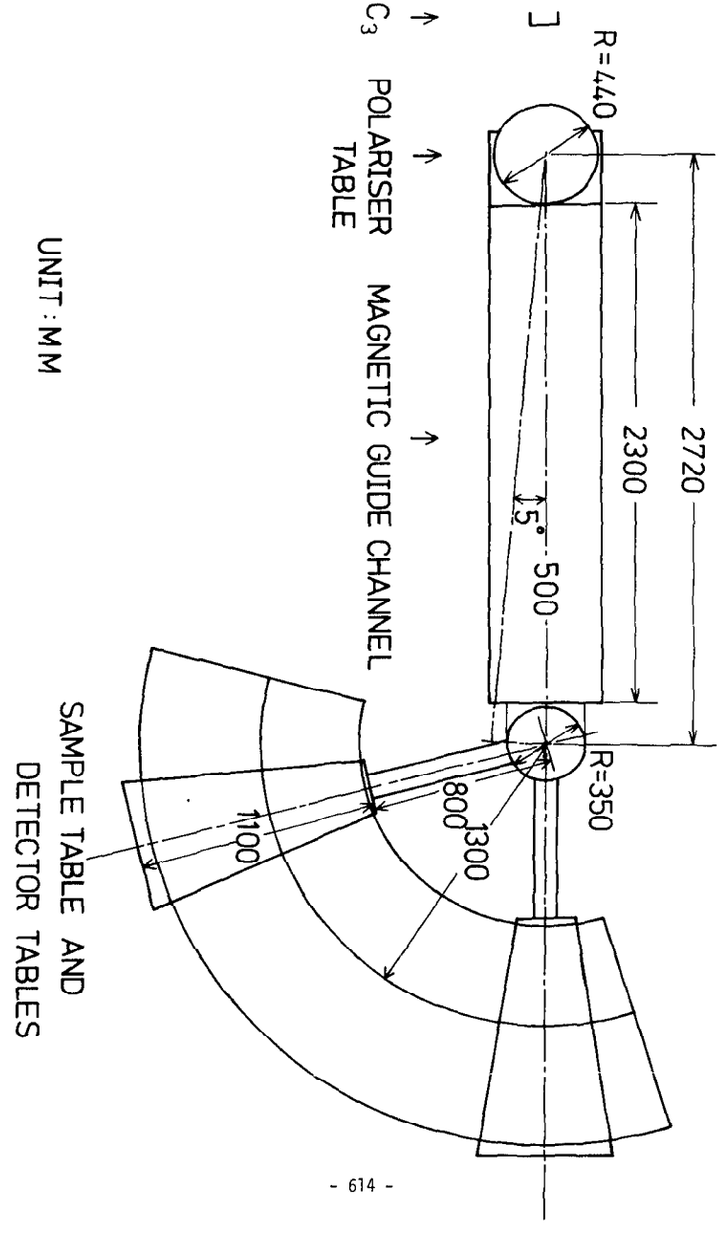

Fig. 1. Schematic drawing of the TOP spectrometer

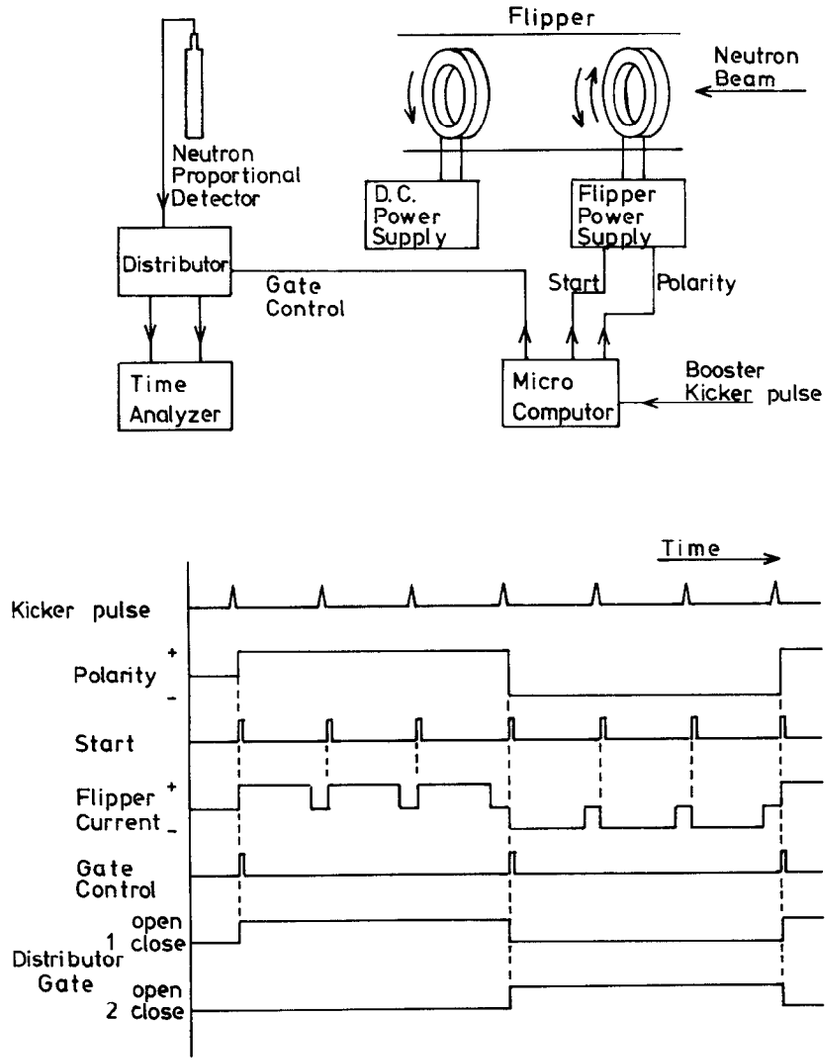

Fig. 2. Diagrams of TOP operation and its time chart

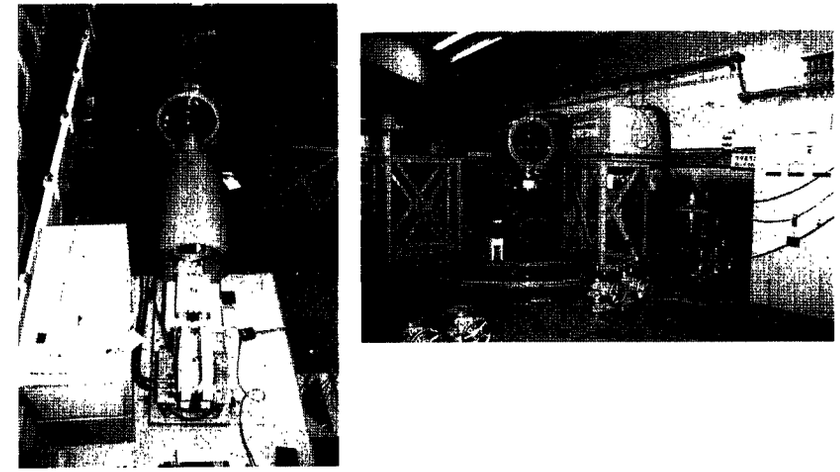

Fig. 3. Overview of TOP

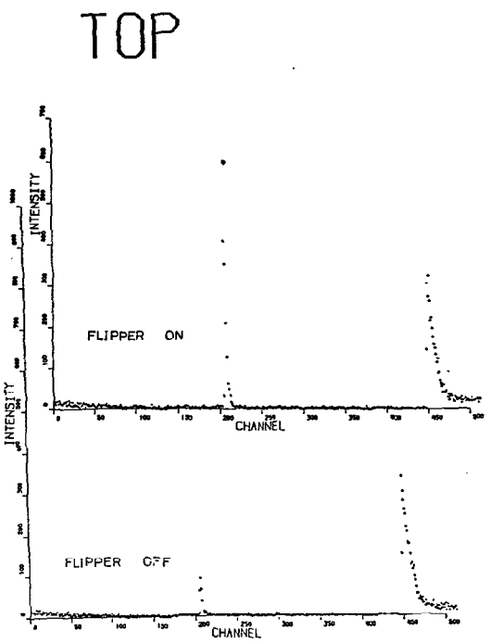

Fig. 4. TOF diffraction patterns of the 111 reflection from the Heusler analyser. The analyser crystal was in a field of 0.95 Tesla. The Bragg angle θ was 45°, so that 4.0 Å neutrons were counted by the detector.

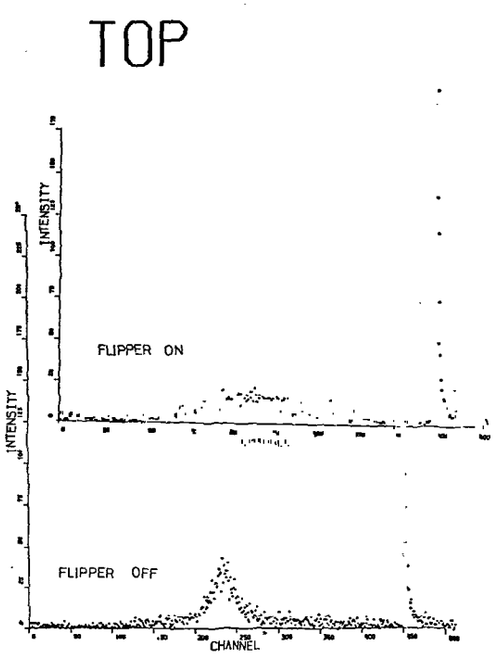

Fig. 5. TOF diffraction patterns from Fe-Pd bilayers at ambien temperature. The period of a bilayer is 55 Å and the present sample has 100 layers. The Bragg angle θ wa set at 3.2°.

Polarised Neutrons

W G Williams
Neutron Division, Rutherford and Appleton Laboratories

1. Introduction

The large majority of polarised beam neutron diffraction work on steady state sources has been carried out using the magnetised ferromagnetic single crystals $Co_{0.92}Fe_{0.08}$ and the Heusler Alloy Cu_2MnAl as polarising monochromators. These polarisers have only a very limited applicability on pulsed sources, where we are concerned with white beams, sometimes up to eV energies. This paper is chiefly devoted to describing polarising filter methods which can be used either for white or epithermal beams. Efficient optical polarisers are readily available for cold neutrons[1,2]; their properties are well-understood and will not be discussed in this paper.

Polarised neutron measurements on pulsed sources will ultimately require full polarisation analysis[3], ie spin selection in both the incident and scattered beams. In the case of elastic measurements the best instrumental arrangement is to use two wide-band polarising filters (Figure 1a). Inelastic experiments will probably best be performed with an inverse geometry instrument, since this only requires changing the analyser arrangement in Figure 1a. Possible designs include using polarising crystals[4] to combine spin/energy analysis (Figure 1b), or a focussing analyser system where a conventional 'curved' crystal analyser bank is used with a polarising filter (Figure 1c), as suggested by Scherm[5]. A detailed investigation of the optimum method to carry out inelastic polarisation analysis experiments will commence shortly at the Rutherford Laboratory.

2. Polarising Filters

Polarising filters operate by having substantially different linear attenuation coefficients for the two neutron spin states. The spin selection process can be either by preferential scattering or by preferential absorption. The main advantages of polarising filters are

that they can accept wide beam divergences and that they are often efficient over a very broad energy range.

The important parameters which determine the effectiveness of a neutron polarising filter are:

(i) the polarising efficiency, p, ie the polarisation attained by an unpolarised neutron beam on being transmitted through the filter,

$$p = (T_+ - T_-)/(T_+ + T_-), \qquad (1)$$

(ii) the total transmittance, T, ie the (Total number of transmitted neutrons)/(Number of neutrons incident on filter) ratio,

$$T = (T_+ + T_-)/2 \qquad (2)$$

where T_+ and T_- are the transmittances for the "up" and "down" neutron spins. The maximisation of a quality factor $p\sqrt{T}$ is often used to optimise the filter thickness, though in general the best thickness should be evaluated by taking into account several parameters. In polarisation analysis experiments where there is a small amount of spin-flip scattering, it is more beneficial to increase p at the expense of T, ie to use a thicker filter than that given by maximising $p\sqrt{T}$[6]. The different types of polarising filters that may be used on pulsed neutron sources will now be described.

3. Polarised Proton Filters

Protons have a sufficiently large neutron spin dependent scattering cross-section that a target of polarised protons can act as a useful polarising filter. High proton polarisations ($P_p \gtrsim 0.7$) are required, and there now seems to be two technically feasible methods of achieving this. Both use methods for transferring the easily-attainable electron polarisation in a paramagnetic dope into the proton spin system.

The first, and historically the most-tried technique, is to use dynamic polarisation (see Figure 2). In this method some of the protons are in dipolar coupling with the saturated electron spins of the dope and by irradiating at well-defined frequencies above and below that of the main ESR transition it is possible to create both positive and negative proton polarisations. The method is technically rather difficult, though it is

now being applied to polarise neutrons by Japanese workers[7]. There is a substantial amount of data available on polarising both resonance and thermal energy neutrons by transmission through a $La_2Mg_3(NO_3)_{12}.24H_2O$ (LMN) polarised proton target [8]. Under typical experimental conditions the target is saturated with 4 mm microwaves at a temperature $\sim$ 0.8K with a 1.87T magnetic field applied along the c-axis[9]. The possibility now exists of also using hydrogen-rich organic compounds doped with Cr^{5+} as filter materials; their main advantage over LMN for the neutron polariser application is that they are not required in single crystal form. There is however one difficulty - that of restricting the quantity of ^3He (used as refrigerant) in the path of the neutron beam.

The proton polarisation method being developed at the Argonne Laboratory uses the spin refrigerator principle first introduced by Langley and Jeffries [10]. The best results have been obtained with single crystals of yttrium ethyl sulphate (YES) in which 0.01% of the Y^{3+} atoms are replaced by the paramagnetic dope Yb^{3+} [11]. Yb^{3+} acts as an effective $s = \frac{1}{2}$ paramagnetic ion with a highly ansotropic g-factor ($g_c \sim 3.3$, $g_a \sim 0$) and when a single crystal is rotated about the b axis the spin dynamics is such that the high Yb^{3+} polarisation can be transferred to the proton spin system (see Figure 3). Typical experimental conditions are: magnetic field (poor homogeneity) $\sim$ 1.5T, temperature T $\sim$ 1K, spinning frequency $\omega \sim 100$ Hz. The main attraction of the technique is its simplicity compared with dynamic polarisation. Neutron tests are scheduled for Los Alamos for early 1981 [11].

The principal advantage of polarised proton filters is that it is the only method available for polarising true white beams even up to keV energies. The expected performances of an LMN polarising filter over a range of neutron energies, a range of filter thicknesses t, and for various values of the proton polarisation p_p have been calculated using the experimentally determined cross-section data of Lushchikov et al[8], and an optimum filter thickness $t_{opt} = 1.5$ cm was selected after maximising for $p\sqrt{T}$ over the thermal and epithermal neutron range. The calculated polarising efficiencies and transmittances of this filter for several values of the proton polarisation, and over the neutron energy range 0-0.6 eV are shown in Figures 4 and 5 respectively. The total and polarisation dependent cross-sections approach constant values at a neutron energy $\sim$ 0.8 eV, thus the p and T values at energies > 0.8 eV are essentially the same as those shown for the higher energy limits of the curves. Polarised proton targets can now be built to give proton polarisations $p_p > 0.80$, and the curves show that this gives an efficient performance at all thermal and epithermal energies.

4 Resonance Absorption Filters

If an unpolarised neutron beam whose energy corresponds to a resonance is transmitted through a target in which the nuclear spins are polarised, then one of the two neutron spin states is preferentially absorbed, and the transmitted beam is polarised. The absorption cross-sections ($\sigma_{A_\pm}$) for the two neutron spins is given by:

$$\sigma_{A_\pm} = \sigma_A (1 \pm p_N \rho) \qquad (3)$$

where σ_A is the absorption cross-section for zero nuclear polarisation p_N, $\rho = I/(I+1)$ if the compound nucleus formed has spin $(I+\frac{1}{2})$, and $\rho = -1$ if it has spin $(I-\frac{1}{2})$. This spin-dependence of the capture has been used extensively in nuclear physics to measure the spins of resonant states. A polarising filter operating by this principle has a total transmittance

$$T = A \exp(-\sigma_A Nt) \cosh(\rho p_N \sigma_A Nt) \qquad (4)$$

and polarising efficiency

$$p = -\tanh(\rho p_N \sigma_A Nt) \qquad (5)$$

where the direction of p_N is defined as for the neutron polarisation, N and t are the nuclear density of the absorbing nucleus and filter thickness respectively, and A is an attenuation factor due to the non-absorbing nuclei in the filter. Equations (4) and (5) give the requirements for a good polarising filter functioning by selective capture, ie (1) it must be possible to obtain a high nuclear polarisation ($P_N > 0.8$); this can often be obtained statically by cooling materials which have a large hyperfine field at the nucleus to dilution refrigerator temperatures, (2) $|\rho|$ should approach unity, which means that the resonance should be of the $(I-\frac{1}{2})$ type, or if of the $(I+\frac{1}{2})$ type I should be large so that $I/(I+1) \rightarrow 1$, and (3) σ_A should be much greater than the total cross-sections for the non-absorbing nuclei in the filter.

A filter containing polarised ^{149}Sm nuclei has been successfully developed at the Rutherford Laboratory[12] and new absorption filters are being investigated in order to extend the applicability of this method into the epithermal neutron region. Absorption filters offer particular advantages over scattering filters as spin analysers since the latter will almost certainly give higher detector backgrounds.

5. Polarised samarium filter

A material containing polarised ^{149}Sm (I = 7/2) nuclei acts as a good polarising filter for thermal neutrons since ^{149}Sm has a strong resonance capture peak at E_0 = 0.97 eV ($\lambda \sim 0.92$ Å) which has been well-characterised by neutron measurements to be predominantly of the $(I+\frac{1}{2})$ type[13]. The polarising filter material used at the Rutherford Laboratory was a deuterated cerous magnesium nitrate single crystal $Ce_2Mg_3(NO_3)_{12}24D_2O$, in which ∿ 6% of the Ce atoms were replaced by ^{149}Sm atoms (CSMN). The deuterated salt was used rather than the hydrated one so as to reduce the neutron spin-independent attenuation factor A. The ^{149}Sm nuclear polarisation was produced by applying a magnetic field H ∿ 0.1 Tesla along the crystal c-axis and by cooling the crystal to temperatures T < 0.02K in the mixing chamber of a $^3He/^4He$ dilution refrigerator. The ^{149}Sm nuclear polarisation was therefore set up by a static process, the Rose-Gorter method[14, 15]; the mechanism involves the electron-nuclear spin interaction, the electrons being essentially fully polarised at the temperatures and magnetic fields used. The hyperfine interaction along the c-axis of CSMN is ∿ 0.041K in temperature units, and this corresponds to a hyperfine field at the nucleus ∿ 300 Tesla.

The polarising efficiency and transmittance values for the filter are strongly neutron energy dependent, due to the resonant nature of σ_A. This will not in general be disadvantageous in a polarised beam measurement of flipping ratios. Polarising efficiency and transmittance measurements at two wavelengths (λ = 0.96 Å and λ = 1.18 Å) gave values which were within a few per cent of the theoretically predicted ones. Figure 6 shows the calculated spin-dependent transmittances and polarising efficiencies of the filter at the refrigerator base temperature (16 mK) as a function of neutron energy, calculated on the basis of the measurements at the two wavelengths. The obvious disadvantage of the Sm filter for pulsed source applications is that it does not perform at neutron energies E $\gtrsim$ 0.14 eV. This is not a severe limitation in low Q elastic measurements since in order to operate without frame overlap (dictated by the machine p.r.f. and instrument length) it turns out that for our first experiments we are not able to operate at E $\gtrsim$ 0.2 eV. There are now plans in the UK for constructing a two samarium filter polarisation analysis spectrometer at the Harwell Linac pulsed neutron facility. A large Q-scan (0.3 < Q(Å^{-1}) < 1.7) in total scattering measurements of magnetic diffuse scattering will be possible

at one scattering angle setting of the filter analyser by using a polychromatic beam (12 meV < E < 130 meV). Metallic polarising filter materials containing ^{149}Sm, eg $SmCo_5$ with better thermal conductivities than CSMN are being developed for this instrument[16].

6. Polarised europium filter

^{151}Eu has two broad resonances which extend up to a neutron energy E ∿ 0.6 eV. Calculations show that it should be possible to polarise Eu-containing materials at temperatures ∿ 10-15 mK to produce a polarising filter with good transmittance and polarising efficiencies up to this energy[17]. The spin selection is not quite as efficient as that for ^{149}Sm thus one would probably use a $^{149}Sm/^{151}Eu$ two-foil combination to perform well over the entire range 0 < E (eV) < 0.6. The predicted performance of such a combination is shown in Figure 7; the calculations assumed that the filters are cooled to 15 mK, that the electron magnetisation is fully saturated, and that the hyperfine field at the ^{151}Eu nucleus is the free ion value H_{eff} ∿ -34 Tesla.

This filter combination could be used to extend the Q range possible in elastic experiments but, more importantly, it could be used as the polariser in an inverse geometry inelastic instrument to study magnetic excitations up to $\hbar\omega$ ∿ 0.25 eV.

7. Polarised erbium filter

^{167}Er has two narrow resonances at energies E = 0.584 eV ($J = I-\frac{1}{2} = 3$) and E = 0.460 eV ($J = I+\frac{1}{2} = 4$). Further, ferromagnetic intermetallic materials such as Fe_2Er are known with a sufficiently high hyperfine field at Er (H_{eff} ∿ 850 Tesla) to enable high nuclear polarisations to be achieved at temperatures T ≲ 30 mK. Calculations of the performance of a polarised ^{167}Er have been carried out[18] with typical results (for Nt ∿ 1.37 x 10^{21} at cm^{-2}):

Neutron Energy eV	Polarising Efficiency p	(+) Spin Transmittance T_+	(-) Spin Transmittance T_-
0.460	0.99	0.454	0.0023
0.584	-0.985	0.0072	0.976

The performance at E = 0.584 eV is close to the theoretical maximum for any polariser; this is a result of the $I-\frac{1}{2}$ nature of the resonance (see equation (3)).

This filter could be used in the incident beam of a chopper spectrometer to provide 'monochromatic' highly polarised beams at the resonance energies. The main scientific applications would be in studying magnetic excitations in aligned samples where $\hbar\omega \gtrsim 0.25$ eV by partial polarisation analysis.

8. Polarised holmium filter

^{165}Ho has a sharp (FWHM $\sim$ 0.15 eV) resonance peak at E = 3.92 eV with a compound nucleus spin $J = I+\frac{1}{2} = 4$[19]. Ho is also known to be one of the easier nuclei to polarise[20], for example a polarisation $P_N \sim 0.95$ can be generated in a magnetically saturated sample at a temperature $T \sim 0.1$K. We here speculate that such a filter might be used in an inverse geometry instrument to combine the functions of spin analysis and detection by using the resonance detector principle. An extension of this idea to combine it with a spin precession coil to Fourier chop the scattered beam so as to improve the inherent resolution of the resonance detector spectrometer has been proposed recently at the Argonne Laboratory[21]. The 3.92 eV resonance could be used to study magnetic and electronic excitations at low Q up to $\hbar\omega \sim 1.0$ eV.

9. Conclusions

Polarised beam work on pulsed neutron sources will rely heavily on developing effective polarising filters. The Rutherford Laboratory programme will concentrate on extending the range of applicability of the resonance absorption method and some of the possibilities have been described.

REFERENCES

1. J B Hayter, J Penfold and W G Williams, J Phys E Sci Instrum 11 453 (1978).
2. F Mezei, Commun Phys 1 81 (1976).
3. R M Moon, T Riste and W C Koehler, Phys Rev 181 (1969) 920.
4. W G Williams, B D Rainford and J H Clarke, 'Inelastic and total scattering polarisation analysis instruments for the SNS', Rutherford Internal Memorandum. Unpublished.
5. R Scherm, private communication.
6. W G Williams, Rutherford Laboratory Report No. RL-73-034 (1973).
7. Y Ishikawa and N Watanabe, KEK-78-19 (1978).
8. V I Lushshikov, Yu V Taran and F L Shapiro, Dubna Report, Brookhaven Translation BNL-TR-295 (1969).
9. H H Atkinson, Proc Int Conf on Polarised Targets and Ion Sources, Saclay, France 41 (1966).
10. K H Langley and C D Jefferies, Phys Rev 152 358 (1966).
11. G Felcher, private communication.
12. F F Freeman and W G Williams, J Phys E Sci Instrum 11 459 (1978).
13. H Marshak, H Postma, V L Sailor, F J Shore and C A Reynolds, Phys Rev 128 1287 (1962).
14. M E Rose, Phys Rev 75 213 (1949).
15. C J Gorter, Physica 14 504 (1948).
16. W G Williams, Rutherford Laboratory Report No RL-74-036 (1974).
17. J Mayers and W G Williams, Unpublished.
18. W G Williams, 'High performance polariser for monochromatic neutrons at energies E = 0.460 eV and E = 0.584 eV', Rutherford Laboratory Memorandum, November 1979.
19. H Postma, H Marshak, V L Sailor, F J Shore and C A Reynolds, Phys Rev 126 (1962) 979.
20. G Brunhart, H Postma and V L Sailor, Phys Rev 137 (1965) B1484.
21. G Felcher and J Carpenter, private communication.

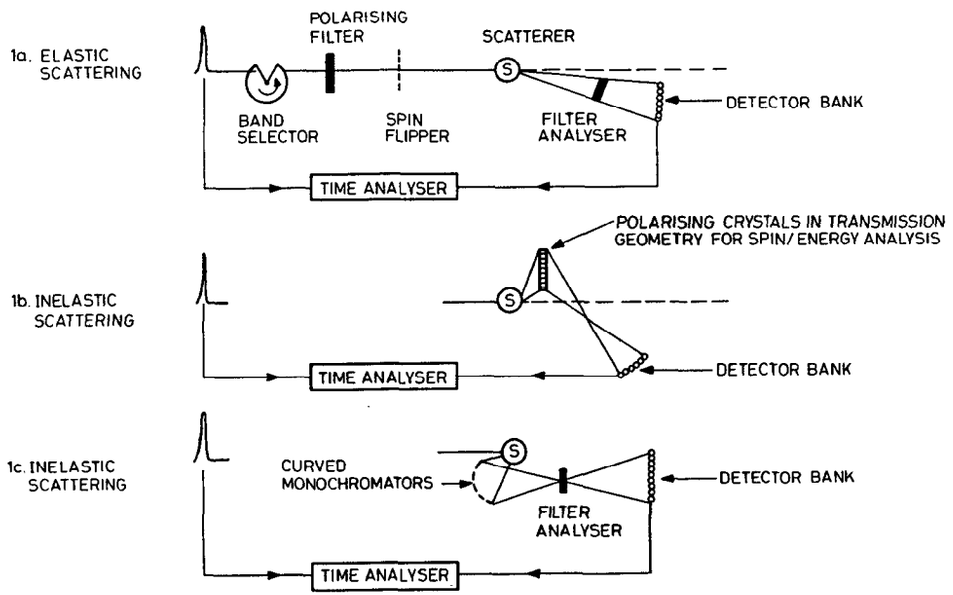

FIGURE 1. POLARISATION ANALYSIS ON PULSED SOURCES

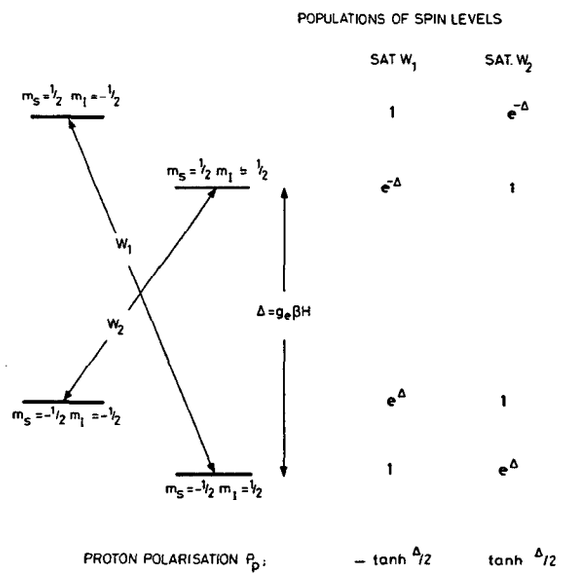

PROTON SPIN I AND ELECTRON SPIN S IN DIPOLE COUPLING
eg Nd^{3+} IN LMN, Cr^{5+} IN ETHYLENE GLYCOL.

FIGURE 2. DYNAMIC PROTON POLARISATION

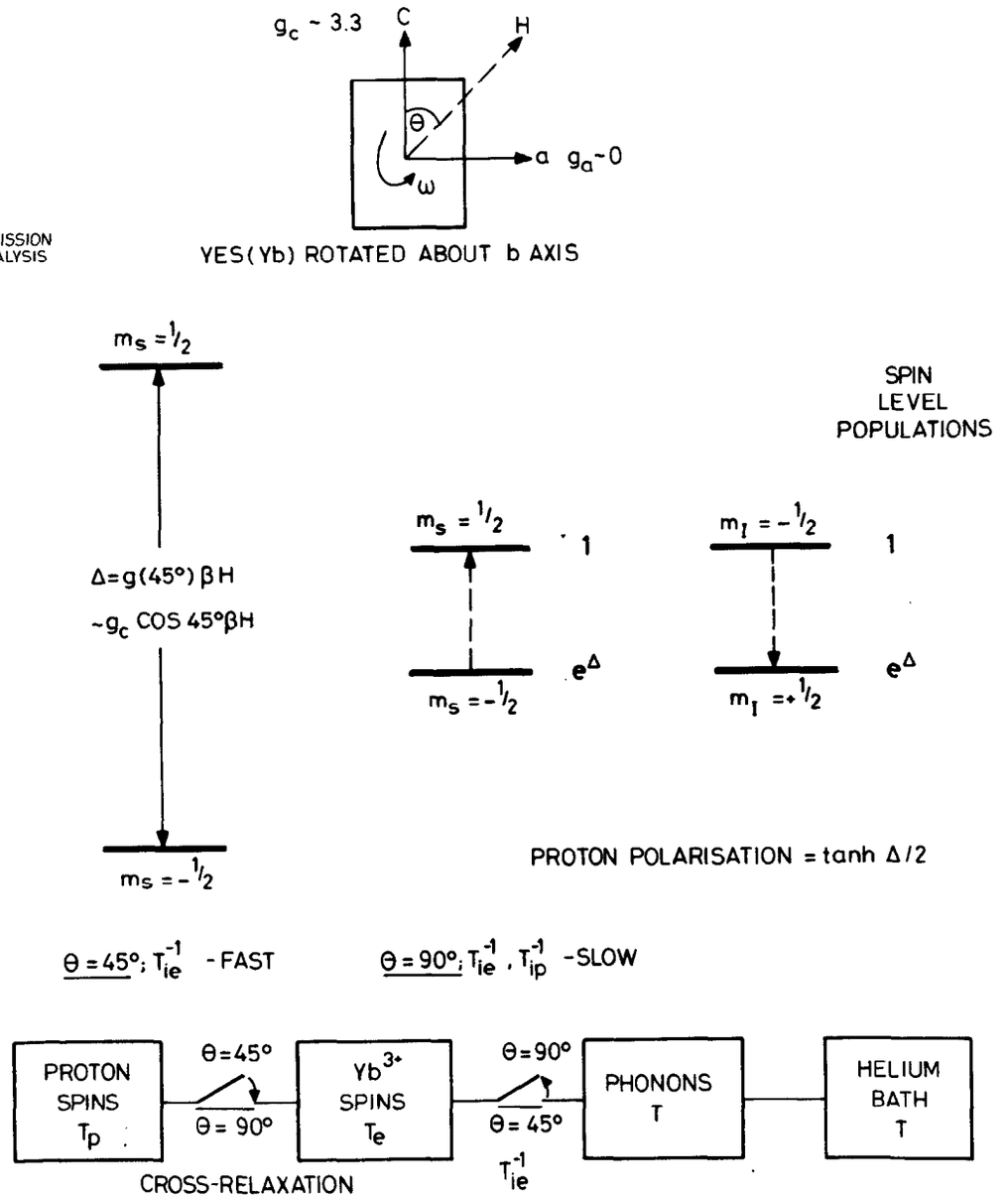

FIGURE 3. PROTON POLARISATION IN SPIN REFRIGERATOR

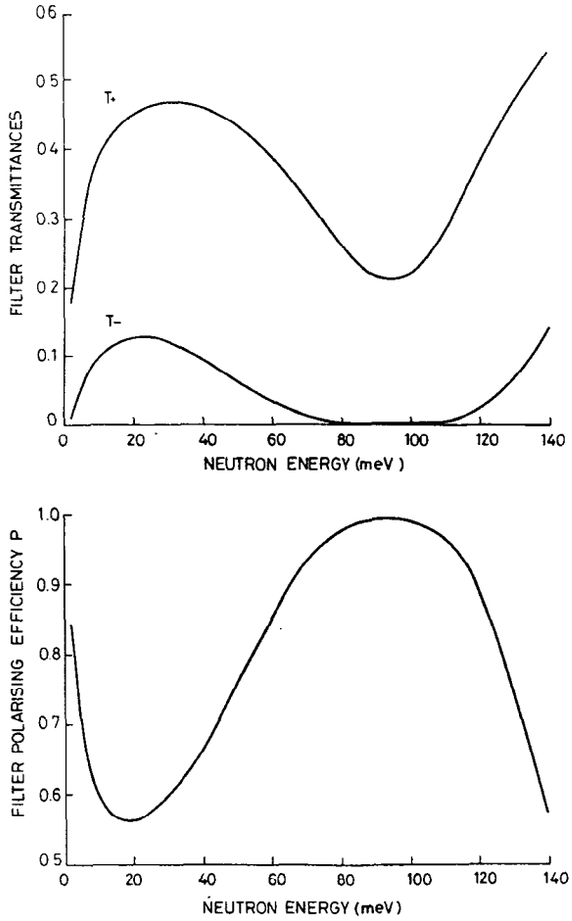

FIGURE 6. SPIN-DEPENDENT TRANSMITTANCES AND POLARISING EFFICIENCY OF Sm FILTER vs NEUTRON ENERGY

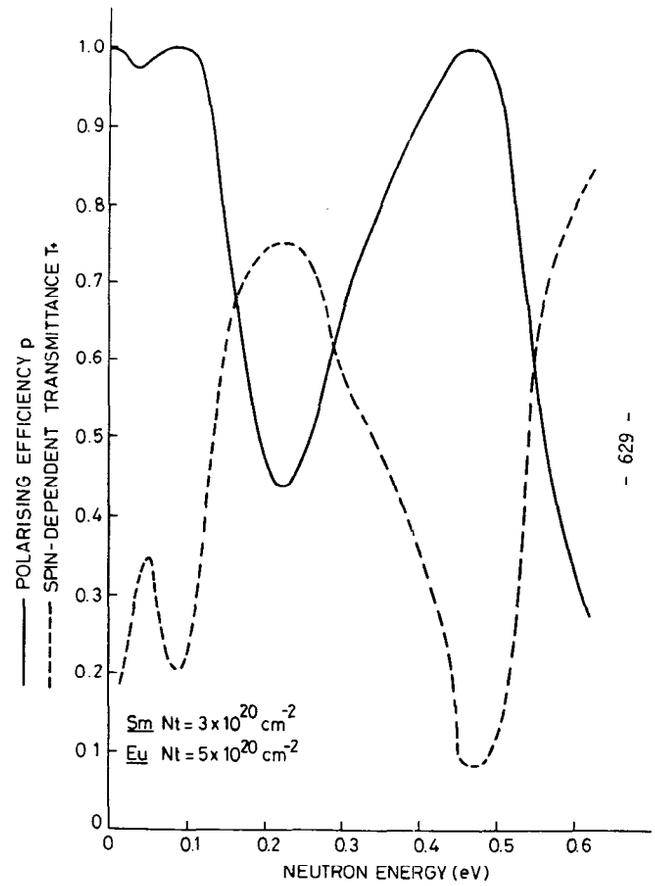

FIGURE 7. SPIN-DEPENDENT TRANSMITTANCE AND POLARISING EFFICIENCY OF Sm/Eu FILTERS IN SERIES vs NEUTRON ENERGY

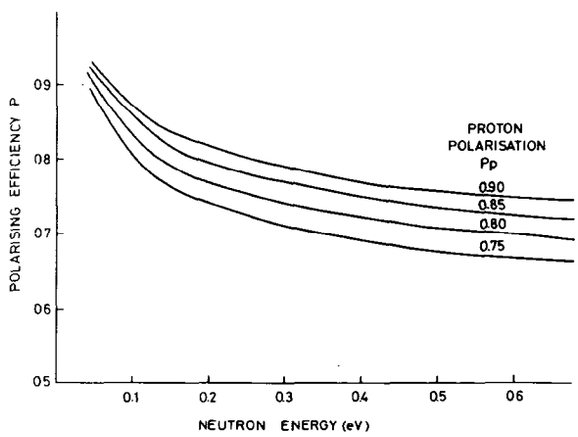

FIGURE 4. NEUTRON ENERGY DEPENDENCE OF THE POLARISING EFFICIENCY OF A 1.5cm THICK LMN POLARISING FILTER OVER THE PROTON POLARISATION RANGE $0.75 < Pp < 0.90$

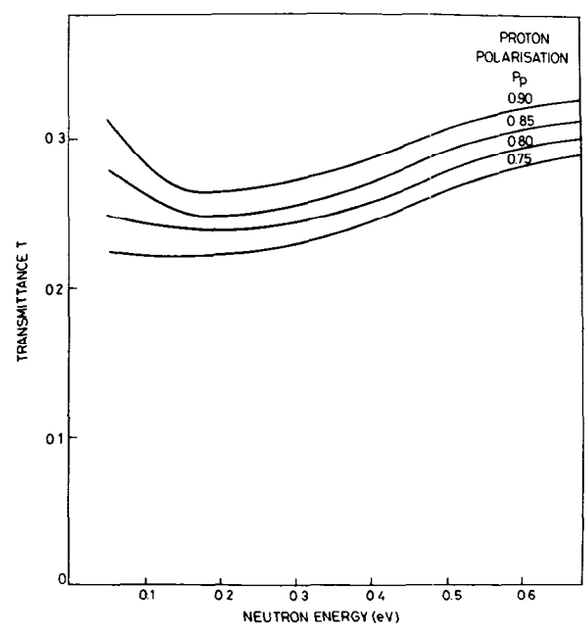

FIGURE 5. NEUTRON ENERGY DEPENDENCE OF THE TRANSMITTANCE OF A 1.5cm THICK LMN POLARISING FILTER OVER THE PROTON POLARISATION RANGE $0.75 < Pp < 0.90$

Neutron Polarization by Polarized Proton Filter

Shigeru Ishimoto

National Laboratry for High Energy Physics, Ibaraki, Japan

1. Introduction

A white beam of cold, thermal and epithermal neutrons transmitted through a polarized proton filter becomes highly polarized, because the cross section for neutron-proton scattering in the singlet state is much larger than that for the triplet state within the energy range 10^{-3}eV - 10^{5}eV.

The use of a polarized proton filter therefore makes it possible to obtain a polarized neutron beam of higher intensity and covering a wider energy range than that available by other techniques.

2. Thermal Neutron

The performance of a polarized proton filter as a slow neutron polarizer was tested using apparatus installed at the JRR-2 reactor. The experimental procedure and the polarization of thermal neutron beams (80 meV) by the filter are discribed in reference 1). Fig.1 shows a schematic view of the experimental arrangement. Fig.2 displays a diagram of the He^3 cryostat. The protons in a sample of ethylene glycol containing a few percent of Cr^V complexes were dynamically polarized in a He^3 cryostat in magnetic field of 25KG. The polarization of neutrons transmitted through the filter as a function of the proton polarization is depicted in Fig.3. The solid line indicates the neutron polarization calculated according to

$$P_n = \tanh P_p n \sigma_p t$$

where P_n and P_p are newtron and proton polarizations, n is the number of protons per cm^3 in the filter and t is the filter thickness. A value for the polarization cross-section of σ_p = 27b was determined from this curve.

Fig. 1

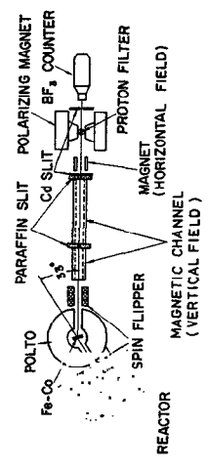

Fig. 3

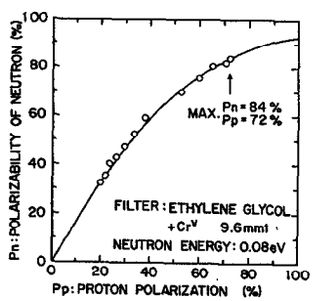

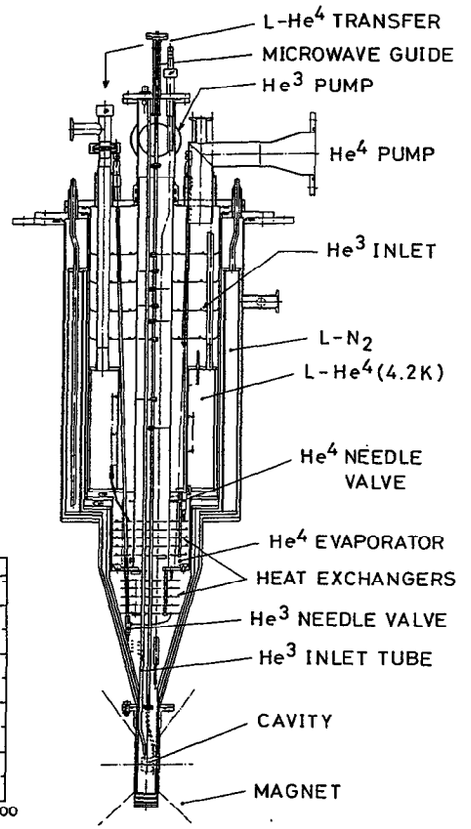

Fig. 2

3. Application to Epithermal Neutron and Scattering of Coaxial n-p Spins Along the Beam

Fig.4 shows the calculated polarizations of neutron beams transmitted through a filter composed of an organic material with 80 % transversely polarized proton and with thicknesses of 10 mm and 20 mm. For the polarization cross section we used the value determined in our experiment for an energy of 80 meV and calculated values from the expression given by Lushchikov et al. 2). The method will open a way for the polarization of intense neutron beams covering wide energy range without serious restrictions on the angular divergence.

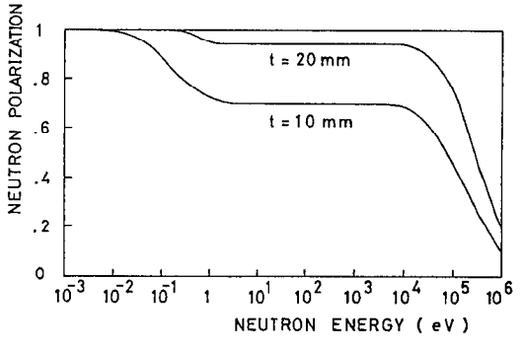

Fig.4 Calculated neutron polarizations (proton filter is an organic material with 80 % polarization)

The polarization cross sections for n-p scattering in which the spins are parallel transverse to the beam and parallel coaxial (II) with the beam direction were estimated by N. Hoshizaki 3).

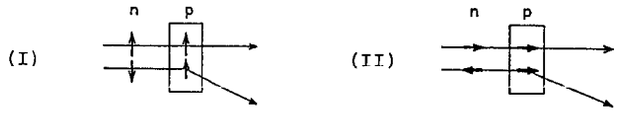

The calculated value of the polarization cross section in case (II) is almost the same as in case (I). We are going to confirm this fact in our next experiments at KENS. For this experiment the apparatus will consist of a holizontal He^3 cryostat and a superconducting solenoid magnet of 25 KG. (Fig.5)

Recently, stable Cr^V-complexes were developed for use as the paramagnetic species in dynamic polarization experiments 4) 5). Proton polarizations of 70 - 80 % have been obtained using such samples at 0.5 K and 25 KG. For our project, we will use such complexes in the polarized proton filter.

Fig.6 shows a proposed schematic plan view of the project of polarized epithermal neutron beam (PEN) at KENS. These partrs are in preparation and the experiment will be started at the beginning of 1982.

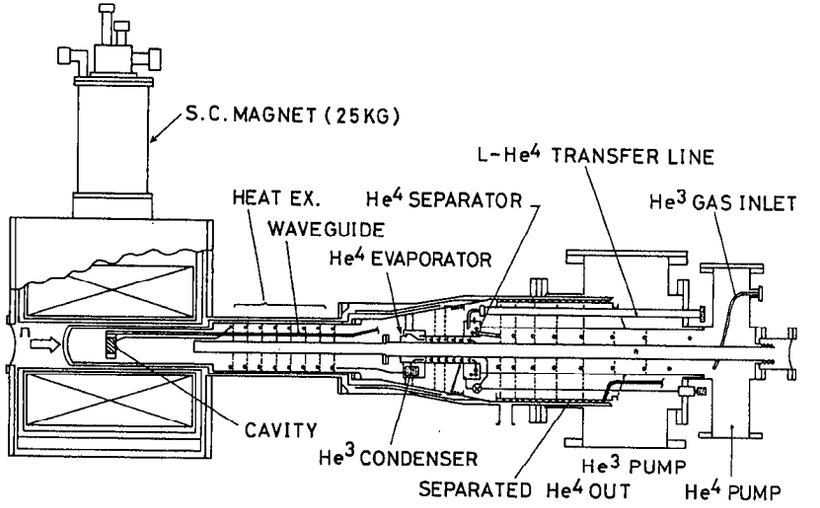

Fig.5 Side view of a He^3 cryostat and a superconducting magnet

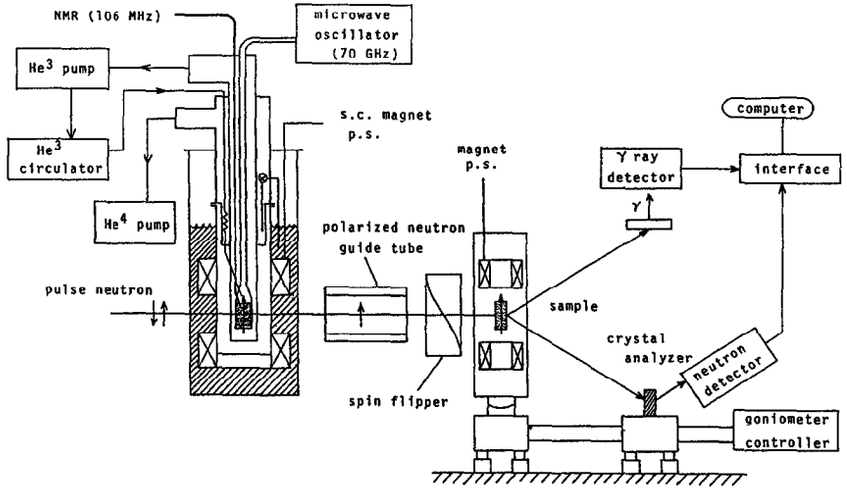

Fig.6 Schematic plan view of the PEN

References

1) S. Hiramatsu, S. Isagawa, S. Ishimoto, A. Masaike, K. Morimoto, S. Fukuhashi, Y. Hamaguchi, N. Minagawa and Y. Yamaguchi, J. Phys. Soc. Japan 45 (1978) 949.

2) V. I. Lushchikov, Yu. V. Taran and F. L. Shapilo, Yad. Fiz. 10 (1969) 1178. [Sov. J. Nucl. Phys. 10 (1970) 669]

3) N. Hoshizaki; private communications

4) D. Hill, R. Miller, M. Krumpolc and J. Rocek, Nucl. Instr. and Meth. 150 (1978) 331.

5) S. Hiramatsu, S. Isagawa, S. Ishimoto, A. Masaike, and K. Morimoto, Nucl. Instr. and Meth. 160 (1979) 193.

Development of ^{6}Li glass scintillator in Japan

Nobuo Niimura
Laboratory of Nuclear Science
Faculty of Science, Tohoku University
982 Sendai, Japan

Akira Matsumoto, Michio Kariya
Nikon, 1773 Asamizodai,
Sagamihara, Japan

and

Sadao Hoshino
Institute for Solid State Physics,
Tokyo University,
Roppongi, Japan

The conventional gas proportional counter is often used because of its high efficiency of neutron detection. The gas amplification in the proportional region gives a good signal to noise ratio. However, it has one disadvantage, namely, a long dead time (i.e. several μsec) because it takes more than several μsec for ions to reach to the cathode. In time-of-flight measurements the dead time of detectors is a big problem, since in the TOF method the peak flux of neutrons is more important than the time-averaged flux. Unless

all the neutrons reaching the detectors in one burst can be separately detected, high flux pulsed neutron source cannot be used efficiently. The pulse created in the detector by an incident neutron must therefore be prompt. A type of detector which appears to meet the dead time requirement is the scintillator. We attempted to make a ^{6}Li-glass scintillator with the co-operation of the NIKON camera-company, and two kinds of scintillators were successfully produced. The ^{6}Li-glass scintillators which are shown in Fig. 1, have diameters of 2" and thicknesses of 0.6 mm, 1 mm and 2 mm respectively.

The performance of our ^{6}Li-glass scintillator was tested by using a ^{226}Ra-Be neutron source, ISSP-spectrometers at JAERI and the Tohoku PNS. Figure 2 shows the pulse height distribution of the ^{6}Li-glass scintillator when the Ra-Be neutron source was used. Since Ra-Be also emits γ-rays, a γ peak is also apparent. When neutrons diffracted from a Cu-single crystal are used, the intensity of the γ-peak decreases to a low value as shown in Figure 3.

We monitored the thickness dependence of the neutron peak position, intensity, signal to noise ratio and resolution by making measurements with the 0.6 mm, 1.0 mm, and 2.0 mm scintillators. The results are summarized in Table 1. The peak position reflects the efficiency, of which the P.M.T. receives the scintillation photons. The intensity corresponds to the neutron detection efficiency of the scintillator. Good resolution implies that we can separate the neutron peak easily by using a single channel discriminator. The scintillators which had a good S/N ratios also had a low background. Both the peak position and resolution appear not to depend on the thickness in this

region. Overall, the scintillator of 1 mm thickness appears to represent the best choice, although if a lower background is required, that of 0.6 mm might be preferred.

The neutron detection efficiency of the ^{6}Li glass scintillator was tested by comparing its efficiency with that of a $^{10}BF_3$ proportional counter. Figure 4 shows the results. The measurement was carried out with monochromatic neutron beams (λ = 2.44 Å). The rocking curve of the 200 reflection from a single crystal of Ag_3SI was measured with both a $^{10}BF_3$ counter (2" in diameter and about 30 cm in length) and a ^{6}Li-glass scintillator (2" in diameter and 1 mm in thickness). The neutron detection efficiency of the ^{6}Li-glass scintillator is about 90 % at λ = 2.44 Å, which is close to the value calculated from the estimated the cross section of ^{6}Li in the scintillator.

ANL groups have tested the pulse height distribution of our glass scintillator, making as direct a comparison as possible with a 1 mm thick sample of similar material sold by Nuclear Enterprises, NE 905. Their results indicate that our glass scintillator gives 90 % of the light output of NE 905.

The glass scintillator has the advantage of allowing the possibility of the large area detectors. If a proper method for defining the position of the scintillation event can be developed, it may be used in a PSD.

We considered the possibility of using the optical fibres to link the scintillator to the photomultiplier tube in a similar fashion to that reported by workers at the Rutherford Laboratory.

The pulse height after the photomultiplier for this system is

estimated by the following expression:

$$I = N_p \cdot \xi \cdot \eta \cdot \zeta \cdot G \cdot q \cdot \sigma / j$$

where

N_p is the number of emitted photons per captured thermal neutron in the glass,

ξ is the efficiency of the collection of photons in the photomultiplier,

η is the quantum efficiency of the photocathode,

ζ is the collection efficiency of the first dynode,

G is the gain of the photomultiplier,

q is the charge of one electron,

σ is the transmission efficiency of the fibre optic bundles, and

j is the number of branches in one fibre optic bundles.

When we use the following values;

N_p = 4000 photons/n, ξ = 70 %, η = 20 %, ζ = 50 %, G = 1.3 x 10^7 (R 1250), q = 1.6 x 10^{-19}C, σ = 20 %, j = 3, the pulse height, I, is estimated as 39 pico coulomb. If we use a charge sensitive preamplifier (4.5 mV/pc), the pulse height on output is about 170 mV which is enough for the signal to be distinguished above background level. We are currently producing such a position sensitive scintillator detector. The number of scintillator elements is 84 and the number of photomultiplier is 9.

Table 1 Performance of Glass Scintillators of various thickness

	Peak Position	Intensity	S/N	Resolution
0.6 mm thickness	1	1	1	1
1.0 mm thickness	∿1	∿1.2	0.6∿0.7	∿1
2.0 mm thickness	∿1	∿1.1	0.3∿0.4	∿1

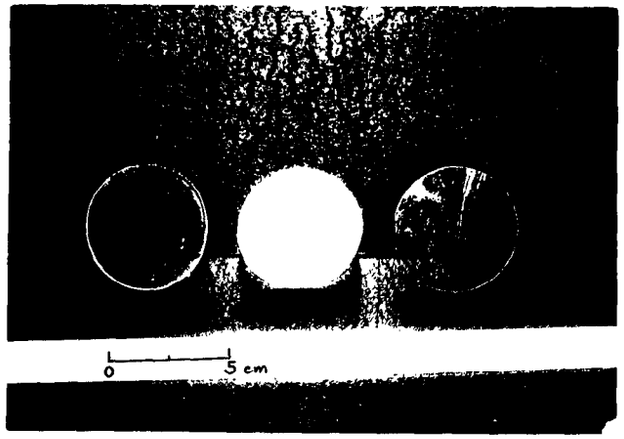

Fig. 1 ^{6}Li glass scintillators. The thicknesses are 0.6 mm, 1.0 mm and 2.0 mm respectively. A layer of TiO_2 has been painted on the surface of the 1.0 mm scintillator to use as a reflector.

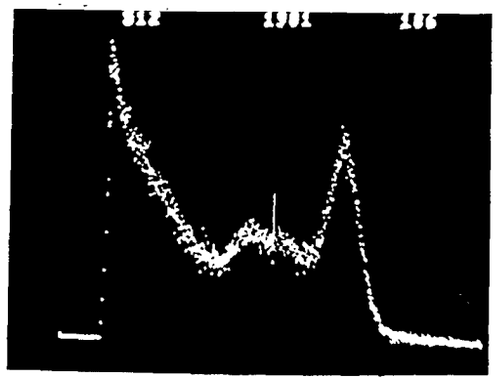

Fig. 2 The pulse height distribution obtained with the Ra-Be neutron source.

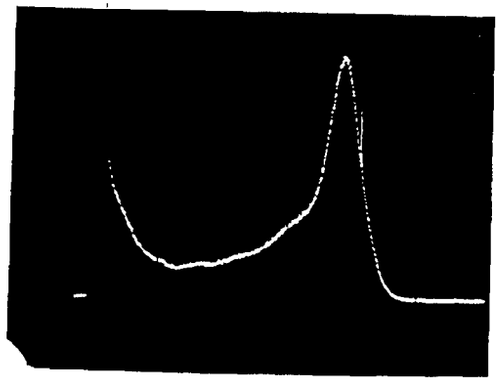

Fig. 3 The pulse height distribution measured using diffracted neutrons.

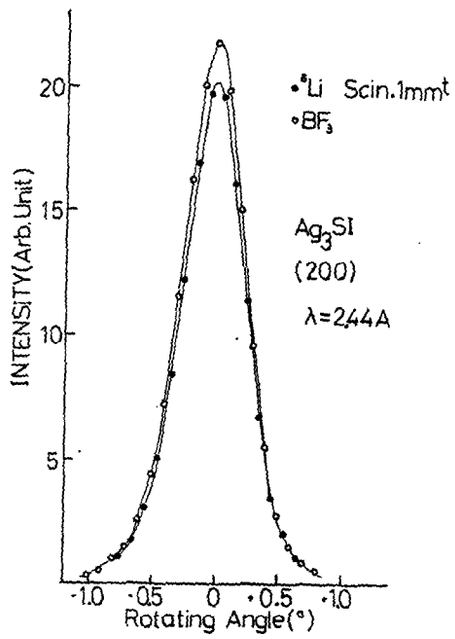

Fig. 4 A comparison of the neutron detection efficiencies of the glass scintillator (1.0 mm in thickness) and a $^{10}BF_3$ proportional counter (30 cm in length) at λ = 2.44 Å.

Position Sensitive Slow Neutron Detectors Using Fibre Optic Encoding

P L Davidson and H Wroe
Neutron Division, Rutherford & Appleton Laboratories.

1. Introduction

The advantages of using "position sensitive detectors" (PSD's) in neutron scattering measurements have been recognised for a number of years[1]. Hitherto, the most successful PSD's have been based on the gas proportional counter principle[2][3] in which a gas containing ^{3}He or ^{10}B in the form of borontrifluoride is used both to absorb the slow neutrons and to obtain gas multiplication of the resulting ionisation. An outstanding example of the application of these detectors has been to small angle scattering such as the D11 instrument at the Institut Laue-Langevin. The recent interest in intense pulsed neutron sources such as the Spallation Neutron Source (SNS) being constructed at the Rutherford Laboratory or the Intense Pulsed Neutron Source at the Argonne National Laboratory, has created new requirements for PSD's. These arise from the time-of-flight technique used for all measurements and from the fact that the neutron energy spectrum from these new sources is much richer in epithermal neutrons than that from reactor sources. It is anticipated that much of the new science will arise from the use of these higher energy neutrons. The requirements of a detector for use at a high intensity pulsed source are summarised below:

a. the thickness must be less than about 20 mm for most types of measurement to avoid uncertainties in the flight path length. Some instruments such as quasi-elastic scattering devices require detectors not more than a few mm thick.

b. dead time of about 100 ns to cope with the high instantaneous count rates with acceptable dead time corrections.

c. adequate detection efficiency over a wide range of neutron energies extending up to epithermal energies, eg an efficiency of about 30% at a neutron energy of 1 eV.

d. positional information with a spatial resolution about 10 mm or more.

It is very difficult to meet these requirements with the gas proportional counter technique. The dead time is limited by the drift velocity of electrons in the gas and cannot be much less than 1 μs in practical detectors. Also the need for adequate efficiency at epithermal neutron energies implies a high pressure gas filling with the attendant need for thick windows.

Detection methods using a solid neutron convertor are more likely to meet the needs of instruments at pulsed neutron sources. The use of gadolinium foils together with conventional multiwire proportional counters to detect directly the charged particle products of the neutron interaction have been proposed[4]. The foils must be thin (< 10m micrometres) to allow the escape of a reasonable fraction of the charged particles, which results in a low detection efficiency for a single foil at epithermal neutron energies. The rapid fall of the gadolinium absorption cross-section with increasing neutron energy above about 0.2 eV accentuates this problem for epithermal neutron detection. For example a foil of ^{157}Gd of thickness 5 micrometres would have a stopping power for 1 eV neutrons of 0.2%. The method is promising however for beams of cold neutrons. Furthermore, if the cost of multiwire proportional counters could be greatly reduced in the future so that several could be placed in series, at reasonable cost, then the detection efficiency could be increased. At the present time, however, it is considered that the scintillator technique offers the best solutions for pulsed source detectors.

Scintillators

2. Two types of neutron scintillator have been used in the present work, both incorporating ^{6}Li as the neutron convertor. Both are well known and commercially available.

2.1 Lithium Loaded Glass

Silicate glass containing ^{6}Li and using cerium as an activator[5] has the following properties as a slow neutron detector:

a. it is transparent to its own light emission which has a wavelength of 3900 Å at the peak of the emission spectrum[6].

b. about 10^4 photons are emitted per neutron absorbed[7] the light output decaying to half peak intensity in ∿ 20 ns and to one-tenth peak intensity in ∿ 100 ns[8].

c. the absorption efficiency of 2mm thick scintillator is typically 80% for neutrons of energy 0.08 eV (wavelength ∿ 1Å). The efficiency as a function of neutron energy is shown in Fig.1

d. scintillator of thickness 2 mm has appreciable gamma sensitivity[9] but this can be reduced by arranging it in the form of 0.5 mm thick wafers interspaced with 1 mm thick sheets of plain glass. The predominant mode of interaction with gamma rays is via Compton scattering producing a recoil electron. The range of the electron in glass is such that it deposits most of its energy in the non-scintillating parts of the sandwich thus reducing the pulse height and enabling simple pulse height discrimination to be used. The ranges of the charged particles produced from the neutron interaction (an alpha particle of energy 2.1 MeV and a triton of energy 2.7 MeV) are short and contained within the layers of scintillator. This technique will be described more fully elsewhere. In the present work with glass scintillator it has been found possible to use pulse shape discrimination against noise but not gammas.

2.2 Lithium Loaded Zinc Sulphide

Silver activated zinc sulphide is a well-known phosphor and it is combined with ^{6}LiF and a plastic binder to form a slow neutron scintillator which has been used for many years for neutron radiography. It has the following properties:

a. it is translucent with strong absorption and scattering of its own light which has a wavelength of 4500 Å at the peak of the emission spectrum[10]. It can only be used in thin sheets

(thickness ≥ 0.6 mm) if all neutrons absorbed are to be "seen" by a photomultiplier.

b. about 10^5 photons are emitted per neutron absorbed[7], the light output decaying to half peak intensity in ∿ 150 ns and to one-tenth peak intensity in ∿ 1 μs[11].

c. the absorption efficiency of 0.6 mm thick scintillator is ∿ 20% for neutrons of energy 0.08 eV and ∿ 6% for an energy of 1 eV.

d. the gamma sensitivity is low and, in addition, pulse shape discrimination can be used.

e. the cost is very roughly one-tenth of that of lithium glass scintillator.

3. Principle of Operation

For PSD's using the scintillation technique and requiring many spatial resolution elements, the obvious method of optically coupling a photomultiplier (PM) to each element is impracticable due to the cost and complexity of a system containing many thousands of PM's. The present system uses a fibre optic encoder to couple a large number of resolution elements to a much smaller number of PM's. Each resolution element is a separate piece of scintillator and is connected by 3 fibre optic channels to a unique combination of 3 PM's out of a bank of N. Thus a coincident output signal on 3 particular PM's identifies the resolution element in which a neutron capture event took place. The number of resolution elements, n, which can be encoded by N PM's using a triple coincidence is given by:

$$n = \frac{N!}{3!(N-3)!}$$

and the number of elements connected to each PM, M, is given by:

$$M = \tfrac{1}{2}(N-1)(N-2)$$

Also, any group of 3 PM's is connected to a large fraction of the total number of resolution elements and so a neutron detected in one element

"linear" detector in the form of a spiral, an area detector with "r-θ" resolution can be made.

4 Methods of Construction

4.1 Use of Zinc Sulphide Scintillator

The zinc sulphide scintillator is useful for cold neutrons where moderate stopping power is not a disadvantage, in an environment with high γ background and where moderate count rates only are encountered (about 10^4c/s over a whole detector for example). The scintillator must be viewed normally to its surface with an arrangement shown schematically in Fig.2. A prototype detector system has been used successfully in a neutron scattering experiment on the D7 instrument at the Institut Laue Langevin[14]. This system used bundles of glass fibre optics in the encoder, but much better results are now achieved using coated plastic fibres. These have better transmission for blue light, are much easier to handle and finish and are of lower cost. The method of making an encoder is illustrated in Fig.3. Spacer bars with 'V' grooves spaced at the pitch corresponding to the resolution required are mounted on a simple winding machine. Three fibres are wound into each groove, the 'V' shape ensuring self alignment. A cover strip is then glued on top to trap the fibres. Twelve strips can be wound simultaneously. The strips are then stacked up as shown and the fibres encoded by hand into the appropriate number of output channels. This whole process can be completed easily in 2 days for a detector module having a few thousand resolution elements. The assembly is then encapsulated in a neutron absorbing material to form a strong monolithic block.

4.2 Use of Glass Scintillator

The light output from the glass scintillator is not high enough for good optical coupling to the fibres in the manner described above. However, its good transmission for its own light output enables good coupling to be made to the edges of the scintillator elements, the light being transmitted to the fibres by total internal reflection. An arrangement using this principle is illustrated in

paralyses many other elements until the detection and decoding process is complete. The number of elements, P, coupled to any group of 3 PM's is given by:

$$P = \tfrac{1}{2}(3N^2 - 15N + 20)$$

We note that the code is free of ambiguities if the decoder accepts 3 and only 3 coincident PM output signals. Thus two neutrons arriving simultaneously on two different resolution elements would produce more than 3 PM outputs and no ambiguity in spatial information would result though the counts would be lost. Table I shows some sets of these quantities by way of illustration.

Table I

No. of PM's	No. of Elements Encoded	No. of elements coupled to each PM	No. of elements coupled to any group of 3 PM's
N	n	M	P
15	455	91	235
20	1140	171	460
30	4060	406	1135
40	9880	741	2110

Still higher economies in PM's could be achieved by using a higher order coincidence, but for the geometries required for neutron work, it would be difficult to pack more than 3 or 4 fibre optic channels behind each resolution element and still achieve enough light collection efficiency for reliable operation. The present system uses triple coincidence and a 3 out of N code as a practical arrangement.

A similar scheme was developed independently by Hoftiezer et al.[12] who used a binary code in a detector for high energy charged particles.

The particular arrangement of the resolution elements can vary widely. For example they can be of any shape and be arranged on any surface such as a cylinder or sphere. Furthermore an area detector having resolution in two dimensions is simply a folded linear one. By arranging a

Fig.4. Fibres wound on spacer strips, as described above, can still be used. The scintillator elements are no longer in one plane but this is not important for most applications. Gamma discrimination can be achieved by arranging the scintillator in a sandwich as described in section 2.1(d). A variation of this principle would be to construct the sandwich without the plain glass, each scintillator layer being coupled with fibre optics as a separate detector element. A gamma event producing light in more than one layer would result in more than 3 simultaneous signals and would therefore be rejected by the decode electronics. An interesting outcome of the capability of collecting light from individual layers of a scintillator sandwich is that there is no limit to the number of layers, so that thick assemblies could be built up (say 10 layers of 1 mm thickness) without increasing the γ sensitivity. Such a device would have an efficiency of over 50% for 10 eV neutrons (see Fig.1).

A detector module of 400 channels with 1 cm resolution and 1 mm thick glass scintillator is being constructed. It is expected that this module will have a count rate capability of over 10^6c/s with pulse pair resolution time of $\sim$ 100 ns.

5. Electronics

Light levels at the outputs of the encoders are low and a photon counting technique is used to identify neutron events in the scintillator[13]. A fast system for use with the glass scintillator has been built which uses a time window of 100 ns opened on the detection of any pulse. A further 3 or more pulses counted within the window indicates a neutron event. A high voltage bias curve for a three channel unit is shown in Fig.5. In this measurement 6 plastic fibres 1 mm diameter were coupled to the edge of a 1 mm thick piece of scintillator, 0.6 cm wide and 4 cm long, the fibres being connected to the narrow edge. A good plateau is achieved.

6. Conclusions

The successful operation of the fibre optic encoding principle has been demonstrated in a neutron scattering experiment and recent developments

have enabled the method to be extended to the use of lithium glass scintillator with the advantages of high count rate capability and good detection efficiency. Methods of manufacture have been developed which use straightforward technology. The cost of detector modules of a few thousand elements should be between £1 and £3 per channel including electronics depending on geometry required and on which scintillator is used.

REFERENCES

1. B H Meardon and D C Salter, Rutherford Laboratory Report RHEL/R.262, 1972.
2. R Allemand et al., Nuclear Instruments and Methods, 126 (1975) 29-42.
3. M K Kopp and C J Borkowski, Oak Ridge National Laboratory Report, ORNL-TM-5083, December 1975.
4. A P Jeavons et al., CERN Report, CERN 77-01, January 1977.
5. D G Anderson et al., Proceedings of the 5th International Instrumentation and Measurements Conference, Stockholm, pp.616-630.
6. A R Spowart, Nuclear Instruments and Methods, 140 (1977) 19-28.
7. A R Spowart, Nuclear Instruments and Methods, 75 (1969) 35-42.
8. E J Fairley and A R Spowart, Nuclear Instruments and Methods, 150 (1978) 159-163.
9. L A Wright et al., Nuclear Instruments and Methods, 33 (1965) 181-183.
10. J B Birks, The Theory and Practice of Scintillation Counting, Pergammon Press, 1964, p.543.
11. J C Barton and P W Ranby, Journal of Physics E: Scientific Instruments, 10, (1977) 437-438.
12. J H Hoftiezer et al., Nuclear Instruments and Methods, 147 (1977) 465-469.
13. R Bond, D K Ross, C J Carlile and I S Anderson, Annual Conference of the Condensed Matter Division of the European Physical Society, Antwerp 1980. Proceedings to be published in Solid State Communications.
14. P L Davidson, Rutherford Laboratory Report RL-77-106/A.

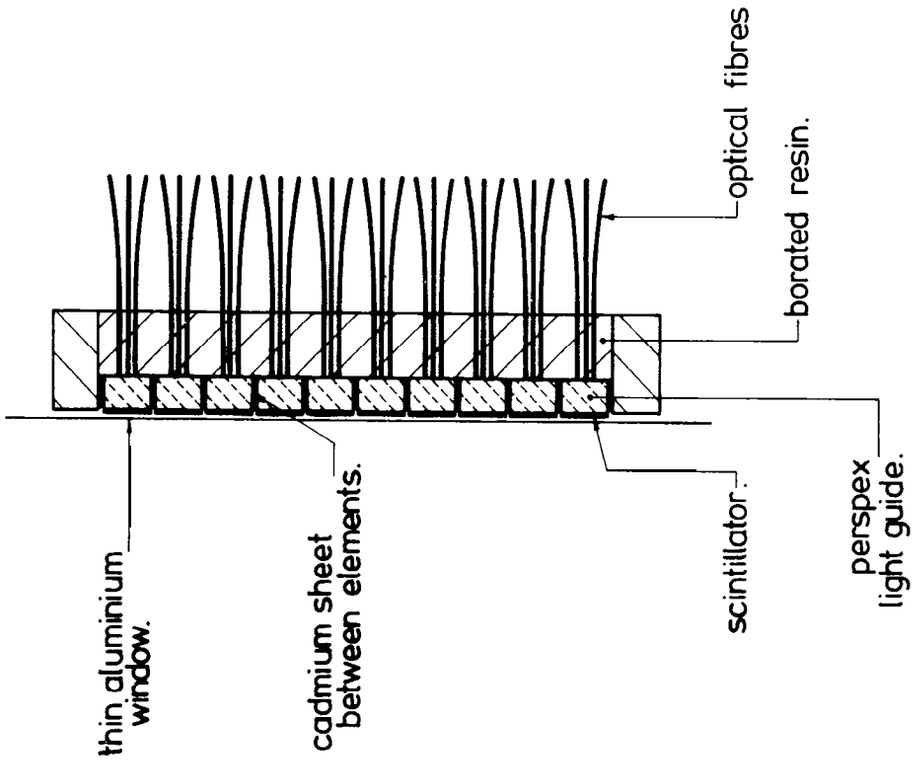

Fig.2 Schematic Cross-Section Of Input End Of Detector.

λ	E	μ	EFFICIENCY FOR VARIOUS THICKNESSES IN MM						
			0.5	1	2	3	5	10	20
Å	eV	cm^{-1}							
0.1	6.190	0.830	.041	.080	.153	.220	.340	.564	.810
0.15	3.640	1.245	.060	.117	.220	.312	.463	.712	.917
0.3	.910	2.49	.117	.220	.392	.526	.712	.917	.993
0.5	.328	4.15	.187	.340	.564	.712	.874	.984	1.000
1	.0819	8.30	.340	.564	.810	.917	.984	.999	1.000
2	.0205	16.60	.564	.810	.964	.993	.999	1.000	1.000
4	.00512	33.20	.810	.964	.999	1.000	1.000	1.000	1.000
6	.00228	49.80	.917	.993	1.000	1.000	1.000	1.000	1.000

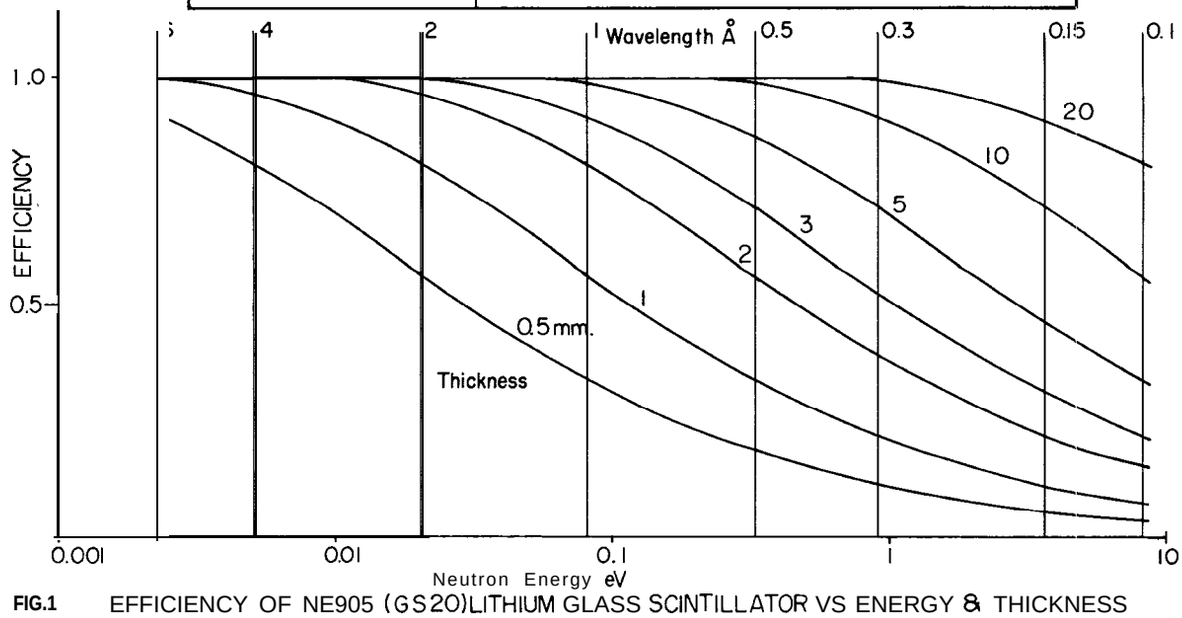

FIG.1 EFFICIENCY OF NE905 (GS20) LITHIUM GLASS SCINTILLATOR VS ENERGY & THICKNESS

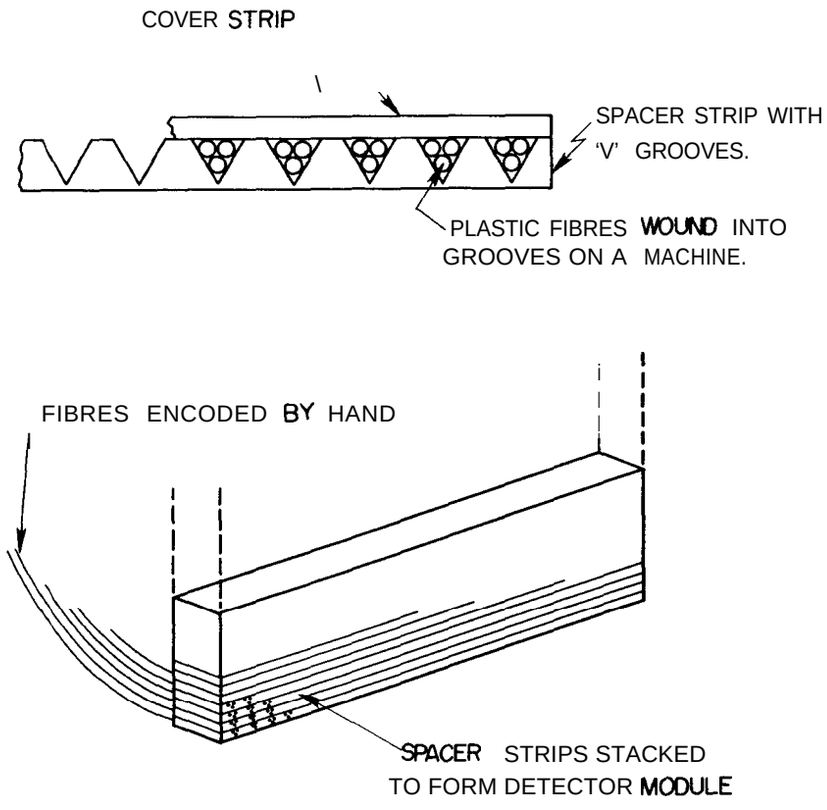

FIG.3. ILLUSTRATING METHOD OF MANUFACTURE OF FIBRE OPTIC ENCODER.

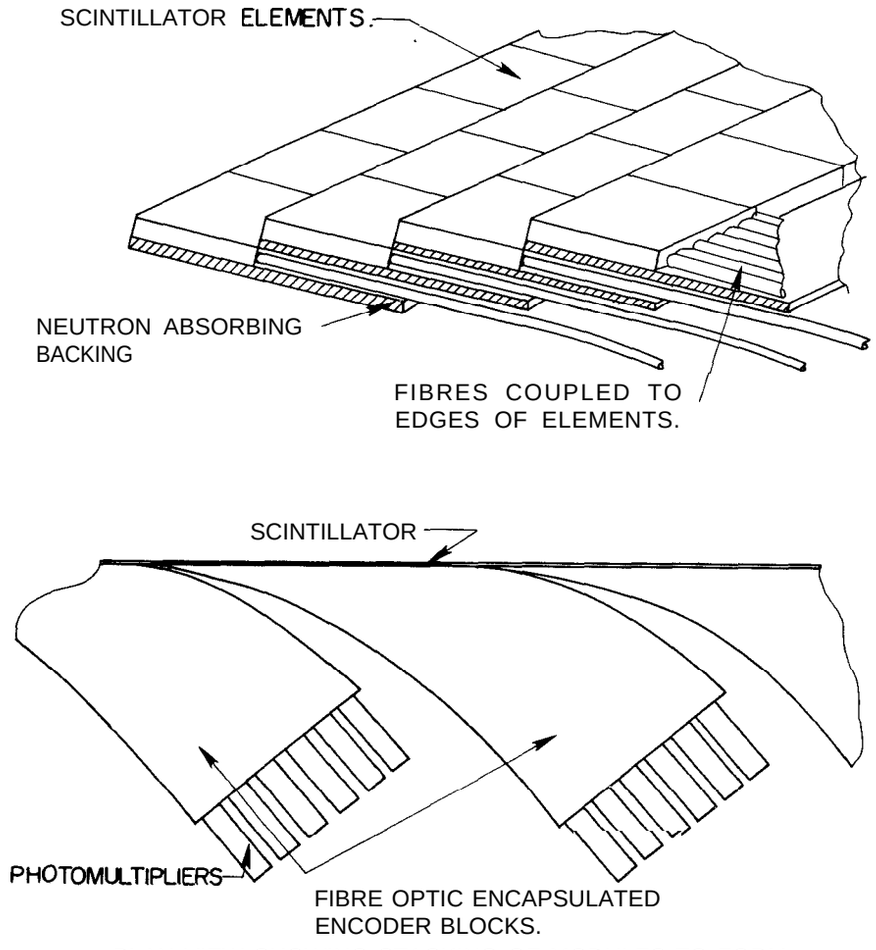

PLAN VIEW SHOWING STACKING OF MODULES TO FORM LARGE DETECTOR AREA.

FIG.4. ILLUSTRATING METHOD OF BUILDING AN ENCODER USING EDGE COUPLING OF PLASTIC FIBRES.

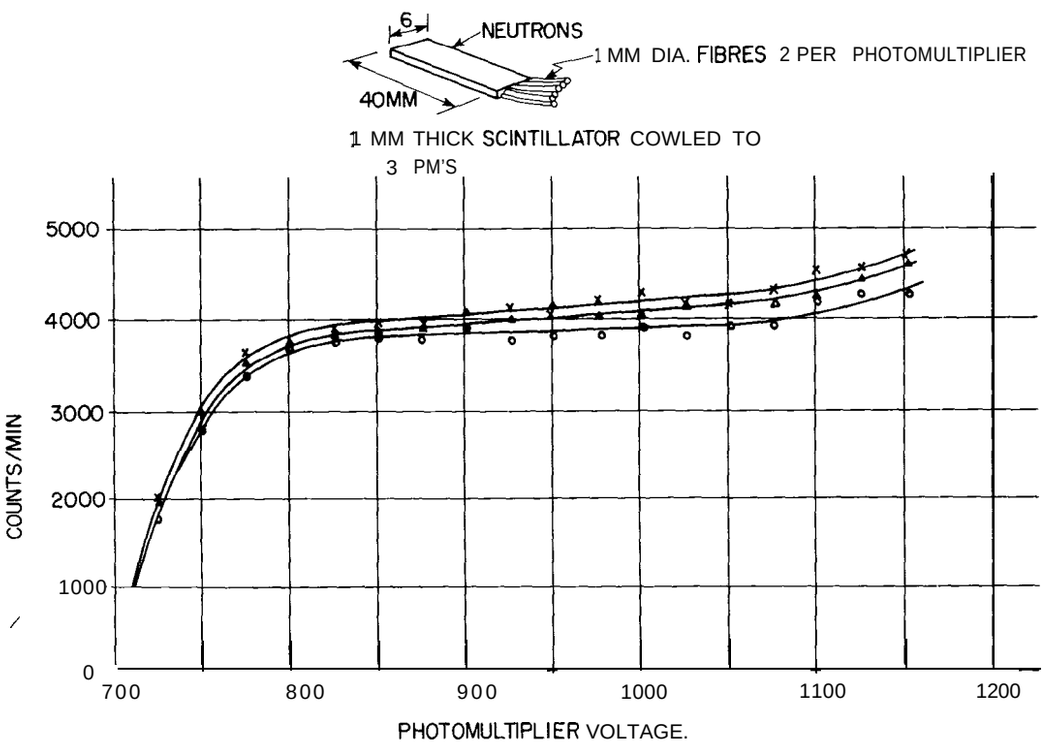

FIG.5. HIGH VOLTAGE CURVES FOR 3 CHANNEL, EDGE COUPLED TEST PIECE

Data Acquisition and Analysis Systems on SNS

M W Johnson
Neutron Division, Rutherford and Appleton Laboratories

1 Introduction

The whole system has been give" the acronym PUNCH: PUlsed Neutron Computer Hierachy.
The PUNCH system will be organised at four levels:

i) The data acquisition electronics (DAE) at each instrument will record the arrival of each detected neutron by incrementing the appropriate word in a memory whose size is determined by the required number of space-time channels. Prototypes of this level have already bee" built in the Rutherford Laboratory's Instrumentation Division.

ii) Each neutron instrument will have its own front-end minicomputer (FEM) to control the course of the experiment and to collect the data. Its

iii) The FEMs will all be linked to a single, medium sized RUB computer having a large disk data base (2 - 3 Gbytes), capable of storing some 2 - 3 weeks of experimental data as well as programs. The HUB

iv) Tbe RUB computer will be linked to the Rutherford Laboratory main-frame computers and hence to remote stations via the SRC network.

Figure 1 Illustrates the four-level hierachy described above.

A simple prototype of an external memory incrementing DAR system coupled to a PDP11/34 has been built and tested. It awaits field trials on the Harwell linac.

A detailed design of the SNS DAE is in progress and is described below.

A hardware/software specification for the FEM/HUB computers has bee" drawn up and circulated to 21 manufacturers (Nov '79), in a pre-tender exercise. Ten manufacturers responded. A very brief summary of this specification is included below under the headings FEM. ROB and Communications. Since

2 Data Acquisition Electronics

The DAE is being designed by the Instrumentation Division at the Rutherford Laboratory and is shown in Figure 2. It consists of up to 16 TOF crates and a system crate. Bach TOF crate contains up to 23 TOF modules and a crate control module.

Each TOF module houses two separate channels. A channel may be fed by a single detector or a number of detectors via a position encoder module. I" the latter case positional information is passed to the module via a front panel connector. When an event occurs on one of these detectors the appropriate space (from the detector) and time (from the TOF bus) information is stored in one of the dual 256 wd memory buffers located in each channel ('DUAL BUFF' in Figure 2a). Thus during a neutron frame (20 ms on SNS) one of the dual buffers is filled while the other is being read (via the data section of the TOF bus). The fact that all of the information for one frame is stored in the TOF module before being incorporated in the bulk memory means that it may be verified before transmission. If any of the error conditions are set (eg due to an overflow in a dual memory buffer) the frame is not read and the 'frame-lost' counter incremented.

The output from a single detector or a position encoder module may also be splayed (via a splay module) to two or more TOF modules. Using the splay technique the effective depth of the dual memory buffers may be increased in units of 256 wds. From each TOF crate the information stored during the previous frame is read out via the instrument bus to the systems crate. Within the crate the instrument bus interface introduces the frame counter information (used in experiments studying relaxation phenomena) resulting in a total of 41 bits of information being presented to the descriptor generator. This is reduced in two stages. A hardware patch removes those bits which are redundant for all experiments on the particular instrument. Secondly a programable section (show" as the ROM and COMPACTOR in Figure 2b) produces the compacted descriptor in a manner that may be tailored to each experiment. This, final, descriptor is the" passed to the bulk store via a" INTEL multibus to effect a Read Increment-Write (RIW) cycle on the appropriate address.

The FEM will be connected, via a suitable interface, to the Intel multibus for DMA transfer of the Bulk store contents to the FEM memory (not show" in figure 2).

3 Front-End Minicomputer

Hardware Configuration

CPU + optional hardware multiply/divide.
OS + 80 Kbyte of < 1 µs main memory

Hardware bootstrap and programmer's console.
20 Mbyte of disk storage which at least 2 Mbyte must be demountable.
Inexpensive hardcopy alphanumeric terminal.
Interactive graphics terminal (ie with graphics cursor facilities).
> 5 Kbyte/s serial synchronous interface to HUB or communications computer.
BUS interface supplied by the Rutherford Laboratory.
CAMAC crate controller.

4 FEM Software

i) The operating system. The minimum requirements of the operating system are to permit two real-time tasks to execute in conjunction with the network software. The OS could be single-user.

ii) The network software. This should permit remote log-in to the HUB from FEM terminals and file transfer facilities. It should be possible to initiate file transfer by terminal commands or under program control.

iii) Applications software PEANO for experiment control

iv) Application software DEDEKIND for data display

vi) Other specialist applications software will deal with subsequent data treatment.

5 HUB and Workstation

Hardware Configuration

32 bit (or larger) word CPU and ancillary hardware such as cache and hardware floating point unit to provide 0.2 IBM 360/195 equivalent processor.
Operator's console and VDU.
1 Mbyte of main memory which can be expanded to at least 2 Mbyte.
2 Gbyte of disk storage which can be expandable to 3 Gbyte.
600 lpm line printer.
3 x 6250 bpi tape drives.
Interface(s) for network connections from FEM's and RLM or communications computers.
Interfaces to HUB workstations.

Two HUB workstations. Each will comprise:

i) workstation control processor and suitable communications interface(s);

ii) 10 x interactive graphics terminals with graphics cursor facilities. These "nits should be identical to those on the FEMs. Shared hardcopy facilities are necessary;

iii) 600 lpm line printer;

iv) High speed, high quality hardcopy graphics plotter;

v) a demountable cartridge disk drive or floppy drive, of the same type as used on the FEM computers. This device is required on one workstation only.

6 HUB Software

operating system

A virtual, multi-user, multi-tasking operating system should provide the following facilities:

Up to 30 simultaneous, logged-on users. It is expected that ∿ 40% of these users will be executing existing data reduction programs requiring a high floating arithmetic activity.

A further ∿ 40% will be viewing/editing their data "sing the interactive graphics terminals and obtaining hardcopy graphics output.

The remainder will be developing new programs (compiling, editing, linking etc).

In addition to the logged-on users there will be continual file transfer from all the FEMs to the HUB (at a mean rate of ∿ 1000 byte/sec). (5 FEMs in 1984 increasing to a maximum of approximately 20).

A virtual memory management system permitting all user programs at least 4 Mbyte of storage (program + data).

A File Management System with the following features:

a) A unified file structure such that files on the FEM and HUB computers are compatible.

b) The system should also provide monitor/restriction functions to a users available file space.

c) An archiving facility, new files should be automatically identified and copied to tape at pre-set time intervals.

d) The system should permit the production of non-standard formats on magnetic tape.

e) All sequential output devices shall have spooling facilitites.

A batch processing mode should be available.

ii) Network Software

iii) Data Base Software

An applications package which will keep track of the runs performed, their location within the various storage mediums and the analysis Performed on them.

iv) Users Applications Programs

7 Communications

The basic design requirements are:

a) That all terminals should be able to communicate with all processors In the PUNCH hierarchy above the one they are physically connected to.

b) File transfer should be possible between adjacent members of the hierarchy. It should be possible under (application) program control.

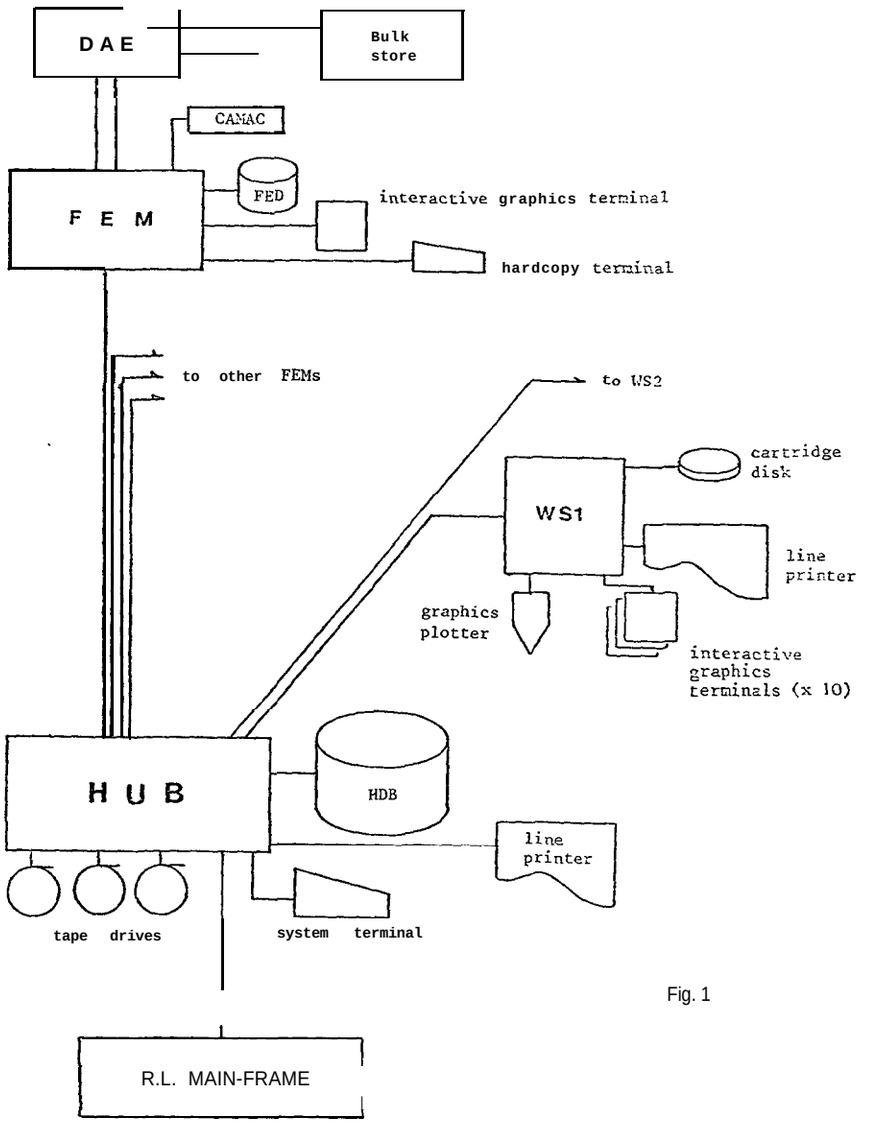

Fig. 1

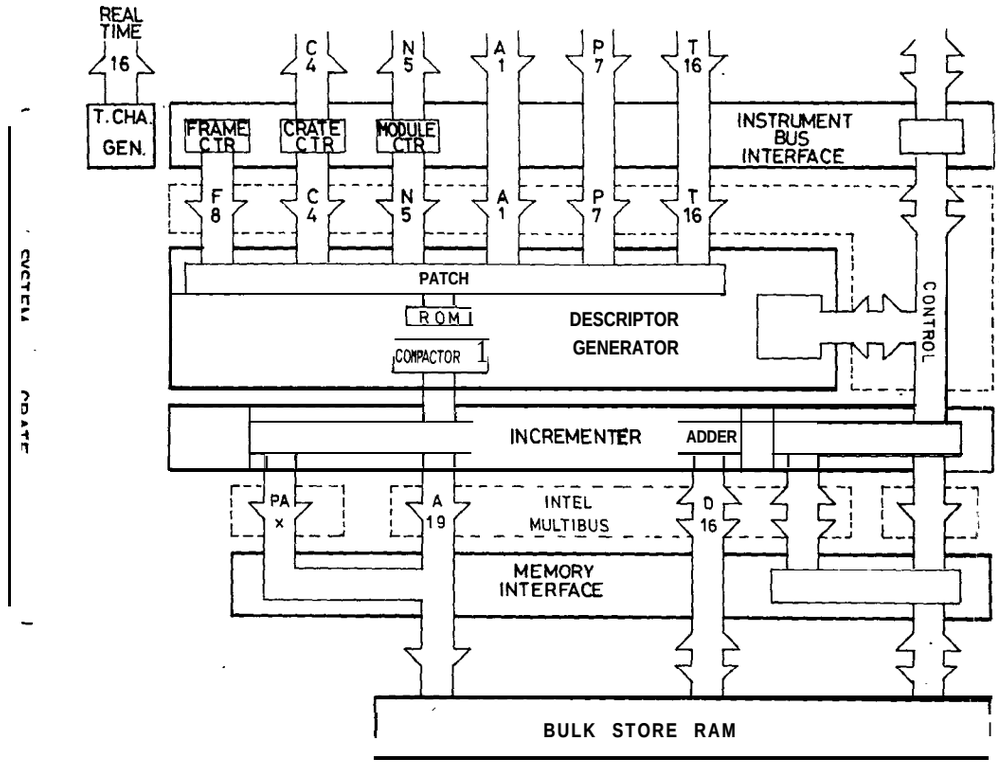
REAL TIME 16
T.CHA. GEN.
FRAME CTR
CRATE CTR
MODULE CTR
C 4
N 5
A 1
P 7
T 16
INSTRUMENT BUS INTERFACE
F 8
PATCH
ROM 1
COMPACTOR 1
DESCRIPTOR GENERATOR
CONTROL
INCREMENTER
ADDER
PA x
A 19
INTEL MULTIBUS
D 16
MEMORY INTERFACE
BULK STORE RAM

Fig 2b

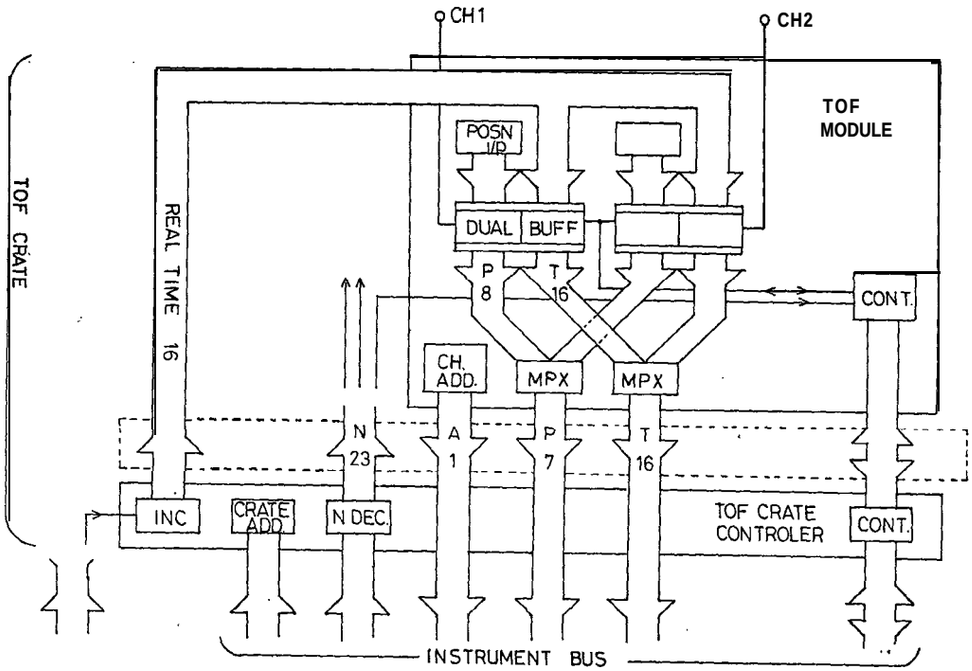
CH1
CH2
TOF MODULE
POSN I/P
DUAL
BUFF
P 8
T 16
CONT.
CH. ADD.
MPX
MPX
TOF CRATE
REAL TIME 16
N 23
A 1
P 7
T 16
INC
CRATE ADD.
N DEC.
TOF CRATE CONTROLER
CONT.
INSTRUMENT BUS

(cont.)

KENS data acquisition system

N. Niimura, M. Kohgi* and Software Group**
Laboratory of Nuclear Science, Faculty of Science*
Tohoku University, Sendai Japan

**M. Arai, S. Tomiyoshi, K. Tajima, M. Isobe,
M. Furusaka and Y. Fujino

§ 1 *Introduction*

Some parts of the KENS data acquisition system have been reported in KENS REPORT 1.1) Here, we wish 'to outline the manner in which the flow of data is controlled. We include photographs of the computer system, the camac system and some specially designed modules which were complted in April 1980. For an outline of the general philosophy of the system and for further details of the functions of each module, readers are referred to the previous paper. [1)]

§2 *System configuration*

The sytem configuration is shown in Fig. 1. The data from 5 spectrometers (SAN, LAM, MAX, TOP, HIT) are accepted, manipulated and stored by this system. The data from the two-dimensional position sensitive detector of SAN are input through the specially designed multi-dimensional

time analyzer (MDTA) interface. The CAMAC system is adopted for the interface. The central process unit (CPU) of the computer is OKITAC SO/model 60. The peripherals are magnetic disc (DK), magnetic tape (MT), electric typewriter (ET) photo-tape reader (PTR), line printer (LP), graphic display (GD), hard copy (HC) and dotted line printer (DLP).

§ 3 *Flow of the data and their control signal*

A chart depicting the flow of data and corresponding control signal is shown in Fig. 2. The thick and thin arrows refer to the data and control signal respectively. The data flow can be managed by the operation of switches on the control panel (CP). Each spectrometer has its own dedicated control panel.

3 - 1 *Count Start*

When a START button is pushed, an interruption signal is sent *to* the branch driver (BD) through the inter-ruption module (IT). The CPU central process unit (CPU) accepts the signal from the BD, and recognises the status of the interruption and sends a count-start-signal both to the time analyzer (TA) and *to* the monitor module (MM) through BD. The booster trigger signal is directed to the trigger control module (TC) which distributes the booster trigger signal to the TA and the MM. When the count-start-signal from the CPU synchronizes with the booster trigger signal, the TA and the MM are opened and measurement commences. The neutron data from each spectrometer are

stored in direct access buffer memory (8 KW RAM) in the TA Monitor signals are counted by a 12 bits-scaler in the MM. During the measurement, the data in the TA are copied to the CPU memory, edited there and copied to the X-Y-display control module (XYD) through the BD so that the raw data may be displayed on the cathode ray tube (CRT),. The portion of the data in the TA to be displayed and the scale are selected by rotary switches. It is also possible to display previous data which is stored on magnetic disc (DK) by using a combination of the DISPLAY/OUTPUT AREA button and DETECTOR switch. The status of these swiches is read by the digital input/output module (DIO), and, if required, data are transferred from the DK to the CPU memory. After editing the data are output as before.

3 - 2 *Count Stop*

Operation of the STOP button sends a stop signal which follows the same path as the start signal above. When this signal is received the TA and MM gates are closed and, the data stored in the TA are transferred to a file on disc as specified by the ACCUMULATION AREA button.

3 - 3 *Data Clear*

Data clear is executed by pushing the DATA CLEAR button on the CP. The data-clear-signal follows the same cource as above although to prevent the data being erased accidentally,

several limitations are imposed. When the measurement is in progress or when the status of the DISPLAY/OUTPUT AREA and ACCUMULATION AREA switches differ, the DATA CLEAR button has no effect. Moreover, only the data currently being displayed on the CRT can be cleared.

3 - 4 *Data Output*

The output device such as the line printer (LP), magnetic tape (MT) and dotted line printer (DP) can be selected by pushing the respective button. A data-output -signal is then sent as above and the data currently being displayed on the CRT is output to the chosen peripheral. Typical examples of LP and DP output are shown in Figures 3 and 4. In addition to the neutron intensity data some relevant experimental parameters such as the delay time, channle width, monitor value etc. are also included.

A reference

1) KENS REPORT I, KEK Internal 80-l (1980) 163-180

Figure Captions

Fig. 1. The system configuration.

Fig. 2. Flow of the data and their control signal.

Fig. 3. An example of LP output.

Fig. 4. An example of DP output.

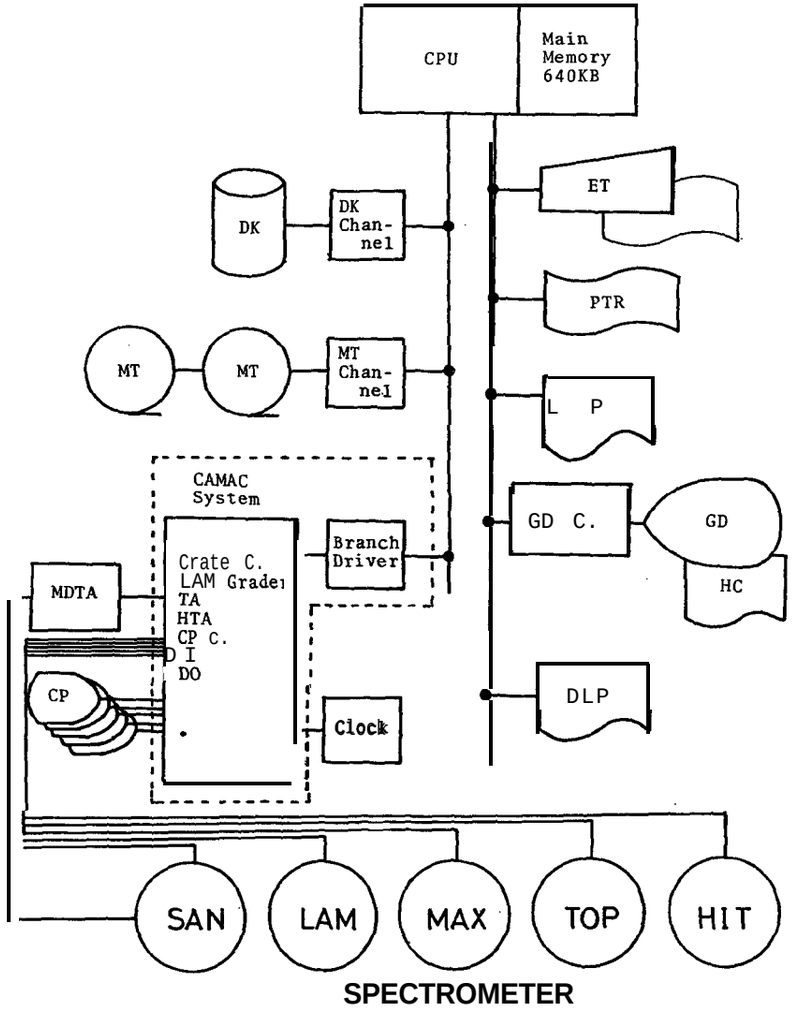
CPU
Main Memory 640KB
DK
DK Chan-nel
ET
PTR
MT
MT
MT Chan-nel
L P
CAMAC System
Crate C.
LAM Grader
TA
HTA
CP c.
I
DO
Branch Driver
GD C.
GD
HC
MDTA
CP
Clock
DLP
SAN
LAM
MAX
TOP
HIT
SPECTROMETER

Fig.

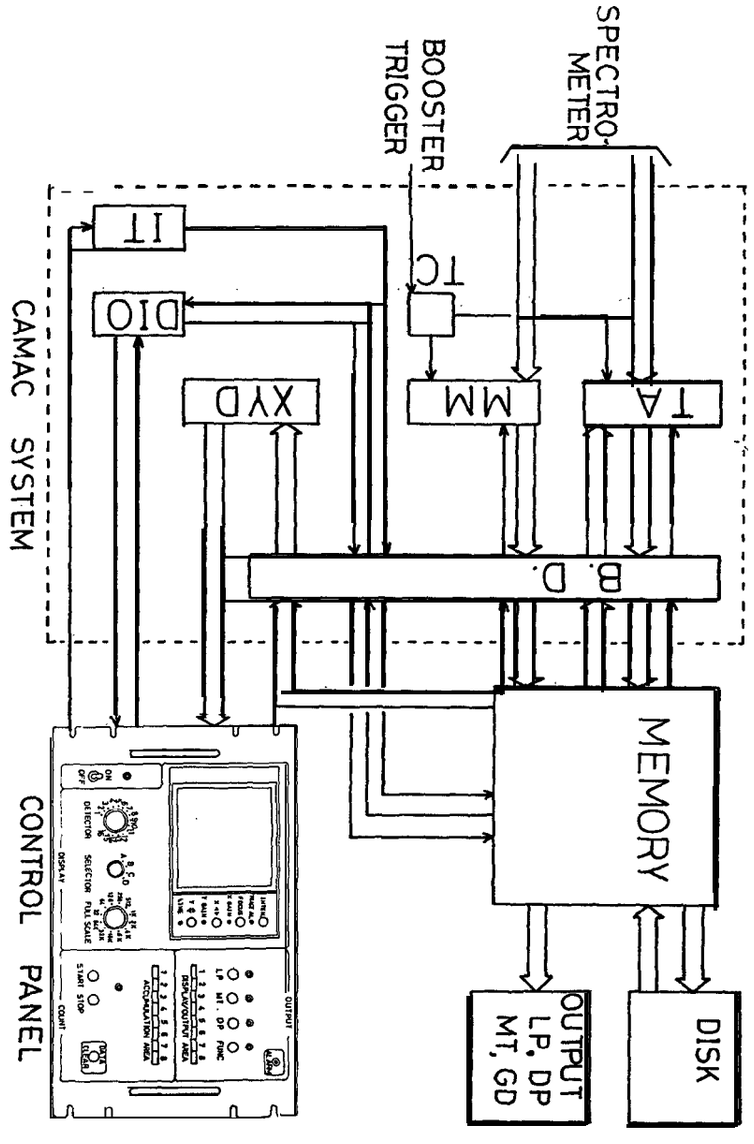
SPECTRO-METER
BOOSTER TRIGGER
IT
TC
DIO
XYD
MM
TA
CAMAC SYSTEM
B. D.
MEMORY
CONTROL PANEL
OUTPUT LP, DP MT, GD
DISK

Fig. 2

LAM

START : 80 - 12 - 13 / 20 : 57
STOP : 80 - 12 - 14 / 1 : 20
CH. WIDTH : 32 - 32 - 32 - 32
DELAY TIME : 1
NO. OF CH. : 512
NO. OF DET. : 8
COMMENT : PAA NO.2

MONITOR 0
DETECTOR - 2
DATA AREA - 4

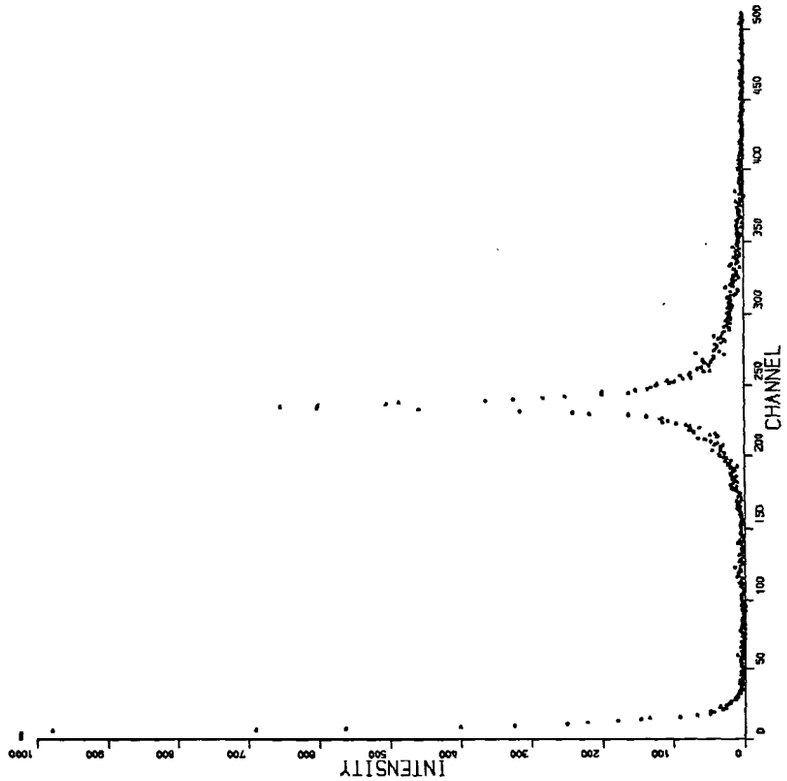

Fig. 4

DATE : 80.12.13 STAR: 20:57 AREA : 4 NET: 253 CH.WIDTH: 32- 32- 32- 32
MONIT: 0 STOP : 1:20 DETEC: 2 DEL: 1 COMMENTS:PAA NO.2

	0	50	133	155	200	251	300	353	400	450	500
1	39143	4	5	6	36	104	20	9	3	1	1
2	13525	6	6	7	28	93	18	8	4	4	1
3	4246	6	6	5	33	108	18	6	4	3	1
4	2222	5	5	6	45	86	22	9	5	4	5
5	1474	7	4	5	33	75	15	4	4	1	2
5	979	7	3	3	33	90	18		3	3	0
7	591	4	2	6	30	77	21	108	7	2	3
8	564	7	4	6	42	76	20	9	1	1	2
9	401	5	7	5	3 8	57	18	10	6	1	1
10	325	12	6	8	48	49	19	4	1	4	1
11	251	5	4	6	56	66	23	11	5	4 0	2
12	223	3	9	7	65	60	19	10	3		12950
13	180	6	7	9	39	50	14	3	4	2	
14	147	3	6	12	3 7	51	11	3	1	1	
15	135	3	5	.	59	55	18	11	4	5	
16	92	7	12	11	41	47	8	8	3	2	
17	68	4	10	10	7.	58	9	3	1	.	
18	50	4	10	8	77	44		5	5	4	
19	44	2	10	12	75	42	25	8	2	0	
23	49	6	6	5	63	43	18	8	5	4	
21	3 2	2	6	5	77	27	15	9	2	2	
22	27	1	8	10	82	67	12	6	2	1	
23	36	2	14	8	96	34	16	8	3	1	
24	28	5	7'	7	115	42	16	10	.		
25	25		5	9	107	40	8	4	3	.	
25	21	4	4	12	118	38	15	7	1	.	
27	23	6	9	15	115	38	10	5	4	.	
23	14	3	7	18	138	41	12	11	1	.	
29	14	1	4	12	163	32	11	4	2	2	
3 3	11	5	2	20	218	26	14	6	2	1	
31	12	4	9	16	241	28	13	1	1	1	
32	11	5	6	11	315	36	6	3	5	0	
33	7	1	4	14	458	52	19	5	3	2	
34	2	3	4	17	602	12	17	4	5		
35		5	5	15	554	30	11	12	2		
35	7	2	2	12	6 3 .	30	8	4	3	3	
37	6	4	4	19	504	28	9	4	2		
38	6	2	5	19	487	20	10	3	5	2	
39	4	2	6	16	364	23	14	4	2	3	
40	9	1	11	14	325	21	7	2	4	0	
41	5	3	5	15	285	28	11	7	3	1	
42	9	0	8	19	2 5 2	24	6	7	0	2	
43	5	5	2	11	200	19	12	3	2	1	
44	4	4	5	24	163	22	10	6	3	.	
45	4	0	4	2.	230	25	6	3	.	3	
46	7	6	6	27	153	18	15	2	5	1	
47	3	1	7	19	136	22	9	5	2	2	
48	7	3	6	25	131	2.	9	2	3		
49	4	5	4	29	124	20	10	4	0	2	
50	3	5	6	34	122	23	7	7	4	1	

Fig. 3

Advantage of Neutron Sources with Time Structure for Special Neutron Spectrometers

N. Nicker and W. Schmatz

Kernforschungszentrum Karlsruhe, Institut fir Angewandte Kernphysik I
7500 Karlsruhe, Postfach 3640, Federal Republic of Germany

Expansion of neutron scattering research requires better neutron sources, even better than the HFR Grenoble. Research reactors seem to be at the limit of development. pulsed sources, especially accelerator pulsed sources, offer a break-through to considerably better sources. For nearly all neutron scattering experiments using neutron energies larger than 100 meV the flux versus energy distribution and the pulse characteristics make accelerator pulsed neutron sources superior to reactors with continuous flux. For cold and thermal neutrons (E smaller than 109 meV) the comparison of continuous and pulsed sources - both in competition and complementarity - is very complex. It obviously depends among many other aspects on the type of sources compared. In this paper we report on some general and also on some very specific considerations to compare the HFR Grenoble (HFRG) with the German Spallation Source Project (SNQ) /1,2/.

The hybrid version of the SNQ with a lead target offers an average flux at the hydrogeneous moderator (below the target wheel) of $\Phi_t = 8\times10^{14}$ n/sec cm^2 and a perturbed flux of $\Phi_c = 5\times10^{14}$ n/sec cm^2 at the position of the cold source in the moderator (above the target wheel). The WFRG-values are $\Phi_t = 10^{15}$ n/sec cm^2 and $\Phi_c = 5\times10^{14}$ n/sec cm^2, respectively. We see, the average fluxes of HFRG and SNQ are about the same. Any gain factor obtainable from the time-structure of SNQ is a full gain compared to the HFRG.

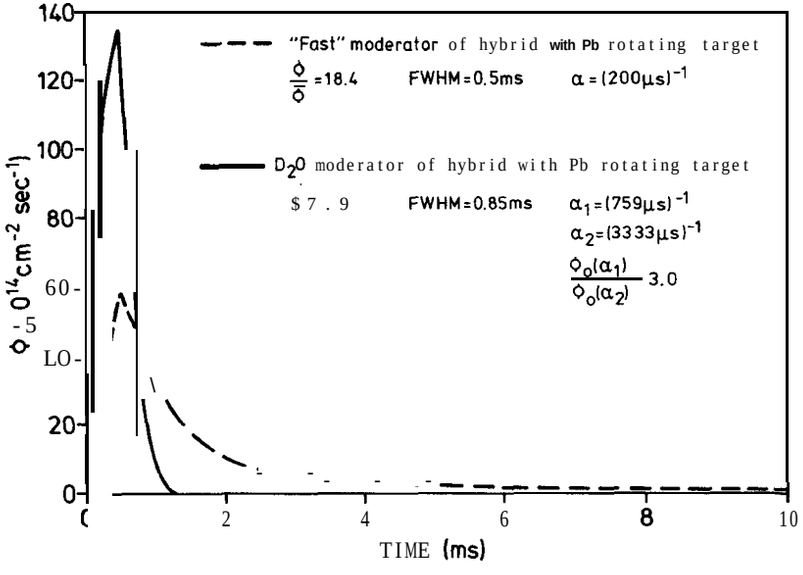

Fig. 1 Neutron pulse forms in the SMQ for H_2O and D_2O moderators /2/.

The 500 μsec proton-pulse of the SNQ is supposed to produce a peak-flux $\hat{\Phi}_H$ of $1{,}5\times10^{16}$ n/sec cm^2 at the hydrogeneous moderator and a peak-flux $\hat{\Phi}_D$ of 4×10^{15} n/sec cm^2 at the position of the cold source in the D_2O moderator (Fig. 1), thus the maximum gain for SNQ compared to HFRG is 15 and 8, respectively. Typical time-of-flight-spectrometers (tof); as IN4, IN5, IN6, and D7 at the HFRG, would fully benefit from this gain, provided the higher duty cycle normally used at reactors could be compensated by larger sample to detector distances keeping the total solid angle constant by some additional costs for detectors. There are about ten neutron diffractometers at the HFRG, all of them operating with single crystal monochronator.About two third of the activity (powder diffraction, structure analysis at single

crystals with large unit cells, diffraction at biological substances) would benefit appreciably from the time- structure provided the large multidetector units are backed-up by electronics and computers able to handle data collection e.g. for 4000 detector elements and a few hundred time-of-flight-channels.

There are, however, special cases (structure analysis for single crystals with small unit cells, fine structure of bragg peaks), where discussions have not revealed full use of time-structure yet. At least a factor of two can be taken as granted for these cases taking into account that i) second order can be eliminated. ii) fast neutron background appears in definite time windows only and iii) inelastic scattering contributions can be separated. In total SNQ would be superior to HFRG for neutron diffractometry somewhere between 2 and 15, somewhat like a factor 7.

As already said in neutron spectroscopy tof-spectrometers fully qain from time-structure. At SNQ probably the fraction of tof-spectrometers would be considerably higher, including new developments like constant q-tof, a renewal of statistical chopper techniques and an adaptation of back-scattering spectrometer to the specific time structure of GSP /3/. An old technique - triple axis spectrometry (tas) - and a new technique - neutron spin echo - seem to tend more towards continuous flux. Neutron spin echo can probably be superimposed to tof as well as it is on the way to be superimposed on tas. The question remains what must be the ratio of $\hat{\Phi}$ to $\bar{\Phi}$ to convert a tas-specialist to tof-phonon-spectroscopy, having in mind that a conventional tas at SNQ already has some advantage (second order diminuation, background free time window). A ratio of 7 to 10 for $\hat{\Phi}/\bar{\Phi}$ probably is necessary to obtain this conversion. To get an idea, whether this guess is reasonable, we sketched an Eo = 100 meV phonon spectrometer (Fig. 2) and considered its efficiency:

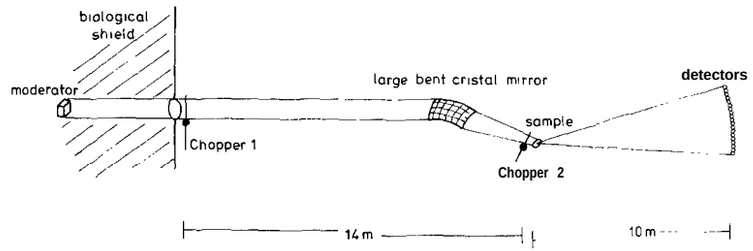

Fig. 2 A 100 meV TOF spectrometer.

With a 25 µsec chopper placed at the biological shielding and a second at 14 m distance just before the sample for E_0 = 100 meV the energy resolution would be 2.2%. In order to keep both the vertical and horizontal divergence comparable to normal tas-conditions a large size double-bent monochromator is placed between the choppers as a "mirror" element. The pulsing reduces the "apparent" source flux from $1{,}5 \times 10^{16}$ n/sec cm^2 by a factor 25 µsec/10 msec down to 4×10^{13} n/sec cm^2, which is a factor 25 below the HFRG-value. Thus, at least 25 detector-tof-channels have to carry useful information. For optical phonons and low-dispersion acoustical phonons a much higher number seems to be achievable.

A great number of experiments will be installed, at neutron guide tubes. Similar to a classical multichopper time-of-flight spectrometer (as IN5 of HFRG) the time structure of the SNQ may be used for energy selection using the long distances in the neutron guide tubes combined with high duty cycle disc choppers. We may first consider a neutron guide installed on a cold source. It should cover an energy range of about 1 meV $\lesssim$ E $\leq$ 15 meV and will be 50 m in length. According to the pulse

width in the D_2O moderator of about 2 msec disc choppers with 30% duty cycle running at 100 Hertz will be suitable. In Fig. 3 it is shown that 4 choppers will be necessary for monochromatizing the beam. The neutron wavelength may be chosen by simply setting the phase between the choppers. The resulting resolution varies between $\Delta\lambda/\lambda$ = 0.026 at 9 Å and 0.105 at 2,3 Å.

In some cases such as small angle scattering experiments poorer resolution may be of interest. This may be achieved with 40% duty cycle choppers at smaller distances. Then, at least 5 choppers are needed. A rather flexible instrument may consist of 6 disc choppers (for example at 20 m, 22 m, 25.7 m, 27.2 m, 30 m, and 50 m from the cold source). The lowest resolution of $\Delta\lambda/\lambda$ = 0.13 at = 4 Å results when choppers 1 to 5 operate at 100 Hertz and chopper 6 is at rest. Running-all 6 choppers at 200 Hertz will improve the resolution to give $\Delta\lambda/\lambda$=0.04 for typical 4 Å or $\Delta\lambda/\lambda$ = 0.018 for 9 Å neutrons. If still a better resolution is wanted the phase of chopper 4 may be changed and thereby cutoff a portion of the monochromatic pulse. This will of course reduce the intensity in a higher rate.

Choppers in a thermal neutron guide looking on an hydrogeneous moderator will allow much better resolutions since the pulse length will be about 500 µsec in the SNQ or about 200 µsec with a storage ring. As an example we may consider a neutron guide 80 m in length designed for an energy range of 15 meV to 50 meV. An energy resolution of 2% at 25 meV will result for a 500 µsec pulse.

As shown for the cold neutron guide the resolution may be variable when using high duty cycle choppers. The resolution may be changed in steps from $\Delta\lambda/\lambda$ = 0.5% to $\Delta\lambda/\lambda$ = 8% (E = 25 meV) without losses in the wavelength center of the pulse. Still better resolution need longer guides or cutting away of monochromatic neutrons.

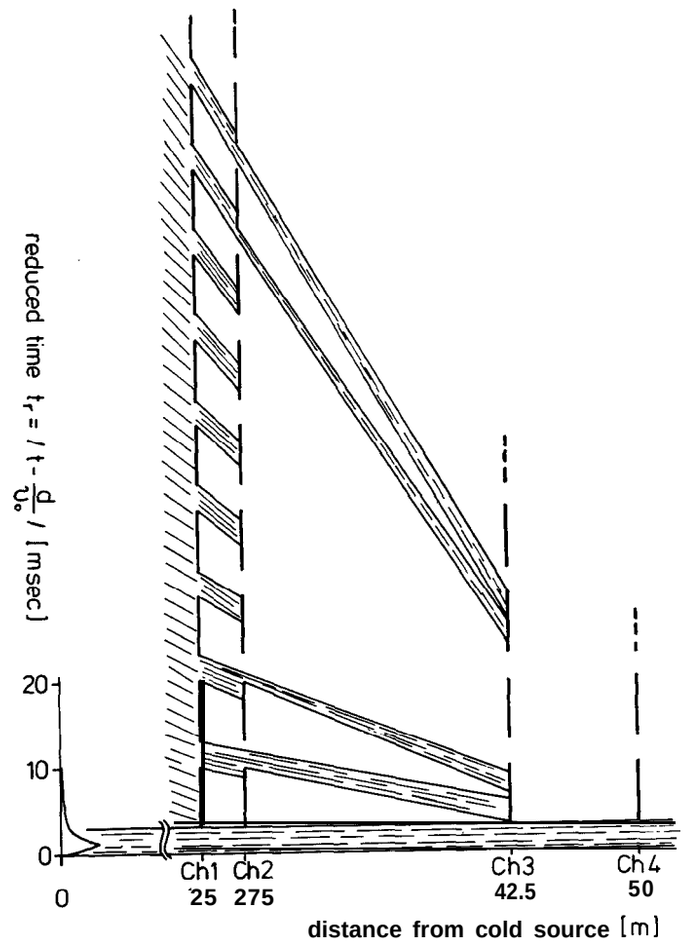

Fig. 3 Energy selection by disc choppers in neutron guides. In the reduced scale the neutrons of the selected speed v_0 follow horizontal lines. Up to the 10th order all neutrons with different speed are shielded by the chopper discs.

In total it can be expected that SNQ would be superior to HFRG in neutron spectroscopy at least a factor 7. It should be mentioned at this point that SNQ contains two options - uranium target, storage ring - which would improve the gain factor considerably. On the other hand, however, there would be some instruments, like high resolution tas, which would have no dramatic gain compared to HFRG.

References

1. Review on the status of the German project, W. Klose, H. Stiller, This meeting
2. Layout of the target station for the German high power spallation neutron source project, G.S. Bauer, This meeting
3. Some new instruments designed to utilize the time structure of a Spallation source, B. Alefeld, This meeting.

Some New Instruments Designed To Use The Time Structure Of A Quasi Continuous Spallation Neutron Source

B. Alefeld, Institut fiir Festkörperforschung der KFA Jülich GmbH, D-5170 Jiilich, Federal Republic of Germany

1. Introduction

The instrumentation on continuous neutron sources has become more and more standard, only few novel instruments have been developed recently, for example the spin echo instrument in Grenoble. The situation is quite different for a quasi continuous source like the spallation neutron source for which a feasibility study is performed in Germany. For our discussion it is not necessary to consider details of the time structure, for this reason we idealize this time structure as one with a periodic sequence of rectangular pulses with a width τ of 0.5 msec, a repetition rate ν of 100 Hz and a peak flux $\hat{\phi}$. With thesedefinitions the mean flux $\bar{\phi}$ is given by $\bar{\phi} = \hat{\phi} \cdot \nu \cdot \tau$. The time structure of such a neutron source offers the possibility to use existing instruments more efficiently and to develop new instruments.

In this paper three instruments are described which have not been built up to now on a neutron source and which are especially well suited to be used on a quasi continuous neutron source. The first instrument described is a time-focusing high resolution time of flight spectrometer which was proposed already in 1967 by H. Maier-Leibnitz /1/, which we call "Bunching Spectrometer". The second example is a high resolution

backscattering spectrometer, a modification of the existing backscattering instruments in Jiilich and Grenoble. The third instrument is designed to produce either polarized neutrons or ultra cold neutrons with a new technique, the dynamical polarization of neutrons by neutron magnetic resonance.

I. Bunching Spectrometer

Looking on the space-time diagram, Fig. 1, we see immediately that is is possible to obtain time focusing of different neutron velocities after a flight length L_o, if the different neutrons start at L = 0 with a special time dependence. In any case the slow neutrons have to start earlier than the faster neutrons. With special approximations (the velocity spread Av has to be small compared to the mean velocity v_o) we obtain the bunching condition

$$v(t) = \frac{v_o^2}{L_o} t$$

This linear dependence of the neutron velocity on time can be obtained easily by reflecting a neutron beam from a sinusoidally vibrating crystal during the linear part of the sin-function. This is shown in the lower part of Fig. 1.

The intrinsic uncertainty of the time of flight AT is given by

$$A\ T = \frac{L_o}{\theta'} \frac{\Delta v}{v_o} + \frac{\Delta L}{L_o}$$

The width of the reflecting curve $\Delta v/v_o$ of a silicon crystal in

back-reflection due to primary extin tion is given by

$$\frac{\Delta v}{v} = \frac{4F}{\pi \pi_c \tau_c^2}$$

F: structure factor

vc: Volume of the unit cell

τ_c: Reciprocal lattice vector

and has a numerical value of $2 \cdot 10^{-5}$ for the (111)-reflex. With this value and an uncertainty AL (thickness of the sample and detector, amplitude of the vibrating crystal) of 6 cm, a length L_o of 60 m and the neutron velocity of 631 m/sec we obtain a pulse length of $12 \cdot 10^{-6}$ sec.

The vibrating amplitude of the crystal is obtained by the equation

$$\frac{dv}{dt} = \frac{v_o^2}{L_o} = a\omega^2 \quad \text{or} \quad a = \frac{v_o^2}{L_o \omega^2}$$

with ω = 628 we obtain a = 1.7 cm.

A schematic picture of this instrument is shown in Fig. 2. Immediately after the shielding of the reactor the neutron beam is deflected by a rotating graphite crystal to the vibrating silicon crystal. The back-reflected neutrons are conducted in a neutron guide tube to the sample. The focussing length L_o from the sample to the detector is dependent on the energy transfer and is shown in Fig. 3.

II. Modified High Resolution Back-scattering Spectrometer

The back-scattering spectrometer is a special version of a triple axis crystal spectrometer with the Bragg-angle of the monochromator and the analyser being 90° /2/. The energy scan is performed by Doppler moving the monochromator parallel to the reflecting τ_c vector resulting in a change of the incoming energy. If this instrument is used on a quasi continuous source the time averaged counting rate is proportional to the mean flux $\bar{\phi}$. However, the useful neutrons appear in the detector during a time interval which is equal to the pulse length of the source. With the time structure given in the introduction only 5 % of the time neutrons are counted. Here we propose a back-scattering instrument which gives at least ten times more intensity in the time average by utilizing not only 0.5 msec of one period (10 msec) but 5 msec. The principle is as follows:

The Doppler moved monochromator is replaced by ten silicon crystals which have different lattice constants given by the intrinsic reflection width. The relative intrinsic width of the (111)-reflex is $2 \cdot 10^{-5}$. The thermal expansion coefficient of silicon near room temperature is $2.5 \cdot 10^{-6}$. It follows that in order to establish a relative lattice parameter difference of 2.10^{-5} a temperature difference of 8° is necessary. In order to be able to measure the different energies of the neutrons separately we have to accomplish that they arrive at the detector at different times. This effect can easily be obtained by imposing to each of the ten different energies a different flight time to the detector. If we want that the reflexes of

the crystals arrive at the detector one after the other and without a time gap between them, the difference of the flight time between two reflexes has to be 0.5 msec. From the equation $L = vT$ we obtain

$$\Delta L = L \frac{\Delta v}{v} + v\Delta T$$

Inserting into this equ. $L = 10$ m, $v = 631$ m/sec, $\Delta v/v = 2\cdot 10^{-5}$ and $\Delta T = 0.5\cdot 10^{-3}$ sec, we see that the first term can be neglected and we obtain $\Delta L = 31.5$ cm.

A schematic picture of this instrument is shown in Fig. 4. A rotating graphite crystal (frequency 100 Hz, in phase with the source) deflects the neutron beam to the silicon crystals which are adjusted perpendicular to the deflected beam and are separated by a distance of 15.7 cm. The crystals are kept on different temperatures with a temperature difference of 8°. If the crystal which is nearest to the sample has the highest temperature we obtain the time-energy diagram of Fig. 5. Each of the ten rectangular regions represents the reflected energy of the ten silicon crystals. The long horizontal bar represents the reflection curve of the analyser crystal. The counting rate is stored time dependently in a multi channel analyser. In Fig. 5 we expect an elastic line with a line width of $0.5\cdot 10^{-3}$ sec at the indicated time. An energy shift of the scattered neutrons produces a time shift given by the slope of the diagram in Fig. 4.

$$\frac{\Delta E}{\Delta t} = \frac{2E\Delta v/v}{\Delta t_s}$$

With $\Delta v/v = 2\cdot 10^{-5}$ and $\Delta t_s = 0.5\cdot 10^{-3}$ sec we obtain

$$\Delta t = 6.25\cdot 10^{3}\ \Delta E$$

Inserting for the energy transfer a value of 10^{-7} eV we obtain a time shift of the line of 0.62 msec, a value which can be measured easily. The fact that we can only measure neutrons half of the available time has the same reason as already described for the existing back-scattering spectrometers /2/. In contrast to these spectrometers the above described instrument profits from the peak flux and not from the time averaged flux of the neutron source.

III. Dynamical Polarization On A Pulsed Neutron Source

Preliminary experiments /3/ have shown that neutron magnetic resonance can be used to produce a completely (not only 50 % but 100 %) polarized neutron beam. If monochromatic neutrons with kinetic energy E enter a magnetic field B_o, the beam is split into two subbeams, one with the spin direction parallel to B_o and the kinetic energy $E + \mu B_o$, the other beam with the spin direction antiparallel to B_o and the kinetic energy $E - \mu B_o$. If the spin directions are reversed within B_o by an oscillating magnetic field B_s perpendicular to B_o, the kinetic energy of both subbeams outside the magnetic field B_o is different by $4\ \mu B_o$. An experimental proof of this energy splitting is shown in Fig. 6. This effect can be used to produce a completely polar-

ized neutron beam on a pulsed source /4/. In Fig. 7 a white neutron pulse is "monochromized" after a flight path L according to the relation $\Delta E_{TOF} = h^3 \Delta t / m^2 \lambda^3 L$ (h: Plancks constant, Δt: pulse length). If this resolution is better than the total energy separation ΔE_N of the two spin states after the N-stage neutron magnetic resonance system, the two polarization directions can be turned into the same direction by a spin precession difference of π of the two polarized subbeams in a magnetic field B_p (spin precession region in Fig. 6). This condition is fulfilled for all neutron velocities, when B_p is given by

$$\int_{\frac{L+a}{v(t)}}^{\frac{L+a+l}{v(t)}} B_p(t)dt = \frac{mv^2(t)\pi}{\gamma \Delta E_N}$$

A solution of this equation is given by

$$B_p(t) = \frac{B_p(o)}{t^3}$$

with $B_p(o) = \frac{2m\pi}{\gamma \Delta E_N} \left(\frac{1}{(L+a)^2} - \frac{1}{(L+a+l)^2}\right)^{-\frac{1}{2}}$

With the following numbers

N = 10	B_o = 2 T	
L = 20 m	$B_p(o)$ = 0.02 T	l = 1.7 m
a = 5 m	t = 10 μsec	

we obtain a polarized wavelength interval between 4 Å and 5.3 Å where the last value is determined by frame overlap.

IV. Time of flight correlation spectroscopy

When the correlation spectroscopy was discovered for neutron scattering about ten years ago, many people expected a revolution of the neutron spectroscopy by this in principle very powerful technique. But things were a little more complicated than envisaged at the very beginning. The main disadvantage of this technique was early discovered and is very crudely described here. We consider a very simple frequency spectrum of our sample, consisting of one weak and one strong line. If this frequency spectrum is measured with the correlation technique the two lines of the frequency spectrum produce a structured intensity distribution which is the sum of two structured intensity distributions of the two lines. In the worst case the intensity modulation due to the weak line is lost in the statistical noise of the intensity produced by the strong line. This extremly bad property of the correlation technique can be removed at a quasicontinous source by an additional time of flight separation of the intensities o both lines. This aspect is one of the most promising things of a quasicontinous neutron source and I would not be astonished if a new experimental period would come up with the spallation source, the "Correlation Time".

References

/1/ H. Maier-Leibnitz, Sonderdruck 16 aus den Sitzungsberichten 1966 der Bayrischen Akademie der Wissenschaften C.H. Beck'sche Verlagsbuchhandlung, München

/2/ B. Alefeld, Kerntechnik 14, 15 (1972)

/3/ B. Alefeld, G. Badurek, H. Rauch, to be published

/4/ G. Badurek, H. Rauch, A. Zeilinger, Z. Physik B 38, 303 (1980)

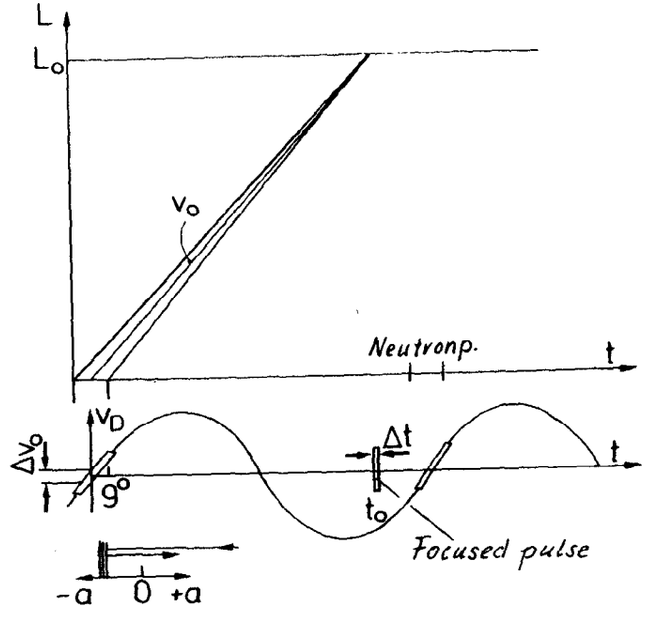

Fig .1 Time-space diagramm and time focusing for the Bunching Spectrometer

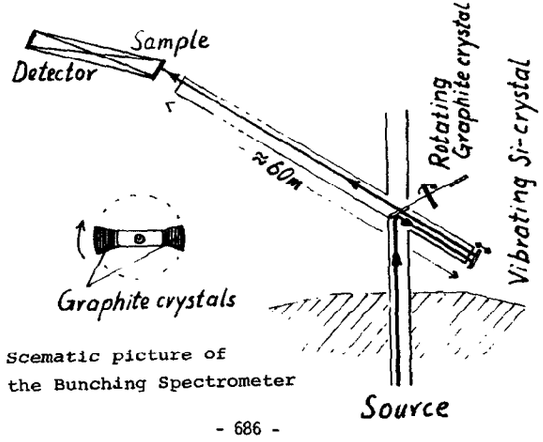

Fig. 2 Scematic picture of the Bunching Spectrometer

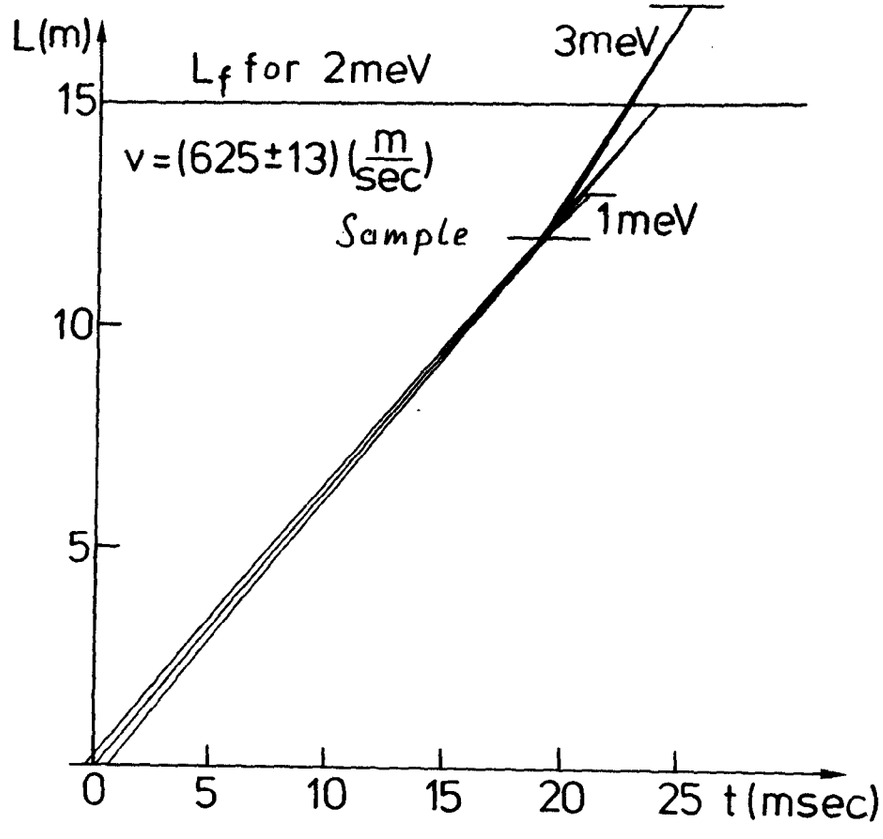

Fig. 3 Time focusing of the Bunching Spectrometer for energy transfers of zero meV, 1meV energy loss and 1meV energy gain.

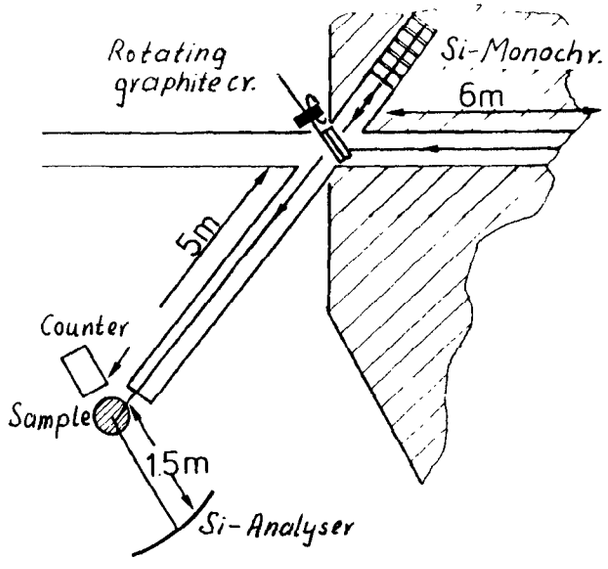

Fig. 4 Modified Backscattering Spectrometer. The distance between the Si-monochromators is 15.7 cm, the temperatur difference between two monochromators is 8° C.

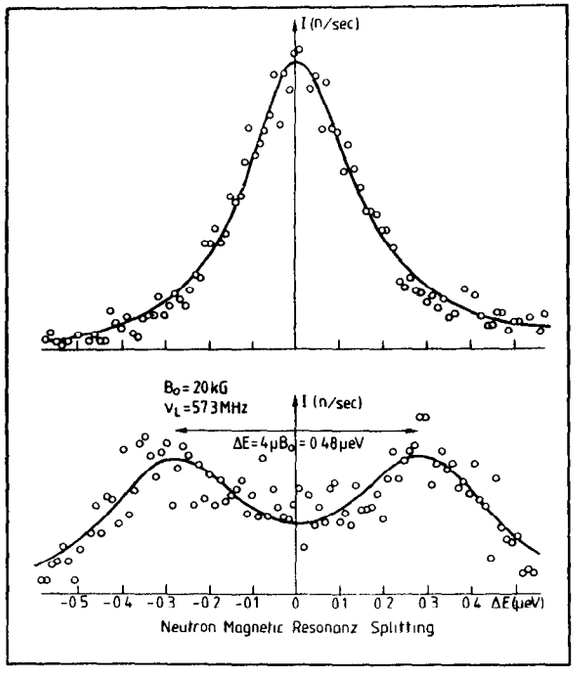

Fig. 6 Neutron magnetic resonance splitting measured with a Backscattering Spectrometer. The upper curve shows the energy resolution (without resonance), the lower curve the energy splitting at resonance.

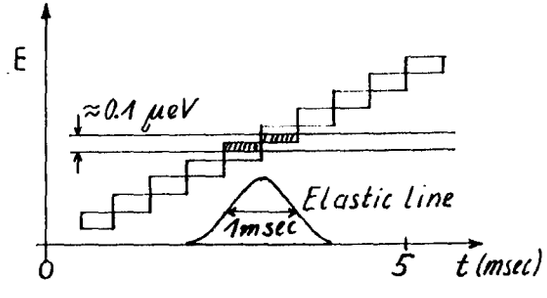

Fig. 5 Energy-time diagramm of the modified Backscattering Spectrometer. The elastic line is shown at the crossing region of the monochromators and the analyser.

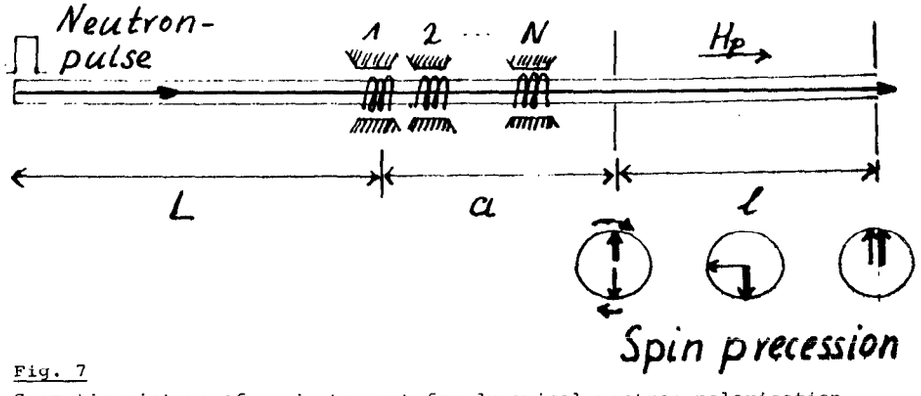

Fig. 7
Scematic picture of an instrument for dynamical neutron polarisation on a pulsed neutron source.

Instrumentation: report on the presentation and discussions

C.G. Windsor and Y. Endoh

Choice of Spectrometers

The instrumentation sessions began by presentations on the WNR, ZING P', IPNS-1, Harwell and KENS spectrometers which have been constructed, or at least fully designed. It was interesting to see how the different laboratories had followed rather different selections from the available instrument ideas. The table summarises these and other instrument portfolios.

		WNR	ZING P'	(IPNS-1)	Harwell	(Rutherford)	KENS	Tohoku
Total	Total scattering (>1%)	2			1	(1)	1	3
	Total scattering (<0.3%)		1	(2)	1	(1)		
	Total scattering (0.03%)					(1)		
	Small angle diffraction	(1)	1	1	1	(2)	1	
	Single crystal diffraction	1	1	(1)	1	(1)	(1)	2
Inelastic	Direct geometry inelastic	1	1	(2)	1	(2)		1
	Incoherent inelastic	2	1	1	(1)	(1)		1
	Incoherent quasielastic					(1)	1	
	Coherent inelastic				1	(2)	1	
Special	Active Sample				1			
	UCN		1	1				
	Polarised neutron				1		1+(1)	1
	Resonance detector	1			1			
	Epithermal diffractometer				1			

( ) means designed but not constructed.

Thus while total scattering is universally represented, there are interesting differences in emphasis. Liquid and amorphous structure factors can be measured with minimum (>1%) resolution. Powder refinements can be made at this resolution, but high order peaks overlap, so that much better refinements are possible at <0.3% resolution spectrometers.

Small angle scattering is being almost universally attempted because of its importance. On the whole however the table shows few cold neutron instruments. This is in keeping with the principle that pulsed neutron sources will compete best against steady sources for high energy incident neutron experiments.

Single crystal instruments are again universally being tried and, although single crystal measurements will usually be necessary for the solution of unknown structures, it is not yet clear how well these can compete for structural refinements against powder measurements. Intrinsically they are less efficient as much of each time-of-flight spectrum measures empty background. However the use of position sensitive detectors may well give them back the advantage.

While all centres are trying direct geometry spectrometers with a pulsed monochromatic beam, there is no consensus as to the best method. Most centres have chosen a double rotor design with the main thermal neutron chopper preceded by a fast neutron "stopper." However the Tohoku spectrometer uses a rotating crystal method, the Harwell spectrometer a combined function reactor-style fast neutron stopping rotor, and WNR plans to run without any fast neutron chopping at all with the philosophy of letting the fast neutrons go past the spectrometer.

The division of crystal analyser/beryllium filter spectrometers

into vibrational and diffusional spectrometers became apparent. Nearly all laboratories plan such spectrometers for high Q, high ω vibrational spectrometry. On the other hand LAM at KENS and IRIS at SNS are designed for quasi-elastic studies with long wavelength incident neutrons. From the point of view of machine design they must be quite different with the high energy transfer machines designed with good scattered flight time focussing and the quasi-elastic machines designed with good scattered energy resolution.

The coherent inelastic machines are all inverted geometry crystal analyser spectrometers. The two designs of the Constant Q Spectrometer using the MARX principle, and the High Symmetry Spectrometer using independent analyser crystals have been the only geometries yet tried.

Most laboratories have chosen their own selection of special purpose spectrometers, reflecting their special interests. The active sample diffractometer with its short L_0 and long L_1 has yet to be tested but has many applied research applications for nuclear laboratories. Ultra-cold neutrons (UCN) have certain advantages on pulsed sources. In particular, access to the "source" is easy, heat fluxes into the moderator are low, and the "turbine" method is naturally suited to pulsed sources. Polarised neutrons have also been linked to cold neutrons in the past, where magnetic supermirrors give easy and efficient polarisation. Their use on epithermal beams depends on the development of good white beam polarisers and this is reported on later. We saw no consensus of design on polarised neutron spectrometers.

It is not yet clear how far up in energy neutron scattering will extend in the future. The total-cross-section, resonance

detector, and epithermal diffractometer all have in common that they use >1000 meV incident energy neutrons. These spectrometers did not receive much attention at the meeting, although if background problems can be solved, these spectrometers allow perhaps our best opportunity to break into new fields of neutron scattering physics quite impossible on reactor sources.

Instrumentation on Long-Pulse Sources

We heard from our German colleagues, Alefeld, Bauer, and Nücker, many new ideas on instrumentation for their 500 μs pulselength 1/20 duty cycle SNQ source. Clearly there are many new instrument ideas waiting to be discovered or exploited in this field. We had one example each of the use of moving samples, multiple monochromators, correlation methods and polarisation control.

The suggestion of Price to pseudo-randomly pulse a semi-continuous source at a relatively fast speed commensurate with the moderation time at the wavelength of interest ($\sim 10\lambda$ μs Å^{-1}), left echoes which reverberated throughout the week. Clearly such a source would give very high performance for all experiments which could exploit the correlation methods. These seem to include most of the important spectrometers. For example it was suggested in the summary presentation that time-of-flight diffraction would be particularly easy and effective on such a source as shown in figure A. The problem with the pseudo-random source is its optimisation for all wavelengths simultaneously. The SNQ is well suited to cold neutron generation, but in the case of say 6 Å neutrons the moderation time is $\sim$100 μs, so that optimum performance

is nearly attainable by reducing the total pulse length to around this value rather than by pseudo-random pulsing.

The use of the SNQ for coherent inelastic scattering was explored in private discussions. A possible method analogous to MAX is shown in figure B.

The SIN spectrometers were not presented as they will be so similar to existing reactor designs. The big uncertainty in many minds was how far it will be possible to shield the counters in the spectrometers from the fast neutron pulse as the proton beam fires. Existing experience on pulsed sources suggests that background neutrons within 100 μs of the time of fast neutron generation are not stopped by conventional spectrometer shielding (∿20 cm borated paraffin). However unconventional methods may bring a solution. For example it may be necessary for monochromator housings to have a "get lost" beam tube leading to a carefully designed beam dump which will moderate and absorb the fast neutrons at an area remote from the spectrometer itself.

Instrument Design

During the instrumentation sessions several interesting differences of design became apparent.

Liquids and Amorphous Diffractometers

Perhaps the most important was that of total scattering. Figure C shows the two extreme views.

(1) The conventional approach uses discrete counter banks each optimised to give the best performance at its own scattering angle. Usually there are massive high angle counter banks with full time focussing. At lower angles there are Debye-Scherrer ring collimators at each angle, and for small angles a separate longer flight path detector bank. Each bank is surrounded by a massive fast neutron shield.

(2) The new approach of IPNS-1 followed in some respects at WNR and KEK is to surround the sample with a "blanket" of counters at all angles. Each counter must then be electronically processed to give a cross-section $S(Q, \lambda)$. The background problem is tackled by the use of a large vacuum chamber. Experience at KENS with the diffractmeter HIT suggests that background can be kept tolerable in such a spectrometer at any rate above 0.5 Å.

Powder Diffractometers

In the case of powder spectroscopy it was clear that the back scattering banks are the crucial ones for giving precision in profile refinements. The SNS project powder spectrometers were described. They include a 0.03% resolution spectrometer incorperating a 100 m guide tube in the incident flight path with a very large flat back scattering position sensitive detector.

Small Angle Diffractometers

This important subject received much discussion inside and outside the sessions. There are several points of principle still not settled. For example, is a 22K source essential or can we work in the 1-4 Å range where ambiant or 77K moderators give good neutron fluxes? Do we need to shield our detector from fast neutrons or can we simply ignore the 500 μs after the fast neutron pulse?

The results from the prototype spectrometers at WNR and ZING P' were not presented in any detail. The KENS spectrometer results suggested that we cannot count through the fast neutron pulse, but that background was no problem in a cadmium shielded enclosure over the 500 to 20,000 μs time range. We heard from Stewart a most interesting discussion of the problems of combining data from different wavelength ranges. Because of the absorption, multiple scattering and various background corrections, there is very little point in trying to combine raw data from a wide range of wavelengths. A good fit of cross-sections from the full range can only emerge after full processing on a main frame computer. While the results from KENS looked very promising in that intense scattering was seen in minutes, we must await a full study before this important spectrometer can be added to the pulsed source portfolio.

Single crystal diffraction

We heard accounts of the ZING P', Tohoku and WNR Spectrometers. Tohoku uses a one-dimensional counter, the others much smaller two dimensional counters. In fact a wide angular range seems highly desirable if we are to achieve the objective of measuring each reflection as a function of wavelength. The real need is to assess the accuracy of the data quantitatively. Both ZING P' and Tohoku have studied NaCl with the object of obtaining a full data set. Both reported preliminary data but the data processing problems are large simply because of the vast amounts of data produced. An hours run produces perhaps 64 x 64 position x 512 time channels! The Tohoku group described an automated analysis procedure for locating peak centroids, in reciprocal space, evaluating their structure factor corrected for local background, and discriminating against

spurious peaks from noise fluctuations.

Direct Geometry Inelastic

For once there was a general conformity of design. Most discussion centred on the difficult problems of rotor phasing. It now seems generally realised that different energy ranges can be covered by just one spectrometer according to the value of the chopper pulse width. The incident flight path L_0 determines the overall resolution. The optimisation of L_1/L_0, the ratio of scattered to incident paths, was discussed. This can only be done for some assumed ratio of energies E_1/E_0. This leads naturally to the SNS designs when a larger L_1/L_0 is specified for low angles where $E_1 \sim E_0$, than for high angles when $E_1 \sim \frac{1}{2}E_0$ and a smaller $\frac{L_1}{L_0}$ is optimum.

Incoherent Inelastic

There are two quite different concepts for this type of measurement, as shown in figure D. In (i) a crystal analyser defines the k_1 value while k_0 is defined by time-of-flight. In (ii) a beryllium filter is used to select only neutrons with energies below the Bragg cut-off (0-5 meV). We thus select a "window" of scattered energies 5 meV wide and again determine E_0 from time-of-flight.

We saw from WNR the interesting comparison of results from the same sample at the same flightpath by the two methods. The analyser method gave of course the cleanest spectra but the filter method gave 100 times the intensity with only 10 times the background! In addition the filter method gave sharp "edges" on most peaks which define the peak energy essentially to as good an accuracy as the analyser method. Thus the question as to which method to use is

still wide open.

Coherent Inelastic

We saw early results from MAX and phonons and magrons from a single crystal of iron. It is clear that lining up the spectrometer with its 15 independent analysers is an important preliminary to obtaining accurate results. Methods using time-of-flight to determine angles directly with respect to their zero angles ($2\theta_s - 2\theta_s^{zero}$) and ($2\theta_A - 2\theta_A^{zero}$) will probably be most precise. The choice of scan in reciprocal space is crucial. Only around certain reciprocal lattice points will the scan around a given reduced $\underline{q}$ and $\hbar\omega$ be with an appropriate E_0 and ratio E_1/E_0 to give a "nice" scattering triangle. Higher order reflections from the analyser are certainly a problem. This is partly because if one order, say graphite (002), gives a high symmetry direction scan through the (111) reciprocal lattice point, the (004) gives a parallel scan through the (222) point. Thus there is an enhanced opportunity for Bragg or low energy phonon scattering from the high orders. On the other hand the higher order scans are often well separated from the low order scan and offer an alternative set of measurements along the same symmetry direction.

Spectrometer Results

Liquid and Amorphous Structures

The many results from amorphous materials, shown by Suzuki, have already brought worldwide fame to Tohoku. An extension of the pulsed method to study transient structures was described by Shinohe. He presented structure factors from super-cooled and just

solidified materials. This type of measurement is highly suited to the pulsed source.

Powder Profile Refinement

Outstanding results were presented from ZING P'. The results of refinement of a beta" alumina, for example (see Borso et al.), show clearly that the pulsed method gives as good a fit as conventional reactor methods. The fact that the important high $\sin\theta/\lambda$ region is extended means that the spatial precision of structural and thermal parameters will in general be better than with reactor data. The 3 pages of experiment titles completed on the ZING P' spectrometer means that the method is now entering a routine stage.

Incoherent Inelastic

Data from the ZING P' spectrometer were presented on several hydride materials, organic materials and even biological samples. The hydride samples showed up to four harmonics---perhaps a record! Again a list of completed experiments convinced one that the spectrometer is fully established.

Quasielastic

Inoue's results from the LAMDA spectrometer at Hokkaido and LAM at KENS provided a welcome contrast as a fully developed spectrometer with an extensive list of important experiments completed. We saw the excellent capability of the spectrometer to measure diffusion constants in the water range and therefore to distinguish free and bound water.

The Use of Peak Fluxes

In the summary session Windsor presented a plea for restraint in the use of peak fluxes or equivalent reactor fluxes in contexts where they will be compared with reactor fluxes. The reason is partly that the true figure of merit for most experiments is

$$\frac{\text{(peak flux)} \times \text{(moderator area)} \times \text{(pulse repitition frequency)}}{\text{(pulse width)}}$$

Thus "hot" neutron performance is underestimated relative to cold neutron performance because of the change in pulse width. Perhaps of more importance is the fact illustrated below that while the pulsed flux shines directly onto one sample where it can be wavelength analysed by time-of-flight, the reactor source must be monochromated (or chopped) before it is useful. Thus the comparison depends on the detailed performance of crystal monochromators. A valid comparison is between the monochromated neutron current at resulution $\Delta\lambda$ at the sample position, and the time averaged neutron current at the sample position for the same wavelength resolution, over the useful wavelength range from λ_{min} to λ_{max} in the particular experiment.

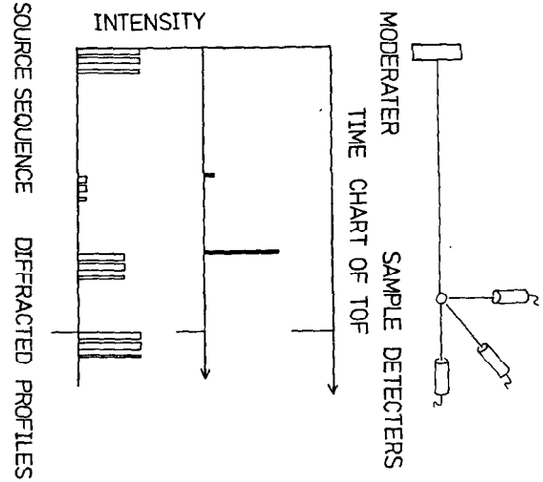

Figure A A diffraction (powder, single crystal or small angle) employing a pseudo-random sequence on the proton beam. Each diffraction pattern is identified from the sequence. The semi-pulsed nature of the source ensures that the "background of ignorance" from intense peaks does not contaminate weak peaks.

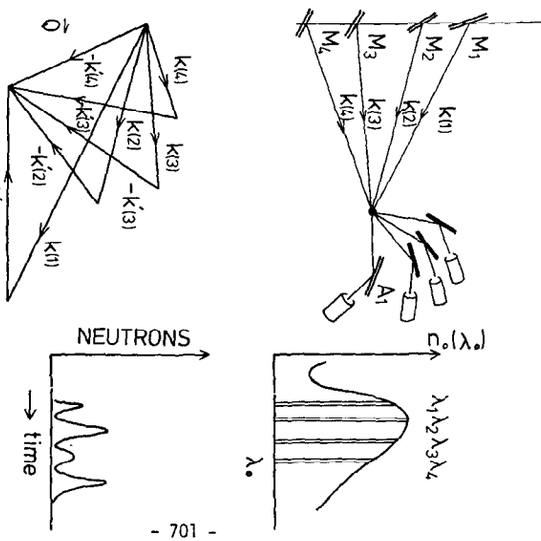

Figure B Coherent inelastic scattering on a long pulse source. The "three axis" spectrometer can use several different incomin wavelengths λ_1, λ_2, λ_3, λ_4. The excitations from each are roughly separated by time-of-flight.

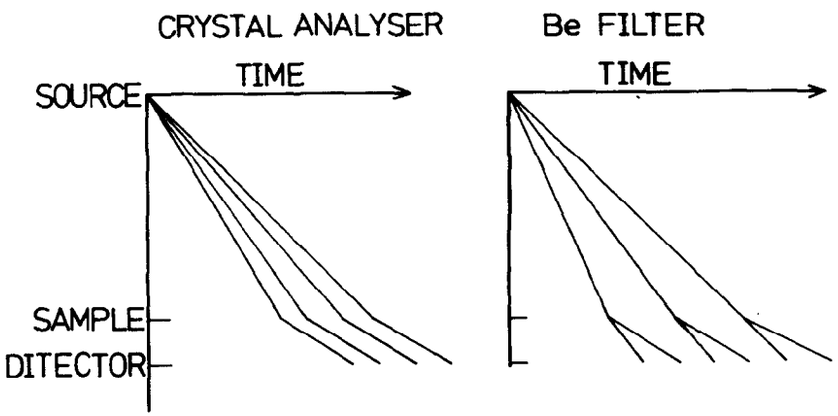

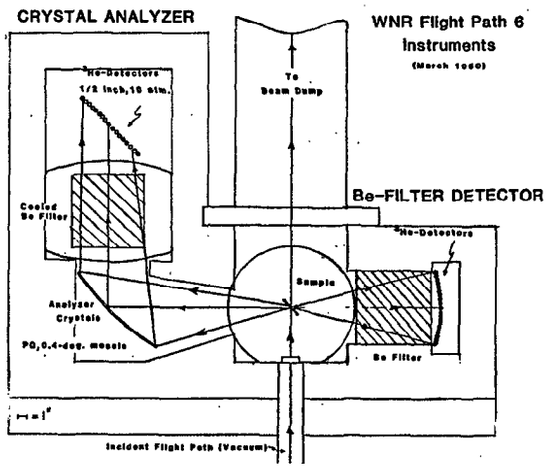

Figure D Two quite different types of incoherent inelastic spectrometers.

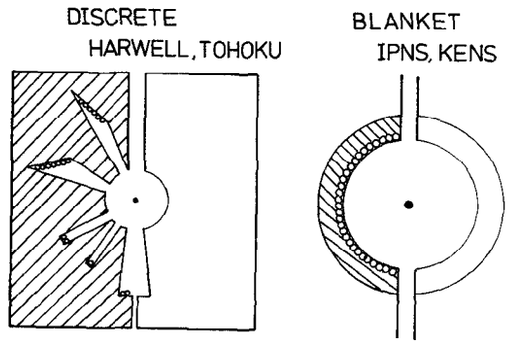

Figure C Two types of total scattering spectrometer.

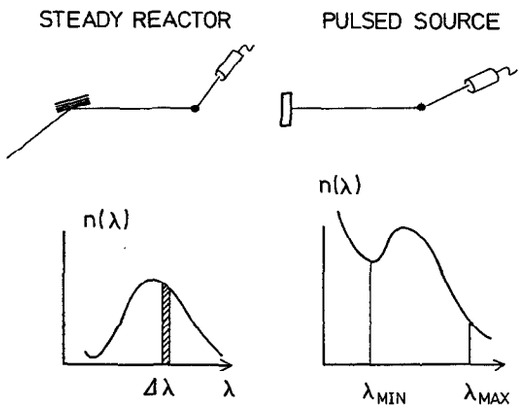

Figure E The comparison between reactor and pulsed source diffraction depends on the neutron current at the sample. The reactor monochromatic current can be compared with the time-averaged pulsed current at the same resolution $\Delta\lambda$ over the useful range of wavelengths.

Report on the Data Acquisition and Detector Session

by J.M. Newsam and N. Niimura

Three themes are common to the contributed papers on data acquisition systems and detectors and to the discussions which followed their presentation.

1) the desirability of standardising both hardware equipment and software on different instruments which might have widely differing intermediate data storage and control requirements.

2) the increasing reliance on the use of Li^6 glass scintillators.

3) the problems associated with the sheer number of arithmetic operations that are required to correct and display the data recorded by large area position-sensitive detectors (PSD).

The speed with which corrections may be applied to the measured data and intermediate results obtained depends on the available on-line computational capacity which, in turn, depends on the philosophy behind the computer configuration. The star or hub approach planned for SNS and IPNS-I and installed at the new Harwell Linac allows each instrument a dedicated mini-computer with intermediate storage capacity. This minimizes the reliance of a given

instrument on the central hub computer although perhaps at the expense of a reduction in the amount of on-line processing that is possible.

The problem is particularly acute for small angle scattering instruments that are equipped with large-area PSD's and, during operation, a two-dimensional display obtained by summing the data for difficult time channels or positions may be all that is possible. As Stewart pointed out, however, this arrangement is unsatisfactory when the scattering is anisotropic. It is possible that parallel array processors will prove useful in reducing the total time required for correcting the raw data.

In TOF scans there are advantages to allowing flexibility in the number and width of the time channel gates. For some situations it may be desirable to match the width of these gates to the widths of the corresponding resolution elements. If electronic time focussing is employed, short-channel widths may be necessary for accuracy in combining the data from different detectors. Further, in particular experiments where only certain portions of the time scan are of interest, it may be advantageous to group the channels in a bunched or 'concertina' fashion.

At the Institut Laue-Langevin all measured data is archived and is therefore readily available to users even several years after their measurements were made. Howells outlined how a similar scheme for data storage and management was envisaged for the SNS facility. This scheme would be consistent with the requirements of the other centres supported by the Science Research Council so that a single data management system would control access to all data

measured at these facilities.

On the question of standardisation, Windsor suggested that ICANS might provide a medium for the exchange of software. As Fortran is the most commonly used programming language, such an exchange would help to standardise the systems at different centres and facilitate new development. Stewart explained that such standardisation at different centres had already ocurred in the case of many European small angle scattering machines. Following the proposal of Price, a member from each ICANS laboratory was then selected to act as the software and computing representative. Questions or information should therefore be addressed to the following

KENS:	N. Niimura/M. Kohgi
Harwell Linac:	D. Johnson
IPNS:	T. Worlton
SNS:	M. Johnson
LASL:	J. Eckert

The question of beam monitors was raised by Crawford who described the flat-plate BF_3 detectors which were successfully used for this purpose at Zing-P'. These detectors have efficiencies which are variable within the range 10^{-5}-10^{-3} for thermal neutrons. They have better pulse height distributions than fission counters which have

the added disadvantage that their signal depends on atmospheric conditions and on the level of discriminators. Howells mentioned the possibility of using low-efficiency edge-coupled scintillation detectors as monitors. In TOF measurements it is usually necessary to monitor the energy dependance of both the incident intensity and sample absorption. Two or more beam monitors may therefore be required.

Stewart pointed out the problems of calibrating area detectors, particularly for small angle scattering and he further elaborated on this issue in a subsequent additional meeting. Vanadium powder is acceptable at high Q ($\gtrsim 0.1$ Å^{-1}) but for lower Q values down to 0.05 Å^{-1} a single crystal is preferable (suitable single crystals of vanadium are obtainable from Metals Research, Cambridge, UK) or, for wavelengths greater than 8 Å, a thin sample of distilled water may be used. It would be desirable to have a standard sample, such as irradiated Ni in the case of small angle X-ray scattering, which would both allow the intercalibration of intensities and provide an internationally accepted standard.

In conclusion, there has been much recent progress, particulary in position sensitive detector research, although there remain some difficulties in very fast arithmetic processing for data correction and display and in the calibration and cross-calibration of large area detectors.

Report on the Guide, Chopper and Polarised Beam Session

by J.M. Newsam and W.G. Williams

Ideally, a neutron guide would allow the transport of neutrons within a particular energy range over the required distance without loss and without disturbing the intensity distribution within the beam. In practice such conditions cannot be realised and to estimate the effect of the various influencing factors on the properties of the transported beam, a Monte-Carlo type computer simulation is necessary. Such simulations have highlighted problems such as that of illumination and indicated interesting variations in beam asymmetry with guide configuration. However, the experience at KENS suggests that even sophisticated simulations may give optimistic predictions of guide performance. The transmission of guides may be improved some 10 % by using Ni^{58} in place of natural Ni for the neutron reflector although, because of cost and availability, natural Ni has been chosen for the KENS and SNS guides. Alefeld suggested that a less costly way to improve the effective performance would be to use a single tapered Ni^{58}-coated section at the end of the guide. Alefeld also queried the necessity of curving guide tubes, it being possible to remove the signal from fast neutrons electronically. Williams, however, explained that although curved

guides were not mandatory for removing the fast neutrons, for many reasons, such as the difficulty in estimating the fast neutron background, it was undesirable to view the moderator directly.

Considerable progress has been made at both ANL and the Rutherford Laboratory in the techniques of manufacture, control and phasing of high angular velocity choppers. The SNS and ANL choppers have similar slit packages although their frame and support systems differ (see Figures 1 and 2). Both designs have evolved over a long period and their present operational status represents no mean technical achievement. The difficulty of phasing choppers rotating at ≥16000 r.p.m. to an impishly varying mains frequency had long been a worry at the operating facilities of ANL and LASL.

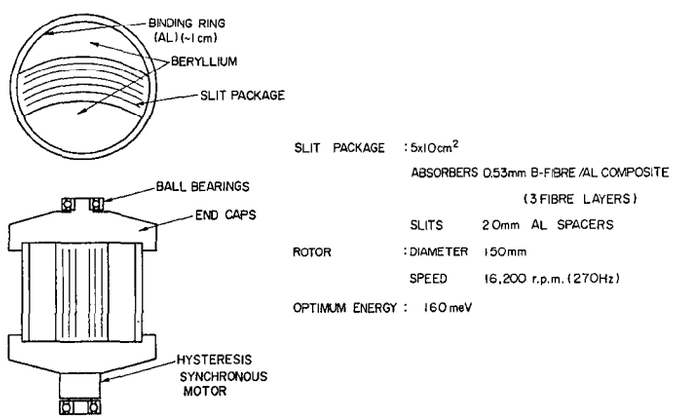

FIGURE. 1. SCHEMATIC DIAGRAM AND SOME CHARACTERISTICS OF THE PRESENT ANL FAST CHOPPERS

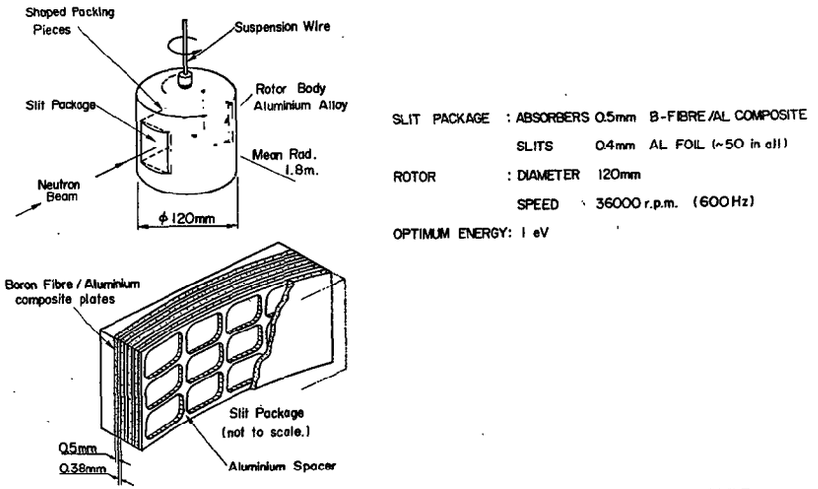

FIGURE. 2 SCHEMATIC DIAGRAM OF THE CONSTRUCTION AND SOME CHARACTERISTICS OF THE PRESENT SNS FAST CHOPPERS

The performance of the SNS and ANL choppers appears to be quite similar and the discussions about these velocity selectors were mainly concerned with mechanical details, in particular the chopper bearings. Carpenter described how at ANL, heating in the bearings due to their rotation in the earth's magnetic field was reduced by using magnetic shielding and that ca 0.5 torr of He gas was preferred to a complete vacuum to increase heat dissipation and prevent loss of grease. These bearings are also elastically mounted and have light shells so as to minimise load. Stewart mentioned that self-aligning bearings were found necessary at the tests for the SNS to prevent a skipping-rope action during running. It is clear that the design of these high velocity choppers is a considerable technical achievement and the associated technology may well find applications in fields far removed from neutron scattering.

The operation of the low-velocity choppers used as tail-cutters before the curved guide tubes at KENS was described by Furusaka. Rather than using a feed-back circuit to control phasing, these choppers are driven by stepping motors which are activated by pulses derived from a signal received from the accelerator control. By supplying only the number of pulses required to complete one revolution between each neutron burst the phase of the chopper can be maintained to within the required accuracy. Further details of the control circuit are available in KENS Report I.

On the subject of polarised beams, all the participating laboratories agreed that any future programs on pulsed sources will depend heavily on the development of successful polarising filters. This is the only type of neutron polariser that has a broad band polarising capacity. They can also accept the full incident beam divergence.

Polarising filters operate by either spin-dependent scattering or spin-dependent resonance absorption. Of the three independent development programs in progress, two are based on the former and one on the latter.

1. Spin-dependent scattering

A target of polarised protons acts as an efficient polarising filter for neutrons over a wide energy range $0 < E < 1$ meV. Such filters will therefore be useful for producing incident polarised beams although, because they operate through differential scattering of the two spin states, they are unlikely to be used as analysers in full polarisation analysis instruments. High proton polarisations ($\sim$ 70%) are required and there now seems to be two technically feasible methods of achieving this.

Both use methods for transferring the easily-attainable electron polarisation in a paramagnetic dope ion into the proton spin system.

(a) Dynamic Polarisation

This is historically the most tried technique and is being pursued at KEK in a collaborative effort with the High Energy Physics group. A spectrometer designed by Newsam et al. employing a dynamically polarised proton filter will be installed at KENS in early 1981. One difficulty in the neutron application is that of restricting the quantity of He^3 in the beam path. This is used as a refrigerant and has a large absorption cross-section. Masaike, however, explained that by careful design He^3 could be completely excluded from the line of the beam.

(b) Spin Refrigerator

The spin refrigerator principle for polarising protons, first introduced by Langley and Jeffries some 15 years ago, is now being applied as a neutron polarising filter in a collaboration between the Argonne and Los Alamos Laboratories. The best results have been obtained with single crystal of yttrium ethyl sulphate (YES) in which 0.01% of the Y^{3+} atoms are replaced by the paramagnetic dope Yb^{3+}. Yb^{3+} acts as an effective $s = \frac{1}{2}$ paramagnetic ion with a highly anisotropic g-factor ($g_c \sim 3.3$, $g_a \sim 0$) and when a single crystal is rotated

about the b axis with an applied H in the ac plane, the spin dynamics is such that the high Yb^{3+} polarisation which is generated when H//c can be transferred to the proton spin system. Typical experimental conditions are:
magnetic field (poor homogeneity) $H \sim 1.5T$, temperature $\sim$ 1K, spinning frequency $\omega \sim 100$ Hz. The main attraction of the technique is its simplicity compared with dynamic polarisation though there is a limitation with materials – YES is the only suitable material so far found. However, unlike dynamic polarisation, the method has received very little development attention in the past. A prototype system is nearing completion and neutron tests are scheduled for early 1981. To date, about 60% proton polarisation has been achieved,as indicated by ^1H-nuclear magnetic resonance measurements. There do remain some experimental difficulties such as the change in filter thickness during rotation. However, the nuclear relaxation time at 1K is ca 20hrs and pumping takes typically 2 mins so that it may be feasible to halt crystal rotation while neutron measurements are made. If further improvements can be made, this technique may well prove the most attractive and further work should therefore be encouraged.

2 Spin-dependent resonance absorption

The resonance absorption method first demonstrated for polarised 149 Sm nuclei is now being applied to other polarised nuclei by the Rutherford Laboratory. The method is technically

simpler than those previously described since it relies on the static polarisation of appropriate nuclei when they are cooled to dilution refrigerator temperatures. The main disadvantage of the method is that it can only be used at the nuclear resonance energies, although it is clear from the paper of Williams (see above) that the useful energy range may be extended by a suitable choice of nucleus or of combimations of nuclei.

Any polarised beam work on the new pulsed sources will rely on the development of polarising filters. These filters are expensive to produce in comparison with other instrument components. It is gratifying to note that three fundamentally different methods are being investigated within ICANS, thus making the optimum use of our resources and effort. This should ensure that polarising filters will be in routine use within the next few years.

he Ultra Cold Neutron Production at KENS

H. Yoshiki
National Laboratory for High Energy Physics, Oho, Tsukuba, 305 Japan

1. Introduction

Golub and Pendlebury[1] proposed the super-thermal helium converter to produce ultra cold neutrons (UCN) from a cold (9Å) neutron source. In the ordinary thermal reactors, the heat, in the order of a few watts/gram, is dissipated inside the reactor, therefore it is difficult to install such a device except on the external cold beam line. This reduces the initial cold neutron flux integrated over the solid angle by a factor of 10^4.[2] The recent success of solid methane moderator at KENS[3] suggests that the heat produced at the target and the radiating heat can be put well under control. It looks therefore that the neutron spallation source is not only suited for TOF measurements by its pulsed beam structure as quoted often, but for gaining an enormous amount of solid angle, e.g. to install the helium converter next to the target.

2. The cross sections

When a cold neutron is led into super-thermal helium, there is a certain chance that the neutron emits a phonon reducing its energy and momentum into the UCN region. For the sake of our calculation, by UCN we define that its energy lies below $E_{max} = 7.6 \times 10^{-7}$eV. At this energy the reflectivity of UCN from beryllium becomes 1%. The beryllium is known to have the highest potential barrier among metals used for the UCN confinement. There are two solutions for the incident cold neutron energy, E_{in}, which produces a UCN having E_{max} : E_{in} = 1.013 and 1.061 meV corresponding 0=0 and 180° UCN production. The excitation function of the super-thermal helium was compiled from the experimental results to our best knowledge. Any E_{in} between these two values produces UCN below E_{max}. The cross section of the neutron-phonon interaction in Born approximation is given by Cohen and Feynman[4]. It was assumed that the initial state of the helium is in its ground state and the matrix element between the initial and final states is equated to the liquid structure factor given by Reekie and Hutchison[5]. We divided the UCN energy between 0 and E_{max} into 40 equal bins and the differential

cross sections were computed at the center of each bin. Since the differential cross sections have poles when E_{in} = 1.043 ± .006 meV, care must be taken neither to loose the accuracy nor the computation time too much in this region. The 40 sets of differential cross sections were tabulated then onto a disk. The total cross section vs. the incident neutron energy is shown in Fig 1.

3. Mote Carlo calculation

Using the tabulated differential cross sections, a Monte Carlo calculation was performed to determine the average store time of UCN in a box of differnt shape, material, surface contamination, with differnt degree of contamination. In regard to the contamination, we were specially interested in that with hydrogen and deuterium. We briefly quote here our findings. 1) The rounder the shape of the container, the longer the store time. 2) When the surface is covered with 10^{15} hydrogen/cm^2, the store time is about 200 sec in a SiO_2 box of $(0.3m)^3$. This number and other sources of information seem to support the theory that the present experimental limit on the store time is due to the hydrogen contamination. 3) If the hydrogen is replaced by the deuterium, due to its larger mass and smaller scattering cross section, the store time becomes about eight times as large.

4. The test apparatus

In order to verify what have been described in the previous sections, the test of UCN production by means of super-thermal helium has been planned (Fig 2). The vessel to contain super-thermal helium will be fabricated out of single piece of Al block whose inner wall is plated with Ni. The size of the vessel is 8cm in diameter, 30cm in length. The figure shows the main part of the cryostat. The upper part is the 4.2°K helium bath in which commercial liquid helium is stored. The outer radiation shield is anchored to this. Through a needle valve the liquid of this bath will be transfered to a 1°K bath below, whose atomosphere will be pumped out through an orfice, to bring down the liquid to the desired temperature. The inner radiation shield is anchored to this bath. The liquid which is partly super-thermal will be led to the vessel through a super-leak, eliminating

He^3 in the process. A He^3 pot attached to the vessel will cool down the He^4 in the vessel to 0.5°K. He^3 will be pumped out and recirculated through the system. A horizontal valve which is not shown in the figure will be pressed down against the opening of the vessel during the time UCNs are produced and is lifted when they are counted by a thin windowed He^3 counter attached to the verticl pipe. The counting rate determined by the present (October, 1980) KENS performance (Mizuki, this meeting) will be only 0.5 UCN/sec. But this is expected to be improved.

5. Check of Neutron Oscillations making use of UCN

Apart from electric dipole moment measurement of the neutron and other topics related to UCN, we discuss the possibility of detecting this phenomenon by means of UCN in this section. Recently Mohapatra and Marshak[6-7] discussed the phenomenology of neutron-antineutron oscillations within a frame work of gauge models with sponteneously broken local B-L symmetry which leads to large $\Delta B=2, \Delta L=0$ nucleon transition amplitudes. A proposal was made to detect this effect by Wilson[7] using thermal neutrons of $\Phi=5\times10^{13}$ neutrons/sec for a period of $t=10^{-2}$ sec. Kamae[8] proposed a similar experiment at a lower neutron energy using a cold neutron source recently installed at KEK. For both experiments it is important to degauss the earth's magnetic field to the order of 10^{-2} gauss along the beam paths of meters or tens of meters. For both experiments the counting rate $R/sec/(\delta m)^2$ is Φt^2, where δm is explained below.

δm is the $\Delta B=2$ transition mass between $|n\rangle$ and $|\bar{n}\rangle$ states, which are placed in a magnetic field B only. The new eigenstates of the $|n\rangle-|\bar{n}\rangle$ complex, $|n_1\rangle$, $|n_2\rangle$, are then,

$$|n_1\rangle=\cos\theta.|n\rangle+\sin\theta.|\bar{n}\rangle=(|n\rangle+|\bar{n}\rangle.\delta m/(\mu B+\sqrt{(\mu B)^2+(\delta m)^2})).\cos\theta \quad (1a)$$

$$|n_2\rangle=-\sin\theta.|n\rangle+\cos\theta.|\bar{n}\rangle=(|\bar{n}\rangle-|n\rangle.\delta m/(\mu B+\sqrt{(\mu B)^2+(\delta m)^2})).\cos\theta \quad (1b)$$

where μ is the magnetic moment of the neutron and θ is the mixing angle, a relation $\tan2\theta=\delta m/\mu B$ thereby holds. The corresponding mass values, m_1, m_2, are

$$m_1, m_2 = m_0 \pm \sqrt{(\mu B)^2+(\delta m)^2}. \quad (2)$$

Mohapatra and Marshak[7] found $\delta m \lesssim 10^{-20}$eV, whereas for B=1 gauss, μB becomes as large as $\sim 6.3\times10^{-12}$eV.

Supposing the state was a pure $|n\rangle$ state at t=0, the state vector

$|\tilde{n}(t)\rangle$ in terms of $|n\rangle$ and $|\bar{n}\rangle$ will be,

$$|\tilde{n}(t)\rangle \cong (|n\rangle+2i\theta\sin\Delta mt/2.e^{-i\Delta mt/2}|\bar{n}\rangle).e^{im_1t}, \quad (3)$$

where $\Delta m=m_1-m_2$. The probability to observe $|\bar{n}\rangle$ at t, is

$$|\langle\bar{n}|\tilde{n}(t)\rangle|^2=1/2.(\delta m/\mu B)^2.(1-\cos2\sqrt{(\mu B)^2+(\delta m)^2}\ t). \quad (4)$$

The maximum effect of oscillation can be seen when the argument of cos-term becomes π, and for the measurment periods proposed like above (10^{-2} sec), B is most preferably in the order of $10^{-2}\sim10^{-3}$ gauss. This is why the earth's magnetic field must be degaussed to this order in the above experiments(fig 3).

Major problems of the $n-\bar{n}$ oscillation experiments with UCN are 1) the phase-shifts produced each time they are reflected from the metal walls, which will mar the relative phase between $|n\rangle$ and $|\bar{n}\rangle$ in eq.(3), and 2) the question of absorption from the wall. The relative phase between $|n\rangle$ and $|\bar{n}\rangle$ in eq.(3) is illustrated in fig 3. If they are reflected in time interval of $\langle\Delta t\rangle$, however, $|\bar{n}\rangle$ is most likely to start a random walk, changing its directions in relative phase angles as shown in fig 4. The step of random walk in this case is $\theta\Delta m\langle\Delta t\rangle$, therfore after t, the square of distance from the starting point to the last point is,

$$N(t) = (\theta\Delta m\langle\Delta t\rangle)^2.t/\langle\Delta t\rangle \simeq (\delta m)^2\langle\Delta t\rangle.t. \quad (5)$$

The effect of absorption is not included in eq(5). If the absorption to the wall takes place at a rate of Γ/sec, eq(5) must be modifed to

$$N(t) \simeq (\delta m)^2\langle\Delta t\rangle\ (1 - e^{-\Gamma t})/\Gamma. \quad (6)$$

The production and absorption rates of $\bar{n}$ per unit time becomes equal after $t \gg \Gamma^{-1}$. If we assume that all absorbed $\bar{n}$'s are detected, the number of $\bar{n}$'s up to time T is,

$$\int_0^T N(t)\Gamma dt = (\delta m)^2(\Delta t).T, \quad (7)$$

if $T \gg \Gamma^{-1}$. Eq(7) times Φ, the inflow of source neutrons to the system per unit time, is the number of $\bar{n}$ observed in unit time. In this calculation the use of the area reserved for the neutron irradiation therapy is envisaged. Since the average velocity υ of UCN is about 3 m/sec, in a box of about $(30cm)^3$ in dimension, $\langle\Delta t\rangle$ is in the order of 10^{-1} sec. Γ can be defined as the absorption coefficient per bounce divided by $\langle\Delta t\rangle$ and not well known. After a reasonable estimate, we assume that the absorption coefficient is ~20%, or $\Gamma^{-1} \sim 0.5$sec. On the other hand UCN can be stored as long as about several hundreds of

seconds therefore $T \gg \Gamma^{-1}$ holds.

Fig.5 shows an example of UCN source to meet such experimental requirements. As was pointed out in sec.1, the use of wide solid angle against the cold neutron sources of solid methane is to be noted. Further, the use of reflectors around the super-thermal bath should enhance the flux of cold neutrons through the converter. With this set-up, it should produce 2×10^5 UCN/sec at KENS assuming the reflector gain of 20%. This type of set-up should be incorporated into a UCN target station independently from other stations. In this case the counting rate $R/sec/(\delta m)^2$ will be $10^7/sec/(\delta m)^2$. The UCN target station will be a very efficient source of UCN in improving the upper bound of the electric dipole moment as well.

References

1) Golub,R. and Pendlebury,J.M. Phys.Lett.53A 133 (1975)
2) Golub,R. and Pendlebury,J.M. Phys.Lett.62A 337 (1977)
3) Watanabe,N. et al This meeting
4) Feynman,R.P. and Cohen,M. Phys.Rev.107 13 (1957)
5) Reekie,J. and Hutchison,T.S. Phys.Rev. 92 827 (1953)
6) Mohapatra,R.M. and Marshak,R.E. Phys.Rev.Lett. 44 (20) 1316 (1980)
7) Mohapatra,R.N. and Marshak,R.E. VPI-HEP-80/4
8) Kamae,T. private communication

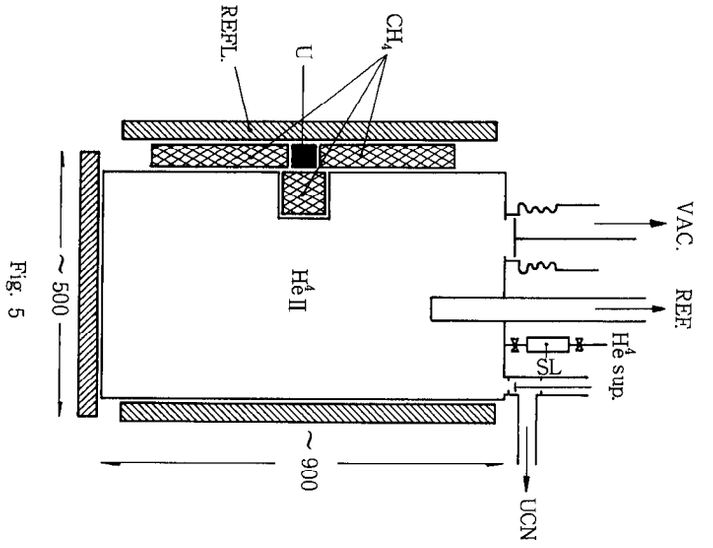

Fig. 5

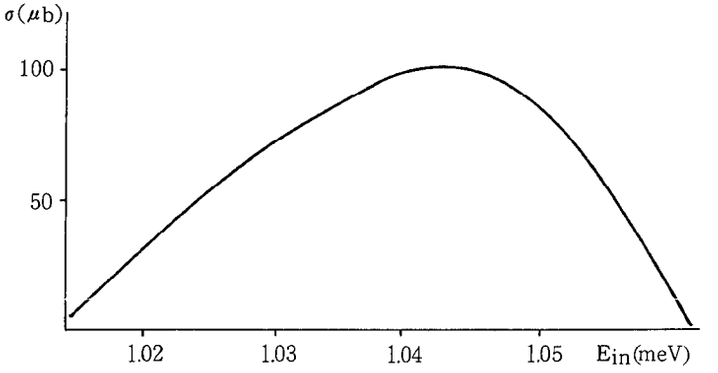

Fig. 1

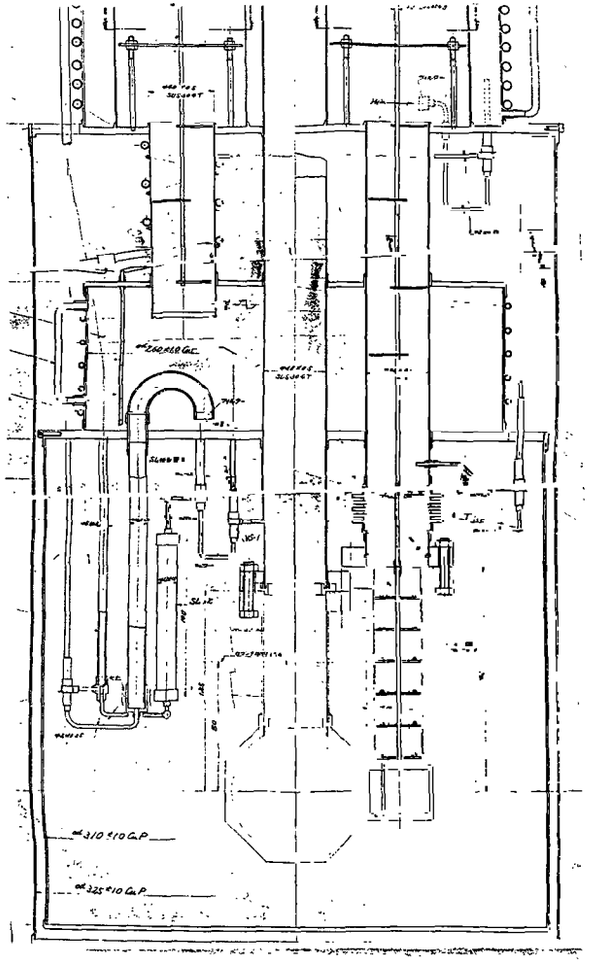

Fig. 2

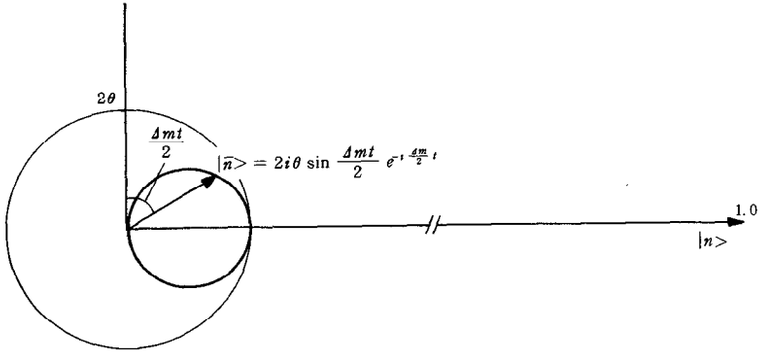

Fig. 3

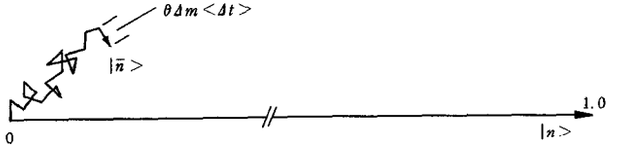

Fig. 4

A NEUTRON SPECTROMETER FOR USE IN THE LONG WAVELENGTH LIMIT

by

Thomas Dombeck

Physics Department, University of Maryland

In this paper I want to describe a possible neutron spectrometer for long wavelengths ($\lambda \sim 50$ to 1000 Å, $v \sim 80$ to 4 m/s, $E \sim 40$ to 0.1 μ eV) which uses Bragg scattering off a moving crystal to produce a narrow velocity band of Doppler shifted neutrons. There are several long wavelength spectrometers currently in use with applications in biological measurements and macroscopic effects in materials science.[1,2,3] The proposed spectrometer would have the advantage of time-of-flight (TOF) determination of the neutron energy.

For adequate TOF measurements in the energy range of interest, a flight path of only a few meters can be tolerated because of absorption losses. The pulse width at the source must be narrow, 10 times narrower than is possible from current pulsed sources in the 1000 Å region. It may also be difficult to extract long wavelength neutrons out of the pulsed source due to absorption losses in moderators and beam tubes. The design which I am considering utilizes a crystal mounted on the end of a rotor[4] such as the arrangement appearing in another paper in these proceedings (the Doppler shifting converter for the production of ultra cold neutrons). It has been demonstrated that moving crystals are good velocity selectors and can shift

the neutron wavelengths on reflection,[5,6] but I want to emphasize that the Bragg scattering occurs only in a short time interval ($\sim$ 400 μs for our present rotor). This permits an intense source of long wavelength neutrons with narrow pulse width generated close to a TOF spectrometer.

Our present rotor design with a thermica crystal generates neutrons with a perpendicular velocity component ($v_\perp$) from 3 to 20 m/s as shown on Fig. 1. Other velocity intervals can probably be produced by either changing rotor speed, crystal angle or working at higher order reflections.[6] Though we generate reasonable counting rates (0.6 n/(m/s) - pulse), the disadvantage of the rotor is the wide beam divergence ($\sim 80^0$). Use of collimation would severely reduce the counting rates; however, there is a class of experiments where angle information is not required (large energy transfer experiments and transmission experiments where only $v_\perp$ is important).

We have tested the principle of such a spectrometer using the Argonne rotor with the experimental setup shown on Fig. 2. We used two magnetic foils arranged in series where we could alter the transmission of neutrons by polarization.[7] The foils were 0.1 mil Ti coated with a 500 to 1500 Å-thick layer of natural iron. Electromagnets were used to saturate the magnetization in the foils. When very low velocity neutrons of the appropriate spin orientation strike the foils, the magnetic and nuclear amplitudes in Fe add together and the neutrons are reflected. In the other spin state the amplitudes subtract allowing some of the neutrons to pass through the foils. For an unpolarized beam and two foils magnetized in the same direction, the transmission T is greater in the magnetized case. (In the unmagnetized case the transmission varies as T^2.) An example of data taken with a 1500 Å Fe layer is shown on Fig. 3 showing a clear separation in the two cases. (The

separation would be even more pronounced with Fe^{54} because the magnetic and nuclear scattering amplitudes are close to the same magnitude.)

Another phenomenon occurs for particular incident velocities on thin layered foils; the neutrons resonate or get trapped.[1] This is easily demonstrated by a calculation where the material layers are represented by square potentials in a simple one-dimensional Schroedinger problem. The resonances give rise to preferential absorption in the various layers which can be detected by changes in transmission as a function of incident velocity. On Fig. 4, data showing this effect are presented. The calculated curves agree with the data for an Fe thickness $\sim$ 450 Å. We see one resonance near 10 m/s and evidence for a second near 12.5 m/s. (The unmagnetized data is again related to the square of the transmission in the magnetized case.)

The physical flight path was 56.89 cm from the crystal center to the He^3 counter. The uncertainty was 4.0% due to lack of knowledge in where these neutrons originated in the crystal ($\pm$ 1.35 cm), where they stopped in the detector ($\pm$ 0.5 cm), and the horizontal motion of the crystal ($\pm$ 0.4 cm) as it swung in front of the spectrometer. Folding in the pulse width ($\sim$ 400 μs) yields a TOF precision given by

$$\Delta v/v = \sqrt{(0.04)^2 + (0.0008v)^2} \qquad (1)$$

where v is in m/s. $\Delta v/v$ is 4% at 3 m/s, 4.1% at 10 m/s and 4.3% at 20 m/s. The energy sensitivity is $\Delta E/E = 2\,\Delta v/v$.

Using the data on Fig. 4 the observed spectrometer sensitivity can be estimated. The full width of the first transmission dip at 10 m/s is 0.2 μ eV, centered at an energy of 0.5 μ eV. The dip spans 5 data points (plotted

in 0.5 m/s bins) which follow the predicted curve. This is true in both the magnetized and unmagnetized data. Therefore, the sensitivity is estimated to be

$$\frac{\Delta E}{E} \approx \frac{0.2}{5} \times \frac{1}{0.5} = 8\% \qquad (2)$$

which yields $\Delta E \approx 0.04$ μ eV. This result agrees with the calculation using (1) for our spectrometer.

The data on Fig. 4 took about 25 minutes to collect at 5 Hz pulse rate on the Argonne ZING-P' source ($\sim$ 7500 pulses). This yields about 0.01 counts/0.5 (m/s) - pulse with a background of 10^{-3} counts/0.5 (m/s) - pulse. The count rates are lower than expected from the data on Fig. 1 ($\sim$ 0.3 counts/0.5 (m/s) - pulse), and this is due in part to a different Thermica crystal package mounted on the rotor for our spectrometer test which had a lower reflectivity, but also it is due to the accentuated losses in the longer flight path in our spectrometer. (Losses for long wavelength neutrons in long tubes have been measured to be $\sim 1/(1 + 1.2L)$ where L is the flight path in meters.[8])

Finally, I want to describe the expected performance for a spectrometer that could be used at IPNS with a 1% energy sensitivity. A 2.95-m long flight path is required as well as a reduction in the source pulse rate to 3 Hz to achieve a velocity descrimination at 9 m/s. The guide losses yield 20% of the counting rate observed above, but this is offset by an expected increase in flux of 10 at IPNS over ZING-P'. In the 10 m/s range (0.5 μ eV) we expect a count rate of 0.18 n/0.05 (m/s) - s (bins of 5 nano eV) at a 3 Hz pulse rate. In the 4 m/s range (0.1 μ eV) we require a pulse rate of 1 Hz with an expected counting rate of 0.024 n/0.02 (m/s) - s (bins of 1 nano eV).

REFERENCES

1. K. Steinhauser et al., PRL 44, 1306 (1980).

2. M. Scheckenhofer and A. Steyerl, PRL 39, 1310 (1977).

3. "Neutron Beam Facilities at the HFR Available for Users," Grenoble Publication, (ILL, Grenoble, Sept., 1977).

4. T. Dombeck et al., NIM 165, 139 (1979).

5. C. G. Shull and N. S. Gingrich, J. of Appl. Phys. 35, 678 (1963).

6. B. Buras and J. Kjems, NIM 106, 461 (1973).

7. V. Lobashov et al., Preprint No. 37, Konstantinov Inst. of Nucl. Phys., (Leningrad, 1973). [The magnetic polarizing foils are a part of an experiment to search for the neutron electric dipole moment.]

8. J. Pendlebury, Private Communication (Univ. of Sussex, Sussex, England).

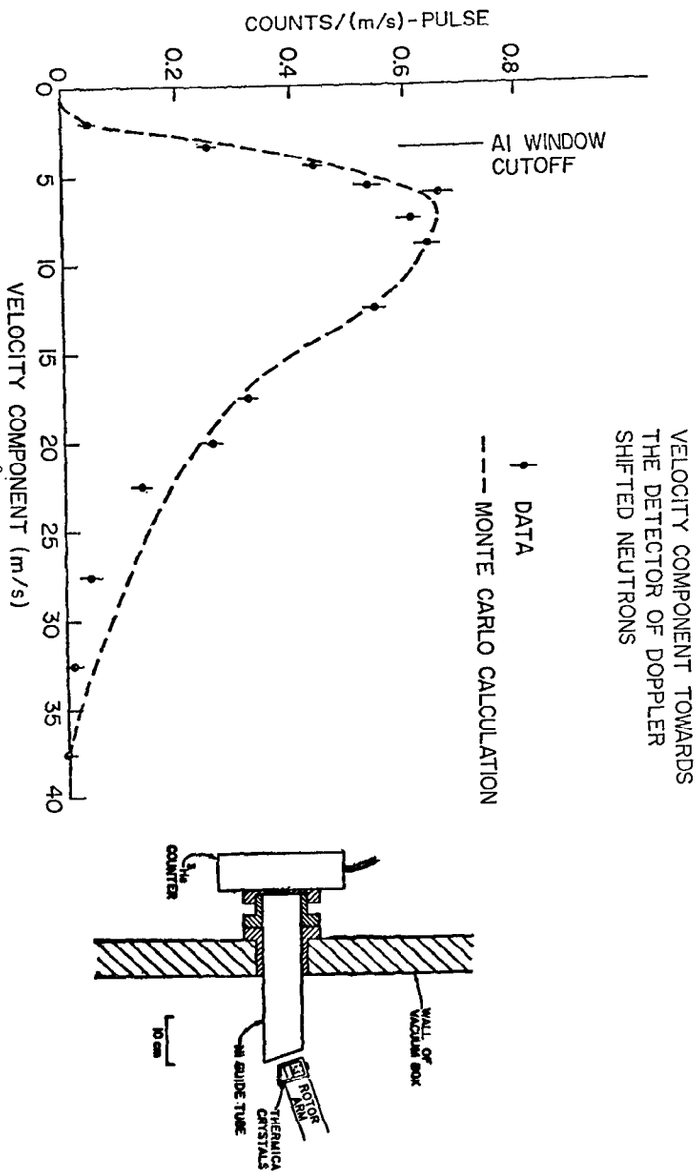

Fig. 1. The velocity spectrum into a He^3 detector is shown for Bragg scattered neutrons off a moving crystal. The experimental arrangement is shown in the insert. For details about the rotor refer to the ultra cold neutron paper in these proceedings.

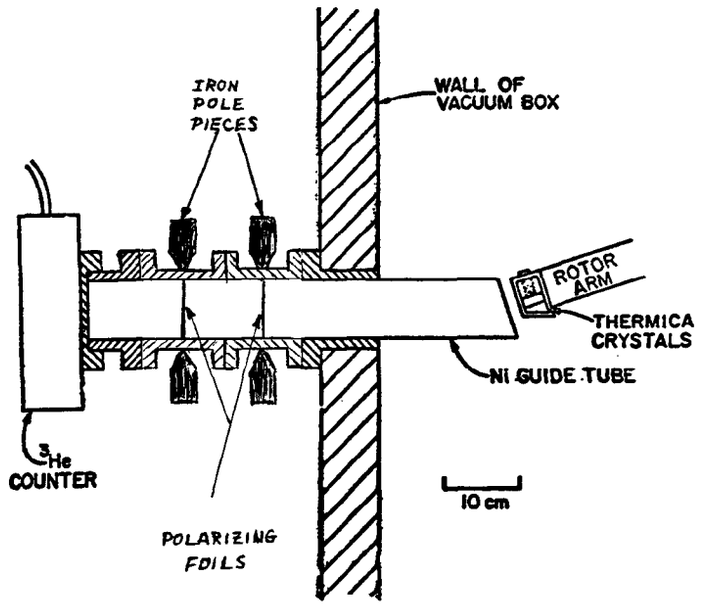

Fig. 2. The time-of-flight spectrometer with two thin foil polarizers is shown schematically. The foils are magnetized perpendicular to the neutron direction by external electromagnets.

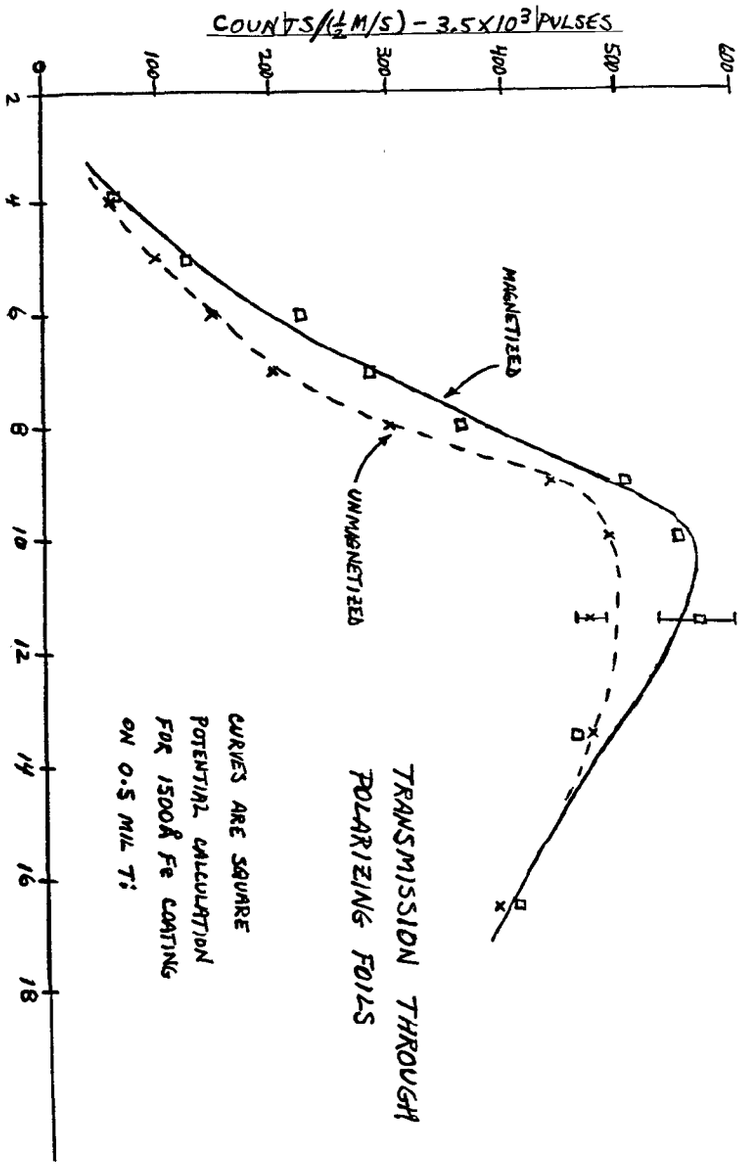

Fig. 3. Transmission data are shown for two foils with parallel magnetization. Refer to the text for a discussion of the curves.

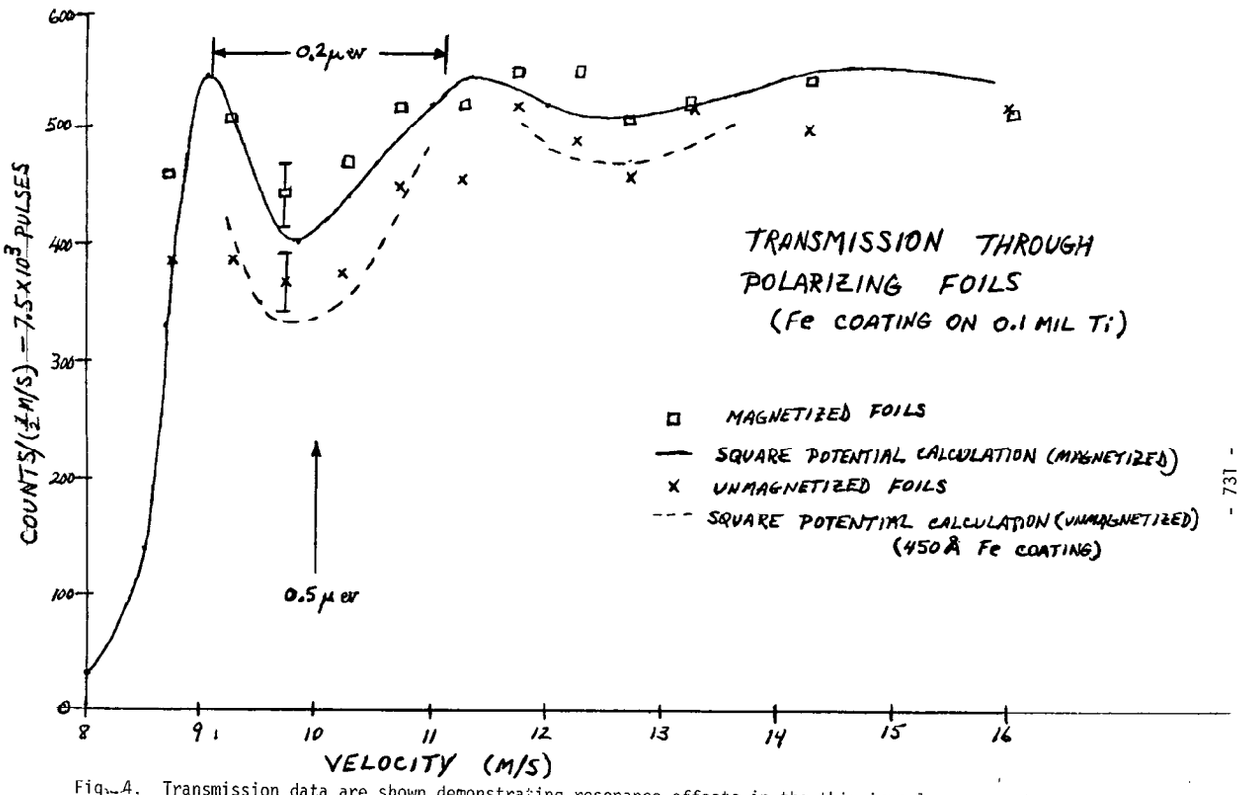

Fig. 4. Transmission data are shown demonstrating resonance effects in the thin iron layers on the polarizing foils. The energy sensitivity at 0.5 μ eV is 0.04 μ eV determined from the width of the dip in the transmission curves.

THE OPERATION OF AN ULTRA-COLD NEUTRON SOURCE AT THE ARGONNE ZING-P' PULSED NEUTRON FACILITY

by

Thomas Dombeck

Physics Department, University of Maryland

This report describes the operation of a converter, based on a Doppler shifting principle, for producing ultra-cold neutrons (UCN). Interest in long wavelength neutrons ($\lambda \sim 1000$ Å, $v < 7$ m/s) has grown in recent years with their possible application in interferometry, spectrometry, and studies of the fundamental properties of the neutron itself.[1] As a probe in material and biological sciences, UCN may provide new information in low momentum transfer interactions; but perhaps the most noteable advantage for UCN is the ability to confine them in material containers for long periods of time.[2] At Argonne we are designing a nuclear magnetic resonance spectrometer to search for the neutron electric dipole moment (EDM) in which we store UCN in a bottle in the central part of the apparatus.[3] With the increased sensitivity which this technique offers, we hope to improve the present experimental limits on the existence of the EDM by one to two orders of magnitude.

I will begin with a brief description of the Doppler shifter converter (for a more detailed description of the principles of operation, see Ref. 4). Neutrons generated in the ZING-P' uranium target are progressively cooled by a

room temperature and finally a liquid H_2 moderator to 20° K. A vertical beam tube looks at the moderator through a cooled Be filter, approximately 2/3 of the 5-m long tube is a Ni guide. Neutrons with a velocity near 400 m/s ($\lambda \sim 10$ Å) are transported up the tube toward the converter as shown on Fig. 1. A crystal of synthetic mica (Thermica, d = 9.963 Å) is mounted on the end of a 1.2-m long rotor spinning at 30 Hz (231 m/s on the periphery). The crystal angle on the rotor is set to Bragg reflect neutrons near 61.2° in the crystal frame and due to the large crystal mosaic spread ($\sim 3^{\circ}$, which is induced artificially), neutrons within a sphere in velocity space with $|v| < 7$ m/s are reflected. Because of the orientation, the reflected neutrons are Doppler shifted off the moving crystal into the UCN range in the laboratory and proceed as a slow moving cloud down a Ni guide tube leading to a bottle.

In principle the Bragg scattering process does not change the phase space density in the reflected cloud of UCN from that in the source. The spatial density in the cloud of 1000 Å neutrons is expected to be the same as the peak density in the source of 10 Å neutrons. In practice there are inefficiencies in the scattering which yield an overall efficiency near 10% for producing UCN from the available neutrons. The sources of the inefficiency are crystal reflectivity (47%), pulse broadening in the 5-m beam tube which reduces density at the crystal (32%), absorption losses, etc. (66%).

Due to the pulsed nature of the source, we take special measures to insure a maximum density of UCN in the bottle. In the present design the opening to the guide tube is fitted with a polished Ni shutter in the form of a rotating disk with a slot cut into it. The disk rotates synchronously with the rotor and opens the guide when each neutron pulse arrives and closes

between pulses to keep the UCN from escaping. In this way the bottle is filled asymptotically over many pulses.

The design parameters for the Doppler shifter are given in Table I. The phase space density near 400 m/s in ZING-P' was determined to be 0.0075 n/cm^3 - $(m/s)^3$ using gold foils and direct time-of-flight (TOF) measurements in the incident beam (the source strength was measured to be $\phi_p = 1.2 \times 10^{13}$ n/cm^2 - s equivalent peak thermal flux). For a sphere of 7 m/s neutrons in velocity space, we expected 1.0 UCN/cm^3 in the reflected cloud for a 10% efficiency. From TOF spectral measurements[5] performed with a He^3 counter at the end of the UCN guide tube (see insert on Fig. 2), we deduced a cloud density of 0.15 UCN/cm^3. A representative example of such a measurement is shown as circles on Fig. 2. A Monte Carlo calculation was performed, and the results are in good agreement with the data. The measurement is sensitive to one component of the velocity, thus 70% of the neutrons below 7 m/s are true UCN. The detector also had a thin Al window which reflected neutrons below 3 m/s, so we were insensitive to the lowest part of the spectrum.

The observed lower density of UCN from what was expected is due to a distortion of the sphere in velocity space in the Bragg scattering process. As confirmed by a detailed examination with our Monte Carlo calculation, only a pancake-shaped region near the center of the reflected sphere was populated adequately. This suggested that the flux of UCN varied with direction. We redesigned the opening to the UCN guide to exclude the lower flux regions by adding a grooved plate as shown on Fig. 3. The computer simulation of the new guide suggested a possible gain of 3 to 7 in UCN density.

We tested a plate fashioned out of triangular sections of stainless steel

placed perpendicular to the motion of the crystal. The resulting grooves reduced the open area of the guide by a factor of 3. The measured spectrum is shown on Fig. 2 as crosses. For the spectrum below 5.6 m/s (the maximum velocity that can be reflected by stainless steel), the crosses agree with the circles indicating that the same number of neutrons per unit time entered the guide even though the opening was restricted. Therefore, we observed an increase in UCN flux by a factor of 3. (To obtain a corresponding increase in the bottle density, however, a three-fold increase in the filling time is necessary.)

We tested the effect of surrounding the UCN cloud with Cu reflectors. The number of neutrons in this spectrum is shown on Fig. 2 as squares. We observe a factor of 2 increase in counts in the UCN range. The use of reflectors does not yield a higher density in the bottle; however, it reduces the fill time. Reflectors also reduce our reliance on the shutter because the opening to the bottle can remain open twice as long before the UCN flux begins to drop. In our configuration, the resulting shutter interval would be 14 ms or about one-half the time between pulses. (Thus, for a 60 Hz source with reflectors we would have approximately a continuous beam of UCN.)

The final proof that we are producing UCN rests in our ability to confine them for periods of time. We placed a crude bottle consisting of a section of Ni-coated Cu pipe with two flapper valves at the end of the UCN guide. The results on the storage time are shown on Fig. 4 with the mean lifetime of about 4 seconds. This is far from hundreds of seconds observed in other experiments,[2,6] but may be understandable in view of the poor vacuum and loose fitting valves in our bottle. Nevertheless, the intercept of the lifetime curve gives us information on how well we are transporting neutrons

into the bottle and whether we are coming close to the expected stored density. We observed an intercept of 6 counts/cycle. (A cycle consists of a 5-second fill time, a variable holding time and a 1.5-second count time).

For the conditions under which the data were taken, we expected 15 counts/cycle for a source density of 0.15 UCN/cm^3. (Because of the short lifetime of the bottle, we filled over 5 secs. even though the 6 ℓ volume would have required 35 secs. to fill. The expected count rate also includes counter efficiency, losses due to gaps in the guide tube and the lower velocity, $\sim$ 6 m/s, that can be contained by the Ni bottle.) The results indicate a loss of a factor of 2.5 probably occurring in transmission between the crystal and the bottle. We do not have an explanation for this loss as yet.

In conclusion, we have successfully produced UCN at the Argonne ZING-P' pulsed neutron facility with a source density of 0.45 to 1.0 UCN/cm^3. To date, we have been able to transport about 1/3 of these UCN into a bottle. These results are comparable to the stored densities observed at ILL, Grenoble[6] which are about 0.15 UCN/cm^3, even though the ZING-P' source strength is much below the HFR reactor. At the IPNS facility to be operational next year, we should have a better H_2 moderator and in general a tighter construction of the target cell which may yield an increase in flux by a factor of 10 over ZING-P'.

I would like to thank my colleagues on the neutron EDM experiment who helped design the equipment described in this paper: J. Carpenter, M. Freedman, V. Krohn, J. Lynn, R. Ringo, and S. Werner.

REFERENCES

1. R. Golub et al., Scientific American, 134 (June, 1979).
   H. Scheckenhofer and A. Steyerl, PRL 39, 1310 (1977).
   N. F. Ramsey, in Atomic Physics (eds. R. Marrus, M. Prior and H. Shugart; Premium Press, NY, 1977).
   T. Dombeck, Preprint No. 78-074, University of Maryland (1977).

2. A. Steyerl, Springer Tracts Mod. Phys. 80, 57 (1977).

3. T. O. Brun et al., "A Proposed Measurement of the Electric Dipole Moment of the Neutron," Argonne National Laboratory (Oct. 1979).

4. T. Dombeck et al., NIM 165, 139 (1979).

5. T. Brun et al., PL 75A, 223 (1980). [We quoted a density of 0.12 UCN/cm^3, but since that measurement we placed a cooled Be filter over the moderator yielding a 25% increase in flux.]

6. W. Mampe, Private Communication (ILL - Grenoble).

Table I.

PARAMETERS FOR THE ARGONNE DOPPLER SHIFTER UCN SOURCE

A. ZING-P'

Pulse Rate	30 Hz
Peak Equivalent Thermal Flux	1.2×10^{13} n/cm^2 - s
Phase Space Density	0.0075 n/cm^3 - (m/s)^3
Pulse Width at Source	140 μs
Velocity Range Reflected	388 - 402 m/s
Distance Source to Crystal	4.78 m

B. ROTOR AND CRYSTAL

Radius	1.202 m
Bragg Angle	61.2^o
d-Spacing	9.963 Å
Mosaic Widths (Broadened by Al Wedges)	3° x 1.2^o
Crystal Dimensions	5.7 cm x 2.7 cm
Crystal Package Thickness	1.1 cm
Reflectivity	0.47
Absorption and Inelastic Scattering	0.36

C. COLLECTION SYSTEM

Guide Tube (Polished Ni)	9.5 cm diam.
Shutter Time Interval	7 ms
Volume In Guide Tube (Reservoir)	3.3 ℓ
Bottle Volume	3.0 ℓ
Velocities Contained (Ni)	$\leq$ 6.2 m/s

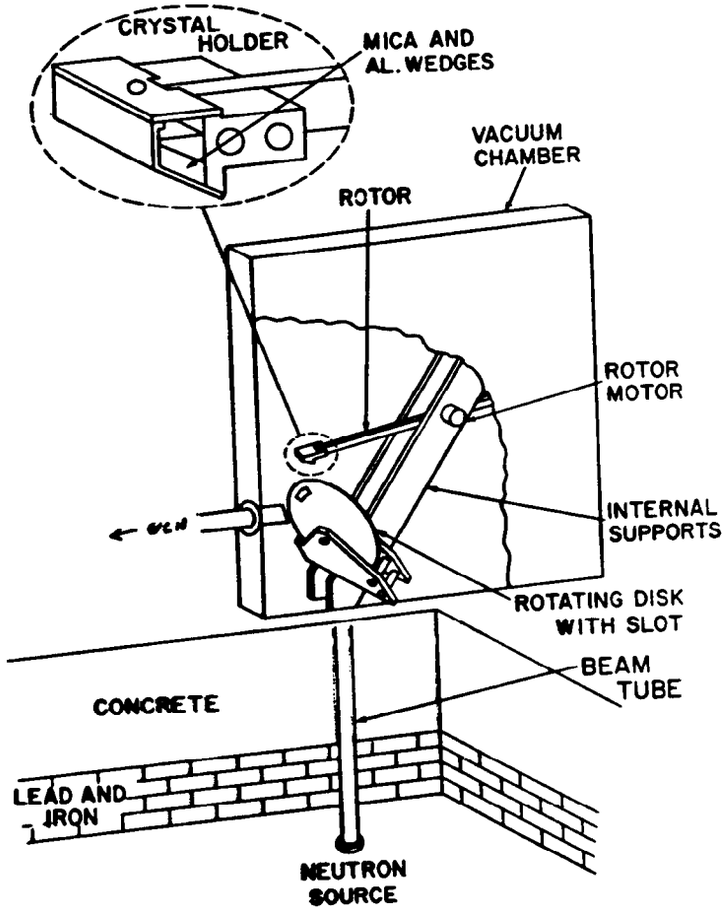

Fig. 1. The layout is shown schematically for the Doppler shifting converter.

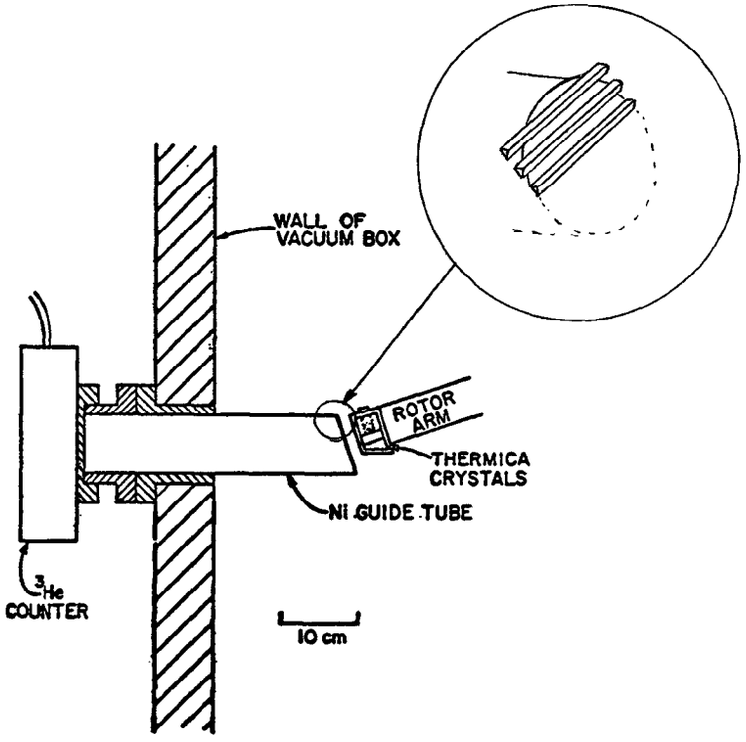

Fig. 3. The experimental arrangement for the grooved plate test is shown. The insert shows schematically how the stainless steel wedges were placed over the end of the Ni guide tube.

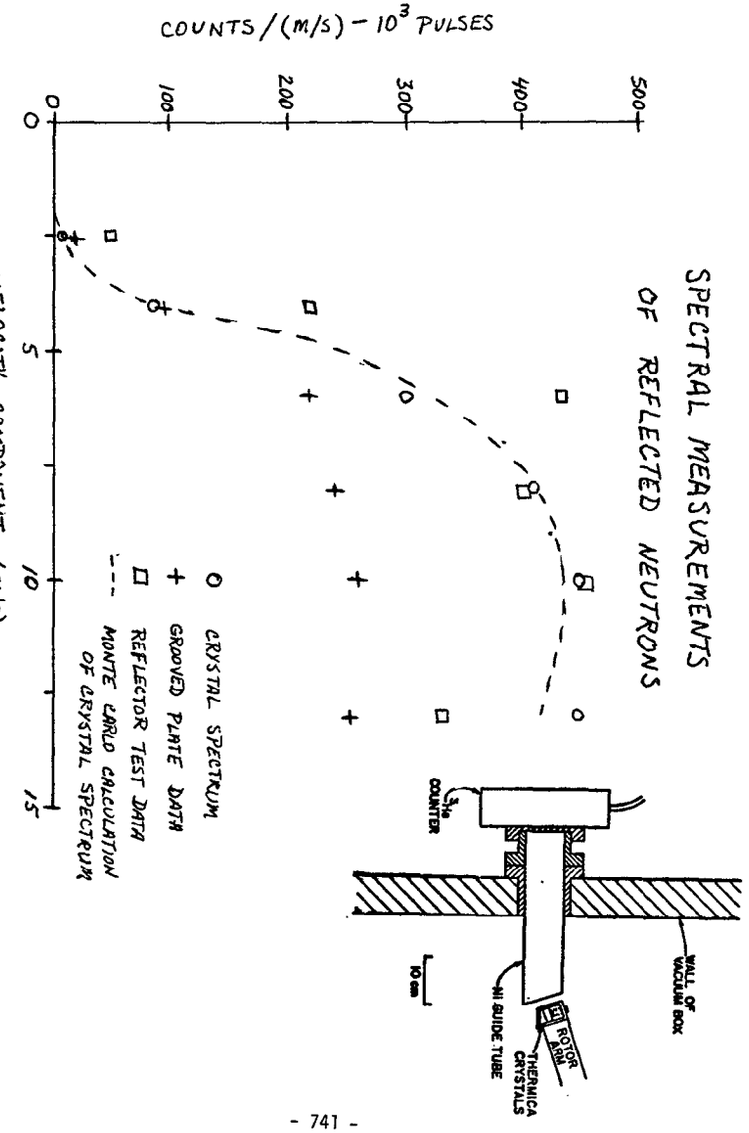

Fig. 2. The spectral measurements of the reflected neutrons is shown comparing the grooved plate, reflector test and open guide data. The insert shows the experimental arrangement for these measurements.

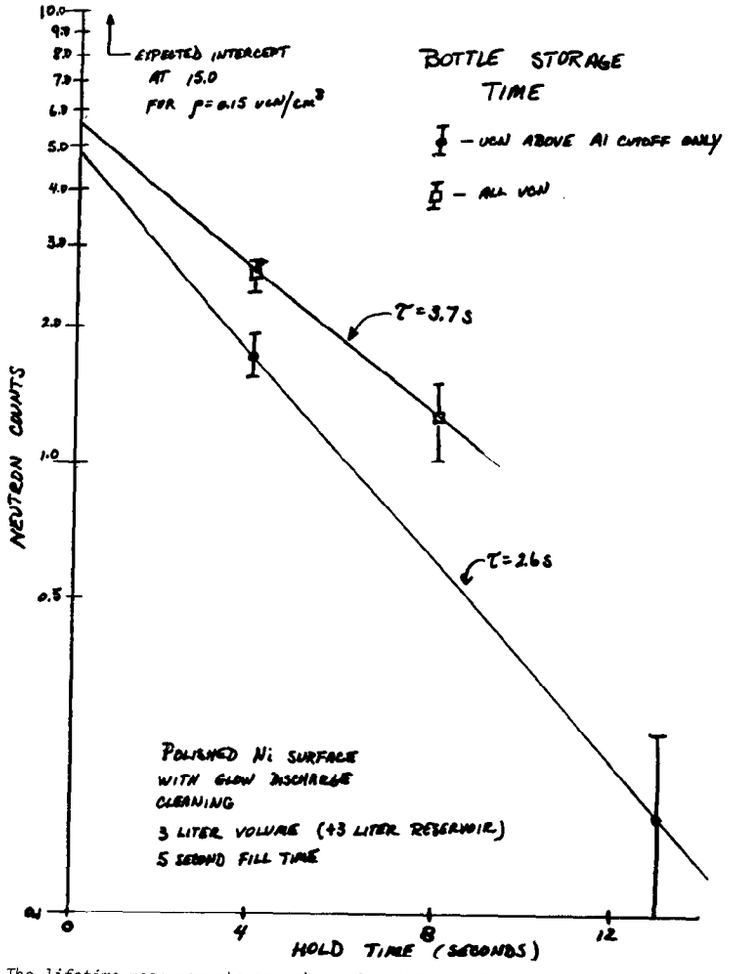

Fig. 4. The lifetime measurements are shown for UCN in a Ni coated bottle.

Construction of KUR Ultra Cold Neutron Source
with a Supermirror Neutron Turbine

M. Utsuro, S. Shirahama*, K. Okumura, Y. Ishikawa
and T. Ebisawa
Research Reactor Institute, Kyoto University. Osaka
Department of Nuclear Engineering, Kyoto University*. Kyoto

1. Introduction

Ultra Cold Neutrons (UCN) with the velocity below about 10 m/s are recently becoming valuable tools for some kinds of physical experiments, because of their long observation time in a closed vessel of neutron bottle, or their long wavelength comparing to cold or thermal neutrons. However, actual extractions of UCN from the inside of a reactor accompany various extraction losses, due to a number of reflections at non-ideal mirror surfaces in UCN guide tubes, window effects at the ends of guide tubes and so on, and severe intensity decreases of $10^{-2} \sim 10^{-3}$ comparing to those in a source neutron intensity are reported.

To overcome these intensity losses, a special machine called "Neutron Turbine" which converts cold neutrons or Very Cold Neutrons (VCN) to UCN and reconstructs the low energy tail of the spectrum becomes useful[1]. The fundamental principle of neutron turbine is described in Fig. 1. The velocity V_1 of an incident neutron in a laboratory system gives the relative velocity V_r in a rotating wheel of a turbine (Fig. 1 (a)). The neutron with the velocity V_r is transformed to one with a much different direction of the velocity V_r' in the wheel, due to the working of a turbine blade (Fig. 1 (b)). Again returning to the laboratory system, we obtain an exit neutron with the velocity V_1' (Fig. 1 (c)), which can be designed to become UCN. In a turbine in FRM Reactor, Munich, curved copper mirrors are used as the turbine blades[1], and the direction of the neutron velocity is reversed through many times of successive total

* Now at Kyushu Electric Power Co. Ltd..

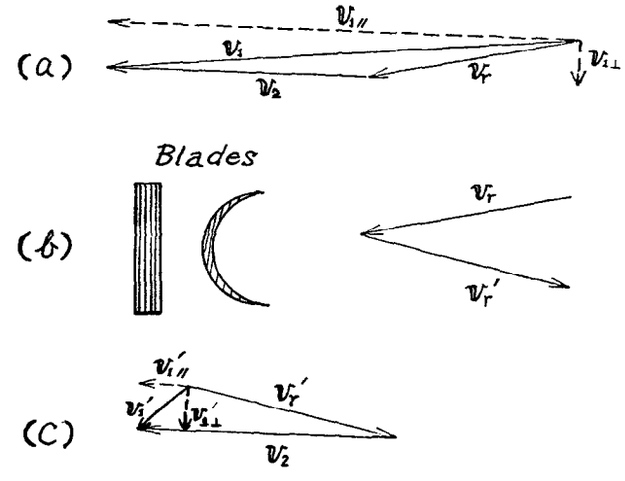

Fig. 1 Working principle of neutron turbine.
(a) at the inlet of turbine blade
(b) working of blade
(c) at the exit of blade

reflections in the blade. On the other hand, Bragg reflections of cold neutrons in a thermica crystal are used in a turbine at the pulsed spallation source in ANL.[2,3]

In the present paper, we report on the design and construction of another type of a neutron turbine which uses supermirror reflection blades having the shape as shown in Fig. 2. Supermirrors with a critical velocity of reflection of neutrons of about 15 m/s can be readily prepared in our laboratory,[4,5] and therefore a combination of three flat mirrors as shown in the Figure is enough to reverse the direction of incident VCN. A neutron turbine with this type of blades was constructed and set at the exit of a VCN guide tube apparatus in the thermal column of 5 MW Kyoto University Reactor (KUR).

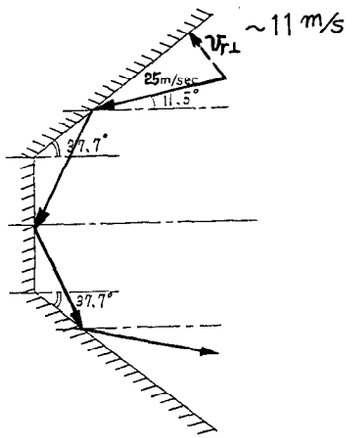

Fig. 2 Performance of the present supermirror turbine blade.

2. Preparation of Supermirror Blades

Supermirror[6] is a neutron mirror consisting of alternative multilayers of two kinds of materials (referred here as N and T) with positive and negative coherent scattering amplitudes, respectively, and further with gradually varied layer thicknesses

$$2d \sin\theta = \lambda \qquad 2d \approx \frac{\lambda}{\theta}$$

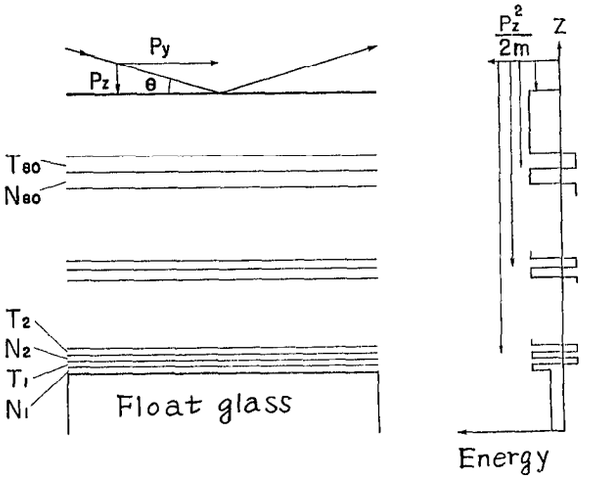

Fig. 3 Layer structure and effective potential in a supermirror.

as shown in Fig. 3. Incident neutrons with long wavelength see a scattering potential with various periodicities in this mirror. As the result, the condition of the Bragg scattering can be satisfied for neutrons in a wide wavelength region at some depth in the multilayers.

In our laboratory, nickel and titanium are used as these mirror materials[4,5] and high quality supermirrors are readily prepared by a vacuum evaporation on a float glass with an electron beam heating of the mirror materials. Some results of design calculations for Ni-Ti supermirrors with various total

number of layers are given in Fig. 4. From this Figure, we decided to use Ni-Ti supermirrors consisting of about 170 total layers for our turbine blades having a critical neutron velocity for reflection of about 15 m/s.

The reflectivity of supermirrors thus prepared as turbine blades (size of a mirror is 100 mm^H x 47 mm^W on a 5 mm^t float glass) were measured in the experimental arrangement of Fig. 5 at the thermal neutron beam tube B-1 of KUR. Pulsed neutrons from a chopper (2) are well collimated by a slit (6) and a collimator (7), and reflected by the sample mirror (8) on a holder (9) with a fine adjustment. Reflected neutrons are counted by a detector (11). The time-of-flight spectrum of reflected neutrons devided by that of the incident neutrons gives the reflectivity of the sample mirror.

One of the results obtained from the experimental conditions of chopper speed 1500 rpm, flight path length 6.39 m, and the

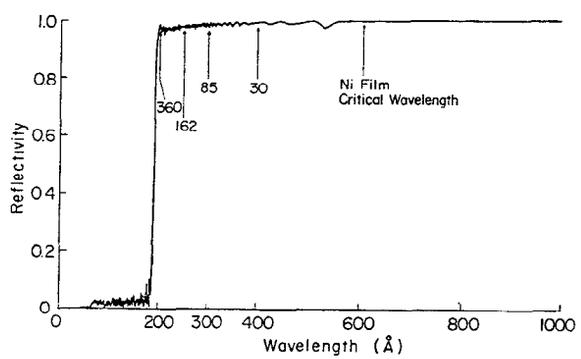

Fig. 4 Theoretical reflectivity calculated for Ni-Ti supermirrors.[4] (Numerals mean total number of layers.)

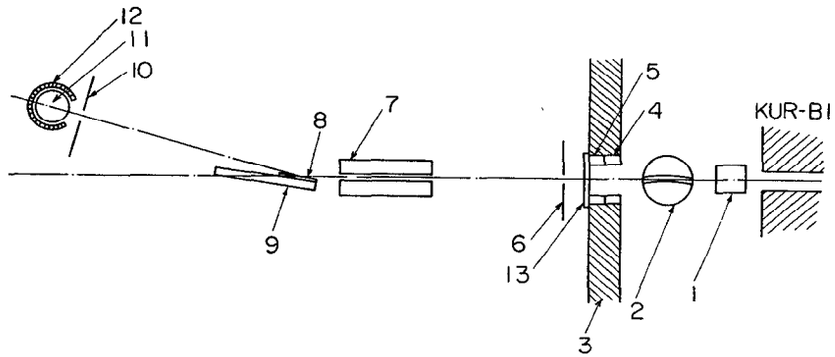

Fig. 5 Experimental arrangement for measurement of supermirror reflectivity. 1; stator slit 2; curved rotor slit 3; heavy concrete shielding 4; boric acid 5; lead 6; cadmium slit 7; collimator 8; sample mirror 9; mirror holder 10; boron carbide slit 11; He^3 detector 12; boron carbide shielding 13; monitor counter.

incident angle of neutrons of 8.30×10^{-3} rad. is given in Fig. 6. In Fig. 6, the abscissa means the neutron wavelength corresponding to the velocity component normal to the mirror surface. Most of mirrors prepared showed similar results with Fig. 6 and satisfy the reflectivities greater than about 70 % in the wavelength region beyond about 260 Å (∿15 m/s).

3. Design and Construction of Neutron Turbine

A simple analysis of neutron motions in our turbine blade with the shape of Fig. 2 is illustrated in a velocity diagram of Fig. 7. Incident neutrons to the turbine are fed by a VCN

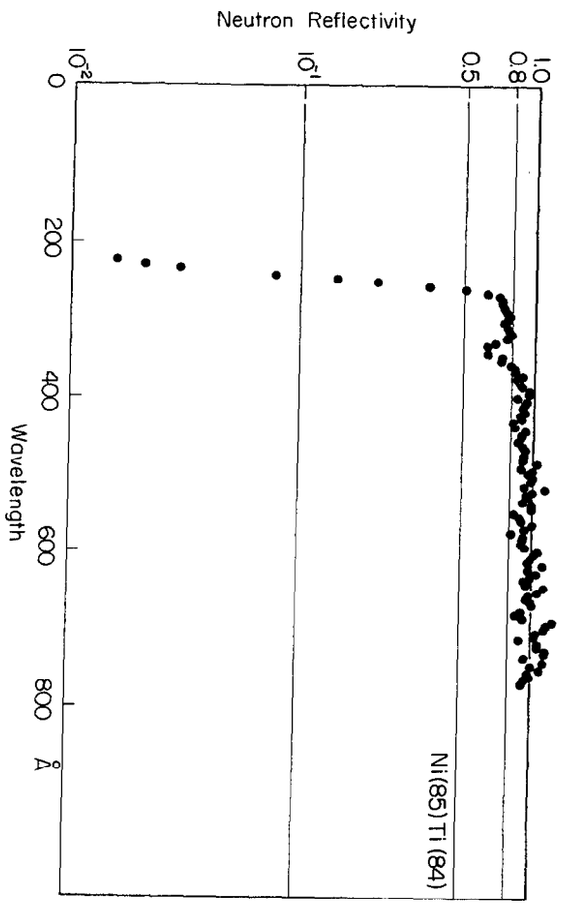

Fig. 6 An example of measured neutron reflectivities of Ni-Ti supermirrors prepared for turbine blades.

guide tube of Ni-coated glass and installed in a reactor. The feeding guide tube in the turbine is adjusted to have a little inclination of an angle of 5.7^{o} to the direction of motion of the blades. Therefore, the velocity vectors of the incident neutrons lie within a band with a total width of about 13 m/s, having the origin at O. Rotating speed of the blade 25 m/s shifts the origin of the neutron velocity from O to O_1 in the system of the relative velocity of neutrons to the blade. Thus, the incident neutrons with the velocity within the hatched region 1 can be reflected by the first reflection plane of the mirrors, and converted into the unhatched region 2. After second and third reflections, similarly, the velocity vectors of the exit neutrons come to lie within another hatched region 4. Again returning to the laboratory system, we can obtain UCN component with the velocity from the origin O at the exit of the turbine.

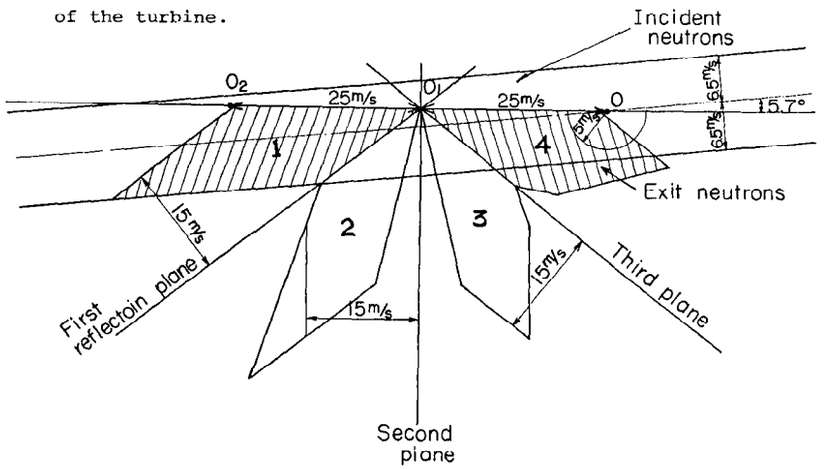

Fig. 7 Velocity diagram showing the working of supermirror turbine blade.

This is one of the simplest analyses of neutron motions in the blade. Concerning actual turbine blades with a finite size, a more sophisticated geometrical analysis is necessary for an exact estimation of the turbine efficiency, taking into consideration about the incident point dependence of the reflection condition for various values of the incident angle. From the result of such an analysis, it can be concluded that about 80 % of incident neutrons to the turbine within a velocity region of 45 m/s ∿ 55 m/s satisfy the reflection condition in our blade.

The essential structure of our neutron turbine is shown in Fig. 8. About 30 turbine blades are fixed around a wheel (3) with a diameter of 100 cm, and the wheel rotates at a speed of about 420 rpm in a vacuum vessel (1), drived from the outside through a non-contact coupling (9). The VCN feeding guide tube (5) has an inner size of 8 cm^H x 2 cm^W. Exit neutrons from the blades are detected by UCN detectors (7) through a short UCN guide tube (6).

In the first stage of the test run of the turbine, only a few pairs of blades are attached symmetrically on the wheel and the exit neutrons in a pulsed form can be measured. In this case, the parts without the blades on the wheel are shielded by cadmium plates. This test running of the pulsed production of UCN is now being carried out by setting the turbine at the VCN guide tube in KUR described in the next chapter.

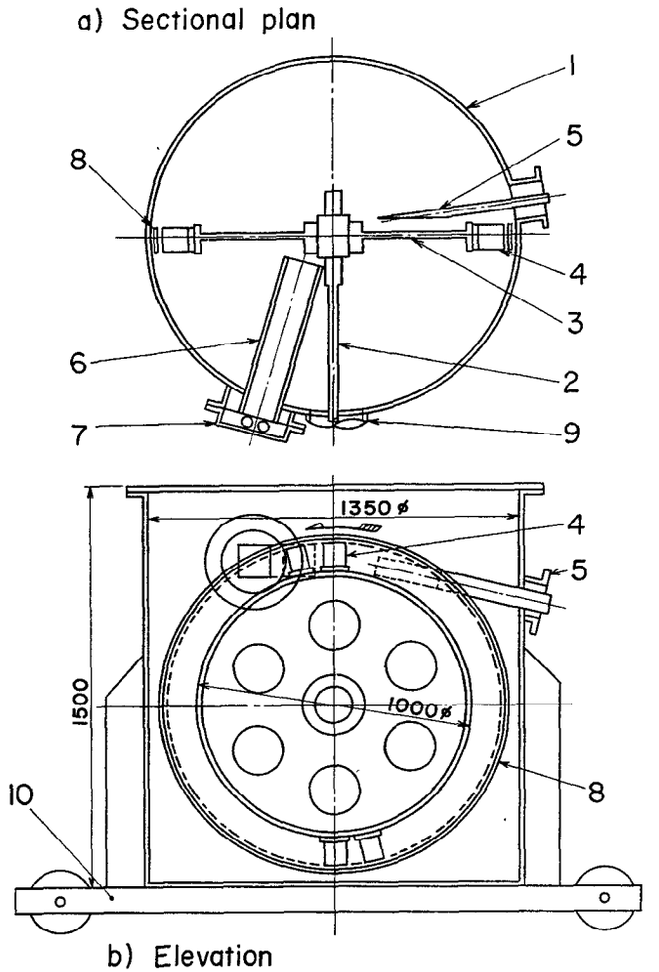

Fig. 8 Essential structure of the supermirror turbine. 1; vacuum vessel 2; driving shaft 3; turbine wheel 4; reflection blades of supermirrors 5; VCN feed guide tube 6; UCN guide tube 7; UCN detectors 8; guard ring 9; non-contact driving mechanism 10; carriage.

4. VCN Guide Tubes at KUR Thermal Column

Our neutron turbine was designed for incident neutrons with the velocity of about 45 ∿ 55 m/s, and therefore a VCN feeding apparatus was also constructed at KUR. The VCN apparatus is S-curved guide tubes consisting of Ni-coated float glass and inserted into a graphite thermal column of the reactor. ($\Phi_{th} \sim 10^{12}$ n/cm²sec) The graphite thermal column is selected here as the VCN source because of its high neutron flux with low fast neutron backgrounds and a large illuminating area easily accessible by the guide tube in order to obtain a large glancing angle. The whole arrangement of the apparatus is given in Fig. 9.

The guide tube is curved not only in horizontal direction but also in vertical, in order to decrease the fast neutron background and to fit the height of the entrance window of the turbine. Geometrical parameters of each sections of the guide tubes are listed in Table 1. The ends of each sections are sealed by thin aluminium foils of 0.1 mm^t, and the insides are filled with helium gas in order to eliminate air effects.

In Fig. 9, a simple VCN chopper is inserted in the midway of the guide tube sections for the measurement of the time-of-flight spectra of the exit neutrons. One of the measured spectra is shown in Fig. 10 for the experimental conditions of chopper speed 655 rpm, effective flight path length 3.01 m and the channel width of time analyser 64 μsec. From the present result, the VCN intensity in the velocity region of 45 m/s ∿ 55 m/s at the exit of the guide tube was obtained

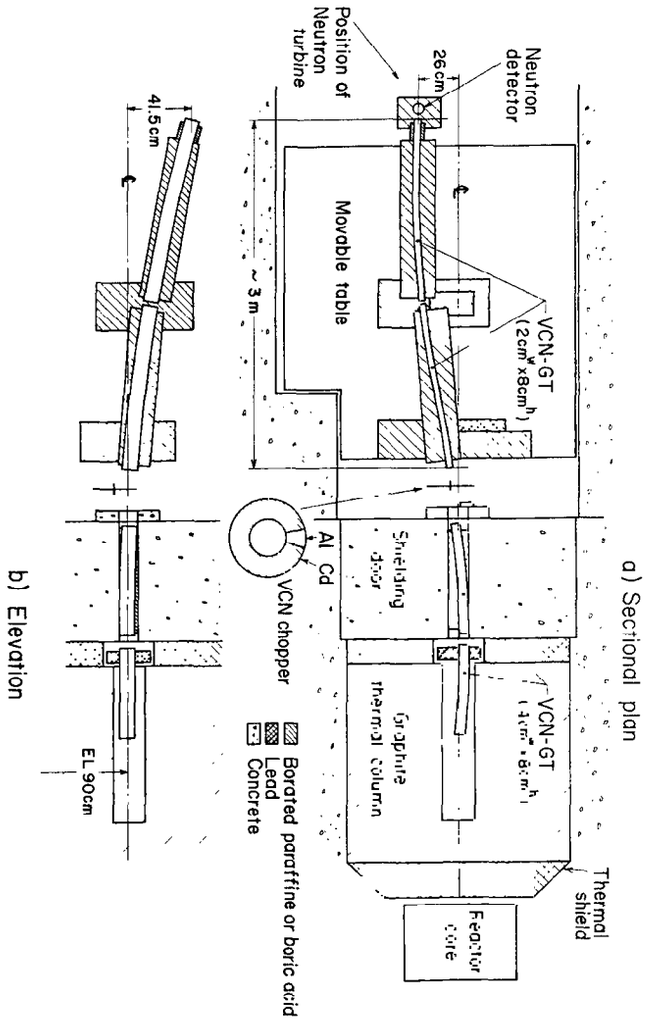

Fig. 9 VCN feeding apparatus for the neutron turbine.

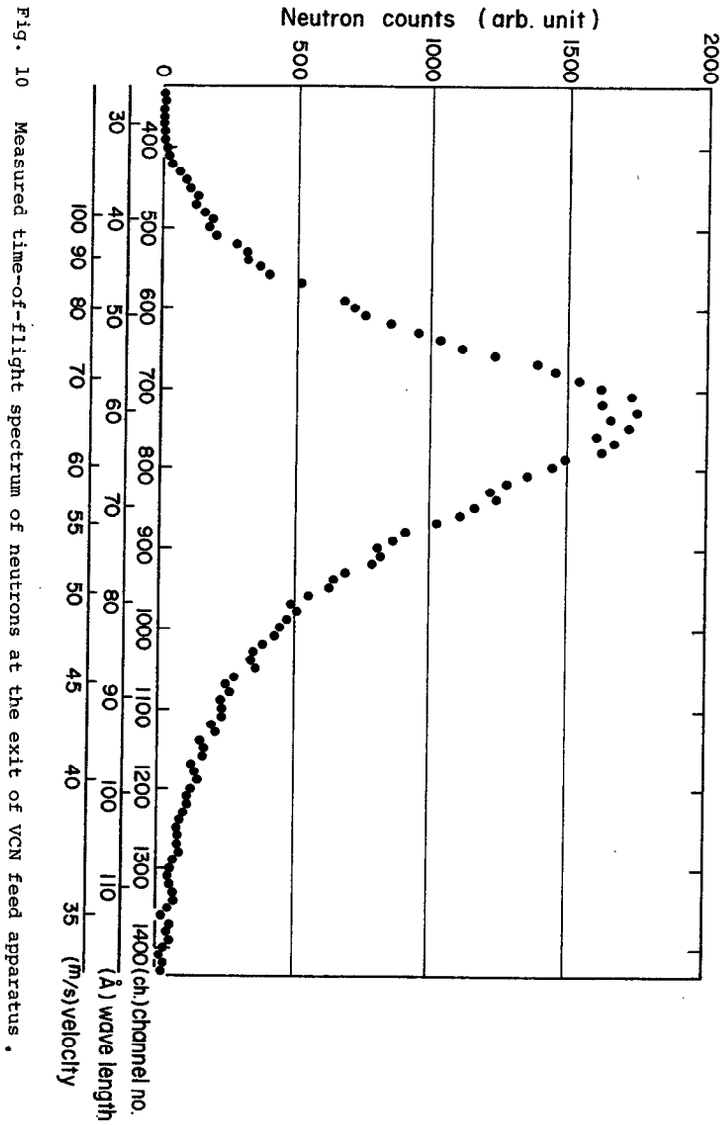

Fig. 10 Measured time-of-flight spectrum of neutrons at the exit of VCN feed apparatus.

Table 1 Parameters of VCN feeding guide tubes.

Sections		Radius of curvature	Width	Charactr. velocity	Minimum length*	Actual length
Former sections		8 m	4 cm	62 m/s	1.6 m	1.9 m
Latter sec-tions	H	8 m	2 cm	88 m/s	1.1 m	1.5m
	V	16 m	8 cm	62 m/s	3.2 m	3.0m

H; horizontal direction V; vertical direction
*; minimum length necessary for stopping direct beam.

to be about 27 $n/cm^2min.$, which agreed well with the expected intensity of 35 $n/cm^2min.$. The background counts due to faster neutrons and gamma rays were sufficiently low.

Our turbine is set at the exit of the present VCN guide tube, removing the chopper and eliminating the distance between the guide tube sections in that place. These modifications and a better alignments of the guide tube sections will improve the VCN intensity by at least a factor of 4.

5. Concluding Remarks

The reflectivity of the supermirrors presently used and the geometrical efficiency of the blades give the expected efficiency of our turbine of about 35 %. Therefore, the intensity of the UCN output of the present turbine will become about 0.6 n/cm^2sec at the present KUR. Some improvement in the intensity is considered to be possible by decreasing various loss factors in the VCN extraction and VCN guide tubes.

Furthermore, the intensity will be greatly enhanced by the insertion of a liquid deuterium cold source[7] into the present thermal column beam hole which is now under preparation.

Acknowledgements

The authors express their thank to Prof. A. Steyerl of Technical University of Munich for his encouragement and valuable discussions with him. They also appreciate the skilfull work of the machine shop in our laboratory.

References

1) A. Steyerl; Nucl. Inst. Methods 125 (1975) 461.

2) T.O. Brun et al.; IPNS Newsletter Vol. 2 (1979) No. 3.

3) T.W. Dombeck et al.; "Production of Ultra-Cold Neutrons Using Doppler-Shifted Bragg Scattering and an Intense Pulsed Neutron Spallation Source."; Nucl. Instrum. Methods 165 (1979) 139.

4) S. Yamada et al.; Annu. Rep. Res. Reactor Inst. Kyoto Univ. 11 (1978) 8.

5) T. Ebisawa et al.; J. Nucl. Sci. Technol. 16 (1979) [9] 647.

6) F. Mezei; Commun. Phys. 1 (1976) 81.

7) M. Utsuro and M. Hetzelt; Proc. Symp. Neutron Inelastic Scattering 1977, IAEA Vol. I (1978) 67.

A Comment on the Ultra Cold Neutron Session

H. Yoshiki

The application of Ultra Cold Neutrons to the fundamental physics and the applied physics has drawn considerable attention in recent years. One of the present major problems of the study is how to produce a strong UCN source in space and time. The Liouville's theorem states that unless the energy-non-conserving external force is applied, the phase space density of UCN is equal to that of source neutrons. The allowed volume of UCN in velocity space is minute, in the order of 7 m/sec in radius. It is however important to note that this limit on the density can be lifted by introducing whatever an externally controlled cooling device which functions in accordance with the velocity coordinates of the source neutrons in bringing them down to the UCN region. This principle has been applied to "stochastic cooling" in the field of high energy physics to increase the luminosity of particle beam in a storage ring. The velocities of source neutrons prior to cooling can be easily known by TOF method. Thus an attractive possibility to produce UCN in conjunction with the pulsed neutron source opens up. Utsuro at University of Kyoto in fact tested such a device, where a magnetic bottle produced by a series of solenoids traveled along its axis while it was decelerating its own speed. The rate of deceleration was carefully adjusted to match the arrival of slower neutrons. He claimed the observation of polarized UCN. It is hoped that any UCN production device which functions periodically as presented in the first two papers here should have the same end. In the present particular contribution, Dombeck, after his successful production of UCN by Doppler-shifted Bragg scattering, showed that by placing a blind which was fashioned out of triangular sections of stainless steel perpendicular to the motion of the crystal the spacial UCN density increased by a factor of three, and placing a copper reflector around the produced UCN cloud the collection efficiency increased by a factor of two. The acceptance energy width is 60 μeV at incident source neutron energy of 815 μeV. Utsuro reported the construction of a neutron turbine where each blade is assembled out of three pieces of supermirror which reflects neutrons totally whose perpendicular component of wavelength is 260Å or over. The acceptance

energy width is 5.2 μeV at 13 μeV. It is to be noted that both devices have high cooling efficiencies, which are essentially equal to reflectivities. The superthermal helium converter, proposed by Golub and Pendlebury, on the other hand works on the direct current basis (i. e. the device is always ready regardless of the neutron arrival time. Although the neutron turbine's duty cycle is nearly 100%, it should be classified into the category of periodic machine from its functioning.) Therefore the final UCN densities are limited by the Liouvulle's theorem. It has also a disadvantage of all neutrons not being converted to UCN because of the limited cross section of the process. The acceptance width is 45 μeV at 1038 μeV. However this scheme has some merits. Since the source neutron can penetrate into the helium vessel and the produced UCN can not leave it, the collection efficiency is high compared to the scheme where diffusing UCN cloud produced in space is trapped into a storage vessel by means of an opening shutter at the moment of UCN production. With the superthermal helium converter, the UCN density in the vessel thus stacks proportionally with time. Although this scheme looks at first best fit to the direct-current source neutrons from nuclear reactors, because of the heat, it is necessary to use the external beam. With the spallation source on the other hand this production device itself can be wrapped up with slabs of cold sources, if not the radiation in helium become too much a problem. The consequent gain in solid angle is in the order of 10^4 which compensates more than the loss due to duty cycle of the accelerator compared to the use of reactors. The third contribution deals with a test of a superthermal helium converter with an emphasis on the elimination of hydrogen contaminating the vessel.

Excursion to Mt. Tsukuba

← Visit to Tsukuba Shrine

↑

At the top of Mt. Tsukuba

Many participants went down
the mountain on foot →

IV APPENDICES

ICANS-IV PROGRAM (Oct.20-Oct.24)

MONDAY October 20

Registration		9:00- 9:30
Technical report	Y. Ishikawa	9:30- 9:45
Welcome address	T. Nishikawa	9:45-10:00
Plenary Session (Room A)		**10:00-15:30**
	Chairman M. Kimura	
* Present status and future development of WNR	G.A. Keyworth	10:00-10:30
Coffee Break		10:30-10:50
* Status of the IPNS program	D.L. Price	10:50-11:20
* Review talk on the present status of SNS facility	G. Manning	11:20-11:50
* Review on the status of the German project	W. Klose/H.H. Stiller	11:50-12:20
Lunch		12:30-14:00
	Chairman G. Manning	
* Present state and planning of the spallation neutron source at SIN	Ch. Tschalär	14:00-14:30
* KEK Booster Synchrotron Utilization Facility (BSF)	H. Sasaki	14:30-14:50
* KEK neutron scattering facility (KENS)	Y. Ishikawa	14:50-15:10
Photograph		15:10-15:30
Coffee Break		15:30-16:00
Excursion to BSF and other facilities in KEK		16:00-17:30
Bus		18:00

Proceedings Reporter: Carpenter/Ishikawa

TUESDAY October 21 A.M.

Technical session, Target I (A) (T-1)		**9:00-12:30**
Target station (Engineering)		
	Chairman W. Klose/N. Yamamuro	
* Status of IPNS construction	N.J. Swanson	9:00- 9:20
* Review of SNS target station	A. Carne	9:20- 9:35
* KENS target-moderator-reflector system	N. Watanabe	9:35- 9:55
* KENS cold neutron source	S. Ikeda	9:55-10:10
* Studies of cold neutron sources for spallation targets	N. Nücker	10:10-10:30
Coffee Break		10:30-11:00
* Measurements of spallation target-moderator-reflector neutronics at the Weapons Neutron Research Facility	G.J. Russell	11:00-11:25
* Layout of the target station for the German project	G.S. Bauer	11:25-11:50
* Experimental results on ZING-P' target	J. Carpenter	11:50-12:15
Discussions		12:15-12:30
Lunch		12:30-14:00

Proceedings Reporter: Carpenter/Bauer/Watanabe

TUESDAY October 21 A.M.

Instrument I (B) (I-2) 9:00-12:30

Data aquisition system and detectors (I-2)

Chairman R.K. Crawford/S. Hoshino

* Discussions on meeting		9:00- 9:10
* SNS data acquisition system	N.W. Howells	9:10- 9:25
* KENS data acquisition system	M. Kohgi	9:25- 9:40
* IPNS data acquisition system	R.K. Crawford	9:40- 9:55
Discussions		9:55-10:30
Coffee Break		10:30-11:00
* Development of Li^6 glass scintillator in Japan	N. Niimura	11:00-11:15
* Neutron position sensitive scintillation detector	R.K. Crawford	11:15-11:30
* Position sensitive slow neutron detector using fiber optic encoding	N.W. Howells	11:30-11:45
* Data acquisition and handling of TOF-2dPSD	M. Arai	11:45-12:00
Discussions		12:00-12:30
Lunch		12:30-14:00

Proceedings Reporter: J. Newsam/N. Niimura

TUESDAY October 21 P.M.

Instrument II (A) 14:00-18:00

Spectrometers (constructed)

Chairman C.G. Windsor/Y. Endoh

* Instrument development for materials science research at WNR	J. Eckert	14:00-14:30
* Experimental results with ZING-P'	D.L. Price	14:30-14:50
* IPNS-1 scattering instrument	R.K. Crawford	14:50-15:10
* Harwell spectrometers	C.G. Windsor	15:10-15:30
Coffee Break		15:30-16:00
* Performance of KENS spectrometers		16:00-17:10
LAM and LANDAM (Hokkaido)	K. Inoue	16:00-16:20
HIT	N. Watanabe	16:20-16:40
MAX	K. Tajima	16:40-17:00
SAN	Y. Ishikawa	17:00-17:20
TOP	Y. Endoh	17:20-17:40
* Experimental results with Tohoku Linac		17:40-18:20
Experiments on liquid and amorphous materials	K. Suzuki	17:40-18:00
Performance of TOF-PSD spectrometer	M. Arai	18:00-18:20
Bus		18:30

Proceedings Reporter: Windsor/Endoh

TUESDAY October 21 P.M.

Technical session, Target II (B) (T-1/2) 14:00-18:00

Target station (Physics)

Chairman G.J. Russell/Y. Nakahara

* Neutron production and neutron production cross section measurements	G.J. Russell	14:00-14:20
* Studies on high energy spallation and fission reactions	Y. Nakahara	14:20-14:40
* Neutronics of continuous and quasi-continuous sources (Theoretical results)	D. Filges	14:40-15:00
* Some remarks on the neutronics in the spallation target	W.E. Fischer	15:00-15:20
Coffee Break		15:30-16:00
* Calculated performance of SNS target assembly	T.A. Broome	16:00-16:15
* Liquid metal target development	J.E. Vetter	16:15-16:35
* Molten salt target and blancket concept	K. Furukawa	16:35-16:55
* Alternative liquid metal target system	Ch. Tschalär	16:55-17:15
Discussions		17:15-18:00
* WNR target-moderator-reflector system	G.J. Russell	17:15-17:25

Proceedings Reporter: Russell/Nakahara

WEDNESDAY October 22 A.M.

technical session, Instrument III (A) (I-1/2)

Spectrometers (Designed)

Chairman J. Carpenter/K. Suzuki

* Advantage of neutron sources with time structure for special neutron spectrometer	N. Nücker	9:00- 9:20
* Some new instruments designed to utilize the time structure of a spallation neutron source	B. Alefeld	9:20- 9:40
* Discussions on various designed spectrometers		
Liquid diffraction	W.S. Howells	9:40-10:00
Small angle scattering	R.J. Stewart	10:00-10:15
Powder diffraction	W.S. Howells W.G. Williams	10:15-10:30
Coffee Service		10:30-
Inelastic spectrometer	B.C. Boland	10:30-10:45
Discussions		10:45-11:00

Ultra cold neutrons (I-1)

* The operation of a new ultra cold neutron source at the Argonne ZING-P' Pulsed Neutron Facilities	T. Dombeck	11:00-11:20
* KUR ultra cold neutron source	M. Utsuro	11:20-11:40
* KENS ultra cold neutron source	H. Yoshiki	11:40-12:00
Lunch		12:00-13:30
Excursion to Tsukuba Mountain		13:30-17:30

Proceedings Reporter: Windsor/Endoh/Yoshiki

WEDNESDAY October 22 A.M.

Technical session, Accelerator I and Target III (B) (T-1/2) 9:00-12:00

Chairman N.J. Swanson

* Review of accelerator development at LASL relevant to intense neutron source	A. Jameson	9:00- 9:20
* Linear accelerator for the German spallation neutron	J.E. Vetter	9:20- 9:40
* Material problems in beam window and structural component of the target	W. Lohman	9:40-10:00
Discussions		10:00-10:30
Coffee Break		10:30-10:50

Target III (B) (Discussions on target stations)

* Energy deposition in and head removal from moderators	A. Carne	10:50-11:20
* Target station systems	A. Carne	11:20-11:30
	T.A. Broome	11:30-11:40
	N.J. Swanson	11:40-11:50
	Open Discussion	11:50-12:00
Lunch		12:00-13:30
Excursion to Tsukuba Mountain		13:30-17:30

Proceedings Reporter: Bauer/Carne/Sasaki/Watanabe

THURSDAY October 23 A.M.

Technical session, Target station IV (A) (T-1) 9:00-12:30

Shielding, Activity handling, Safety

Chairman A. Carne/K. Katoh

* Discussions on meeting		9:00- 9:10
* Shielding	C.G. Windsor	9:10- 9:25
* KENS radiation shield	S. Ban	9:25- 9:45
* Shield materials for neutron source and their costs	M.M. Barbier	9:45-10:00
* Beam hole design	W.S. Howells	10:00-10:15
Discussions		10:15-10:30
Coffee Break		10:30-11:00
* Mechanical layout and activity handling of a high power target	H. Stechemesser	11:00-11:20
* KENS radiation activity		
Structural materials	H. Hirayama	11:20-11:30
Water and cold moderator	K. Kondoh	11:30-11:40
* Radioactivities induced in U-238 target	K. Katoh	11:40-12:00
* BSF beam control system	Y. Irie	12:00-12:15
* Safety and emergency system	H. Stechemesser	12:15-12:30
Lunch		12:30-14:00

Proceedings Reporter: Carne/Watanabe

THURSDAY October 23 A.M.

Technical session, Instrument IV (B) (I-2) 9:00-12:30

Accessary

Chairman W.G. Williams

* Discussions on meeting		9:00- 9:10
* SNS neutron guide	W.G. Williams	9:10- 9:25
* KENS neutron guide	J. Mizuki	9:25- 9:40
* SNS chopper	B.C. Boland	9:40- 9:55
* IPNS chopper	R.K. Crawford	9:55-10:10
* KENS chopper	M. Furusaka	10:10-10:25
Coffee Break		10:30-11:00

Polarized neutrons

* SNS polarized neutrons	W.G. Williams	11:00-11:20
* Polarized epithermal neutrons by polarized proton	S. Ishimoto	11:20-11:40
Discussions on polarized neutrons		11:40-12:30

Lunch

Proceedings Reporter: Newsam/Endoh

THURSDAY October 23 P.M.

Technical session 14:00-17:00

Discussions in separate groups

Target V (A)

Chairman G.S. Bauer

* Flux distribution in the reflector of continuous spallation sources (Theoretical and experimental) W.E. Fischer
* Neutronics of decoupled and undecoupled target-moderator-reflector systems (Experimental results) G.S. Bauer
* Measurement of neutron yield and fast neutron spectra from spallation target N. Nücker
* Angular distribution of high energy nucleous from 500 MeV proton on thick lead target I.M. Thorson
* State of the art of computer-codes in KFA Jülich D. Filges
* Integral experiment of neutron production cross section induced by 52 MeV protons based on MECC calculation T. Nakamura

Target VI (B)

Chairman N.J. Swanson

Special discussions on common problems

* Material problems-general (e.g. radiolysis of cooling water, radiation damage of ceramics, corrosion problems) W. Lohman
* Reentrant (finger) moderator techniques G.S. Bauer
* Material problems-liquid metals (e.g. corrosion,renting, seals, safety) Ch. Tschalär
* Cold neutron problems
* Quasi continuous neutron sources
* Open discussion

Proceedings Reporter: G.S. Bauer/N.J. Swanson

THURSDAY October 23 P.M.

Technical session

Discussions in separate groups

Instrument V (C)

Chairman R.J. Stewart/D.L. Price

Discussions on Diffractometers

* Dynamical correction of liquid diffraction with pulsed neutron source T. Matsumoto
* Small angle neutron scattering S. Komura

Discussions on Spectrometers

* High resolution TOF spectrometers in the long wave length region T.W. Dombeck
* Some remarks on the design of optimized thermal neutron scattering spectrometers W. Kley

Coffee Break

Free Discussions

Discussions for tomorrow's summary meeting **17:00-17:30**
(All attendants)

Chairman J. Carpenter

Bus 18:00

Meeting for next ICANS late evening
(Only for the representatives from each ICANS laboratories)

Summary of ICANS-IV

1.	Target (A) (Engineering)			9:10
	incl. Re-entrant Moderators	G.S. Bauer	(20 min)	
2.	Target (B) (Physics)			9:30
	incl. Neutron Yields	G.J. Russell	(20 min)	
3.	Shield & Safety + Energy Deposition	A. Carne	(20 min)	9:50
4.	Activity	N.J. Swanson	(15 min)	10:10
5.	Instrumentation	C.G. Windsor	(25 min)	10:25
6.	Data Acquisition	R.K. Crawford	(10 min)	10:50
7.	Polarized Target	W. Williams	(10 min)	11:00
8.	Ultra Cold Neutrons	T.W. Dombeck	(10 min)	11:10
				11:20
				(11:30)
Closing		H. Sasaki		11:30-12:00
Bus				12:00

APPENDIX: COMMON ABBREVIATIONS

Facilities

ANL	Argonne National Laboratory, USA
BSF	Booster Synchrotron Utilisation Facility, KEK Japan
ILL	Institut Max von Laue-Paul Langevin, Grenoble, France
IPNS	Intense Pulsed Neutron Source Project at ANL, USA
JAERI	Japan Atomic Energy Research Institute
KEK	Japan National High Energy Physics Laboratory, Tsukuba
KENS	KEK Neutron Source
KFA-KFK	Kernforschungszentrum Karlsruhe, Kernforschungsanlage Jülich, Germany
KUR	Kyoto University Reactor Kumatori, Japan
LASL	Los Alamos Scientific Laboratory, New Mexico, USA
RL	Rutherford and Appleton Laboratories, England
SIN	Schweizerisches Institut für Nuklearforschung, Switzerland
SNQ	Spallation Neutron Quelle (German spallation source project)
SNS	Spallation Neutron Source, Rutherford Laboratory, England
WNR	Weapons Neutron Research Facility, Spallation Neutron Source at LASL, USA
ZING-P'	Prototype Spallation Neutron Source at ANL, USA

Technical Terms and Instruments

FWHM	Full Width at Half Maximum
GM	Geiger-Müller
HIT	High Intensity Total scattering spectrometer at KENS
IRIS	High Resolution Quasielastic Spectrometer for the SNS
LAM	Large Analyser Mirror quasielastic spectrometer at KENS
MARX	Multi Angle Reflecting Crystal
MAX	Multi Analyser Crystal spectrometer at KENS
PG	Pyrolytic Graphite
PND	Powder Neutron Diffraction
PSD	Position Sensitive Detector
SAN	Small Angle Neutron spectrometer at KENS
SN	Signal: Noise ratio
TOF	Time of Flight
TOP	Time of Flight spectrometer with Optical Polariser at KENS
UCN	Ultra Cold Neutron

ICANS-IV PARTICIPANTS

(Participants from abroad)

Name	Affiliation	Photo
Alefeld, Berthold	KFA Jülich	3
Armstrong, Tony W.	KFA Jülich	25
Barbier, Marcel	Scientific Consulting	4
Bauer, Günter S.	KFA Jülich	28
Boland, Brian C.	RL	72
Broome, Timothy A.	RL	55
Burgerjon, J. J.	TRIUMF	57
Carne, Alan	RL	56
Carpenter, John M.	ANL	13
Crawford, Roy K.	ANL	18
Dombeck, Thomas W.	University of Maryland	62
Eckert, Juergen	LASL	54
Filges, Detlef	KFA Jülich	64
Fischer, Walter E.	SIN	42
Grand, Pierre	BNL	33
Howells, William S.	RL	75
Jameson, Robert A.	LASL	22
Keyworth, Geoffrey A.	LASL	8
Kley, Walter	Joint Research Centre EURATOM	61
Klose, Wolfgang	KFK Karlsruhe	15
Lohmann, Wolfgang	KFA Jülich	63
Manning, Geoffrey	RL	12
Nücker, Nikolaus H. H.	KFK Karlsruhe	2
Price, David L.	ANL	9
Russell, Gary J.	LASL	6
Stechemesser, Horst	KFA Jülich	65
Stewart, Roger J.	RL	17
Swanson, Norman J.	ANL	7
Thorson, Ian M.	TRIUMF	5
Tschalär, Christoph	SIN	1
Vetter, Joerg E.	KFK Karlsruhe	21
Williams, William G.	RL	19
Windsor, Colin G.	Harwell	70

(Participants from Japan)

Name	Affiliation	Photo
Adachi, Toshikazu	KEK	
Arai, Masatoshi	Tohoku Univ.	44
Arai, Toshihiro	Univ. of Tsukuba	
Asano, Hajime	Univ. of Tsukuba	
Ban, Shuichi	KEK	
Endoh, Yasuo	Tohoku Univ.	68
Fujino, Yutaka	Tohoku Univ.	43
Fukumoto, Sadayoshi	KEK	34
Fukunaga, Toshiharu	Tohoku Univ.	50
Furukawa, Kazuo	JAERI	26
Furusaka, Michihiro	Tohoku Univ.	67
Hamaguchi, Yoshikazu	JAERI	41
Hatta, Shin-ichiro	Gakushuin Univ.	
Hirayama, Hideo	KEK	
Hoshino, Sadao	Univ. of Tokyo	30
Inoue, Kazuhiko	Hokkaido Univ.	31
Ikeda, Susumu	KEK	36
Irie, Yoshiro	KEK	47
Ishida, Masayoshi	Tohoku Univ.	49
Ishikawa, Yoshikazu	Tohoku Univ.	16
Ishimaru, Hajime	KEK	
Ishimoto, Shigeru	KEK	
Kai, Kenzo	Tohoku Univ.	23
Kanai, Ken-ichi	Tohoku Univ.	46
Katoh, Kazuaki	KEK	38
Kawada, Isao	NIRIM	59
Kimura, Motoharu	Tohoku Univ.	10
Kiyanagi, Yoshiaki	Hokkaido Univ.	35
Kohgi, Masahumi	Tohoku Univ.	71
Kojima, Seiji	Univ. of Tsukuba	
Komura, Shigehiro	Hiroshima Univ.	
Kondoh, Kenjiro	KEK	
Kunitomi, Nobuhiko	Osaka Univ.	

Name	Affiliation	Photo
Masaike, Akira	KEK	
Matsumoto, Takaaki	Hokkaido Univ.	60
Mizoguchi, Tadashi	Gakushuin Univ.	
Mizuki, Jun-ichiro	Tohoku Univ.	74
Nakahara, Yasuaki	JAERI	24
Nakajima, Tetsuo	Tohoku Univ.	29
Nakamura, Takashi	Univ. of Tokyo	
Newsam, John M.	Tohoku Univ.	66
Niimura, Nobuo	Tohoku Univ.	69
Nishina, Kojiro	Nagoya Univ.	37
Nishikawa, Tetsuji	KEK	11
Ogawa, Shinji	Electrotechnical Lab	
Okamura, Fujio	NIRIM	
Ono, Hitoshi	Tohoku Univ.	48
Sasaki, Hiroshi	KEK	14
Shinohe, Takashi	Tohoku Univ.	
Suzuki, Kenji	Tohoku univ.	27
Suwa, Shigeki	KEK	
Tajima, Keisuke	Tohoku univ.	73
Takeda, Yasushi	Tohoku Univ.	53
Utsuro, Masahiko	KUR	39
Watanabe, Noboru	KEK	20
Yamada, Kazuyoshi	Tohoku Univ.	58
Yamaguchi, Sadae	Tohoku Univ.	41
Yamamuro, Nobuhiro	Tokyo Institute of Technology	32
Yashiki, Hajime	KEK	40

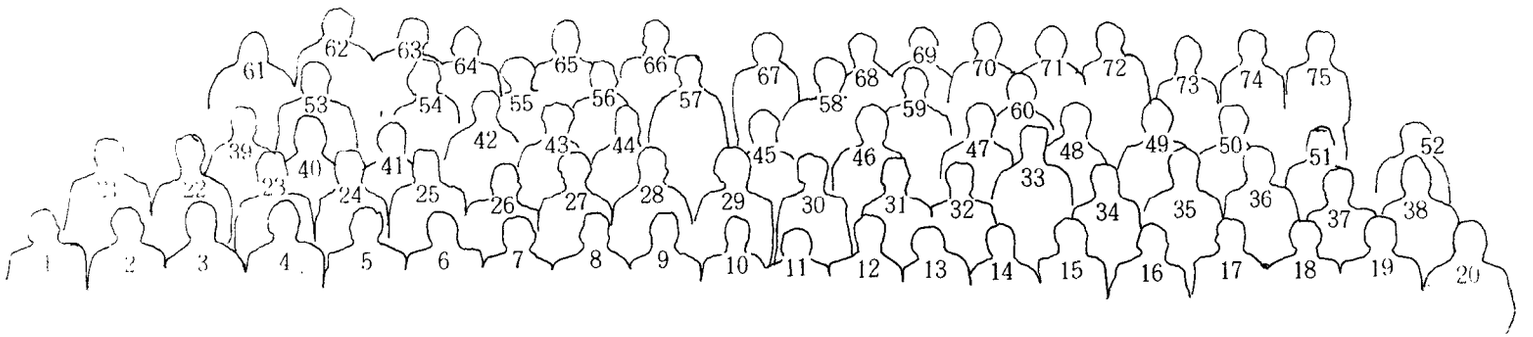

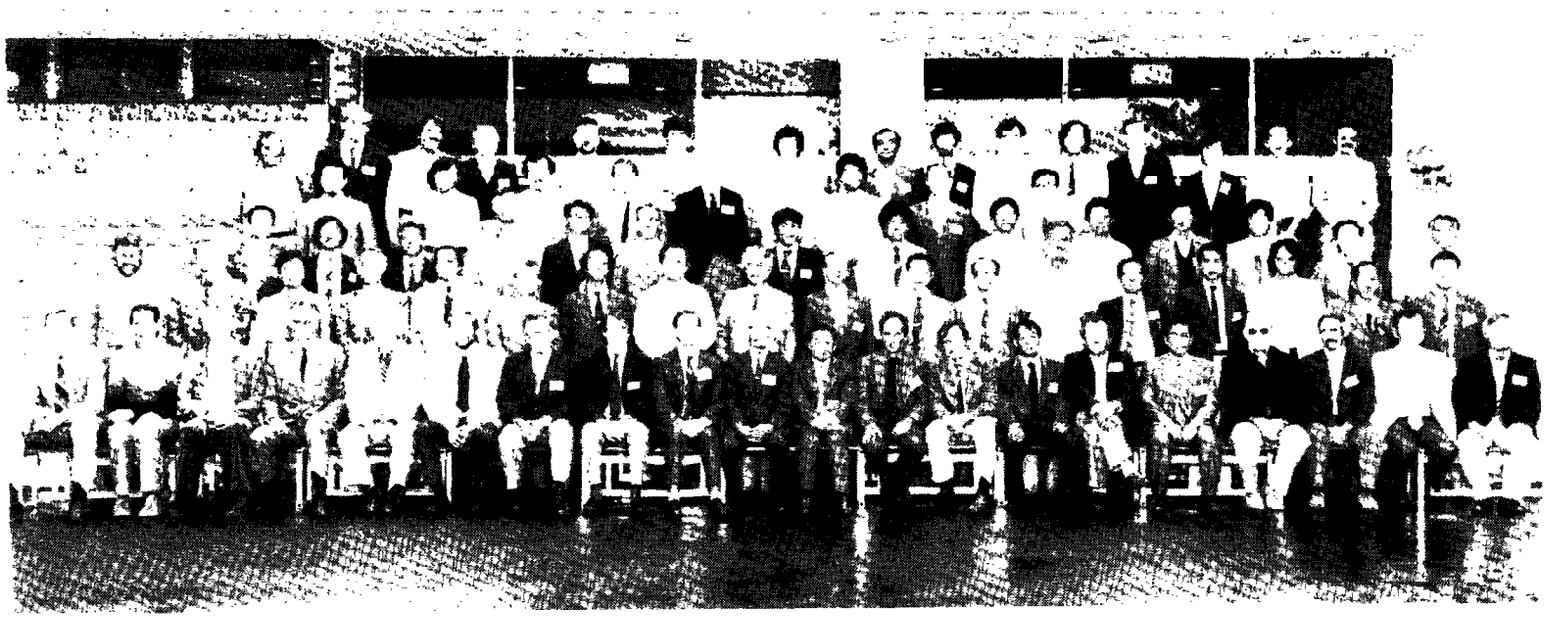

ICANS—IV October 20 to 24 1980 KEK Tsukuba Japan